TESIS DE LA UNIVERSIDAD DE ZARAGOZA

2017

39

Alexandre Lancelot

New dendritic derivatives for applications in nanomedicine: drug delivery and gene transfection

Departamento
Química Orgánica

Director/es
Serrano Ostáriz, José Luis
Sierra Travieso, Teresa

ISSN 2254-7606

Prensas de la Universidad
Universidad Zaragoza

ISSN 2254-7606

Universidad Zaragoza
1542

Tesis Doctoral

NEW DENDRITIC DERIVATIVES FOR APPLICATIONS IN NANOMEDICINE: DRUG DELIVERY AND GENE TRANSFECTION

Autor

Alexandre Lancelot

Director/es

Serrano Ostáriz, José Luis
Sierra Travieso, Teresa

UNIVERSIDAD DE ZARAGOZA

Química Orgánica

2017

TESIS DOCTORAL

NEW DENDRITIC DERIVATIVES FOR APPLICATIONS IN NANOMEDICINE: DRUG DELIVERY AND GENE TRANSFECTION

Author

Alexandre LANCELOT

Directors

José Luis SERRANO OSTÁRIZ

Teresa SIERRA TRAVIESO

Departamento de Química Orgánica
Facultad de Ciencias

Instituto de Nanociencia de Aragón (INA)
Instituto de Ciencias de Materiales de Aragón (ICMA)

Zaragoza, marzo de 2017

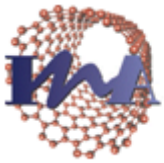

Instituto Universitario de Investigación
en Nanociencia de Aragón
Universidad Zaragoza

TESIS DOCTORAL

NEW DENDRITIC DERIVATIVES FOR APPLICATIONS IN NANOMEDICINE: DRUG DELIVERY AND GENE TRANSFECTION

Memoria presentada en la Universidad de Zaragoza para optar al grado de Doctor

Alexandre LANCELOT

Departamento de Química Orgánica
Facultad de Ciencias
Universidad de Zaragoza - CSIC

Instituto de Nanociencia de Aragón (INA)
Instituto de Ciencias de Materiales de Aragón (ICMA)

Zaragoza, marzo de 2017

Departamento de
Química Orgánica
Universidad Zaragoza

Prof. JOSÉ LUIS SERRANO OSTÁTRIZ, Catedrático del departamento de Química Orgánica de la facultad de Ciencias de la Univerisdad de Zaragoza perteneciendo al Instituto de Nanociencia de Aragón y

Dra. TERESA SIERRA TRAVIESO, Investigador Científico del Consejo Superior de Investigaciones Científicas del Instituto de Ciencia de Materiales de Aragón de la Universidad de Zaragoza-CSIC.

HACEN CONSTAR:

Que la memoria titulada: "New dendritic derivatives for applications in nanomedicine: drug delivery and gene transfection" ha sido realizada bajo nuestra dirección por Don ALEXANDRE LANCELOT en el Departamento de Química Orgánica de esta Universidad y reúne las condiciones requeridas para su presentación como tesis doctoral.

Zaragoza, a 31 de marzo de 2017

Fdo.: Prof. José Luis Serrano Ostariz Fdo.: Dra. Teresa Sierra Travieso

A mes grands-pères,
A mon frère,

Pour le savant, croire la Science achevée
est toujours une illusion aussi complète que le serait
pour l'historien de croire l'Histoire terminée.

Louis Victor de Broglie
(Dieppe, 1892 - Paris, 1987)

Agradecimientos

Me gustaría agradecer a mis directores de tesis, José Luis y Teresa, para ofrecerme la posibilidad de realizar una tesis doctoral y para su ayuda y consejos a lo largo de estos 4 años.

Quiero agradecer también a todos los miembros del grupo de Cristales Liquídos y polímeros de la Universidad de Zaragoza así como el departamento de Química Orgánica de la Universidad de Zaragoza, el Instituto de Nanociencia de Aragón (INA), el Laboratorio de Microscopias avanzadas (LMA) y el Instituto de Ciencias de Materiales de Aragón (ICMA).

Quiero agradecer a la Dra. Olga Abián y a Rafael Clavería-Gimeno del Instituto de Biocomputación y Física de Sistemas Complejos (BIFI) para su fructífera colaboración durante el estudio de los derivados dendríticos como transportadores de camptotecina.

Quiero agradecer a la Dra. Pilar Martín-Duque y a Rebeca González-Prado del Centro de Investigación Biomédica de Aragón (CIBA) para su ayuda y colaboración durante el estudio de los derivados dendríticos como vectores no-virales de material genético.

Quiero agradecer al Dr. Xavier Fernàndez-Busquets perteneciendo al Instituto de Bioengeneria de Cataluña (IBEC) y al Instituto de Salud Global de Barcelona (ISGlobal) para ofrecerme la posibilidad de realizar una estancia en su grupo. Así mismo quiero agradecer a todos los miembros del grupo Nanomalaria y en particular a Elisabet Martí Coma-Cros para su ayuda, disponibilidad y el estudio de los derivados dendríticos como transportadores de fármacos antimaláricos.

Finalmente, quiero agradecer al ministerio de educación, cultura y deporte (MECD) para ofrecerme la posibilidad de realizar una tesis doctoral a través de une beca FPU nº12/05210, al ministerio de economía y competitividad por la financiación económica a través de los proyectos "*nuevas plataformas multifuncionales basadas en estructuras dendrímericas auto-organizables para aplicaciones en biomedicina y materiales avanzados*" (CTQ2015- 70164-P) y " Dendrímeros funcionales: nuevas herramientas para la obtención de materiales avanzados y aplicaciones biomédicas" (CTQ2012-35692) y al Gobierno de Aragón-FSE (E04- Grupo de Investigación).

Acronyms

^{1}H-NMR	Proton nuclear magnetic resonance
^{13}C-NMR	Carbon-13 Nuclear magnetic resonance
A_n	Absorbance at *n* nm
a_0	Surface area of the hydrophilic part
AIDS	Acquired immune deficiency syndrome
BIFI	Biocomputation and Physics of Complex Systems
bis-GMPA	*2*,2'-*bis*(glyciloxymethyl) propionic acid
bis-MPA	2,2'-*bis*(hydroxymethyl)propionic acid
bis-GMPA monomer*	t-Boc-protected bis-GMPA monomer
bis-MPA monomer*	ketal-protected *bis*-MPA monomer
CAC	Critical aggregation concentration
CC_{50}	Half-maximal cytotoxic concentration
CDI	N,N'-carbonyldiimidazole
CIBA	Center of Biomedical Investigation of Aragon
COSY	Correlation spectroscopy
CPT	Camptothecin
CQ	Chloroquine
CQb	Chloroquine in its lipophilic base form
CQs	Chloroquine in its hydrophilic salt form
cryoTEM	Cryogenic transmission electron microscopy
CuAAC	Copper(I) azide-alkyne cycloaddition
EC_{50}	Half-effective heparin complexation
EC_{100}	Effective heparin complexation
Đ	Polydispersity index
DB	Degree of branching
DCC	N,N'-dicyclohexylcarbodiimide

DCM	Dichloromethane
DCU	N,N'-dicyclohexylurea
D_H	Hydrodynamic diameter
dend.	Dendritic derivative
DHP	Dendronized hyperbranched polymers
DL	Detection limit
DLS	Dynamic light scattering
DMSO	Dimethyl sulfoxide
DNA	Deoxyribonucleic acid
DMAP	Dimethylaminopyridine
DMEM	Dublecco's Modified Eagle's Medium
DMF	Dimethylformamide
dnc	Dendritic nanocarrier
DPTS	(dimethylamino)pyridinium 4-toluenesulfonate
EPR	Enhanced permeability and retention
EA	Elemental analysis
EDC·HCl	N-(3-dimethylaminopropyl)-N'-ethylcarbodiimide hydrochloride
EE	Encapsulation efficiency
EGFP	Enhanced green fluorescent protein
ESI^+	Positive electrospray inonization
EtOAc	Ethyl acetate
FDA	Food and drug administration
FTIR	Fourier transform infrared spectroscopy
G	Generation
GATG	Gallic acid-triethylene glycol
GFP	Green fluorescent protein
GIA	Growing inhibiton assay
HCV	Hepatitis C virus

Hela	Human epithelial carcinoma cells
Hep	Heparin
HDLDBC	Hybrid dendritic-linear-dendritic block copolymer
HLDBC	Hybrid linear-dendritic block copolymer
HIV	Human immunodeficiency virus
HOBt	1-hydroxybenzotriazole hydrate
HSQC	Hetero nuclear single-quantum correlation spectroscopy
Huh	Human heptoma cell lines
H/L	Hydrophilic lipophilic ratio
IBEC	Institute for Bioengineering of Catalonia
IC_{50}	Half-maximal inhibition concentration
ICP-AES	Inductively coupled plasma atomic emission spectroscopy
ISGlobal	Barcelona Institute for Global Health
Ka	Acid dissociation constant
l	Length of the lipophilic part
LADMET-R	Liberation, absorption, distribution, metabolism, excretion, toxicity and activity/response
L-Asc	(*L*)-ascorbate
LCST	Lower critical solution temperature
LOQ	Limit of quantification
MALDI-Tof	Matrix assisted laser desorption/ionization - time of flight
MB	Methylene blue
MeOH	Methanol
MDSK-GFP	Epithelial kidney cells from dog expressing GFP
mMSC	Mousse origin mesenchymal stem cells
MSC	Mesenchymal stem cells

mRNA	Messenger ribonucleic acid
Mn	Number average molecular weight
MS	Mass spectrometry
Mw	Mass average molecular weight
MW	Molecular weight
NHS	N-hydroxysuccinimide
N^+/P^-	N^+ peripheral atoms P^- atoms of the genetic material ratio
pDNA	Plasmid deoxyribonucleic acid
p	Packing parameter
PAMAM	Poly(amidoamine)
PBS	Phosphate saline buffer
PEI	Poly(ethylene imine)
PEG	Polyethylene glycol
PEO	Polyethylene oxide
PG	Polyglycerol
PGLSA	Polyglycerolsuccinic acid
PLL	Poly-(*L*)-lysine
PLU	Pluronic® F-127
PMMA	poly(methyl methacrylate)
PPI	Poly(propylene imine)
PPO	Polypropylene oxide
PQ	Primaquine
PQb	Primaquine in its lipophilic base form
PQs	Primaquine in its hydrophilic salt form
QN	Quinacrine
QNb	Quinacrine in its lipophilic base form
QNs	Quinacrine in its hydrophilic salt form
RBC	Red blood cells

RES	Reticulo-endothelial system
RNA	Ribonucleic acid
SEC	Size exclusion chromatography
SKOV3-Luc	Cancerous human ovary cells expressing luciferease
siGFP	GFP specified small interfering RNA
siLuc	Luciferease specified small interfering RNA
siRNA	Small interfering ribonucleic acid
sub.	Substance
t-Boc	*Tert*-butoxycarbonyl
TBTA	Tris(benzyltriazolylmethyl)amine
t-Boc glycine	*N*-(*tert*-butoxycarbonyl)glycine
TEM	Transmission electon microscopy
TI	Therapeutic index
THF	Tertahydrofuran
U251 MG	Human neuronal glycobastoma (astrocytoma) cell line
U_b	Fully branched internal groups
U_p	Peripheral terminal groups
USP	U.S. Pharmacopeial
U_t	Internal terminal groups
UV-VIS	Ultraviolet-visible
V	Volume of the lipophilic part
w	weight
WHO	World Health Organisation
%w	Percentage in weight

Index

Chapter 1- Introduction **1**

Chapter 2- State of the art **9**

2.1- Drug and gene delivery, two attractive nanomedicine applications 13
2.1.2- Smart nanocarriers for drug delivery 13
2.1.1.1- General aspects of advanced drug delivery systems 13
2.1.1.2- Designing new smart nanocarriers and nanocarrier/ drug conjugation 18
2.1.2- Gene therapy 24
2.1.2.1- An innovative, precise and versatile new therapy 24
2.1.2.2- Vectorisation of gene therapy for a better efficiency 27

2.2- Dendritic derivatives, alluring materials for nanomedicine applications 33
2.2.1- Dendrimer, an overview 34
2.2.1.1- General properties of dendrimers 34
2.2.1.2- Synthesis of dendrimers 37
2.2.2- Dendritic-polymer hybrids, derivatives at the intersection of classical polymers and dendrimers 44
2.2.2.1- Hyperbranched polymers 44
2.2.2.2- Hybrid dendritic-linear-dendritic block copolymers 50
2.2.3- Self-assembly in water of amphiphilic dendrimers and hybrid linear-dendritic block copolymers 53
2.2.3.1- Amphiphilic derivatives in water 53
2.2.3.2- Amphiphilic dendritic derivatives, interesting supramolecular aggregates 56
2.3- An extended library of dendritic materials for drug and gene delivery 62
2.3.1- Most common dendrimers and dendritic derivatives based on nitrogen functions 62
2.3.1.1- Poly(amidoamine) dendrimers 62
2.3.1.2- Poly(imine) dendrimers 66
2.3.1.3- Polyamide dendrimers 68
2.3.2- Most common dendrimers and dendritic derivatives based on oxygen functions 70

2.3.2.1- Bis-MPA and other polyester dendrimers 70
2.3.2.2- Polyether dendrimers 75
2.3.3- Other dendrimers used for nanomedicine 77

Chapter 3- Objective and working plan 79

Chapter 4- Amphiphilic *bis*-MPA and *bis*-GMPA dendritic derivatives for camptothecin delivery 89

4.1- *Bis*-MPA and *bis*-GMPA dendrons 93
4.1.1- Bis-MPA dendrons 95
4.1.1.1- *t*-Boc protected amino terminated bis-MPA dendrons 95
4.1.1.2- Lipophilic bis-MPA dendrons 100
4.1.2- *Bis*-GMPA dendrons 104
4.1.3- Biocompatibility and degradability 114
4.2- Amphiphilic *bis*-MPA and *bis*-GMPA dendritic derivatives 118
4.2.1-Synthesis and chemical characterization 124
4.2.1.1- Amphiphilic Janus dendrimers 124
4.2.1.2- Hybrid dendritic-linear-dendritic block copolymers 131
4.2.2- Self-assembly in water 137
4.2.2.1- Amphiphilic Janus dendrimers 138
4.2.2.2- Hybrid dendritic-linear-dendritic block copolymers 152
4.3- Amphiphilic Janus dendrimers and HDLDDBCs as camptothecin nanocarriers 157
4.3.1- Nanocarriers/camptothecin conjugates 162
4.3.1.1- Camptothecin encapsulation 162
4.3.2.2- Morphological studies 166
4.3.2- In vitro evaluation of the nanocarriers/camptothecin conjugates 172
4.3.2.1- Antiviral activity against HCV and cytotoxicity 172
4.3.2.2- Cell internalization 181
4.4- General remarks 195

Chapter 5- *Bis*-GMPA and *bis*-MPA globular dendritic derivatives for gene transfection 197

5.1- *Bis*-GMPA and *bis*-MPA globular dendritic derivatives 201
5.1.1- Synthesis and chemical characterization 202
5.1.1.1- *Bis*-GMPA dendrimers 202
5.1.1.2- Bis-MPA dendronized hyperbranched polymers 208

5.1.2- Properties 217
5.1.2.1- Biocompatibility 217
5.1.2.2- pH change response 220
5.1.2.3- Aggregation in water 224
5.2- Gene therapy 227
5.2.1- Dendriplex formation and characterization 229
5.2.1.1- Dendriplex formation 229
5.2.1.2- Morphological studies 235
5.2.2- siRNA and pDNA transfection 242
5.2.2.1- siRNA transfection 243
5.2.2.2- pDNA transfection 246
5.3- General remarks 250

Chapter 6- *Bis*-MPA and bis-GMPA HDLDBCs and *bis*-MPA DHPs as antimalarial drug nanocarriers 251
6.1- Hybrid dendritic-linear-dendritic block copolymers (HDLDBCs) 261
6.1.1- Chloroquine, primaquine and quinacrine encapsulation 261
6.1.1.1- Preparation of the lipophilic base form of the drugs 261
6.1.1.2- Drugs encapsulation 265
6.1.2- *In vitro* targeting studies 268
6.1.2.1- Labeling with rhodamine B 268
6.1.2.2- Targeting experiments 270
6.2- Dendronized hyperbranched polymers coated with heparin 272
6.2.1- Chloroquine, primaquine and quinacrine encapsulation 274
6.2.2- Heparin complex formation 277
6.2.2.1- DHP-heparin complexes 278
6.2.2.2- DHP/drug-heparin complexes 279
6.2.3- Morphological studies 283
6.2.4- *In vitro* targeting studies 285
6.2.4.1- Synthesis of a *bis*-MPA DHP labeled with rhodamine B 285
6.2.4.2- Targeting experiments 288
6.3- *In vitro plasmodium* growing inhibition assays (GIAs) 292
6.4- General remarks 294

Chapter 7- Experimental part 297

7.1 Synthesis and chemical characterization 299
7.1.1- Materials and equipments 299

7.1.2- *Bis*-MPA and *bis*-GMPA dendrons 301
7.1.2.1- *Bis*-MPA dendrons 301
7.1.2.2- *Bis*-GMPA dendrons 320
7.1.3- Amphiphilic dendritic derivatives for camptothecin delivery 333
7.1.3.1- Amphiphilic Janus dendrimers 333
7.1.3.2- Amphiphilic hybrid dendritic-linear-dendritic block copolymers (HDLDBCs) 348
7.1.4- Globular dendritic derivatives for gene transfection 357
7.1.4.1- *Bis*-GMPA dendrimers 357
7.1.4.2- *Bis*-MPA dendronized hyperbranched polymers 363
7.1.5- Other derivatives 372
7.1.5.1- Rhodamine B derivatives 372
7.1.5.2- Antimalarial drug in their lipophilic base form 378
7.1.5.3- Tris(benzyltriazolylmethyl)amine (TBTA) 382
7.2- Working protocols 383
7.2.1- General working protocols and apparatus 383
7.2.2- Study of the amphiphilic dendritic derivatives for camptothecin delivery 385
7.2.3- Study of the globular dendritic derivatives for gene transfection 392
7.2.4- Study of the dendritic derivatives as antimalarial nanocarriers 396

Chapter 8- Resumen y conclusiones 403

Annexes 417

Chapter 1

Introduction

Nanoscience and nanotechnology refer to a recent scientific approach situated at the convergence of physics, chemistry, biology and engineering. They deal with the production and manipulation of materials that have at least one dimension between 1 and 100 nm. Although nanoscience and nanotechnology broke into scientific literature in the 1980s, nanomaterials were actually used since ancient times. Two of the most famous examples are the Damascus steel, which was produced by Persians from the twelfth to the seventeenth century and resulted of material changes at the nanometric scale, and the red ruby stain glass of cathedrals built in the Middle Age. However, these old techniques remained empirical and were only based on people's know-how. It was not until 1959 that the nanotechnology concept was first described during Richard Feynman's lecture, "*there's plenty of room at the bottom"*. He claimed that new properties should be reached by modifying the materials directly at the atomic level. Indeed, the properties of materials may change at this tiny scale. Therefore, mechanical properties, electric or thermal conductivity, magnetism, *etc*. might be enhanced while comparing a nanometric material with its homologous macroscopic material.[1]

[1] R. Feynman, *There's plenty of room at the bottom*, American Physical Society meeting, Caltech, **1959**, December 29th.

A large **variety of nanomaterials** exists (**figure C_1-1**). They can be organic, inorganic or hybrids and adopt different morphologies. They are found as spheres, helixes, rods, fibers, *etc*. Some of them are natural whereas others are synthetic. Undoubtedly, numerous nanomaterials can be found in biological systems. For example, the protein membrane of viruses, the capsid, is a highly functionalized nanomaterial, the size of which ranges between 10 and 400 nm. Keratin is a natural biopolymer that can self-assemble into helix-forming fibers of micrometer length and with nanometric width. It can be found in hair, nails or other horny materials.

Synthetic nanomaterials can be based on metals or oxides, such as gold or silica, or organic compounds. As examples, fullerene and graphene are well-known nanomaterials that are usually added to improve the properties of other materials. Besides, giant polymeric molecules can rapidly reach the nanometric size and small organic molecules, such as surfactants, can spontaneously self-assemble into nanosized structures. A large number of procedures have been engineered for the synthesis of nanomaterials with a homogenous size and morphology. In parallel, other procedures have been developed to modify the nanomaterials in order to improve their properties.[2]

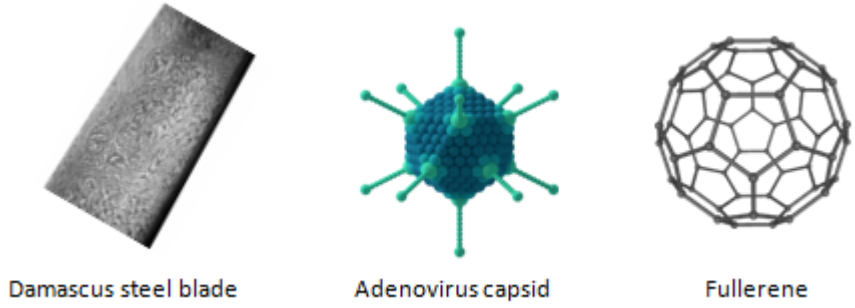

Figure C_1-1: Examples of nano- or nanostructured materials.

In the last centuries, medicine, jointly to science, has evolved and some acute or fatal diseases, such as small pox, have been eradicated. France, Japan,

[2] J.J. Ramsden, Nanotechnology: an introduction, 2nd edition, **2016**, Elsevier, Oxford, UK.

Canada and Australia are the countries in which the life expectancy is the highest: it rises to more than 83 years for women and more than 78 years for men. However, as population became older, degenerative and cardiovascular diseases, such as cancers or Alzheimer's disease, started to spread. For instance, the OMS predicted that cancer death would increase by 45 % in the world between 2007 and 2030. At the same time, new severe diseases have appeared like the acquired immune deficiency syndrome (AIDS), Ebola virus disease, Creutzfeldt–Jakob disease, *etc.* while other older ones, like influenza or malaria, still provoke numerous deaths worldwide.

New treatments have been developed to cure patients that have contracted these severe diseases although they usually cause painful side effects. For example, chemotherapeutic cancer treatments are usually based on cytotoxic agents that interfere with the cell division. Thus, they naturally target cancer cells that have an abnormal replication. Unfortunately, they also damage healthy cells that divide rapidly such as cells located in the bone narrow, in the digestive system and in the hair or the skin, generating side effects that are hardly endured by patients. Triple therapies, used as treatments against AIDS or hepatitis C viral infection, are also known to produce harsh side effects. As these diseases present a slow evolution with generally few symptoms, patients might be tempted to stop the treatment, provoking its failure. Brain diseases, such as Alzheimer's or Parkinson's diseases, are particularly difficult to cure in part due to the difficulty for the drugs to reach the brain tissues. Therefore, the development of novel innovative therapies that can reduce the side effects of these treatments or improve their efficacy is a current need.

It is in this context of development of new nanomaterials and social expectancies for new therapies easier to handle that **nanomedicine** rose in the 2000's. Thanks to their nanometric size that facilitates their mobility in physiological media, inside and outside the cells, combined with the evolution

of the procedures for nanomaterial preparation, nanomaterials specially designed to improve various biomedical applications are nowadays available. Thus, nanomedicine actually investigates medical diagnostic and imaging, smart drug delivery, drugs resistance, tissue reparation as well as new therapies like gene delivery or new antibacterial therapies against multi-resistant bacteria (**Figure C_1-2**).[3]

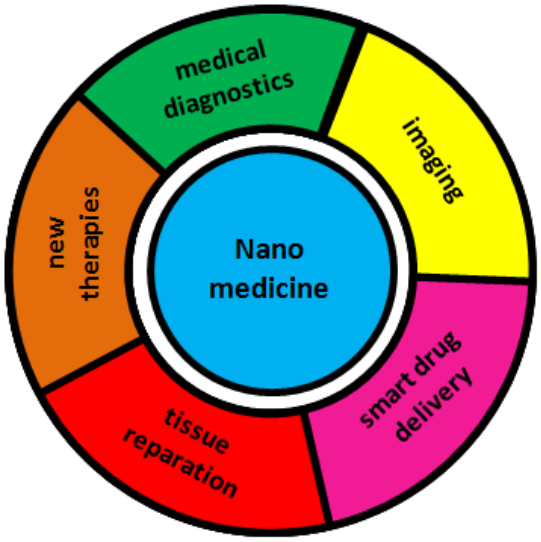

Figure C_1-2: Nanomedicine applications.

Even if nanomedicine is a **young and interdisciplinary field**, hundreds of nanomedical products have been approved or are under **clinical investigation**. Probably, it is for drug delivery purposes that the benefits of nanomedicine have gone the farthest.[4] For example, paclitaxel is an anticancer drug, commercialized under the name Taxol®, that is generally administrated using a formulation based on ethanol associated with a heterogeneous mixture of surfactantcs (Cremophor EL®). This formulation allows increasing the water solubility of the drug but may cause allergic

[3] T.L. Doane, C. Burda, The unique role of nanoparticles in nanomedicine: imaging, drug delivery and therapy, *Chem. Soc. Rev.*, **2012**, 41, 2885-2911.
[4] Y. Min, J.M. Caster, M.J. Eblan, A.Z. Wang, Clinical translation of nanomedicine, *Chem. Rev.*, **2015**, 115, 11147-11190.

reactions and precipitation during its administration to the patients.[5] Two new formulations based on nanomaterials have been developed, approved and commercialized to overcome these drawbacks. Genexol-PM® formulation associates the drug with nanosized amphiphilic polymers[6] while Abraxane® associates the drug with protein-based nanoparticles.[7] Another example is Vivagel®; this condom lubricant contains a nanometric dendrimer that is able to stack on the surface of the human immunodeficiency virus (HIV) limiting its transmission. The active ingredient is the dendritic nanomaterial and any other antiviral drug has to be include in this formulation.[8]

Among all the new possibilities offered by nanomedicine, this thesis will focus on drug delivery and gene therapy. New dendritic systems, based on previously existing polyester structures or novel poly(esteramide) architectures, are proposed to afford new solutions to these nanomedical applications. The synthesis and the properties of these new materials are described and their possible applications are discussed in comparison with other well-known standard systems.

[5] A.K. Singla, A. Garg, D. Aggarwal, Paclitaxel and its formulations, *Int. J. Pharm.*, **2002**, 235, 179-192.

[6] S.C. Kim, D.W. Kim, Y.H. Shim, J.S. Bang, H.S. Oh, S. Wan Kim, M.H. Seo, *In vivo* evaluation of polymeric micellar paclitaxel formulation: toxicity and efficacy, *J. Control. Release*, **2001**, 72, 191-202.

[7] F. Dosio, P. Brusa, P. Crosasso, S. Arpicco, L. Catte, Preparation, characterization and properties *in vitro* and *in vivo* of a paclitaxel–albumin conjugate, *J. Control. Release*, 1997, 47, 293-304.

[8] J. O'Loughlin, I.Y. Millwood, H.M. McDonald, C.F. Price, J.M. Kaldor, J.R. Paull, Safety, tolerability, and pharmacokinetics of SPL7013 Gel (Vivagel): a dose ranging, phase I study, *Sex. Transm. Dis.*, **2010**, 37, 100-104.

Chapter 2

State of the art

2.1- Drug and gene delivery, two attractive nanomedicine applications

Important concepts related with the application of nanomedicine to drug and gene delivery, as well as relevant previous works are discussed in this section.

2.1.1 - Smart nanocarriers for drug delivery

2.1.1.1 - General aspects of advanced drug delivery systems

Drug delivery carriers are defined as vehicles employed for the delivery of drugs in order to target the sites of their pharmacological actions. They can be nanometrically sized or bigger. Their goal is to provide a more effective way to deliver the drugs, modifying their physicochemical properties and/or allowing them to overcome some biological barriers. Drug delivery systems started to be used in the 1960's when the first sustained drug release devices based on silicone rubber was employed to control the diffusion of ocular (pilocarpine) or contraceptive (progesterone) drugs in the body.[9] Sustained release was then extended to other drugs by controlling their diffusion or dissolution into the physiological medium employing oral or topical administration routes.[10]

[9] J. Folkman, D.M. Long, The use of silicone rubber as a carrier for prolonged drug therapy, *Surg. Res.*, **1964**, 4, 139-142.

[10] A.S. Hoffman, The origins and evolution of "controlled" drug delivery systems, *J. Control. Release*, **2008**, 132, 153-163.

Later, in 1980's, a new class of drug delivery carriers emerged and was defined as ***"smart carriers"***. They were designed to extend the available drug library and improve their selectivity, effectiveness and/or safety. To do so, aspects other than sustained drug release were taken into account, *i.e*. drug aqueous media solubility and stability, drug pharmacokinetics, targeted drug release, etc.[10]

Solubility in aqueous media and stability are important factors to consider in **drug design**. Low water solubility and/or stability can impede the use of new drugs as effective therapeutic agents. Camptothecin drug is a good example to illustrate these two limitations. This drug shows a remarkable anticancer activity but it has failed to pass clinical trials. Indeed, it presents really low water solubility associated to low water stability (**figure C_2-1**). To overcome these drawbacks, camptothecin has been chemically modified in order to increase both its water solubility and its stability. Currently, topotecan® and irinotecan® are two camptothecin analogues approved by the Food and Drug Administration (FDA) for chemotherapy. Another way is to associate camptothecin with drug delivery nanocarriers that would increase its water

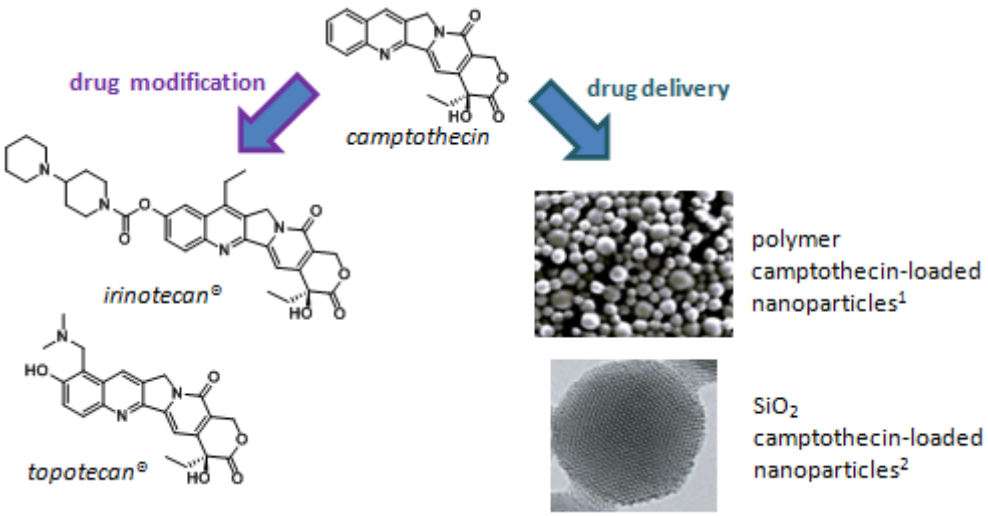

Figure C_2-1: Camptothecin drug and its two FDA (Food and Drug Administration) approved chemotherapeutic analogues and two drug delivery carriers based on organic and inorganic nanoparticles. [1] Adapted from refs. [11b], [2] adapted from ref. [11c].

solubility and activity. Hence, good *in vitro* and *in vivo* anticancer activity have been observed after administration of covalent or non-covalent camptothecin loaded carriers.[11]

Drug pharmacokinetics refers to the study of a drug and its metabolites in the body over time and gathers other parameters that can be tuned by drug delivery. These parameters correspond to seven properties: liberation, absorption, distribution, metabolism, excretion, toxicity and activity/response, also called ***LADMET-R* properties**. Liberation and absorption are responsible of the bioavailability of the drug and are the first two steps. They correspond to the liberation of the active form of the drug form the formulated medication and its entry into the bloodstream. The third property is distribution, which corresponds to the repartition of the drug into the different tissues. Metabolism and excretion processes modify the presence of the active form of the drug within the body. Two other parameters must be taken in account: the toxicity of the drug and of its metabolites and how the diseased tissues would response to the drug activity (**figure C_2-2**).[12]

Drug delivery nanocarriers can easily modify some of these parameters in order to **improve the pharmacokinetics** of a drug.[13] Thus:

- They can increase the drug penetration into the bloodstream, affording a better and less factors dependent drug bioavailability.[14]

[11] a) P. Botella, E. Rivero-Buceta, Safe approaches for camptothecin delivery: structural analogues and nanomedicines, *J. Control. Release*, **2017**, 247, 28-54; b) J. Lu, Z. Li, J.I. Zink, F. Tamanoi F, *In vivo* tumor suppression efficacy of mesoporous silica nanoparticles-based drug-delivery system: enhanced efficacy by folate modification, *Nanomedicine*, **2012**, 8, 212-220; d) K.T. Householder, D.M. Di Perna, P.E. Chung, G.M. Wohlleb, H.D. Dhruv, M.E. Berens, R.W. Sirianni, Intravenous delivery of camptothecin-loaded PLGA nanoparticles for the treatment of intracranial glioma, *Int. J. Pharm.*, **2015**, 479, 374-380.

[12] A. Ruiz-Garcia, M. Bermejo, A. Moss, V.G. Casabo, Pharmacokinetics in drug discovery, *J. Pharm. Sci.*, **2008**, 97, 654-690.

[13] M. Hamidi, A, Azadi, P. Rafiei, H. Ashrafi, A pharmacokinetic overview of nanotechnology-based drug delivery systems: an ADME-oriented approach, *Crit. Rev. Ther. Drug Carrier Syst.*, **2013**, 30, 435-467.

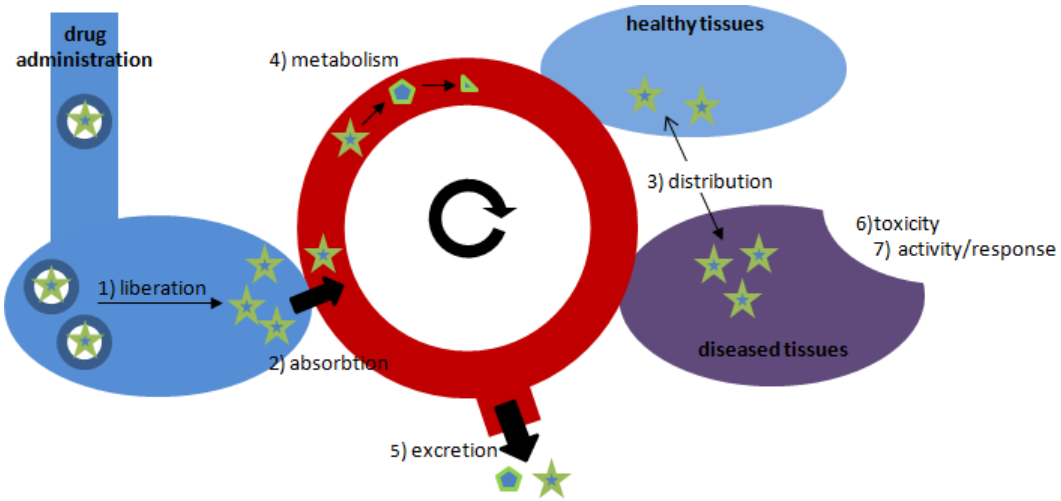

Figure C_2-2: schematic representation of the LADMET-R properties.

- They can improve the circulation time of the drug in the bloodstream, avoiding rapid clearance by the kidneys or the reticulo-endothelial system (RES). Low molecular drugs, with size inferior to 10 nm, are particularly affected by renal clearance whereas high molecular drugs with size of hundreds of nanometers, such as proteins, may be quickly detected by RES and eliminated from the bloodstream.[15]

- They can ameliorate the drug concentration within the desired tissues, by especially targeting the diseased ones.[16]

- They can limit the drug side effects, such as cytotoxicity, as a consequence of a better bioavailability and a higher drug concentration within the diseased tissues,[17]

- *etc*.

[14] C. Feng, J. Li, Y. Mu, M. Kong, Y. Li, M.A. Raja, X.J. Cheng, Y. Liu, X. Guang Chen, Multilayer micro-dispersing system as oral carriers for co-delivery of doxorubicin hydrochloride and P-gp inhibitor, *Int. J. Biol. Macromolec.*, **2017**, 97A, 170-180.

[15] L.X. Long, J. Zhao, K. Li, L.G. He, X.M. Qian, C.Y. Liu, L.M. Wang, X.Q. Yang, J. Sun, Y. Ren, C.S. Kang, X.B. Yuan, Synthesis of star-branched PLA-b-PMPC copolymer micelles as long blood circulation vectors to enhance tumor-targeted delivery of hydrophobic drugs *in vivo*, *Mater. Chem. Phys.*, **2016**, 180, 184-194.

[16] L. B-Peppas, J.O. Blanchette, Nanoparticle and targeted systems for cancer therapy, *Adv. Drug Deliv. Rev.*, **2004**, 56, 1649-1659.

[17] I. Ojima, E.S. Zuniga, W.T: Berger, J.D. Seitz, Tumor-targeting drug delivery of new-generation taxoids, *Future Med. Chem.*, 2012, 4, 33-50.

Many efforts have been made in order to develop **targeted drug delivery nanocarriers**. Indeed, these carriers can carry drugs into the diseased tissues improving specific drug distribution and therefore reducing both the quantity of drug that has to be administrated to patients and the drug side effects. Targeting can be either active or passive.

Passive targeting is based on the **enhanced permeability and retention** (EPR) effect, which has shown a good selectivity for solid tumors. Indeed, solid tumors need high supply of nutrients and oxygen to sustain their quick growth. This results in the formation of blood vessels with a defective architecture, more permeable than normal ones, and favors the absorption and retention of nanocarrier/drug conjugates within the interstitial space between the blood vessels and the tumors (**figure C_2-3**).[18]

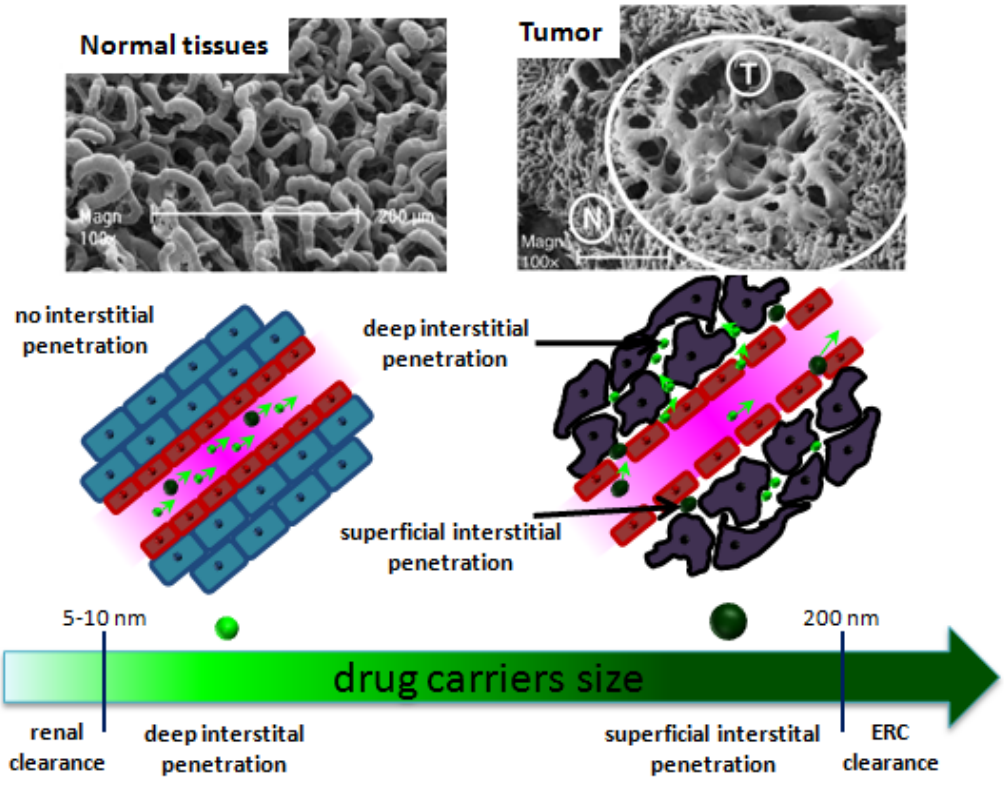

Figure C_2-3: Blood vessels of normal tissues and solid tumor (T points the tumor whereas N points normal tissues), adapted from ref. [18]. Schematic representations of the normal and tumor tissues. Drug carrier size schematic scale and its relation with penetration into tumors.

[18] J.W. Nichols, Y.H. Bae, EPR: Evidence and fallacy, *J. Control. Release*, **2014,** 190, 451-464.

The **circulation time** in the bloodstream of the drug delivery system and its **size** are the two key parameters that **favor the EPR effect**. To reach and be able to accumulate in the tumor tissues, drug delivery systems must have a long circulation time, avoiding renal and RES rapid clearance. Moreover, small carriers (light green in **figure C_2-3**), with sizes lower than 50 nm, would penetrate deeper into the interstitial spaces between blood vessels and solid tumors cells and their therapeutic effect would therefore affect a higher proportion of cancerous cells. In contrast, bigger carriers (dark green in **figure C_2-3**) would stay on the surfaces of the tumors, affecting less cancerous cells and being eventually dragged by the bloodstream flow. Besides, the EPR effect can be promoted by increasing the blood flow to the tumor tissues by inducing hypertension or employing vasodilators, such as nitric oxide.[19]

Active targeting is much more versatile than passive one and many **different tissues and cells** can be reached. Two distinct strategies are commonly followed to achieve it (**figure C_2-4**):

- the nanocarrier can specifically target a receptor that is currently overexpressed by the diseased cell, or
- the release of the drug from the nanocarrier can be triggered only after exposure to one or various stimulus.

Many different moieties have been employed to achieve active targeted drug delivery. As examples, **antibodies**, **peptides** or **folic acid**, receptor of which is highly overexpressed in various tumor cells, have enabled effective drug targeting during *in vivo* assays.[20] **Stimulus mediated drug targeting** can be

[19] a) Lammers T, Smart drug delivery systems: back to the future vs. clinical reality, *Int. J. Pharm.*, **2013**, 454, 527-529; b) J. Fang, H. Nakamura, H. Maeda, The EPR effect: unique features of tumor blood vessels for drug delivery, factors involved, and limitations and augmentation of the effect, *Adv. Drug Deliv. Rev.*, **2011**, 63, 136-151.

[20] a) S.C. Alley , N.M. Oakley, P.D. Senter, Antibody–drug conjugates: targeted drug delivery for cancer, *Curr. Op. Chem. Biol.*, **2010**, 14, 529-537; b) S. Majumdar, T.J. Siahaan, Peptide-mediated targeted drug delivery, *Med. Res. Rev.*, **2012**, 32, 637-658; c) J. Sudimack, R.J. Lee, Targeted drug delivery via the folate receptor, *Adv. Drug Deliv. Rev.*, **2000**, 41, 147-162.

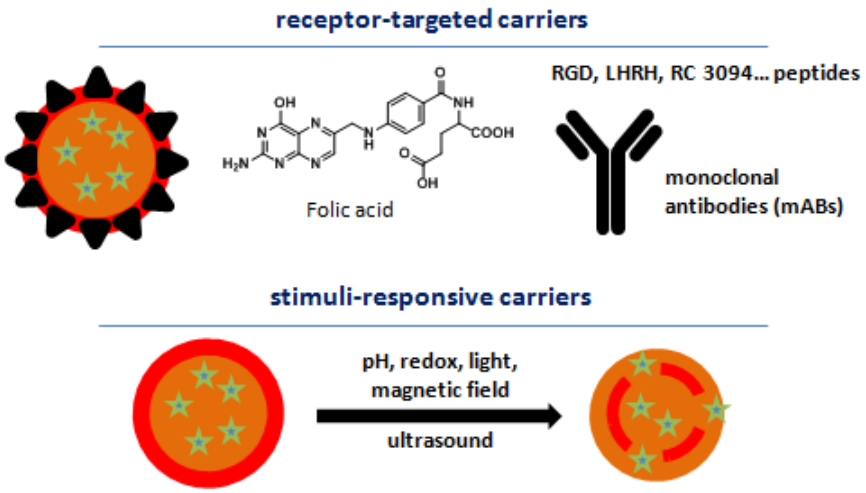

Figure C_2-4: Representation of receptor-targeted and stimuli-responsive carriers.

attained by playing with the specific physiological conditions of the target diseased tissues. For example, tumor cells have lower **pH** than healthy cells and may present a hypoxic reductive disorder; several drug carriers have been designed to respond to these stimuli and successfully release their cargo in such tissues.[21] The **stimulus** may also be **external**; therefore drug nanocarriers that respond to light,[22] temperature,[23] magnetic field[24] and ultrasounds[25] have been designed as well as drug carriers that are able to respond to various stimuli.[26]

[21] a) Y. Liu, W. Wang, J. Yang, C. Zhou, J. Sun, pH-sensitive polymeric micelles triggered drug release for extracellular and intracellular drug targeting delivery, *Asian J. Pharm. Sci.*, **2013**,8, 159-167; b) H. Alimoradi, S.S. Matikonda, A.B. Gamble, G.I. Giles, K. Greish, Hypoxia responsive drug delivery systems in tumor therapy, *Curr. Pharm. Des.,* **2016**, 22, 2808-2820.

[22] G. Yang, J. Liu, Y. Wu, L. Feng, Z. Liu, Near-infrared-light responsive nanoscale drug delivery systems for cancer treatment, *Coord. Chem. Rev.*, **2016**, 320-321, 100-117.

[23] M. Karimi, P.S. Zangabad, A. Ghasemi, M. Amiri, M. Bahrami, H. Malekzad, H.G. Asl, Z. Mahdieh, M. Bozorgomid, A. Ghasemi, M.R.R.T. Boyuk, M.R. Hamblin, Temperature-responsive smart nanocarriers for delivery of therapeutic agents: applications and recent advances, *ACS Appl. Mater. interfaces*, **2016**, 8, 21107-21133.

[24] M. Bonini, D. Berti, P. Baglioni, Nanostructures for magnetically triggered release of drugs and biomolecules, *Curr. Opin. Colloid Interface Sci.*, **2013**, 18, 459-467

[25] Boissenot, A. Bordat, E. Fattal, N. Tsapis, Ultrasound-triggered drug delivery for cancer treatment using drug delivery systems: from theoretical considerations to practical applications, *J. Control. Release*, **2016**, 144-163.

[26] R. Cheng, F. Meng, C. Deng, H.A. Klok, Z. Zhonga, Dual and multi-stimuli responsive polymeric nanoparticles for programmed site-specific drug delivery, *Biomaterials*, **2013**, 34, 3647-3657.

2.1.1.2- Designing new smart nanocarriers and nanocarrier/drug conjugation

Important features have been defined to be considered in order to design drug nanocarriers that, in a smart way, would deliver the drug they carry into the diseased tissues (**figure C_2-5**).

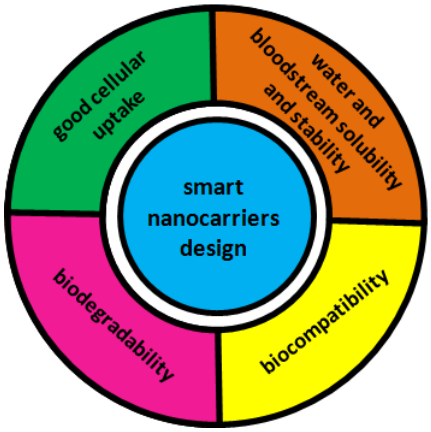

Figure C_2-5: "*Smart nanocarriers*" properties.

Firstly, drug nanocarriers must be water **soluble and stable in aqueous physiological media** and in the bloodstream to afford a good drug bioavailability and capacity to reach the desired tissues. Self-aggregation of nanocarriers, which may reduce their water solubility and mobility, must be avoided. Thus, polyethylene glycol (PEG) moieties are usually added at the nanocarriers' periphery as PEG repulsion between chains impedes the aggregation between various nanocarriers and also limits the RES clearance, increasing the bloodstream stability.[27] The insertion of chemical groups that can be ionized at physiological pH, such as carboxylic acids or primary amino groups, is another possibility. These groups increase the water solubility of the nanomaterials and limit their aggregation by electrostatic repulsion.[28]

[27] P. Mishra, B. Nayak, R.K. Dey, PEGylation in anti-cancer therapy: An overview, *Asian J. Pharmacol.*, **2016**, 11, 337-348.

[28] P. Charoongchit, J. Suksiriworapong, K. Sripha, S. Mao, A. Sapin-Minet, P. Maincent, V.B. Junyaprasert, Self-aggregation of cationically modified poly(ε-caprolactone)2-co-poly(ethylene glycol) copolymers: Effect of cationic grafting ligand and poly(ε-caprolactone) chain length, *Mat. Sci. Eng. C*, **2017**, 72, 444-455.

Secondly, drug nanocarriers must be fully **biocompatible**. Biocompatibility is defined as the property of not producing a toxic, injurious, or immunologic response in living tissues. A large variety of materials are *per se* biocompatible and can be used without further modification like natural or synthetic polyethers, polyesters, *etc*. For example, natural polysaccharides, like chitosan, or natural poly(amino acids) like proteins and synthetic polyethers, like Pluronic®, or synthetic polyesters like, polylactic acid, have been successfully used as biocompatible drug carriers.[29] The biocompatibility of some slightly cytotoxic materials can generally be improved by chemical modifications that affect the surface of the nanocarrier. The most common ones are the addition of polyethylene chains, but fatty acid, amino acid or sugars derivatives have also been employed.[30]

Thirdly, they must be **biodegradable** to avoid nanocarrier accumulation in the tissues. Besides, the degradation processes must limit the formation of cytotoxic fragments. Organic materials and in particular those based on polyesters, polyamides and polyethers that can be easily degraded in small biocompatible fragments by either enzymatic activity or water hydrolysis appear as attractive materials. Furthermore, the degradation reactions of the materials can be used to improve the drug release. Indeed, chemical groups sensitive to acidic pH or reductive environment such as carbonate groups or disulfide bonds

[29] a) J. Nicolas, S. Mura, D. Brambilla, N. Mackiewicz, P. Couvreur, Design, functionalization strategies and biomedical applications of targeted biodegradable/biocompatible polymer-based nanocarriers for drug delivery, *Chem. Soc. Rev.*, **2013**, 42, 1147-1235; b) Y. Cheng, L. Zhao, Y. Li, T. Xu, Design of biocompatible dendrimers for cancer diagnosis and therapy: current status and future perspectives, *Chem. Soc. Rev.*, **2011**, 40, 2673-2703.

[30] M. Ciolkowski, J.F. Petersen, m. Ficker, A. Janaszewska, J.B. Christensen, B. Klajnert, M. Bryszewska, Surface modification of PAMAM dendrimer improves its biocompatibility, *Nanomedicine*, **2012**, 8, 815-817.

may be inserted into the nanocarriers structure to favor an optimal and controlled release of drugs.[31]

Fourthly, **good cellular uptake** is another important requirement. Various pathways can occur during cellular uptake; they are principally regulated by the size, morphology and surface functionalization of the nanocarriers (**figure C_2-6**).

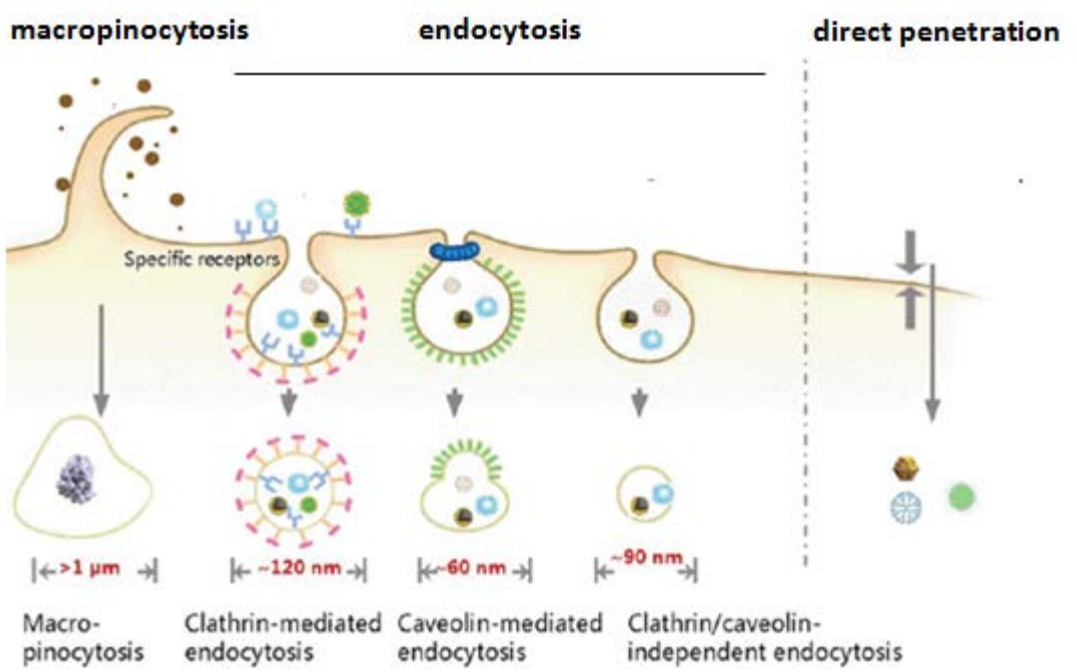

Figure C_2-6: Different pathways of cellular uptake, adapted from ref. [32].

Small nanoparticles with size under 10 nm usually enter into the cells by **simple diffusion** across the cell membrane. Particles with size comprised between 10 and 150 nm usually enter into the cell according to **endocytic pathways**. The cell membrane deforms itself into an alveolus that contains the nanocarriers. This hole closes up forming an endosome. Later, the nanocarriers must leave this endosome to enter into the cytoplasm. Endocytic pathways can be receptor mediated, with clathrin or caveolin, or receptor independent.

[31] N. Kamaly, B. Yameen, J. Wu, O.C. Farokhzad, Degradable controlled-release polymers and polymeric nanoparticles: mechanisms of controlling drug release, *Chem. Rev.*, **2016**, 116, 2602-2663.

[32] Z. Mao, X. Zhou, C. Gao, Influence of structure and properties of colloidal biomaterials on cellular uptake and cell functions, *Biomater. Sci.*, **2013**, 1, 896-911.

Finally, bigger particles can enter the cells mediating **macropinocytosis** and **phagocytosis**.

It is commonly assumed that a spherical morphology with a diameter bellow 100 nm favors the cellular uptake. Cellular uptake can also be promoted by the functionalization of the nanocarriers with peripheral cationic groups. Indeed, electrostatic interactions between cationic nanocarriers and negatively charged membrane may occur resulting in a better cellular internalization.[33]

Finally and prior to its delivery, the **drug must be loaded** inside the nanocarriers. Drugs can be inserted into the nanocarriers by non-covalent and covalent strategies (**figure C_2-7**).[34]

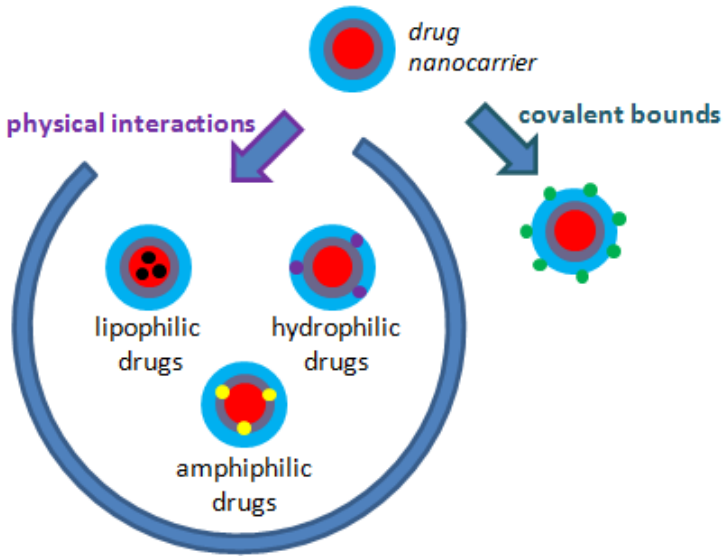

Figure C_2-7: Covalent and non-covalent strategies for loading drugs into nanocarriers.

[33] a) X. Hu, J. Hu, J. Tian, Z. Ge, G. Zhang, K. Luo, S. Liu, Polyprodrug amphiphiles: hierarchical assemblies for shape-regulated cellular internalization, trafficking, and drug delivery, *J. Am. Chem. Soc.*, **2013**, 135, 17617-17629; b) M. Elsabahy, K.L. Wooley, Design of polymeric nanoparticles for biomedical delivery applications, *Chem. Soc. Rev.*, **2012**,41, 2545-2561; c) M. Adabi, M. Naghibzadeh, M. Adabi, M.A. Zarrinfard, S.S. Esnaashari, A.M. Seifalian, R. Faridi-Majidi, H.T. Aiyelabegan, H. Ghanbari, Biocompatibility and nanostructured materials: applications in nanomedicine, artificial cells, nanomedicine, and biotechnology, ***in press***, DOI: 10.1080/21691401.2016.1178134.

[34] K. Ulbrich, K. Holá, V. Šubr, A. Bakandritsos, J. Tučekand, R. Zbořil, Targeted drug delivery with polymers and magnetic nanoparticles: covalent and noncovalent approaches, release control, and clinical studies, *Chem. Rev.*, **2016**, 116, 5338-5431.

Non-covalent strategies are based on various equilibria, which must be shifted to a better affinity of the drug for the nanocarrier than for the external medium. In the case of lipophilic drugs, loading is mainly based on favorable **lipophilic interactions** between the drug molecules and the lipophilic parts of the nanocarriers. The low water solubility of lipophilic drugs usually shifts the equilibrium towards the formation of stable drug/nanocarrier conjugates. Hydrophilic and amphiphilic drugs may also be encapsulated within the nanocarriers; they are respectively located in the hydrophilic parts or at the frontiers between the two parts. The conjugate formation can be reinforced by other favorable interactions, such as **hydrogen or halogen bounds**.

Drug encapsulation based on non-covalent interactions has the advantages to be easy to carry out and versatile. Therefore, many encapsulation techniques are currently described in the literature. However, the release of drugs might be too fast ("*burst release*"), especially during *in vivo* experiments in which the drug/nanocarrier conjugates are highly diluted and constantly washed by human plasma (*"sink-conditions"*). Such "*burst release*" can be avoided by closing up the nanocarriers after drug encapsulation by covalent cross-linking. The encapsulated drug molecules remain therefore entrapped within the nanocarriers and can only be expelled after reopening or destruction of the nanocarriers. This effect can be stimuli dependent in order to favor a targeted release.[35]

Drugs can also be **covalently linked** to the nanocarrier structures. Covalent bonds between nanocarriers and drugs are advantageously highly stable. A more controlled drug release can be induced, allowing a perfect

[35] a) E.V. Skorb, H. Möhwald, "Smart" surface capsules for delivery devices, *Adv. Mater. Interfaces*, **2014**, 1, 1400237; b) C. Pinto Reis, R.J. Neufeld, A.J. Ribeiro, F. Veiga, Nanoencapsulation I. Methods for preparation of drug-loaded polymeric nanoparticles, *Nanomedicine*, **2006**, 2, 8-21.

control of the drug pharmacokinetics, favoring good drug bioavailability and constant drug concentration into the bloodstream.

Furthermore, **stimuli-sensitive covalent bonds**, such as hydrazone linkages, can be employed to attach the drugs on the nanocarriers and induce targeted drug release after exposure to mild acidic pH. Nevertheless, drug/nanocarrier covalent linkages are almost always based on costly chemical synthesis with usually expensive and unstable drugs and are tedious to be scaled-up.[36]

A wide variety of nanocarriers fulfill the above mentioned criteria of water solubility and stability, biocompatibility, biodegradability and favored cellular uptake, in which various drugs have been loaded by covalent and non-covalent strategies. Thus, many organic, inorganic and hybrid materials have been used for the design of drug delivery nanocarriers such as polymers and dendrimers, liposomes, inorganic nanoparticles (based on silica, gold, iron, *etc*.), quantum dots, fullerene, graphene, carbon nanotubes and nanodiamonds, metal organic frameworks, *etc*.[34]

[36] a) Y. Chen, T. Xu, The effect of dendrimers on the pharmacodynamic and pharmacokinetic behaviors of non-covalently or covalently attached drugs, *Eur. J. Med. Chem.*, **2008**, 43, 2291-2297; b) K.R. Est, S. Otto, Reversible covalent chemistry in drug delivery, *Curr. Drug Discov. Technol.*, **2005**, 2, 123-160.

2.1.2- Gene therapy

2.1.2.1- An innovative, precise and versatile new therapy

Gene therapy is defined as the **therapeutic delivery of exogenous genome** into specific cells in order to treat diseases. It can be used to treat genetic diseases, such as muscular dystrophy, but also other diseases such as cardiovascular, neurological, or infectious diseases and cancer. The exogenous genetic material would modify the natural production of proteins in the target cells, altering the expression of specific genes or triggering the production of cytotoxic proteins in order to kill cancerous cells, for example.[37]

Various forms of genetic material can be administered to the patient; the most common ones are **plasmid deoxyribonucleic acid** (pDNA) and **small interfering ribonucleic acid** (siRNA) (**figure C_2-8**). pDNAs are circular DNA molecules that contain a gene that would induce, after recombination with the original host cell DNA in its nucleus, the production of a desired protein. siRNA can specifically knock down the expression of a deleterious gene in the cell cytoplasm. To express a gene, the cell produces a messenger RNA (mRNA) that transcripts and transports the genetic information from the nucleus, where the DNA is located, to the ribosomes. The ribosomes are located in the cell cytoplasm and, after receiving the mRNA information, start the production of the corresponding protein. siRNA is complementary to a given messenger RNA and forms a stable complex with it. The mRNA can no longer be translated by the ribosomes and the production of the corresponding protein stops.[38]

[37] H.M. Blau, M.L. Springer, Gene therapy - a novel form of drug delivery, *N. Engl. J. Med.*, **1995**, 333, 1204-1207.

[38] L. Naldini, Gene therapy returns to centre stage, *Nature*, **2015**, 526, 351-360.

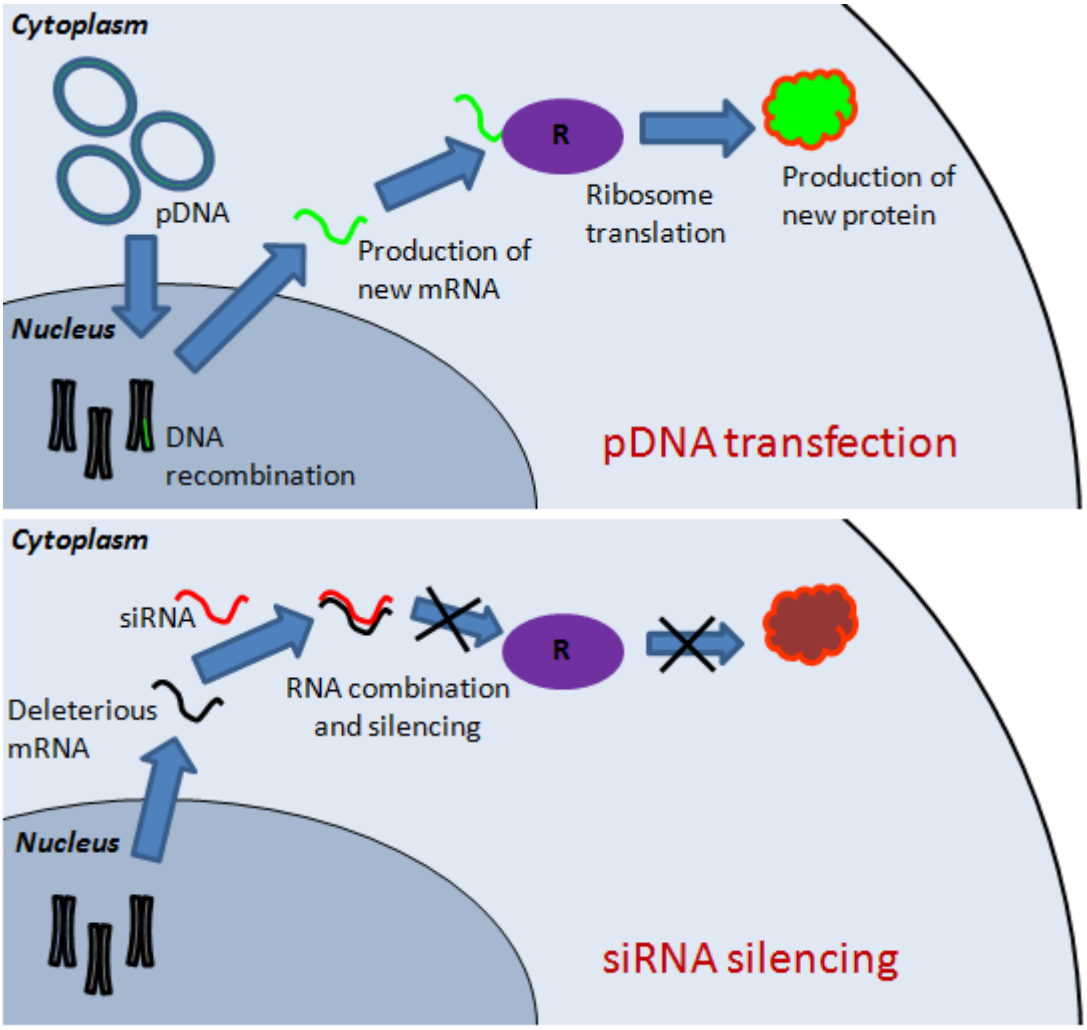

Figure C_2-8: pDNA transfection (up) and siRNA silencing (down) mechanisms.

The concept of gene therapy appeared in the 1970's and the first approved and successful gene therapy investigations in humans occurred in the beginning of the 1990's.[39] In 2016, 2409 clinical trials had been conducted with 94 trials in phase III or IV.[40] Only two gene therapies are currently approved in Europe. The first one treats a rare genetic condition called "*lipoprotein lipase*

[39] a) T. Friedmann, R. Roblin, Gene therapy for human genetic disease?, *Science*, **1972**, 175, 949-955; b) S.A. Rosenberg, P. Aebersold, K. Cornetta, A. Kasid, R.A. Morgan, R. Moen, E.M. Karson, M.T. Lotze, J.C. Yang, S.L. Topalian, M.J. Merino, K. Culver, A.D. Miller, R.M. Blaese, W.F. Anderson, Gene transfer into humans — immunotherapy of patients with advanced melanoma, using tumor-infiltrating lymphocytes modified by retroviral gene transduction, *N. Engl. J. Med.*, **1990**, 323, 570-578

[40] Gene therapy clinical trials worldwide database, *http://www.abedia.com/wiley/phases.php*, Wiley, **2016**.

deficiency" that affects digestion and impedes the degradation of fatty acids.[41] The second one treats children with severe combined immunodeficiency syndrome, known as "*bubble babies*".[42] A third therapy was approved in China and treats squamous cell malignant cancer.[43]

Three principal barriers need to be overcome to convert gene therapy into a safe and efficient therapy:[44]

- As a drug, genetic material must **reach and be internalized by the target cells** while being protected from the physiological medium and immune system aggressions. *Ex vivo* procedures have been developed to administrate genetic material in addition to classical *in vivo* procedures. During *ex vivo* administration, selected cells are collected from the patient, then treated *in vitro* with genetic materials and, finally, after having being successfully modified genetically, reintroduced to the patient.
- The **expression of exogenous genome must be time sustained** and must not be lost during cell division or after natural epigenetic modifications. Otherwise, gene therapy would be limited to quiescent tissues like brain that have a low cell turnover or to treat episodic diseases, such as cancers or infections.
- The **host immune response** is the final major concern. The immune system tends to eliminate all foreign genome and this bothers the gene therapy administration procedures. Furthermore, it can also be activated during the transcription of the genome by classifying the new proteins as foreign and invasive, triggering their destruction.

[41] A. Pollack, European agency backs approval of a gene therapy, *New York Times*, July, 21th, **2012**, B1.

[42] A. Coghlan, Gene therapy gets approval for 'bubble kids' in world first, *New Scientist*, April, 9th, **2016**, issue 3068.

[43] S. Pearson, H. Jia, K. Kandachi, China approves first gene therapy, *Nat. Biotechnol.*, **2004**, 22, 3-4.

[44] M.A. Kay, State-of-the-art gene-based therapies: the road ahead, *Nat. Rev.*, **2011**, 12, 316-328.

2.1.2.2- Vectorisation of gene therapy for a better efficiency

Gene therapy may be carried out by directly injecting naked pDNA into the tissues. However, this technique presents a really low efficiency since foreign genetic material is usually rejected and rapidly destroyed.[45]

In order to favor the delivery of exogenous genome to target cells, **gene vectors** have been introduced. They can be viral or synthetic. **Viral vectors** were the first ones to be developed and are still the most commonly exploited. Indeed, viruses are infectious agents that transport their own RNA or DNA into cells where they replicate. They effectively protect the genetic material they carry from physiological medium and are rather stable in the bloodstream. They naturally target specific cells and easily release their genetic cargo inside them. A large variety of viruses have been employed to successfully deliver foreign genetic material into cells such as retroviruses, lentiviruses, adenoviruses, adeno-associated viruses, simplex herpes virus and vaccinia virus. The three currently approved gene therapies are based on three distinct types of viruses: the retroviruses, the adenoviruses and the adeno-associated viruses.[46]

However, viral vectors are associated to issues that cannot be ignored. First of all, viral vectors are expensive and their manufacturing production is harsh to be handled. Secondly, the size of the genetic material is limited by the size of the virus cavity and restrains gene delivery to small plasmid DNA and RNA. Thirdly, the virus may induce an immunogenic response after being administrated to the patient, limiting the efficiency of further administration. Besides, this immunogenic response might have even been acquired by the

[45] H. Herweijer, J.A. Wolff, Progress and prospects: naked DNA gene transfer and therapy, *Gene Therapy*, **2003**, 10, 453-458.

[46] a) M.A. Kay, J.C. Glorioso, L. Naldini, Viral vectors for gene therapy: the art of turning infectious agents into vehicles of therapeutics, *Nat. Med.*, **2001**, 7, 33-40; b) O.W. Mertena, B. Gaillet, Viral vectors for gene therapy and gene modification approaches, *Biochem. Eng. J.*, **2016**, 108, 98-115.

patient before any gene treatment (after a normal exposure to unmodified viruses). Finally, long term safety and patient tolerability is still unknown.[46]

Therefore, **biocompatible and biodegradable synthetic vectors** are being investigated and developed to compete with viruses and outstrip the viruses' inherent drawbacks. They form complexes with genetic material that would enable the administration and uptake of the exogenous genome into target cells. The complexes are principally based on **physical electrostatic interactions** between anionic phosphate groups belonging to the DNA with cationic groups belonging to the non-viral vector. An excess of cationic vectors would form stable, dense and positively charged complexes wherein the genetic material is located in the center of the complexes, protected from external aggressions (**figure C_2-9**).[47,28b]

After being formed, the vector-genome complex must act like a virus and pass through the natural barriers that impede the delivery of foreign genetic material into the cell. The cell internalization of the complexes usually follows endocytic pathways. Once in the cell, the complexes must escape from the endosome to enter into the cytoplasm. While siRNA can be released anywhere in the cytoplasm to be active, pDNA must be released close to the cell nucleus to be able to penetrate inside it and modify the endogenous DNA (**figure C_2-10**).[47]

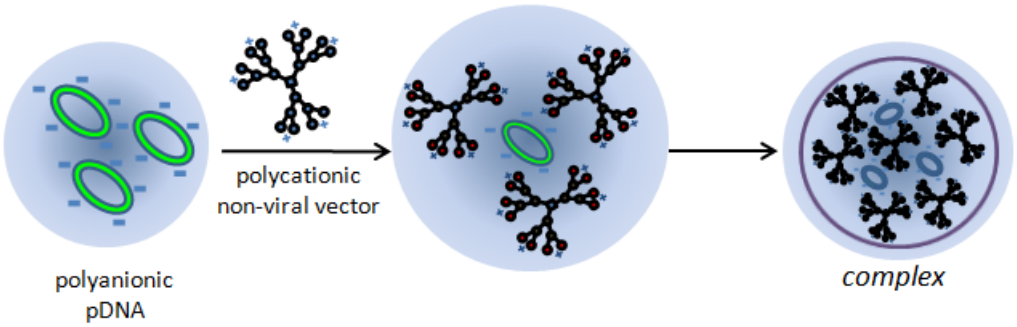

Figure C_2-9: pDNA complexation by cationic non-viral vector.

[47] D.W. Pack, A.S. Hoffman, S. Pun, P.S. Stayton, Design and development of polymers for gene delivery, *Nat. Rev.*, **2005**, 4, 581-593.
[28b] M. Ramamoorth *et al.*, *J. Clin. Diagn. Res.*, **2015**, 9, GE01-GE06.

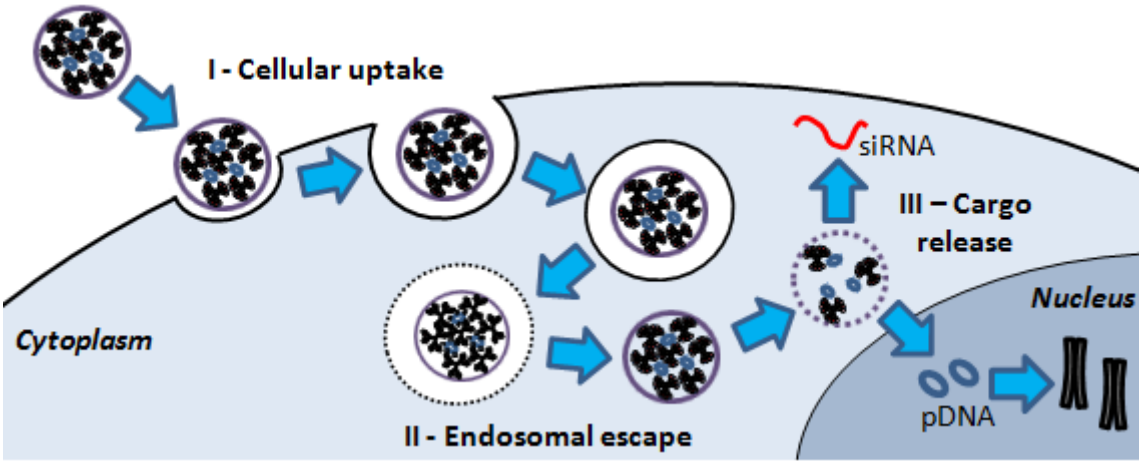

Figure C_2-10: pDNA and siRNA complexes routes to efficient gene transfection.

As described for drug delivery vectors, synthetic vectors for gene therapy can be intelligently designed to reach efficient gene therapy in a safety way. Biocompatible and biodegradable cationic vectors that can interact with polyanionic pDNA o siRNA usually contain numerous tertiary amino groups that are protonated at physiological pH or other quaternary amino groups. The complex they form with genetic material must be stable in the bloodstream to be able to reach the target cells for *in vivo* gene therapy procedures. The **cellular internalization** by means of endocytosis is favored for particles with size up to 100 nm that are positively charged to interact with the negatively charged cell membrane.[48]

Endosomal escape can be favored by the addition of moieties that naturally destabilize the endosome. Indeed, various proteins and peptides or chemical agents, such as chloroquine, can induce pore formation in the endosome membrane or can fusion with it, destabilizing the membrane and breaking it down. Interestingly, some polymers that possess secondary and tertiary amino groups are able to catch protons and may promote the breakdown of the endosome membrane. This property is known as the ***"proton sponge effect"***. After endosome formation, the pH of the endosome naturally

[48] A.E. Nel, L. Madler, D. Velegol, T. Xia, E.M.V. Hoek, P. Somasundaran, F. Klaessig, V. Castranova, M. Thompson, Understanding biophysicochemical interactions at the nano-bio interface, *Nat. Mater.*, **2009**, 8, 543-557.

decreases, starting from physiological pH, at 7.4, to more acidic pH, near 5.0. Secondary and principally tertiary amino groups are being gradually protonated while the pH decreases and disturb this natural process. Thus, to counteract the "*proton sponge effect*" of these polymers, more and more protons are injected inside the endosome by the cell. As a water molecule and a chlorine ion are injected jointly to a proton, the endosome starts to swell until it blows up, liberating its contents into the cytoplasm (**Figure C_2-11**).[48,49]

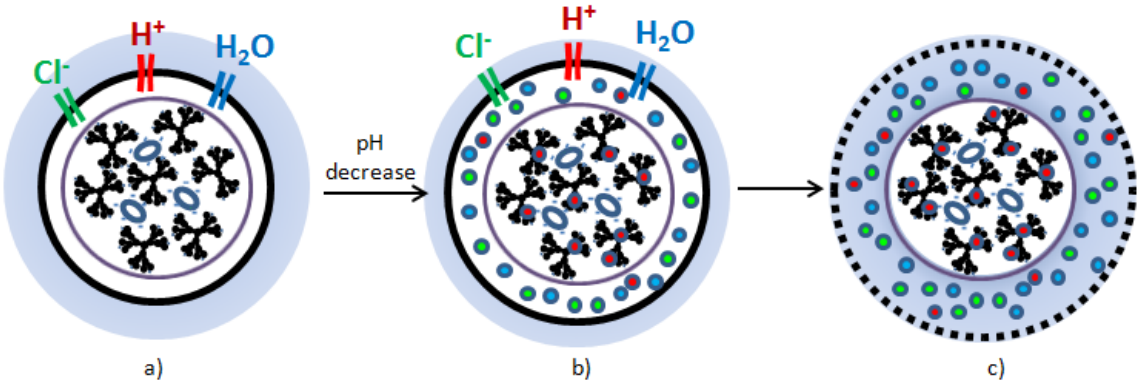

Figure C_2-11: Schematic representation of the "*proton sponge effect*". a) The pDNA/vector complex is located within the endosome. b) H^+ ions sent by the cell to decrease the pH of the endosome are catch by the gene vector and the endosome starts to swell. c) The endosome blows up before reaching ph 5.0.

After entering the cytoplasm, the complexes that bear pDNA must approach the nearest possible to the nucleus to avoid the destruction of pDNA. It has been observed that complexes can naturally move into the cytoplasm and reach the cell nucleus. The addition of some peptide sequences that naturally go to the nucleus might assist this approach. The internalization of the complexes into the cell nucleus is highly challenging and the exogenous DNA is usually recombined with the DNA host cell during the cell division when the nucleus membrane is open.[50]

[49] a) A.K. Varkouhi, M. Scholte, G. Storm, H.J. Haisma, Endosomal escape pathways for delivery of biological, *J. Control. Release*, **2011**, 151, 220-228; b) J. Behr, The proton sponge: a trick to enter cells the viruses did not exploit, *Chimia*, **1997**, 51, 34-36.

[50] C.M. Roth, S. Sundaram, Engineering synthetic vectors for improved DNA delivery: insights from intracellular pathways, *Annu. Rev. Biomed. Eng.*, **2004**, 6, 397-426.

Finally, both **siRNA and pDNA must be released** from the complexes to be expressed. A good balance between efficient packing for extracellular protection and intracellular release must be reached to obtain good transfection efficiency. Thus, some synthetic vectors have shown enhanced gene transfection efficiency after being partially degraded. The non-viral vector degradation can proceed before the complex formation with pDNA[51] or during the gene transfection by the cytoplasm reductive environment or by the lower pH in the endosomes.[52]

As with drug delivery, many synthetic gene vectors based on a variety of organic, inorganic and hybrid materials have been successfully used for *in vitro* and *in vivo* assays. Among them, cationic lipids, lipid nanoemulsions, solid lipidic nanoparticles, peptides, polymers and dendrimers, inorganic nanoparticles (based on gold, silica or calcium phosphate, *etc*.) have received enormous attention from research groups.[28b]

Additionally, some organic synthetic **non-viral vectors are commercially available**:[53]

- lipofectamine® 2000 or 3000 are the most effective commercial agents. They are based on cationic lipids that naturally self-assemble in water forming stable liposomes in which DNA can intercalate,
- FuGENE® 6 or HD are another lipid formulations,
- jetPEI® is based on linear polyethylenimine polymer,
- ExpressFect™ is a cationic polymer,

[51] M.X. Tang, C.T. Redemann, F.C. Szoka, *In vitro* gene delivery by degraded polyamidoamine dendrimers, *Bioconjugate Chem.*, **1996**, 7, 703-714.

[52] a) D. Ouyang, N. Shah, H. Zhang, S.C. Smith, H.S. Parekh, Reducible disulfide-based non-viral gene delivery systems, *Mini Rev. Med. Chem.*, **2009**, 9, 1242-1250; b) P. Venugopalan, S. Jain, S. Sankar, P. Singh, A. Rawat, S.P. Vyas, pH-sensitive liposomes: mechanism of triggered release to drug and gene delivery prospects, *Pharmazie*, **2002**, 57, 659-671.

[28b] M. Ramamoorth *et al*., *J. Clin. Diagn. Res.*, **2015**, 9, GE01-GE06.

[53] S. Yamano, J. Dai, A.M. Moursi, Comparison of transfection efficiency of nonviral gene transfer reagents, *Mol. Biotechnol.*, **2010**, 46, 287-300.

- Superfect® reagents are based on poly(amido amine) dendrimers,

- Arrest-In™ is a formulation that combines lipids and polymers,

-*etc*.

2.2 - Dendritic derivatives alluring materials for nanomedicine applications

Dendrimers show interesting features that have prompted their investigation and the development of new dendritic derivatives for drug delivery and non-viral gene therapy. Indeed, dendrimers are macromolecules that can be easily designed by convenient and precise modifications to afford relevant vectors with engaging properties, and have been therefore extensively studied as drug and gene nanocarriers. During the last decade, a big number of reviews and books dealing with dendrimers and their nanomedicine applications have been published.[54] Among them, a specially relevant review deals with some clinical applications of dendrimers as biomedical materials.[55]

[54] a) H.J. Hsu, J. Bugno, S. Lee, S. Hong, Dendrimer-based nanocarriers: a versatile platform for drug delivery, *WIREs Nanomed. Nanobiotechnol.*, **2017**, 9, e1409; b) M. Selin, L. Peltonen, L.M. Bimbo, Dendrimers and their supramolecular nanostructures for biomedical applications, *J. Drug Deliv. Sci. Tech.*, **2016**, 10; c) A. Mascaraque , A. Sousa-Herves , J. Rojo, Medicinal applications of dendrimers, *Reference Module in Chemistry, Molecular Sciences and Chemical Engineering*, **2016**, DOI: 10.1016/B978-0-12-409547-2.12571-5; d) H. Yang, Targeted nanosystems: advances in targeted dendrimers for cancer therapy, *Nanomedicine*, **2016**, 12, 309; e) A.K. Sharma, A. Gothwal, P. Kesharwani, H. Alsaab, A.K. Iyer, U. Gupta, Dendrimer nanoarchitectures for cancer diagnosis and anticancer drug delivery, *Drug Discov. Today*, **2016**, *In press*, DOI: 0.1016/j.drudis.2016.09.013; f) L.P. Wu, M. Ficker, J.B. Christensen, P.N. Trohopoulos, S.M. Moghimi, Dendrimers in medicine: therapeutic concepts and pharmaceutical challenges, **2015**, 26, 1198-1211; g) A. J. Perisé-Barrios, D. Sepúlveda-Crespo, D. Shcharbin, B. Rasines, R. Gómez, B. Klajnert-Maculewicz, M. Bryszewska, F. J. de la Mata and M. A. Muñoz-Fernández, Dendrimers, Chapter 7 In J. Callejas-Fernández, J. Estelrich, M. Quesada-Pérez, J. Forcada, Soft nanoparticles for biomedical applications, **2014**, *RSC*, London; h) A.M. Caminade, C.O. Turrin, Dendrimers for drug delivery, *J. Mater. Chem. B*, **2014**, 2, 4055-4066; i) P. Kesharwani, K. Jain, N.K.Jain, Dendrimer as nanocarrier for drug delivery, *Progress Polym. Sci.*, **2014**, 39, 268-307.

[55] R.M. Kannan, E. Nance, S. Kannan, D.A Tomalia, Emerging concepts in dendrimer-based nanomedicine: from design principles to clinical applications, *J. Intern. Med.*, **2014**,276, 576-617.

2.2.1- Dendrimers, an overview

2.2.1.1- General properties of dendrimers

Dendrimers are **ramified polymers** with a repetitive tree-like structure. They present a perfectly defined skeleton, resulting in almost uniform and monodisperse polymers with a large number of functional groups at the periphery. Their name describes their original structure; the Greek words "*dendron*" and "*meros*" respectively mean tree and part. Each wedge moiety of a dendrimer is called dendron **(figure C_2-12)**.

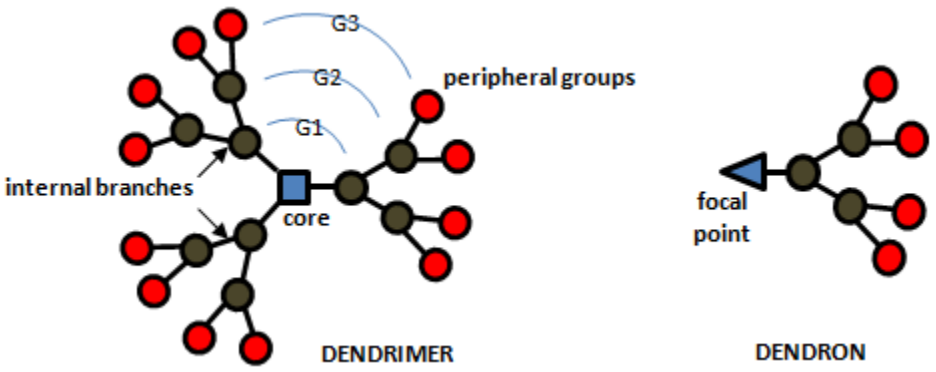

Figure C_2-12: Schematic representations of a dendrimer and a dendron.

Dendrimers are composed of three parts: the core, the internal branches and the peripheral groups. The **core** of the dendrimers is multifunctional and determines both the shape of the dendrimers and their directionality. Starting from its central core, the dendrimer grows up in a repetitive manner forming the **internal branches**. The number of repetitive units conditions the generation of the dendrimer and its size.[56]

[56] a) F. Vögtle, G. Richardt, N. Werner, Dendrimer chemistry, **2009**, WILEY-VCH, Weinheim; b) E. Abbasi, S.F. Aval, A. Aknarzahed, M. Milani, H.T. Nasrabadi, S.W. Joo, Y. Hanifeh, K. Nejati-Koshki, R. Pashaei-Asl, Dendrimers: synthesis, applications, and properties, *Nanoscale Res. Lett.*, **2014**, 9, 247; c) S. Hernández-Ainsa, M. Marcos, J.L: Serrano, Chapter 3: Dendrimeric and hyperbranched liquid crystal structures In: Handbook of liquid crystals, 7 volume ses, 2nd

One of the most interesting features of the dendrimer structure is the presence of **numerous and accessible peripheral groups**. The number of these groups increases exponentially with the generation of the dendrimer and allows an easy functionalization with many different moieties. Moreover, the stimuli-response and activity of the moieties located at the periphery of the dendrimers may be increased when compared to one of the free moieties diluted in solution. This property is known as the "*dendritic effect*".[57]

In addition, dendrimers adopt preferentially a **spherical shape with few interactions between molecules**. In contrast with linear polymeric chains, which usually form random coils that are entangled like "*cooked spaghettis*", dendrimers generally appear as spherical and dispersed molecules, like "*green peas*". This property is related with the generation of the dendrimer: dendrimers of low generations are generally flexible and open molecules whereas dendrimers of high generations usually adopt a spherical and dense shape showing a closed surface. Hence, dendrimers are more soluble than their corresponding linear polymers and their solutions have a lower viscosity.[58]

Finally, the density of the dendrimeric molecules varies from their core to their periphery. Dendrimers present **holes in their architecture** that are situated between internal branches making them appropriate macromolecules for "*host-guest*" systems. Indeed, these internal void spaces can be filled with small molecules like solvent molecules or other molecules of interest, like drugs. In 1994, Meijer *et al.* introduced the term of "*dendrimer box*" to describe this

edition by J.W. Goodby, P.J. Collings T.Kato, C. Tschierske, H. Gleeson, P. Raynes, 2013, Wiley-VCH, Weinheim, Germany.

[57] a) A.M. Caminade, A. Ouali, R. Laurent, C.O. Turrin, J.P. Majoral, The dendritic effect illustrated with phosphorus dendrimers, *Chem. Soc. Rev.*, **2015**, 44, 3890-3899; b) E.M Munoz, J. Correa, R. Riguera, E. Fernandez-Megia, Real-time evaluation of binding mechanisms in multivalent interactions: a surface plasmon resonance kinetic approach, *J. Am. Chem. Soc.*, **2013**, 135, 5966-5969.

[58] J.M.J. Fréchet, Functional polymers and dendrimers: reactivity, molecular architecture, and interfacial energy, *Science*, **1994**, 263, 1710-1715.

phenomenon. A solid shell made of *ter*-butoxyphenylalanine amino acid were synthesized at the periphery of a flexible poly(propyleneimine) dendrimer in the presence of guest molecules. The guest molecules that were inside the internal dendrimer void spaces remained entrapped and could only get out of the dendrimer after being exposed to an external stimulus (**figure C_2-13**).[59]

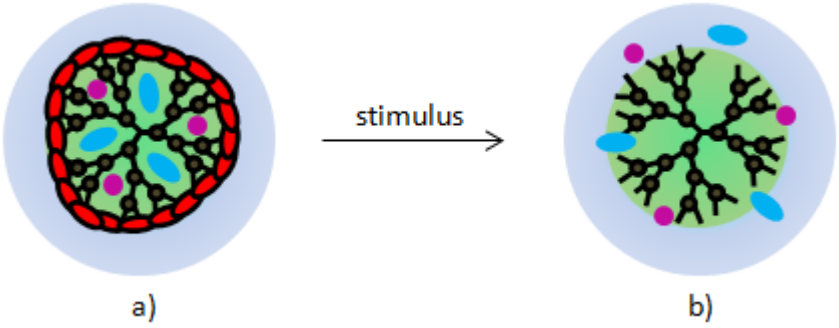

Figure C_2-13: Meijer's "*dendritic box*". a) The guest molecules are entrapped in the dendrimer. b) After exposition to a stimulus, the shell of the dendrimer is removed and the guest molecules are released outside the dendrimer.

[59] J.F. Jansen, E.M. de Brabander-van den Berg, E.W. Meijer EW, Encapsulation of guest molecules into a dendritic box, *Science*, **1994**, 266, 1226-1229: b) J.F. Jansen, E.W. Meijer, E.M. de Brabander-van den Berg , The dendritic box: shape-selective liberation of encapsulated guests, *J. Am. Chem. Soc.*, **1995**, 117, 4417-4418.

2.2.1.2- Synthesis of dendrimers

Dendrimers constitute a **relatively recent research line** in the field of polymers. The first dendritic structure was published by Vötgle *et al.* in 1978 when this group synthesized a series of new macromolecules named "*cascade polymers*".[60] Later, in 1981, Denkewalter *et al.* patented a new type of dendrimer based on poly-(*L*)-lysine (PLL).[61] Due to the limitations of the synthetic and analytic methods available at this time, the synthesis of new dendrimers remained undeveloped until 1985. During this year, Tomalia *et al.* and Newkome *et al.* described independently the synthesis of two new dendrimers. On the one hand, Tomalia's group synthesized poly(amidoamine) dendrimers (PAMAMs) that were described as "*starburst-dendritic macromolecules*", using the term dendrimer for the first time.[62] On the other hand, Newkome's group prepared polyethers "*arborol*".[63] Five years later, in 1990, Hawker, Fréchet *et al.* described a new synthetic process to synthesize the dendrimers. These years marked a turning point for dendrimeric macromolecules, and they started to spread among the scientific community (**figure C_2-14**).[64]

Two principal synthetic methods are employed to synthesize the dendrimers: the divergent one and the convergent one. The **divergent way** was first employed by Tomalia's and Newkome's groups. The dendrimer starts

[60] E. Buhleier, W. Wehner, F. Vögtle, Cascade"- and "nonskid-chain-like" synthesis of molecular cavity topologies, *Synthesis*, **1978**, 9, 155-158.

[61] R.G. Denkewalter, J.F. Kolc, W.J. Lukasavage, in US Pat. 4.360.646, **1979**.

[62] D.A. Tomalia, H. Baker, J. R. Dewald, M. Hall, G. Kallos, S. Martin, J. Roeck, J. Ryder, P. Smith, A new class of polymers: starburst-dendritic macromolecules, *Polym. J.*, **1985**, 17, 117-132.

[63] G.R. Newkome, Z.Q. Yao, G.R. Baker, V.K. Gupta, Micelles part 1. Cascade molecules: a new approach to micelles. A [27]-arborol, *J. Org. Chem.*, **1985**, 50, 2003-2004.

[64] C. Hawker, J.M.J. Fréchet, A new convergent approach to monodisperse molecules, *J. Chem. Soc., Chem. Commun.*, **1990**, 15, 1010-1013.

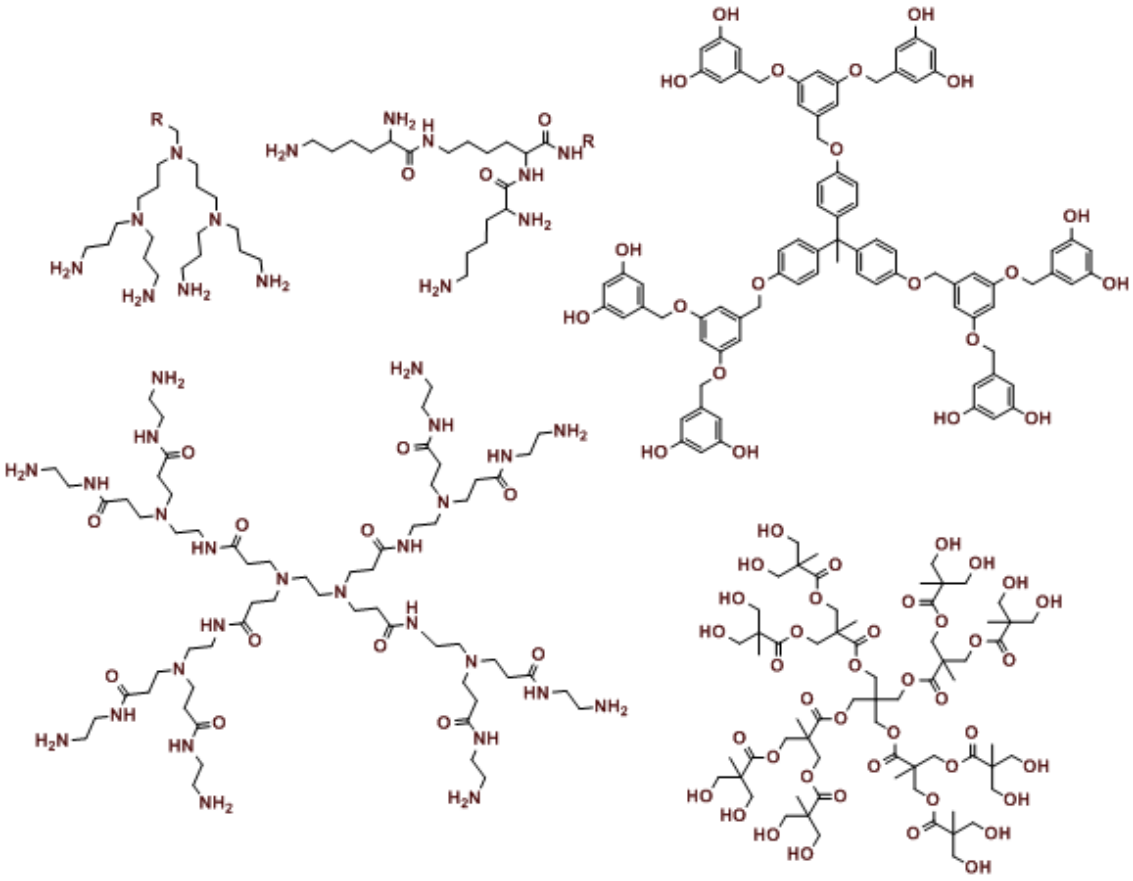

Figure C_2-14: Vötgle's cascade molecule, Denkenwalter's poly-(*L*)-lysine, Fréchet's dendrimer, Tomalia's dendrimer and 2,2'-*bis*(hydroxymethyl)propionic acid based *(bis*-MPA) polyester dendrimer.

growing from its core to its periphery by iterative synthetic steps: in each step a new generation of the dendrimer is formed by the addition of an appropriate amount of monomer. Briefly, a multifunctional core bearing nB active groups reacts with n AB_n* monomers, in which A is a chemical group that can react with the B group. To avoid side reactions that would decrease the yield, B chemical groups must be protected (B* corresponds to B protected group). Hence, each step of generation growth has to be followed by the deprotection of the B* chemical groups to continue building the dendrimer. This two-step process "*addition of monomer/deprotection of peripheral reactive groups*" has to be repeated until the desired dendrimer generation is reached (**figure C_2-15**).[62,63]

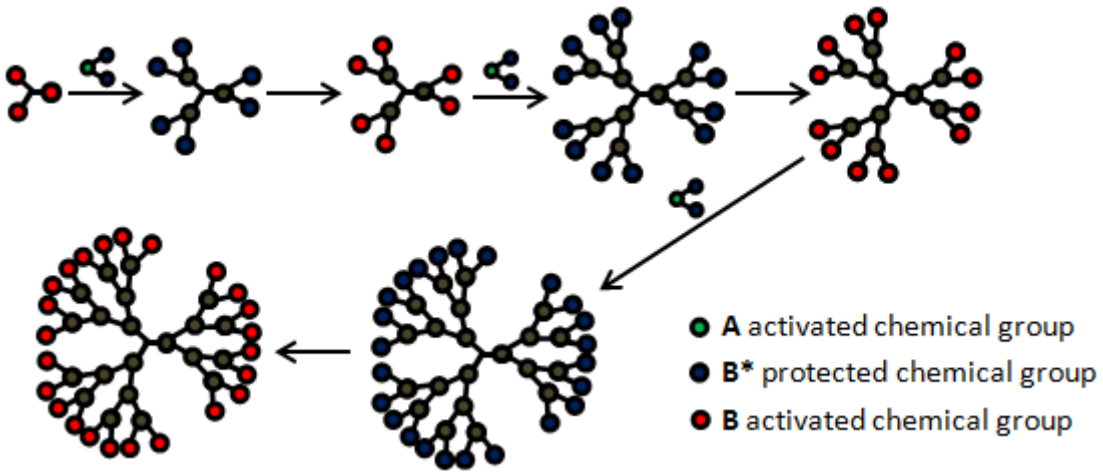

Figure C_2-15: Synthesis of dendrimers following the divergent pathway.

The AB_n* monomers are generally cheap and easily available allowing the addition of a large excess of monomer during the growing step and assuring a complete addition of the monomer to each of the peripheral reactive groups of the dendrimer. Nevertheless, and even using an excess of monomer, the principal limitation of this synthetic pathway is the difficulty to obtain pure monodisperse high generation dendrimers for which the risk of uncompleted growing reactions is big and leads to imperfect macromolecules. For instance, during many years, it was though that dendrimers had a maximum size that could not be exceeded, according to De Genes' theory,[65] until Simanek's group reached the synthesis of a 13th generation dendrimer with a size similar to that of small viruses.[66]

The **convergent method** was first employed by Hawker and Fréchet's group. A dendron, made of *AB_n monomers, is synthesized following the same two steps procedure employed by the divergent method. In this case, the chemical group A, located at the focal point of the dendron, must be protected to avoid side reactions (*A). When the desired generation is reached, the *A

[65] P.G. de Gennes, H. Hervet, Statistics of « starburst » polymers, *J. Phys. Lett. Fr.*, **1983**, 44, 351-360.

[66] J. Lim, M. Kostiainen, J. Maly, V.C.P. da Costa, O. Annunziata, G.M. Pavan, E.E. Simanek, Synthesis of large dendrimers with the dimensions of small viruses, *J. Am. Chem Soc.*, **2013**, 135, 4660-4663.

group is deprotected and reacts with the corresponding dendrimer core (**figure C_2-16**). The final reaction must proceed with an elevated yield as the synthesis of dendrons is costly and this avoids the addition of a large excess of dendron. Besides, the steric hindrance may limit the addition of various large dendrons to a small core.[45]

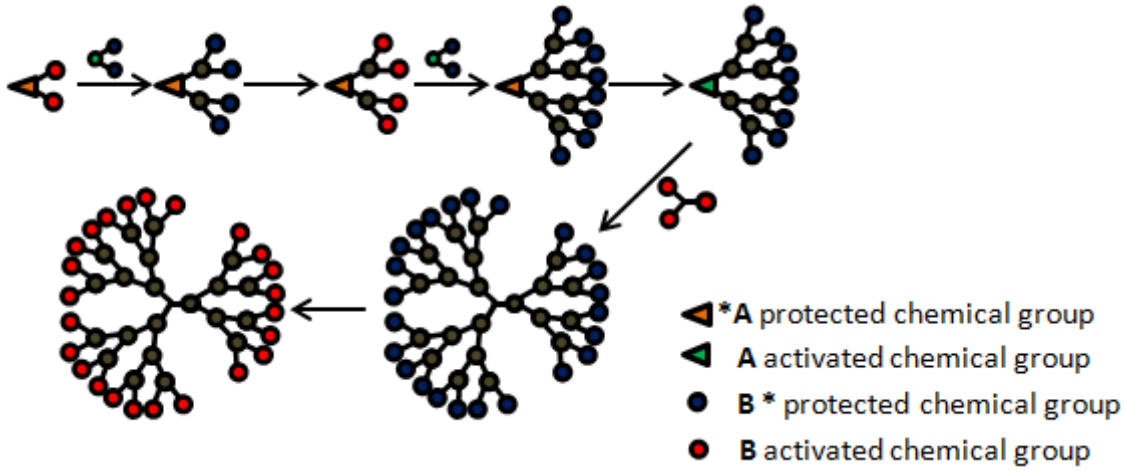

Figure C_2-16: Synthesis of dendrimers following the convergent pathway.

More recently, new synthetic pathways have been described to synthesize dendrimers. The **double growth methods** are surely the most common ones. They consist on the synthesis of low generation dendrons and/or dendrimers, which can be easily obtained and combined to afford high generation dendrimers and dendrons without requiring excessively complicated reactions (**figure C_2-17**).[67] In the *"double-exponential method"*, two low generation dendrons are allowed to react to form a new high generation dendron. For example, this strategy allows the easy synthesis of a 4th generation dendron starting from two 2nd generation dendrons. This strategy presents the advantage of simplifying the synthesis and purification of high generation intermediate dendrons. In another synthetic pathway, the *"double-stage convergent method"*, low generation dendrons are allowed to react with a low generation dendrimer that would act as the new dendrimer core. For example,

[67] M.V. Walter, M. Malkoch, Accelerated approaches to dendrimers. Materials science and technology, **2006**, Wiley-VCH, London, UK.

when 2nd generation dendrons react with a 2nd generation dendrimer, a 4th generation dendrimer is obtained. In this modified convergent synthetic pathway, the steric hindrance is less important as the core is bigger and the dendrons are smaller.

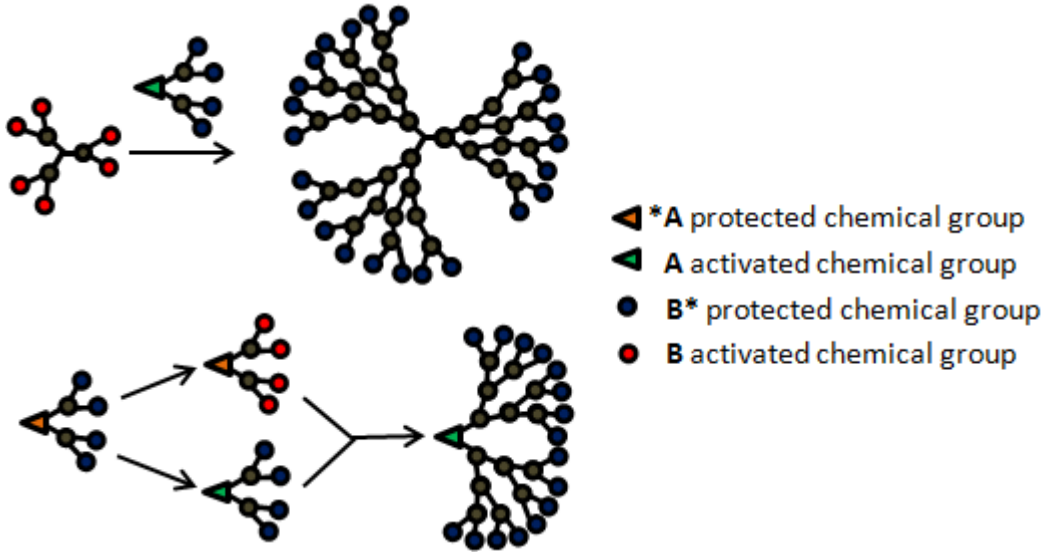

Figure C_2-17: Double stage convergent and double exponential synthetic pathway.

Another new strategy is the **orthogonal growth** that can be employed in either a divergent or a convergent pathway. Dendrimers are composed of two monomers AB_n and CD_n. A groups only react with D groups, whereas C groups only react with B groups. This strategy allows bypassing the deprotection reaction steps of the peripheral group. Therefore, the synthesis of dendrimers is much faster and, for instance, a 6th generation dendrimer could be synthesized in one single day (**figure C_2-18**).[68]

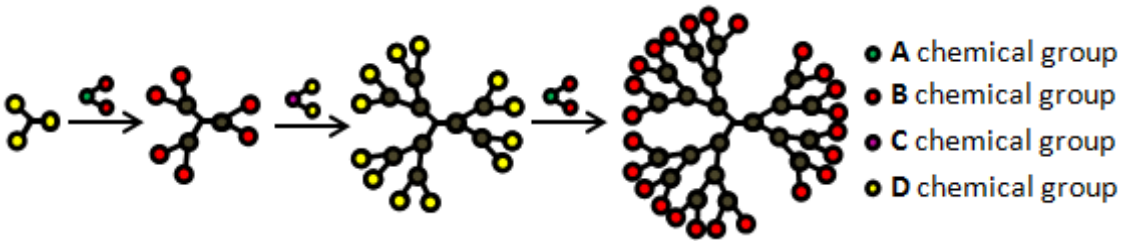

Figure C_2-18: Divergent orthogonal growth synthetic pathway.

[68] P. Antoni, M.J. Robb, L. Campos, M. Montanez, A. Hult, E. Malmström, M. Malkoch, C.J. Hawker, Pushing the limits for thiol-ene and CuAAC reactions: synthesis of a 6th generation dendrimer in a single day, *Macromolecules*, **2010**, 43, 6625-6631.

Recent advances in organic synthesis have been applied to dendrimer synthesis in order to obtain dendrimers in a faster way and/or of higher generations. The **"*click chemistry*"** concept was first described by Sharpless *et al.* in 2001. The dendritic community was interested in the high yields and the good orthogonality of the click chemistry reactions. Nowadays, they are commonly employed to synthesize a large variety of dendrimers. The most used click chemistry reactions are the copper(I) azide-alkyne cycloaddition (CuAAC), the thiol-ene and thiol-yne reactions and the Diels-Alder reaction.[69] In particular, these reactions have been used to obtain new and more complex dendrimers with heterofunctional groups, like Janus dendrimers,[70] onion-peel[71] and 3-faces dendrimers[72] (**figure C_2-19**).

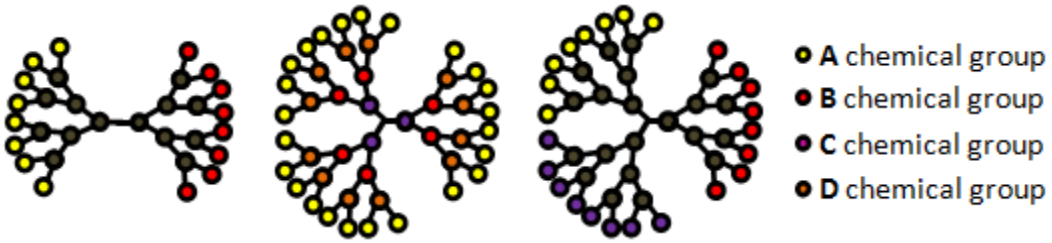

Figure C_2-19: Janus, onion-peel and 3-face dendrimers.

Dendrimers **heterofunctionality** has also been introduced by employing innovative monomers with more than one reactive groups, *eg.* A-(BC) monomers, or by employing AB_2* monomers with different protective groups

[69] a) M. Sowinska, Z. Urbanczyk-Lipkowska, Advances in the chemistry of dendrimers, *New J. Chem.*, **2014**, 38, 2168-2203; b) M. Arseneault, C. Wafer, J.F. Morin, Recent advances in click chemistry applied to dendrimer synthesis, *Molecules*, **2015**, 20, 9263-9294.

[70] A.M Caminade, R. Laurent, B. Delavaux-Nicot, J.P. Majoral, "Janus" dendrimers: syntheses and properties, New J. Chem., **2012**, 36, 217-226.

[71] R. Sharma, K. Naresh, Y.M. Chabre, R. Rej, N.K. Saadeh, R. Roy, "Onion peel" dendrimers: a straightforward synthetic approach towards highly diversified architectures, *Polym. Chem.*, **2014**, 5, 4321-4331

[72] M. Arseneault, P. Dufour, I. Levesque, J.F. Morin, Synthesis of a controlled three-faced PAMAM particle, *Polym. Chem.*, **2011**, 2, 2293-2298.

that can be selectively deprotected.[73]

Other synthetic approaches, like **supramolecular chemistry**, have been studied in order to facilitate the synthesis of dendrimers. Supramolecular chemistry is based on non-covalent bonds between atoms. It allows the formation of large structures by self-assembly of small molecules.[74] In convergent synthesis, supramolecular chemistry is generally used to bind the dendrons to the core. Among others, metal coordination[75] and H bonds[76] have been used as non-covalent interactions. Supramolecular chemistry has also been used in the double stage convergent synthetic pathway. Small dendrons were linked *via* supramolecular chemistry to small dendrimers in order to obtain a new assembly named megamer.[77]

[73] a) R.S. Navath, A.R. Menjoge, B. Wang, R. Romero, S. Kannan, R.M. Kannan, Amino acid-functionalized dendrimers with heterobifunctional chemoselective peripheral groups for drug delivery applications, *Biomacromolecules*, **2010**, 11, 1544-1563; b) A.P. Goodwin, S.S. Lam, J.M.J. Fréchet, Rapid, efficient synthesis of heterobifunctional biodegradable dendrimers *J. Am. Chem. Soc.*, **2007**, 129, 6994-6995.

[74] J.M.J. Fréchet, Dendrimers and supramolecular chemistry, *PNAS*, 99, 4782-4787.

[75] G.R. Newkome, R. Güther, C.N. Moorefield, F. Cardullo, L. Echegoyen, E. Pérez-Cordero, H. Luftmann, Routes to dendritic networks: *bis*-dendrimers by coupling of cascade macromolecules through metal centers, *Angew. Chem. Int. Ed.*, **1995**, 34, 2023-2026

[76] S.C. Zimmerman, F. Zeng, D.E.C. Reichert, S.V. Kolotuchin, Self-assembling dendrimers, *Science*, **1996**, 271, 1095-1098.

[77] S. Uppuluri, D.R. Swanson, L.T. Piehler, J. Li, G.L. Hagnauer, D.A. Tomalia, Core–shell tecto(dendrimers): I. synthesis and characterization of saturated shell models, *Adv. Mat.*, **2000**, 12, 796-800.

2.2.2- Dendritic-polymer hybrids, derivatives at the intersection of classical polymers and dendrimers

2.2.2.1- Hyperbranched polymers

Despite the significant progress in dendrimer synthesis, high generation dendrimers are still obtained after a long, multi-step and challenging process. A new class of macromolecules has emerged at the intersection of linear polymers and dendrimers: the **hyperbranched polymers**. They combine both, some advantages of linear polymers and some advantages of dendrimers. As the linear polymers, they can be synthesized in one-pot reaction and, as dendrimers, they have numerous and available chemical groups at their periphery and present a globular shape (**figure C_2-20**).[78]

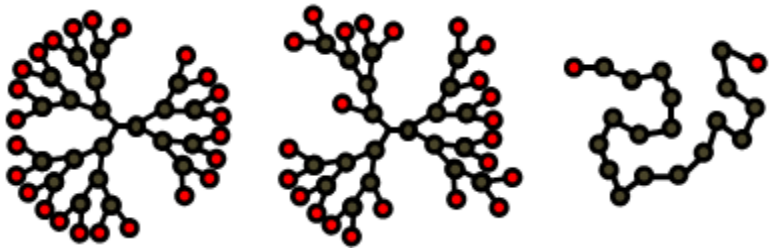

Figure C_2-20: Schematic representation of a dendrimer (left), a linear polymer (right) and a hyperbranched polymer (middle).

Hyperbranched polymers are, as their name suggests, highly ramified macromolecules, and like the dendrimers, they are characterized by a generation number that defines their average size and their average number of peripheral groups.

The first hyperbranched polymer was synthesized in 1982 by Kricheldorf *et al.*, who reported the synthesis of a new poly(3-hydroxybenzoate), a highly

[78] M. Jikei, M.A. Kakimoto, Hyperbranched polymers: a promising new class of materials, *Prog. Polym. Sci.*, **2001**, 26, 1233-1285.

ramified polyester synthesized in bulk.[79] Like in the case of dendrimers, some years were necessary after this first report for hyperbranched polymers to catch the interest of the scientific community. Nowadays, a large variety of hyperbranched polymers exists including polyesters, polyethers, polyamines, polyamides, polystyrene derivatives, *etc*.[80] Due to their easy synthesis in one-pot reaction, some of them have been commercialized at very competitive prices. Thus, for example, in Sigma-Aldrich©, 1 g of polyester hyperbranched polymer of 3rd generation costs 18.50 € whereas 1 g of polyester dendrimer of 3rd generation costs 1302.00 €.

Hyperbranched polymers are mainly synthesized using the **polycondensation of AB_x monomers**. In general, the self-polycondensation of AB groups needs the addition of a catalyst to activate either A or B chemical groups (**figure C_2-21**).[81] Two other ones are currently used for the synthesis of hyperbranched polymers: the self-condensing vinyl polymerization[82] and the multibranching ring-opening polymerization.[83]

[79] H.R. Kricheldorf, Q.Z. Zang, G. Schwarz, New polymer syntheses: 6. Linear and branched poly(3-hydroxy-benzoates), *Polymer*, **1982**, 23, 1821-1829.

[80] a) Y.H. Kim, O.W. Webster, Water soluble hyperbranched polyphenylene: "a unimolecular micelle?", *J. Am. Chem. Soc.*, **1990**, 112, 4592-4593; b) Y. Zheng, S. Li, Z. Weng C. Gao, Hyperbranched polymers: advances from synthesis to applications, *Chem. Soc. Rev.*, **2015**, 44, 4091-4130.

[81] a) E. Malmström, A. Hult, Kinetics of formation of hyperbranched polyesters based on 2,2-bis(methylol)propionic acid, *Macromolecules*, **1996**, 29, 1222-1228; b) C. J. Hawker, R. Lee, J.M.J. Fréchet, One-step synthesis of hyperbranched dendritic polyesters, *J. Am. Chem. Soc.*, **1991**, 113, 4583-4588; c) A. Blencowe, L. Davidson, W. Hayes, Synthesis and characterization of hyperbranched polyesters incorporating the AB2 monomer 3,5-bis(3-hydroxylprop-1-ynyl)benzoic acid, *Eur. Polym. J.*, **2003**, 39, 1955-1563.

[82] J.A. Alfurhood, P.R. Bachlera, B.S. Sumerlin, Hyperbranched polymers via RAFT self-condensing vinyl polymerization, *Polym. Chem.*, **2016**, 7, 3361-3369.

[83] A. Sunder , R. Hanselmann , H. Frey ,R. Mülhaupt, Controlled synthesis of hyperbranched polyglycerols by ring-opening multibranching polymerization, *Macromolecules*, **1999**, 32, 4240–4246.

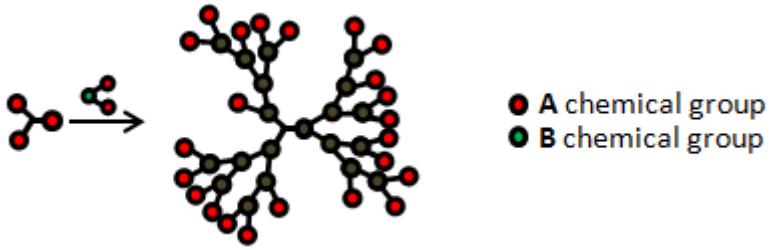

Figure C_2-21: Schematic synthesis of hyperbranched polymers by polycondensation.

The one-step synthesis of hyperbranched polymers is much easier and faster than the multi-step synthesis of the dendrimers but it has the disadvantage to give macromolecules with **higher polydispersity**. This is principally due to the coupling of growing molecules between themselves forming bigger and larger molecules that would have more terminal groups and therefore would have even more probability to couple with other molecules. The polydispersity index is calculated according to the equation *(1)*.[78]

$$(1)\quad Đ = M_w/M_n$$

where Đ is the polydispersity index, M_w, the mass average molecular weight and M_n the number average molecular weight.

Additionally, hyperbranched polymers have a more **irregular structure** than dendrimers and all the terminal groups are not only located at the periphery but also in the internal branches (**figure C_2-22**). Indeed, hyperbranched polymers are not fully branched macromolecules and present pending terminal groups in their inner branches.

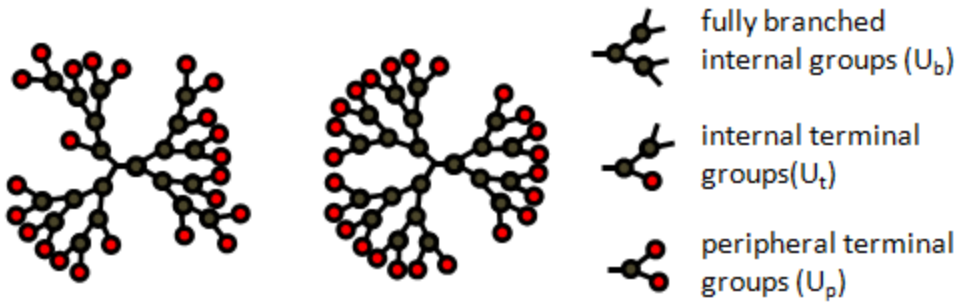

Figure C_2-22: Schematic architectures of a hyperbranched polymer (left) and a dendrimer (right).

[78] M. Jikei *et al.*, *Progr. Polym. Sci.*, **2001**, 26, 1233.

The **degree of branching, DB,** is calculated according to the equation *(2)*.[78]

$$(2)\ DB = \frac{Ub + Up}{Ub + Up + Ut}$$

where U_b is the number of fully branched internal groups, U_t the number of internal terminal groups and U_p the number of peripheral terminal groups.

For dendrimers, both the polydispersity index and the degree of branching are equal to 1. However, for hyperbranched polymers, the polydispersity index is always higher than 1 and, at the contrary, the degree of branching is always lower than 1. Both tendencies rise when the proportion of pending internal terminal groups increases. In fact, the closer these values are to 1, the closer to a dendrimer is the hyperbranched polymer.

Several synthetic processes have been employed to **reduce the polydispersity and the number of internal terminal groups** of hyperbranched polymers. The most common one is the addition of a small multifunctional core upon which the monomers would condensate. This technique is usually combined with a slow addition of the monomer that would favor a regular growing of the macromolecule.[84] Playing with the kinetics of competitive polycondensation reactions may also reduce the macromolecule defects.[85] Recently, click chemistry reactions have been used as coupling reactions between monomers in order to obtain macromolecules closer to dendrimers. Thus, hyperbranched polymers with Đ ≤ 1.3 and DB ≥ 0.7 were synthesized by CuAAC.[86]

[84] R. Hanselmann , D. Hölter , H. Frey, Hyperbranched polymers prepared via the core-dilution/slow addition technique: computer simulation of molecular weight distribution and degree of branching, *Macromolecules*, **1998**, 31, 3790-3801.

[85] Y. Ohta, S. Fujii, A. Yokoyama, T. Furuyama, M. Uchiyama, T. Yokozawa, Synthesis of well-defined hyperbranched polyamides by condensation polymerization of AB2 monomer through changed substituent effects, *Angew. Chem. Int. Ed.*, **2009**, 48, 5942-5945.

[86] a) Y. Shi, R.W. Graff, X. Cao, X. Wang, H. Gao, Chain-growth click polymerization of AB2 monomers for the formation of hyperbranched polymers with low polydispersities in a one-pot process, *Angew. Chem. Int. Ed.*, **2015**, 54, 7631-7635.

Another strategy is the combination of hyperbranched polymers of small generations with dendrons. Indeed, hyperbranched polymers can be used as a core in the double stage convergent synthesis instead of a low generation dendrimer and this allows the preparation of **dendronized hyperbranched polymers (DHPs)** also named pseudo-dendrimers (**figure C_2-23**).[87]

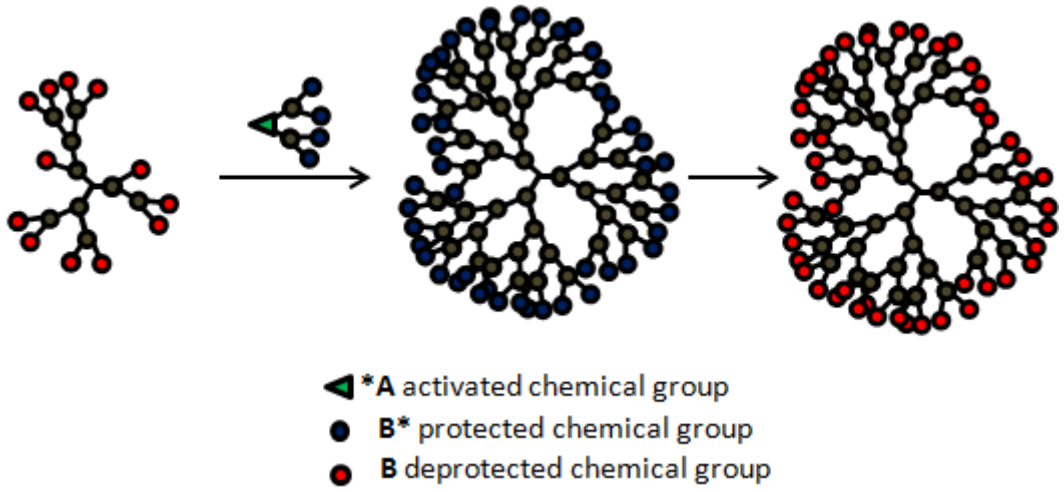

Figure C_2-23: Schematic synthesis of a dendronized hyperbranched polymer (DHP).

In 1998, Frey *et al.* reported for the first time the synthesis of hyperbranched polymer-dendron hybrids by post-functionalizing a hyperbranched polymer with a 1st generation dendron.[88] The coupling of higher generation dendrons with hyperbranched polymers was carried out in 2012 by Lederer *et al*. that reported new DHPs with properties really similar than the ones observed for classical dendrimers.[89] In general, the preparation of the dendrons requires a multi-step synthesis, whereas the hyperbranched polymer is prepared in a one-step reaction. It is important to remark that the reactivity of the terminal internal groups of the hyperbranched polymer is

[87] A. Lederer, W. Burchard, T. Hartmann, J.S. Haataja, N. Houbenov, A. Janke, P. Firedel, R. Schweinds, P. Linder, Dendronized hyperbranched macromolecules: soft matter with a novel type of segmental distribution, *Angew. Chem. Int. Ed.*, **2015**, 54, 12578-12583.

[88] C. Lach, H. Frey, Enhancing the degree of branching of hyperbranched polymers by postsynthetic modification, *Macromolecules*, **1998**, 31, 2381-2383

[89] A. Lederer, T. Hartmann, H. Komber, Sphere-like fourth generation pseudo-dendrimers with a hyperbranched core, *Macromol. Rapid Commun.*, **2012**, 33, 1440-1444.

different from this of the peripheral groups. However, for these high generation derivatives, the final properties of the dendronized hyperbranched polymer are closer to the dendrimer of comparable size as the internal terminal groups are hidden in the deep inner part of the macromolecule.

The recent synthesis of these new hybrid macromolecules, between hyperbranched polymers and dendrimers, represent a good opportunity to synthesize globular polymers with properties similar to high generation dendrimers without requiring a too complicated synthetic procedure.[87-89]

2.2.2.2- Hybrid linear-dendritic block copolymers (HDLBCs)

Another class of hybrid dendritic polymers consists on a linear polymeric chain grafted with one or two dendrons at the ending positions. In the first case, **hybrid linear-dendritic block copolymers** (HLDBCs) are obtained (**figure C_2-24-A**), and in the second case, **hybrid dendritic-linear-dendritic block copolymers** (HDLDBCs) are made (**figure C_2-24-B**). A third type of structure named as dendronized polymers is formed when dendrons are located along the polymer chain, but they won't be discussed herein.[90]

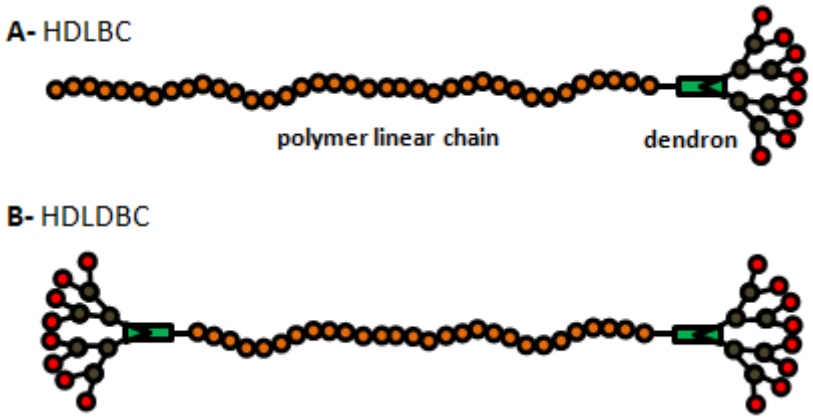

Figure C_2-24: Schematic representations of one hybrid linear-dendritic block copolymer (HDLBC) (**A**) and one hybrid dendritic-linear-dendritic block copolymer (HDLDBC) (**B**).

The first synthesis of a hybrid dendritic-linear-dendritic block copolymer (HDLDBC) was described by Fréchet *et al.* in 1992. This compound was obtained following a convergent approach: the authors coupled a previously synthesized poly(benzylether) dendron with a linear polyethylene oxide (PEO) chain, *i.e. "coupling strategy"* (**figure C_2-25-A**).[91] Two years later, in 1994, Chapman *et al.* published the synthesis of a HLDBC using a divergent approach. In this case, a poly-(*L*)-lysine dendron was grown up in the terminal position of a PEO linear chain, the author named this method as the "*chain first strategy*" (**figure**

[90] D.A. Tomalia, J.M.J Fréchet, Dendrimers and other dendritic polymers, **2002**, John Wiley & Sons, Ltd, Chischester, UK.
[91] I. Gitsov, K.L. Wooley, J.M.J. Fréchet, Novel polyether copolymers consisting of linear and dendritic blocks, *Angew. Chem. Int. Ed.*, **1992**, 31, 1200-1202.

C_2-25-B).[92] During the same year, Fréchet *et al.* described a different approach that consists in growing up the polymer chain at the focal point of the dendron. This strategy was called the "*dendron first strategy*" (**figure C_2-25-C**).[93]

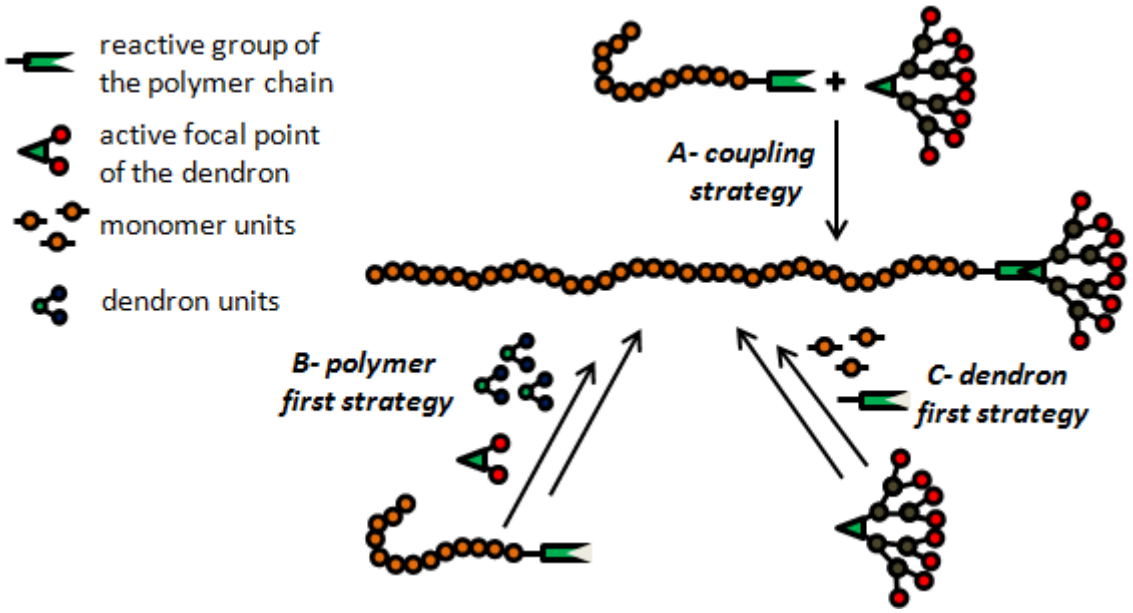

Figure C_2-25: Synthesis of one HLDBC employing the "*coupling strategy*" (**A**), the "*chain first strategy*" (**B**) and the "*dendron first strategy*" (**C**).

The ***"coupling strategy"*** shows some limits as the reactivity of the chemical groups at the extremities of the polymer and at the focal point of the dendron may be low. As a consequence, the coupling reaction is generally uncompleted and the purification of the blends containing the reactive linear polymer and dendron, as well as the final HLDBC, is challenging. Indeed, the new hybrid enhances the compatibility of the two reactants with the final product and hinders their effective separation. Nevertheless, using click chemistry reactions, Oriol *et al.* successfully published the "*coupling*" synthesis of an HLDBC based on linear polyethylene glycol (PEG) chain and *bis*-MPA

[92] T.M. Chapman, G.L. Hillyer, E.J. Mahan, K.A. Shaffer, Hydraamphiphiles: novel linear dendritic block copolymer surfactants, *J. Am. Chem. Soc.*, **1994**, 116, 11195-11196.

[93] I. Gitsov, P.T. Ivanova, J.M.J. Fréchet, Dendrimers as macroiniciator for anionic ring-opening polymerization. Polymerization of ε-caprolactone, *Macromol. Rapid Commun.*, **1994**, 15, 387-393.

polyester dendrons.[94] In parallel, Serrano *et al.* described the successful synthesis of an HDLDBC based on a triblock polyethylene oxide - polypropylene oxide - polyethylene oxide (PEO-PPO-PEO) linear chain, commercialized under the name Pluronic® F-127, with two *bis*-MPA dendrons using the same click chemistry approach.[95]

The **"*chain first strategy*"** procedure is the most common method used to synthesize HLDBCs as it allows the synthesis of a variety of different high generation dendrons upon the linear chain. Among other examples, Meijer *et al.* grew up to the 5th generation a poly(propylene imine) dendron from a polystyrene linear chain,[96] and Fréchet *et al.* synthesized a 6th generation polyester dendron at the terminal position of a PEO linear chain.[97]

The **"*dendron first strategy*"** is the less spread method used to synthesize HLDBCs. Only few examples are described dealing with the synthesis of linear chains of polystyrene and poly(N-isopropylacrylamide) at the focal point of poly(benzylether) dendrons.[98]

[94] E. Blasco, J.L. Serrano, M. Piñol, L. Oriol, Light responsive vesicles based on linear–dendritic block copolymers using azobenzene–aliphatic codendrons, *Macromolecules*, **2013**, 46, 5951-5960.

[95] J. Movellan, P. Urbán, E. Moles, J.M. de la Fuente, T. Sierra, J.L. Serrano, X. Fernàndez-Busquets, Amphiphilic dendritic derivatives as nanocarriers for the targeted delivery of antimalarial drugs, *Biomaterials*, **2014**, 35, 7940-7950.

[96] J.C.M. van Hest, D.A.P. Delnoye, M.W.P.L. Baars, C. Elissen-Román, M. H. P. van Genderen, E.W. Meijer, Polystyrene–poly(propylene imine) dendrimers: synthesis, characterization, and association behavior of a new class of amphiphiles, *J. Eur. Chem.*, **1996**, 2, 1616-1626.

[97] H. Ihre, O.L. Padilla de Jesús, J.M.J. Fréchet, Fast and convenient divergent synthesis of aliphatic ester dendrimers by anhydride coupling, *J. Am. Chem. Soc.*, **2001**, 123, 5908-5917.

[98] a) K. Matyjaszewski, T. Shigemoto, J.M.J. Fréchet , M. Leduc, Controlled/"living" radical polymerization with dendrimers containing stable radicals, *Macromolecules*, **1996**, 29, 4167-4179; b) Z. Ge, S. Luo, S. Liu, Syntheses and self-assembly of poly(benzyl ether)-b-poly(N-isopropylacrylamide) dendritic–linear diblock copolymers, *J. Polym. Sci. Part A. Polym. Chem.*, **2006**, 44, 1357-1371.

2.2.3 - Self-assembly in water of amphiphilic dendrimers and hybrid linear-dendritic block copolymers

2.2.3.1 - Amphiphilic derivatives in water

When an amphiphilic derivative is dissolved in a solvent, such as an aqueous media, it can **self assemble into supramolecular aggregates**. On the one hand, the lipophilic parts of the amphiphilic molecule self-interact and situate themselves in the inner part of the new supramolecular aggregate to avoid unfavorable interactions with external water. On the other hand, the hydrophilic parts are located at the periphery of the supramolecular aggregates and interact with the external water stabilizing the aggregates. A large variety of aggregates with different morphologies can be obtained like micelles, vesicles, sponge phases, *etc*. (**figure C_2-26**).[99]

The different morphologies of the aggregates formed by the amphiphiles are related with the architecture of their components. The **packing parameter**, *p*, was introduced to classify the aggregates and associate their morphology with their components. It is calculated according to the equation *(3)*.

$$(3)\ p = \frac{V}{a0 \times l}$$

where V is the volume of the lipophilic part, a_0 is the surface area of the hydrophilic part and l is the length of the lipophilic part.[100]

[99] M. Ramanathan, L.K. Shrestha, T. Mori, Q. Ji, J.P. Hill, K. Ariga, Amphiphile nanoarchitectonics: from basic physical chemistry to advanced applications, *Phys. Chem. Chem. Phys.*, **2013**, 15, 10580-10611.

[100] J.N. Israelachvili, D.J. Mitchell, B.W. Ninham, Theory of self-assembly of hydrocarbon amphiphiles into micelles and bilayers, *J. Chem. Soc., Faraday Trans. 2*, **1976**, 72, 1525-1568.

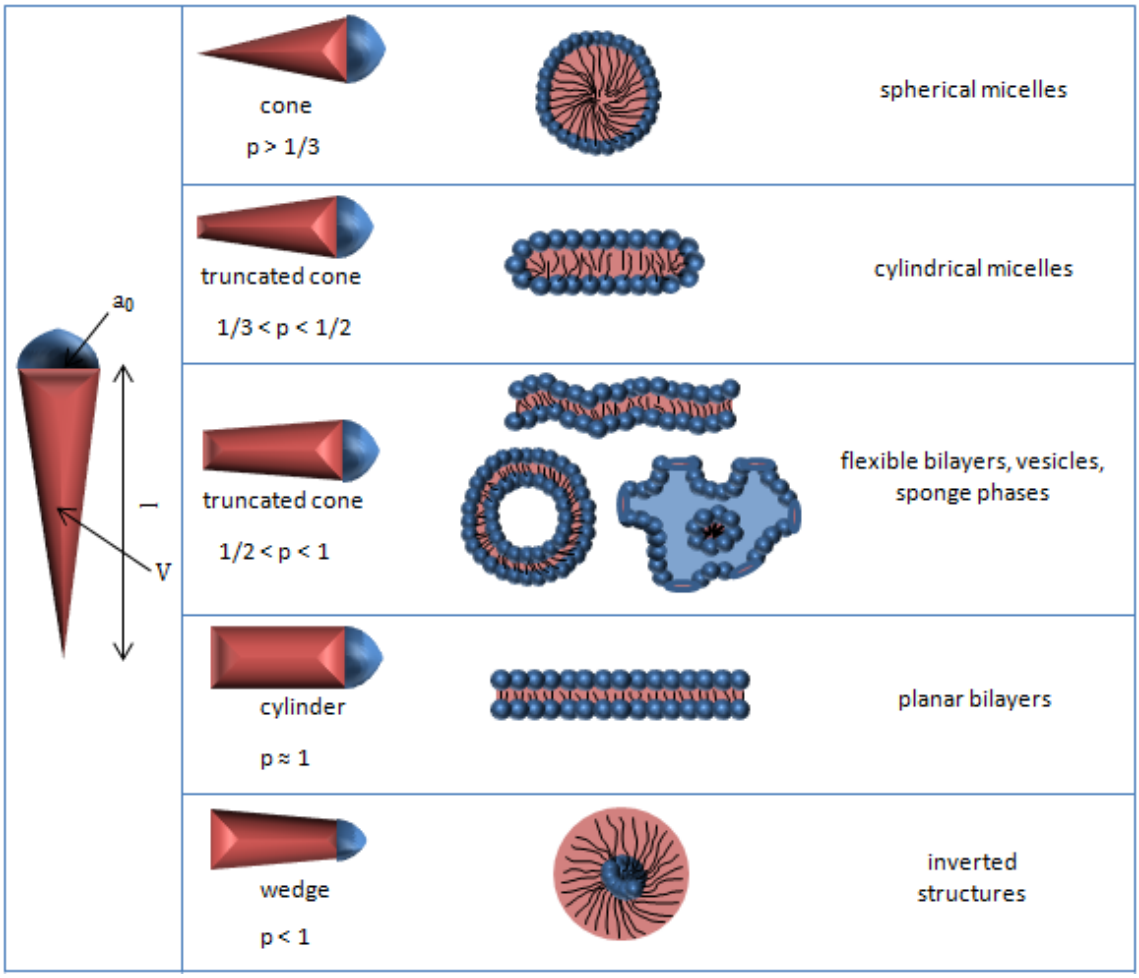

Figure C_2-26: Forms of the amphiphile according to its *p* valor and related to the morphology of the corresponding self-assembled aggregate.

When p is inferior to 1/3, the amphiphile adopts a conical shape and forms spherical micelles in water. When p is comprised between 1/3 and 1, the amphiphile presents a truncated conical shape, and it adopts a cylindrical shape when p becomes equal to 1. When p is comprised between 1/3 and 1/2, cylindrical micelles are formed and when p is comprised between 1/2 and 1, the amphiphiles self-assemble into flexible and curved bilayers (L_α phase) and can form more complex structures like vesicles or sponge phases. In contrast to micelles, vesicles are not dense spheres and present a vacuole in their center. Sponge phases (L_3 phases) are bicontinuous cubic phases. When p is equal to 1, the amphiphiles form planar bilayers that usually stack one on top of each other

(L_β phase). Finally, when p is superior to 1, the amphiphiles form inverted structures.

The formation of supramolecular aggregates by dissolution of an amphiphile in water can only occur when the amphiphile is above a given concentration. This concentration, which depends on the amphiphile nature, the solvent, the temperature, the pressure and the ionic force, is called "***critical aggregation concentration***" (CAC). At concentrations below the CAC, the amphiphile is fully dissolved in the solvent and no interactions between the amphiphilic molecules occur. Some amphiphiles situate themselves at the surface of the solvent where they contribute to reduce the interfacial tension between the air and the solvent. The increase of the amphiphile concentration leads to a saturation of the solvent surface. Above this concentration, the amphiphiles can self-assemble into aggregates (**figure C_2-27**).[101]

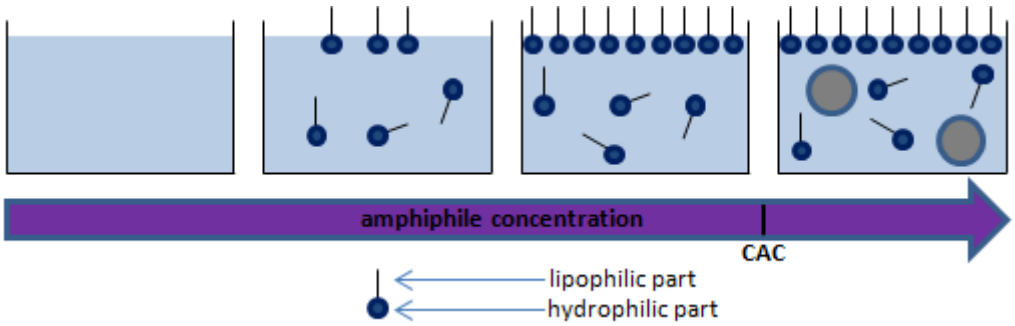

Figure C_2-27: Localization of the amphiphiles in a solution while increasing their concentration and formation of aggregates above the CAC.

[101] M.J. Rosen, J.T. Kunjappu, Surfactants and interfacial phenomena, 4th edition, **2012**, John Wiley & Sons, Inc, Hoboken, USA.

2.2.3.2- Amphiphilic dendritic derivatives, interesting supramolecular aggregates

The most common dendritic amphiphiles are dendrimers and hyperbranched polymers with a lipophilic internal core surrounded with by a hydrophilic shell. These compounds are usually soluble in water and can act as micelles even though they are composed of only one and unique molecule. They were described as ***"unimolecular micelles"*** (**figure C_2-28**).[102] These micelle-like molecules are small, usually between 5 and 20 nm. Therefore, they are not very sensitive to reticuloendothelial system (RES) clearance and can be easily internalized by cells. Moreover, they can encapsulate small lipophilic molecules, such as drugs or dyes, in their inner structure, thus increasing their solubility in water.[103]

Some high generation dendrimers naturally possess the property of forming "*unimolecular micelles*" in water even though aggregation between

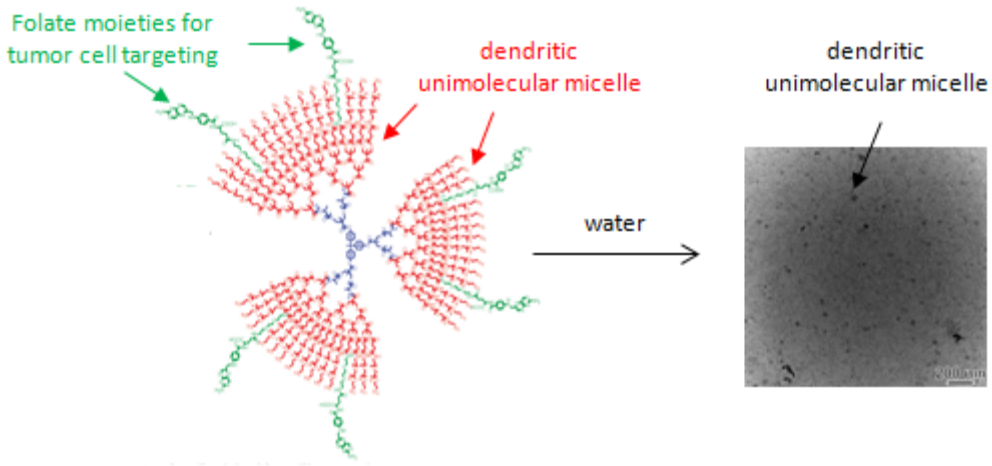

Figure C_2-28: Schematic representation of a "*unimolecular micelle*" and TEM image after dissolution in water, adapted from ref. [108].

[102] G.R. Newkome, C.N. Moorefield, G.R. Baker, M.J. Saunders, S.H. Grossman, Unimolecular micelles, *Angew. Chem. Int. Ed.*, **1991**, 30, 1178-1180.

[103] a) F. Xiaoshan, L. Zibiao, X.J. Loh, Recent development of unimolecular micelles as functional materials and applications, *Polym. Chem.*, **2016**, 7, 5898-5919; b) M. Liu, K. Kono, J.M.J Fréchet, Water-soluble dendritic unimolecular micelles: their potential as drug delivery agents, *J. Control. Release*, **2000**, 65, 121-131.

various macromolecules are generally observed.[104] In order to increase the stability of the "*unimolecular micelles*", dendrimer post-functionalization with hydrophilic chains[105], lipophilic chains[106] or both[107] were performed. Additionally, targeting moieties have been added at the periphery of these structures to reach specific diseased tissues.[108]

In contrast to core-shell amphihilic dendrimers that give unimolecular micelles, numerous amphiphiles based on dendrimers have been synthesized that form aggregates in water. Particularly, because of their controlled and versatile architecture, **amphiphilic Janus dendrimers, and hybrid linear-dendritic block copolymers (HLDBCs)** afford interesting possibilities to form nanoaggregates while encapsulating lipophilic, amphiphilic and hydrophilic drugs within their diverse structures modifying their bioavailability and in particular water solubility, release profile and activity.[109]

Amphiphilic Janus dendrimers are composed of two antagonistic parts: one is hydrophilic whereas the second one is lipophilic. They can consist of two dendrons based on the same monomer forming therefore homodendritic

[104] C. Yu , L. Ma, K. Li, S. Li, Y. Liu, Y. Zhou, D. Yan, Molecular dynamics simulation studies of hyperbranched polyglycerols and their encapsulation behaviors of small drug molecules, *Phys. Chem. Chem. Phys.*, **2016**, 18, 22446-22457

[105] K. Sharma, O.Y. Zolotarskaya, K.J. Wynne, H. Yang, Poly (ethylene glycol)-armed hyperbranched polyoxetanes for anticancer drug delivery, *J. Bioact. Compat. Polym.*, **2012**, 27, 525-539.

[106] L. Ye, K. Letchford, M. Heller, R. Liggins, D. Guan, J.N. Kizhakkedathu, D.E. Brooks, J.K. Jackson, H.M. Burt, Synthesis and characterization of carboxylic acid conjugated, hydrophobically derivatized, hyperbranched polyglycerols as nanoparticulate drug carriers for Cisplatin

[107] Y. Xiao, H. Hong, A. Javadi, J.W. Engle, W. Xu, Y. Yang, Y. Zhang, T.E. Barnhart, W. Cai, S Gong, Multifunctional unimolecular micelles for cancer-targeted drug delivery and positron emission tomography imaging, *Biomaterials*, **2012**, 33, 3071-3082.

[108] W. Cao, J. Zhou, A. Mann, Y. Wang, L. Zhu, Folate-functionalized unimolecular micelles based on a degradable amphiphilic dendrimer-like star polymer for cancer cell-targeted drug delivery, *Biomacromolecules*, **2011**, 12, 2697-2707.

[109] B.N.S. Thota, L.H. Urner, R. Haag, Supramolecular architectures of dendritic amphiphiles in water, *Chem. Rev.*, **2016**, 116, 2079-2102.

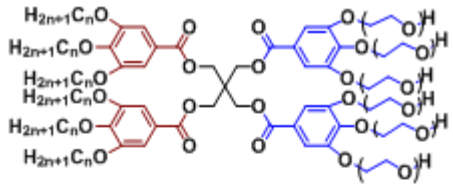

A- Homodendritic amphiphilic Janus dendrimer

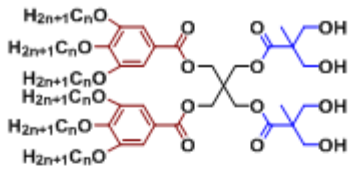

B- Heterodendritic amphiphilic Janus dendrimer

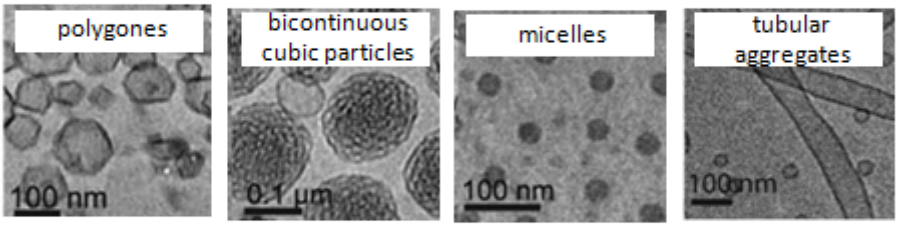

C- Diverse aggregates formed by Amphiphilic Janus dendrimers

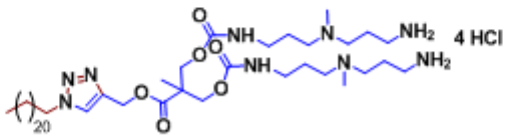

D- Amphiphilic dendron

Figure C_2-29: Chemical structures of a homodendritic (**A**) and a heterodendritic (**B**) amphiphilic Janus dendrimer and cryoTEM images of various aggregates formed by some amphiphilic Janus dendrimers (**C**), adapted from ref. [111]. Chemical structure of an amphiphilic dendron (**D**) (adapted from ref. [112]). The red block represents the lipophilic block and the blue block represents the hydrophilic block.

structures (**figure C_2-29-A**) or, alternatively, they can be formed by two dendrons based on different monomers forming heterodendritic structures (**figure C_2-29-B**).[110]

The difference of hydrophilicity of the two dendrons is usually reached by the addition of hydrophilic or lipophilic moieties at the terminal groups of one of the dendrons constituting the final Janus dendrimer (**figure C_2-29-B**) or by the addition of hydrophilic moieties at the terminal groups of one of the dendrons and the addition of lipophilic moieties at the terminal groups of the other

[110] D.R. Sikwal, R.S. Kalhapure, T. Govender, An emerging class of amphiphilic dendrimers for pharmaceutical and biomedical applications: Janus amphiphilic dendrimers, *Eur. J. Pharm. Sci.*, **2017**, 97, 113-134.

dendron (**figure C_2-29-A**). Playing with the different generations of the hydrophilic and lipophilic dendrons, a large variety of different aggregates with tunable, highly controlled and predictable morphologies and sizes can be obtained (**figureC_2-30-C**).[111]

In parallel, **amphiphilic dendrons** have also been developed (**figure C_2-29-D**). They are more simple structures, based on a hydrophilic dendron and a lipophilic chain.[112] As a result of self-aggregation, the resulting nanostructures can act as high generation dendrimers bearing numerous peripheral groups while they are only based on dendrimers or dendrons of small generation. These non-covalent structures usually afford a lower synthetic cost and a higher biocompatibility and biodegradability than their related high generation dendrimers.

Hybrid linear-dendritic block copolymers (HLDBCs and HDLDBCs) are another dendritic family that can exhibit amphiphilic properties. Three main procedures allow obtaining these amphiphilic hybrids (**figure C_2-30**):

- by coupling hydrophilic dendron(s) with a lipophilic linear polymer,
- by coupling lipophilic dendron(s) with a hydrophilic linear polymer,
- by coupling hydrophilic or lipophilic dendron(s) with an amphiphilic linear polymer.

[111] V. Percec, D.A. Wilson, P. Leowanawat, C.J. Wilson, A.D. Hughes, M.S. Kaucher, D.A. Hammer, D.H. Levine, A.J. Kim, F.S. Bates, K.P. Davis, T.P. Lodge, M.L. Klein, R.H. DeVane, E. Aqad, B.M. Rosen, A.O. Argintaru, M.J. Sienkowska, K. Rissanen, S. Nummelin, J. Ropponen, Self-assembly of Janus dendrimers into uniform dendrimersomes and other complex architectures, *Science*, **2010**, 328, 1009-1014; c) M. Peterca, V. Percec, P. Leowanawat, A. Bertin, Predicting the size and properties of dendrimersomes from the lamellar structure of their amphiphilic Janus dendrimers, *J. Am. Chem. Soc.*, **2011**, 133, 20507-20520.

[112] a) M. Calderón, M.I. Velasco, M.C. Strumia, A.T. Lorenzo, A.J. Müller, M.R. Rojas, A.E. Sáez, Synthesis of amphiphilic dendrons and their interactions in aqueous solutions with cetyltrimethylammonium p-toluenesulfonate (CTAT), *J. Colloid Inter. Sci.*, **2009**, 336, 462-469; b) S.M. Bromfield, P. Posocco, C.W. Chan, M. Calderon, S.E. Guimond, J.E. Turnbull, S. Pricl, D.K. Smith, Nanoscale self-assembled multivalent (SAMul) heparin binders in highly competitive, biologically relevant, aqueous media, *Chem. Sci.*, **2014**; 5, 1484-1492.

As occurs with Janus dendrimers, a large variety or different aggregates with tunable and highly controlled morphologies has been described using amphiphilic hybrid linear-dendritic block copolymers (HLDBCs).[113]

Moreover, **stimuli-responsive amphiphilic HLDBCs** have been described. The morphologies of the aggregates formed by such compounds can be modified after exposure to an external input. For example, spherical aggregates based on thermoresponsive poly(N-isopropylacrylamide) polymer and polyether dendron have been transformed into bigger entangled nanotubes after being heated[114] and spherical aggregates, worm-like micelles, spherical and tubular vesicles have been obtained with a unique polyampholyte HLDBC based on a pH-sensitive poly-(*L*)-lysine linear polymer and a poly(*L*-glutamic acid)-poly(amidoamine) dendritic construct.[115]

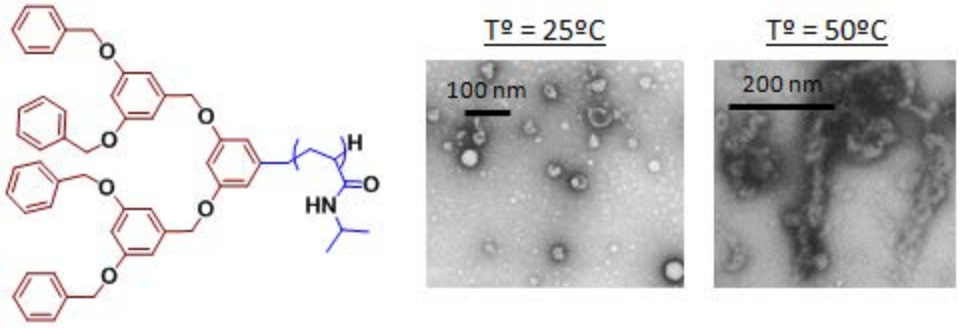

Figure C_2-30: Schematic representation of an amphiphilic HLDBC based on polyether dendron and thermoresponsive poly(N-isoproprylacrylamide); after being heated the spherical aggregates were transformed into entangled nanotubes, adapted from ref. [114].

[113] a) X. Fan, Y. Zhao, W. Xu, L. Li, Linear–dendritic block copolymer for drug and gene delivery, *Mat. Sci. Eng. C*, **2016**, 62, 943-959, b) Q. Yu, J. Liu, D. Chen, R. Wang, Self-assembly of linear-dendritic triblock copolymer dependent on variant generations, *Polymer*, **2015**, 79, 179-186.

[114] L. Zhu, G. Zhu, M. Li, E. Wang, R. Zhu, X. Qi, Thermosensitive aggregates self-assembled by an asymmetric block copolymer of dendritic polyether and poly(N-isopropylacrylamide), *Eur. Polym. J.*, **2002**, 38, 2503-2506.

[115] L. Chen, T. Chen, W. Fang, Y. Wen, S. Lin, J. Lin, C. Cai, Synthesis and pH-responsive "schizophrenic" aggregation of a linear-dendron-like polyampholyte based on oppositely charged polypeptides, *Biomacromolecules*, **2013**, 14, 4320-4330.

An interesting characteristic of the amphiphilic dendritic aggregates based on either Janus dendrimer or hybrid linear-dendritic block copolymers (HLDBCs and HDLDBCs) when compared with the ones based on small molecule surfactants is their **resistance to dilution**. In fact, when administered as a nanomedicine treatment, the aggregates are generally highly diluted and sometimes below their CAC, which should induce their break down. Fortunately, the disassembly of aggregates based on high molecular weight amphiphiles, such as the dendritic amphiphiles, is not kinetically favored and may be delayed from days to weeks making these aggregates highly suitable for drug delivery.[116]

[116] a) H. Gheybi, M. Adeli, Supramolecular anticancer drug delivery systems based on linear-dendritic copolymers, Polym. Chem., **2015**, 6, 2580-2615; b) P. Opanasopit, M. Yokoyama, M. Watanabe, K. Kawano, Y. Maitani, T. Okano, Block copolymer design for camptothecin incorporation into polymeric micelles for passive tumor targeting., *Pharm. Res.*, **2004**, 21, 2001-2008.

2.3- An extended library of dendritic materials for drug and gene delivery

A large variety of dendrimers are currently investigated as vectors for gene and drug delivery purposes. Herein, some relevant examples of the most used dendritic architectures, including dendrimers, hyperbranched polymers, self-assembling amphiphilic dendrimers and hybrid linear-dendritic block copolymers will be commented.

2.3.1- Most common dendrimers and dendritic derivatives based on nitrogen functions

2.3.1.1- Poly(amidoamine) dendrimers

Poly(amidoamine) dendrimers, abbreviated as PAMAMs, are one of the most commonly used dendrimers in nanomedicine as evidenced by the more than 400 articles containing PAMAM in their title and reviews dealing exclusively with it published since 2010,[117] as well as numerous patents.[118]

[117] a) D. Luong, P. Kesharwani, R. Deshmukh, M.C.I.M. Amin, U. Gupta, K. Greish, A.K. Iyer, PEGylated PAMAM dendrimers: Enhancing efficacy and mitigating toxicity for effective anticancer drug and gene delivery, *Acta Biomaterialia*, **2016**, 43, 14-29; b) E.B. Bahadıra, M.K. Sezgintürk, Poly(amidoamine) (PAMAM): an emerging material for electrochemical bio(sensing) applications, *Talanta*, **2016**, 148, 427-438; c) P. Kesharwani, S. Banerjee, U. Gupta, M.C.I.M. Amin, S. Padhye, F.H. Sarkar, A.K. Iyer, PAMAM dendrimers as promising nanocarriers for RNAi therapeutics, *Materials Today*, **2015**, 18, 565-572; d) M. Labieniec-Watala, C. Watala, PAMAM dendrimers: destined for success or doomed to fail? plain and modified PAMAM dendrimers in the context of biomedical applications, *J. Pharm. Sci.*, **2015**, 104, 2-14; e) S. Sadekar, H. Ghandehari, Transepithelial transport and toxicity of PAMAM dendrimers: Implications for oral drug delivery, *Adv. Drug Deliv. Rev.*, **2012**, 64, 571-588.

PAMAM dendrimers were first synthesized by Tomalia's group in 1985[62] and are nowadays commercially available up to the 10th generation with size ranging from 0.1 to 13 nm (**figure C_2-31**).[119]

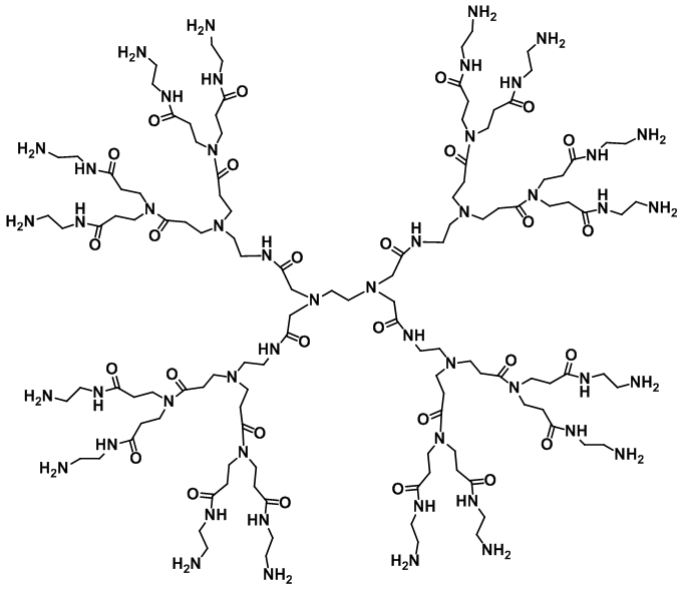

Figure C_2-31: PAMAM dendrimer of 2nd generation.

PAMAM dendrimers have demonstrated their high potential for applications in biomedicine,[116-117] catalysis,[120] material science including liquid crystals[121] and material engineering.[122]

Particularly, in the biomedical field, PAMAM dendrimers were the first dendrimers to show effective *in vitro* plasmid gene transfection in liver, kidney

[118] D. Rajasekhar, P.C Liao, Patents and the development on polymer based nanomaterial (PAMAM dendrimer) for biomedical applications, *Recent Patent Biomed. Eng.*, **2012**, 5, 159-174.

[62] D.A. Tomalia et al., *Polym. J.*, **1985**, 17, 117; cf p.35

[119] www.dendritech.com

[120] D. Wang, D. Astruc, Dendritic catalysis - basic concepts and recent trends, *Coord. Chem. Rev.*, **2013**, 257, 2317-2334

[121] M. Marcos, R. Giménez, J.L. Serrano, B. Donnio, B. Heinrich, D. Guillon, Dendromesogens: liquid crystal organizations of poly(amidoamine) dendrimers versus starburst structures, *Chem. Eur. J.*, **2001**, 7, 1006-1013

[122] L.M. Bronstein, Z.B. Shifrina, Dendrimers as encapsulating, stabilizing, or directing agents for inorganic nanoparticles, *Chem. Rev.*, **2011**, 111, 5301-5344.

and cancerous cells, results reported in 1993.[123] These promising results in **pDNA transfection** with PAMAMs could be extended to other cells and with other genetic material, like siRNA for example.[124]

PAMAM dendrimers have also been deeply studied for **drug delivery**. They can form dendrimer-drug conjugates by means of drug encapsulation or drug-dendrimer covalent bonds, which have been explored to improve the activity of various anticancer or antiviral drugs while reducing their side effects. Thus, anticancer,[125] antiviral,[126] and antiobiotic[127] properties and/or efficacy of various drugs have been successively improved *in vitro* and *in vivo* after conjugation with PAMAMs.

Nevertheless, PAMAM dendrimers are **neither fully biocompatible nor biodegradable**, their cytotoxicity increasing with the dendrimer generation, and this limits their applications in nanomedicine.[128] Several strategies have been pursued to overcome this drawback. The biocompatibility of high generation

[123] J. Haensler, F.C. Szoka, Polyamidoamine cascade polymers mediate efficient transfection of cells in culture, Bioconj. Chem., 1993, 4, 372-379.

[124] a) J.D. Eichman, A.U. Bielinska, J.F. Kukowska-Latallo, J.R. Baker, The use of PAMAM dendrimers in the efficient transfer of genetic material into cells, *PSTT*, **2000**, 3, 232-245; b) Liu, X. Liu, P. Rocchi, F. Qu, J.L. Iovanna, L. Peng, Arginine-terminated generation 4 PAMAM dendrimer as an effective nanovector for functional siRNA delivery *in vitro* and *in vivo*, *Bioconjugate Chem.*, **2014**, 25, 521-532.

[125] Q. Zhong, E.R. Bielski, L.S. Rodrigues, M.R. Brown, J.J. Reineke, S.R.P. Da Rocha, Conjugation to poly(amidoamine) dendrimers and pulmonary delivery reduce cardiac accumulation and enhance antitumor activity of doxorubicin in lung metastasis, *Mol. Pharmaceutics*, **2016**, 13, 2363-2375

[126] J.J. Landers, Z. Cao, I. Lee, L.T. Piehler, P.P. Myc, A. Myc, T. Hamouda, A.T. Galecki, J.R. Baker Jr. Prevention of influenza pneumonitis by sialic acid–conjugated dendritic polymers, *J. Infect. Dis.*, **2002**, 186, 1222-1230

[127] R.S. Navath, A.R. Menjoge, H. Da, R. Romero, S. Kannan, R.M. Kannan, Injectable PAMAM dendrimer–PEG hydrogels for the treatment of genital infections: formulation and *in vitro* and *in vivo* evaluation, *Mol. Pharmaceutics*, **2011**, 8, 1209-1223.

[128] S.P. Mukherjee, H.J. Byrne, *Basic Science*, Polyamidoamine dendrimer nanoparticle cytotoxicity, oxidative stress, caspase activation and inflammatory response: experimental observation and numerical simulation, *Nanomedicine*, **2013**, 9, 202-211.

PAMAMs has been principally enhanced by **PEGylation**.[129] Additionally, the **self-assembly** of low generation amphiphilic PAMAM derivatives, such as Janus dendrimers[130] or amphiphilic dendrons,[131] allows the formation of macromolecular aggregates in water that show the same potential in gene transfection than high generation PAMAMs while showing higher biocompatibility and biodegradability.

[129] D. Luong, P. Kesharwania, R. Deshmukha, Mo. Cairul I.l. Amin, U. Gupta, K. Greish, A.K. Iyer, PEGylated PAMAM dendrimers: Enhancing efficacy and mitigating toxicity for effective anticancer drug and gene delivery, Acta Biomater., 2016, 43, 14-29.

[130] T. Wei, C. Chen, J. Liu, C. Liu, P. Posocco, X. Liu, Q. Cheng, S. Huo, Z. Liang, M. Fermeglia, S. Pricl, X.J. Liang, P. Rocchi, L. Peng, Anticancer drug nanomicelles formed by self-assembling amphiphilic dendrimer to combat cancer drug resistance, *Proc. Natl. Acad. Sci. USA.*, **2015**, 112, 2978-2983.

[131] T. Yu, X. Liu, A.L. Bolcato-Bellemin, Y. Wang, C. Liu, P. Erbacher, F. Qu, P. Rocchi, J.P. Behr, L. Peng, An amphiphilic dendrimer for effective delivery of small interfering RNA and gene silencing *in vitro* and *in vivo*, *Angew. Chem. Int. Ed.*, **2012**, 51, 8478-8484.

2.3.1.2- Poly(imine) dendrimers

Commercial **poly(propylene imine)** (PPI) and **poly(ethylene imine)** (PEI) **dendrimers** were first synthesized by Vögtle's group in 1978 [60,132] and by Imae's group in 2008,[133] respectively (**figure C_2-32**).

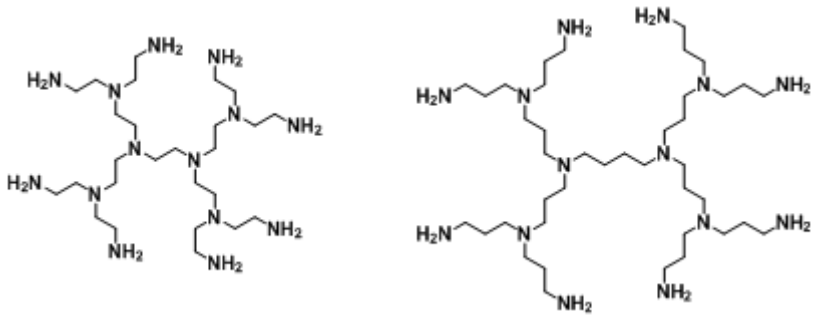

Figure C_2-32: Examples of poly(ethylene imine) (left) and poly(propylene imine) (right) dendrimers.

PPI and PEI dendrimers are widely used in **gene delivery**. They have shown effective gene transfection of pDNA and siRNA *in vitro* and *in vivo*. However, the gene transfection efficacy of these dendrimers is limited by their low biocompatibility.[134] As PAMAM dendrimers, the biocompatibility of PPI dendrimers has been enhanced by either PEGylation or formation of macromolecular aggregates in water based on amphiphilic HLDBC.[135]

[60] E. Buhleier, *Synthesis*, **1978**, 9, 155; cf p.35.

[132] www.signaaldrich.com

[133] a) O. Yemul, T. Imae, Synthesis and characterization of poly(ethyleneimine) dendrimers, *Colloid Polym. Sci.*, **2008**, 286, 747-752; b) www.nanopartica.com.

[134] a) B.H. Zinselmeyer, S.P. Mackay, A.G. Schatzlein, I.F. Uchegbu, The lower-generation polypropylenimine dendrimers are effective gene-transfer agents, *Pharm. Res.*, **2002**, 19, 960-967; b) K. Nam, S. Jung, J.P. Nam, S. Wan Kim, Poly(ethylenimine) conjugated bioreducible dendrimer for efficient gene delivery, *J. Control. Release*, **2015**, 220, 447-455.

[135] a) V. Russ, M. Günther, A. Halama, M.Ogris, E. Wagner, Oligoethylenimine-grafted polypropylenimine dendrimers as degradable and biocompatible synthetic vectors for gene delivery, *J. Control. Release*, **2008**, 132, 131-140. b) J. Gu, J. Hao, X. Fang, X. Sha, Factors influencing the transfection efficiency and cellular uptake mechanisms of Pluronic P123-modified polypropyleneimine/pDNA polyplexes in multidrug resistant breast cancer cells, *Colloids Surf. B*; **2016**, 140, 83-93.

PPI dendrimers have also been used in **drug delivery** after surface modifications. As examples, PEGylated PPI functionalized with folic acid could improve its tumor targeting,[136] and sugar modified PPI could enhance the activity of cytarabine, an anticancer drug.[137]

Additionally, non-commercial **1,3,5-triazine based dendrimers** have been developed by Simanek's group complementary to PPIs and PEIs (**figure C_2-33**).[138] They have been used in nanomedicine and could transfer siRNA *in vitro*,[139] and deliver the low water soluble paclitaxel, an antitumor drug, with higher or similar efficacy *in vivo* than formulations of the commercial agent.[140]

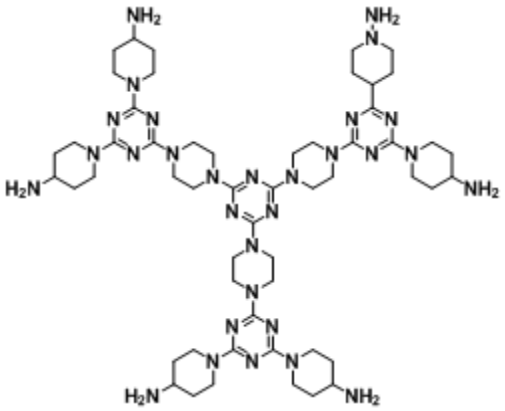

Figure C_2-33: Example of 1,3,5-triazine dendrimer.

[136] S. Thakur, R.K. Tekade, P. Kesharwani, N.K. Jain, The effect of polyethylene glycol spacer chain length on the tumor-targeting potential of folate-modified PPI dendrimers, *J. Nanopart. Res.*, **2013**, 15, 1625.

[137] A. Szulc, L. Pulaski, D. Appelhans, B. Voit, B. Klajnert-Maculewicz, Sugar-modified poly(propylene imine) dendrimers as drug delivery agents for cytarabine to overcome drug resistance, *Int. J. Pharm.*, **2016**, 513, 572-583.

[138] J. Lim, E.E. Simanek, Triazine dendrimers as drug delivery systems: from synthesis to therapy, *Adv. Drug Deliv. Rev.*, **2012**, 64, 826-835.

[139] O.M. Merkel, M.A. Mintzer, D. Librizzi, O. Samsonova, T. Dicke, B. Sproat, H. Garn, P.J. Barth, E.E. Simanek, T.Kissel, Triazine dendrimers as nonviral vectors for *in vitro* and *in vivo* RNAi: the effects of peripheral groups and core structure on biological activity, *Mol. Pharm.*, **2010**, 7, 969-983.

[140] S.T. Lo, S. Stern, J.D. Clogston, J. Zheng, P.P. Adiseshaiah, M. Dobrovolskaia, J. Lim, A.K. Patri, X. Sun, E.E. Simanek, Biological assessment of triazine dendrimer: toxicological profiles, solution behavior, biodistribution, drug release and efficacy in a PEGylated, paclitaxel construct, *Mol. Pharm.*, **2010**, 7, 993-1006.

2.3.1.3 - Polyamide dendrimers

Commercial **poly-(L)-lysine (PLL) dendrimers** were first synthesized by Denkewalter's group in 1979,[61] and are the most common polyamide dendrimers used in nanomedicine (**figure C_2-34**). In contrast to poly(imine) dendrimers mentioned above, PLLs are in general biocompatible at the concentrations used for nanomedicine assays although they still present some biodegradation issues. Nevertheless, successful *in vitro* **gene transfection**[141] and *in vivo* anticancer doxorubicin **drug delivery**[142] with PLL dendritic derivatives have been reported.

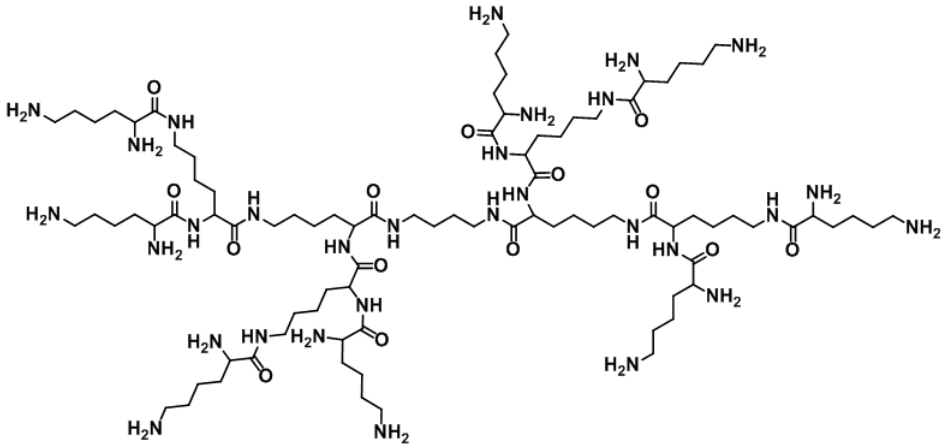

Figure C_2-34: Example of poly-(L)-lysine (PLL) dendrimer.

Other non-commercial polyamide dendrimers are currently used in nanomedicine such as **gallic acid-triethylene glycol** (**GATG**) **dendrons** that showed effective *in vitro* pDNA transfection.[143]

[141] M. Ohsaki, T. Okuda, A. Wada, T. Hirayama, T. Niidome,H. Aoyag, *In vitro* gene transfection using dendritic poly(l-lysine), *Bioconjugate Chem.*, **2002**, 13, 510-517.

[142] K.T. Al-Jamal, W.T. Al-Jamal, J.T.W. Wang, N. Rubio, J. Buddle, D. Gathercole, M. Zloh,K. Kostarelos, Cationic poly-l-lysine dendrimer complexes doxorubicin and delays tumor growth *in vitro* and *in vivo*, *ACS Nano*, **2013**, 7, 1905-1917.

[143] M. De la Fuente, M. Raviña, A. Sousa-Herves, J. Correa, R. Riguera, E. Fernandez-Megia, A. Sanchez, M.A. Alonso, Exploring the efficiency of gallic acid-based dendrimers and their block copolymers with PEG as gene carriers, *Nanomedicine,* **2012**, 7, 1667-1681.

[61] R.G. Denkewalter, *et al.* in US Pat. 4.360.646, **1979**.

Polycarbamate dendrimers (**figure C_2-35**) have also been developed. As the carbamate group can be quickly degraded when exposed to acidic pH or enzymes. Few examples of these dendrimers have been used in drug delivery. Among them, a self-immolative polycarbamate dendrimer could specifically release anticancer melphalan, doxorubicin and camptothecin drugs after being exposed to enzymes thus enhancing their drug activity.[144]

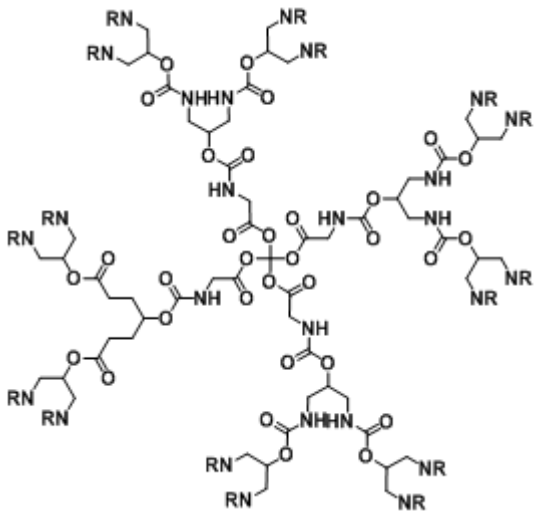

Figure C_2-35: Example of polycarbamate dendrimer.

[144] a) M. Grinda, J. Clarhaut, B. Renoux, I. Tranoy-Opalinski, S. Papo, A self-immolative dendritic glucuronide prodrug of doxorubicin, *Med. Chem. Commun.*, **2012**, 3, 68-70; b) A. Sagi, E. Segal, R. Satchi-Fainaro, D. Shabata, Remarkable drug-release enhancement with an elimination-based AB_3 self-immolative dendritic amplifier, *Bioorg. Med. Chem.*, **2007**, 15, 3720-3727.

2.3.2 - Most common dendrimers and dendritic derivatives based on oxygen functions

2.3.2.1 - *Bis*-MPA and other polyester dendrimers

Among polyester dendrimers, commercial **2,2-*bis*(hydroxymethyl) propionic acid (*bis*-MPA) dendrimers**, based on aliphatic ester groups with hydroxyl groups at the periphery, are the most widespread one (**figure C_2-36**).[145]

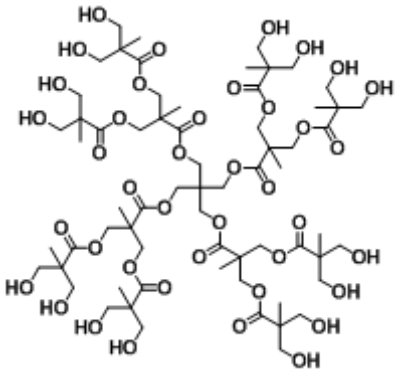

Figure C_2-36: 2,2-*bis*(hydroxymethyl)propionic acid (*bis*-MPA) dendrimers.

Since their first synthesis described by Hult's group in 1996,[146] the synthesis of *bis*-MPA dendrimers has progressed considerably. Indeed, nowadays three protected monomers are currently used to grow the dendrimer up to the 6th generation, carrying out versatile procedures that may be divergent, convergent or double exponential.[96,144-147] Moreover, new

[96] H. Ihre *et al.*, *J. Am. Chem. Soc.*, **2001**, 123, 5908.

[145] A. Carlmark, E. Malmström, M. Malkoch, Dendritic architectures based on *bis*-MPA: functional polymeric scaffolds for application-driven research, *Chem. Soc. Rev.*, **2013**, 42, 5858-5879.

[146] H. Ihre, A. Hult, E. Söderlind, Synthesis, characterization and ^{1}H NMR self-diffusion studies of dendritic aliphatic polyesters based on 2,2-*bis*(hydroxymethyl)propionic acid and 1,1,1-tris(hydroxyphenyl)ethane, *J. Am. Chem. Soc.*, **1996**, 118, 6388-6395.

[147] A.P. Goodwin, S.S. Lam, J.M.J. Fréchet, Rapid, efficient synthesis of heterobifunctional biodegradable dendrimers, *J. Am. Chem. Soc.*, **2007**, 129, 6994-6995.

esterification conditions that differ from the classical Steglich's esterification and anhydride coupling have also been described to grow the dendrimer up. For instance 1,1'-carbonyldiimidazole/cesium fluoride coupling has been employed to synthesize *bis*-MPA dendrimer up to the 6th generation. In this recent procedure, the imidazole moiety activates the carboxylic group of the *bis*-MPA monomer while the fluoride group activates the terminal OH groups of the dendrimer allowing high reaction yields (close to 90 %) and easier purifications processes.[148]

Bis-MPA dendrimers consist of a moderated lipophilic inner part surrounded by a hydrophilic shell that allows the **water solubility** of the whole structure. Moreover, they are highly **biocompatible** and can be easily **degraded**, by simple hydrolysis or by enzymatic activity, into small fragments that do not precipitate in water and are not cytotoxic. These properties make them really interesting for nanomedicine studies when compared to poly(imine) and poly(amidoamine) dendrimers.[149]

Therefore, a large variety of *bis*-MPA dendritic derivatives have been synthesized over the years. For instance, 3-arms and 4-arms *bis*-MPA hyperbranched polyesters, respectively based on *bis*-MPA or pentaerythritol ethoxylate, M_n 270,[150, 151] HLDBCs and HDLDBCs with PEG and Janus type dendrimers are commercially available.[149]

This type of dendritic structure has been widely studied in nanomedicine. *Bis*-MPA dendrimers and hyperbranched polymers have a **lipophilic core -**

[148] S. García-Gallego, D. Hult, J.V. Olsson, M. Malkoch, Fluoride-promoted esterification with imidazolide-activated compounds: a modular and sustainable approach to dendrimers, *Angew. Chem. Int. Ed.*, **2015**, 127, 2446-2449.

[149] N. Feliu, M.V. Walter, M.I. Montañez, A. Kunzmann, A. Hult, A. Nyström, M. Malkoch, B. Fadeel, Stability and biocompatibility of a library of polyester dendrimers in comparison to polyamidoamine dendrimers, *Biomaterials*, **2012**, 33, 1970-1981.

[150] www.polymerfactory.com

[151] www.sigmaaldrich.com

hydrophilic shell structure that may lead to "*unimolecular micelles*", and this makes them suitable derivatives for **drug delivery** purposes. Lipophilic drugs can be encapsulated within the internal voids of the dendritic macromolecules or can be covalently linked to them.[152]

The stability of these "*unimolecular micelles*" has been enhanced by PEGylation resulting in **HLDBC and HDLDBC derivatives**. For example, lipophilic paclitaxel,[153] as well as hydrophilic doxorubicin,[154] two anticancer drugs have been successfully encapsulated within these structures improving their physical properties. Moreover, pH sensitive HDLBCs have been synthesized to release doxorubicin after exposure to mildly acidic pH,[155] as well as light and thermo sensitive HLDBCs.[156]

Bis-MPA based **Janus dendrimers** have also been used as drug nanocarriers. For example, a series of Janus dendrimers functionalized in one of its two sides by aliphatic lipophilic chains have been studied. These dendrimers can self-assemble in water forming a large variety of nanostructures; the morphology of them depends on the balance between the size of

[152] O.L. Padilla de Jesús, H.R. Ihre, L. Gagne, J.M.J Fréchet, F.C. Szoka, Polyester dendritic systems for drug delivery applications: *in vitro* and *in vivo* evaluation, *Bioconjugate Chem.* **2002**, 13, 453-461.

[153] C. Kontoyianni, Z. Sideratou, T. Theodossiou, L.A. Tziveleka, D. Tsiourvas, C.M. Paleos, A novel micellar PEGylated hyperbranched polyester as a prospective drug delivery system for paclitaxel, *Macromol Biosci.*, **2008**, 8, 871-881.

[154] Z. Wu, X. Zeng, Y. Zhang, N. Feliu, P. Lundberg, B. Fadeel, M. Malkoch, A.M. Nyström, Linear-dendritic polymeric amphiphiles as carriers of doxorubicin - *In vitro* evaluation of biocompatibility and drug delivery, *J. Polym. Sci. Part A: Polym. Chem.*, **2012**, 50,217-226

[155] E.R. Gillies, J.M.J. Fréchet, pH-responsive copolymer assemblies for controlled release of doxorubicin, *Bioconjugate Chem.*, **2005**, 16, 361-368.

[156] a) J. del Barrio, L. Oriol, C. Sánchez, JL. Serrano, A. Di Cicco, P. Keller, M.H. Li, Self-assembly of linear-dendritic diblock copolymers: from nanofibers to polymersomes, *J. Am. Chem. Soc.*, **2010**, 132, 3762-3769; b) H. García-Juan, A. Nogales, E. Blasco, J.C. Martínez, I. Šics, T.A. Ezquerra, M. Piñol, L. Oriol, Self-assembly of thermo and light responsive amphiphilic linear dendritic block copolymers, *Eur. Polym. J.*, **2016**, 81, 621-633.

hydrophilic and the lipophilic dendrons (**figure C_2-37**).[157] Furthermore, they could encapsulate lipophilic plitidepsin anticancer drug, increasing its water solubility without altering its activity into various cancer cell lines. Other *bis*-MPA Janus dendrimers bearing doxorubicin in one side and polyethylene glycol chains in the other side has been synthesized. The bloodstream circulation of the drug was increased when compared to the free drug and a complete tumor regression was observed *in vivo*.[158]

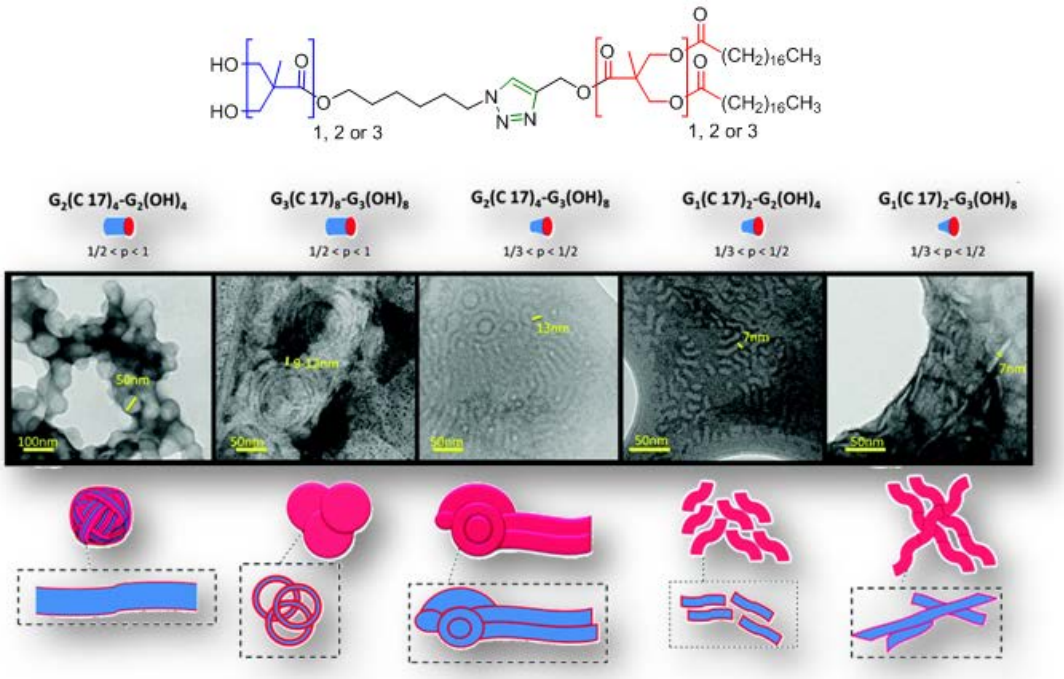

Figure C_2-37: Different morphologies formed by the amphiphilic Janus *bis*-MPA dendrimers observed in TEM, adapted from [157].

In **gene therapy**, *bis*-MPA dendritic derivatives have shown promising results but more investigation efforts are still required to achieve efficient gene transfection. Thus, biocompatible amino functionalized *bis*-MPA dendrimers with tetra ethylene glycol moieties showed good pDNA complexation ability but

[157] E. Fedeli, A. Lancelot, J.L. Serrano, P. Calvo, T. Sierra T, Self-assembling amphiphilic Janus dendrimers: mesomorphic properties and aggregation in water, *New J. Chem.*, **2015**, 39, 1960-1967.

[158] C.C. Lee, E.R. Gillies, M.E. Fox, S.J. Guillaudeu, J.M.J. Fréchet, E.E. Dy, F.C. Szoka, A single dose of doxorubicin-functionalized bow-tie dendrimer cures mice bearing C-26 colon carcinomas, *Proc. Natl. Acad. Sci. USA*, **2006**, 103, 16649–16654.

failed to transfect pDNA.[159] Self-assembling Janus *bis*-MPA dendrimers bearing spermine at the periphery were also synthesized for this purpose and were fully biocompatible and biodegradable. However, and as the previous materials, even showing good pDNA complexation efficiency, they failed to transfect it into the cells.[160] The main reason evoked by the authors was the difficulty of these materials to release the pDNA within the cells. The more promising derivatives are amine modified hyperbranched polymers. They were totally biocompatible and biodegradable and could transfect pDNA *in vitro*. However, the transfection efficiency remained low when compared to commercial agents.[161]

Other **polyester dendrimers** have been synthesized in order to be used as drug delivery systems for lipophilic and hydrophobic drugs. For example, polyglycerolsuccinic acid (PGLSA) dendrimers could encapsulate small lipophilic molecules like anticancer camptothecin while maintaining its activity.[162] Hydrophilic doxorubicin drug was encapsulated within polyester dendrimers based on 2,2-bis(acryloyloxymethyl)propionic acid and 1-thioglycerol monomers.[163]

[159] J. Movellan, R. González-Pastor, P. Martín-Duque, T. Sierra, J.M. de la Fuente, J.L. Serrano, New ionic *bis*-MPA and PAMAM dendrimers: a study of their biocompatibility and DNA-complexation, *Macromol. Biosci.*, **2015**, 15, 657-667.

[160] a) A. Barnard, P. Posocco, S. Pricl, M. Calderon, R. Haag, M.E. Hwang, V.W.T. Shum, D.W. Pack, D.K. Smith, Degradable self-assembling dendrons for gene delivery: experimental and theoretical insights into the barriers to cellular uptake, *J. Am. Chem. Soc.*, **2011**, 133, 20288-20300; b) G.M. Pavan, A. Danani, S. Pricl, D.K. Smith, Modeling the multivalent recognition between dendritic molecules and DNA: understanding how ligand "sacrifice" and screening can enhance binding, *J. Am. Chem. Soc.*, **2009**, 131, 9686-9694

[161] R. Reul, J. Nguyen, T. Kissel, Amine-modified hyperbranched polyesters as non-toxic, biodegradable gene delivery systems, *Biomaterials*, **2009**, 30, 5815-5824.

[162] M. T. Morgan, M.A. Carnahan, C.E. Immoos, A.A. Ribeiro , S. Finkelstein , S.J. Lee,M.W. Grinstaff, Dendritic molecular capsules for hydrophobic compounds, *J. Am. Chem. Soc.*, **2003**, 125, 15485-15489

[163] X. Ma, Z. Zhou,E. Jin, Q. Sun,B. Zhang, J. Tang, Y. Shen, Facile synthesis of polyester dendrimers as drug delivery carriers, *Macromolecules*, **2013**, 46, 37-42.

2.3.2.2- Polyether dendrimers

Commercial **polyglycerol** (PG) **dendrimers** and hyperbranched polymers are the most common polyether dendrimers used for nanomedicine applications.[164] They were first synthesized by Fréchet's group in 1998 (**figure C_2-38**).[165]

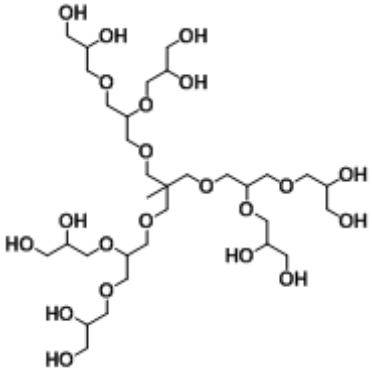

Figure C_2-38: Polyether (PG) dendrimers.

As they are highly biocompatible, PG dendrimers and hyperbranched polymers have been used in **drug delivery**. PG dendrimers that are composed of a lipophilic core surrounded by a hydrophilic shell are more suitable to encapsulate lipophilic drugs, such as paclitaxel,[166] whereas hyperbranched polymers, that present pending hydroxyl groups in their inner structure, are more adapted for hydrophilic drug encapsulation.[167]

This type of dendrimer has also been used in **gene therapy**. For example, amino-functionalized hyperbranched PG could complex pDNA and transfect it *in*

[164]M. Calderón, M.A. Quadir, S.K. Sharma, R. Haag, Dendritic polyglycerols for biomedical applications, *Adv. Mater.*, **2010**, 22, 190-218; b) www.nanopartica.com.

[165]M. Jayaraman, J.M.J. Fréchet, A convergent route to novel aliphatic polyether dendrimers, *J. Am. Chem. Soc.*, **1998**, 120, 12996-12997.

[166] T. Ooya, J. Lee, K. Park, Hydrotropic dendrimers of generation 4 and 5: synthesis, characterization and hydrotropic solubilization of paclitaxedl, *Biconjugate Chem.*, **2004**, 15, 1221-1229.

[167] A. Sunder, M. Krämer, R. Hanselmann, R. Mülhaupt, H. Frey, Molecular nanocapsules based on amphiphilic hyperbranched polycglycerols, *Angew. Chem. Int. Ed.*, **1999**, 38, 3552-3555.

vitro without showing any cytotoxicity,[168] and amphiphiles based on hydrophilic PG dendrons functionalized with amino moieties could self-assemble in water and deliver siRNA at a level similar to commercial agents.[169]

[168] Leto-Aikaterini Tziveleka, A.M.G. Psarra, D. Tsiourvas, C.M. Paleos, Synthesis and evaluation of functional hyperbranched polyether polyols as prospected gene carriers, *Int. J. Pharm.*, **2008**, 356, 314-324

[169] A. Tschiche, A.M. Staedtler, S. Malhotra, H. Bauer, C. Böttcher, S. Sharbati,M. Calderón, M. Koch,T.M. Zollner, A. Barnard, D.K. Smith, R. Einspanier, N. Schmidt, R. Haag, Polyglycerol-based amphiphilic dendrons as potential siRNA carriers for *in vivo* applications, *J. Mater. Chem. B*, **2014**, 2, 2153-2167.

2.3.2.3 - Other dendrimers used for nanomedicine

Phosphorus has been incorporated to various dendritic structures providing **phosphorus containing dendrimers** that are water soluble and biocompatible.[170] They have been used in drug delivery, for example enhancing the *in vivo* biodistribution of carteolol, a drug used to treat glaucoma.[171] Additionally, after functionalization with pyrrolidinium cationic group, they showed effective pDNA transfection *in vitro* although it showed less efficiency than lipofectamine®, a commercial agent.[172]

Organosilicon dendrimers, based on carbosilane (Si-C) and carbosiloxane (Si-O) have also been synthesized and studied for nanomedicine purposes as they are generally biocompatible and biodegradable.[173] For instance, anionic and cationic carbosilane dendrimers have been used in drug delivery associated with antiviral drugs or with ibuprofen.[174] For gene delivery purposes, carbosilane dendrimers have been able to deliver anti-HIV siRNA *in vivo* with high efficiency and low cytotoxicity.[175]

[170] A.M. Caminade, C.O. Turrin, J.P. Majoral, Biological properties of phosphorus dendrimers, *New. J. Chem.*, **2010**, 34, 1512-1524.

[171] G. Spataro, F. Malecaze, C.O. Turrin, V. Soler, C. Duhayon, P.P. Elena, J.P. Majoral, A.M. Caminade, Designing dendrimers for ocular drug delivery, *Eur. J. Med. Chem.*, **2010**, 45, 326-334.

[172] C. Padié, M. Maszewsk, K. Majchrzak, B. Nawrot, A.M. Caminade J.P. Majoral, Polycationic phosphorus dendrimers: synthesis, characterization, study of cytotoxicity, complexation of DNA, and transfection experiments, *New. J. Chem.*, **2009**, 33, 318-326.

[173] C. Kim, J.H. Hong, Carbosilane and carbosiloxane dendrimers, *Molecules*, **2009**, 14, 3719-3730.

[174] a) D. Sepúlveda-Crespo, J.L. Jiménez, R. Gómez, F.J. de la Mata, P.L. Majano, M.Á. Muñoz-Fernández, P. Gastaminza, Polyanionic carbosilane dendrimers prevent hepatitis C virus infection in cell culture, *Nanomedicine*, **2017**, 49-58; b) A.J. Perisé-Barrios, E. Fuentes-Paniagua, J. Sánchez-Nieves, M.J. Serramía, E. Alonso, R.M. Reguera, R. Gómez, F.J. de la Mata, M.Á. Muñoz-Fernandez, Improved efficiency of ibuprofen by cationic carbosilane dendritic conjugates, *Mol. Pharmaceutics*, **2016**, 13, 3427-3438.

[175] M.J. Serramía, S. Álvarez, E. Fuentes-Paniagua, M.I. Clemente, J. Sánchez-Nieves, R. Gómez, J.F. de la Mata, M.Á. Muñoz-Fernández, *In vivo* delivery of siRNA to the brain by carbosilane dendrimer, *J. Controll. Release*, **2015**, 200, 60-70.

Chapter 3:

Objectives and working plan

The main objective of this PhD fits within the main research lines of the Liquid Crystals and Polymers group of the University of Zaragoza:

Design, preparation and study of new dendritic systems for both, gene and drug delivery.

Among the numerous dendritic derivatives used for these nanomedical applications, the poly(amidoamine) dendrimers stands out as the most investigated and alluring materials; however, its biocompatibility and biodegradability issues are hampering its transfer to clinical therapeutic assays.[172] On the other hand, polyester dendritic systems based on 2,2'-*bis*(hydroxymethyl)propionic acid (*bis*-MPA) are fully biocompatible and biodegradable; nevertheless their use has not as widespread as this poly(amidoamines), principally because of their lowest efficiency, especially in gene transfection.[173] Poly(ester amide) dendritic derivatives might appeared as interesting materials combining the efficiency of poly(amidoamine) dendrimers with the biocompatibility of polyester dendrimers but their investigation remained essentially limited to linear polymers.[174]

[172] M. Labieniec-Watala, C. Watala, PAMAM dendrimers: destined for success or doomed to fail? Plain and modified PAMAM dendrimers in the context of biomedical applications, *J. Pharm. Sci.*, **2015**, 104,2-14

[173] S. García-Gallego, A.M. Nyström, M. Malkoch, Chemistry of multifunctional polymers based on *bis*-MPA and their cutting-edge applications, *Progr. Polym. Sci.*, **2015**, 48, 85-110.

[174] a) A. C. Fonseca, M. H. Girl, O. N. Simões, Biodegradable poly(ester amide)s – A remarkable opportunity for the biomedical area: Review on the synthesis, characterization and applications, *Prog. Polym. Sci.*, **2014**, 39, 1291-1311; b) D. Pahovnik, A. Čusak, S. Reven, E. Žagar, Synthesis of poly(ester-amide) dendrimers based on 2,2-*bis*(hydroxymethyl) propanoic acid and glycine, J. Polym. Sci. Part A: Polym. Chem., **2014**, 52, 3292-3301; c) X. Li,X.Lu, Y. Lin, J. Zhan, Y. Li, Z. liu, X. Chen, S. Liu, Syntheis and charachterization of hyperbrnached poly(ester-amide)s from commercially available dicarboxylicacids and multihydroxyl primary amines, *Macromolecules*, **2006**, 39, 7889-7899.

Taking in account the previous works developed in our group, we decided to use two dendron architectures based on 2,2'-*bis*(hydroxymethyl)propionic acid (*bis*-MPA) modified with glycine moieties (**figure C_3-1**):

- In the first case, the glycine moieties were added at the **periphery** of the dendron in order to obtain **amino-terminated *bis*-MPA polyester dendrons**. This dendron structure has been previously studied in our group.

- In the second case, the glycine moieties were added at both, the **periphery and the internal branches** of the dendrons in order to obtain a **new type of poly(ester amide) dendrons** based on 2,2'-*bis*(glyciloxymethyl)propionic acid (*bis*-GMPA).

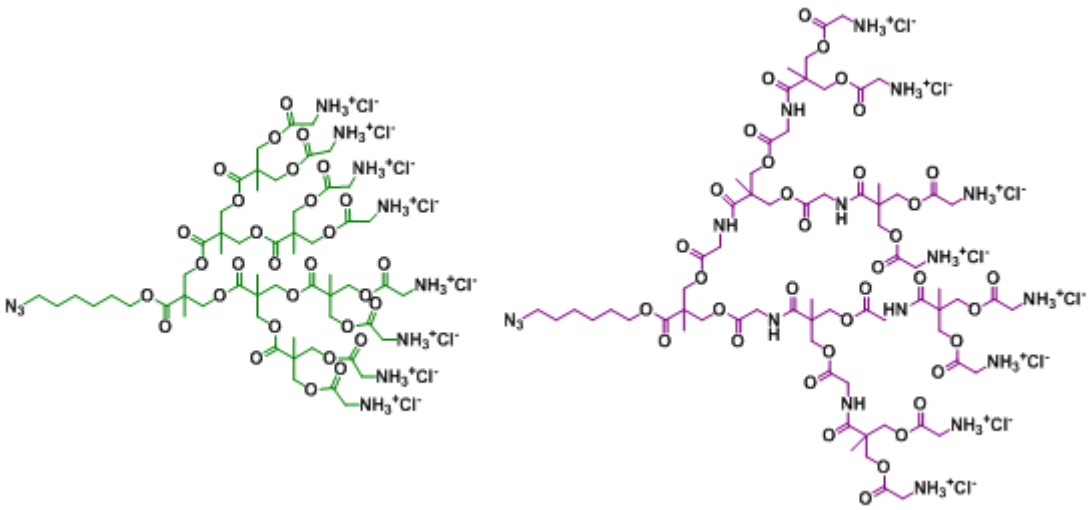

Figure C_3-1: amino-terminated *bis*-MPA polyester dendron of 3rd generation (left) and amino-terminated *bis*-GMPA poly(ester amide) dendron of 2nd generation (right) with an azide group at the focal point.

The insertion of internal amide groups in *the bis*-GMPA architecture would increase its hydrophilic character and might induce the formation of favorable hydrogen bonds among dendrons and/or with small guest molecules, such as drugs.

Using these two dendron structures, we have designed four types of dendritic derivative. In all cases, the possibility of playing with the amphiphilic nature of the compounds has been considered (**figure C_3-2**).

(A) Janus dendrimers:

which are composed in one of the two hydrophilic dendrons mentioned and a lipophilic dendron derived from *bis*-MPA functionalized with terminal stearic acids.

(B) Hybrid dendritic-linear-dendritic block copolymers (HDLDBCs):

which are formed by a commercial amphiphilic linear triblock copolymer based on polyethylene oxide - polypropylene oxide - polyethylene oxide (PEO-PPO-PEO), commercialized under the name, Pluronic® F-127, modified in its terminal positions by the two hydrophilic dendron moieties.

(C) Dendronized hyperbranched polymers (DHPs):

which are composed by a central core derived from commercial bis-MPA hyperbranched polyesters grafted with peripheral amino-terminated *bis*-MPA dendrons.

(D) bis-GMPA dendrimers:

Due to the novelty of the bis-GMPA dendrons, two dendrimers based on these structures have been synthesized by a convergent method using tripropargyl amine as a central core.

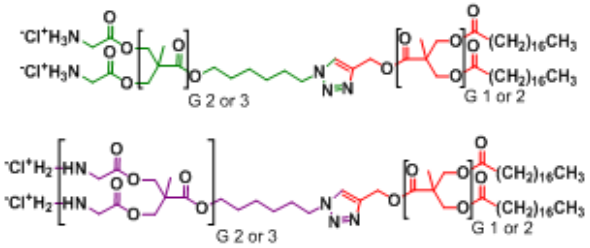

Amphiphilic Janus dendrimers

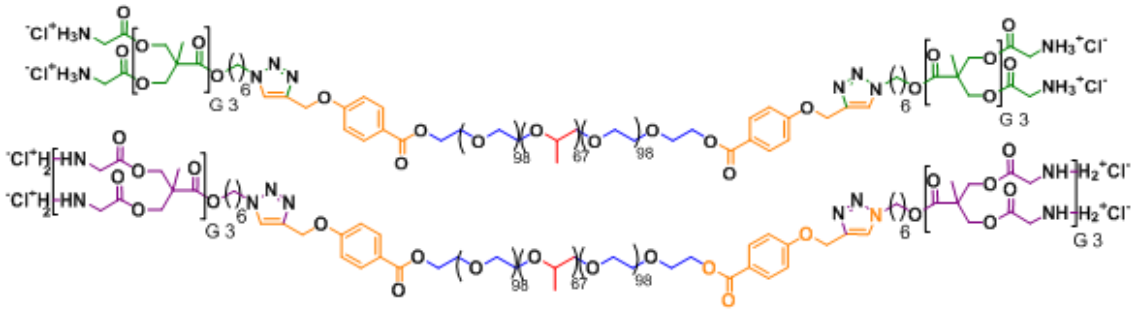

Hybrid dendritic-lineal-dendritic block copolymers (HDLDBCs)

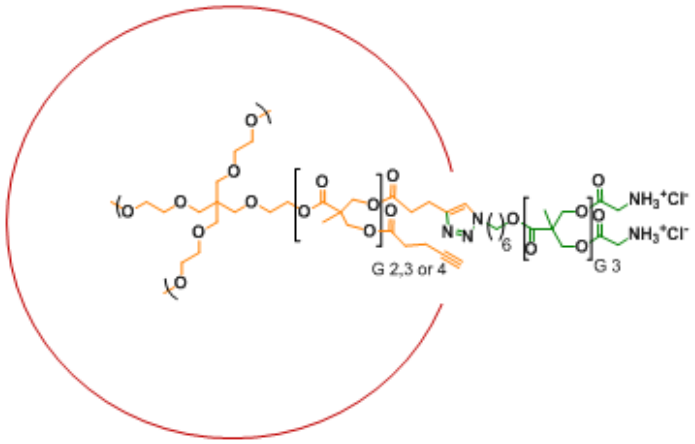

***Bis*-MPA dendronized hyperbranched polymers (DHPs)**

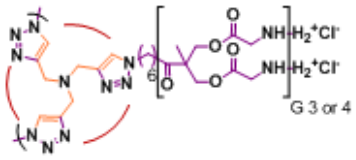

***Bis*-GMPA dendrimers**

Figure C_3-2: Chemical structures of the dendritic systems designed.

Using these four dendritic systems, we have planned the following specific objectives for this work:

(I) Study of the abilities of the amphiphilic Janus dendrimers and the HDLDBCs to transport and deliver **camptothecin for anti-Hepatitis C therapy**.

This work was carried out in collaboration with Dr. Olga Abián of the Biocomputation and Physics of Complex Systems (BIFI).

(II) Study of the potential of the globular *bis*-MPA DHPs and the *bis*-GMPA dendrimers to **transfect siRNA and pDNA**.

This work was carried out in collaboration with Dr. María Pilar Martín-Duque of the Center for Biomedical research of Aragon (CIBA).

(III) Study of the potential of the *bis*-MPA and *bis*-GMPA HDLDBCs and *bis*-MPA DHPs to promote **drug targeting of antimalarial drugs**.

This work was carried out in collaboration with Dr. Xavier Fernàndez-Busquets of the Barcelona Institute for Global Health (ISGlobal) and the Institute for Bioengineering of Catalonia (IBEC).

In order to reach these objectives, some secondary objectives have been necessary and are herein detailed.

Objective (I):

(i) Synthesis and chemical characterization of the amphiphilic derivatives based on the Janus dendrimers and the HDLDBCs.

(ii) Study of the self-assembly in water of these amphiphilic dendritic derivatives and of the size and morphology of the aggregates. Moreover, as Pluronic® F-127 has a lower critical solution temperature (LCST) in water, the size of its aggregates will be studied at different temperatures.

(iii) Encapsulation of camptothecin, CPT, used as anti-hepatitis C drug, into the aggregates formed by the amphiphilic Janus dendrimers and the HDLDBCs and its influence on the size and morphology of the aggregates.

(iv) Evaluation of the activity against the hepatitis-C virus replication and the cytotoxicity of the dendritic derivatives and dendritic nanocarrier/CPT conjugates with respect to the free drug.

(v) Synthesis of a low-water soluble dendritic fluorophore based on the commercial rhodamine B in order to label the aggregates formed by the amphiphilic dendritic derivatives and study their cellular uptake.

(vi) Encapsulation of this low-water soluble fluorophore, together with camptothecin, within the Janus dendrimers and the study of its influence on the morphology, size and drug activity.

Objective (II):

(i) Synthesis and chemical characterization of the *bis*-GMPA dendrimers and the *bis*-MPA dendronized hyperbranched polymers (DHPs).

(ii) Study of their acid-base properties and their aggregation in water.

(iii) Formation of dendriplexes by electrostatic interactions with pDNA and siRNA by the *bis*-GMPA dendrimers and the *bis*-MPA DHPs, as well as study of their morphology, size and net charge.

(xiv) *In vitro* pDNA and siRNA transfection experiments with these derivatives into cancerous and healthy cells.

Objective (III):

(i) Synthesis of the lipophilic base forms of chloroquine, primaquine and quinacrine, three antimalarial drugs from their commercial hydrophilic salt forms.

(ii) Encapsulation of these drugs in their hydrophilic and lipophilic forms within the DHPs and the HDLDBCs.

(iii) Formation of complexes by electrostatic interactions with the *bis*-MPA DHPs and heparin, a polysaccharide that favors the targeting of drug nanocarriers to the parasite infected red blood cells. The formation of the complexes will be study with the DHPs and with the DHP/antimalarial drug conjugates. Their morphology and size of will be studied.

(iv) Labeling of the DHP and HDLDBC with fluorofores based on the commercial rhodamine B in order to study their targeting abilities to the parasite infected red blood cells.

(v) Study of the antimalarial activity of the dendritic nanocarrier/drug conjugates and the dendritic nanocarrier/heparin/drug conjugates with respect with the free drugs.

CHAPTER 4:

Amphiphilic *bis*-MPA and *bis*-GMPA dendritic derivatives for camptothecin delivery

In this chapter, new amphiphilic Janus dendrimers and hybrid dendritic-linear-dendritic block copolymers (HDLDBCs) based on 2,2-*bis*(hydroxymethyl) propionic acid (*bis*-MPA) and 2,2-*bis*(glyciloxymethyl)propionic acid (*bis*-GMPA) are described as nanocarriers to deliver camptothecin as an anti-hepatitis C virus drug.

First, the synthesis and characterization of the dendrons of *bis*-MPA and *bis*-GMPA used to build the dendritic systems as well as their biocompatibility and degradability are described. Second, the synthesis, characterization and self-assembly in water of the amphiphilic Janus dendrimers and the HDLDBCs are studied. Finally, their ability to deliver camptothecin and increase its biological properties so as to decrease the replication of the hepatitis C virus in infected hepatic cells is discussed.

4.1- *Bis*-MPA and *bis*-GMPA dendrons

This first part describes the synthesis, chemical characterization and the properties of dendrons based on 2,2'-*bis*(hydroxymethyl)propionic acid (*bis*-MPA) and 2,2'-*bis*(glyciloxymethyl)propionic acid (*bis*-GMPA) that will be further used to build dendritic derivatives.

On the one hand, polyester *bis*-MPA dendrons are functionalized at their periphery with terminal glycine moieties in order to enhance their cellular internalization[160a] and their abilities to transport both, drugs[179] and genetic material.[180] On the other hand, these dendrons are functionalized at their periphery with lipophilic alkyl chains in order to trigger the self-assembly in aqueous media of amphiphilic dendritic derivatives. The former has an azide group at their focal point while the letter has an alkyne group to allow their coupling by means of a copper(I) azide-alkyne cycloaddition (CuAAC) reaction. As the synthesis and the biological properties of these dendrons have been extensively described in two previous thesis reports of the group[181,182] and three papers[95,157,159], they will be herein briefly commented.

[95] J. Movellan, P. Urbán *et al.*, *Biomacromolecules,* **2014**, 35, 7940.
[157] E. Fedeli *et al.*, *New. J. Chem.,* **2015**, 39, 1960.
[159] J. Movellan *et al.*, *Macromol. Biosci.*, **2015**, 15, 657.
[160a] A. Barnard *et al.*, *J. Am. Chem. Soc.,* **2011**, 133, 20288-20300.
[179] S. Tarvirdipour, E. Vasheghani-Farahani, M. Soleimani, H. Bardaniac, Functionalized magnetic dextran-spermine nanocarriers for targeted delivery of doxorubicin to breast cancer cells, *Int. J. Pharm.*, **2016**, 501, 331-341.
[180] S. Malhotra, H. Bauer, A. Tschiche, A.M. Staedtler, A. Mohr, M. Calderón, V.S. Parmar, L. Hoeke, S. Sharbati, R. Einspanier, R. Haag, Glycine-Terminated Dendritic Amphiphiles for Nonviral Gene Delivery., Biomacromolecules, **2012**, 13, 3087-98.
[181] J. Movellan, Dendritic derivatives as building blocks for biomedical applications, **2013**, Universidad de Zaragoza.

As part of the objectives of the work of this thesis, a new type poly(esteramide) dendrons has been prepared. They are based on 2,2'-*bis*(glyciloxymethyl)propionic acid and contain internal and peripheral glycine moieties. Additionally, these dendrons have an azide group at their focal point so that they can be coupled with complementary moieties by CuAAC reactions. The synthesis, chemical characterization, biocompatibility and degradability of the new *bis*-GMPA dendrons are fully described.

The CuAAC "click chemistry" was performed with the *bis*-MPA and *bis*-GMPA dendrons bearing terminal *t*-Boc protected amino groups in order to avoid the unfavorable complexation of the copper catalyst by the amino-terminated dendrons, since this might reduce the reaction conversion. Hence, each "click chemistry" coupling was always followed by the deprotection of the terminal amino groups in acidic conditions in order to obtain the final dendritic derivatives.

[182] E. Fedeli, Self-assembly of dendrimeric derivatives: possible vectors for drug delivery, **2013**, Universidad de Zaragoza.

4.1.1- *Bis*-MPA dendrons

4.1.1.1- *t*-Boc protected amino terminated *bis*-MPA dendrons

2,2'-*bis*(hydroxymethyl)propionic acid (*bis*-MPA) dendron derivatives bearing peripheral *t*-Boc protected amino groups and an azide group at the focal point were synthesized up to the 3rd generation following a divergent pathway first described by our group in 2014.[95]

First of all, the **ketal-protected *bis*-MPA monomer** was synthesized in one step during which the two terminal hydroxyl groups were protected with a ketal group (**figure C_4-1**). For this purpose, commercial *bis*-MPA reacted with 2,2-dimethoxypropane, in the presence of *p*-toluenesulfonic acid as catalyst, in dry acetone. The final product was purified by several washings with aqueous solutions yielding 69 % of the pure protected *bis*-MPA monomer.

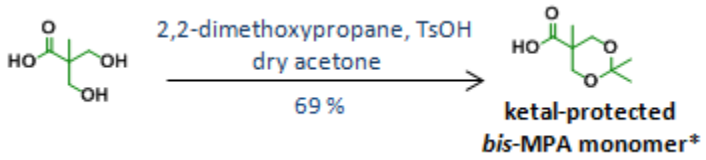

Figure C_4-1: Synthesis of ketal-protected *bis*-MPA monomer*.

In order to perform the subsequent copper(I) catalyzed azide-alkyne cycloaddition with the dendron derivatives, the **focal point** of the pre-hydrophilic dendrons derivatives was functionalized with a **hexan-1-azide** chain (**figure C_{IV}-2-A**). For that purpose, 6-chloro-hexan-1-ol reacted with sodium azide in dimethylformamide at 100ºC. The azide group, according to a nucleophile substitution of type II, replaced the chlorine atom of the alkyl chain and 6-azidehexan-1-ol chain was obtained.

[95] J. Movellan, P. Urbán *et al.*, *Biomacromolecules,* **2014**, 35, 7940.

Then, 6-azidehexan-1-ol chain reacted with the ketal-protected *bis*-MPA monomer in dry dichloromethane according to a Steglich's esterification procedure (**figure C_4-2-A**, general procedure I).

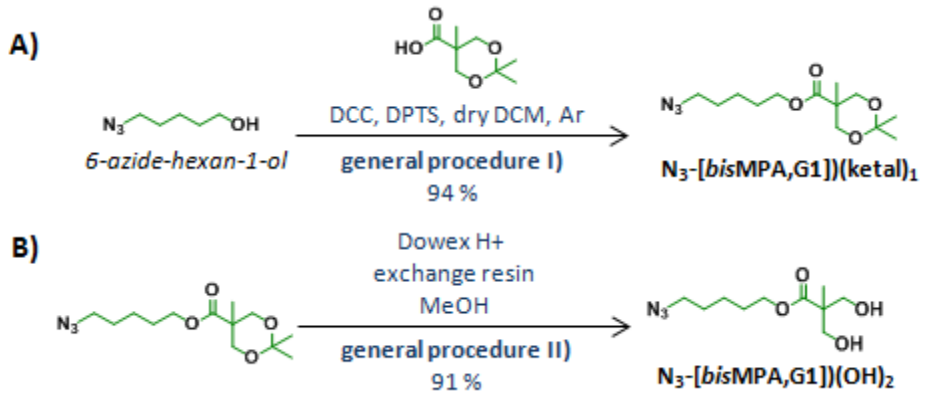

Figure C_4-2 : A) general procedure I): esterification reaction for growing up the *bis*-MPA dendron derivatives and **B**) general procedure II): deprotection of the terminal hydroxyl groups. See chapter 7 for the description of the general procedures.

DCC (dicyclohexylcarbodiimide) acts as a coupling agent and is consumed during the reaction forming dicyclohexylcarbodiurea (DCU) while DPTS (4-(dimethylamino)pyridium 4-toluenesulfonate) acts as a catalyst and is regenerated after the esterification. After completion of the reaction, DCU was removed by filtration and by precipitation in hexanes. Then, the crude product was purified by flash chromatography on silica gel to obtain the pure dendron, named as **N_3-[*bis*MPA,G1]-(ketal)$_1$**.

The deprotection of the terminal hydroxyl groups was carried out by hydrolysis of the ketal using a Dowex® proton exchange resin in methanol (**figure C_4-2-B**, general procedure II). This resin allowed the hydrolysis of the terminal ketal protective groups of the dendron without reacting with their internal ester groups. After completion of the reaction, the resin was easily removed by filtration and any other purification was required to obtain pure **N_3-[*bis*MPA,G1]-(OH)$_2$**.

Following an iterative procedure that used the reaction sequence explained above, *bis*-MPA dendron derivatives bearing an azide group at the

focal point were synthesized up to the 3rd generation. Both, esterification couplings and the ketal deprotections gave high conversion yields even for the highest generation (up to 75 %). Finally, the dendrons of 2nd and 3rd generation reacted with *N*-(*tert*-butoxycarbonyl)glycine (*t*-Boc-glycine) using the Steglich's esterification protocol to obtain *t*-Boc amino protected *bis*-MPA dendrons of 2nd and 3rd generation bearing 4 and 8 *t*-Boc-glycine moieties at their periphery, respectively (**figure C_4-3**, general procedure III). These dendrons were named as **N_3-[*bis*MPA,G2]-$(NHBoc)_4$** and **N_3-[*bis*MPA,G3]-$(NHBoc)_8$**, and were obtained with 19 % and 20 % global yields for the 2nd and 3rd generation, respectively.

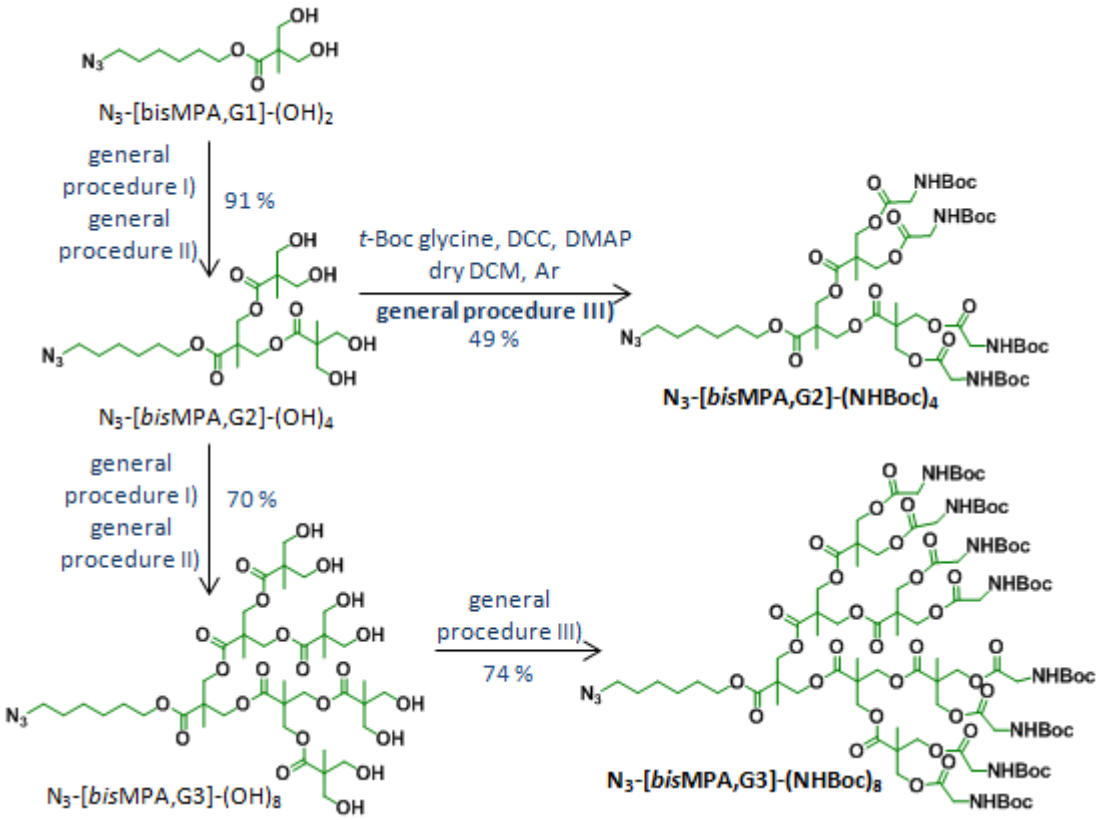

Figure C_4-3: Synthesis of *t*-Boc amino protected *bis*-MPA dendrons of 2nd and 3rd generation bearing the 6-azidehexyloxy chain at their focal point. See chapter 7 for the description of the general procedures.

All the final dendrons and intermediates were characterized by ^1H and ^{13}C nuclear magnetic resonance (NMR), mass spectrometry (MS), Fourier transformed infrared spectroscopy (FTIR) and elemental analysis (EA). Size

exclusion chromatography (SEC) was carried out only for the final *t*-Boc protected amino dendrons (**figure C_4-4**). The complete characterization data are gathered in the chapter 7.

The correct insertion of the terminal *t*-Boc glycine moieties at the periphery of the dendrons was asserted by the presence of two peaks in the ^{1}H NMR spectrum at 1.43 and 3.88 ppm corresponding to the methyl protons of the *t*-Boc protective group (*H-23*) and the methylene protons of the glycine moiety (*H-20*), respectively. Additionally, a broad signal is observed at 5.29 ppm, which corresponds to the protons attached to the nitrogen atom. In the ^{13}C NMR spectrum, the presence of peaks at 28.3, 42.2, 79.8, 155.8 and 170.0 ppm also confirms the correct functionalization of the dendron. Besides, a triplet at 3.27 ppm and a peak at 51.1 ppm corresponding to the methylene protons in the α-position of the azide group (*H-1* and *C-1*) are observed in the ^{1}H and ^{13}C NMR spectra.

Moreover, the presence of the glycine moieties is observed in the FTIR spectra in which a band at 3383 cm^{-1} corresponding to the N-H stretching and another band at 1717 cm^{-1} corresponding to the N-C=O stretching can be seen. Also, a band at 2102 cm^{-1} that corresponded to the azide group is also observed.

In MS and SEC, only one peak is observed for each dendron confirming the monodispersity and the perfect functionalization of the terminal groups of the *bis*-MPA dendrons.

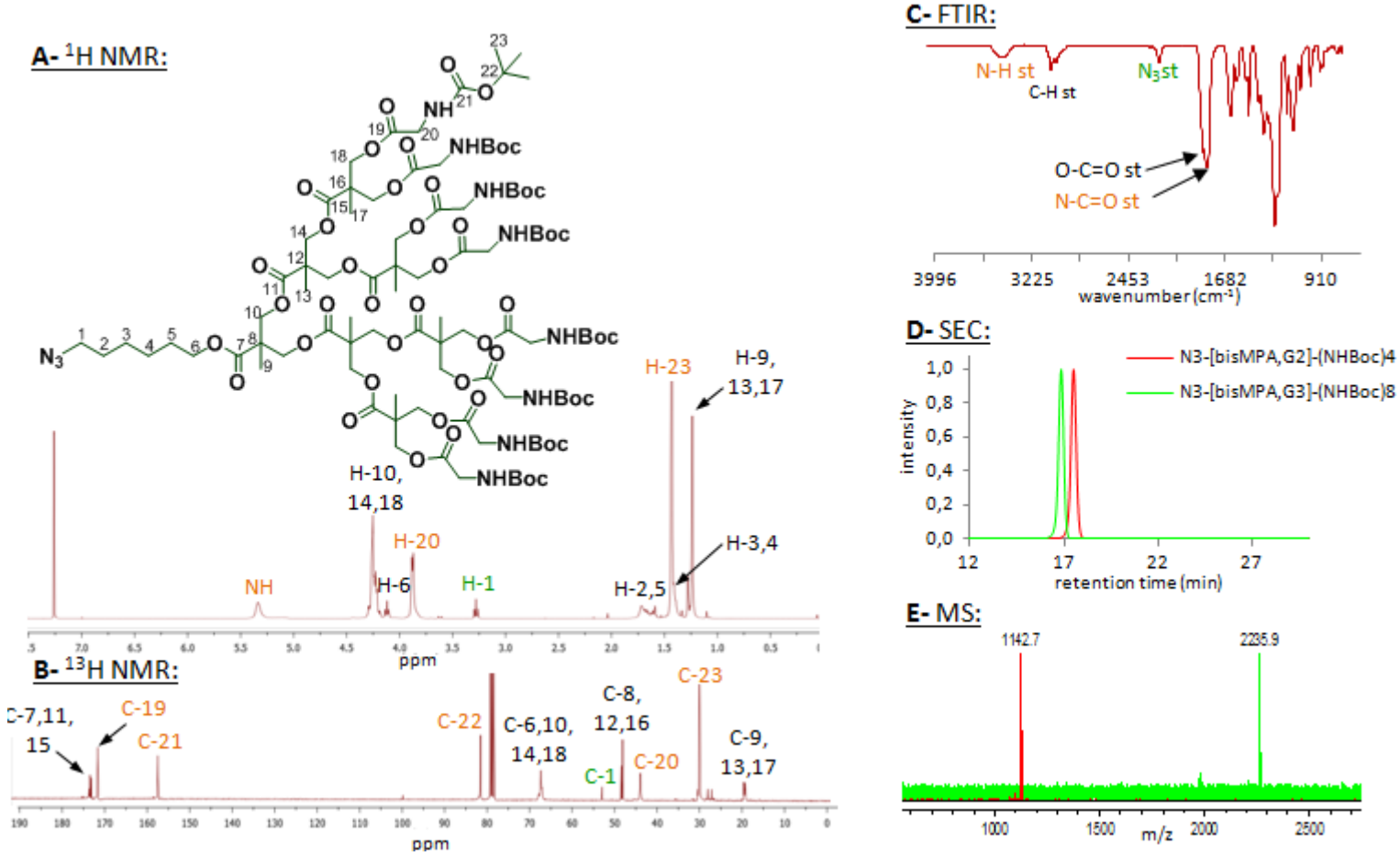

Figure C_4-4: Chemical characterization of **N_3-[*bis*MPA,G3](NHBoc)$_8$**: ^{1}H NMR (**A**) and ^{13}C (**B**) recorded in $CDCl_3$ at 400 MHz and 75 MHz respectively, FTIR (**C**), SEC (**D**) and MS (**E**). The signals corresponding to the t-Boc glycine are colored in orange and the ones characteristics of the azidomethylene group are colored in green.

4.1.1.2- Lipophilic *bis*-MPA dendrons

Lipophilic *bis*-MPA dendrons with terminal aliphatic linear chains of seventeen carbons (C17) and a propargyl group at the focal point were synthesized up to the 2nd generation. As the previous *bis*-MPA dendrons, the synthesis followed a divergent pathway that had been first described by our group in 2015 (**figure C_4-5**).[157]

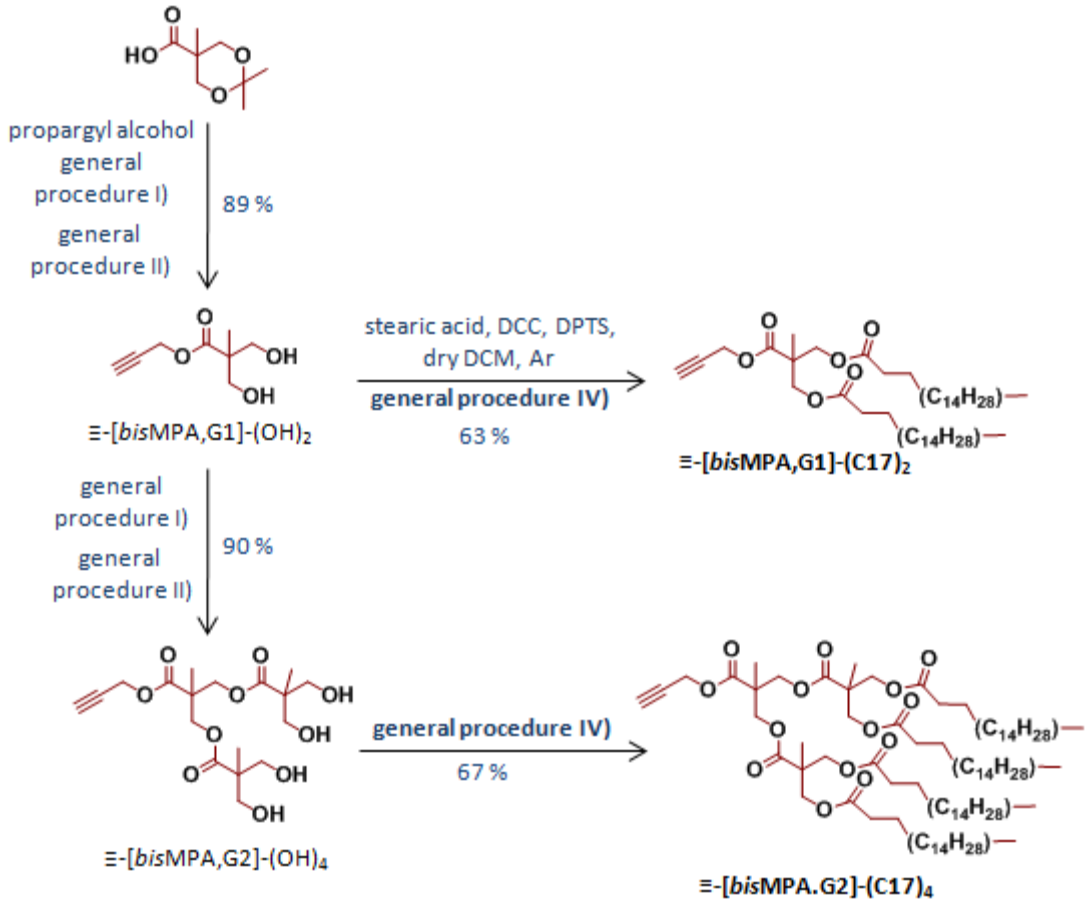

Figure C_4-5: Synthesis of the lipophilic dendron of *bis*-MPA of 1st and 2nd generation with C17 aliphatic linear chains at the periphery and a propargyl group at the focal point. See chapter 7 for the description of the general procedures.

The propargyl group was inserted at the focal point of the ketal-protected *bis*-MPA monomer by means of a Steglich's esterification. The protecting group was removed using the method described before yielding the *bis*-MPA dendron of 1st generation bearing an alkyne group at its focal point,

[157] E. Fedeli *et al.*, *New. J. Chem.*, **2015**, 39, 1960.

≡-[*bis*MPA,G1]-$(OH)_2$. This dendron was grown up in order to obtain the dendron of 2nd generation, **≡-[*bis*MPA,G2]-$(OH)_4$**. Finally, the peripheral hydroxyl groups of the dendrons of the 1st and 2nd generation reacted with stearic acid using the Steglich's esterification conditions (**figure C_4-5**, general procedure IV). Thus, two lipophilic *bis*-MPA dendrons of 1st and 2nd generation were obtained with an alkyne group at their focal point and 2 and 4 terminal aliphatic chains with global yields of 39 % and 37 %, respectively. These dendrons were named as **≡-[*bis*MPA,G1]-$(C17)_2$** and **≡-[*bis*MPA,G2]-$(C17)_4$**.

All the final dendrons and intermediates were characterized by ^1H and ^{13}C nuclear magnetic resonance (NMR), mass spectrometry (MS), Fourier transform infrared spectroscopy (FTIR) and elemental analysis (EA). Size exclusion chromatography (SEC) was carried out only for the final dendrons (**figure C_4-6,** see chapter 7 for the complete chemical characterization of the derivatives).

The correct insertion of the alkyl chains at the periphery of the dendrons was asserted by the apparition of four peaks in the ^1H NMR spectrum at 0.88, 1.25, 1.58 and 2.29 ppm corresponding to the methyl proton (*H-16*) and the methylene protons (*H-15*, *H-14* and *H-13*) respectively. In the ^{13}C NMR spectrum, the presence of the chains was confirmed by the apparition of various peaks at 14.1, between 17.8 and 34.0 and at 173.1 ppm.

In MS, the molecular peak more sodium can be observed for the two dendrons. Some low intense peaks are observed in the spectra although they do not correspond to dendrons with uncomplete functionalization. In SEC, only a monomodal peak is observed attesting the perfect functionalization of the dendrons.

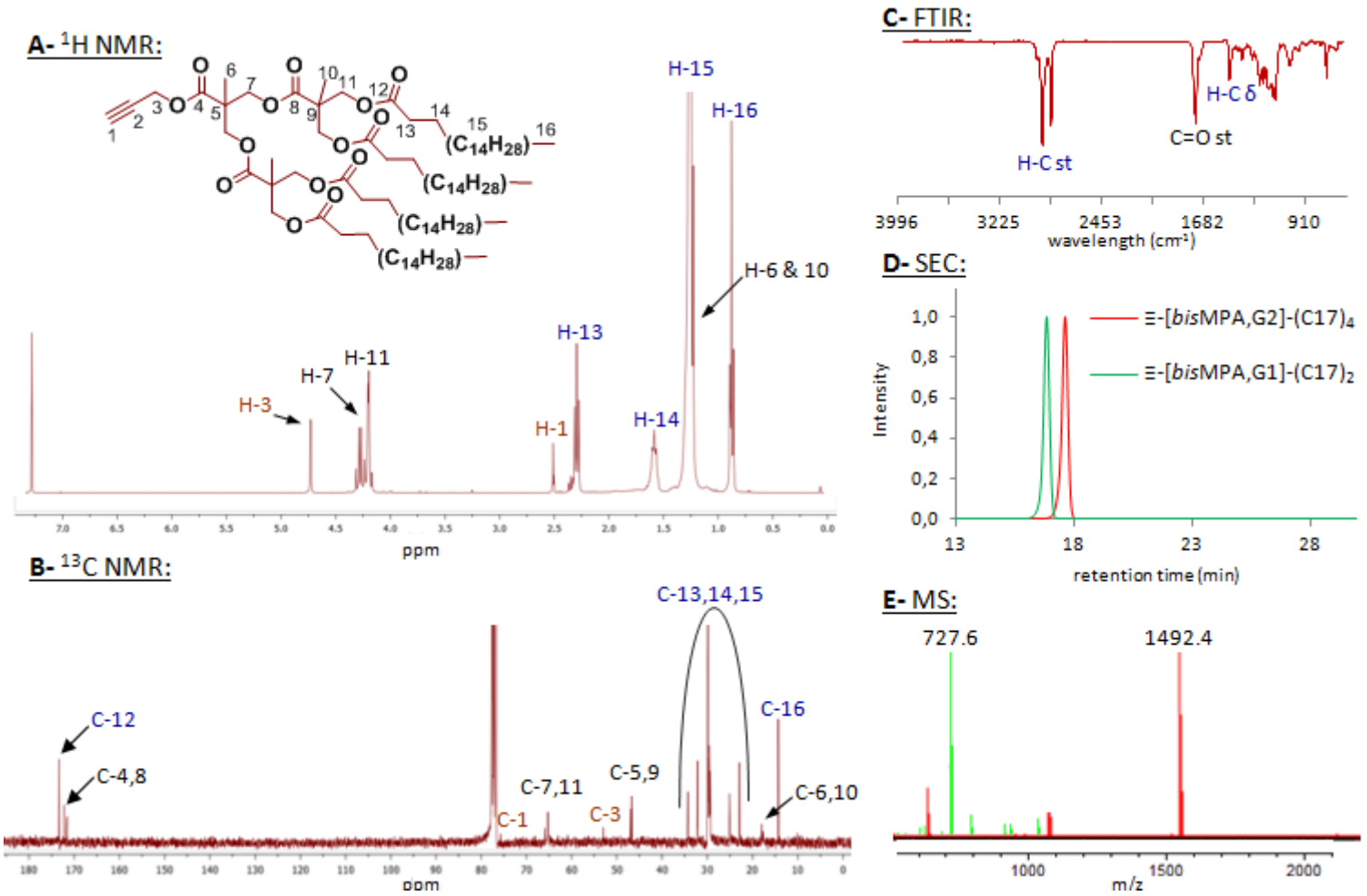

Figure C_4-6: Chemical characterization of **≡-[*bis*MPA,G2]-$(C17)_4$**: ^{1}H NMR (**A**) and ^{13}C (**B**) recorded in $CDCl_3$ at 400 MHz and 75 MHz respectively, FTIR (**C**), SEC (**D**) and MS (**E**). The signals corresponding to the alkyl chains are colored in blue and the ones of the proprargyl moiety are colored in brown.

Additionally, a triplet at 2.50 and a doublet at 4.72 ppm corresponding to the protons of the propargyl moiety (*H-1* and *H-3* respectively) are observed in the ^{1}H NMR spectrum. Likewise, the peaks corresponding to their relative carbons are observed at 75.4 and 52.8 ppm respectively in the ^{13}C NRM spectra.

Due to their low intensity, the bands corresponding to the stretching of the alkyne groups (H-C≡ and C≡C) are not visible in the dendron spectra after the functionalization with the terminal alkyl chains.

4.1.2- *bis*-GMPA dendrons

New hydrophilic *bis*-(glyciloxymethyl)propionic acid (*bis*-GMPA) dendrons with the 6-azidehexyloxy group at the focal point were synthesized up to the 4th generation. They were synthesized according to an original divergent synthesis.

***t*-Boc amino-protected *bis*-GMPA monomer** was synthesized in three steps starting from commercial *bis*-MPA (**figure C_4-7**). First of all, the acid moiety of the *bis*-MPA was protected with a benzyl group. Then, its terminal hydroxyl groups reacted with *t*-Boc protected glycine according to the Steglich's esterification conditions. Finally, the benzyl protecting group was removed by hydrogenation in the presence of Pd/C as catalyst obtaining the *t*-Boc protected *bis*-GMPA monomer with a global yield of 59 %. The terminal amines of the *bis*-GMPA monomer were protected with *t*-Boc groups to avoid side reactions during the dendron growing up reactions. This protecting group can be easily removed in acidic conditions.

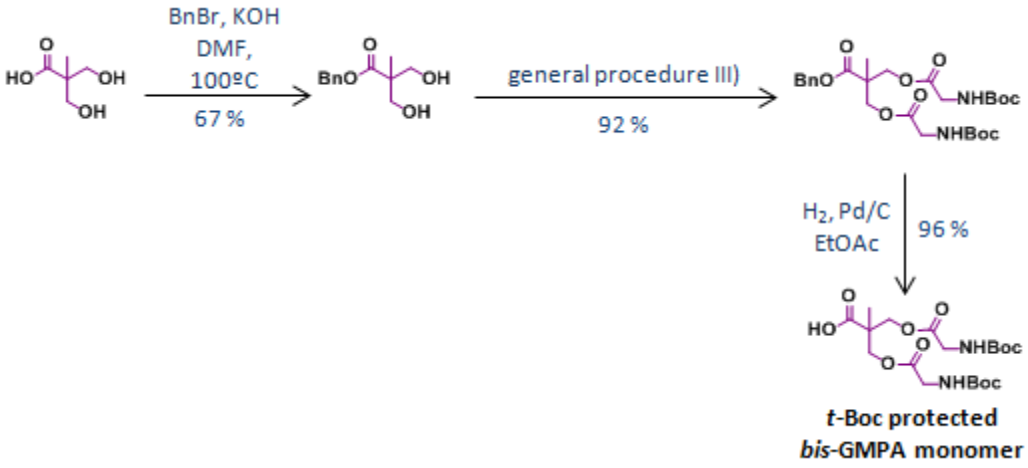

Figure C_4-7: synthesis of the *t*-Boc protected *bis*-GMPA monomer.

The synthesis of the *bis*-GMPA dendrons with an azide group at the focal point started from the *bis*-MPA dendron of 1st generation, **N_3-[*bis*MPA,G1]-$(OH)_2$** (**figure C_4-2**) that reacted with *t*-Boc glycine in order to obtain the new *bis*-GMPA dendron with *t*-Boc terminal amino groups. The protecting groups were removed in acidic conditions in ethyl acetate giving rise to the *bis*-GMPA

dendron of 1st generation with terminal ammonium groups, **N_3-[*bis*GMPA]($NH_3^+Cl^-$)$_2$** with 30% overall yield (**figure C_4-8**).

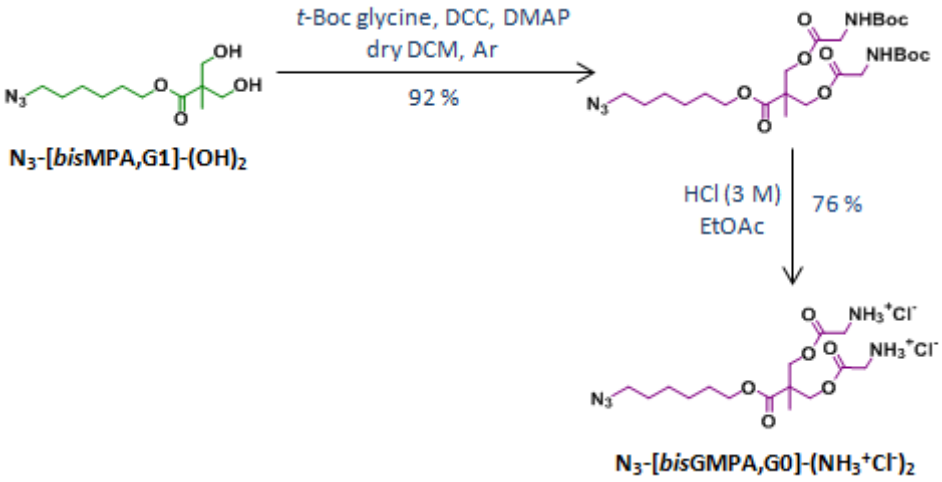

Figure C_4-8: Synthesis of the1st generation *bis*-GMPA dendron.

Bis-GMPA dendrons of 2nd to 4th generation were prepared by subsequent amide couplings (**figure C_4-9-A,** general procedure V).

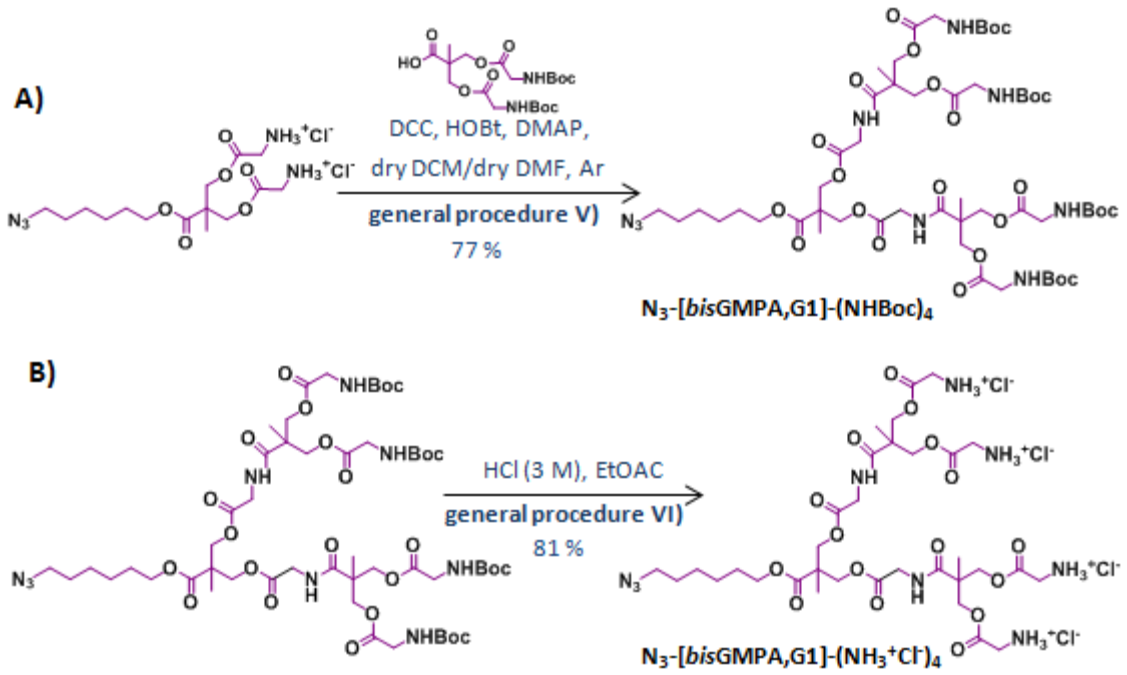

Figure C_{IV}-9: A) general procedure V): generation growing up by amide coupling reaction with the *t*-boc protected *bis*-GMPA monomer and **B**) general procedure VI): deprotection of the terminal amino groups. See chapter 7 for the description of the general procedures.

The reaction conditions were similar to the Steglich's esterification previously described. The *t*-boc-protected *bis*-GMPA monomer was allowed to react with the terminal ammonium groups of dendron **N_3-[*bis*GMPA,G1] $(NH_3^+Cl^-)_2$** in the presence of dicyclohexylcarbodiimide (DCC), 1-hydroxybenzotriazole hydrate (HOBt) and 4-(dimethylamino)pyridine (DMAP), according to a protocol adapted from Fernández-Megía *et al.*[183] DCC and HOBt act as coupling agents whereas DMAP plays a double role: first, it neutralizes the acidic ammonium salts of the dendrons and second, it activates the *bis*-GMPA monomer. The reaction was performed in a mixture of dry dichloromethane and dry dimethylformamide to allow the dissolution of all the reagents. After completion of the reaction, DCU and HOBt precipitates were removed by a primary filtration and by a subsequent precipitation in a mixture of hexanes and ethyl acetate. The crude product was finally purified by flash chromatography on silica gel. The growing up amide couplings showed yields between 43 and 61 %. N,N'-carbonyldiimidazole (CDI) and N-hydroxysuccinimide (NHS) were tested as coupling agents instead of DCC but showed lower reaction yields.

The deprotection of the terminal amino groups was carried out in acidic conditions. The protected dendrimer was dissolved in ethyl acetate in the presence of hydrochloric acid (3 M) (**figure C_4-9-B,** general procedure VI). After the removal of the *t*-Boc protecting groups, the terminal amino groups reacted with hydrochloride acid to form the ammonium salt that precipitated in ethyl acetate. The precipitation not only favors the purification of the compounds, but also protects the internal amide and ester groups of the dendron from acidic hydrolysis. The deprotection of the terminal amines gave yields between 89 and 98 %.

[183] E. Fernández-Megía, J. Correa, I. Rodríguez-Meizoso, R. Riguera, A click approach to unprotected glycodendrimers, *Macromolecules*, **2006**, 39, 2113-2120.

Following this synthetic protocol, and according to a divergent strategy, three new hydrophilic poly(esteramide) dendrons derived from *bis*-GMPA were synthesized, *i.e.* **N_3-[*bis*GMPA,G2]$(NH_3^+Cl^-)_4$**, with a 7 % global yield, **N_3-[*bis*GMPA,G3]$(NH_3^+Cl^-)_8$** with a 4 % global yield and **N_3-[*bis*GMPA,G4] $(NH_3^+Cl^-)_{16}$** with a 2 % global yield (**figure C_4-10**).

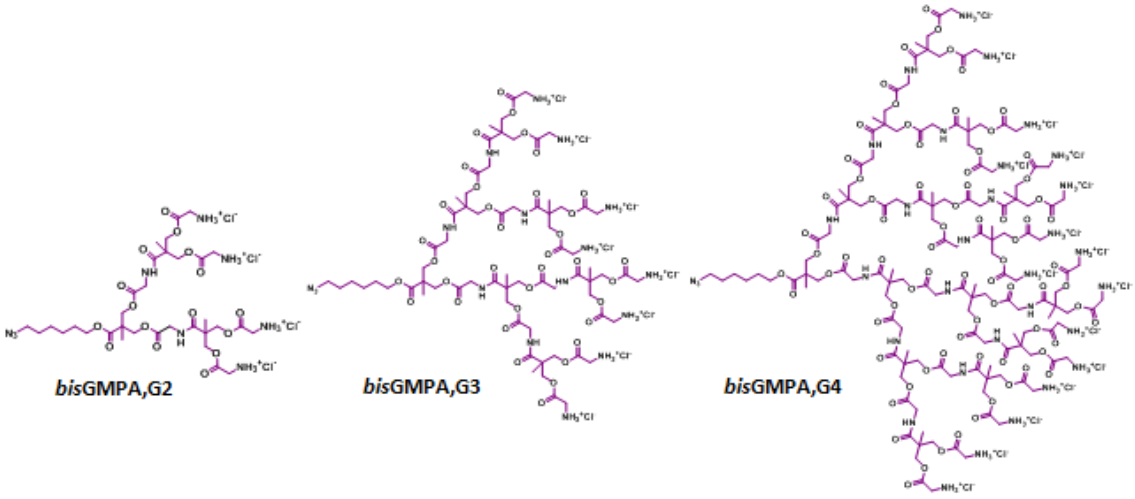

Figure C_4-10: Dendrons of *bis*-GMPA of the 2nd, 3rd and 4th generation.

All the dendrons were characterized by ^1H and ^{13}C nuclear magnetic resonance (NMR), Fourier transform infrared spectroscopy (FTIR) and elemental analysis (EA). Additionally, the dendrons bearing the *t*-Boc protecting groups were characterized by mass spectrometry (MS) and size exclusion chromatography (SEC). The complete characterization data are gathered in the chapter 7.

The analyses of the ^1H and ^{13}C NMR spectra of the *bis*-GMPA dendrons and their comparison with the spectra of an analogous *bis*-MPA dendron helped the signal assignation to the corresponding protons and carbons and assess their correct synthesis (**figure C_4-11**). Moreover, ^1H-^1H correlation spectroscopy (COSY) was performed to corroborate the proton assignation (**annexes 1**).

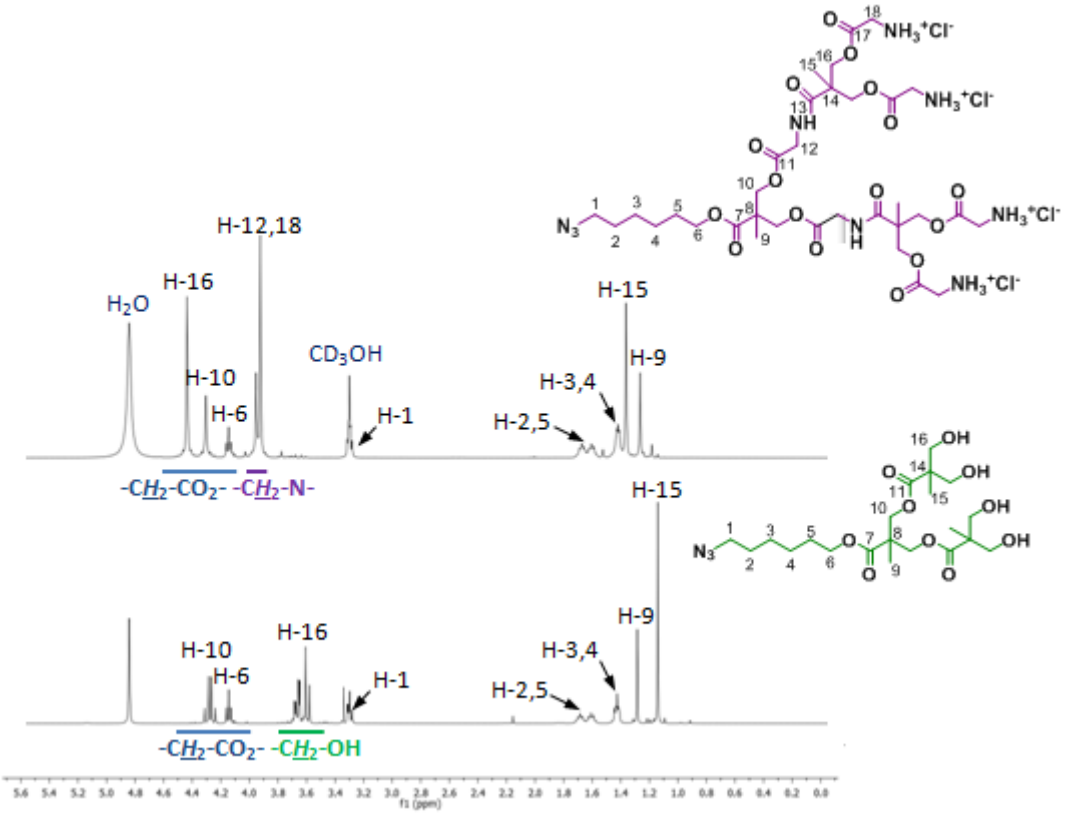

Figure C$_4$-11: ^{1}H-NMR spectrum of **N$_3$-[*bis*GMPA,G2](NH$_3^+$Cl$^-$)$_4$** (up) and **N$_3$-[*bis*MPA,G2](OH)$_4$** (down) recorded in CD_3OD at 400 MHz.

The signals corresponding to the protons that belong to the 6-azidohexyloxy chain of both dendrons (*H-1* to *H-6*) appear almost identical. In the spectrum of the *bis*-GMPA dendrons, the triplet corresponding to the methylene protons in the α-position of the azide group (*H-1*) is overlapped with the signal of the solvent. Nevertheless, the correlation of this triplet with the signal corresponding to its vicinal methylene protons (*H-2*) is observed in ^{1}H-^{1}H COSY (see **annexes 1**). The singlets corresponding to the methyl protons (*H-9* and *H-15*) appear between 1.1 and 1.4 ppm in both dendrons even if their respective signals appear inverted.

The signals corresponding to the other protons appear at different chemical shifts in both spectra. In the spectrum of the *bis*-GMPA dendron, new singlets are observed near 3.9 ppm that correspond to the methylene protons of the glycine groups (*H-12* and *H-18*). Additionally, the signals corresponding to the oxymethylene protons are clearly different. First, the ABq systems

corresponding to the terminal hydroxymethylene protons -C*H*$_2$-OH (*H-16*), which appear between 3.6 and 3.7 ppm in the *bis*-MPA derivative, are not observed in the *bis*-GMPA dendron, pointing out its complete functionalization with terminal glycine groups. Second, an additional peak is observed between 4.2 and 4.6 ppm in the *bis*-GMPA spectrum, which corresponds to the oxymethylene protons of the terminal ester groups, -CH$_2$-OOC- (*H-16*). Also, the signal corresponding to the oxymethylene protons of the internal ester group (*H-10*) is clearly distinct. In the *bis*-MPA spectrum, it appears as a clear ABq system whereas in the *bis*-GMPA spectrum, the ABq system is much less defined.

Figure C$_4$-12 gathers the regions of the ^{1}H-NMR spectra corresponding to the methylene protons -CH$_2$-N- and -CH$_2$-O- of the *bis*-GMPA dendrons from the 1st to the 4th generation. It is possible to distinguish between the peripheral protons and those that belong to the internal branches. The methylene protons of the external glycine moieties, CH$_2$-N-, appear at higher fields (3.94 ppm) than the protons belonging to the internal glycine moieties (3.96 - 4.00 ppm). With respect to oxymethylene groups, -CH$_2$-O-, the ABq signals that correspond to the peripheral *bis*-MPA moieties appear at lower fields (4.40 - 4.60 ppm) than the protons belonging to the internal *bis*-MPA moieties (4.33 ppm). Logically, the triplet that corresponds to the oxymethylene protons of the 6-azidohexyloxy chain appears at the same positions regardless the dendron generation.

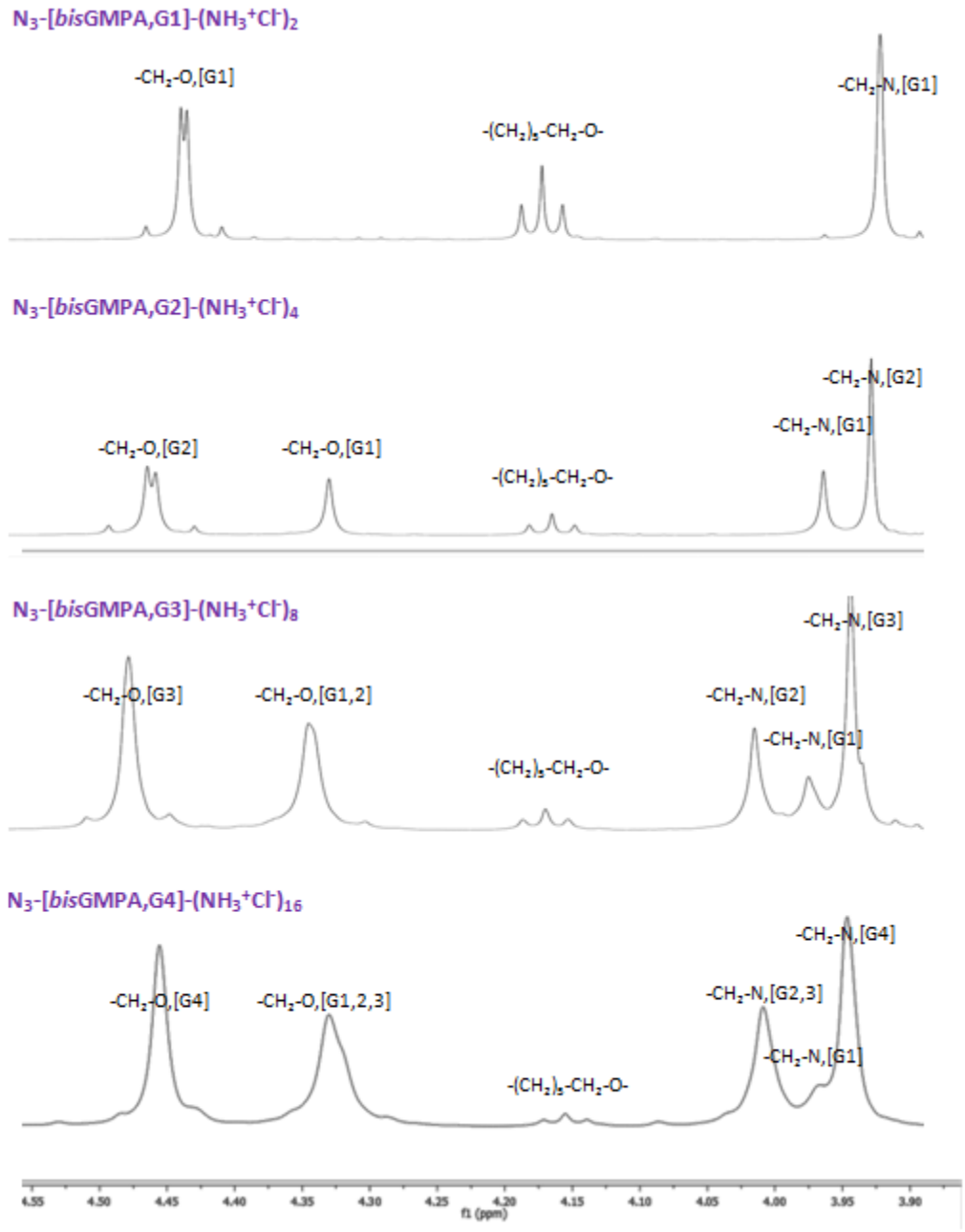

Figure C_4-12: Expansions of the ^{1}H-NMR spectra of *bis*-GMPA dendrons from the 1st to the 4th generation from 3.90 ppm to 4.55 ppm.

The ^{13}C-NMR spectrum of the 2nd generation poly(esteramide) dendron of *bis*-GMPA, **N_3-[*bis*GMPA,G2]-($NH_3^+Cl^-$)$_4$**, is represented and described as an example in **figure C_4-13**, together with it homologous *bis*-MPA dendron. Their comparison helped to interpret the spectrum of the new dendron. Additionally, ^{1}H-^{13}C hetero nuclear single-quantum correlation spectroscopy (HSQC) was performed to corroborate the carbon assignation (**see annexes 1**).

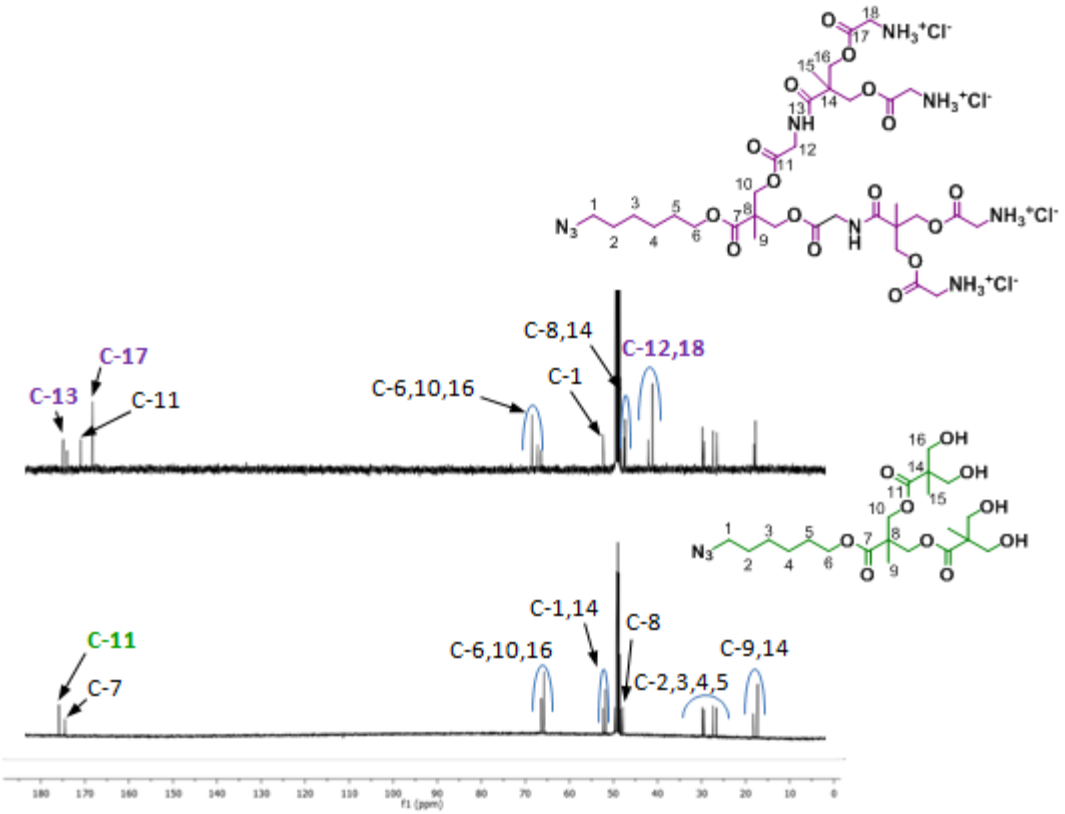

Figure C_4-13: ^{13}C-NMR spectrum of **N_3-[*bis*GMPA,G2]($NH_3^+Cl^-$)$_4$** (up) and **N_3-[*bis*MPA,G2](OH)$_4$** (down) recorded in CD_3OD at 100 MHz.

New peaks corresponding to the internal and peripheral glycine moieties are observed in the *bis*-GMPA spectrum. Thus, two peaks are observed at 41.1 and 42.1 ppm, which correspond to the methylene carbon of the glycine groups (*C-18* and *C-12* respectively). As for carbonyl carbon atoms, two representative peaks that appear at 168.2 and 174.9 ppm confirm the presence of glycine groups within the dendron structure. The first one corresponds to the external ester groups (*C-17*) while the second one corresponds to the amide groups (*C-13*).

The difference between the *bis*-MPA and *bis*-GMPA dendrons is also clearly observed in FTIR spectroscopy (**figure C_4-14**).

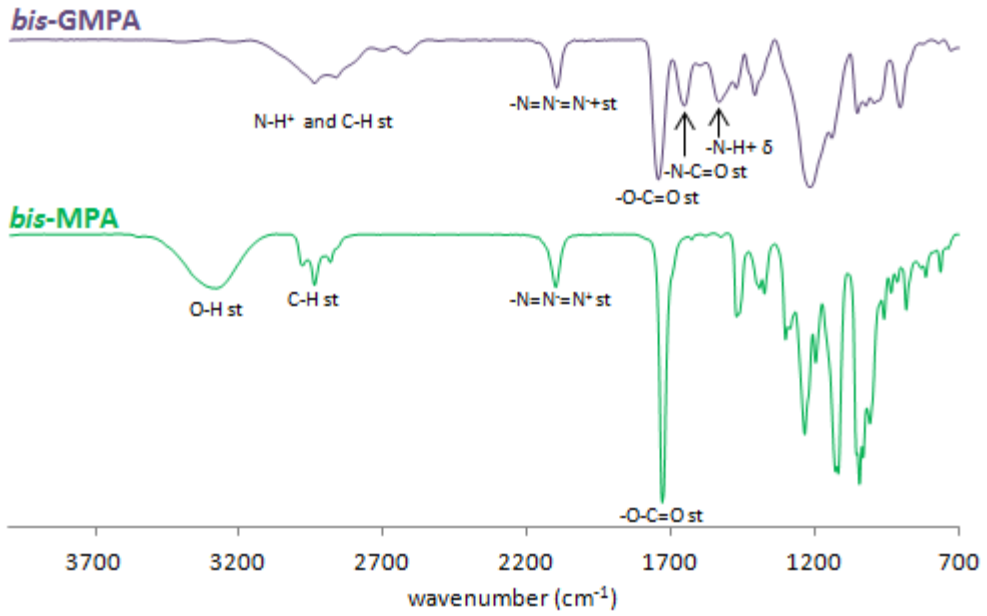

Figure C_4-14: FTIR spectra of the dendron of *bis*-GMPA of 2nd generation (up) and of the dendron of *bis*-MPA of 3rd generation (down).

The spectrum of the *bis*-GMPA dendron shows a broad band with various maxima between 3400 and 2600 cm^{-1} that correspond to the ammonium groups. This is in contrast to the spectrum of the *bis*-MPA dendron that shows an only band at 3283 cm^{-1} belonging to the hydroxyl groups. Whereas the presence of the ester groups was confirmed by an intense band around 1737 cm^{-1} in both dendrons, the *bis*-GMPA dendron exhibits an additional band at 1665 cm^{-1} corresponding to the amide groups, together with a band at 1541 cm^{-1} corresponding to the vibration deformations of the N-H bonds. Finally, the presence of the azide group in both dendrons was confirmed by a sharp band at 2100 cm^{-1}.

The monodispersity of the dendrons was controlled by MS and SEC (**figure C_4-15**).

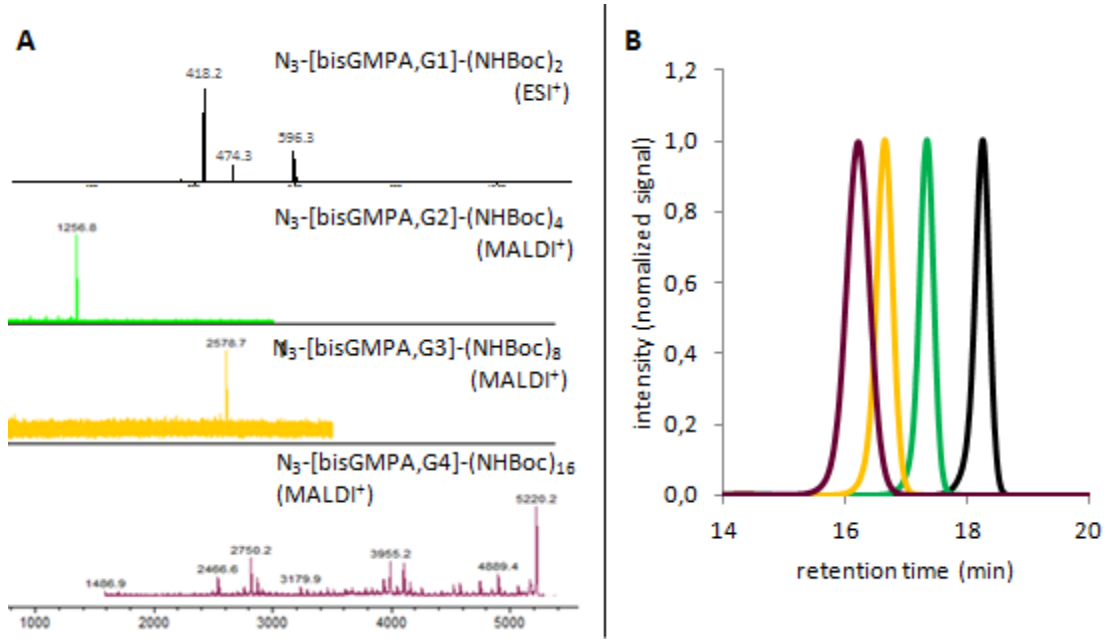

Figure C_4-15: MS spectra (A) and SEC chromatograms (B) of the *bis*-GMPA dendrons with terminal *t*-Boc amino groups from the 1st to the 4th generation.

ESI^+ spectrum was recorded for the smallest *bis*-GMPA dendron. A peak that corresponds to $[M + Na]^+$ is observed together with fragmentation peaks. $MALDI^+$-TOF spectra were recorded for the *bis*-GMPA dendrons of higher generations. Only one peak is observed for the 2nd and 3th generation that correspond to $[M + Na]^+$ in each spectrum. In the case of the 3rd generation dendron, other peaks resulting from the fragmentation of the dendron are visible in addition to the $[M + Na]^+$ peak.

SEC chromatograms show only one monomodal and symmetrical peak for each dendron. The polydispersity of the dendrons was determined using poly(methyl methacrylate) (PMMA) as a reference and had values between 1.01 and 1.04 as expected for monodisperse dendrons.

4.1.3- Biocompatibility and degradability

The biocompatibility, as well as the degradability, of new materials is an important requirement for their further use in nanomedicine. The biocompatibility and biodegradability of *bis*-MPA dendrons has already been intensively studied. In general, they show high biocompatibility and they can be degraded in the body by either enzymatic ester cleavage or by hydrolysis in water.[149]

In a previous work, our group studied the biocompatibility and degradability of a 3rd generation hydrophilic *bis*-MPA dendron with terminal glycine moieties in cancerous human brain cells line (U251 MG) and in mouse origin mesenchymal cells line (mMSCs).[95,159] In both cases, the cell viability was higher to 80 % after 72 hours at concentration 1 mM. The dendron degradability at 37ºC in water was also studied. The dendron was effectively degraded by hydrolysis. In these compounds, the ester linkages of the glycine moieties with the *bis*-MPA dendrons were the first ester groups to be hydrolyzed.

The biocompatibility of the *bis*-GMPA dendrons of 2nd, 3rd and 4th generation that will be further used during *in vitro* assays was studied in human cancerous cells line (HeLa) and in mouse mesenchymal cells line (mMSCs). These studies were carried by Rebeca González and belong to her thesis research work (**figure C_4-16)**.[184 In both cases, cell viability was higher than 70 % at 1 mg·mL^{-1} after 72 hours. The weaker biocompatibility of the 2nd generation dendron can be explained by the higher relative abundance of the toxic azide groups.

[149] N. Feliu *et al.*, *Biomaterials*, **2012**, 33, 1970.

[95] J. Movellan, P. Urbán *et al.*, *Biomaterials*, **2014**, 35, 7940.

[159] J. Movellan *et al.*, *Macromol. Biosci.*, **2015**, 15 657.

[184] R. González, Estudio de dendrímeros y nanopartículas de oro para su uso en tratamientos antitumorales, **2017**, Universidad de Zaragoza.

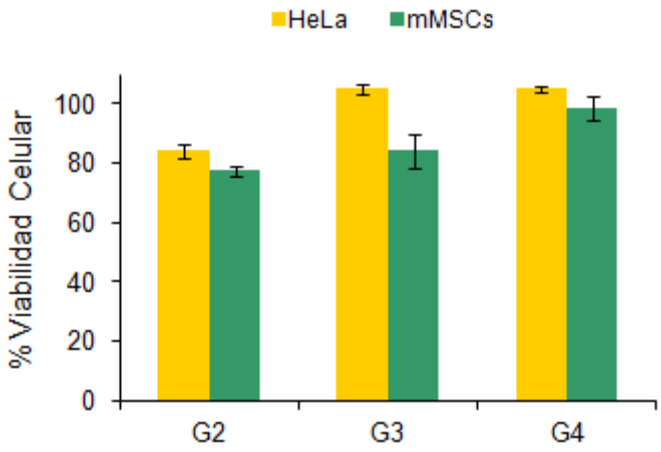

Figure C_4-16: Cell viability of the three *bis*-GMPA dendrons of the 2nd, 3rd and 4th generation at 1 mg/mL after 72 hours.

The degradability of the *bis*-GMPA dendrons of 2nd, 3rd and 4th generation was studied in deuterated water and in deuterated water with H_2SO_4 (pH near 1). ^{1}H NMR experiments were carried out at different times to observe the degradation of the dendrons. The regions of the spectra that give more information about de degradation process are gathered in **figure C_4-17**. The signal of the methylene protons in the α-position of the azide group (3.2 ppm), which should not be modified by hydrolysis, was used as a reference to measure the intensity of the other signals.

In deuterated water, the degradation of all the dendrons was observed. After 5 days, a signal near 3.8 ppm started to be observable and its intensity increases with time. It corresponds to hydroxymethylene protons, -C$\underline{H_2}$-OH, that appear in the periphery of the dendron meaning that the ester groups of the dendrons were slowly hydrolyzed, inducing the destruction of the macromolecular dendrons into small fragments.

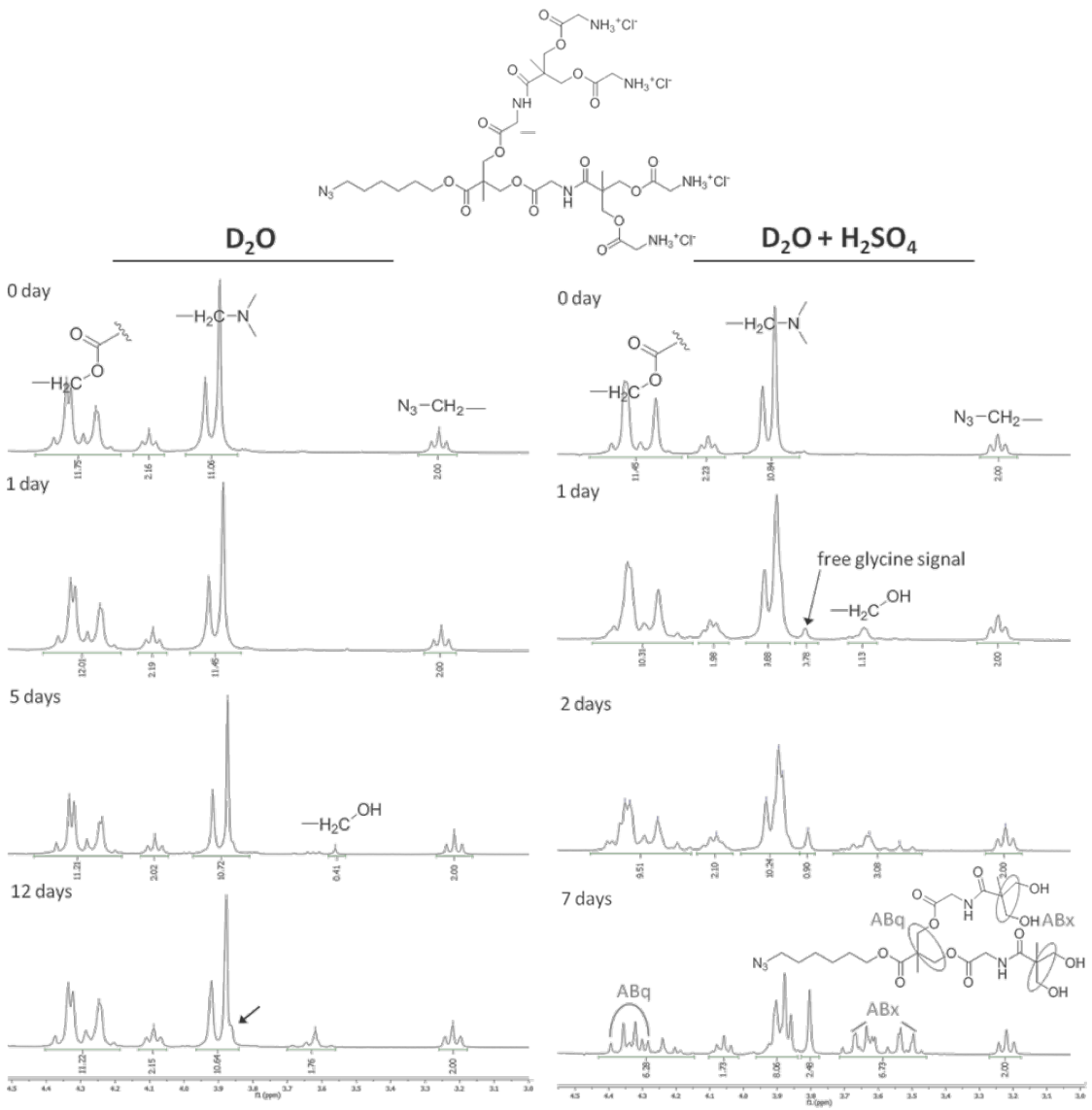

Figure C_4-17: Degradation of N_3-[*bis*GMPA,G2]$(NH_3^+Cl^-)_4$ in D_2O and in D_2O+H_2SO_4 observed in ^1H NMR.

In deuterated water with sulfuric acid, pH near 1, the rate of the degradation of dendrons is accelerated. After only 1 day, the signals corresponding to the hydroxymethylene protons, -C*H*$_2$-OH, could be observed. And, after two days, the general aspect of the signals corresponding to the oxymethylene protons attached to the ester groups, -C*H*$_2$-OC(O)-, and in the α-position of the nitrogen atoms, -C*H*$_2$-N-, were modified indicating that the degradation process was affecting the full dendron structure.

After 7 days, the ABq signal near 4.35 ppm that corresponded to the -C*H*$_2$-OC(O)- of the peripheral generation was replaced by a new ABq signal with

a bigger Δv_{AB}. Moreover, in the hydroxymethylene zone, -C*H*$_2$-OH zone, the ABx system, characteristic of the hydroxyl terminated *bis*-MPA dendrons, started to be clearly observable leading to think that the dendron had lost these four terminal external glycine moieties. The modifications observed in the -C*H*$_2$-N- zone corroborated this supposition. The integration of the peak corresponding to the external methylene protons decreased and a new signal, which relative integration increased with time, appeared at 3.8 ppm and should correspond to the -C*H*$_2$-N of the free glycine.

Additional signals that did not correspond to the undegraded dendron and to the dendron without peripheral glycine moieties were also observed in the spectra. They can correspond to intermediates that have lost only a part of their four peripheral glycine moieties or to other degradation products resulting from the cleavage of internal ester or amide bonds.

The same behavior was observed for the dendrons of the 3rd and 4th generation (**table C$_4$-1**).

Tables C$_4$-1: Degradation of the *bis*-GMPA dendrons of 2nd, 3rd and 4th generation in D_2O and in D_2O+H_2SO_4 .

dendron generation	relative integration of -C*H*$_2$OC(O)-	relative integration of -C*H*$_2$O-OH-	% degradation
in D_2O			
G2	11.12	1.76	14
G3	20.54	2.02	14
G4	40.00	7.24	20
in D_2O + H_2SO_4			
G2	6.28	6.73	52
G3	9.46	13.04	58
G4	14.67	22.21	60

4.2- Amphiphilic *bis*-MPA and *bis*-GMPA dendritic derivatives

Two types of amphiphilic dendritic derivative based on *bis*-MPA and *bis*-GMPA were synthesized: amphiphilic Janus dendrimers and hybrid dendritic-linear-dendritic block copolymers (HDLDBCs).

The amphiphilic Janus dendrimers are divided in two series. Series ***A*** gathers dendrimers in which the hydrophilic block consists on 2nd or 3rd generation *bis*-MPA dendrons with terminal amino groups (***bis*-MPA/*bis*-MPA** series), whereas series ***B*** corresponds to dendrimers in which the hydrophilic block consists on 2nd or 3rd generation *bis*-GMPA dendrons (***bis*-GMPA/*bis*-MPA** series). For the two series, 1st and 2nd generation *bis*-MPA dendrons with terminal C17 alkyl chains constitute the lipophilic block (**figure C_4-18**).

Series ***A*** includes four amphiphilic Janus ***bis*MPA/*bis*MPA** dendrimers:

- **$(NH_3^+Cl^-)_4$[*bis*MPA,G2]-[*bis*MPA,G1]-$(C17)_2$** that consists of a hydrophilic dendron of 2nd generation and a lipophilic one of 1st generation,
- **$(NH_3^+Cl^-)_4$[*bis*MPA,G2]-[*bis*MPA,G2]-$(C17)_4$*** that consist of a hydrophilic dendron of 2nd generation and a lipophilic one of 2nd generation,
- **$(NH_3^+Cl^-)_8$[*bis*MPA,G3]-[*bis*MPA,G1]-$(C17)_2$** that consists of a hydrophilic dendron of 3rd generation and a lipophilic one of 1st generation,
- **$(NH_3^+Cl^-)_8$[*bis*MPA,G3]-[*bis*MPA,G2]-$(C17)_4$*** that consists of a hydrophilic dendron of 3rd generation and a lipophilic one of 2nd generation.

The two Janus dendrimers marked with a star have been previously described by our group.[95]

[95] J. Movellan, P. Urbán *et al.*, *Biomaterials*, **2014**, 35, 7940.

The series ***B*** contained the following three amphiphilic ***bis*-GMPA/*bis*-MPA** Janus dendrimers:

-**$(NH_3^+Cl^-)_4$[*bis*GMPA,G2]-[*bis*MPA,G1]-$(C17)_2$** that consists of a hydrophilic dendron of 2nd generation of *bis*-GMPA and a lipophilic dendron of *bis*-MPA of 1st generation,

-**$(NH_3^+Cl^-)_8$[*bis*GMPA,G3]-[*bis*MPA,G1]-$(C17)_2$** that consists of a hydrophilic dendron of 3rd generation of *bis*-GMPA and a lipophilic dendron of *bis*-MPA of 1st generation,

-**$(NH_3^+Cl^-)_8$[*bis*GMPA,G3]-[*bis*MPA,G2]-$(C17)_4$** that consists of a hydrophilic dendron of *bis*-GMPA of 3rd generation and a lipophilic dendron of *bis*-MPA of 2nd generation.

The Janus dendrimer **$(NH_3^+Cl^-)_4$[*bis*GMPA,G2]-[*bis*MPA,G2]-$(C17)_4$** was not synthesized given the low water solubility and encapsulation abilities shown by its homologous dendrimer in series ***A*** (**$(NH_3^+Cl^-)_4$[*bis*MPA,G2]-[*bis*MPA,G2]-$(C17)_4$**).

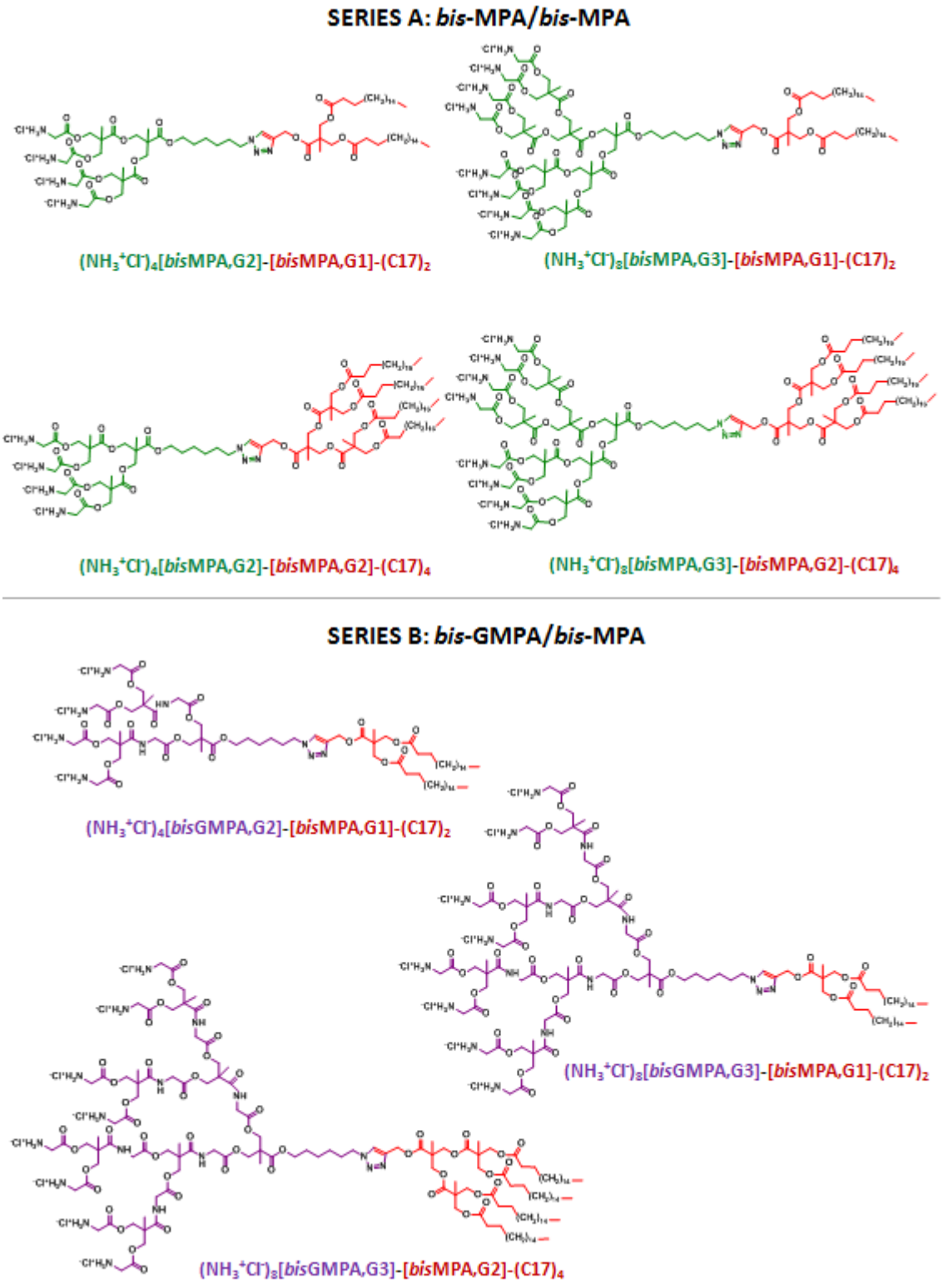

Figure C_4-18: Chemical structures of the four amphiphilic ***bis*-MPA/*bis*-MPA** Janus dendrimers and the three amphiphilic ***bis*-GMPA/*bis*-MPA** Janus dendrimers.

The variation in the chemical composition of the hydrophilic dendron, ***bis*-MPA** or ***bis*-GMPA**, associated to different combinations between the hydrophilic and lipophilic dendrons enabled to obtain amphiphilic Janus dendrimers with different molecular weight and variable hydrophilic/lipophilic ratios (H/L) (**table C_4-2**). H/L ratio was calculated by dividing the number of hydrophilic groups by the number of lipophilic ones. Terminal ammonium salts and internal amide groups were considered as hydrophilic groups whereas the terminal aliphatic chains were considered as lipophilic groups. The other groups, including the aliphatic esters and triazole rings, were not considered for this calculation.

Table C_4-2: Molecular weights (MW) and hydrophilic/lipophilic ratios (H/L) calculated for the two series of amphiphilic Janus dendrimers.

		MW ($g.mol^{-1}$)	relative H/L
hydrophilic *bis*-MPA / lipophilic *bis*-MPA	**$(NH_3^+Cl^-)_4$[G2]-[G1]-$(C17)_2$**	1571	4/2 =2
	$(NH_3^+Cl^-)_4$[G2]-[G2]-$(C17)_4$	2336	4/4 = 1
	$(NH_3^+Cl^-)_8$[G3]-[G1]-$(C17)_2$	2409	8/2 = 4
	$(NH_3^+Cl^-)_8$[G3]-[G2]-$(C17)_4$	3174	8/4 = 2
hydrophilic *b*-GMPA / lipophilic *bis*-MPA	**$(NH_3^+Cl^-)_4$[G1]-[G1]-$(C17)_2$**	1685	(4+2)/2 = 3
	$(NH_3^+Cl^-)_8$[G2]-[G1]-$(C17)_2$	2752	(8+6)/2 = 7
	$(NH_3^+Cl^-)_8$[G2]-[G2]-$(C17)_4$	3517	(8+6)/4 = 3.5

The 3rd series (***C***) brings together two amphiphilic hybrid dendritic-linear-dendritic block copolymers (HDLDBCs), which are represented in **figure C_4-19**. Both derivatives were based on commercial amphiphilic linear triblock copolymer Pluronic® F-127, which was functionalized at its two terminal positions by 3rd generation amino-terminated *bis*-MPA dendrons or by 3rd generation *bis*-GMPA dendrons, named as ***bis*MPA-PLU-*bis*MPA** and ***bis*GMPA-PLU-*bis*GMPA**, respectively. The first HDLDBC was previously published by our group.[95]

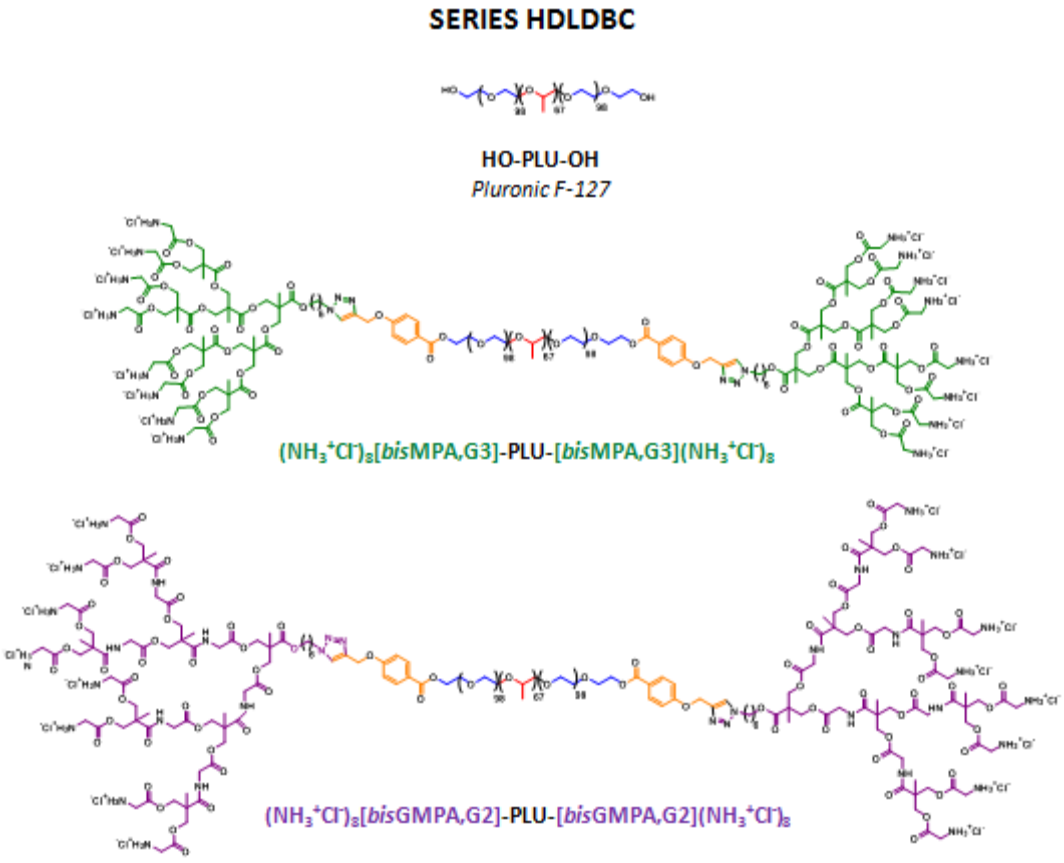

Figure C_4-19: Chemical structures of Pluronic® F-127 and the two HDLDBC derivatives.

[95] J. Movellan, P. Urbán *et al.*, *Biomaterials*, **2014**, 35, 7940.

The derivatives of this series have a much higher molecular weight than the Janus dendrimers (approximately 16 300 and 17 000 $g.mol^{-1}$, respectively). Their corresponding hydrophilic/lipophilic ratio is mainly conditioned by the amphiphilic linear triblock Pluronic® F-127 that consists in two peripheral blocks of poly(ethylene oxide) (PEO) of 99 units each and one central block of poly(propylene oxide) (PPO) of 67 units, resulting in compounds of higher hydrophilicity than that the previous Janus dendrimers.

Moreover, Pluronic® F127 shows a **lower critical solution temperature (LCST) in water**, which means a decrease in solubility attributed to changes in the overall hydrophilicity of the polymer chain upon temperature increase. The effect induces the formation of micelles in water at room temperature whose lipophilic core, based on the PPO blocks, is surrounded by a hydrophilic shell, based on PEO blocks.[185]

[185] a) A.V. Kabanov, E.V. Batrakova, V.Y. Alakhov, Pluronic® block copolymers as novel polymer therapeutics for drug and gene delivery, *J. Control. Release*, **2002**, 82, 189-212; b) W. Zhang, K. Gilstrap, L. Wu, R.K.C. Bahadur, M.A. Moss, Q. Wang, X-n Lu, X. He, Synthesis and characterization of thermally responsive pluronic F127−chitosan nanocapsules for controlled release and intracellular delivery of small molecules, *ACS Nano*, **2010**, 4, 6747-6759; c)T.T.C Nguyen, C.K. Nguyen, T.H. Nguyen, N.Q. Tran, Highly lipophilic pluronics-conjugated polyamidoamine dendrimer nanocarriers as potential delivery system for hydrophobic drugs, *Mat. Sci. Eng. C*, **2017**, 70, 992-999.

4.2.1- Synthesis and chemical characterization

4.2.1.1- Synthesis of the amphiphilic Janus dendrimers

The hydrophilic and lipophilic dendrons were linked *via* copper(I)-catalyzed azide-alkyne cycloaddition (CuAAC) click chemistry. The Huisgen reaction, known from decades, consists on the formation of a triazole ring by heating an azide and alkyne groups together.[186] This reaction used to show low transformation rates and a mixture of different products were generally obtained. However, the introduction of copper(I) as catalyst, as proposed by the Sharpless's group, increased dramatically the reaction rates even at room temperature.[187] This modification widely extended the library of the starting products that could tolerate the reaction conditions and, furthermore, it favors the formation of the 1,4-isomer.[188]

For our syntheses, the copper(I) catalytic species was formed *in situ* by the reduction of copper(II) salt by (*L*)-ascorbate. Tris(benzyltriazolylmethyl) amine (TBTA) was added to increase the stability of the Cu(I) species.[189] This catalytic system was chosen as it is easier to handle, more stable and cheaper than halogen copper derivatives (CuI and CuBr) and had already proved its advantages to synthesize dendrimers and dendritic systems.[190]

[186] R. Huisgen, 1,3-Dipolar cycloadditions. Past and future, *Angew. Chem. Int. Ed. Engl.*, **1963**, 2, 565-598.

[187] H.C. Kolb, M.G. Finn, K.B. Sharpless, Click chemistry: diverse chemical function from a few good reactions, *Angew. Chem. Int. Ed.*, **2001**, 40, 2004-2021.

[188] J.E. Hein, V.V. Fokin, Copper-catalyzed azide–alkyne cycloaddition (CuAAC) and beyond: new reactivity of copper(I) acetylides, *Chem. Soc. Rev.*, **2010**, 39,1302-1315.

[189] T.R. Chan, R. Hilgraf, K.B. Sharpless, V.V. Fokin Copper(I)-catalyzed synthesis of azoles. DFT study predicts unprecedented reactivity and intermediates, *Org. Lett.*, **2004**, 17, 2853-2855.

[190] G. Franc, A.K. Kakkar, "Click" methodologies: efficient, simple and greener routes to design dendrimers, *Chem. Soc. Rev.*, **2010**, 39, 1536-1544.

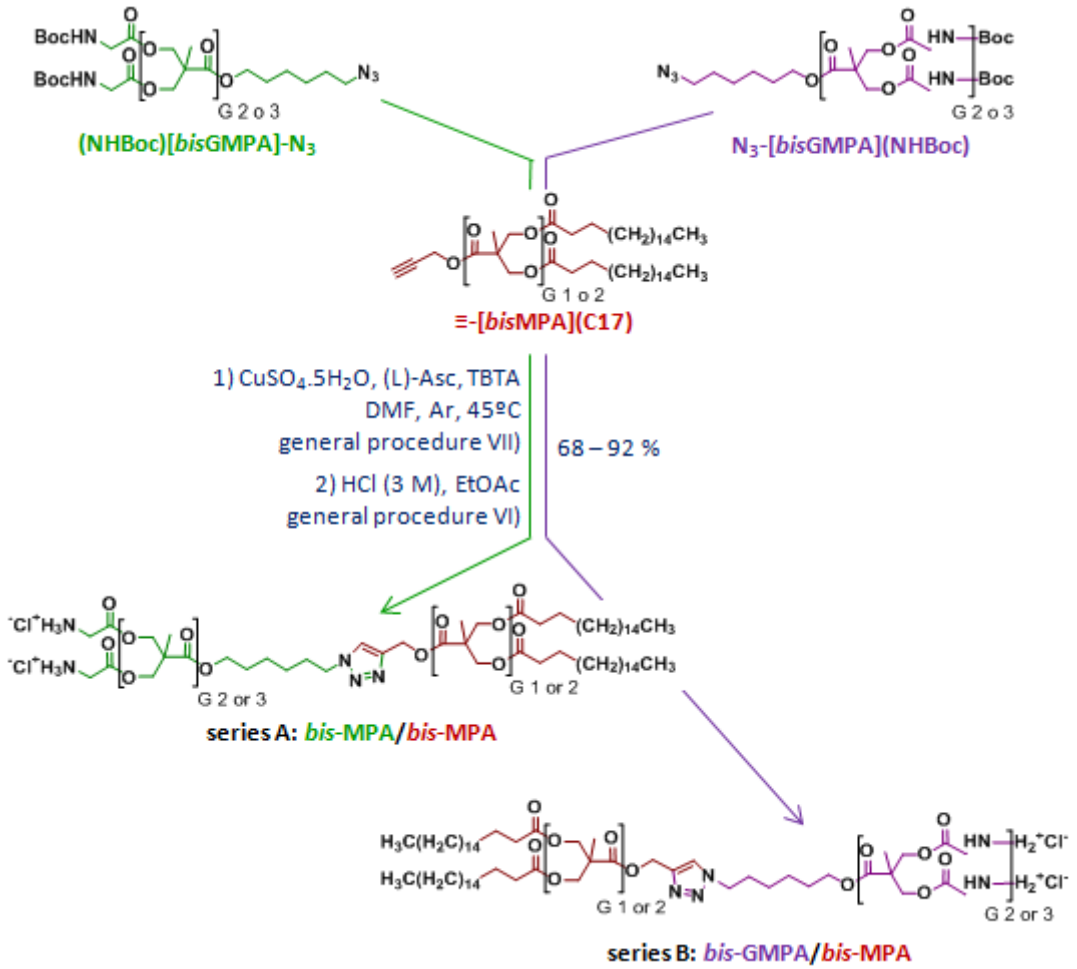

Figure C_4-20: Synthesis of the amphiphilic Janus dendrimers of the two series (see chapter 7 for the detailed description of the synthesis and the general procedures VII) and VI)).

As the terminal primary amines could have complexed the copper species, lowering the conversion of the reaction, the CuAAC coupling reactions were achieved with the *t*-Boc protected dendrons. Besides, the products obtained after the CuAAC were lipophilic allowing their purification by flash chromatography on silica gel.

The *t*-Boc protected and lipophilic dendrons were mixed together in the presence of $CuSO_4.5H_2O$, (*L*)-ascorbate and TBTA into dry dimethylformamide at 45ºC during 1 day (**figure C_4-20**, general procedure VII). The Janus dendrimers were first purified by several washings with brine and an aqueous KCN solution

before performing flash chromatography on silica gel. An excess of the lipophilic dendron (1.2 or 1.5 mole of lipophilic dendron per mole of *t*-Boc protected dendron) was added to consume all the *t*-Boc protected dendrons during the CuAAC. Therefore, the crude products only contained the Janus dendrimer and the excess of lipophilic dendron that could be easily separated.

Finally, the *t*-Boc protecting groups were removed in acidic conditions in ethyl acetate, forming the ammonium salts which precipitated in the reaction medium (**figure C_4-20**, general procedure VI). After removing the hydrochloric acid under vacuum, the final products were recovered by centrifugation and washed with pure ethyl acetate to remove the remaining acid traces. At this point, the Janus dendrimers became amphiphilic: they were composed of a hydrophilic part that had ammonium salts at its periphery and a lipophilic part that had aliphatic chains at its periphery.

The CuAAC reaction yields obtained were in the range of 69 and 92 % for the ***bis*-MPA/*bis*-MPA** series and between 68 and 84 % for the ***bis*-GMPA/*bis*-MPA** series. The *t*-Boc deprotection reactions showed quantitative yields in all cases.

The intermediate Janus dendrimers with the terminal *t*-Boc protecting groups were characterized by means of ^{1}H and ^{13}C nuclear magnetic resonance (NMR), mass spectrometry (MS), Fourier transform infrared spectrometry (FTIR), elemental analysis (EA) and size exclusion chromatography (SEC). The final amphiphilic Janus dendrimers were characterized by ^{1}H and ^{13}C nuclear magnetic resonance (NMR), mass spectrometry (MS) and Fourier transform infrared spectrometry (FTIR). The complete characterization data are gathered in chapter 7.

As an example, the ^{1}H-NMR spectra of **$(NH_3^+Cl^-)_4$[*bis*MPA,G2]-[*bis*MPA,G1](C17)$_2$** and **$(NH_3^+Cl^-)_4$[*bis*GMPA,G2]-[*bis*MPA,G1](C17)$_2$** are depicted in **figure C_4-21**.

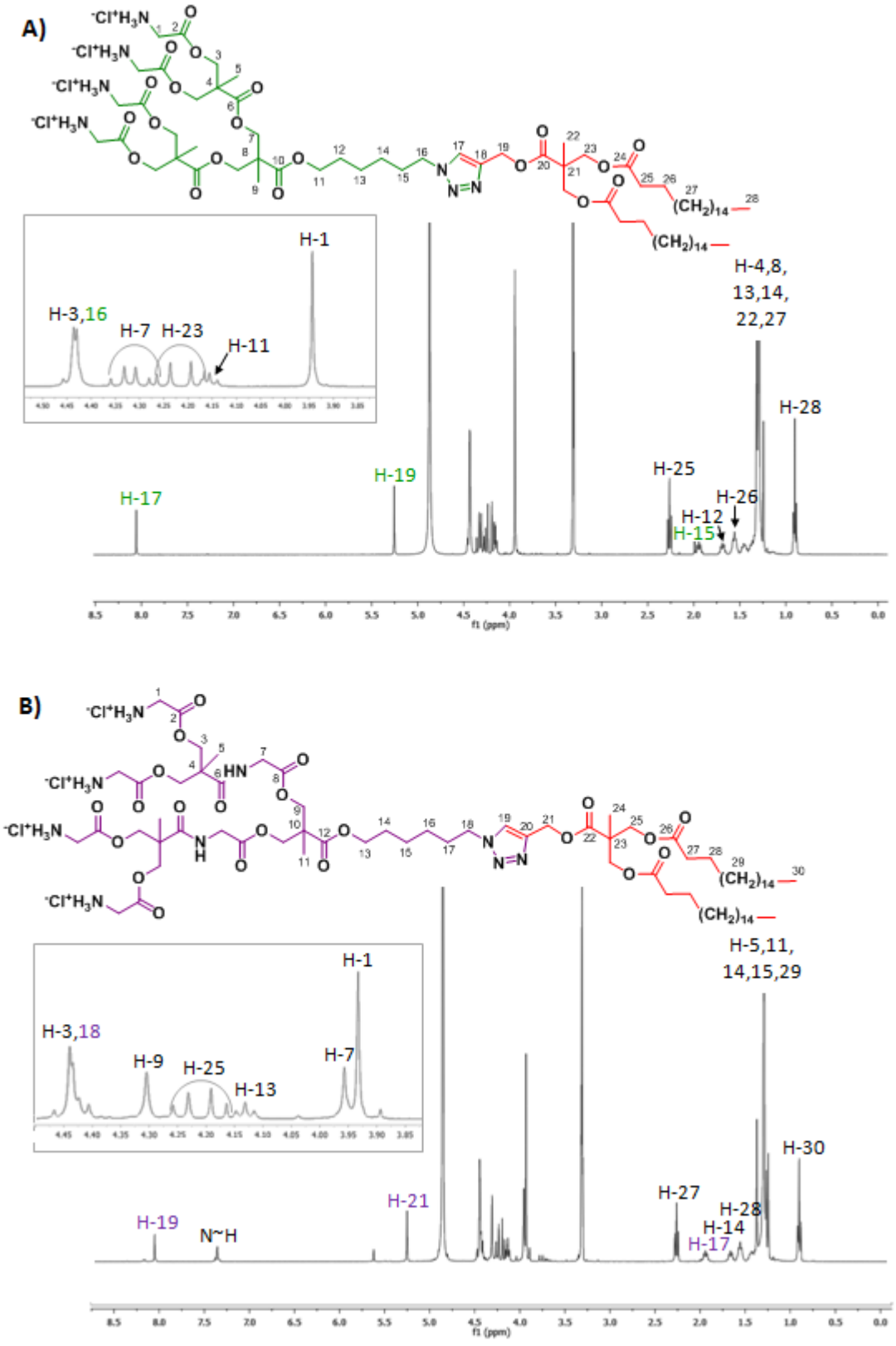

Figure C_4-21: ^{1}H-NMR spectra of **$(NH_3^+Cl^-)_4$[*bis*MPA,G2]-[*bis*MPA,G1](C17)$_2$ (A)** and **$(NH_3^+Cl^-)_4$[bisGMPA,G2]-[*bis*MPA,G1](C17)$_2$ (B)** in CD_3OD recorded at 400 MHz. The overlapping of the peaks corresponding to the protons *H-3* with *H-16* (*bis*-MPA) or *H-18* (*bis*-GMPA) was resolved by ^{1}H-^{1}H COSY experiments (see **annexes 2 & 3**).

For both amphiphilic Janus dendrimers, the formation of the triazole ring was confirmed by the appearance of a peak at 8.06 ppm corresponding to the proton *H-17* (*bis*-MPA) or *H-19* (*bis*-GMPA). Comparing the spectra of these final dendrimers with their corresponding starting dendrons, three signals are shifted downfield. The methylene protons in the α- and β-positions of the triazole ring belonging to the hydrophilic block (*H-16/18* and *H-15/17*) are respectively shifted from 3.25 to 4.43 ppm and from 1.63 to 1.95 ppm, while the signals corresponding to the oxymethylene protons in the α-position of the triazole ring belonging to the lipophilic block (*H-19/21*) are shifted from 4.70 to 5.25 ppm. The other signals remain unchanged and a perfect correlation was observed for the signals integration belonging to the two different blocks.

The ^{13}C NMR spectra of both Janus dendrimers **$(NH_3^+Cl^-)_4$[*bis*GMPA,G2]-[*bis*MPA,G1](C17)$_2$** and **$(NHBoc)_4$[*bis*GMPA,G2]-[*bis*MPA,G1](C17)$_2$** with terminal *t*-Boc protected amino groups and free ammonium groups together with these of their respective starting dendrons, **$(NH_3^+Cl^-)_4$[*bis*GMPA,G2]-N_3** and **$(C17)_2$[*bis*MPA,G1]-(≡)** are depicted in **figure C$_4$-22**.

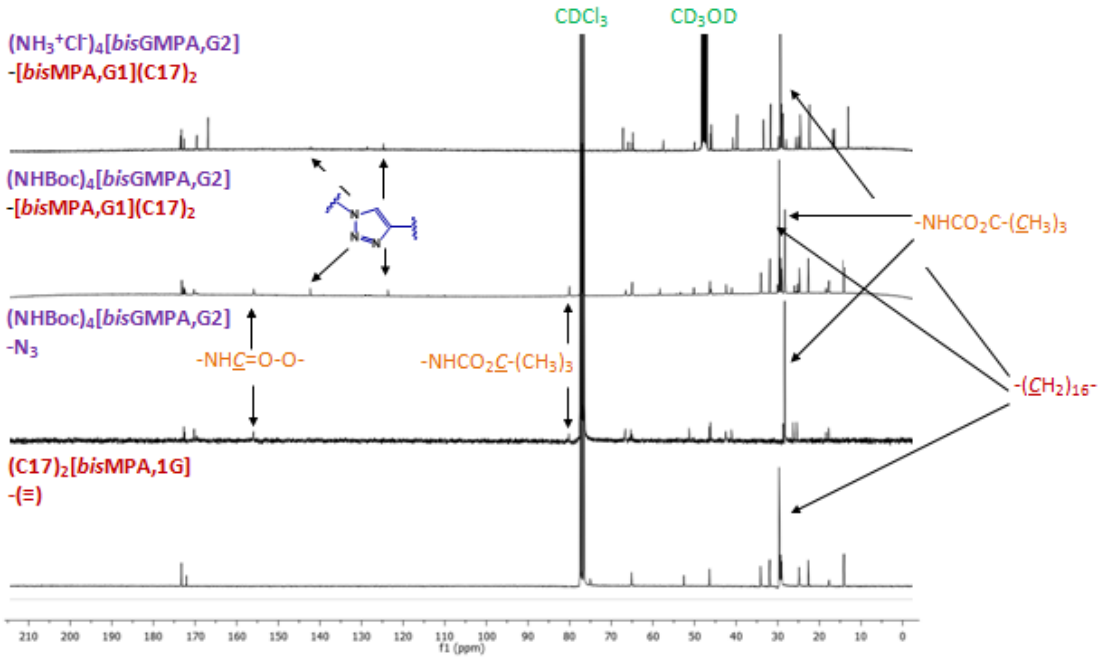

Figure C$_4$-22: ^{13}C-NMR spectra of **$(NHBoc)_4$[*bis*GMPA,G2]-[*bis*MPA,G1](C17)$_2$** and the two starting dendrons **$(NH_3^+Cl^-)_4$[*bis*GMPA,G2]-N_3** and **$(C17)_2$[*bis*MPA,G1]-(≡)** in $CDCl_3$ and **$(NH_3^+Cl^-)_4$[*bis*GMPA,G2]-[*bis*MPA,G1](C17)$_2$** in CD_3OD, at 75 or 100 MHz.

With respect to the spectra of its corresponding starting dendrons, two new peaks are visible for the Janus dendrimers at 124 and 142 ppm (in blue); they correspond to the carbons of the triazole ring, (*C*-19 and *C*-20, respectively). This observation is also valid for the ***bis*-MPA/*bis*-MPA** dendrimers (**annexes 4**).

After the CuAAC, the correct deprotection of the terminal amino groups was confirmed by the disappearance of the signals at 28.3, 80.0 and 155.8 ppm corresponding to the *t*-Boc protecting groups (in orange).

The monodispersity of the Janus dendrimers and the absence of free dendrons that had not reacted during the CuAAC process were confirmed by SEC and MS (**figure C_4-23**). SEC could only be performed with the Janus dendrimers whose amines were protected by the *t*-Boc groups as the final amphiphilic Janus dendrimers showed low solubility in the SEC elution solvent (tetrahydrofuran (THF)).

In all cases, a unique and symmetrical monomodal peak is observed in the SEC chromatogram. The polydispersity was calculated equal to 1.02 using PMMA as standard internal reference as expected for dendrimers.

MS was performed with the Janus dendrimers after the deprotection of the terminal amino groups. A peak that corresponds to the amphiliphilic Janus dendrimers whose amines are unprotected and unprotonated (-NH_2 form) plus sodium is observed for all the Janus dendrimers. Unlike linear polydisperse polymers, the dendrimers don't appear as a distribution of mass peaks, confirming therefore their monodispersity.

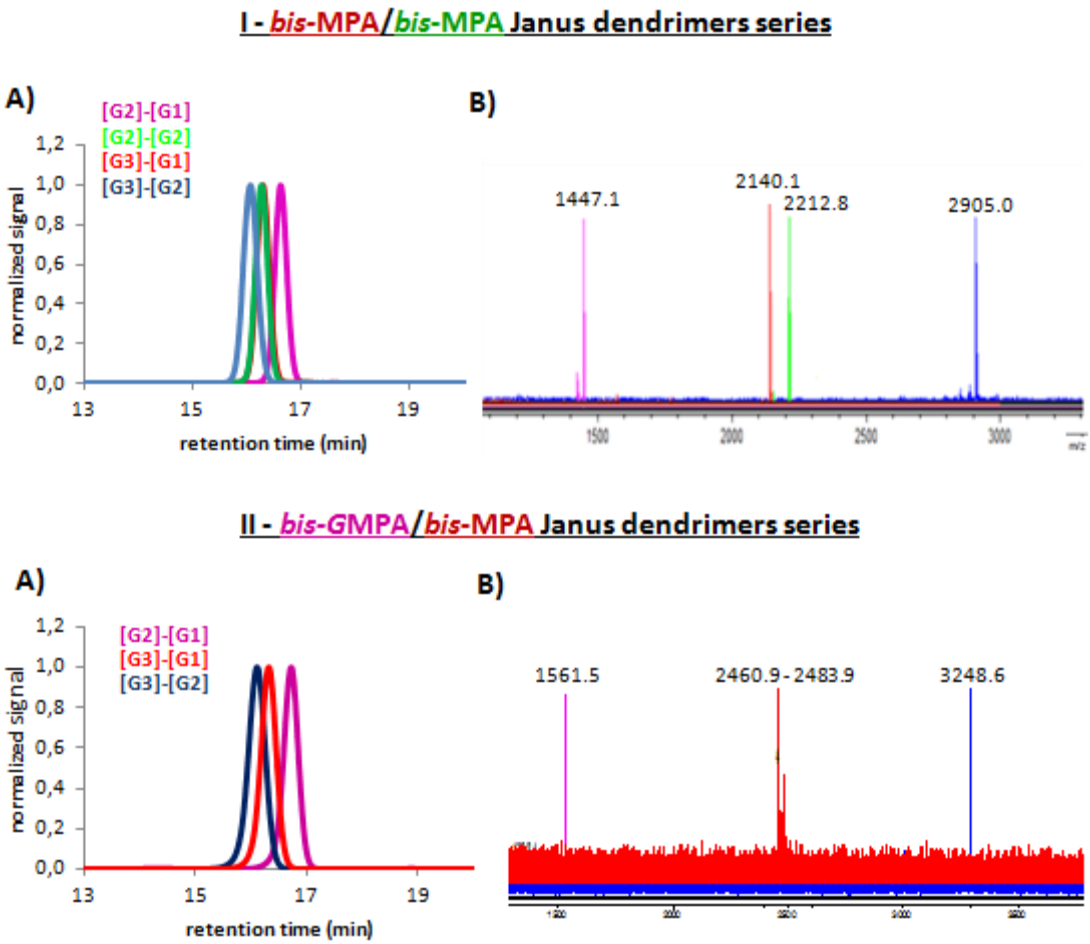

Figure C_4-23: **A**) SEC chromatograms of the *bis*-MPA/*bis*-MPA (**I**) and *bis*-GMPA/*bis*-MPA (**II**) Janus dendrimers series with the *t*-Boc protecting groups (-NHBoc form) and **B**) MS spectra of the *bis*-MPA/*bis*-MPA (**I**) and *bis*-GMPA/*bis*-MPA (**II**) Janus dendrimers after removing the *t*-Boc protecting groups (-NH_2 form).

4.2.1.2- Hybrid dendritic-linear-dendritic block copolymers (HDLDBCs)

Amphiphilic linear tri-block Pluronic® F-127 was decorated at its terminal positions with two hydrophilic dendrons of *bis*-MPA and *bis*-GMPA of 3rd generation bearing 8 terminal amino groups. To perform the CuAAC coupling between the dendrons and the linear polymer, alkyne moieties were incorporated at the terminal position of the Pluronic® F-127 by means of a *bis* (4-propargyloxybenzoate) derivative.

Commercial methyl 4-hydroxybenzoate reacted with propargyl bromide using Williamson etherification conditions to obtain 4-propargyloxybenzoate. Then, the methyl ester was hydrolyzed with lithium hydroxide in a mixture of water and methanol to give 4-propargylbenzoic acid (**figure C_4-24-A**).

4-propargyloxybenzoic acid reacted then with Pluronic® F-127 (**HO-PLU-OH**) according to the **Steglich's esterification conditions** (in presence of DCC and DMAP) in a mixture of dry THF and dry DCM at 45ºC (**figure C_4-24-B**). The final product was purified by precipitation into cold diethyl ether and the dicyclohexylurea (DCU) that was formed during the reaction was removed by precipitation in toluene. Pluronic® F-127 is soluble in toluene whereas the DCU is totally insoluble and can be easily removed by filtration.

The **two 3rd generation dendrons** of *bis*-MPA or *bis*-GMPA bearing 8 terminal *t*-Boc amino groups **were grafted on the Pluronic®** ***via*** **CuAAC** in dimethylformamide at 45ºC under argon atmosphere during 2 days (**figure C_4-24-B**, general procedure VIII)). The Cu(I) catalytic species was formed *"in situ"* by reduction of Cu(II) salt with (*L*)-ascorbate and TBTA was added to increase its stability. An excess of dendron (1.3 mole of dendron per 1.0 mole of alkyne group) was used to obtain a complete functionalization of the linear polymer.

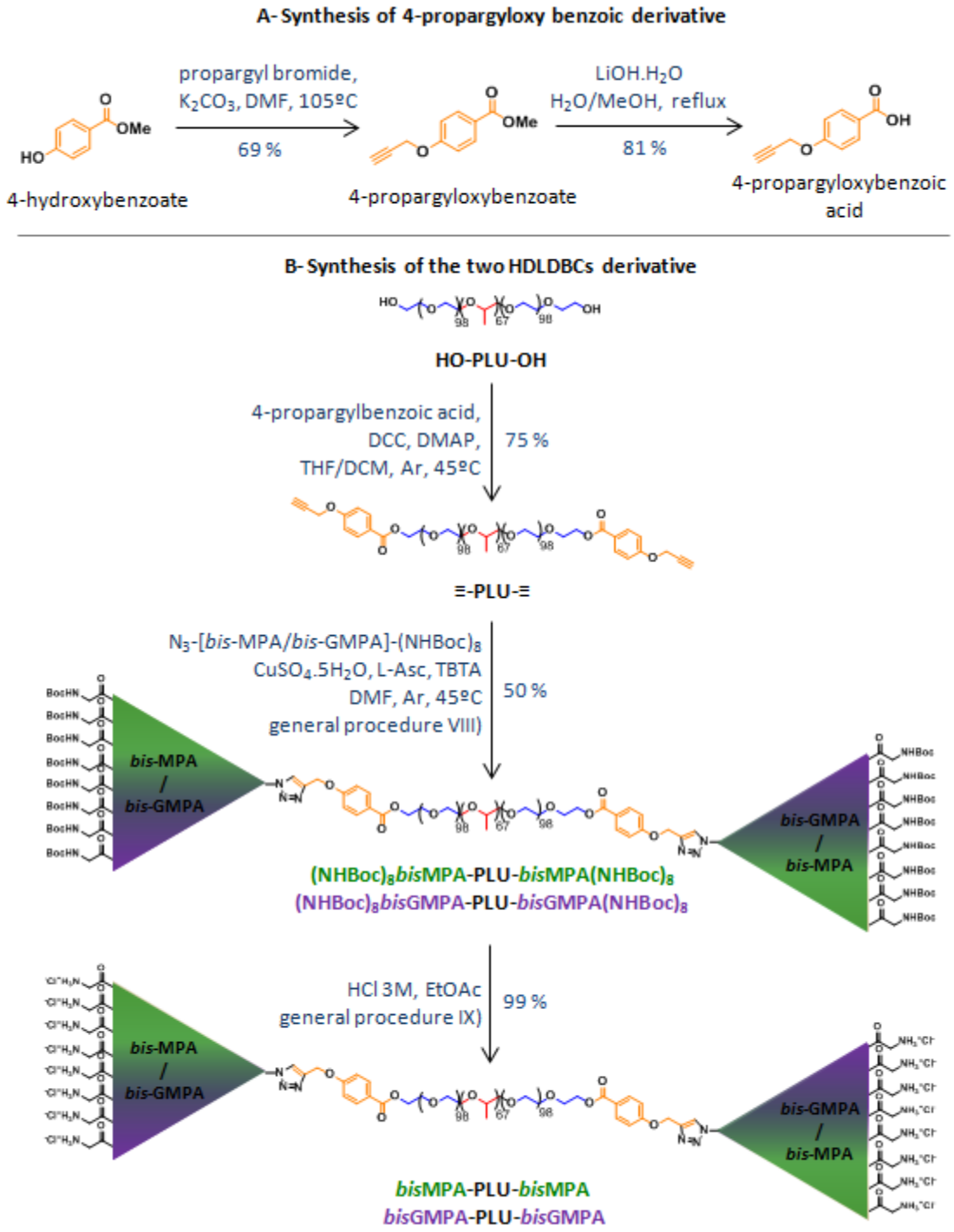

Figure C_4-24: Synthesis of 4-propargylbenzoic acid (**A**) and synthesis of the two HDLDBCs starting from the commercial Pluronic® F-127 (**B**) (see chapter 7 for the detailed description of the synthesis and the general procedures VIII) and IX)).

After completion of the reaction, the reaction mixtures were diluted in dichloromethane and washed several times with hot brine. The final products were precipitated several times into cold diethyl ether and remaining impurities of low molecular weight were removed by dialysis against methanol.

Following this protocol, the complete functionalization of Pluronic® F-127 at its extremities was achieved. Unfortunately, the reaction yields were low-moderate, 38 % for the HDLDBC with the *bis*-MPA dendrons and 61 % for the HDLDBC with the *bis*-GMPA dendrons. The main reason was the numerous but necessary precipitations of the products into cold diethyl in order to obtain the final products with the appropriate degree of purity.

Finally, the ***t*-Boc protecting groups were removed** in acidic conditions into ethyl acetate (**figure C_4-24-B**, general procedure IX)). After completion of the reaction, the HDLDBCs bearing the dendrons with terminal ammonium salt formed a gel in the reaction medium. The hydrochloric acid was removed under vacuum and the gel was washed two times with pure ethyl acetate in order to remove the acid traces. After evaporation of the organic solvent, the pure products were obtained with quantitative yields.

The correct functionalization of the HDLDBC derivatives combining commercial Pluronic® F-127 and *bis*-GMPA or *bis-MPA* dendrons was controlled by ^{1}H and ^{13}C nuclear magnetic resonance (NMR), Fourier transform infrared spectrometry (FTIR) and size exclusion chromatography (SEC). The complete characterization data are gathered in chapter 7.

As an example, the ^{1}H and an expansion of the ^{13}C NMR spectra of **$(NH_3^+Cl^-)_8$*bis*GMPA-PLU-*bis*GMPA$(NH_3^+Cl^-)_8$** are depicted in **figure C_4-25**.

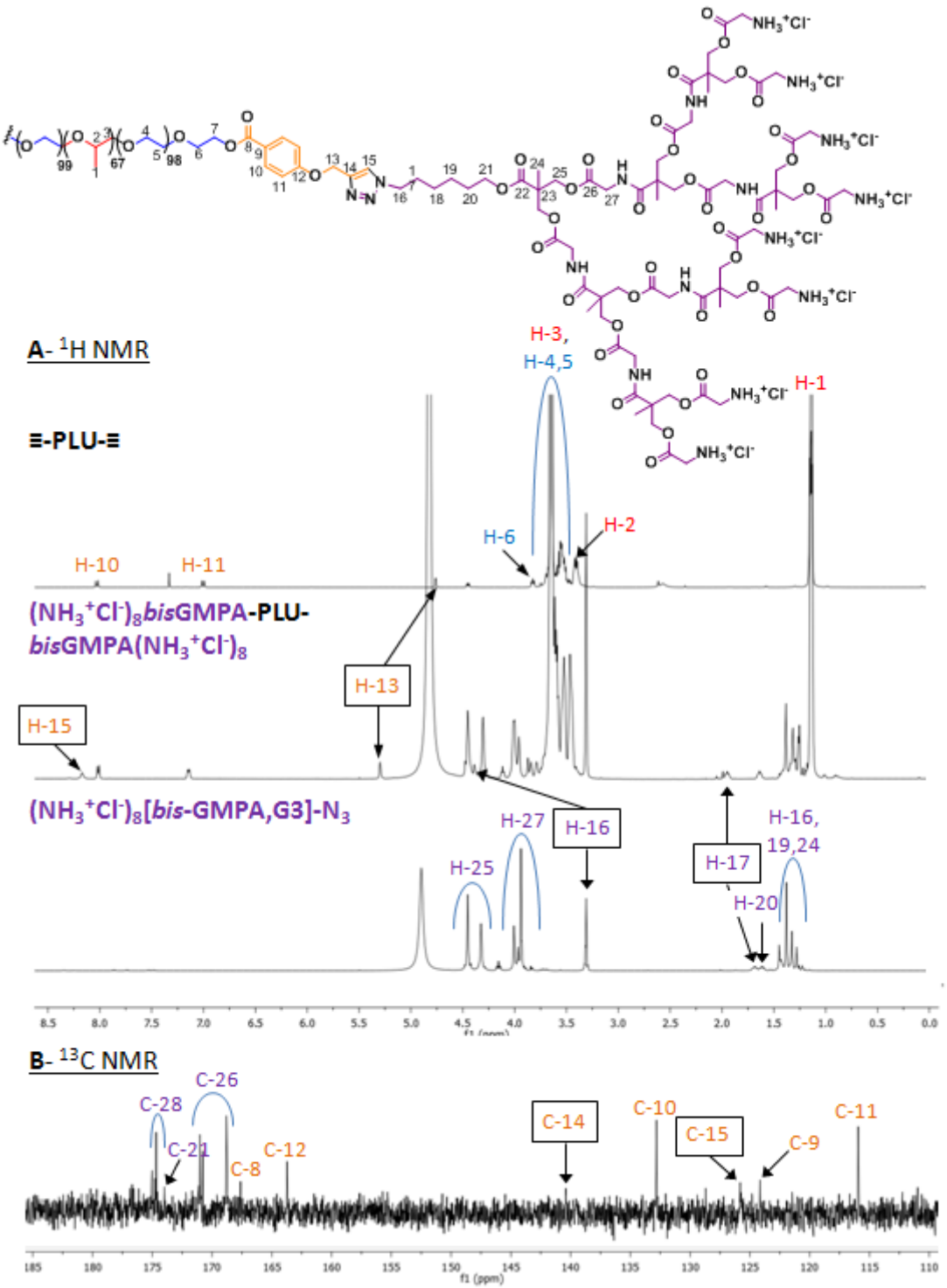

Figure C_4-25: ^{1}H-NMR (**A**) and ^{13}C-NMR (110 to 185 nm) (**B**) spectra in CD_3OD recorded at 400 and 125 MHz, respectively, for **$(NH_3^+Cl^-)_8$*bis*GMPA-PLU- *bis*GMPA$(NH_3^+Cl^-)_8$**. ^{1}H NMR spectra of **≡-PLU-≡** and **$(NH_3^+Cl^-)_8$[*bis*GMPA,G3]-N_3** are included to help the peak assignation.

The correct assignation of the peaks observed in the ^{1}H NMR spectrum was asserted by ^{1}H-^{1}H COSY experiments (see **annexes 5**) and corroborated by their relative integration.

The **formation of the triazole rings** was confirmed by the appearance of a peak at 8.19 ppm (*H-15*) in the ^{1}H NMR spectrum and by the appearance of two peaks at 125.8 (*C-15*) and 140.4 ppm (*C-14*) in the ^{13}C NMR spectrum.

Additionally, three signals are shifted downfield in the ^{1}H NMR spectra of the final HDLDBC when compared with the spectra of its two precursors. Thus, the signal corresponding to the protons in the α-position of the triazole rings belonging to the linear polymeric part (*H-13*) is shifted from 4.72 to 5.30 ppm. With respect to the dendritic part, the signals corresponding to the protons in the α- and β-positions of the triazole rings (*H-16* and *H-17*) are shifted from 3.20 and 1.65 to 4.45 and 1.95 ppm, respectively. The other signals are not modified after the click chemistry reaction.

The characteristic bands of the two *bis*-GMPA dendrons and of the central linear Pluronic® F-127 can be observed in the FTIR spectrum of **$(NH_3^+Cl^-)_8$ *bis*GMPA-PLU-*bis*GMPA $(NH_3^+Cl^-)_8$** (**figure C$_4$-26**).

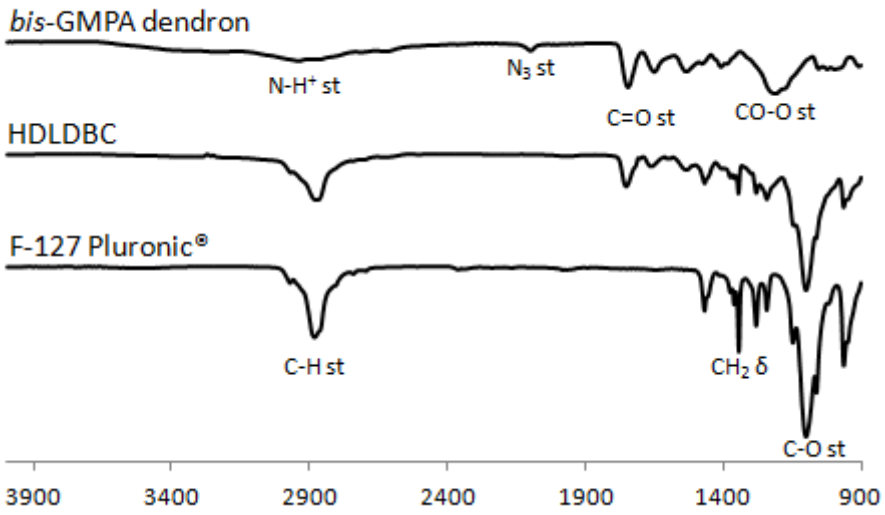

Figure C$_4$-26: FTIR spectra of the 2nd generation *bis*-GMPA dendron (up), the HDLDBC (middle) and the F-127 Pluronic® (down).

The presence of the central Pluronic® F-127 polyether was asserted by the intense band at 1101 cm^{-1} that corresponds to the C-O bonds, and the two intense bands at 2881 and 1344 cm^{-1} corresponding to the C-H bonds. The presence of the poly(esteramide) *bis*-GMPA dendrons was confirmed by the appearance of two bands at 1755 and 1664 cm^{-1} which correspond to the carbonyl groups. The band corresponding to the stretching of the $N\text{-}H^{+}$ bond is difficult to observe in this polymer because it appears as a broad band. Additionally, the band corresponding to the azide group near 2100 cm^{-1} is no longer observed in the HDLDBC spectrum proving the formation of the triazole moiety between the Pluronic® and the two *bis*-GMPA dendrons.

SEC was performed for **$(NHBoc)_8$*bis*GMPA-PLU-*bis*GMPA$(NHBoc)_8$** and its corresponding precursors in THF (**figure C_4-27**).

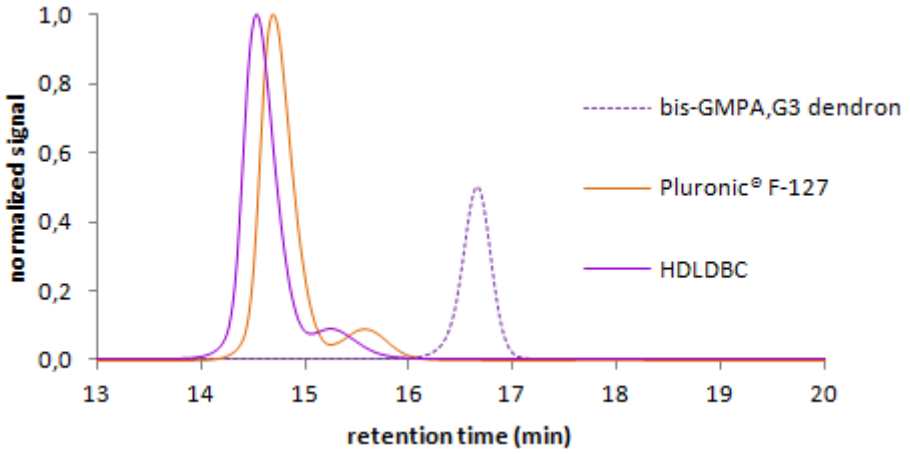

Figure C_4-27: SEC spectra of the starting dendron of 3rd generation of *bis*-GMPA, the commercial Pluronic® F-127 and of the intermediate HDLDBC.

Two peaks, the first one being really more intense than the second one, are observed in the chromatogram of both, the commercial Pluronic® F-127 and the HDLDBC, showing the polydispersity of these compounds. Nevertheless, the correct functionalization of the Pluronic® by the dendrons could be asserted as the two peaks corresponding to the HDLDBC show both lower retention time in comparison with the two peaks of the starting Pluronic® F-127. Additionally, no peak corresponding to residual free *bis*-GMPA dendron can be observed.

4.2.2- Self-assembly in water

Both, the Janus dendrimers and HDLDBCs have been designed to exhibit **amphiphilic character**. Indeed, the Janus dendrimers consist of a lipophilic *bis*-MPA dendron and a hydrophilic *bis*-MPA or *bis*-GMPA dendrons; and the HDLDBCs consist of a central lipophilic block of polypropylene oxide (PPO) and two blocks of polyethylene oxide (PEO) that were linked to *bis*-MPA or *bis*-GMPA hydrophilic dendrons at their terminal position.

The different nature of the blocks can trigger spontaneous self-assembly in water. The poor affinity of the lipophilic block for the external aqueous medium favors intermolecular lipophilic interactions leading to the formation of lipophilic domains surrounded and stabilized by hydrophilic ones. A large variety of different structures can be obtained such as micelles, vesicles, lamellar and sponge phases, etc.[109]

[109] B.N.S. Thota *et al.*, *Chem. Rev.*, **2016**, 116, 2079-2102.

4.2.2.1- Amphiphilic Janus dendrimers

Self-assembly processes

The self-assembly in water of all the Janus dendrimers was carried out using the oil-in-water technique (**figure C_4-28**).[95] According to this method, the Janus dendrimers were first dissolved into dichloromethane, and then an appropriate amount of distilled water was added. The aqueous and organic phases were mixed by vigorous stirring forming an emulsion from which the dichloromethane was slowly evaporated using a ventilation system. When all the dichloromethane was evaporated, a clearly and transparent aqueous solution containing the dendritic nanoaggregates was obtained.

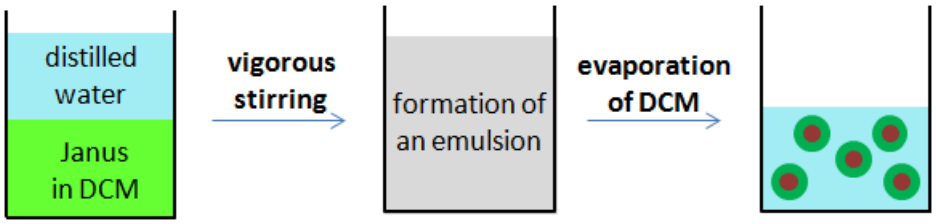

Figure C_4-28: Schematic representation of the formation of the nanoaggregates by self-assembling of the Janus dendrimers using the oil-in-water technique.

[95] J. Movellan, P. Urbán *et al.*, *Biomaterials*, **2014**, 35, 7940.

Critical aggregation concentration (CAC)

The critical aggregation concentration (CAC) in distilled water was determined using **nile red as a solvatochromic fluorophore**.[191] The fluorescence intensity of nile red is low in a hydrophilic environment and high in a lipophilic environment.

Below the CAC, the nile red is located in water and presents weak fluorescence intensity (λ_{max} = 653 nm). In contrast, above the CAC, nile red migrates to the lipophilic inner part of the aggregates and presents an intense fluorescence emission (λ_{max} ≈ 630 nm). Hence, the CAC can be determined by drawing the fluorescence intensity of nile red as a function of the amphiphile concentration. The change of the curve slope corresponds to the beginning of lipophilic domains formation, *i.e.* the CAC.

Figure C_4-29 gathers the plots corresponding to all the dendrimers. An **abrupt change** of the curve slope is observed in each case allowing the determination of the CAC for all the dendrimers (**table C_4-3**).

[191] M.C.A. Stuart, J.C. van de Pas, J.B.F.N. Engberts, The use of Nile Red to monitor the aggregation behavior in ternary surfactant–water–organic solvent systems, *J. Phys. Org. Chem.*, **2005**, 18, 929-934.

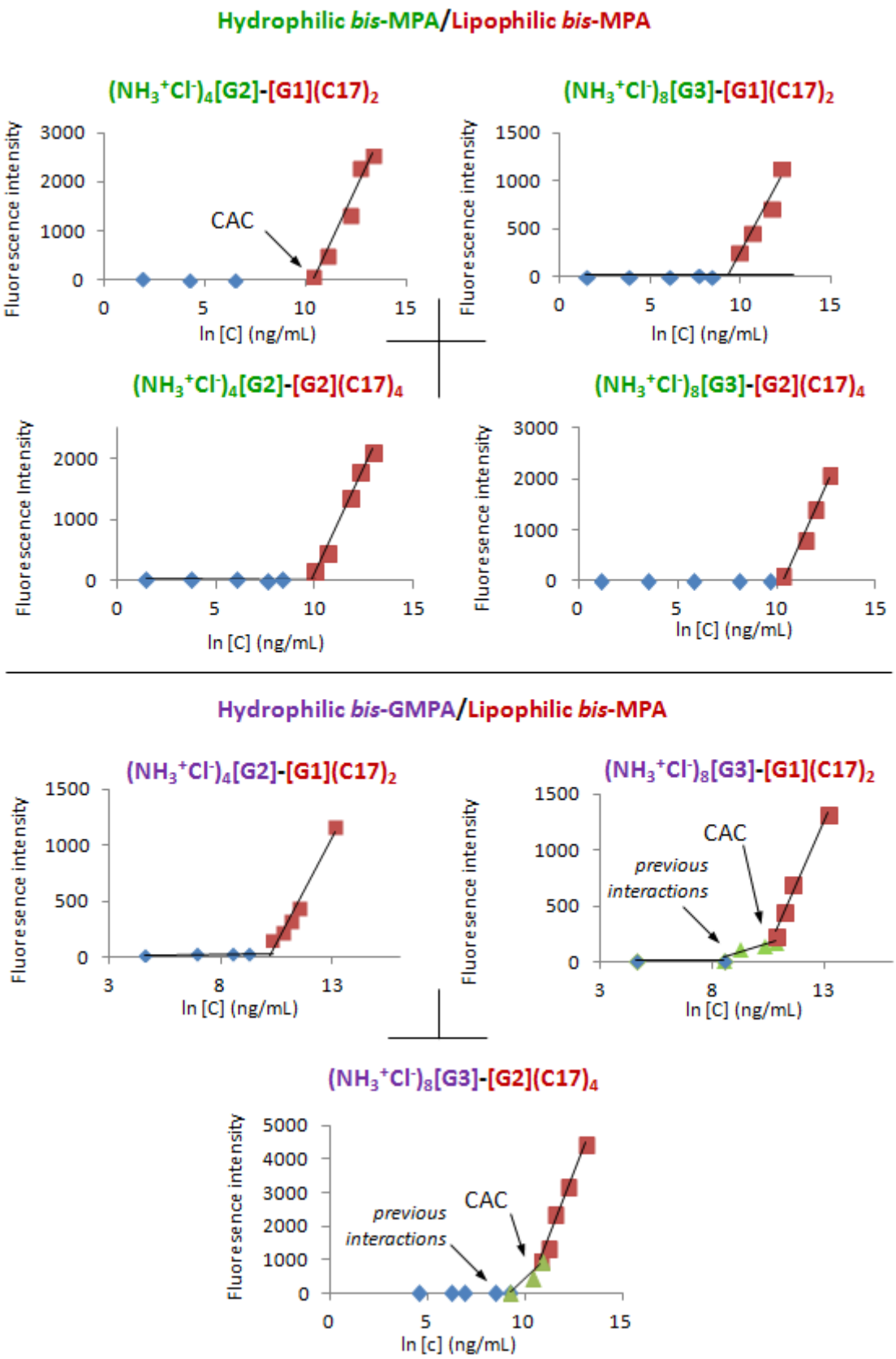

Figure C_4-29: Determination of the CAC employing the nile red technique for the Janus dendrimers.

Table C_4-3: Critical aggregation concentration (CAC) of the Janus dendrimer in distilled water given in mg/mL and in mol/L.

	Janus dendrimer	CAC (mg/mL)	CAC (mol/L)
***bis*-MPA / *bis*-MPA**	$(NH_3^+Cl^-)_4$[G2]-[G1]$(C17)_2$	$5.2 \cdot 10^{-2}$	$3.3 \cdot 10^{-5}$
	$(NH_3^+Cl^-)_8$[G3]-[G1]$(C17)_2$	$2.6 \cdot 10^{-2}$	$1.1 \cdot 10^{-5}$
	$(NH_3^+Cl^-)_4$[G2]-[G2]$(C17)_4$	$4.4 \cdot 10^{-2}$	$1.9 \cdot 10^{-5}$
	$(NH_3^+Cl^-)_8$[G3]-[G2]$(C17)_4$	$9.8 \cdot 10^{-2}$	$3.1 \cdot 10^{-5}$
***bis*-GMPA / *bis*-MPA**	$(NH_3^+Cl^-)_4$[G2]-[G1]$(C17)_2$	$2.8 \cdot 10^{-2}$	$1.7 \cdot 10^{-5}$
	$(NH_3^+Cl^-)_8$[G3]-[G1]$(C17)_2$	$2.8 \cdot 10^{-2}$	$1.0 \cdot 10^{-5}$
	$(NH_3^+Cl^-)_8$[G3]-[G2]$(C17)_4$	$4.3 \cdot 10^{-2}$	$1.3 \cdot 10^{-5}$

All the Janus dendrimers present a CAC near 2×10^{-5} mol/L regardless the nature of the hydrophilic dendron and the different dendron generations. Interestingly, in the case of the ***bis*-GMPA/*bis*-MPA** Janus dendrimers bearing the hydrophilic dendron of the 3rd generation a previous smooth change of the curve slope is observed at lower concentrations, 8.7×10^{-7} mol/L for $(NH_3^+Cl^-)_8$ [*bis*GMPA,G3]-[*bis*MPA,G1]$(C17)_2$ and 3.0×10^{-6} mol/L for $(NH_3^+Cl^-)_8$ [*bis*GMPA,G3]-[*bis*MPA,G2]$(C17)_2$ (**figure C_4-29**). They indicate that two different aggregation processes must exist for these derivatives. Nevertheless, if the abrupt curve slope changes correspond to the formation of aggregates with a sufficiently extended lipophilic domain to encapsulate big amount of nile red, defined as the CAC, further investigation is needed to determine what type of lipophilic interactions between nile red and the dendrimers, or some dendritic aggregates, can take place at these lower concentrations.

Transmission electron microscopy (TEM)

The morphology and the size of the aggregates were investigated using transmission electron microscopy (TEM) at the concentration of 1 mg/mL (above the CAC) (**figure C_4-30 and table C_4-4**). Regarding the ***bis*-MPA/*bis*-MPA** series, the morphology of the aggregates depends on the generation of the lipophilic dendron. The 1st generation dendron promotes **spherical micelles** with an average size about 14.5 ± 3.9 nm for **$(NH_3^+Cl^-)_4$[*bis*MPA,G2]-[*bis*MPA,G1](C17)$_2$** and about 15.5 ± 4.0 nm for **$(NH_3^+Cl^-)_8$[*bis*MPA,G3]-[*bis*MPA,G1](C17)$_2$**. The lipophilic dendron of 2nd generation gives rise to aggregates with a bilayer morphology. When it is combined with the hydrophilic dendron of 2nd generation, **$(NH_3^+Cl^-)_4$[*bis*MPA,G2]-[*bis*MPA,G2](C17)$_4$**, stacked **rigid bilayers** with an average width of 5 nm are observed. When it is linked to the hydrophilic dendron of 3rd generation, **$(NH_3^+Cl^-)_8$[*bis*MPA,G3]-[*bis*MPA,G2](C17)$_4$**, **vesicles and flexible bilayers** are observed. The vesicles have an average diameter of 52.3 ± 11.9 nm and the bilayers have an average width of 7 nm.

With respect to the ***bis*-GMPA/*bis*-MPA** series, micelles were observed in all cases. The Janus dendrimers bearing the small lipophilic dendron form **spherical micelles** with an average size of 13.1 ± 3.6 nm for **$(NH_3^+Cl)_4$ [*bis*GMPA,G2]-[*bis*MPA,G1](C17)$_2$** and 14.6 ± 3.1 nm for **$(NH_3^+Cl^-)_8$ [*bis*GMPA,G3]-[*bis*MPA,G1](C17)$_2$**. The Janus dendrimer bearing the biggest lipophilic dendron, **$(NH_3^+Cl^-)_8$[*bis*GMPA,G3]-[*bis*MPA,G2](C17)$_4$**, forms a mixture of **spherical and ovoidal micelles** with a bigger size, around 18.8 ± 5.6 nm.

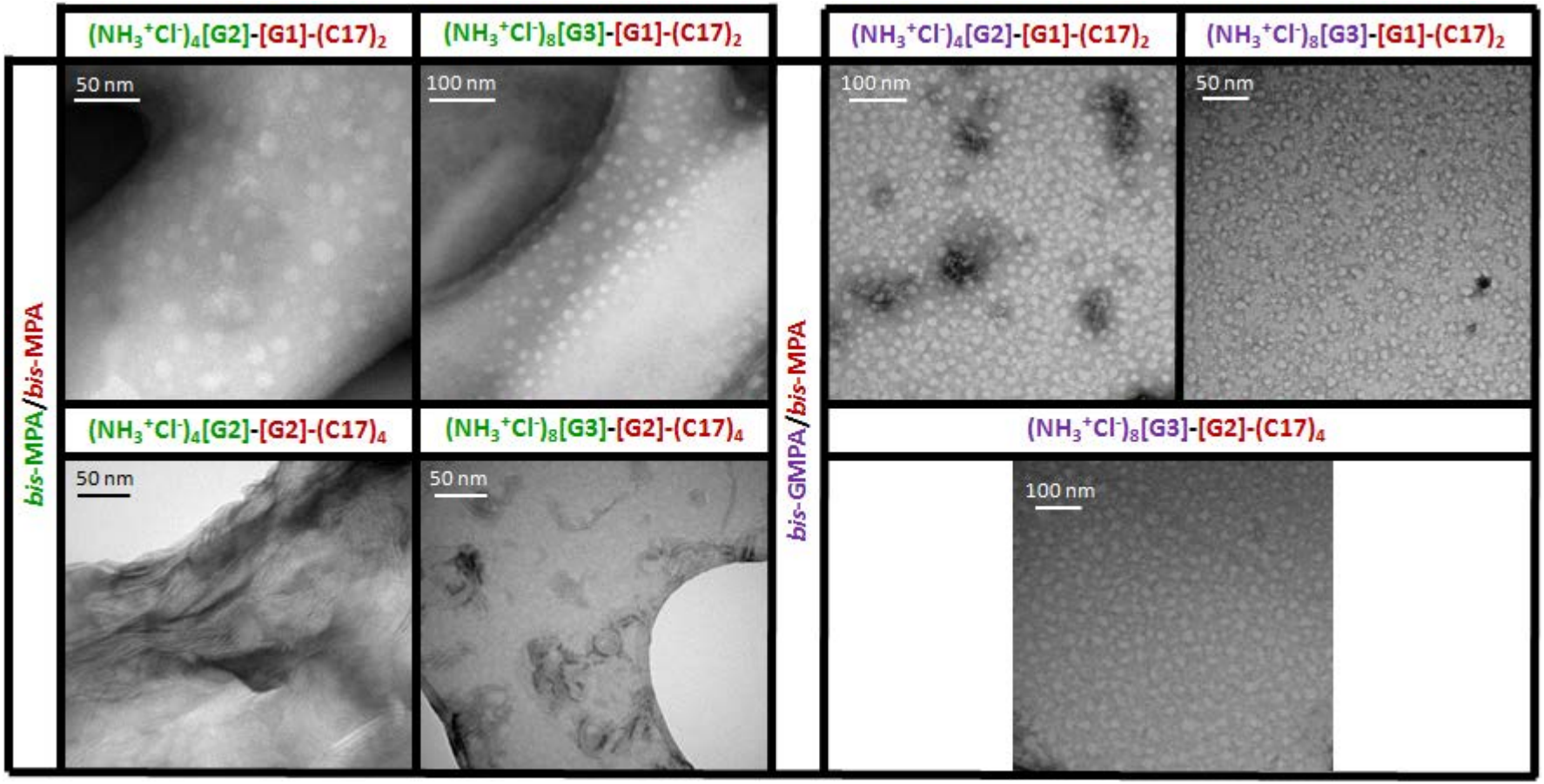

Figure C_4-30: TEM images of the two series of Janus dendrimers at 1.00 mg/mL.

In general the **size of the lipophilic dendron** appeared as the main factor that **determined the morphology** of the final aggregates. For Janus dendrimers based on a 1st generation lipophilic dendron, spherical micelles with relatively similar sizes (between 13.1 and 15.5 nm) are observed, whereas for Janus dendrimers based on a 2nd generation lipophilic dendron, aggregates with variable morphologies are visible. Using this last dendron, a mixture of spherical and ovoidal micelles are observed when it is linked to the 2nd generation *bis*-GMPA dendron (H/L =3.5), a mixture of flexible bilayers and vesicles are observed when it is linked to the 3rd generation *bis*-MPA dendron (H/L =2) and rigid bilayers that tend to stack are formed when it is linked to the 2nd generation *bis*-MPA dendron (H/L =1). The less hydrophilic is the final Janus dendrimer, the larger the lipophilic domains inside the aggregates are.[157]

[157] E. Fedeli *et al.*, *New. J. Chem.*, **2015**, 39, 1960.

Cryogenic transmission electron microscopy (cryoTEM)

The morphology and the size of the aggregates formed by the Janus dendrimers were also investigated using cryogenic transmission electron microscopy (cryoTEM) at the same concentration of 1 mg/mL (**figure C_4-31** and **table C_4-4**). CryoTEM permits to observe the aggregates as they are in aqueous solution, since the liquid sample is not dried but directly and quickly cryogenized employing liquid ethane before observation.

In almost all the cases, two size-population distributions are observed in cryoTEM images: small aggregates with sizes ranged from 20 to 60 nm that should correspond to the micelles, bilayers and/or vesicles observed in TEM together with bigger spherical aggregates with sizes around 200 nm that must be due to self-aggregation. **$(NH_3^+Cl^-)_4$[*bis*MPA,G2]-[*bis*MPA,G1](C17)$_2$** and **$(NH_3^+Cl^-)_8$[*bis*MPA,G3]-[*bis*MPA,G1](C17)$_2$** show aggregates with sizes near 20 nm which correspond to micelles. **$(NH_3^+Cl^-)_8$[*bis*MPA,G3]-[*bis*MPA,G2](C17)$_4$** shows spherical aggregates with diameters close to 60 nm and smaller aggregates with sizes near 20. Finally, in the case of **$(NH_3^+Cl^-)_4$ [*bis*MPA,G2]-[*bis*MPA,G2](C17)$_4$**, only the biggest aggregates are observed; they present either a spherical shape or a more distorted shape which is coherent with the TEM image where the rigid bilayers appear stacked between themselves into bigger structures.

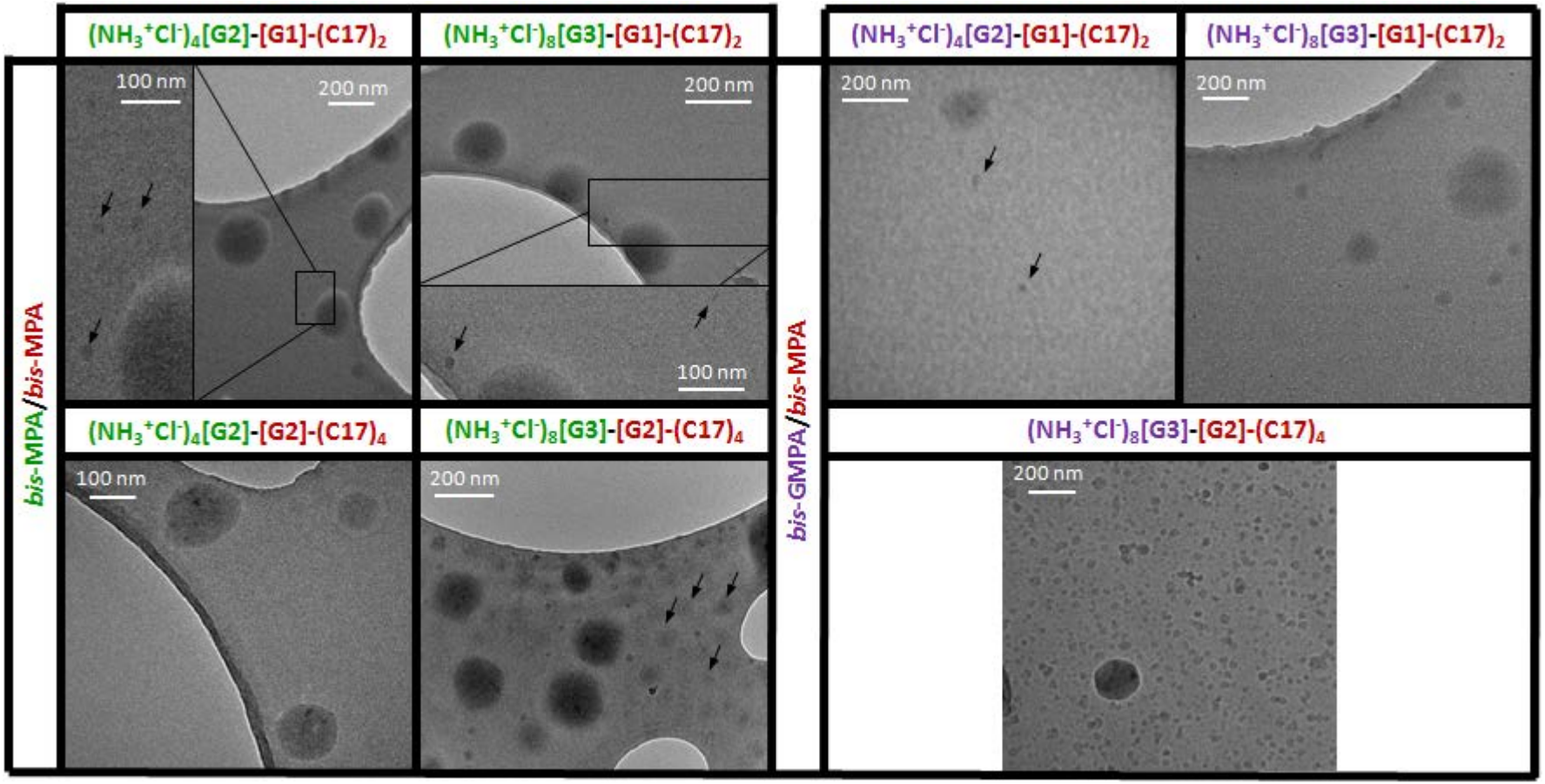

Figure C_4-31: CryoTEM images of the two series of Janus dendrimers at 1.00 mg/mL. The smallest aggregates (micelles, bilayers or vesicles) can be marked with black arrows.

In the case of the **bis-GMPA/bis-MPA** series, two size-population distributions are also observed. **$(NH_3^+Cl^-)_4$[*bis*GMPA,G2]-[*bis*MPA,G1](C17)$_2$** shows small spherical aggregates with sizes near 30 nm and bigger ones with sizes around 150 nm. **$(NH_3^+Cl^-)_8$[*bis*GMPA,G3]-[*bis*MPA,G1](C17)$_2$** forms spherical aggregates with sizes between 20 and 50 nm and bigger ones with sizes between 150 and 500 nm. **$(NH_3^+Cl^-)_8$[*bis*GMPA,G3]-[*bis*MPA,G2](C17)$_4$** forms small spherical aggregates with size between 20 and 50 nm and bigger ones with sizes around 200 nm.

Dynamic light scattering (DLS)

The size of the hydrodynamic volume of the aggregates was measured by dynamic light scattering (DLS), technique that is only valid for spherical aggregates. When possible, the results were treated employing two mathematical approaches: the number average data and the intensity average data. The intensity average data are more sensitive to the largest particles whereas the number average data are more sensitive to the smallest particles. The results are gathered in the table **C_4-4** together with the sizes previously measured in TEM and cryoTEM images.

As observed before in cryoTEM, two size-population distributions were measured in the samples: small particles and bigger ones.

With regard to the number average data treatment, sizes comprised between 1.0 and 3.2 nm were determined for the dendrimers bearing the 1st generation *bis*-MPA lipophilic dendron, **$(NH_3^+Cl^-)_4$[*bis*MPA,G2]-[*bis*MPA,G1]$(C17)_2$**, **$(NH_3^+Cl^-)_8$[*bis*MPA,G3]-[*bis*MPA,G1]$(C17)_2$**, **$(NH_3^+Cl^-)_4$[*bis*GMPA,G2]-[*bis*MPA,G1]$(C17)_2$** and **$(NH_3^+Cl^-)_8$[*bis*GMPA,G3]-[*bis*MPA,G1]$(C17)_2$**. These small particles should correspond to the spherical micelles observed in TEM and cryoTEM. In the case of the dendrimers bearing the 2nd generation *bis*-MPA lipophilic dendron, some major difference were observed between the 3 different dendrimers as previously observed in TEM and cryoTEM. The size calculated for the **$(NH_3^+Cl^-)_8$[*bis*GMPA,G3]-[*bis*MPA,G2]$(C17)_4$** aggregates is about 7.8 nm with a higher polydispersity. This difference can be related to the less spherical shape of the micelles, as observed by TEM. The size calculated for **$(NH_3^+Cl^-)_8$[*bis*MPA,G3]-[*bis*MPA,G2]$(C17)_4$** is bigger, near 62.9 nm, which is relatively close to the size of the vesicles measured in TEM and cryoTEM.

Table C_4-4: Morphology and size of the aggregates formed by the amphiphilic Janus dendrimers determined by TEM, cryoTEM and DLS (with number and data average treatments).

	Janus dendrimer	TEM		DLS number	cryoTEM		DLS intensity
		shape	diameter /width	D_H	shape	size	D_H
bis-MPA / *bis*-MPA	$(NH_3^+Cl^-)_4$[G2]-[G1](C17)$_2$	spherical micelles	14.5 ± 3.9 nm	3.2 ± 0.0 nm	spherical	*ca.*20 nm & 200 nm	95.6 ± 25.6 nm
	$(NH_3^+Cl^-)_8$[G3]-[G1](C17)$_2$	spherical micelles	15.5 ± 4.0 nm	1.1 ± 0.1 nm	spherical	*ca.*20 nm & 200 nm	87.8 ± 26.9 nm
	$(NH_3^+Cl^-)_4$[G2]-[G2](C17)$_4$	rigid bilayers	5 nm	*no spherical aggregates*	spherical & ill-defined	*ca.*200 nm	579.5 ± 77.8 nm
	$(NH_3^+Cl^-)_8$[G3]-[G2](C17)$_4$	vesicles & flexible bilayers	52.3 ± 11.9 & 7 nm	62.9 ± 0.6 nm	spherical	*ca.*20-60 nm & 200 nm	340.4 ± 149.9 nm
bis-GMPA / *bis*-MPA	$(NH_3^+Cl^-)_4$[G2]-[G1](C17)$_2$	spherical micelles	13.1 ± 3.6 nm	2.6 ± 0.4 nm	spherical	*ca.*30 nm & 150 nm	208.2 ± 120.0 nm
	$(NH_3^+Cl^-)_8$[G3]-[G1](C17)$_2$	spherical micelles	14.6 ± 3.1 nm	1.0 ± 0.1 nm	spherical	*ca.*20-50 nm & 100-500 nm	159.4 ± 63.1 nm
	$(NH_3^+Cl^-)_8$[G3]-[G2] (C17)$_4$	spherical & ovoidal micelles	18.8 ± 5.6 nm	7.8 ± 1.4 nm	spherical	*ca.*20-50 nm & 200 nm	260.1 ± 163.0 nm

With respect to the intensity data treatment, bigger aggregates with high polydispersity were detected. These bigger aggregates should correspond to the micellar and bilayered aggregates observed in cryoTEM formed by self-aggregation of various micelles, vesicles and/or bilayers.[192]

As a general trend, it can be noticed that the size and the polydispersity is lower for the ***bis*-MPA/*bis*-MPA** series than for the ***bis*-GMPA/*bis*-MPA** series.

[192] Y. Hed, Y. Zhang, O.C.J. Andrén, X. Zeng, A.M. Nyström, M. Malkoch, Side-by-side comparison of dendritic-linear hybrids and their hyperbranched analogs as micellar carriers of chemotherapeutics, *J. Polym. Sci. Pol. Chem.*, **2013**, 51, 3992-3996.

Overview

Amphiphilic ***bis*-MPA/*bis*-MPA** and ***bis*-GMPA/*bis*-MPA** Janus dendrimers can self-assemble in water forming aggregates with different morphologies. According to the generation of the lipophilic *bis*-MPA dendron, it is possible to design the final morphology of the nanostructures. Employing the lipophilic dendron of 1st generation, spherical micelles are always obtained. In contrast, employing the lipophilic dendron of 2nd generation, micelles, vesicles and flexible or rigid bilayers can be obtained depending on the hydrophilic dendron nature and generation (**figure C_4-32**). Additionally, in all cases, bigger aggregates are observed. They are ascribed to the self-aggregation of various particles.

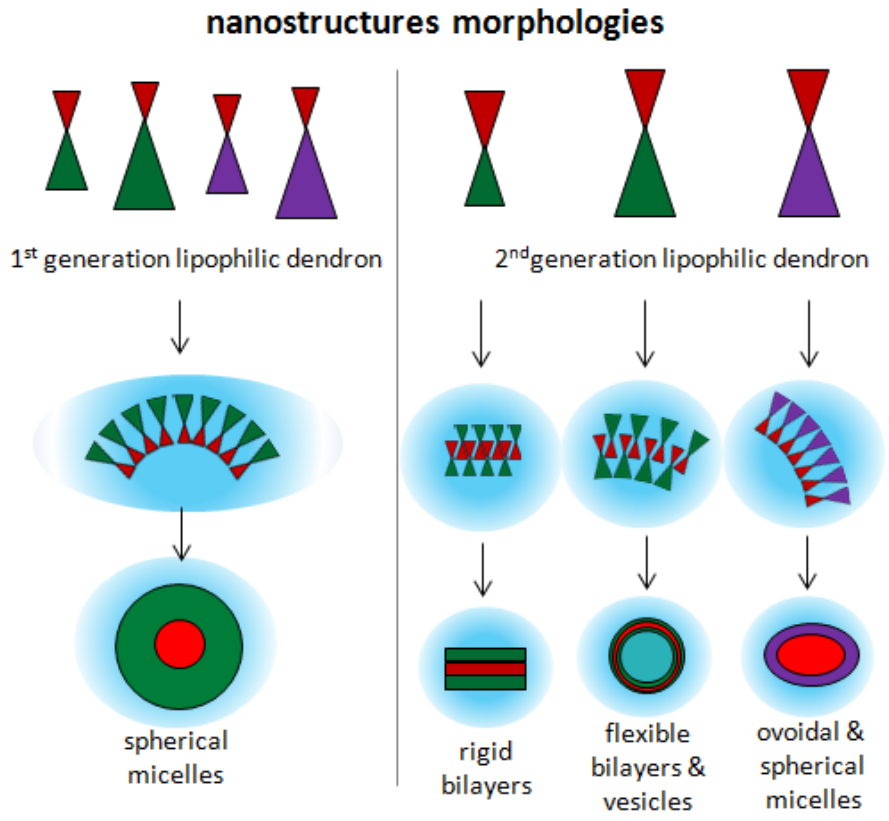

Figure C_4-32: Schematic representation of the amphiphilic Janus dendrimer self-assembly in water.

4.2.2.2- Hybrid sendritic-linear-dendritic block copolymers

Self-assembly process

The two HDLDBCs are formed by Pluronic® F-127, a thermoresponsive amphiphilic tri-block copolymer and hydrophilic *bis*-MPA and *bis*-GMPA dendrons. In this case, micelles can be spontaneously formed by solubilizing the solid HDLDBCs in water at 4ºC and slowly heating their solution to room temperature (**figure C_4-33**).[193]

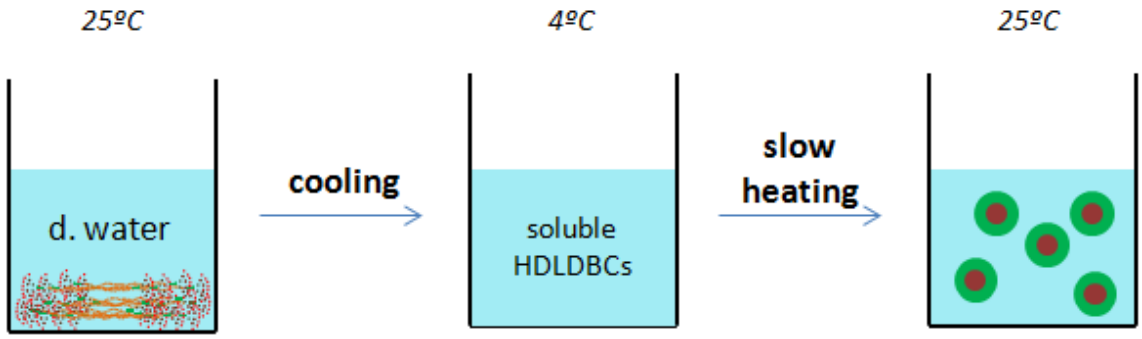

Figure C_4-33: Formation of the micelles by the HDLDBCs by slow heating to room temperature.

Critical aggregation concentration (CAC)

The critical aggregation concentrations were determined for the two HDLDBCs using the nile red fluorophore as it was carried out before for the amphiphilic Janus dendrimers (**figure C_4-34**).

[193] I. Jiménez-Pardo, Hidrogeles termosensibles y fotopolimerizables derivados de Pluronic® para aplicaciones biomédicas, **2014**, Univerisdad de Zaragoza.

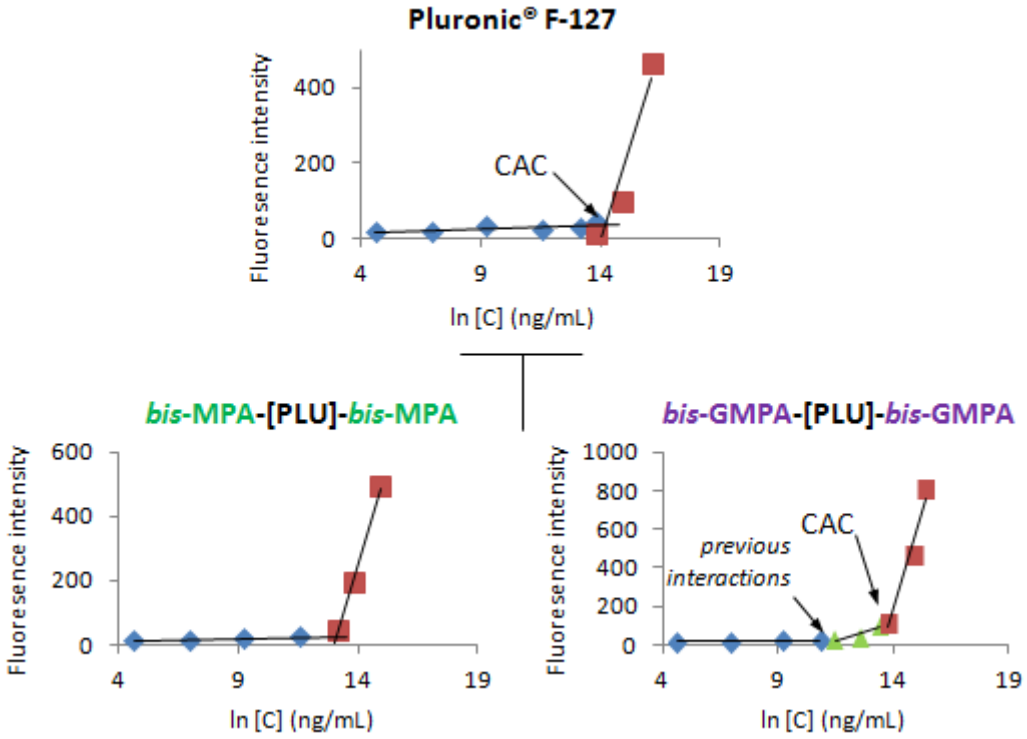

Figure C_4-34: Determination of the CAC employing the nile red technique for the HDLDCs and the commercial Pluronic® F-127.

Pluronic® F127 and the HDLDBC derivatives, show an abrupt change of the curve slope that corresponds to the CAC (**table C_4-5)**. The CACs are lower for the two HDLDBCs in comparison with the commercial F-127 Pluronic®. As observed for some Janus dendrimers, the *bis*-GMPA based HDLDBC shows a previous smooth change in the curve slope at 7.1 x 10^{-6} mol/L that must correspond to lipophilic interactions between nile red and the HDLDC previous to the micelle formation although further investigation is required to fully study this phenomenon.

Table C_4-5: CAC of the Janus dendrimer in distilled water in mg/mL and in mol/L.

Pluronic® derivatives	CAC	
	(mg/mL)	(mol/L)
F-127	1.4	1.1 x 10^{-4}
***bis*MPA-[PLU]-*bis*MPA**	0.5	2.9 x 10^{-5}
***bis*GMPA-[PLU]-*bis*GMPA**	1.0	6.1 x 10^{-5}

Transmission electronic microscopy (TEM) and cryogenic transmission electron microscopy (cryoTEM)

The morphology and the size of the aggregates formed by the HDLDBCs in water at room temperature were studied by TEM and cryoTEM at a concentration of 1.0 mg/mL, which is superior to the CAC (**figure C_4-35**).

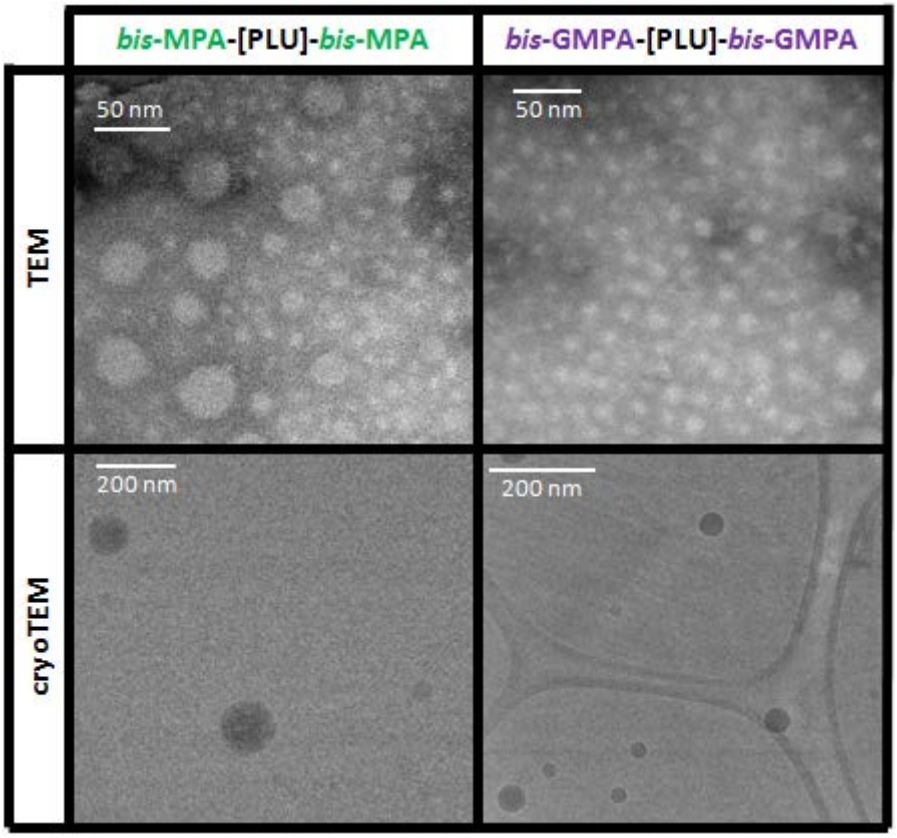

Figure C_4-35: TEM and cryoTEM images of the two HDLDBCs at 1.0 mg/mL in water at room temperature.

Spherical micelles were observed in TEM and cryoTEM images for both HDLDBCs. TEM images show polydisperse micelles for the ***bis*MPA-[PLU]-*bis*MPA** with an average size around 18.7 ± 5.9 nm, whereas monodisperse micelles appear for the ***bis*GMPA-[PLU]-*bis*GMPA**, with an average size around 13.4 ± 2.5 nm. CryoTEM images reveal micelles with two size-population distributions in the case of ***bis*MPA-[PLU]-*bis*MPA**, small micelles with sizes around 60 nm and bigger aggregates with sizes near 150 nm. In the case of ***bis*GMPA-[PLU]-*bis*GMPA**, only one size-population distribution of micelles is observed with sizes in the range of 40 and 70 nm.

Dynamic light scattering (DLS)

The hydrodynamic diameter of the aggregates was also measured employing the dynamic light scattering technique. As Pluronic® F-127 is a thermosensitive polymer,[185a] DLS measurements were carried out at different temperatures, *i.e.* 25, 37 and 45ºC to observe the effect of temperature changes on the size of the aggregates. The results were treated employing two mathematical approaches: intensity average data and number average data (**table C_4-6**).

Table C_4-6: Hydrodynamic diameter of the aggregates measured with DLS according to two different mathematical data approaches (in number and in intensity).

	Pluronic® F-127		
	25ºC	37ºC	
number	4.89 ± 1.3 (100%)	18.4 ± 4.4 (100%)	
intensity	7.8 ± 2.6 (70%) 159.6 ± 96.2 (16%)	25.7 ± 6.7 (100%)	
	***bis*MPA-[PLU]-*bis*MPA**		
	25ºC	37ºC	45ºC
number	20.8 ± 5.6 (67%) 124.8 ± 54.2 (33%)	23.1 ± 4.5 (100%)	16.2 ± 5.1 (100%)
intensity	27.2 ± 3.6 (7%) 222.8 ± 79.5 (90%)	27.5 ± 5.0 (33%) 141.6 ± 25.5 (67%)	21.4 ± 7.3 (29%) 90.3 ± 38.1 (71%)
	***bis*GMPA-[PLU]-*bis*GMPA**		
	25ºC	37ºC	45ºC
number	143.8 ± 56.2 (100%)	24.4 ± 5.6 (100%)	21.6 ± 4.9 (100%)
intensity	224.8 ± 88.9 (96%)	31.7 ± 8.2 (13%) 208.6 ± 65.0 (87%)	25.8 ± 5.6 (18%) 169.7± 42.3 (82%)

At 25 and 37ºC, the aggregates formed by the two HDLDBCs are bigger (more than 100 nm) than the aggregates formed by Pluronic® F-127. Thus, the

[185a] A.V. Kabanov *et al.*, *J. Control. Release*, **2002**, 82, 189-212.

addition of the dendrons must favor the formation of micellar aggregates. Moreover, and as observed before in cryoTEM, two size distributions were measured at 25ºC in the case of ***bis*MPA-[PLU]-*bis*MPA** whereas only one size-population was measured in the case of ***bis*GMPA-[PLU]-*bis*GMPA**. Nevertheless, the diameters measured for the aggregates were always bigger when employing the DLS than when deduced from cryoTEM images.

When increasing the temperature, the average size of the aggregates decreases and the percentage of the smallest aggregates population increases. At higher temperature, polyethylene oxide (PEO) blocks are less hydrophilic and water starts to be expelled out of the hydrophilic shell. Consequently, the average particle-size decreases (**figure C_4-36**). This effect is more significant for the ***bis*MPA-[PLU]-*bis*MPA** than for ***bis*GMPA-[PLU]-*bis*GMPA** derivatives.

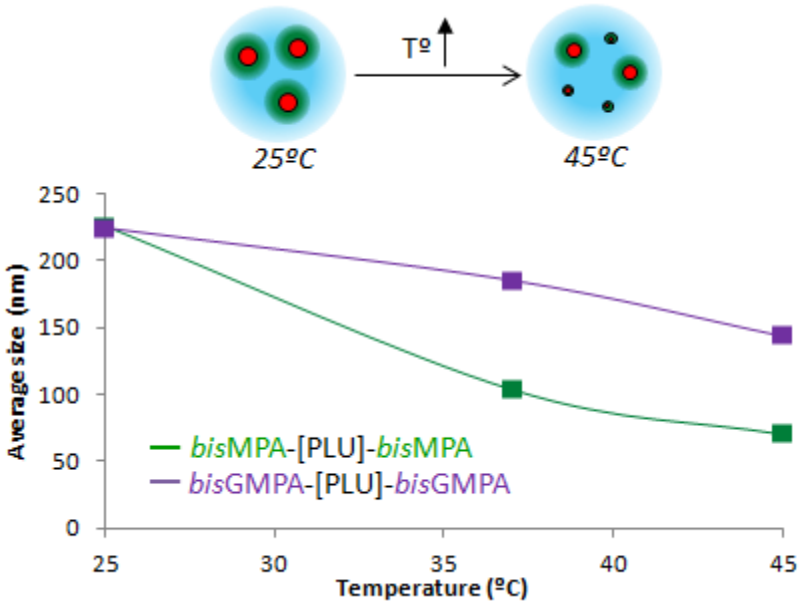

Figure C_4-36: Average particle size decrease of the HDLDBC aggregates when they are heated. The average size represented here was measured applying the intensity average data approach.

4.3- Amphiphilic Janus dendrimers and HDLDBCs as camptothecin nanocarriers

Hepatitis C is an infectious disease caused by the hepatitis C virus (HCV), an RNA virus. It may trigger chronic disorders that particularly affect the liver. HCV causes cirrhosis that might induce hepatocellular carcinoma, a malignant liver cancer. This disease affects between 150 and 200 million people (~3% of the world population) spread all over the globe. In Spain, it is estimated that around 480000 and 760000 people are infected by the virus (~1% of population). HCV is transferred *via* blood-to-blood contact, and the use of deficiently sterilized intravenous injection material is the main reason of HCV spreading.[194]

The hepatitis C viral infection can be effectively treated. A bi-therapeutic treatment based on Ribavirin, a large spectral antiviral drug, and interferons, proteins that defend the organism against pathogens were previously used. Nevertheless, this treatment is responsible for serious and numerous side effects. Patients usually suffer fevers, headaches, dry skin, hair lost, anemia, conjunctivitis, depressions, teratogenic complications, *etc*.

Recently, a variety of new antiviral treatments specific to hepatitis C virus has been developed: ledipasvir, sofosbuvir, paritaprevir, ombitasvir, dasabuvir. They inhibit the action of some HCV enzymes and can be used alone or in association with ribavirin and interferons. As they block specifically the activity of HCV enzymes, they are globally well tolerated by the patients. Moreover, they have shown a spectacular efficiency: near 90 % of the patients could be cured in some cases. However, their complex structure and HCV

[194] M. Bruguera, X. Forns, Hepatitis C in Spain, *Medicina Clínica*, **2006**, 127, 113-117.

specificity makes them challenging to investigate and produce and are highly sensitive to virus mutations. They are, therefore, highly expensive and their availability for the treatment of HCV infected people is restrained.[195]

Thus, in order to extend the library of anti-HCV drugs, in the Institute for Biocomputation and Physics of Complex Systems (BIFI) of the University of Zaragoza, Dr. Olga Abián, Dr. Adrián Velazquez-Campoy and collaborators started to investigate new alleosteric inhibitors of the NS3 protease, an enzyme that belongs to the HCV virus.[196] Whereas competitive inhibitors block the active site of enzymes, allosteric inhibitors interfere with the binding properties of enzymes. They bind the enzymes in a region different of their active site and induce conformational modifications that consequently block their activity. Allosteric inhibitors are generally less specific than competitive inhibitors, easier to synthesize and less sensitive to drug resistance. In this particular case, NS3 protease needs to be coordinated with Zn^{2+} ions and NS4A peptide to pass from an inactive form to the active one. The BIFI group looked for allosteric inhibitors that would increase the stability of the inactive form and would impede its transformation into the active form (**figure C_4-37**).

[195] a) G. Fanjul, E. Villanueva, Hepatitis C: el nuevo campo de batalla por el acceso a medicamentos esenciales, **2016**, ISGlobal, creative commons; b) J. Zhang, J.C. Garrison, L.Y. Poluektova, T.K. Bronich, N.A. Osna, Liver-targeted antiviral peptide nanocomplexes as potential anti-HCV therapeutics, *Biomaterials*, **2015**, 70, 37-47.

[196] a) O. Abián, S. Vega, J. Sancho, A. Velazquez-Campoy, Allosteric inhibitors of the NS3 protease from the hepatitis C virus, *PLoS ONE*, **2013**, 8, e69773; b) R. Clavería-Gimeno, S. Vega, V. Grazu, J.M. de la Fuente, A. Lanas, A. Velázquez-Campoy, O. Abián, Rescuing compound bioactivity in a secondary cell-based screening by using γ-cyclodextrin as a molecular carrier, *Int. J. Nanomedicine*, **2015**, 10, 2249-2259.

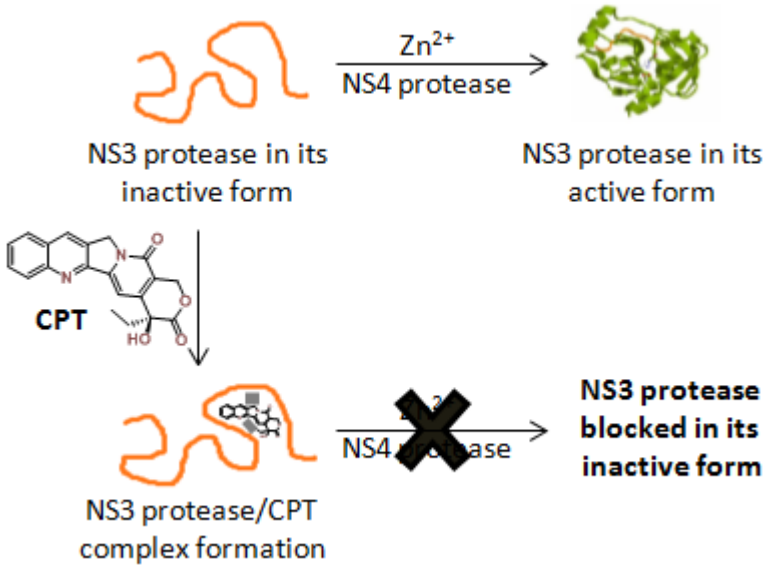

Figure C_4-37: Schematic representation of the allosteric inhibition of NS3 protease by camptothecin (CPT) drug.

Camptothecin (CPT) (**figure C_4-37**), a well-known versatile drug investigated in cancer and antiviral therapy,[197] showed a remarkable potential when used as an NS3 protease allosteric inhibitor.[196] This might convert it into an interesting alternative as anti-HCV drug with respect to the harmful and unspecific old HCV-treatments and to the specific and expensive new treatments. However, CPT presents some drawbacks that may hinder its future as an alternative anti-HCV drug:

- it is a low water-soluble drug; indeed, camptothecin is usually delivered during *in vitro* or *in vivo* experiments after dissolution into organic solvents such as ethanol or dimethyl sulfoxide,
- it is a cytotoxic drug that damages the DNA,
- it is unstable in the physiological serum, camptothecin contains a lactone ring that is spontaneously hydrolyzed at physiological pH turning down its activity.

[197] a) Y.Q. Liu, W.Q. Li, S.L. Morris-Natschke, K. Qian, L. Yang, G.X. Zhu, X.B. Wu, A.L. Chen, S.Y. Zhang, Z.L. Song, K.H. Lee, Perspectives on biologically active camptothecin derivatives, *Med. Res. Rev.*, **2015**, 35, 735-789; b) P. Pantazis, Z. Han, D. Chatterjee, J. Wyche, Water-insoluble camptothecin analogues as potential antiviral drugs, *J. Biomed. Sci.*, **1999**, 6, 1-7; c) A.L. Bodley AL, T.A. Shapiro, Molecular and cytotoxic effects of camptothecin, a topoisomerase I inhibitor, on trypanosomes and Leishmania, *Proc. Natl. Acad. Sci. U S A*, **1995**, 92, 3726-3730.

As a strategy to overcome these issues and improve its natural therapeutic abilities, camptothecin has already been encapsulated within various nanocarrier systems, among which dendritic systems represent a good alternative. For instance, the anticancer activity of CPT has been enhanced after its encapsulation within carbonated poly(glycerol succinic acid) dendrimers[198] and PAMAM dendrimers.[199] CPT was also covalently attached to dendritic structures based on poly-(*L*)-lysine[200] or polycarbamate.[201] Moreover, an interesting Janus dendrimer bearing folic acid moieties at one face and camptothecin drug at the other face was synthesized.[202] This dendrimer was still water soluble even after the covalent incorporation of 16 molecules of camptothecin.

The Liquid Crystals and Polymers Group (CLIP) of the University of Zaragoza had previously encapsulated camptothecin within different types of amphiphilic block copolymers. Linear amphiphilic Pluronic® F-127 triblock copolymer was functionalized at its extremities with two *bis*-MPA dendrons functionalized with acrylate groups, and the stability of the micelles across time was increased by photo-induced reticulation. Camptothecin water solubility was enhanced as well as its biocompatibility while its antiviral activity remained

[198] M.T. Morgan, Y. Nakanishi, D.J. Kroll, A.P. Griset, M.A. Carnahan, M. Wathier, N.H. Oberlies, G. Manikumar, M.C. Wani, M.W. Grinstaff, Dendrimer-encapsulated camptothecins: increased solubility, cellular uptake, and cellular retention affords enhanced anticancer activity in vitro, *Cancer Res.*, **2006**, 66, 11913-11921.

[199] S. Sadekar, G. Thiagarajan, K. Bartlett D. Hubbard, A. Ray L.D. McGill, H. Ghandehari, Poly(amido amine) dendrimers as absorption enhancers for oral delivery of camptothecin, *Int. J. Pharm.*, **2013**, 456, 175-185

[200] M.E. Fox, S. Guillaudeu, J.M.J. Fréchet, K. Jerger, N. Macaraeg, F.C. Szoka, Synthesis and in vivo antitumor efficacy of PEGylated poly(l-lysine) dendrimer−camptothecin conjugates, *Mol. Pharmaceutics*, **2009**, 6, 1562-1572.

[201] A. Gopin, S. Ebner, B. Attali, S. Doron, Enzymatic activation of second-generation dendritic Prodrugs: conjugation of self-immolative dendrimers with poly(ethylene glycol) via click chemistry, *Bioconj. Chem.*, **2006**, 17, 1432-1440

[202] X. Feng, J. Pinaud, E.L. Chaikof, D. Taton, Y. Gnanou, Sequential functionalization of janus-type dendrimer-like poly(ethylene oxide)s with camptothecin and folic acid, *J. Polym. Sci. A Polym. Chem.*, **2011**, 49, 2839-2849.

unaltered (**figure C_4-38**).[203] Also, a lipophilic polymethacrylate block bearing 2,6-diacylaminopyridine pendant units and a hydrophilic poly(ethylene glycol) block of two different molar masses, 2000 and 10000 provided block-copolymers that self-assembled in water forming spherical micelles with a lipophilic core and a hydrophilic shell. These micelles could encapsulate camptothecin and enhance its water solubility (**figure C_4-38**).[204]

Following this research line, camptothecin was chosen to be encapsulated within the different nanostructures formed by the amphiphilic Janus dendrimers and by the hybrid dendritic-linear-dendritic block copolymers (HDLDBCs), in order to investigated their potential as anti-HCV drug carriers. The lipophilic drug encapsulation abilities as well as the biocompatibility and antiviral activity of the encapsulated drug is discussed and related to the different nature and morphologies of the dendritic nanocarriers.

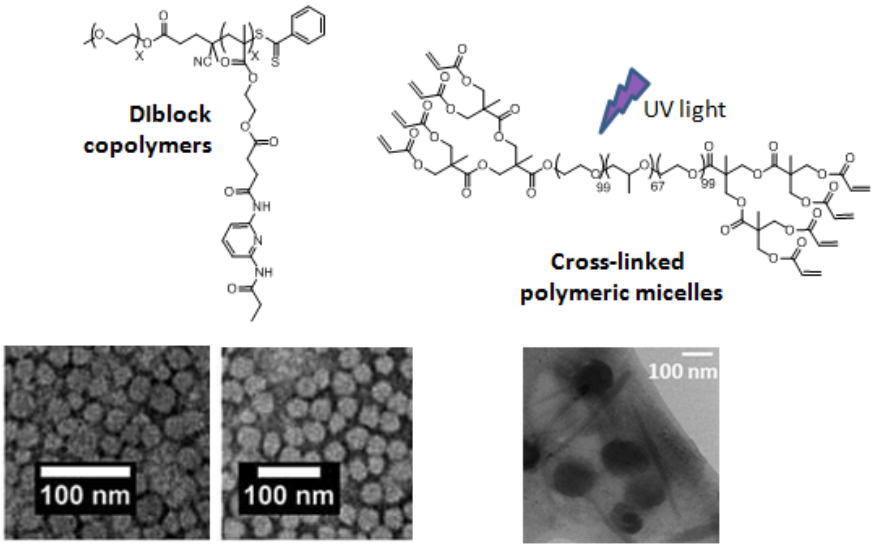

Figure C_4-38: Representation of the chemical structure of the amphiphiles and respective TEM images of the spherical micelles they formed in water, adapted from ref. [203] and [204].

[203] I. Jiménez-Pardo, R. González-Pastor, A. Lancelot, R. Clavería-Gimeno, A. Velázquez-Campoy, O. Abián, M.B. Ros, T. Sierra, Shell Cross-Linked Polymeric Micelles as Camptothecin Nanocarriers for Anti-HCV Therapy, *Macromol. Biosci.*, **2015**, 15, 1381-1391.

[204] Concellon, R. Clavería-Gimeno, A. Velázquez-Campoy, O. Abian, M. Pinol, L. Oriol, Polymeric micelles from block copolymers containing 2,6-diacylaminopyridine units for encapsulation of hydrophobic drugs, *RSC Adv.*, **2016**, 6, 24066-24075.

4.3.1- Nanocarrier/camptothecin conjugates

4.3.1.1- Camptothecin encapsulation

Camptothecin (CPT) was encapsulated within the nanostructures formed by the two types of dendritic derivatives, the Janus dendrimers and the hybrid dendritic-linear-dendritic block copolymers (HDLDBCs), employing the solvent diffusion technique (**figure C_4-39**).

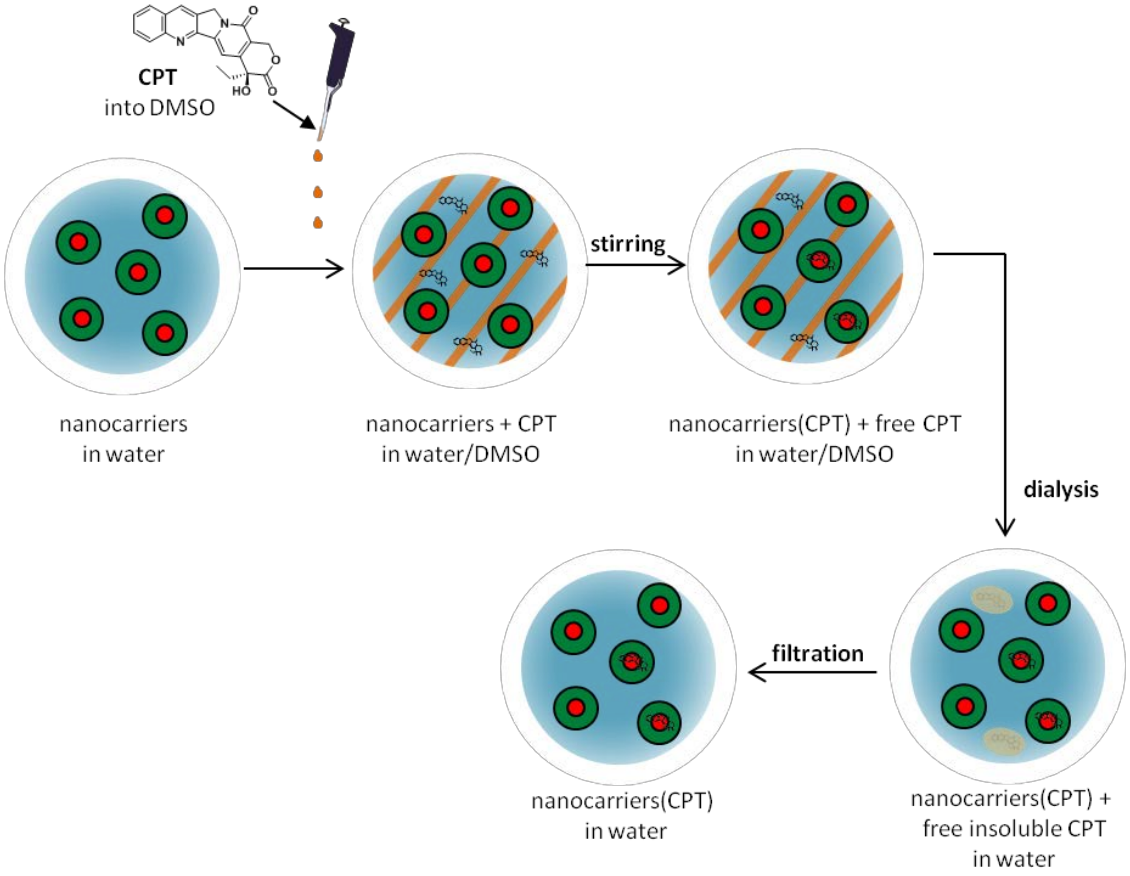

Figure C_4-39: Schematic drawing of the camptothecin (CPT) encapsulation process within the dendritic nanocarriers by the solvent diffusion technique.

The empty nanocarriers were prepared in distilled water using the solvent evaporation technique for the Janus dendrimers (see p. 138) and the slow heating procedure for the HDLDBCs derivatives (see p 152). Interestingly, the pH of the corresponding final aqueous solutions was acid, between 3.08 and

3.82.[a] At acidic pH, the equilibrium between the insoluble and active lactone form of camptothecin and its water soluble inactive sodium salt form is shifted to the lactone form, favoring the stability of the active form of the drug (**figure C_4-40**).[205]

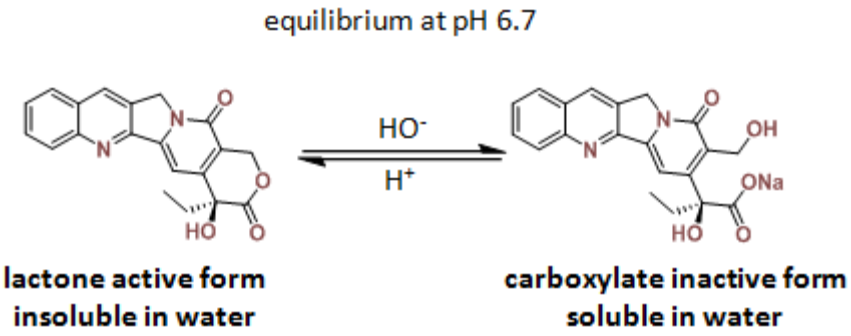

Figure C_4-40: equilibrium of the two forms of camptothecin in water.

A solution of camptothecin in dimethyl sulfoxide (DMSO) was added into the nanocarrier aqueous solutions. They were stirred overnight to let enter the drug inside the lipophilic core of the nanocarriers. Then, DMSO was removed by dialysis against distilled water. The drug that couldn't be encapsulated within the nanocarrier, insoluble in water, precipitated and it was removed by filtration. The amount of encapsulated drug was directly measured by fluorescence (see chapter 7 for detailed protocol).

Camptothecin was encapsulated within the dendritic nanocarriers at a feeding ratio of 0.1/1 ($w_{CPT}/w_{dend.}$). The final ratio of camptothecin encapsulated within the dendritic nanocarriers is given in weight and in mole in **table C_4-7** together with the corresponding encapsulation efficiencies.

[a] *cf.* chapter 7 to see the pH of each dendritic derivatives dissolution at 1 mg/mL in distilled water.

[205] Fassberg, V.J. Stella, A kinetic and mechanistic study of the hydrolysis of camptothecin and some analogues, *J. Pharm. Sci*., **1992**, 81 676-684.

Table C_4-7: Amount of camptothecin encapsulated within the dendritic nanocarriers. [a]*d*nc means dendritic nanocarrier and [b]EE means encapsulation efficiency; it was calculated by dividing the mass of camptothecin encapsulated within the dendritic nanocarriers by the mass of camptothecin added at the beginning of the encapsulation process. The aggregates morphology corresponds to TEM observations.

		Janus dendrimers					
		H/L	MW (g/mol)	aggregates morphology	mg CPT / mg *d*nc[a]	mol CPT / mol *d*nc[a]	EE[b] (%)
hydrophilic *bis*MPA / lipophilic *bis*MPA	**[G2]-[G1]**	2	1571	spherical micelles	0.014	0.0631	14
	[G3]-[G1]	4	2409	spherical micelles	0.013	0.0899	13
	[G2]-[G2]	1	2336	X	< 0.001	< 0.001	< 1
	[G3]-[G2]	2	3174	flexible bilayers	0.006	0.0547	6
hydrophilic *bis*GMPA / lipophilic *bis*MPA	**[G2]-[G1]**	3	1685	spherical micelles	0.061	0.295	60
	[G3]-[G1]	7	2752	spherical micelles	0.059	0.466	61
	[G3]-[G2]	3.5	3517	cylindrical micelles	0.054	0.546	54
		HDLDBCs					
		H/L	MW (g/mol)	aggregates morphology	mg CPT / mg *d*nc[a]	mol CPT / mol *d*nc[a]	EE[b] (%)
***bis*MPA-[PLU]-*bis*MPA**		≈ Plu. F-127	16 320	sph. & ovoidal micelles	0.029	1.361	29
***bis*GMPA-[PLU]-*bis*GMPA**			17 000	sph. & ovoidal micelles	0.046	2.24	46

Encapsulation efficiencies (EE) depends significantly on the nature of the hydrophilic dendron. The highest EE values, in the range of 54 and 61 %, correspond to ***bis*-GMPA/*bis*-MPA** Janus dendrimers series. The **HDLDBC** series also shows high encapsulation efficiency with values of 29 and 46 %. Finally, the ***bis*-MPA/*bis*-MPA** Janus dendrimers series show the lowest efficiency, < 15 %. In fact, the insertion of hydrophilic dendrons derived from *bis*-GMPA instead of

bis-MPA clearly increased the amount of camptothecin encapsulated inside the dendritic nanocarriers. This effect is very significant when comparing the two Janus dendrimer series, in which the amount of encapsulated camptothecin is more than 6 times higher when the *bis*-GMPA hydrophilic dendrons are used. It is also different for the two HDLDBCs, the HDLDBC bearing the two *bis*-GMPA dendrons encapsulates 1.5 times more CPT than the one bearing the two *bis*-MPA dendrons.

All the ***bis*-GMPA/*bis*-MPA** dendrimers can encapsulate similar amounts of **CPT** with negligible influence of their hydrophilic/lipophilic ratio (H/L) and size. In contrast, for the ***bis*-MPA/*bis*-MPA** dendrimers, the two dendrimers bearing the smallest lipophilic dendron could encapsulate higher amount of **CPT**, than the other two. Thus, the most lipophilic **$(NH_3^+Cl^-)_4$ [*bis*MPA,G2]-[*bis*MPA,G2]$(C17)_4$** (H/L =1) showed an EE below 1 % demonstrating its inability to form stable dendrimer/CPT conjugates in water.

The higher drug contents observed for the amphiphilic derivatives bearing the *bis*-GMPA hydrophilic dendron may be explained by the possible formation of favorable H-bonding interactions between the lactone, hydroxyl and ketone groups of the drug with the internal amide groups of the dendron.

3.3.1.2- Morphological studies

The size and the different morphologies of all the nanocarrier/**CPT** conjugates were investigated by TEM and cryoTEM together with DLS measurements.

Amphiphilic Janus dendrimer/CPT conjugates

Within the *bis*-MPA/*bis*-MPA series, TEM images (**figure C_4-41** and **table C_4-8**) show spherical micelles for **$(NH_3^+Cl^-)_4$[*bis*MPA,G2]-[*bis*MPA,G1]$(C17)_2$/CPT** and **$(NH_3^+Cl^-)_8$[*bis*MPA,G3]-[*bis*MPA,G1]$(C17)_2$/CPT**, with diameters significantly bigger than those of the empty nanocarriers. **$(NH_3^+Cl^-)_4$[*bis*MPA,G2]-[*bis*MPA,G1]$(C17)_2$/CPT** shows aggregates with sizes of around 35.5 ± 7.8 nm, 2.5 times bigger than the aggregates without CPT, whereas **$(NH_3^+Cl^-)_8$ [*bis*MPA,G3]-[*bis*MPA,G1]$(C17)_2$/CPT** forms aggregates with sizes around 19.9 ± 4.1 nm, 1.5 times bigger than the aggregates without CPT. In both cases and as before, two size-population distributions are visible in cryoTEM images (**figure C_4-41** and **table C_4-8**): small rounded micelles (*ca*. 20-40 nm) appear together with big aggregates (*ca.* 100-400 nm). In contrast, **$(NH_3^+Cl^-)_8$[*bis*MPA,G3]-[*bis*MPA,G2]$(C17)_4$/CPT** conjugates appear as interconnected flexible bilayers in TEM images. CryoTEM images show ill-defined shapes, although small micelles can also be detected. It seems that the incorporation of camptothecin within these aggregates destabilized them and promoted the formation of less spherical nanostructures.

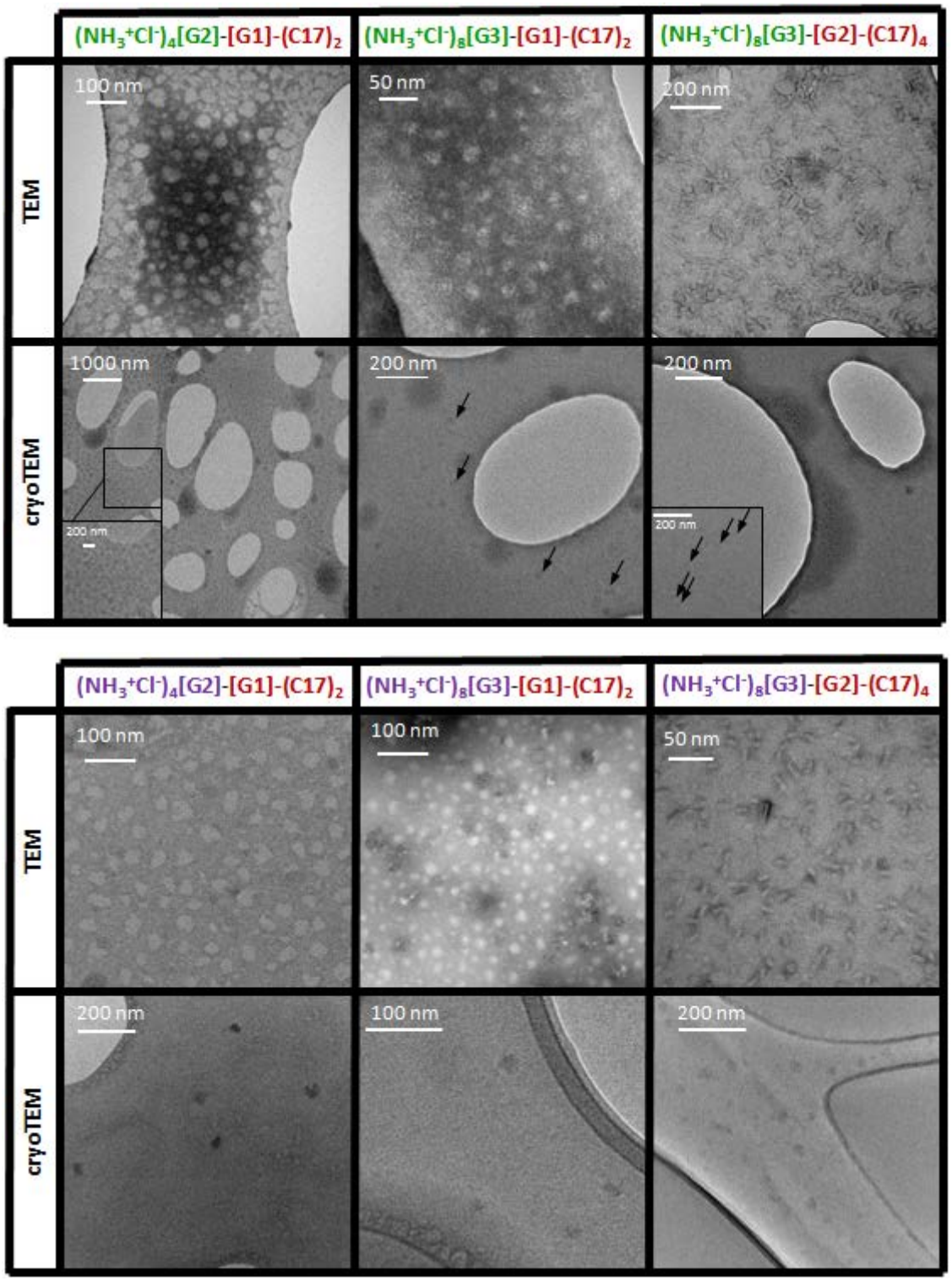

Figure C_4-41: TEM and cryoTEM images of the nanocarriers/**CPT** conjugates formed by the two series of amphiphilic Janus dendrimers, ***bis*-MPA/*bis*-MPA** series (up) and ***bis*-GMPA/*bis*-MPA** (down). Smaller aggregates are marked with black arrows.

Within the *bis*-GMPA/*bis*-MPA series, **$(NH_3^+Cl^-)_4$[bisGMPA,G2]-[*bis*MPA,G1](C17)$_2$/CPT** and **$(NH_3^+Cl^-)_8$[bisGMPA,G3]-[*bis*MPA,G1](C17)$_2$/CPT** conjugates appear as spherical micelles in TEM images (**figure C_4-41**). **$(NH_3^+Cl^-)_4$ [bisGMPA,G2]-[*bis*MPA,G1](C17)$_2$/CPT** formed micelles with sizes of around 29.6 ± 6.2 nm, 2.3 times bigger than the aggregates without CPT, while **$(NH_3^+Cl^-)_8$[bisGMPA,G3]-[*bis*MPA,G1](C17)$_2$/CPT** formed micelles with diameters around 18.0 ± 4.2 nm, 1.2 times bigger than the aggregates without CPT. In both cases, these micelles appear slightly bigger in cryoTEM images, 30 - 50 nm and 20 - 30 nm, respectively. Some bigger aggregates (*ca.* 100 - 400 nm) are also observed but in a lower proportion than the ones observed for the *bis*-MPA/*bis*-MPA series. In contrast, the spherical and ovoidal micelles formed by **$(NH_3^+Cl^-)_8$[*bis*GMPA,G3]-[*bis*MPA,G2](C17)$_4$** in water (**figure C_4-30,** p. 143) were deformed after the formation of the nanocarrier/**CPT** conjugates. In TEM, they appear as cylindrical micelles with a width *ca.* 5 nm while in cryoTEM, ovoidal and ill-defined aggregates with diameters in the range of 20 and 40 nm are observed alongside with bigger aggregates with sizes higher than 100 nm.

The hydrodynamic diameters of the nanocarrier/**CPT** conjugates were measured by DLS although these measurements showed little reliability since CPT is a photosensitive drug and interacts with light, disturbing DLS measurements. For this reason, the results are not included in the discussion but are gathered in **annexes 6**. Qualitatively, it can be said that, as observed in microscopy images, the size of the aggregates increases after camptothecin encapsulation.

Table C_4-8: Morphology and size of the amphiphilic Janus dendrimer/CPT conjugates determined by TEM and cryoTEM.

	amphiphilic Janus dendrimers/CPT conjugates			
	TEM		**cryoTEM**	
	morphology	diameter/width	morphology	diameter
[G2]-[G1]	spherical micelles	35.5 ± 7.8 nm	spherical aggregates	*ca.*20-40 nm & ≥ 100 nm
[G3]-[G1]	spherical micelles	19.9 ± 4.1 nm	spherical aggregates	*ca.*20-40 nm & ≥ 100 nm
[G3]-[G2]	flexible bilayers	9 nm	ill-defined shape & sph. aggregates	*ca.*20-40 nm & ≥ 100 nm
[G2]-[G1]	spherical micelles	29.6 ± 6.2 nm	spherical aggregates	*ca.*30-50 nm & ≥ 100 nm
[G3]-[G1]	spherical micelles	18.0 ± 4.2 nm	spherical aggregates	*ca.*20-30 nm & ≥ 100 nm
[G3]-[G2]	cylindrical micelles	5 nm	ill-defined shape	*ca.*20-40 nm & ≥ 100 nm

It can be summarized that camptothecin encapsulation certainly affects the aggregates formed by the amphiphilic Janus dendrimers. On the one hand, the amphiphilic dendrimers bearing the smallest lipophilic dendron, 1st generation, that preferentially form spherical micelles, maintain their spherical morphology although, their size increases. On the other hand, the amphiphilic dendrimers bearing the biggest lipophilic dendron, 2nd generation, undergo morphological changes through the formation of nanostructures containing more extended lipophilic domains. Indeed, **$(NH_3^+Cl^-)_8$[*bis*GMPA,G3]-[*bis*MPA,G2](C17)$_4$** changes from a mixture of spherical and ovoidal micelles to cylindrical ones, while **$(NH_3^+Cl^-)_8$[*bis*MPA,G3]-[*bis*MPA,G2](C17)$_4$** changes from a mixture of flexible bilayers and vesicles to interconnected flexible bilayers.

Amphiphilic HDLDBC/CPT conjugates

As it can be observed in TEM images (**figure C_4-42**), the morphology of the aggregates formed by both HDLDBCs results modified after the encapsulation of camptothecin. They change from regular spherical aggregates (**figure C_4-35, p. 154**) to a mixture of ovoidal and spherical aggregates with bigger size. ***bis*MPA-[PLU]-*bis*MPA/CPT** conjugates formed aggregates with an average size of 21.0 ± 4.9 (1.1 times bigger than the empty aggregates) while ***bis*GMPA-[PLU]-*bis*GMPA/CPT** conjugates formed aggregates with an average size of 30.9 ± 9.4 nm (2.3 times bigger than the empty aggregates). The more elevated standard deviation observed for the *bis*-GMPA based HDLDBC must be due to the formation of less spherical **HDLDBC/CPT** conjugates.

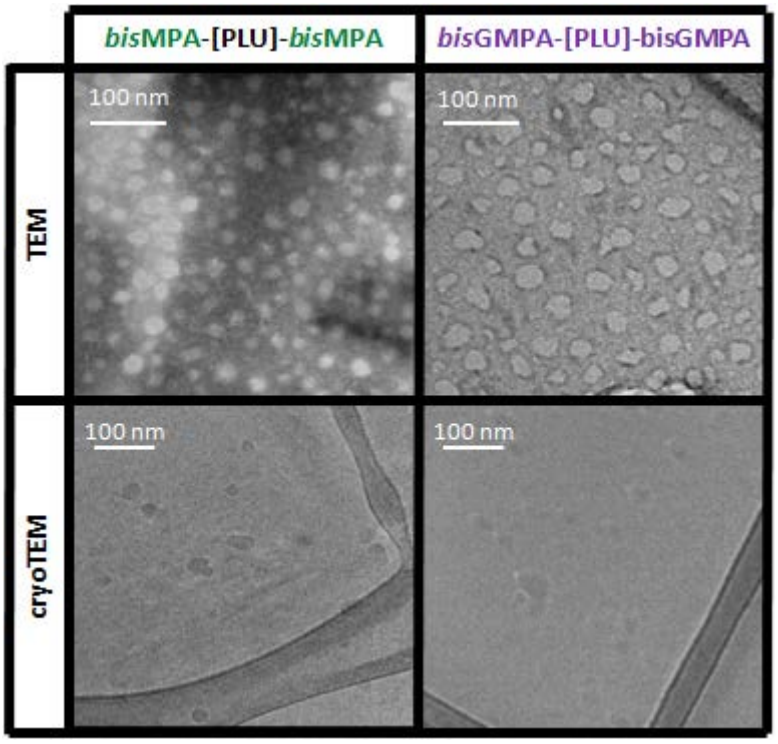

Figure C_4-42: TEM and cryoTEM images of the HDLDBCs/**CPT** conjugates.

These small aggregates are also visible in cryoTEM images in which ***bis*MPA-[PLU]-*bis*MPA/CPT** conjugates appear as spherical aggregates with an average size of *ca.* 25 - 30 nm while ***bis*GMPA-[PLU]-*bis*GMPA/CPT** conjugates appear as a mixture of spherical and ovoidal aggregates with an average size of

ca. 25 - 35 nm. In both cases, no bigger aggregates with size superior to 100 nm, corresponding to self-aggregation of various micelles, can be observed.

The hydrodynamic diameters of the aggregates were measured by DLS (see **annexes 6**). Again and although these data are not fully reliable, it can be notice that the portion of the size-population composed of small hydrodynamic diameters increases after camptothecin encapsulation, limiting the micelles self-aggregation.

The encapsulation of camptothecin within the HDLDBCs aggregates had a comparable effect than temperature on the size and dispersion of the aggregates formed by the HDLDBCs in water. Both limit the self-aggregation of micelles (**figure C_4-43**).

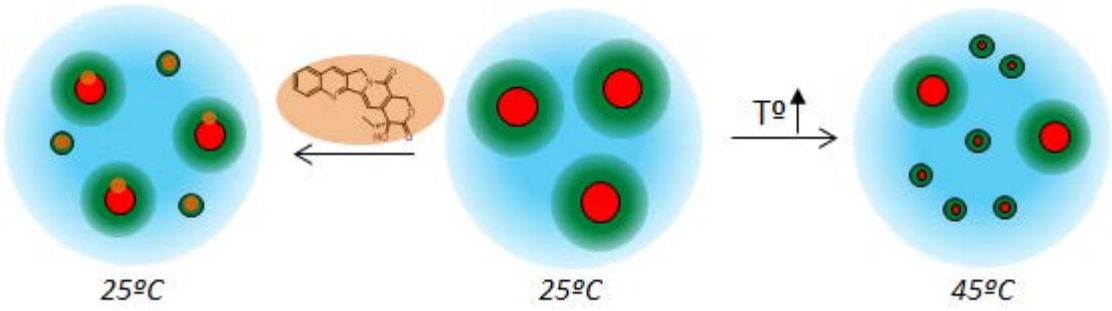

Figure C_4-43: Schematic representation of the effect of the temperature (right) or the encapsulation of camptothecin (left) on the aggregates formed by the HDLDBCs in water.

4.3.2- *In vitro* evaluation of the nanocarrier/CPT conjugates

All the nanocarrier/CPT conjugates described in this chapter were studied *in vitro* in order to determine their potential as inhibitors of HCV replication. The experiments were carried out in the laboratories of the Institute for Biocomputation and Physics of Complex Systems (BIFI), in collaboration with Dr. Olga Abián, Dr. Adrián Velázquez-Campoy and Rafael Clavería-Gimeno. In this section, the most relevant results that allow the discussion about the potential of these systems are presented. Detailed studies of the bioactivity are gathered in the thesis report of Rafael Clavería-Gimeno.

4.3.2.1- Antiviral activity against HCV and cytotoxicity

Prior to the activity studies of the different nanocarrier/CPT conjugates, the cytotoxicity and antiviral activity of the empty nanostructures formed by the dendritic derivatives were evaluated with HCV infected human heptoma cell lines (Huh). The concentrations tested were related to their CPT load (**figure C_4-44**).

The cell viability of all the **amphiphilic Janus dendrimers** was found to be higher than 70 % at all the concentrations tested. This value corresponds to the accepted limit to distinguish biocompatible materials from toxic ones.[200] These results allowed to assert the interest of these dendrimers to form biocompatible nanocarrier drugs vectors for hepatic diseases. In particular, **$(NH_3^+Cl^-)_4$ [*bis*MPA,G2]-[*bis*MPA,G1](C17)$_2$**, **$(NH_3^+Cl^-)_8$[*bis*MPA,G3]-[*bis*MPA,G2](C17)$_4$**, **$(NH_3^+Cl^-)_4$[*bis*GMPA,G2]-[*bis*MPA,G1](C17)$_2$** and **$(NH_3^+Cl^-)_8$[*bis*GMPA,G3]-[*bis*MPA,G2](C17)$_4$** show remarkable biocompatibility with hepatic cell viability

[200] Norm UNE-EN ISO-10993-5, 2009. Biological evaluation of medical devices- part 5: tests *in vitro* for cytotoxicity.

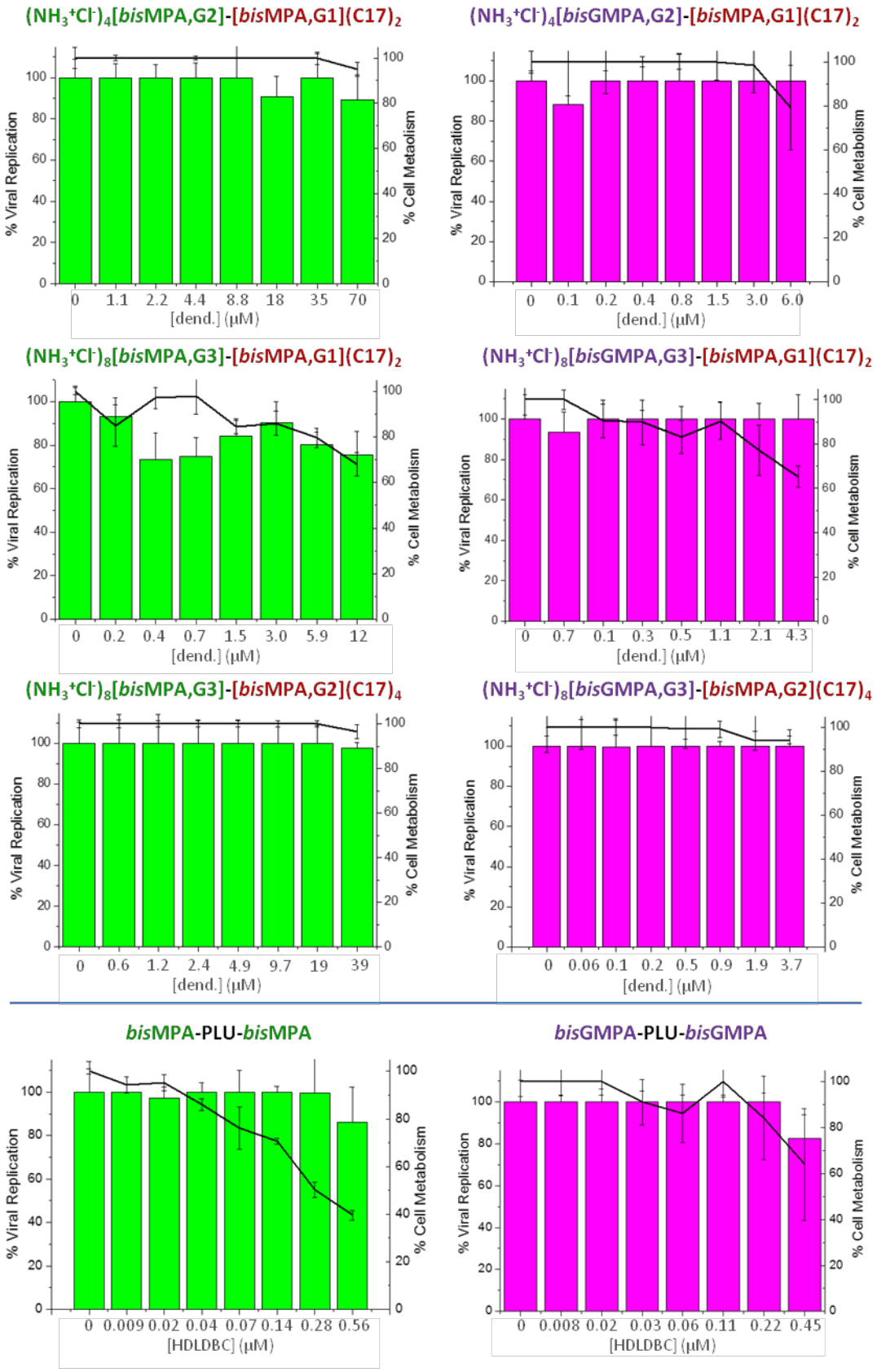

Figure C_4-44: Cell viability (lines) and antiviral activity (bars) of the ***bis*MPA/*bis*MPA** (up & left) and ***bis*GMPA/*bis*MPA** (up & right) amphiphilic Janus dendrimers series and of the HDLDBCs series (down).

superior to 90 %. The two most hydrophilic Janus dendrimers of each series, **$(NH_3^+Cl^-)_8$[*bis*MPA,G3]-[*bis*MPA,G1](C17)$_2$** and **$(NH_3^+Cl^-)_8$[*bis*GMPA,G3]-[*bis*MPA,G1](C17)$_2$** are slightly more cytotoxic than the other dendrimers.

As for antiviral activity, the aggregates formed by the Janus dendrimers **$(NH_3^+Cl^-)_4$[*bis*MPA,G2]-[*bis*MPA,G1](C17)$_2$**, **$(NH_3^+Cl^-)_8$[*bis*MPA,G3]-[*bis*MPA,G2](C17)$_4$**, **$(NH_3^+Cl^-)_4$[*bis*GMPA,G2]-[*bis*MPA,G1](C17)$_2$** and **$(NH_3^+Cl^-)_8$[*bis*GMPA,G3]-[*bis*MPA,G2](C17)$_4$** do not affect the viral replication that is over 90 % in all the cases. The most hydrophilic dendrimers of each series, **$(NH_3^+Cl^-)_8$[*bis*MPA,G3]-[*bis*MPA,G1](C17)$_2$** and **$(NH_3^+Cl^-)_8$[*bis*GMPA,G2]-[*bis*MPA,G1](C17)$_2$** are again slightly different from the other Janus dendrimers. A decrease of the viral replication to 70 % and 80 % is observed, respectively, but it must be associated to a cytotoxic effect.

The **amphiphilic HDLDBCs** are less biocompatible than the Janus dendrimers in human heptoma cell cultures (**figure C$_4$-44**). ***bis*GMPA-[PLU]-*bis*GMPA** shows high viability at the lowest concentrations that decreases below the 70 % threshold at the highest concentration tested (0.45 µM). ***bis*MPA-[PLU]-*bis*MPA** is the less biocompatible system with this cell line, cell viability decreases below 70 % for concentrations higher than 0.14 µM.

***bis*GMPA-[PLU]-*bis*GMPA** does not present any antiviral activity. The viral replication is close to 100 % at all the tested concentrations with the exception of the highest concentration, at which the cytotoxic effect is present. In a similar way, ***bis*MPA-[PLU]-*bis*MPA** does not present any antiviral activity. In this case, the viral replication was close to 100 %, even when the HDLDBC biocompatibility decreased.

The biocompatibility and the antiviral activity of all the nanocarrier/**CPT** conjugates were then evaluated with HCV infected cells with increasing concentrations of camptothecin (from 0 to 1 or 2 µM). As the cells might respond differently after their exposure to camptothecin, each nanocarrier/**CPT** conjugate was compared to its own control, consisting on a solution of free camptothecin in DMSO. The concentration-effect curves for each nanocarrier/**CPT** conjugate and its free camptothecin control are represented in **figure C_4-45**.

For each conjugate, three parameters that permit to assess their potential as anti-HCV systems are given in **table C_4-9**: the half-maximal cytotoxic concentration (CC_{50}), which represents the concentration of drug at which cell viability is reduced to 50 %, the half-maximal inhibition concentration (IC_{50}), which represents the concentration at which the viral replication is reduced to 50%, and the therapeutic index (TI), which compares the efficacy of a drug with its cytotoxicity. CC_{50} and IC_{50} were determined from the concentration-effect curves (**figure C_4-47**) and the TI was calculated according to the following equation (4):

$$(4)\ \mathrm{TI} = \frac{\mathrm{CC50}}{\mathrm{EC50}}$$

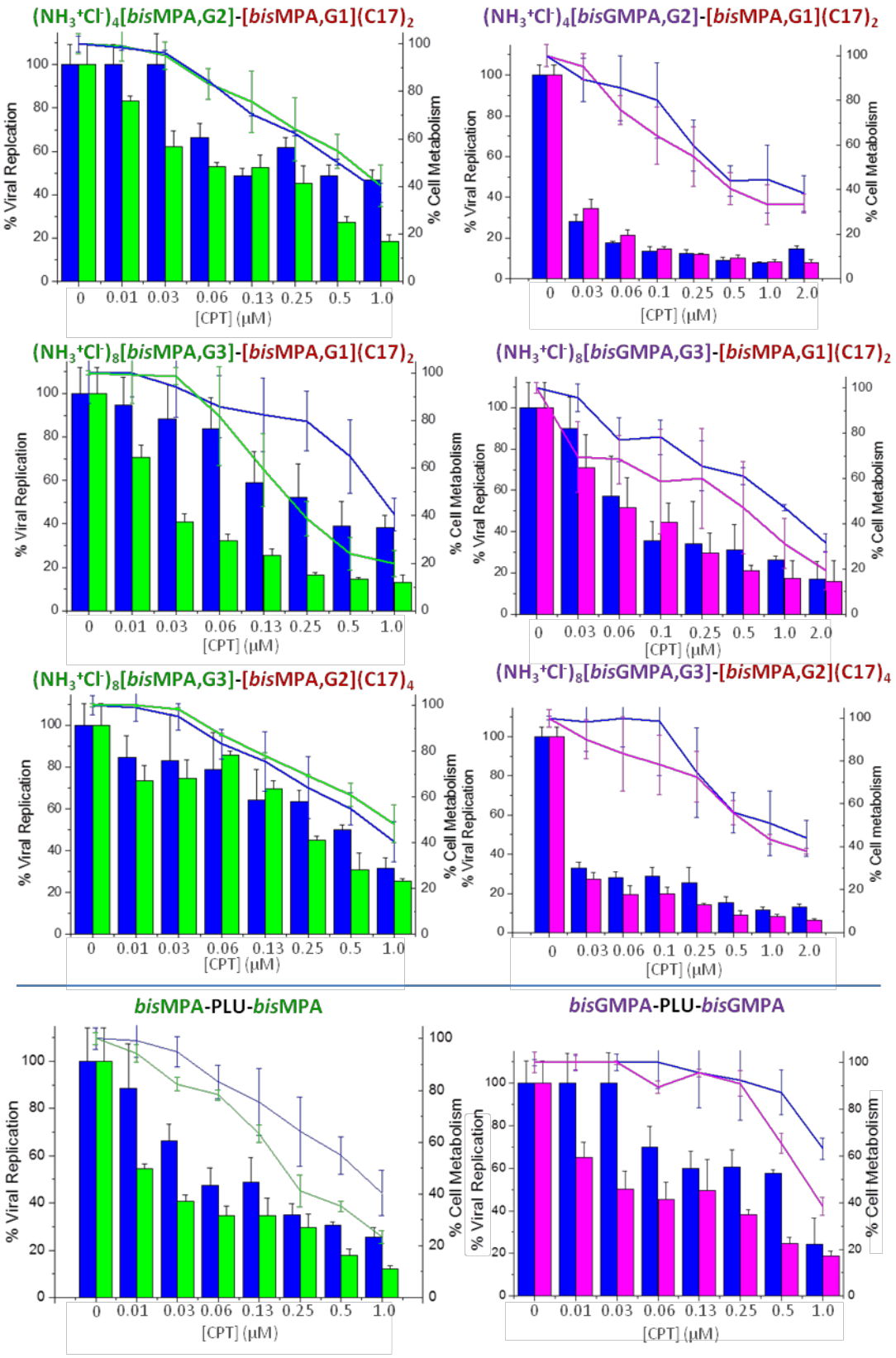

Figure C_4-45: Cell viability (lines) and antiviral activity (bars) of the nanocarrier/drug conjugates of the ***bis*MPA/*bis*MPA** series (up & left), ***bis*GMPA/*bis*MPA** series (up & right) and the **HDLDBCs** series (down). Free camptothecin is represented in blue and nanocarrier/CPT conjugates are represented in green or violet.

Table C_4-9: IC_{50}, CC_{50} and TI values determined for the nanocarrier/CPT conjugates and their internal free CPT control. CC_{50} and IC_{50} values are given in µM. The different CC_{50} and IC_{50} obtained for each free CPT control are due to the variation of the cell response overtime. [a] *dnc* means dendritic nanocarrier. ** inferior TI values for the dnc/CPT conjugates than the free drug.*

Amphiphilic Janus dendrimers					
			CC_{50}	**IC_{50}**	**TI**
***bis*-MPA / *bis*-MPA**	**[G2]-[G1]**	***dnc*[a]/CPT**	**0.5**	**0.1**	**5.0**
		free **CPT**	0.5	0.2	2.5
	[G3]-[G1]	***dnc*/CPT**	**0.2**	**0.03**	**6.7**
		free **CPT**	0.6	0.3	3.0
	[G3]-[G2]	***dnc*/CPT**	**0.9**	**0.3**	**3.0**
		free **CPT**	0.6	0.4	1.5
***bis*-GMPA / *bis*-MPA**	**[G2]-[G1]**	***dnc*/CPT**	**0.4**	**< 0.03**	*
		free **CPT**	0.5	< 0.03	*
	[G3]-[G1]	***dnc*/CPT**	**0.5**	**0.06**	*
		free **CPT**	1.0	0.08	*
	[G3]-[G2]	***dnc*/CPT**	**0.5**	**< 0.03**	*
		free **CPT**	0.7	< 0.03	*
HDLDBCs					
			CC_{50}	**IC_{50}**	**TI**
***bis*MPA-[PLU]-*bis*MPA**		***dnc*/CPT**	**0.1**	**0.03**	**3.3**
		free **CPT**	0.5	0.2	2.5
***bis*GMPA-[PLU]-*bis*GMPA**		***dnc*/CPT**	**0.7**	**0.06**	**11.7**
		free **CPT**	0.4	0.4	4.0

As a general and first observation, camptothecin **maintained its activity against the hepatitis C viral replication after being encapsulated** within all the nanocarriers hereby tested. All of them were therefore able to enhance the water solubility of the camptothecin, protect the drug from hydrolysis in physiological media and deliver it to infected human heptoma cells without requiring the addition of any organic solvent. Interestingly, the different nanocarrier/**CPT** conjugates do not trigger the same cell response when compared to their corresponding free CPT control.

With respect to the *bis*-MPA/*bis*-MPA amphiphilic Janus dendrimers series, all the three nanocarrier/**CPT** conjugates tested show better therapeutic index (TI) values than the free camptothecin. In particular **$(NH_3^+Cl)_8$ [*bis*MPA,G3]-[*bis*MPA,G1](C17)$_2$/CPT**, the amphiphilic Janus dendrimer with the highest hydrophilic/lipophilic ratio (H/L), shows the highest therapeutic index. Indeed, even if the CC_{50} of this nanocarrier/**CPT** conjugate is lower than that measured for its free camptothecin control (0.2 and 0.6 µM, respectively), its antiviral activity is 10 times higher (0.03 and 0.3 µM, respectively). Impressively, at low drug concentrations, this nanocarrier/**CPT** conjugate can certainly inhibit the virus replication while remaining highly biocompatible. For example at a concentration of drug equal to 0.03 µM, the virus replication is reduced down to 33 % and the cell viability is still high, 79 %.

$(NH_3^+Cl^-)_4$[*bis*MPA,G2]-[*bis*MPA,G1](C17)$_2$/CPT and **$(NH_3^+Cl^-)_8$ [*bis*MPA,G3]-[*bis*MPA,G2](C17)$_4$/CPT** conjugates also show better therapeutic indexes than free camptothecin, 5.0 and 3.0, respectively. The **$(NH_3^+Cl^-)_4$ [*bis*MPA,G2]-[*bis*MPA,G1](C17)$_2$/CPT** conjugate is more effective than its free drug control while presenting similar biocompatibility. The **$(NH_3^+Cl^-)_8$ [*bis*MPA,G3]-[*bis*MPA,G2](C17)$_4$/CPT** conjugate shows similar antiviral activity than its free drug control but exhibits higher biocompatibility.

Unfortunately, all the three nanocarrier/CPT conjugates derived from dendrimers of the ***bis*-GMPA/*bis*-MPA** series show cell viabilities and antiviral activities slightly lower than their corresponding free drug control making pointless the calculation of the therapeutic index.

Finally, the **HDLDBC/CPT** conjugates showed different results depending on the nature of the dendritic blocks. ***bis*GMPA-[PLU]-*bis*GMPA/CPT** conjugate has a remarkable therapeutic index of 11.7, 3 times higher than that of its free camptothecin control (4.0). The antiviral activity of the encapsulated camptothecin was enhanced at low concentrations while its biocompatibility

remained highly elevated. For instance, at a concentration of encapsulated drug of 0.03 µM, the viral replication went down to 50 % while the biocompatibility was equal to 89 %. In contrast, ***bis*MPA-[PLU]-*bis*MPA/CPT** conjugate showed poorer biological abilities. As for the other HDLDBC, the activity of the drug results enhanced at low concentrations. For instance, at a concentration of encapsulated drug of 0.03 µM, the viral replication goes down to 41 % while the biocompatibility is equal to 82 %. However, the rapid decrease of the cell viability of the nanocarrier/**CPT** conjugate restrains its use to only really low concentrations. Its lower biocompatibility must certainly be a consequence of the lower biocompatibility of the empty nanocarriers formed by this HDLDBC (**figure C_4-44,** p. 173).

Summarizing, eight of the nine nanocarriers described in this chapter result interesting candidates to promote the use of camptothecin as an anti-HCV drug. All of them are able to enhance the solubilization of its active lactone form in water, avoiding the use of an organic co-solvent during drug administration. Moreover, five of them improve the camptothecin activity against the hepatitis C virus at low drug concentrations, resulting into better therapeutic indexes when compared with free camptothecin.

The ***bis*-GMPA/*bis*-MPA** amphiphilic Janus dendrimer series that shows the most interesting capacity to encapsulate camptothecin, shows the poorest biological activities related to CPT therapeutic action. In contrast, the ***bis*-MPA/*bis*-MPA** amphiphilic Janus dendrimer series that shows the poorest abilities to encapsulate the drug, shows more interesting biological activities in this respect.

The ***bis*GMPA-[PLU]-*bis*GMPA** HDLDBC appears as the most promising material to deliver camptothecin. It combines good abilities to encapsulate the drug providing a nanocarrier/**CPT** conjugate that improves the drug activity

against the hepatitis C virus replication, while reducing its cytotoxicity for hepatic cells.

4.3.2.2- Cell internalization

Because of the novelty of the ***bis*-GMPA/*bis*-MPA** amphiphilic Janus dendrimers and their good encapsulation abilities, they were chosen to perform a study of cell internalization that involves double encapsulation using a drug (CPT) and a fluorescent probe. The objective was to study by imaging flow cytometry, technique that combines flow cytometry with fluorescence, the cellular uptake of these nanocarriers while evaluating the bioactivity of the systems.

In order to label the nanocarriers with a fluorescent probe, we synthesized a fluorophore derived from rhodamine B (**figure C_4-48**), specially designed to integrate within the structure of the micelles formed by amphiphilic dendrimers. The new fluorophore consists on rhodamine B linked to a 1st generation lipophilic dendron of *bis*-MPA, **RhB-[*bis*MPA,G1](C17)$_2$** (abbreviated as **RhB(C17)$_2$**), by means of click chemistry. The aim was to prepare a fluorescent probe versatile enough to be used within many micellar carriers, while minimizing the possibilities of fast release of water soluble fluorescent probes, such as rhodamine B.

Synthesis of RhB(C17)$_2$

Red rhodamine B fluorophore is commonly used to efficiently mark materials in order to carry out biological experiments. This affordable water soluble fluorophore has an elevated absorption coefficient and broad fluorescence in the visible region. Moreover, it is highly stable and its acid moiety allows easy and versatile modifications.[206]

[206] M. Beija, C.A.M. Afonso, J.M.G. Martinho, Synthesis and applications of rhodamine derivatives as fluorescent probes, *Chem. Soc. Rev.*, **2009**, 38, 2410-2433; b) X. Chen, Q. Wu, L. Henschke, G. Weber, T. Weil, An efficient and versatile approach for the preparation of a rhodamine B ester bioprobe library, *Dyes Pigm.*, **2012**, 94, 296-303.

Commercial rhodamine B fluorophore was linked to a 1st generation lipophilic dendron of *bis*-MPA by means of CuAAC in order to obtain a modified red fluorophore with a low water solubility which interestingly presents a lipophilic block similar to that of the Janus dendrimers (**figure C_4-46**). Thus, the acid moiety of the commercial rhodamine B was first modified with 6-azidohexan-1-ol to incorporate an azide group on the fluorophore. The CuAAC was carried out with the 1st generation lipophilic dendron of *bis*-MPA in conditions similar to those employed during the synthesis of the Janus dendrimers (see chapter 7 for detailed procedure).[203]

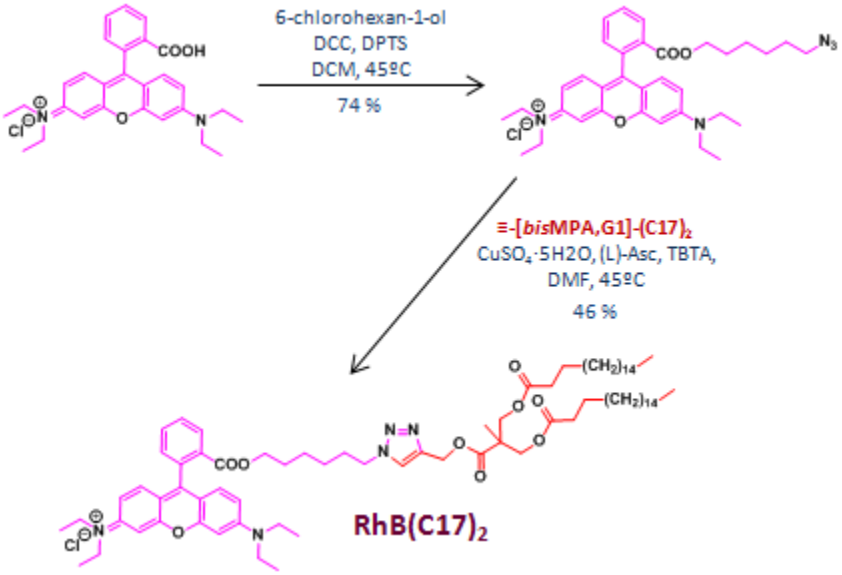

Figure C_4-46: Synthesis of the low-water soluble modified rhodamine (***RhB(C17)$_2$***) starting from the commercial rhodamine B fluorophore (see chapter 7 for the detailed procedure employed for the synthesis).

The modified rhodamine B derivative (***RhB(C17)$_2$***) was readily synthesized in a scale of hundred of milligrams, with a global yield of 34 %. This fluorophore is insoluble in water, and was characterized by ^{1}H and ^{13}C nuclear magnetic resonance (NMR), mass spectrometry (MS), Fourier transform infrared spectroscopy (FTIR) and elemental analysis (EA). The complete chemical characterization data are gathered in chapter 7.

[203] I. Jiménez-Pardo et al., *Macromol. Biosci.*, **2015**, 15, 1381.

The completion of the CuAAC reaction was first asserted by ^{1}H NMR. A singlet corresponding to the proton of the triazole ring, *H-17*, appears at 7.97 ppm in the ***RhB(C17)$_2$*** spectra. Additionally, two peaks corresponding to the protons in the α-positions of the triazole ring, *H-16* and *H-19*, are shifted downfield when compared to the spectra of the corresponding starting compounds, from 3.23 to 4.40 ppm and from 4.71 to 5.24 ppm, respectively (**figure C$_4$-47**). Unfortunately, the peaks corresponding to the carbon atoms of the triazole ring cannot be observed in the ^{13}C NMR spectrum; however, the coupling between proton *H-17* and the carbon *C-17* of the triazole ring can be observed in ^{1}H-^{13}C HSQC experiments (see **annexes 7**).

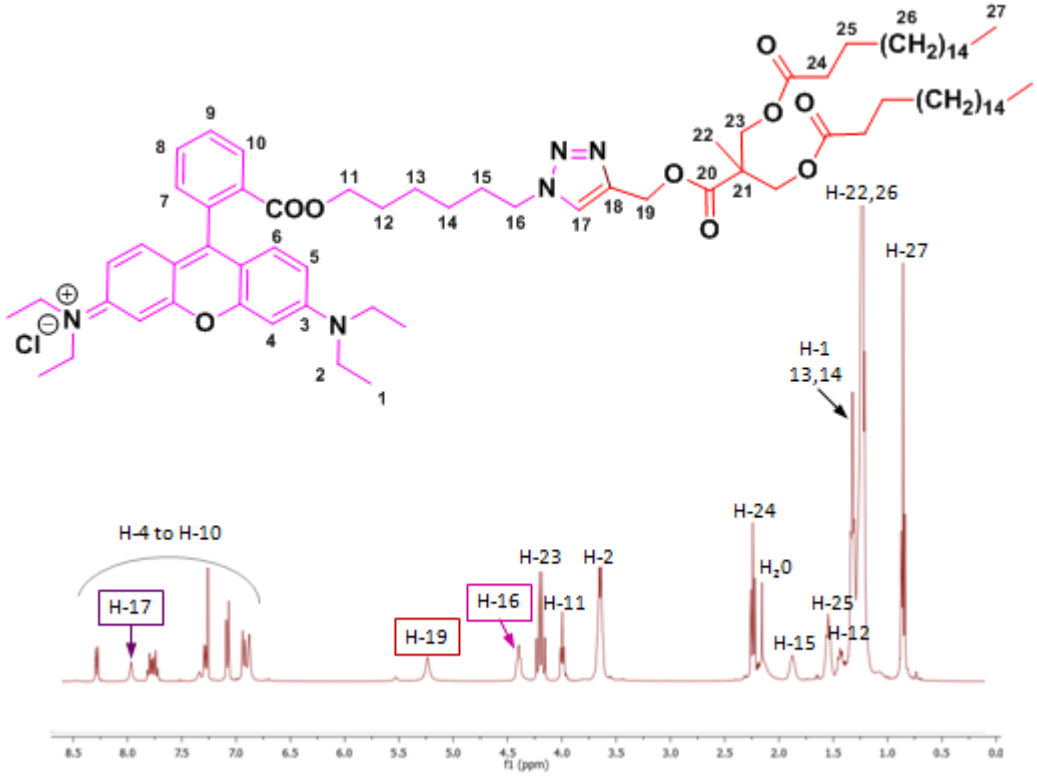

Figure C$_4$-47: ^{1}H NMR spectrum of low-water soluble modified rhodamine B, ***RhB(C17)$_2$***.

The FTIR spectrum doesn't show the characteristic bands corresponding to the azide and alkyne groups (**figure C$_4$-48-A**), and an only peak is observed in the MS spectrum that corresponds to the correctly functionalized cationic fluorophore without chlorine (**figure C$_4$-48-B**).

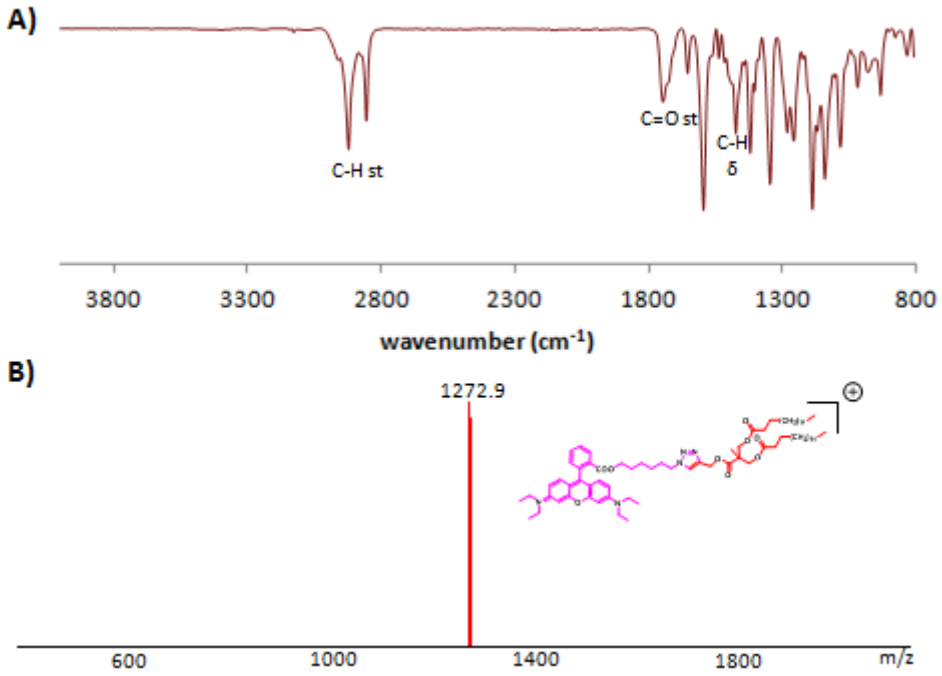

Figure C_4-48: FTIR (**A**) and MALDI$^+$-Tof (**B**) spectra of the low-water soluble modified rhodamine B (**RhB(C17)$_2$**).

Encapsulation of RhB(C17)$_2$

The lipophilic modified rhodamine was encapsulated within the three ***bis*-GMPA/*bis*-MPA** amphiphilic Janus dendrimers employing the oil-in-water emulsion method (**figure C_4-49**).

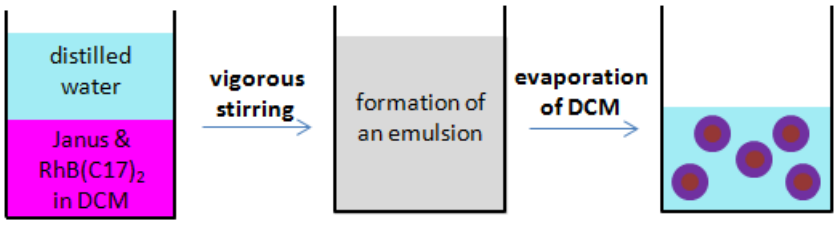

Figure C_4-49: Solubilization and encapsulation of low-water soluble rhodamine B, **RhB(C17)$_2$**, using the oil-in-water emulsion method.

The amphiphilic Janus dendrimers and **RhB(C17)$_2$** were dissolved into dichloromethane and an appropriate amount of distilled water was added to the solution. The biphasic system was vigorously stirred to form an emulsion from which the volatile organic solvent was slowly removed by evaporation using a ventilation system. When all the organic solvent was evaporated, a clear

violet solution of the nanocarriers/**RhB(C17)$_2$** conjugates was obtained (see chapter 7 for detailed protocol).

At a feeding ratio of 0.15/1 ($w_{RhB(C17)}/w_{dend.}$), any precipitate could be observed after the formation of the nanocarrier/**RhB(C17)$_2$** conjugates in water. Therefore, it was assumed that all the new red fluorophore **RhB(C17)$_2$** was encapsulated within the nanocarriers.

As the nanocarrier/**RhB(C17)$_2$** conjugates were based on non-covalent interactions between the amphiphilic Janus dendrimers and the non-water soluble rhodamine B fluorophore, release studies were carried out to assert the time-persistence and effectiveness of the fluorescent labeling of the nanocarriers. **Release experiments** were carried out by dialysis of a solution of nanocarrier/**RhB(C17)$_2$** conjugates against a volume 100 times higher of distilled water (*"sink conditions"*) (**figure C$_4$-50**).

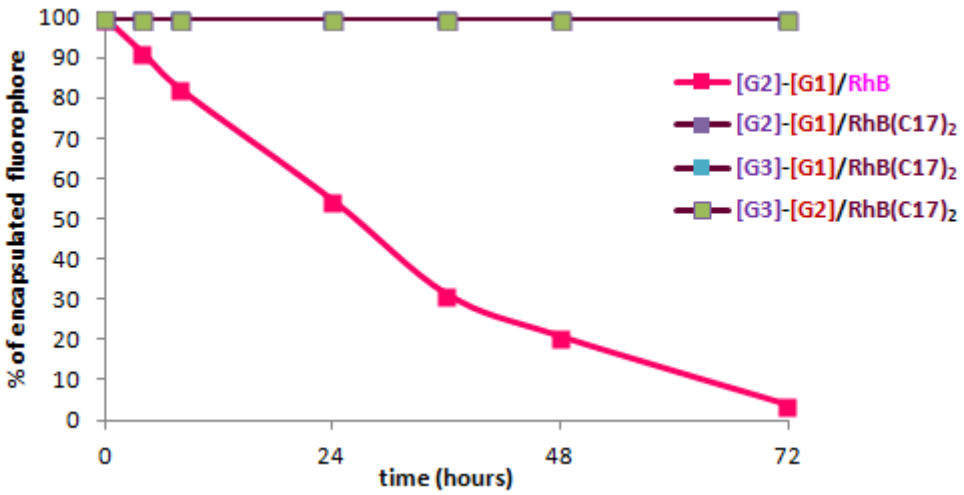

Figure C$_4$-50: **RhB(C17)$_2$** release curves from the three nanocarriers/**RhB(C17)$_2$** conjugates and **RhB** release curve from **$(NH_3^+Cl^-)_4$[*bis*GMPA,G2]-[*bis*MPA,G1](C17)$_2$/RhB** conjugate.

While the unmodified commercial rhodamine B (**RhB**) was released in a continuous way from the nanocarrier/**RhB** conjugates, the low-water soluble modified rhodamine B (**RhB(C17)$_2$**) was efficiently retained within the three nanocarriers/fluorophore conjugates. After 72 hours, between 99.8 and 99.9 %

of the encapsulated modified rhodamine remained in the nanocarriers/**RhB(C17)$_2$** conjugates whereas only 3 % of commercial rhodamine remained within the nanocarrier/**RhB** conjugate.

Hence, by a simple chemical modification achieved in two steps, the commercial rhodamine B fluorophore was modified into a less water soluble fluorophore (**RhB(C17)$_2$**) that can effectively and easily label the nanocarriers by non-covalent interactions during at least 72 hours.

RhB(C17)$_2$ and CPT co-encapsulation

Co-encapsulation of the low-water soluble modified rhodamine B and camptothecin was carried out in two steps. First, the nanocarrier/**RhB(C17)$_2$** conjugates were prepared according to the oil-in-water emulsion method (see section 4.2.2.1, p. 138). Second, and as before, camptothecin was encapsulated within the nanocarrier/**RhB(C17)$_2$** conjugates employing the solvent diffusion technique (see section 4.3.1.1, p. 162) in order to obtain the final nanocarrier/**RhB(C17)$_2$**/**CPT** conjugates (**figure C$_4$-51**, see chapter 7 for detailed protocol).

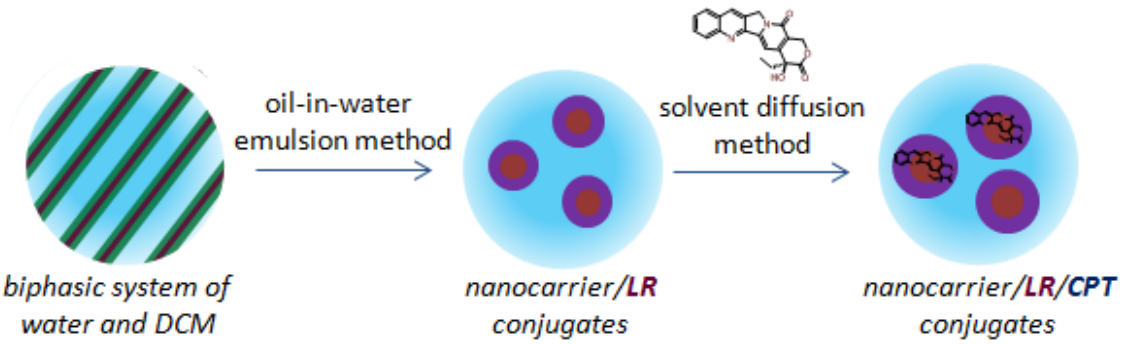

Figure C$_4$-51: Preparation of the ***bis*-GMPA**/***bis*-MPA** based amphiphilic Janus dendrimers/**RhB(C17)$_2$**/**CPT** co-conjugates.

RhB(C17)$_2$ was encapsulated within the ***bis*-GMPA/*bis*-MPA** amphiphilic Janus dendrimers at a feeding ratio of 0.15/1 ($w_{RhB(C17)}/w_{dend.}$) while camptothecin was encapsulated within the nanocarriers at a feeding ratio of 0.10/1 ($w_{CPT}/w_{dend.}$). The amounts of **RhB(C17)$_2$** and **CPT** encapsulated within the dendritic nanocarriers were calculated in weight and in mole and their encapsulation efficiencies (EE) were determined (**table C$_4$-10**).

Table C$_4$-10: Amount of **RhB(C17)$_2$** and **CPT** encapsulated within the dendritic nanocarriers. [a]*d*nc means dendritic nanocarrier and [b]EE means encapsulation efficiency and was calculated dividing the amount of substance at the end of the encapsulation process by the amount added at the beginning.

	Amphiphilic *bis*-GMPA/*bis*-MPA dendrimers				
	loaded substance	aggregates morphology	mg sub. / mg *d*nc[a]	mol sub. / mol *d*nc[a]	EE[b] (%)
[G2]-[G1]	**CPT**	spherical micelles	0.061	0.295	60
	RhB(C17)$_2$	spherical micelles	0.15	0.193	100
	RhB(C17)$_2$ /CPT	elongated micelles	0.15 /0.018	0.193 /0.087	100 /19
[G3]-[G1]	**CPT**	spherical micelles	0.059	0.466	61
	RhB(C17)$_2$	spherical & ovoidal micelles	0.15	0.315	100
	RhB(C17)$_2$ /CPT	spherical micelles	0.15 /0.024	0.315 /0.186	100 /24
[G3]-[G2]	**CPT**	cylindrical micelles	0.054	0.549	54
	RhB(C17)$_2$	spherical micelles	0.15	0.403	100
	RhB(C17)$_2$ /CPT	ovoidal micelles & vesicles	0.15 /0.039	0.403 /0.394	100 /39

As no colored precipitate was observed during the co-encapsulation process, it was assumed that all the modified rhodamine B remained encapsulated within the conjugates. However, a white precipitate appeared during the co-encapsulation process that corresponded to camptothecin. The precipitate was removed by filtration and the amount of camptothecin encapsulated within the nanocarrier/**RhB(C17)$_2$**/**CPT** conjugates was determined by fluorescence. The presence of the modified rhodamine B within the nanocarriers affected negatively the camptothecin encapsulation efficiency. However and fortunately, the amount of camptothecin encapsulated within the nanocarriers remained relatively high and the camptothecin encapsulation efficiency ranged from 19 to 39 %.

(NH$_3^+$Cl$^-$)$_8$[*bis*GMPA,G3]-[*bis*MPA,G2](C17)$_4$, the biggest amphiphilic Janus dendrimer, was the less affected. The encapsulation efficiency of camptothecin goes down from 54 to 39 % with the presence of the modified rhodamine B. In the cases of **(NH$_3^+$Cl$^-$)$_4$[*bis*GMPA,G2]-[*bis*MPA,G1](C17)$_2$** and **(NH$_3^+$Cl$^-$)$_8$[*bis*GMPA,G3]-[*bis*MPA,G1](C17)$_2$**, the camptothecin encapsulation efficiency decreases significantly from 60 to 19 % and from 61 to 24 %, respectively. Clearly, the size of the amphiphilic Janus dendrimer appears as a key factor for the co-encapsulation efficiency.

Size and morphology of the nanocarrier/RhB(C17)$_2$/CPT conjugates

The size and morphology of the Janus dendrimers/**RhB(C17)$_2$**/**CPT** conjugates was studied by TEM and cryoTEM (**figure C$_4$-52 and table C$_4$-11**).

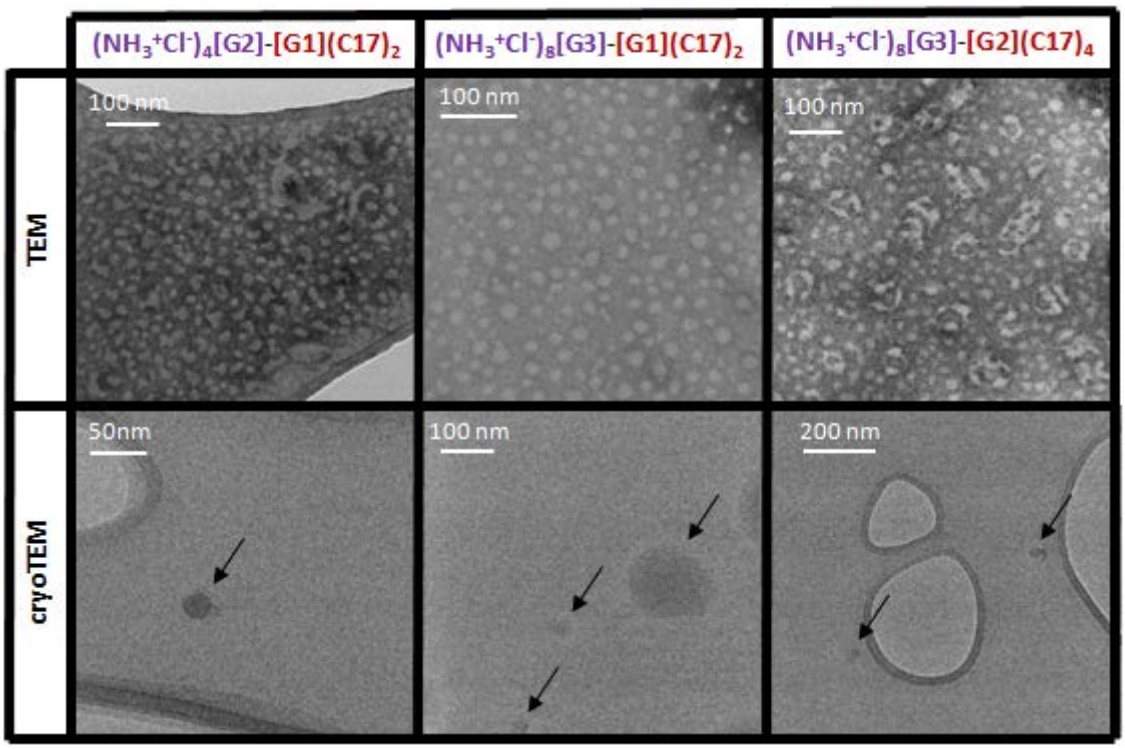

Figure C$_4$-52: TEM (up) and cryoTEM (down) images of the Janus dendrimer/**RhB(C17)$_2$**/**CPT** conjugates.

Table C$_4$-11: Size and morphology of the Janus dendrimers/**RhB(C17)$_2$**/**CPT** conjugates determined by TEM and cryoTEM.

	amphiphilic *bis*-GMPA/*bis*-MPA Janus dendrimers			
	TEM		**cryoTEM**	
	morphology	size	morphology	size
[G2]-[G1]	elongated micelles	21.7 ± 4.9 nm	spherical aggregates	*ca.*30-50 nm & ≥ 200 nm
[G3]-[G1]	spherical micelles	19.0 ± 4.1 nm	spherical aggregates	*ca.*20-30 nm & ≥ 200 nm
[G3]-[G2]	micelles & vesicles	22.3 ± 8.3 nm 40.4 ± 7.9 nm	spherical aggregates	*ca.*20-60 nm & ≥ 200 nm

The **$(NH_3^+Cl^-)_4$[*bis*GMPA,G2]-[*bis*MPA,G1](C17)$_2$/RhB(C17)$_2$/CPT** and **$(NH_3^+Cl^-)_8$[*bis*GMPA,G3]-[*bis*MPA,G1](C17)$_2$/RhB(C17)$_2$/CPT** conjugates give rise to micelles whose sizes are close to those formed by the Janus dendrimer/**CPT** conjugates (see **table C_4-8**, p. 169) . In cryoTEM images, these spherical aggregates are also observed together with some bigger aggregates that should correspond to micelle self-aggregation.

In contrast, the **$(NH_3^+Cl^-)_8$[*bis*GMPA,G3]-[*bis*MPA,G2](C17)$_4$/RhB(C17)$_2$/CPT** conjugate underwent some morphological changes when compared to its respective nanocarrier/CPT conjugate (see **table C_4-8**, p. 169), forming now a mixture of ovoidal micelles and small vesicles. In cryoTEM images, two size-population distributions are observed: spherical aggregates with sizes ranged from 20 to 60 nm together with some bigger aggregates with sizes bigger than 200 nm.

As a summary, the labeling of the nanocarrier/drug conjugates by the modified rhodamine B fluorophore did not induce morphological changes in two of the three nanocarrier/**RhB(C17)$_2$/CPT** conjugates.

In vitro antiviral activity and cytotoxicity

The biocompatibility and the antiviral activity of the nanocarrier/**RhB(C17)$_2$/CPT** conjugates were evaluated in human hepatoma cells in order to determine if the presence of the fluorophore has an influence on the biological properties of the encapsulated camptothecin. Two systems were studied: **$(NH_3^+Cl^-)_4$[*bis*GMPA,G2]-[*bis*MPA,G1](C17)$_2$/RhB(C17)$_2$/CPT** as a model for the micelles whose morphology are nor modified by the incorporation of **RhB(C17)$_2$** and **$(NH_3^+Cl^-)_8$[*bis*GMPA,G3]-[*bis*MPA,G2](C17)$_4$/RhB(C17)$_2$/CPT** that underwent morphological changes after the addition of **RhB(C17)$_2$**

The incorporation of modified rhodamine B, **RhB(C17)$_2$**, within the two dendritic nanocarriers affected only slightly their biocompatibility and antiviral activity (**figure C$_4$-53-A**). They appear almost identical as the one previously measured for the nanocarriers without **RhB(C17)$_2$**. Likewise, the two nanocarrier/**RhB(C17)$_2$**/**CPT** conjugates show similar biocompatibility with this cell line and antiviral replication than their respective nanocarriers/**CPT** conjugates (**figure C$_4$-53-B**).

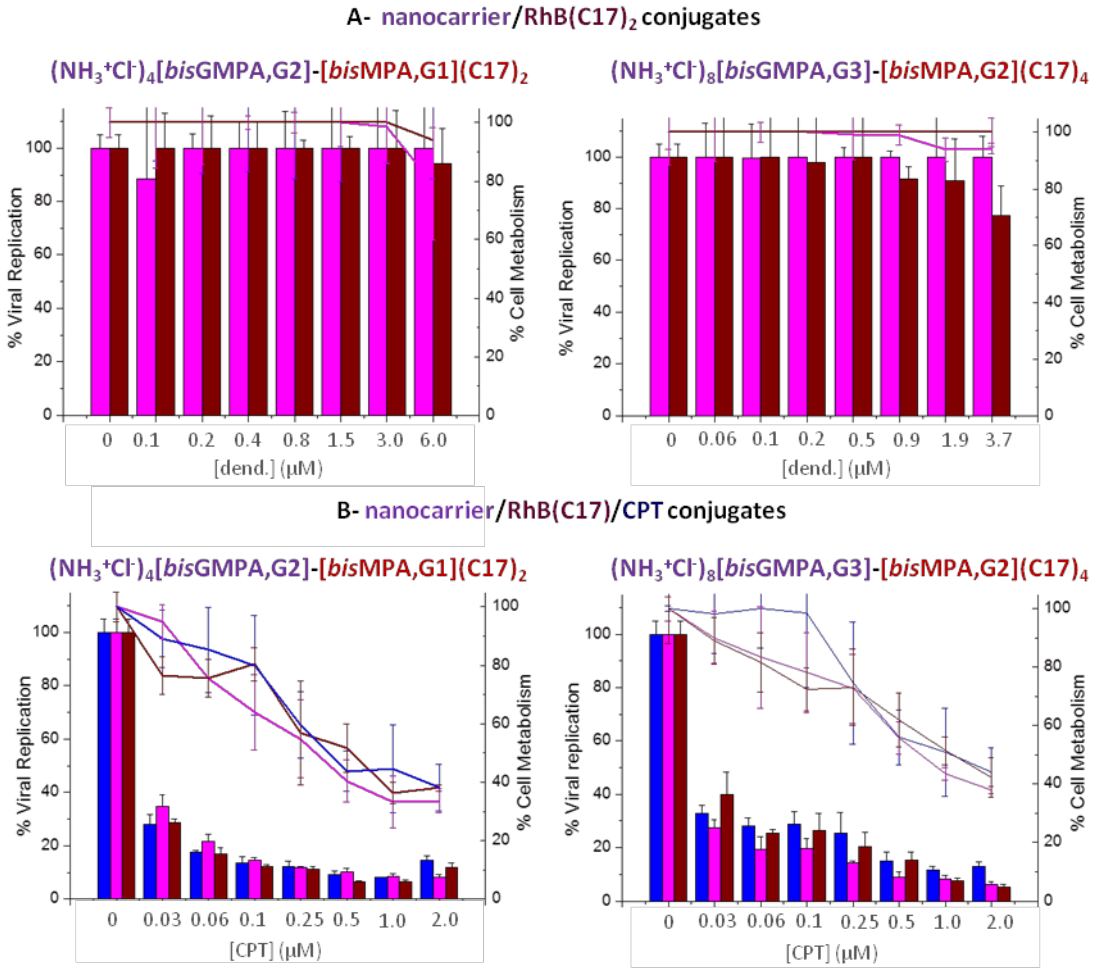

Figure C$_4$-53: Cell viability (lines) and antiviral activity (bars) of the empty nanocarriers in violet and of the nanocarrier/**RhB(C17)$_2$** conjugates in burgundy (**A**) and of the nanocarriers/**CPT** and nanocarriers/**RhB(C17)$_2$**/**CPT** conjugates (**B**). Free **CPT** is represented in blue.

Therefore, the labeling of these nanocarrier/**CPT** conjugates by the modified rhodamine B (**RhB(C17)$_2$**) does not alter their biological properties in HCV-infected human hepatoma cells.

Cellular internalization

Flow-cytometry assays were carried out with the two ***bis*-GMPA/ *bis*-MPA** dendritic nanocarriers to determine if they were effectively capable of delivering camptothecin into the hepatic cells in spite of showing different morphologies. Two parameters were measured: the presence of modified rhodamine B in the cells and the correct organization of the cellular cycle. Camptothecin forms stable complexes with DNA and this hampers the regular cell division, disorganizing the cellular cycle. Propidium iodide stoichiometrically stains the DNA cell and allows classifying the cells that can replicate (which show n and 2n DNA population) from those that cannot replicate (which only show n DNA population).

The empty nanocarriers, nanocarrier/**RhB(C17)$_2$** conjugates, nanocarrier/**CPT** conjugates and nanocarrier/**RhB(C17)$_2$/CPT** conjugates were studied. Two cell controls were carried out, one without adding anything to the cells and the other one adding camptothecin to the cells to quantify its activity. An organized cellular cycle (n and 2n DNA population) would testify the absence of active camptothecin, whereas a disorganized cellular cycle (only n DNA population) would confirm the presence of active camptothecin (**table C$_4$-18**).

Table C_4-18: Lipophilic modified rhodamine (**RhB(C17)$_2$**) internalization level and organization of the cellular cycle measured by flow-cytometry assays. [a]DL means detection limit.

	***bis*-GMPA/*bis*-MPA Janus dendrimers**		
	channel	**[G2]-[G1]**	**[G3]-[G2]**
free CPT	**RhB(C17)$_2$** (%)	< DL[a]	< DL
	cellular cycle	**disorganized**	**disorganized**
nanocarriers	**RhB(C17)$_2$** (%)	< DL	< DL
	cellular cycle	organized	organized
nanocarriers/ RhB(C17)$_2$	**RhB(C17)$_2$** (%)	**34.7**	**67.3**
	cellular cycle	organized	organized
nanocarriers/CPT	**RhB(C17)$_2$** (%)	< DL	< DL
	cellular cycle	**disorganized**	**disorganized**
nanocarriers/ RhB(C17)$_2$/CPT	**RhB(C17)$_2$** (%)	**46.1**	**51.6**
	cellular cycle	**disorganized**	**disorganized**

$(NH_3^+Cl^-)_4$[*bis*GMPA,G2]-[*bis*MPA,G1](C17)$_2$ and **$(NH_3^+Cl^-)_8$[*bis*GMPA,G3]-[*bis*MPA,G2](C17)$_4$** show the same results. As expected, the empty nanocarriers does not give any positive signal for **RhB(C17)$_2$** and **CPT**, while the nanocarrier/**RhB(C17)$_2$** conjugates only give a positive signal for the rhodamine channel, which is coherent with the results obtained during the biocompatibility assays. Neither the empty nanocarriers, nor the nanocarrier/**RhB(C17)$_2$** conjugates were cytotoxic; they did not perturb the normal cellular cycle of hepatic cells.

All the nanocarrier conjugates with camptothecin disturbed the cellular cycle, confirming that the encapsulation of the drug within the diverse conjugates does not affect its activity. Besides, the nanocarrier/**RhB(C17)$_2$/CPT** conjugates additionally give a positive signal for **RhB(C17)$_2$** that proves the correct internalization of the whole nanocarrier/**RhB(C17)$_2$/CPT** conjugates in the cells.

The low-water soluble modified rhodamine B appears as an efficient fluorophore that allows the labeling of various amphiphilic nanocarriers while inducing few morphological changes in the nanocarrier/drug conjugates, and showing similar anti-HCV activity than the unlabeled nanocarrier/drug conjugates.

As the labeling is based on non-covalent interactions, various dendritic nanocarriers could be effectively labeled by the same modified fluorophore without requiring additional covalent synthesis.

4.4- General remarks

Summary of results

Three series of amphiphilic dendritic derivatives were synthesized in order to transport and deliver camptothecin, an alleosteric inhibitor of the hepatitis C virus, into human hepatic cells.

The nature of the amphiphilic dendritic derivatives, either Janus dendrimers or hybrid dendritic-lineal-dendritic block copolymers, as well as the variety of hydrophilic and lipophilic dendrons employed for their synthesis allowed the formation of diverse nanocarriers to transport camptothecin.

One of the series of the amphiphilic Janus dendrimers was fluorescently labeled with a commercial fluorophore modified with a lipophilic dendron, and this permitted to confirm their cellular internalization into hepatic cells.

Conclusions

Eight of the nine dendritic systems presented hereby could effectively encapsulate and deliver camptothecin into HCV-infected hepatic cells.

Among them, the amphiphilic hybrid dendritic-lineal-dendritic block copolymers based on *bis*-GMPA dendrons and Pluronic® F-127 appeared to be the best candidate as it presented good level of camptothecin encapsulation (46 µg of camptothecin per mg of derivative) and a better therapeutic index than the free drug (almost 3 times higher).

The addition of a lipophilic dendron to the rhodamine B allows a simple, versatile and time-persistent labeling by non-covalent interactions of the amphiphilic Janus dendrimer/drug conjugates without altering their biological properties.

Future investigation

In order to perform further in vivo tests, the release of camptothecin from the nanocarriers/CPT conjugates must be studied. The reticulation of the nanocarriers might be studied to perform a sustained drug release, as well as the design of "*on/off systems*" to favor targeting abilities.

The targeting abilities of the nanocarriers might be promoted following a protocol similar than the one employed with rhodamine B. The addition of a lipophilic dendron on small targeting molecules might favor stable and time-persistent non-covalent interactions between these modified targeting molecules with the nanocarriers avoiding covalent synthesis.

Chapter 5:

Bis-GMPA and *bis*-MPA globular dendritic derivatives for gene delivery

In this chapter, new globular dendrimers based 2,2-*bis*(glyciloxymethyl)propionic acid (*bis*-GMPA) and dendronized hyperbranched polymers (DHPs) based on 2,2-*bis*(hydroxylmethyl)propionic acid (*bis*-MPA) are described as vectors for gene transfection.

Firstly, the synthesis and the characterization of the materials are commented. Secondly, their potential as gene transfection vector for pDNA and siRNA is reported.

5.1- *bis*-GMPA and *bis*-MPA globular dendritic derivatives

In order to perform non-viral gene transfection, a high number of amino groups is required to efficiently complex the genetic material. Therefore, two dendrimers based on *bis*-GMPA of 3rd and 4th generation were synthesized with respectively 28 and 48 terminal ammonium groups and 18 and 46 internal amide groups. In addition, three commercial *bis*-MPA hyperbranched polyesters decorated with hydrophilic dendrons of *bis*-MPA bearing terminal amino groups were synthesized. It resulted into three new dendronized hyperbranched polymers (DHPs) with theoretically 128, 256 and 512 terminal ammonium groups. (**figure C_5-1**).

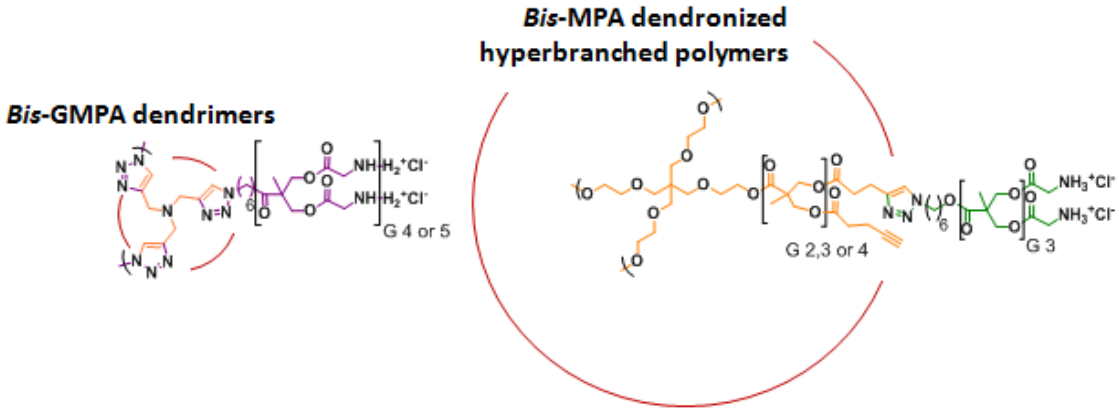

Figure C_5-1: Gneral chemical structure of the two *bis*-GMPA dendrimers and the three *bis*-MPA dendronized hyperbranched polymers.

5.1.1- Synthesis and chemical characterization

5.1.1.1- *Bis*-GMPA dendrimers

2,2'-*bis*(glyciloxymethyl)propionic acid (*bis*-GMPA) dendrimers were synthesized following an original convergent pathway (**figure C_5-2**). *Bis*-GMPA dendrons of the 3rd and 4th generation were linked to a core of tripropargyl amine by means of CuAAC. Because of its high conversion yields and the few by product generated, CuAAC "click chemistry" has been widely used for the convergent synthesis of dendrimers.[69,207] For example, a tripropargyl amino core permits the construction of globular dendrimers consisting of three dendrons in a convergent way using this methodology.[208] In our case, a hexamethylenic chain was used as spacer between the core and the *bis*-GMPA dendrons in order to favor the complete functionalization of the core and afford flexibility of the final dendritic structure which might help their abilities to form dendriplexes with pDNA and siRNA.[209]

[69] a) M. Sowinska *et al.*, *New J. Chem.*, **2014**, 38, 2168; b) M. Arseneault *et al.*, *Molecules*, **2015**, 20, 9263.

[207] W. Lee, J. H. Kim, B.K. Kim, J.H. Kim, W.S. Shin, S.H Jin, Convergent synthesis of PAMAM dendrimers using click chemistry of azide-functionalized PAMAM dendrons, *Tetrahedon Lett.*, **2006**, 62, 9193-9200.

[208] J.W. Lee, B.K. Kim, A facile route to triazole dendrimers via click chemistry linking tripodal acetylene and dendrons, *Bull.Korean Chem. Soc.*, **2005**, 6, 658-600.

[209] J.A. Kretzmann, D. Ho, C.W. Evans, J.H. C. Plani-Lam, B. Garcia-Bloj, E. Mohamed, M.L. O'Mara, E. Ford, D.E. K. Tan, R. Lister, P. Blancafort, M. Norret, K.S. Iyer, Synthetically controlling dendrimer flexibility improves delivery of large plasmid DNA, *Chem. Sci.*, **2017**, *in pres press press press*, DOI: 10.1039/c7sc00097a.

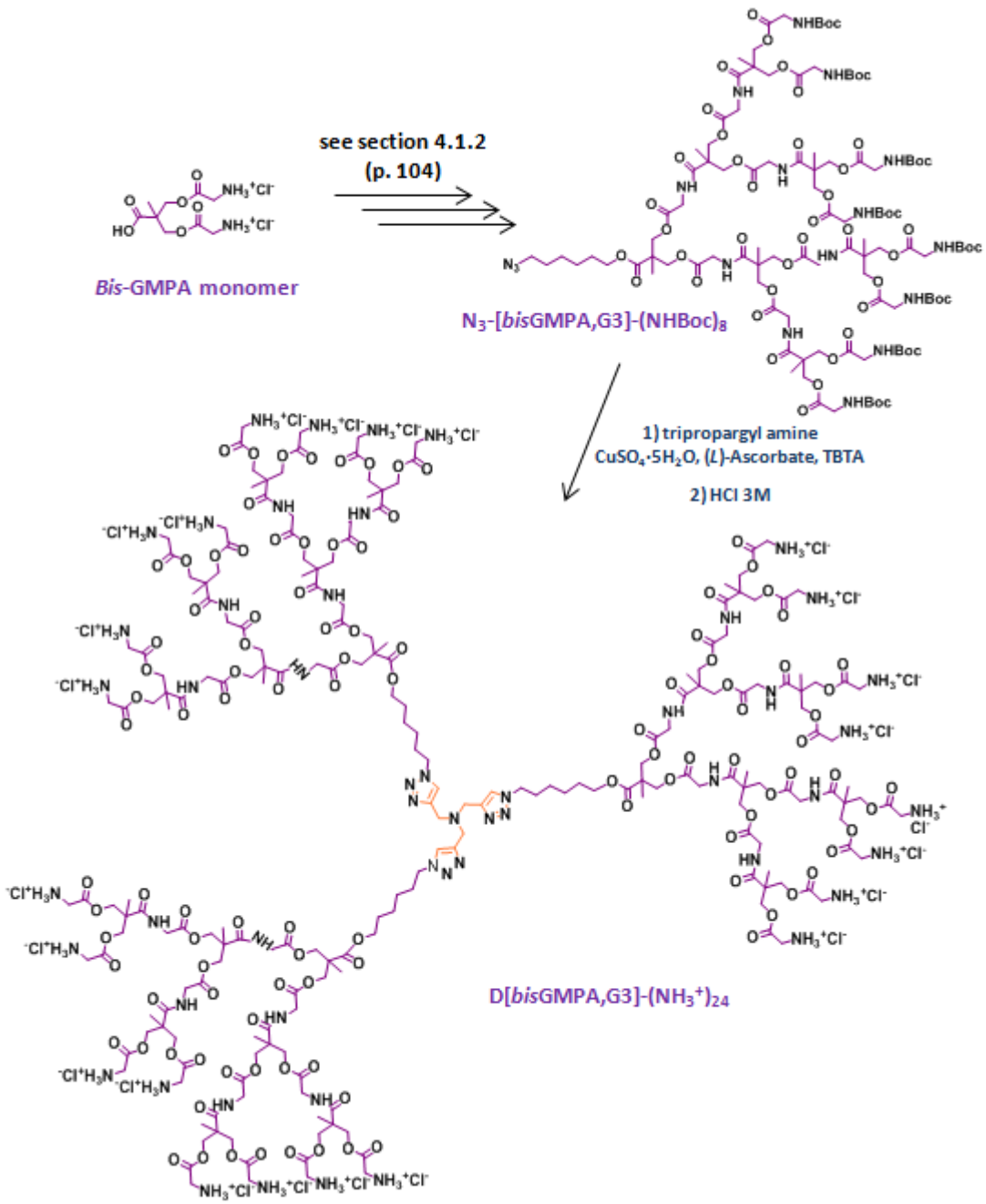

Figure C_5-2: Synthesis of the *bis*-GMPA dendrimer of 3rd generation (see chapter 7 for detailled general procedure X) and VI)).

The synthesis of the *bis*-GMPA dendrons of the 3rd and 4th generation with t-*Boc* protected amino groups with an azide group in the focal point is described in section 4.1.2 (see p. 104). These dendrons were made to react with tripropargyl amine by means of Copper(I) azide-alkyne cycloaddition (CuAAC) in dimethylformamide (**figure C_5-2**, general procedure X). An excess of dendron (1.2 mole of dendron per mole of alkyne groups) was added to ensure a

complete functionalization of the dendrimer core. The Cu(I) catalytic species was formed "*in situ*" by reduction of Cu(II) salts of $CuSO_4 \cdot 5H_2O$ using (*L*)-ascorbate in the presence of TBTA to increase its stability.[189]

After completion of the reaction, the reaction mixture was washed several times with different aqueous solutions, including a KCN solution, in order to eliminate the dimethylformamide solvent and the catalytic system. The crude products were precipiated in a mixture of ethyl acetate and hexanes to remove the dendron that had not reacted. Then, dialysis against methanol was carried out to remove all the small impurities.

Finally, the *t*-Boc protecting groups were quantitatively removed in acidic conditions in ethyl acetate, forming the ammonium salts that precipitated from the reaction mixture. Hydrochloric acid was, then, removed under vacuum. The final products were recovered by centrifugation and washed with pure ethyl acetate to remove the remaining acid traces.

The total yield of both reactions was quite high, *i.e.* 85 % and 78 % for the 3^{rd} and 4^{th} generation dendrimer, respectively.

The final dendrimers were characterized with ^{1}H and ^{13}C nuclear magnetic resonance (NMR), Fourier transform infrared spectroscopy (FTIR). Elemental analysis (EA) and size exclusion chromatography (SEC) were performed with the *t*-Boc protected precursors. The complete chemical characterization data are gathered in chapter 7. The correct formation of the triazole ring was first confirmed by ^{1}H NMR and ^{13}C NMR spectrometry (**figure C_5-3**).

[189] T. R. Chan *et al.*, *Org. Lett.*, **2004**, 6, 2853.

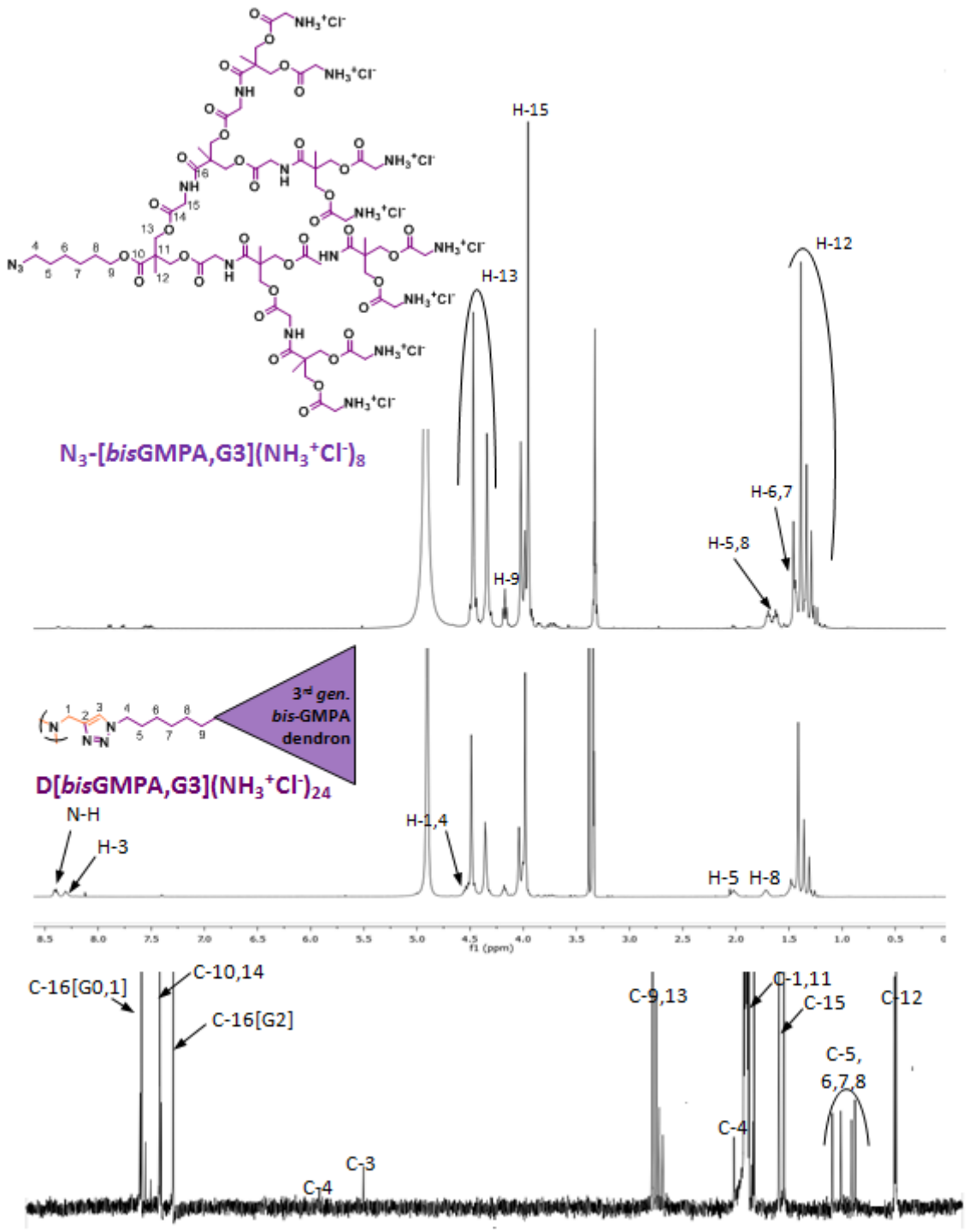

Figure C_5-3: ^{1}H NMR spectrum of **N_3-[*bis*GMPA,G3]($NH_3^+Cl^-$)$_8$** (up) and ^{1}H NMR (middle) and ^{13}C NMR (down) spectra of **D[*bis*GMPA,G3]($NH_3^+Cl^-$)$_{24}$** recorded in CD_3OD at 400 and 100 MHz, respectively.

The **^{1}H NMR** spectrum of the dendrimer shows a singlet at 8.50 ppm that corresponds to the proton of the triazole ring, *H-3*. Additionally, the methylene

protons in the α-position of the triazole belonging to the core, *H-1*, as well as the protons in the α- and β-positions of the triazole belonging to the dendrons, *H-4* and *H-5*, were shifted downfield with respect to the signals observed in the dendron spectrum. They moved from 3.49 to 4.55 ppm (*H-1*), from 2.3 to 4.55 ppm (*H-4*) and from 1.70 to 1.95 ppm (*H-5*). The correct assignation of the peaks was confirmed by ^{1}H-^{1}H COSY and ^{1}H-^{13}C HSQC experiments (see **annexes 8 & 9**).

Furthermore, the **^{13}C NMR** shows two peaks that correspond to the carbon atoms of the triazole ring, *C-2 and C-3*, which appear at 137.9 and 128.7 ppm, respectively.

The absence of dendron that had not reacted with the core was confirmed by FTIR and SEC (**figure C$_5$-4**).

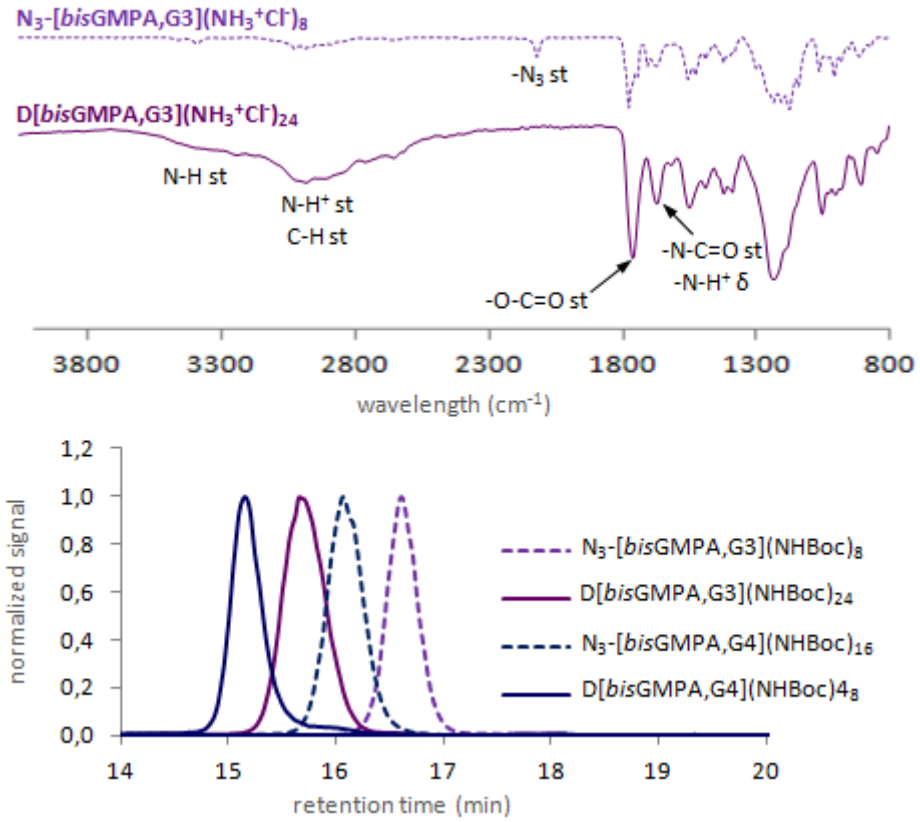

Figure C$_5$-4: FTIR spectra of a dendron and a dendrimer of *bis*-GMPA and SEC chromatogram of the dendrons and dendrimers of 3rd and 4th generation of *bis*-GMPA.

The characteristic band at 2100 cm^{-1}, which corresponds to the azide group of the dendron, is not visible in the FTIR spectrum of the dendrimer. **SEC** chromatograms show an only monomodal peak for the dendrimer of 3^{rd} generation, and a peak with a small shoulder for the dendrimer of 4^{th} generation, although this shoulder doesn't correspond to the maximum of its dendron precursor. The polydispersity of the dendrimers was low, 1.02 and 1.05 respectively using PMMA as a reference, in accordance with their dendritic nature.

In summary, *bis*-GMPA dendrimers of small or medium generations can be easily synthesized following a convergent pathway by means of CuAAC. The two dendrimers showed very few defects and were synthesized with good yields.

5.1.1.2- *Bis*-MPA dendronized hyperbranched polymers (DHPs)

The typical synthesis of high generation dendrimers using either the divergent or convergent method requires many steps followed in all cases by complicated purification processes making them long and tedious. In this context, hyperbranched polymers were developed as an alternative to dendrimers. These polymers are easily obtained in only one step. Although they are polydisperse compounds, their properties, size and terminal groups are very similar in different batches. Today, a lot of commercial hyperbranched polymers is available.[80]

Recently, dendronized hyperbranched polymers (DHPs) have been investigated. They consist on a core based on a hyperbranched polymer of small or medium generation which is decorated with peripheral dendrons. Following this strategy, high generation dendritic macromolecules with low polydispersity can be obtained quite easily. The term pseudodendrimer was also introduced to describe them.[87-89]

In our case, commercial *bis*-MPA hyperbranched polymers of 2nd, 3rd and 4th generation were decorated with *bis*-MPA dendrons of 3rd generation with peripheral glycine moieties following a double stage convergent synthetic pathway (**figure C_5-5**).

In a first step, *bis*-MPA commercial hyperbranched polymers were allowed to react with 4-pentynoic acid according to **Steglich's esterification** conditions (in the presence of N-(3-dimethylaminopropyl)-N'-ethylcarbodiimide

[80] a) Y.H. Kim *et al.*, *J. Am. Chem. Soc.*, **1990**, 112, 4592; b) Y. Zheng *et al.*, *Chem. Soc. Rev.*, **2015**, 44, 4091.
[87] A. Lederer *et al.*, *Angew. Chem. Int. Ed.*, **2015**, 54, 12578.
[88] C. Lach *et al.*, *Macromolecules*, **1998**, 31, 2381.
[89] A. Lederer *et al.*, *Macromol. Rapid Commun.*, **2012**, 33, 1440.

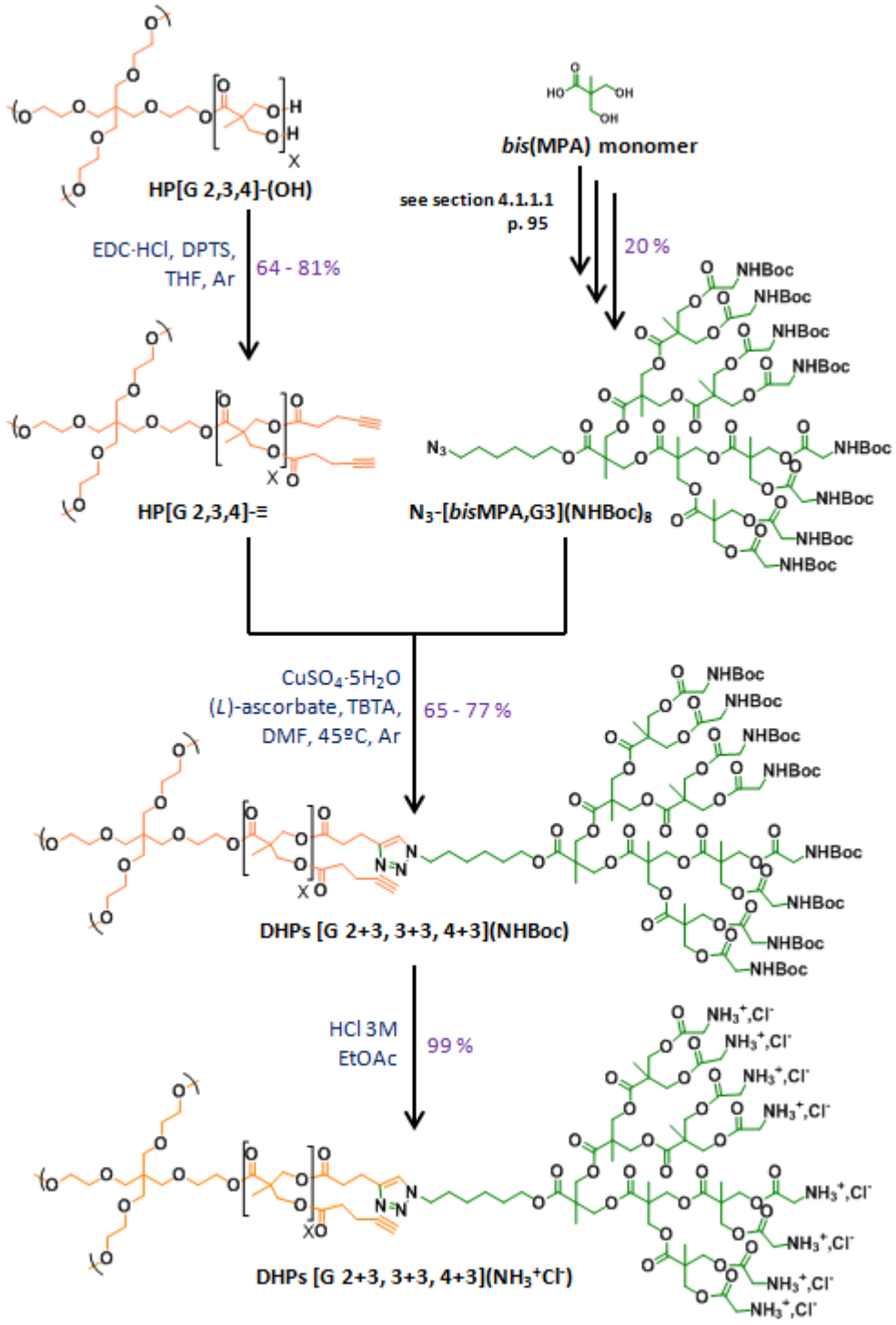

Figure C_5-5: Synthesis of the three *bis*-MPA dendronized hyperbranched polymers of generations 2+3, 3+3 and 4+3.

hydrochloride (EDC·HCl) and DPTS) to insert peripheral alkyne groups at the periphery of the polymers, **HP-[G2,3,4]-≡** (**figure C_5-5**, general procedure XI)). An excess of the acid (1.25 mole per mole of hydroxyl groups) was used to favor a complete functionalization of the terminal hydroxyl groups. In this specific case, EDC·HCl was preferred to DCC as coupling agent as it induces the formation of a water soluble urea derivative that can be easily removed by several washings with aqueous solutions. The hyperbranched polymers were further purified by precipitation into hexanes.[210]

The so prepared hyperbranched polymers **HP-[G2,3,4]-≡** were grafted with the previously synthesized 3rd generation of the *bis*-MPA dendrons with t-Boc glycine moieties at the periphery and with an azide group at the focal point (see section 4.1.1.1, p. 95). As before, the Cu(I) catalytic species was formed *"in situ"* by reduction of Cu(II) salts by (*L*)-ascorbate in presence of TBTA (**figure C_5-5**, general procedure XII)). An excess of the corresponding dendron (1.2 mole of dendron per mole of alkyne group) was used to favor a high level of dendron grafting. The catalytic system was removed by washings with aqueous solutions, including a KCN solution, and filtrated through silica gel in order to remove the catalytic system. Then, the **DHP[G 2+3, 3+3, 4+3](NHBoc)** were precipitated into a mixture of hexanes and ethyl acetate (9/1) to remove the unreacted dendron.

Finally, the *t*-Boc protecting groups of the terminal amino groups were removed under **acidic conditions** (HCl 3M) in ethyl acetate, forming the ammonium salts that precipitated in the reaction medium. Hydrochloric acid was then removed under vacuum. The final products were recovered by centrifugation and washed with pure ethyl acetate to remove remaining acid traces. **DHP[G2+3]($NH_3^+Cl^-$)**, **DHP[G3+3]($NH_3^+Cl^-$)** and **DHP[G4+3]($NH_3^+Cl^-$)** were obtained with **global yields** between 49 and 55 %.

[210] M. Lomba, L. Oriol, R. Alcalá, C. Sánchez, M. Moros, V. Grazú, J.L. Serrano, J.M. de la Fuente, *In situ* photopolymerization of biomaterials by thiol-yne click chemistry, *Macromol. Biosci.*, **2011**, 11, 1505-1514.

All the final DHPs and their respective intermediates were characterized by ^{1}H and ^{13}C nuclear magnetic resonance (NMR) and Fourier transform infrared spectroscopy (FTIR). Additionally, size exclusion chromatography (SEC) were performed for the hyperbranched polymers bearing terminal alkyne groups and with the DHPs bearing terminal *t*-Boc protected amino groups. Elemental analysis (EA) was performed with the DHPs with *t*-Boc protected and unprotected amino groups (see chapter 7 for the complete chemical characterization of the derivatives).

^{1}H NMR was used to confirm the **completion of the reactions** (**figure C_5-6**). The correct insertion of the alkyne groups was confirmed by the apparition of a peak at 1.94 ppm, corresponding to the protons of the alkyne groups *H-13'*, and two other signals at 2.54 and 2.44 ppm that corresponded to the methylene protons in the α- and β-positions of the alkyne groups *H-10'* and *H-11'*, respectively.

The grafting of the *bis*-MPA dendrons after the CuAAC was verified by the apparition of a new peak at 7.41 ppm that corresponded to the proton of the triazole rings, *H-13*. Additionally, four other peaks corresponding to the *bis*-MPA dendrons appeared in the spectra. They corresponded to the methyl groups of the *t*-Boc protecting groups, *H-27* (1.43 ppm), the methylene protons in the β-position of the triazole rings, *H-15* (1.89 ppm), the methylene protons in the α-position of the amino groups, *H-26* (3.87 ppm) and the protons belonging to the amido groups, *N-H* (5.48 ppm).

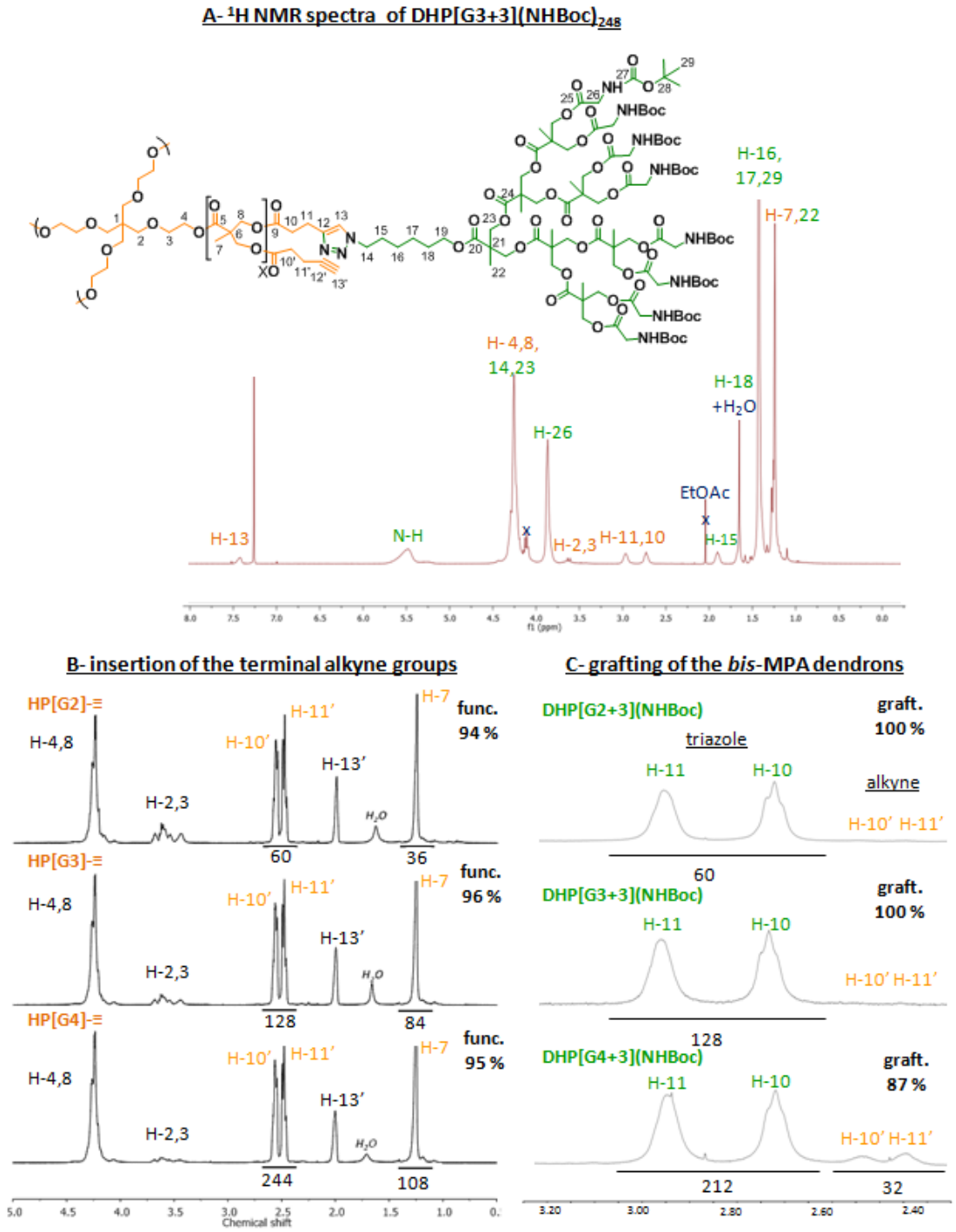

Figure C_5-6: Full ^{1}H NMR spectrum of **DHP[G3+3](NHBoc)** (**A**) and enlargements of the ^{1}H NMR spectra of the 3 hyperbranched polymers **HP[G2,3,4]-≡** (**B**) and the 3 dendronized hyperbranched polymers **DHP[G2+3,3+3,4+3](NHBoc)** (**C**) recorded in $CDCl_3$ at 400 MHz. 1H-1H COSY experiments were carried out to confirm the correct peak assignation (see **annexes 10**).

The **^{1}H NMR** spectrum also permitted to estimate the **proportion of alkyne groups and dendrons that could be effectively grafted** onto the hyperbranched polymer cores.

After the insertion of the terminal alkyne groups, the relative integration of the peaks corresponding to the protons in the α- and β-positions of the alkyne groups (*H-10'* and *H-11'*) were compared with the relative integration of the peak corresponding to the methyl groups of the hyperbranched polymer (*H-7*). This allowed to estimate that the hyperbranched polymer of 2nd generation could be grafted with an average of 15 terminal peripheral alkyne groups while the 3rd and 4th generation ones could be grafted with an average of 31 and 61 peripheral alkyne groups, respectively. These values correspond to degrees of functionalization between 94 % and 96 %.

After the CuAAC reaction, the peaks corresponding to these methylene protons are downfield shifted and move from 2.54 and 2.44 ppm (*H-10'* and *H-11'*) to 2.73 and 2.96 ppm (*H-10* and *H-11*), respectively. In the case of **DHP[G2+3](NHBoc)** and **DHP[G3+3](NHBoc)**, no remaining signals could be observed at 2.44 and 2.54 ppm, leading to affirm that all their terminal alkyne groups were grafted with *bis*-MPA dendrons. However, in the case of **DHP[G4+3](NHBoc)**, remaining signals at 2.44 and 2.54 ppm could be observed and by comparing the relative integrations, it was estimated that 87 % of the alkyne groups could be grafted with dendrons. Thus, after the two reactions, an average of 15 dendrons, 31 dendrons and 53 dendrons were respectively grafted on the hyperbranched polymers of 2nd, 3rd and 4th generation, and this correspond to 120, 248 and 424 terminal amino groups.

Other characterization studies were carried out to control the correct synthesis of the final DHPs. In **^{13}C NMR**, the signals corresponding to the carbon atoms belonging of the triazole rings, *C-12* and *C-13*, appeared at 122.1 and 145.2 ppm together with peaks corresponding to the hyperbranched polymer core (in orange) and to the peripheral dendrons (in green) (**figure C_5-7**).

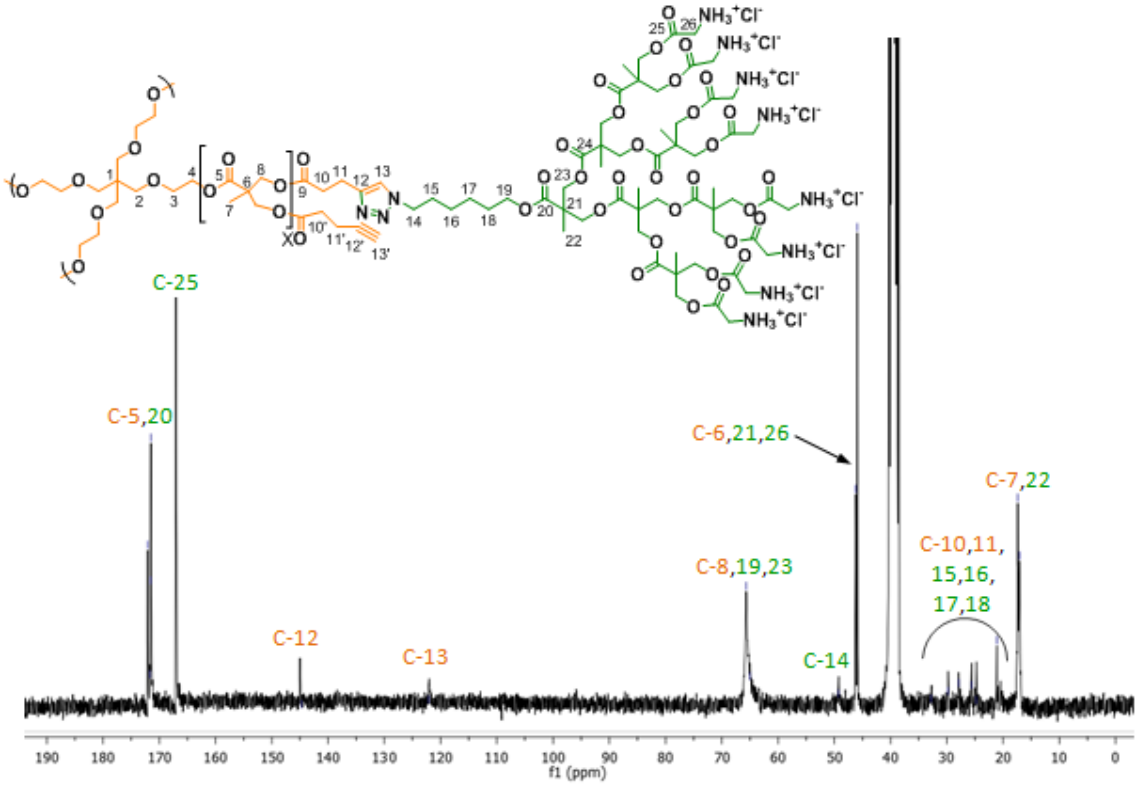

Figure C_5-7: ^{13}C NMR spectra of **DHP[G3+3](NH$_3^+$Cl$^-$)$_{248}$** recorded in $(CD_3)_2SO$ at 75 MHz.

According to the **FTIR** spectra (**figure C_5-8**), the insertion of the terminal alkyne groups was confirmed by the disappearance of the stretching band of the O-H bonds at 3387 cm^{-1} and the apparition of the bands at 3309 and 2119 cm^{-1} corresponding to the stretching of the ≡C-H and C≡C bonds, respectively. After the CuAAC reaction, these two bands were no longer visible and a band at 3354 cm^{-1} corresponding to the stretching of the N-H bond appeared and the band corresponding to the stretching of the C=O bonds (near 1700 cm^{-1}) was modified due to the introduction of carbamate groups. Finally, after removing the *t*-Boc protecting groups, the stretching band of the N-H bonds became much larger, and an only peak due to the C=O bonds of the ester groups could be seen.

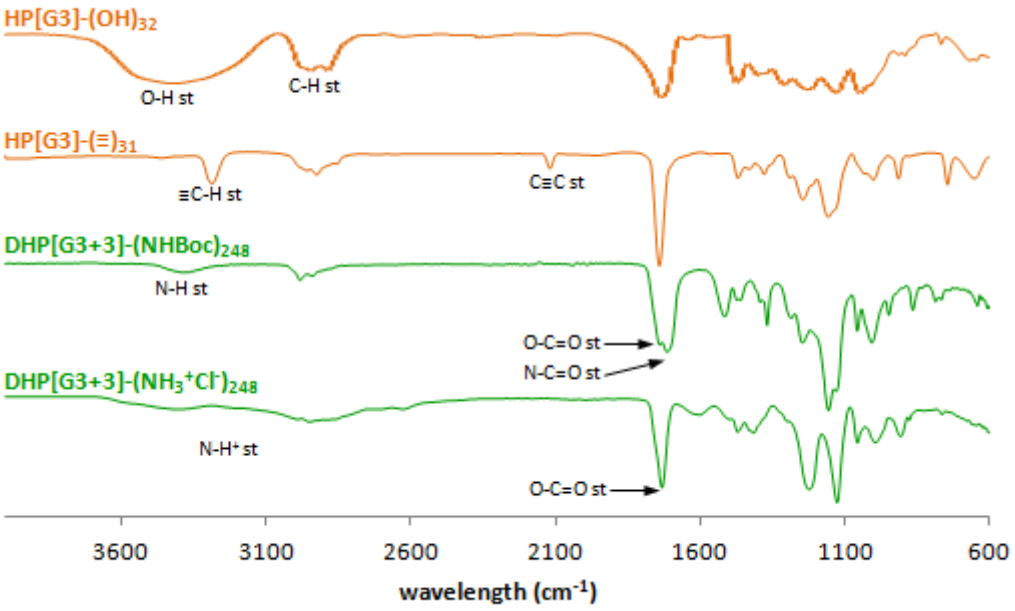

Figure C_5-8: FTIR spectra of **HP[G3]-$(OH)_{32}$**, **HP[G3]-$(≡)_{31}$**, **DHP[G3+3]$(NHBoc)_{248}$** and **DHP[G3+3]$(NH_3^+Cl^-)_{248}$**.

SEC chromatograms show peaks much sharper and at lower retention times (**figure C_5-9**) than the corresponding commercial hyperbranched polymers (HPs), which show broad peaks with several maxima. Additionally, no peak corresponding to free *bis*-MPA dendron can be observed in the chromatograms. The polydispersity of the three DHPs was calculated finding values between 1.13 and 1.22 using PMMA as a reference. The grafting of monodisperse dendrons on hyperbranched polymers of small and medium generations contributes to the low polydispersity of the final compounds.

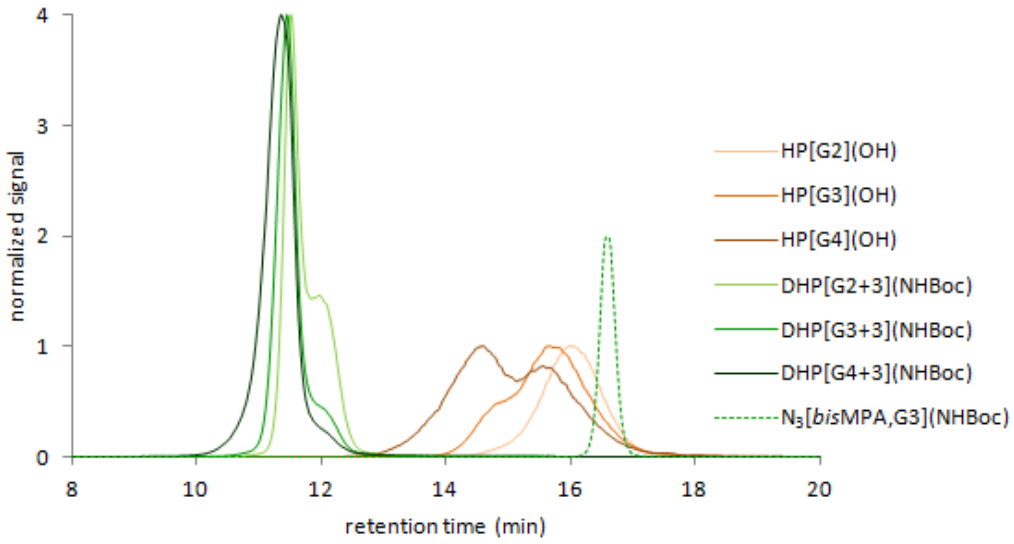

Figure C_5-9: SEC chromatograms of **HP[G2,3,4](OH)**, **HP[G2+3,3+3,4+3](NHBoc)** and **N_3-[*bis*MPA,G3]-$(NHBoc)_8$**.

Following this novel procedure, high generation *bis*-MPA dendronized hyperbranched polymers (DHPs) could be easily synthesized. These macromolecules, also called pseudodendrimers, present a high number of terminal ammonium groups (up to 424) and show a low polydispersity.

5.1.2. Properties

Both types of globular dendritic derivative were considered so as to be employed as gene delivery carriers. For this reason, properties such as bicompatibility, their response to pH changes and aggregation in water were studied.

5.1.2.1. Bicompatibility

These studies carried out in the laboratories of the Center for Biomedical Research of Aragon (CIBA) in collaboration with Dr. M. Pilar Martín-Duque and Dr. Rebeca González-Pastor. Further details of these studies as well as deeper research belong to the thesis work and are gathered in her thesis report.[184] Part of these studies are already published in Bioconjugate Chemistry.[211] This article is added at the end of this chapter for supporting information.

The biocompatibility of non-viral vectors used for gene delivery is undoubtedly an essential issue. However, only few dendrimers are both biocompatible and highly efficient gene vectors.[212] Indeed, classical dendrimers

[184] R. González, Estudio de dendrímeros y nanopartículas de oro para su uso en tratamientos antitumorales, **2017**, Universidad de Zaragoza.

[211] A. Lancelot, R. González-Pastor, A. Concellón, T. Sierra, P. Martín-Duque, J.L. Serrano, DNA transfection to mesenchymal stem cells using a novel type of pseudodendrimer based on 2,2-bis(hydroxymethyl)propionic acid, *Bioconjugate Chem.*, **2017**, *In press*, DOI: 10.1021/acs.bioconjchem.7b00037

[212] a) Y. Wang, L.Li, N. Shao, Z.hu, H.Chen, L. Xu, C. Wang, Y. Cheng, J. Xiao, Triazine-modified dendrimer for efficient TRAIL gene therapy in osteosarcoma, *Acta Bioamat.*, **2015**, 17, 115-124; b) A. Kobayashi, Y. Yokoyama, Y. Osawa, R. Miura, H. Mizunuma, Gene therapy for ovarian cancer using carbonyl reductase 1 DNA with a polyamidoamine dendrimer in mouse models, *Cancer Gene Ther.*, **2016**, 23, 24-28; c) y. Wang, M. Wang, H. Chen, H. Liu, Q. Zhang, Y. Chen, Fluorinated dendrimer for TRAIL gene therapy in cancer treatment, *J. Mater. Chem. B*, **2016**,4, 1354-1360; d) L.Y. Lim, P.Y. Koh, S. Somani, M. Al Robaian, R. Karim, Y.L. Yean, J. Mitchell, R.J. Tate, R. Edrada-Ebel, D.R. Blatchford, M. Mullin, C. Dufès, Tumor regression following intravenous administration of lactoferrin- and lactoferricin-bearing dendriplexes, *Nanomedicine*, **2015**, 1445-1454.

such as naked PAMAMs, PPIs, *etc*. usually showed high gene transfection gene efficacy but notable cytotoxicity whereas others like *bis*-MPA based dendrimer derivatives showed high biocompatibility but low gene transfection efficiency.[213]

The cytotoxicity of the *bis*-GMPA dendrimers and *bis*-MPA DHPs was studied with human cervix cancer cells HeLa and mouse mesenchymal stem cells (MSCs) (**figure C_5-10**).

All the derivatives were biocompatible for these two cell lines. Thus, the cell viability measured for the *bis*-MPA DHPs was high and appeared superior to 85 % in all the cases. The *bis*-GMPA dendrimers also showed elevated biocompatibility with cell viabilities superior to 75 % in both cases.

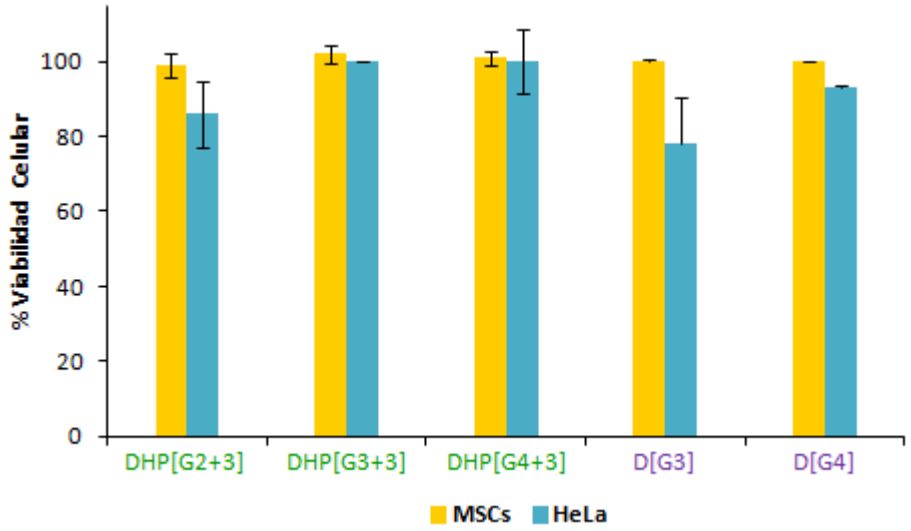

Figure C_5-10: Cell viability measured for HeLa cells and MSCs after 72 hours after 72h with 1 mg/mL of globular dendritic derivatives.

Additionally, the amounts of copper that might have remained in the compounds were measured by inductively coupled plasma atomic emission spectroscopy (ICP-AES) (**table C_5-1**). Indeed, copper is quite cytotoxic and might

[213] a) M. Breunig, U. Lungwitz, R. Liebl, A. Goepferich, Breaking up the correlation between efficacy and toxicity for nonviral gene delivery, *Proc. Natl. Acad. Sci. USA.*, **2007**, 104, 14454–14459; b) L. Jin X. Zeng, M. Liu, Y. Deng, N. He, Current progress in gene delivery technology based on chemical methods and nano-carriers, *Theranostics*, **2014**, 4, 240–255.

accumulate in the tissues, limiting the long-term biocompatibility of the compounds.

Table C_5-1: Amount of copper remaining in the globular dendritic derivatives measured by ICP-AES. [a]The limit of quantification (LOQ) for this technique was of 15 ppm.

globular dendritic derivatives	amount of copper (µg/mg)
D[G3]$(NH_3^+Cl^-)_{24}$	16
D[G4]$(NH_3^+Cl^-)_{48}$	54
DHP[G2+3]$(NHBoc)_{120}$	< LOQ[a]
DHP[G3+3]$(NHBoc)_{248}$	< LOQ
DHP[G4+3]$(NHBoc)_{424}$	< LOQ

The amounts of copper that remained in all the dendritic derivatives were really low and always far below the recommended dietary allowance.[214]

[214]Dietary Reference Intakes Tables and Application, The national academy of sciences, engineering, medicine, Table DRI Values Summary- A com

5.1.2.2 pH change response

The "*proton sponge ability*" of the dendrimers at pH values comprised between 7.4 and 5.0 is entailed during the endosomal escape process and favor transfection efficiency.[49] It is known that a large portion of 2nd and 3rd amino groups in the backbone of the synthetic vectors clearly promotes this ability.[215] Thus, the buffering effect of the two *bis*-GMPA dendrimers and the three *bis*-GMPA DHPs was determined and compared to water and commercial PAMAM dendrimer as negative and positive controls, respectively (**figure C_5-11**).

To decrease the pH from 7.5 to 5.0, 15 µL of HCl 0.1M are required in the case of water (in blue) whereas 130 µL of HCl 0.1 M are required for PAMAM (in red). Surprisingly, and although *bis*-MPA DHPs only contain primary amino groups, they show a "*proton sponge ability*" close to that of PAMAM and better than that of the *bis*-GMPA dendrimers. Indeed, between 90 and 100 µL of HCl 0.1 M are required to decrease the pH in the case of the DHPs while 30 and 50 µL are required for the *bis*-GMPA dendrimers of respectively 3rd and 4th generation. Interestingly, the 4th generation *bis*-GMPA dendrimer shows better proton sponge abilities than the 3rd generation one.

[49] a) A.K. Varkouhi *et al.*, *J. Control. Release*, **2011**, 151, 220; b) J. Behr, *Chimia*, **1997**, 51, 34.
[215] a) J.C. Sunshine, D.Y. Peng, J.J. Green, Uptake and transfection with polymeric Nanoparticles are dependent on polymer end-group structure, but largely independent of nanoparticle physical and chemical properties, *Mol. Pharm.*, **2012**, 9, 3375-83; b) J. Zhou, J. Wu, N. Hafdi, J.P. Behr, P. Erbacher, L. Peng L, PAMAM dendrimers for efficient siRNA delivery and potent gene silencing, *Chem. Comm.*, **2006**, 22, 2362-2364; c) A. Akinc, M. Thomas, A.M. Klibanov, R. Langer, Exploring polyethylenimine-mediated DNA transfection and the proton sponge hypothesis, *J. Gene Med.*, **2005**, 657-663; d) D. Ouyang, H. Zhang, H.S. Parekh, S.C. Smith, The effect of pH on PAMAM dendrimer–siRNA complexation — Endosomal considerations as determined by molecular dynamics simulation, *Biophys. Chem.*, 2011, 158, 2–3, 126–133.

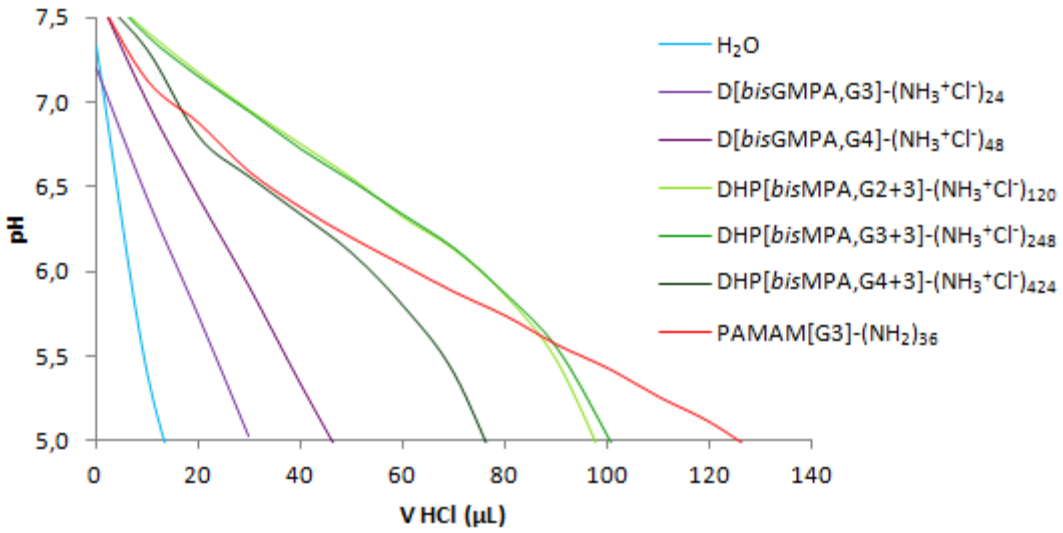

Figure C_5-11: "*Proton sponge*" titration curves of the *bis*-GMPA dendrimers, *bis*-MPA DHPs and commercial PAMAM in presence of 0.1 M NaCl.

In order to explain the good proton sponge ability of the DHPs, **DHP[G3+3](NH$_3^+$Cl$^-$)$_{248}$** was titrated with NaOH (0.1 M). The pH of the solution was measured after each addition of NaOH (**figure C_5-12-A**). As it can be observed in the curve, the pH changes were smooth. This observation confirms some theoretical calculations[216] that predict different pKa values for each terminal amino groups of the **N$_3$-[*bis*MPA,G3]-(NH$_3^+$Cl$^-$)$_8$** dendron, ranged from 6.19 to 7.99 (**figure C_5-12-B**). Due to the important electrical repulsions between the terminal ammonium groups located at the periphery of the dendron, the dissociation of the ammonium group is favored at lower pH, reducing the basic character of the terminal amino groups. As a consequence, some primary amino groups change from their neutral form to their protonated at endosomal pH values and disturb the normal pH decrease of the endosome, acting as a "*proton sponge*".

The poorer proton sponge ability of **DHP[G4+3](NH$_3^+$Cl$^-$)$_{424}$** in comparison with the two other DHPs may be explained by the lowest dendron density on

[216] Calculations performed by MarvinSketch program (www.chemaxom.com).

this hyperbranched polymer core. The electrostatic repulsions between the terminal ammonium groups are lower and, as a consequence, their basicity is higher. They change from their neutral form to their protonated form at higher pH and are therefore less sensitive to the pH changes that take place in the endosomes.

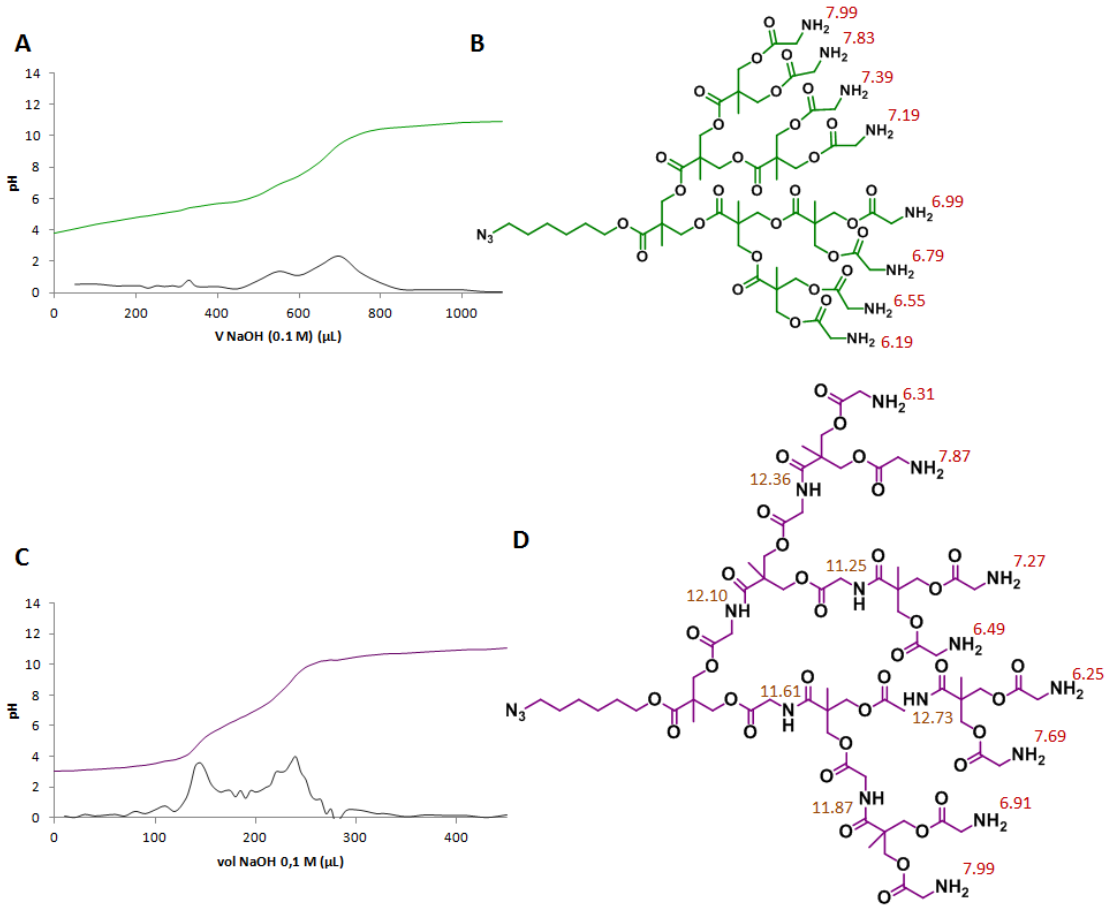

Figure C_5-12: Acid-base titration of **DHP[G3+3]($NH_3^+Cl^-$)$_{248}$** (**A**) and **D[G4]($NH_3^+Cl^-$)$_{48}$** (**C**); colorcurves represent the pH values after each addition of NaOH while grey curves represent the derivative pH curves. Representations of **N_3-[*bis*MPA,G3](NH_2)$_8$** (**B**) and **N_3-[*bisG*MPA,G3](NH_2)$_8$** (**D**) dendrons with pKa values of their terminal amino groups and internal amido groups calculated with MarvinSketch program.

D[G4]($NH_3^+Cl^-$)$_{48}$ was also titrated with NaOH (0.1M) (**figure C_5-12-C**). The derivative of the curve clearly shows two distinct maxima: one corresponding to pH = 4-6 and the other one corresponding to pH = 8-9. This observation does not confirm the theoretical calculations that predicted pKa values for the terminal amino groups comprised between 6.25 and 7.87 (**figure C_5-12-D**).

These results suggest that the insertion of amido groups in the internal branches of the dendrimers modified the protonation of the peripheral amino groups.

5.1.2.3- Aggregation in water

The globular dendritic derivatives were observed by TEM in order to study the morphology they adopt in water and their ability to self-aggregate (**figure C_5-13**).

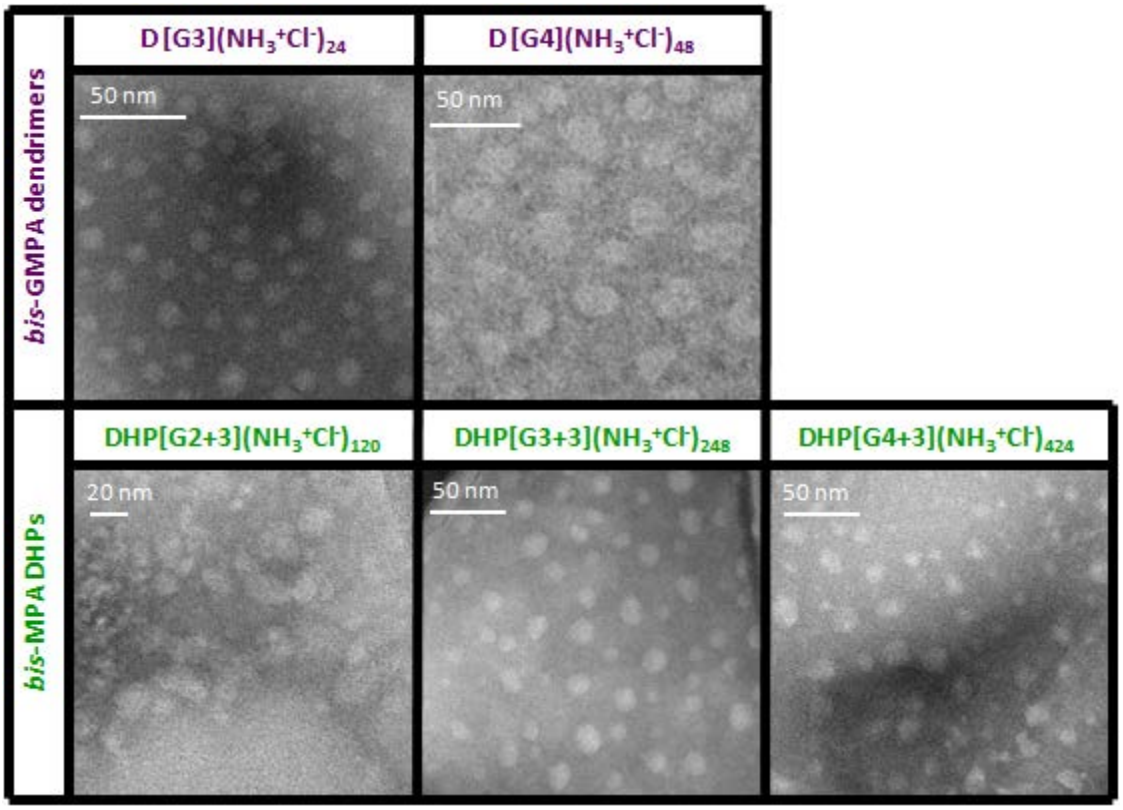

Figure C_5-13: TEM images of the *bis*-GMPA dendrimers and the *bis*-MPA DHPs at 1 mg/mL in distilled water.

Both *bis*-GMPA dendrimers appear as **spherical objects** with average diameters around 10.42 ± 2.63 for **D[G3]($NH_3^+Cl^-$)$_{24}$** and 14.32 ± 2.94 nm for **D[G4]($NH_3^+Cl^-$)$_{48}$**.The *bis*-MPA DHPs appear as **spherical objects** with average diameters around 7.52 ± 4.21, for **DHP[G2+3]($NH_3^+Cl^-$)$_{120}$**, 9.80 ± 2.71 for **DHP[G3+3]($NH_3^+Cl^-$)$_{248}$** and 13.47 ± 3.50 nm for **DHP[G4+3]($NH_3^+Cl^-$)$_{424}$**.

The diameters measured for the ***bis*-MPA DHPs** reveal that they form **unique and independent molecules** dispersed in solution like the "*green peas*" culinary model described by Fréchet.[58] This observation is in accordance with

[58] J.M.J Fréchet, *Science*, **1994**, 263, 1710.

the literature. While the commercial hyperbranched polyester can aggregate in water forming bigger nanoobjects stabilized by lipophilic interactions and/or H bonds,[217] the surface of amino terminated DHPs is positively charged and their aggregation must be impeded by electrostatic repulsion between molecules.

In contrast, ***bis*-GMPA dendrimers**, give rise to TEM images of rounded nanoobjects the diameter of which is too big to correspond to an only molecule. This indicates that **self-aggregation** must have occured. Indeed, these dendrimers can fold upon themselves to adopt a conical shape and several folded dendrimers can self-assemble to form a sphere. This sphere must be stabilized by the H bonds between the internal amide groups of the dendrimers and destabilized by the electrostatic repulsion between the terminal ammonium groups (**figure C_5-14**).

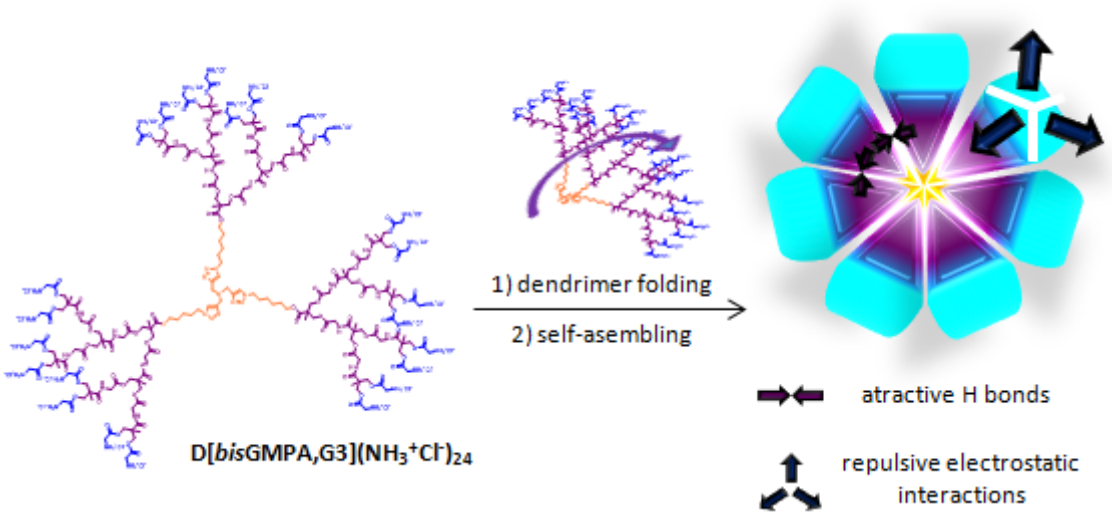

Figure C_5-14: Self-assembly of the dendrimers into bigger spheres.

[217] a) M. Prabaharan, J.J. Grailer, S. Pilla, D.A Steeber, S. Gong, Folate-conjugated amphiphilic hyperbranched block copolymers based on Boltorn® H40, poly(l-lactide) and poly(ethylene glycol) for tumor-targeted drug delivery, *Biomaterials*, **2009**, 30, 3009-19; b) G. Chen, L. Wang, T. Cordie, C. Vokoun, K.W. Eliceiri, S. Gong, Multi-functional self-fluorescent unimolecular micelles for tumor-targeted drug delivery and bioimaging, *Biomaterials*, **2015**, 47, 41-50.

To conclude, two *bis*-GMPA dendrimers and three *bis*-MPA dendronized hyperbranched polymers (DHPs) were synthesized. Both compounds present numerous peripheral cationic ammonium groups to effectively complex pDNA and siRNA. Moreover, as they are biocompatible and as they present proton sponge abilities, they are good candidates to be explored as gene transfection agents.

5.2 - Gene transfection

The ability of both, *bis*-GMPA and *bis*-MPA globular dendritic derivatives, to transfect genetic material was studied. The dendriplexes formation and their characteristics were studied as well as their transfection efficiency. The *bis*-GMPA dendrimers and *bis*-MPA dendronized hyperbranched polymers (DHPs) were used to transfect both pDNA and siRNA.

For pDNA transfection, plasmid enhanced green fluorescent protein (pEGFP) was chosen. This small plasmid (4733 base pairs) induces the fabrication of a green fluorescent protein by the cells that permits to attest the efficiency of the gene transfection and facilitates the comparison between various non-viral vectors, including commercial agents.

For siRNA transfection, green fluorescent protein specified small interfering RNA (siGFP) and luciferease specified small interfering RNA (siLuc) with approximately 20 and 21 base pairs respectively were chosen. siGFP silences the production of GFP by epithelial cells and siLuc silences the production of luciferease by cancerous cells. After gene transfection, the decrease of fluorescence or luminescence allows attesting the efficiency of the gene silencing and facilitates the comparison of various non-viral vectors with commercial agents.

These studies herein detailed were carried out in collaboration with the Center for Biomedical Research of Aragon (CIBA) in collaboration with Dr. M. Pilar Martín-Duque and Rebeca González-Pastor whom performed gel retardation and transfection assays. Complementary investigations such as dendriplexes stability and cellular internalization are gathered in the thesis

report of Rebeca González-Pastor[184] and in one article[218] published in "*Bioconjugate Chemistry"* inserted at the end of this chapter.

[184] R. González, Estudio de dendrímeros y nanopartículas de oro para su uso en tratamientos antitumorales, **2017**, Universidad de Zaragoza.

[218] A. Lancelot, R. González-Pastor *et al.*, *Bioconjugate Chem.*, **2017**, *In press*, DOI: 10.1021/acs.bioconjchem.7b00037

5.2.1- Dendriplex formation and characterization

5.2.1.1- Dendriplex formation

The electrostatic complexation of pDNA and siRNA by the two *bis*-GMPA dendrimers of 3rd and 4th generation and the three *bis*-MPA DHPs of the generations 2+3, 3+3 and 4+3 give rise to the formation of dendrimer/nucleic acid complexes, *i.e.* dendriplexes. Their formation was studied by agarose gel retardation assays and ζ potential measurements.

Agarose gel retardation assays

Electrophoresis studies were carried out with the two *bis*-GMPA dendrimers to observe the migration of the negatively charged genetic material to the positive pole at different ratios $weight_{dendrimer}/weight_{pDNA\ or\ siRNA}$ ($w_{dend.}/w_{pDNA\ or\ siRNA}$). When the genetic materials are totally and strongly complexed by the dendritic derivatives, they don't move and any remaining trace is observed at the same level than the free genetic material (**figure C_5-15**).

The *bis*-GMPA dendrimer of 3rd generation, **D[G3]($NH_3^+Cl^-$)$_{24}$**, can complex the pDNA from a ratio ($w_{dend.}/w_{pDNA}$) 50/1 and fails to totally complex the siRNA at any of the ratios tested. The dendrimer of 4th generation, **D[G4]($NH_3^+Cl^-$)$_{48}$**, shows much better complexation abilities and can totally complex the pDNA from a ratio ($w_{dend.}/w_{pDNA}$) 5/1 and the siRNA from a ratio ($w_{dend.}/w_{siRNA}$) of 80/1. As previously described in the literature for other dendritic derivatives,[219] **the dendrimer of the highest generation showed better siRNA and pDNA complexation abilities than the smallest one**. Contrary to the flexible circular pDNAs, siRNA strands are rigid. Therefore, they cannot wrap around the

[219] L. Albertazzi, F.M. Mickler, G.M. Pavan, F. Salomone, G. Bardi, M. Panniello , E. Amir, T. Kang, K.L. Killops, C. Bräuchle, R.J. Amir, C.J. Hawker, Enhanced bioactivity of internally functionalized cationic dendrimers with PEG cores, *Biomacromolecules*, **2012**, 13, 4089-4097.

dendritic derivatives and more dendritic macromolecules are required to effectively complex all the siRNA, as previously observed in the literature.[220]

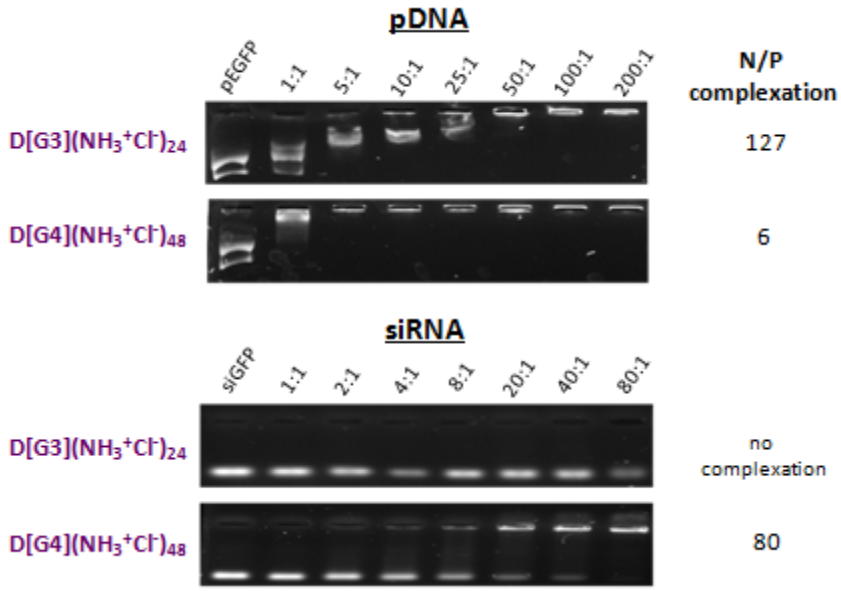

Figure C_5-15: Gel retardation of pDNA (up) and siRNA (down) with increasing concentrations of 3rd and 4th generation *bis*-GMPA dendrimers. The N/P ratio corresponds to the number of N^+ peripheral atoms of the dendritic derivatives required to complex all the P^- atoms of the genetic material.

Electrophoresis studies were also carried out with the three *bis*-MPA DHPs at different ratios ($w_{dend.}/w_{pDNA\ or\ siRNA}$) to estimate their pDNA and siRNA complexation abilities (**figure C_5-16**). The two biggest DHPs, **DHP[G3+3]$(NH_3^+Cl^-)_{248}$** and **DHP[G4+3]$(NH_3^+Cl^-)_{424}$**, **show similar complexation abilities**. They can totally complex the pDNA at ratios ($w_{dend.}/w_{pDNA}$) superior or equal to 3/1 for and the siRNA at ratios ($w_{dend.}/w_{siRNA}$) superior or equal to 25/1. The smallest DHP, **DHP[G2+3]$(NH_3^+Cl^-)_{120}$**, shows lower complexation abilities. It can totally complex pDNA and siRNA starting from ratios ($w_{dend.}/w_{pDNA\ or\ siRNA}$) equal to 5/1 and 200/1, respectively. In addition, and as observed before for the *bis*-GMPA dendrimers, siRNA is fully complexed by the DHPs at higher ratios ($w_{dend.}/w_{pDNA}$ or $_{siRNA}$) than pDNA.

[220] S. Biswas, V.P. Torchilin, Dendrimers for siRNA Delivery, *Pharmaceuticals*, **2013**, 6, 161-183.

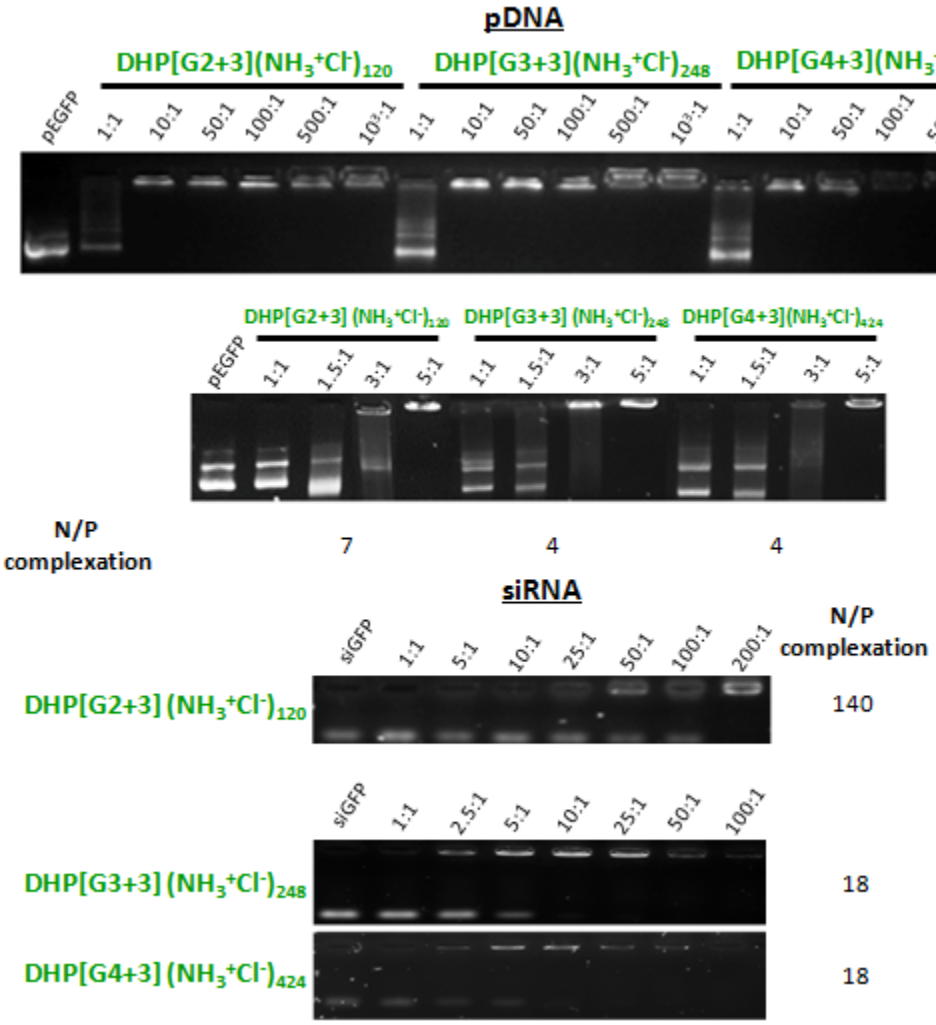

Figure C_5-16: Gel retardation assays of pDNA (up) and siRNA (down) with increasing concentrations of the three *bis*-MPA DHPs. The N/P ratio corresponds to the number of N^+ peripheral atoms of the dendritic derivatives required to complex all the P^- atoms of the genetic material.

Even if **D[G4]-$(NH_3^+Cl^-)_{48}$** has much less terminal protonated amino groups than the **DHPs** (48 versus 120, 248 and 424), it shows similar abilities to complex pDNA (N/P ratios 6 versus 7 or 4). On the other hand, it possess superior abilities than **DHP[G2+3]$(NH_3^+Cl^-)_{120}$** to complex siRNA (N/P ratio 80 versus 140). These results can be explained by the higher flexibility of *bis*-GMPA dendrimers, which allows them to easily wrap pDNA or siRNA, when compared with the rigid unimolecular micelles formed by the DHPs.

ζ potential titration

The ζ potential of different solutions of genetic material with increasing quantity of *bis*-GMPA dendrimers or *bis*-MPA DHPs was measured (**figure C_5-17**).

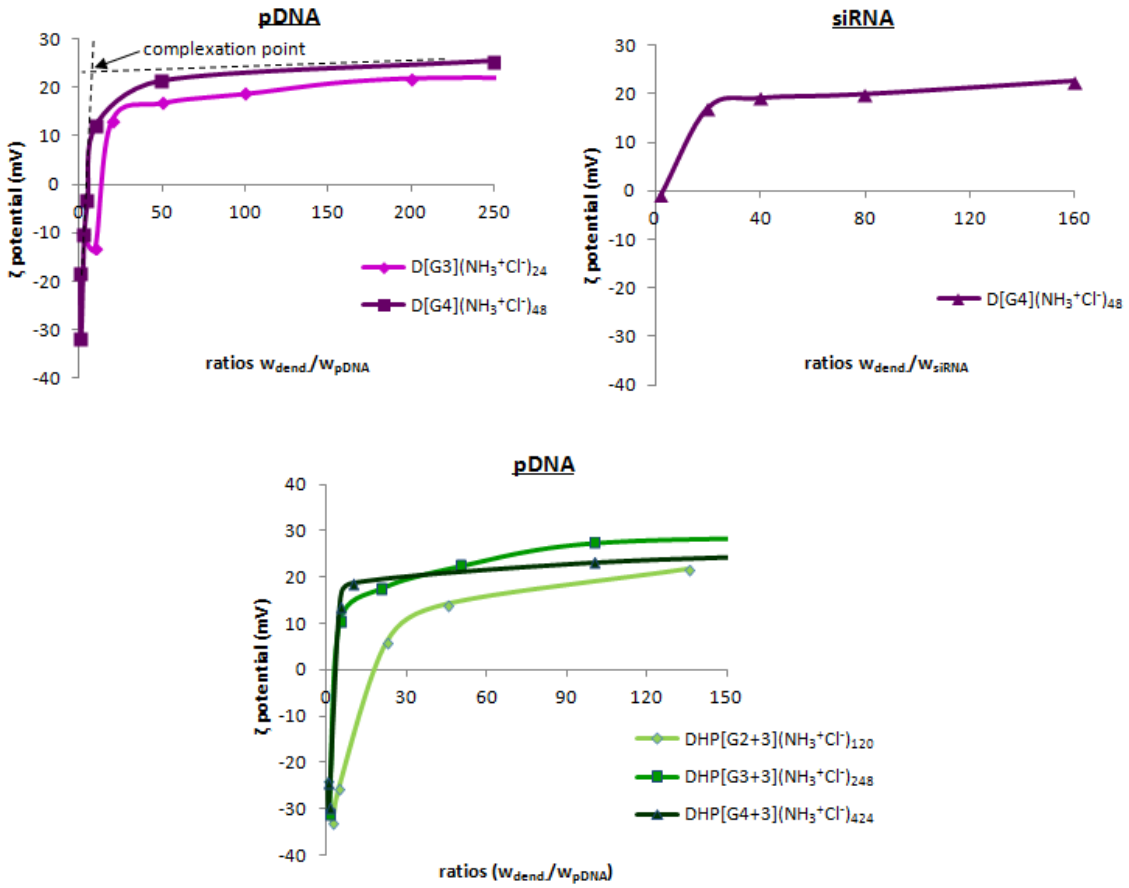

Figure C_5-17: ζ potential of dissolutions of pDNA and siRNA and *bis*-GMPA dendrimers (up) and of dissolution of pDNA and *bis*-MPA DHPs (down) at different ($w_{dend.}/w_{pDNA\ or\ siRNA}$) ratios.

In all cases, the global charge of the particles in solution changes from negative values at low ($w_{dend.}/w_{pDNA\ or\ siRNA}$) ratios to positive values at high ratios drawing curves that present two slopes. The first pronounced slope corresponds to the neutralization of the negative charges of the genetic material by the dendrimers. When the majority of the negative charges of the pDNA or the siRNA are neutralized, the slope of the curve becomes much smoother.

According to this technique, it was determined that **D[G4](NH$_3^+$Cl$^-$)$_{48}$** could complex pDNA at a ratio ($w_{dend.}/w_{pDNA}$) equal to 8.0 and siRNA at a ratio

($w_{dend.}/w_{siRNA}$) equal to 21.4, and **D[G3]($NH_3^+Cl^-$)$_{24}$** could complex pDNA at a ratio ($w_{dend.}/w_{pDNA}$) equal to 22.3. Likewise, **DHP[G3+3]($NH_3^+Cl^-$)$_{248}$** and **DHP[G4+3]($NH_3^+Cl^-$)$_{424}$** could complex pDNA ratios ($w_{dend.}/w_{pDNA}$) equal to 5.6 an 5.4, respectively, whereas **DHP[G2+3]($NH_3^+Cl^-$)$_{120}$** could complex pDNA at a ratio equal to 24.9.

The **($w_{dend.}/w_{pDNA}$) ratios determined by this technique** turn to be **lower** than those determined by the **agarose gel retardation assays** but the **results show similar trends**. The biggest *bis*-GMPA dendrimer **D[G4]($NH_3^+Cl^-$)$_{48}$** can form complexes with pDNA at lower ratios than the smallest dendrimer, **D[G3]($NH_3^+Cl^-$)$_{24}$**, and **DHP[G3+3]($NH_3^+Cl^-$)$_{248}$** and **DHP[G4+3]($NH_3^+Cl^-$)$_{424}$** can complex pDNA at ratios smaller than **DHP[G2+3]($NH_3^+Cl^-$)$_{120}$**. Also, pDNA is complexed by the all the derivatives at lower ratios than siRNA. Additionally, and as observed with the agarose gel retardation assay, **D[G4]($NH_3^+Cl^-$)$_{48}$** has similar abilities to complex pDNA than **DHP[G3+3]($NH_3^+Cl^-$)$_{248}$** and **DHP[G4+3]($NH_3^+Cl^-$)$_{424}$**.

At the end of the titration, the ζ potential values of the dendriplexes were ranged between + 21.6 and + 28.9 mV. The highest values were obtained for the two biggest *bis*-MPA DHPs with pDNA (+ 25.2 and + 28.9 mV) and for the biggest *bis*-GMPA dendrimers with pDNA (+ 25.6 mV). These values are promising: first, they are sufficiently elevated to promote **good cellular internalization** favoring interactions between the dendriplexes and the cellular membrane while, second, as they remain moderated, they should not break down the membrane inducing cell death.[221]

The differences observed between agarose gel retardation assays and ζ potential titration might be explained by the conditions employed to perform

[221] E. Fröhlich, The role of surface charge in cellular uptake and cytotoxicity of medical nanoparticles, *Int. J. Nanomedicine*, **2012**, 7, 5577–5591.

the studies. In particular, the retardation assays were carried out during long time (45 min) and with high voltage applied (95 V) whereas ζ potential measurements were carried out during shorter time (2-3 min) and with lower voltage applied. Moreover, the ζ potential is a value determined for the totality of the sample whereas the gel agarose assay permits to separate the fully complexed, partially complexed and uncomplexed genetic material. Thus, the average ζ potential of the solution can be positive although all pDNA or siRNA are not fully complexed. For example, the **D[G4](NH$_3^+$Cl$^-$)$_{48}$/siRNA** dendriplexes showed a ζ potential equal to + 19.2 mV (**figure C$_5$-17**) at the ratio 50/1 whereas two populations, corresponding to fully complexed and partially complexed siRNA, were observed in agarose gel retardation assay (**figure C$_5$-15**).

5.2.1.2- Morphological studies

Dendriplexes based on bis-GMPA dendrimers

The hydrodynamic diameter of the dendriplexes formed by the dendrimers and the pDNA or siRNA were measured by DLS at the ratios ($w_{dend.}/w_{pDNA}$) 10/1 and 100/1 for pDNA and at the ratios ($w_{dend.}/w_{siRNA}$) 50/1 and 100/1 for siRNA (**table C_5-2**). The results are given employing two mathematical data treatments: the intensity average and the number average hydrodynamic diameter.

Table C_5-2: Hydrodynamic diameters, d_H, and ζ potential of the dendriplexes at different ($w_{dend.}/w_{pDNA\ or\ siRNA}$) ratios at 1 mg/mL.

	dendriplexes	**DLS (D_H, nm)** number	intensity	**ζ potential (mV)**
pDNA	**D[G3](NH$_3^+$Cl$^-$)$_{24}$/pDNA** 10/1	97.2 ± 6.9	97.2 ± 6.9 327.3 ±25.5	- 13.2
	D[G3](NH$_3^+$Cl$^-$)$_{24}$/pDNA 100/1	56.9 ± 11.3	76.7 ± 18.6	+ 18.6
	D[G4](NH$_3^+$Cl$^-$)$_{48}$/pDNA 10/1	55.7 ± 3.6	57.2 ± 3.7 243.7 ±20.9	+ 12.4
	D[G4](NH$_3^+$Cl$^-$)$_{48}$/pDNA 100/1	40.2 ± 15.7	84.7 ± 21.9	+ 22.5
siRNA	**D[G4](NH$_3^+$Cl$^-$)$_{48}$/siRNA** 50/1	56.6 ± 6.9	63.1 ± 9.2	+ 19.2
	D[G4](NH$_3^+$Cl$^-$)$_{48}$/siRNA 100/1	126.3 ± 22.8	178.8 ± 29.4	+20.7

With respect to dendriplexes formed with **pDNA**, two size-populations of aggregates were measured upon applying the intensity average data treatment at the ratio ($w_{dend.}/w_{pDNA}$) 10/1: diameters bigger than 250 nm and diameters smaller than 100 nm. The dendriplexes have a low ζ potential (-13.2 and + 12.4 mV) that promote the self-aggregation of dendriplexes. When the proportion of dendrimer increases, ratio of 100/1, the ζ potential of the dendriplexes is higher

and this impedes dendriplex aggregation.[222] Thus, only a population of small objects was detected in both, number and intensity averages, with diameters smaller than 100 nm.

The **D[G3](NH$_3^+$Cl$^-$)$_{24}$/pDNA** dendriplexes formed at the ratio 10/1 were bigger, more polydisperse and with a negative ζ potential because all the pDNA was not complexed at this ratio in agreement with the agarose gel retardation assays (**figure C$_5$-15**, p. 230).

For dendriplexes formed with **siRNA**, only a size-population was detected for **D[G4](NH$_3^+$Cl$^-$)$_{48}$/siRNA** dendriplexes in number and in intensity average diameters, regardless the ($w_{dend.}/w_{siRNA}$) ratio. Small aggregates were identified at the ratio 50/1, with average diameter *ca.* 60 nm, whereas bigger and more polydisperse aggregates with average diameters *ca.* 120-180 nm were identified at the ratio 100/1.

The results obtained from **DLS measurements were in general confirmed by cryoTEM observation** (**figure C$_5$-18**), although the dendriplexes appeared with smaller diameters in the latter.

In the case of the dendriplexes formed with pDNA, two size-population distributions of spherical objects are observed for the dendriplexes at the ratio 10/1. Big nanoobjects with sizes between 120 and 300 nm and small nanoobjects, more abundant, with sizes between 15 and 35 nm or between 30 and 70 nm for **D[G3](NH$_3^+$Cl$^-$)$_{24}$/pDNA** and **D[G4](NH$_3^+$Cl$^-$)$_{48}$/pDNA** dendriplexes, respectively. At the ratio 100/1, an only population distribution of spherical dendriplexes is observed for the **D[G4](NH$_3^+$Cl$^-$)$_{48}$/pDNA** dendriplexes with sizes comprised between 30 and 120 nm. In contrast to DLS measurements, two size-

[222] I.C. Bellettini, S.J. Fayad, V.G. Machado, E. Minatti, Properties of polyplexes formed through interaction between hydrophobically-modified poly(ethylene imine)s and calf thymus DNA in aqueous solution, soft matter, **2017**, ASAP, DOI: 10.1039/c6sm02835g.

population distribution of spherical objects are observed for **D[G3]$(NH_3^+Cl^-)_{24}$/pDNA** dendriplexes, one with sizes between 15 and 40 nm and another scarce one with sizes superior to 200 nm.

As for dendriplexes formed with siRNA, **D[G4]$(NH_3^+Cl^-)_{48}$/siRNA** dendriplexes at the ratio 50/1, at which the siRNA strands are not fully complexed by the dendrimer, appear as a mixture of objects with two different morphologies, either spherical or elongated, whose sizes ranged from 35 to 60 nm. At the ratio 100/1, all the siRNA was complexed by the dendrimer and this result in an only size-population of elongated objects with sizes *ca.* 50-120 nm. As siRNA is more rigid than pDNA, it cannot wrap the dendrimers and this must induce the formation of bigger and less spherical aggregates.

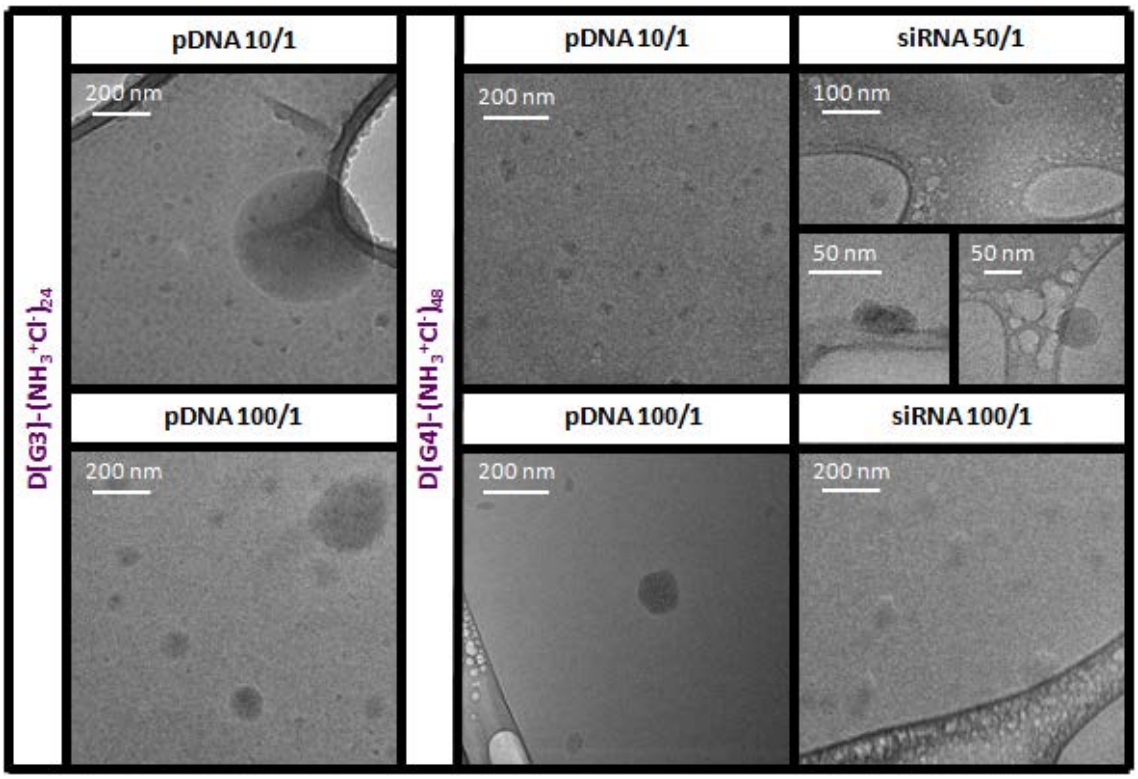

Figure C_5-18: CryoTEM images of the dendriplexes at different ($w_{dend.}/w_{pDNA\ or\ siRNA}$) ratios at 1 mg/mL.

Dendriplexes based on bis-MPA DHPs

The hydrodynamic diameter of the dendriplexes formed by the *bis*-MPA DHPs and the pDNA or siRNA was measured by DLS at the ratios ($w_{dend.}/w_{pDNA}$) equal to 10/1 and 100/1 and at the ratio ($w_{dend.}/w_{siRNA}$) 50/1 (**table C_5-3**). The results are given employing two mathematical data treatments: the intensity average and the number average.

Table C_5-3: Hydrodynamic diameters and ζ potential of the dendriplexes at different ($w_{dend.}/w_{pDNA\ or\ siRNA}$) ratios at 1 mg/mL.

	dendriplexes	DLS (D_H nm) number	DLS (D_H nm) intensity	ζ potential (mV)
pDNA	**DHP[G2+3](NH$_3^+$Cl$^-$)$_{120}$/pDNA** 10/1	18.0 ± 0.1	121.9 ± 42.6	- 17.2
	DHP[G2+3](NH$_3^+$Cl$^-$)$_{120}$/pDNA 100/1	69.6 ± 12.1	87.8 ± 18.7	+ 18.7
	DHP[G3+3](NH$_3^+$Cl$^-$)$_{248}$/pDNA 10/1	38.5 ± 3.3	40.3 ± 3.6 186.3 ± 17.9	+ 17.5
	DHP[G3+3](NH$_3^+$Cl$^-$)$_{248}$/pDNA 100/1	112.7 ± 16.3	127.6 ± 19.5	+ 27.4
	DHP[G4+3](NH$_3^+$Cl$^-$)$_{424}$/pDNA 10/1	39.0 ± 4.3	75.3 ± 36.5	+18.8
	DHP[G4+3](NH$_3^+$Cl$^-$)$_{424}$/pDNA 100/1	41.9 ± 4.6	63.9 ± 27.4	+23.2
siRNA	**DHP[G3+3](NH$_3^+$Cl$^-$)$_{248}$/siRNA** 50/1	47.8 ± 2.8	48.9 ± 2.9 160.7 ± 13.5	X

For **DHP[G2+3](NH$_3^+$Cl$^-$)$_{120}$/pDNA** and **DHP[G3+3](NH$_3^+$Cl$^-$)$_{248}$/pDNA**, at the ratio ($w_{dend.}/w_{pDNA}$) 10/1, two size-population distributions were detected. A population of aggregates with sizes around ca. 20-40 nm according to the number average data treatment and another population of aggregates with sizes around *ca.* 120-190 nm employing the intensity average data treatment. When the amount of DHPs increased up to the ratio 100/1, an only population of dendriplexes with sizes around *ca.* 70 - 90 nm and *ca.* 110 - 130 nm was detected, respectively.

The **DHP[G4+3](NH$_3^+$Cl$^-$)$_{424}$/pDNA** dendriplexes appeared as a unique size-population in both number and intensity averages with sizes around *ca.* 40 - 75 nm at the ratio 10/1 and with sizes around *ca.* 40 - 60 nm at the ratio 100/1. This DHP clearly induces the formation of smaller and stable dendriplexes with positive ζ potential even at the lowest ratios.

The dendriplexes formed with siRNA, **DHP[G3+3](NH$_3^+$Cl$^-$)$_{248}$/siRNA**, showed two size-population distributions at the ratio ($w_{dend.}/w_{pDNA}$) 50/1 applying the intensity average data treatment, a big one with sizes *ca.* 160 nm and a smaller one with size *ca.* 50 nm. Only the population of small aggregates was detected applying the number average data treatment.

CryoTEM observations (**figure C$_5$-19**) **showed good agreement with DLS measurements**. All the dendriplexes containing pDNA appear as spherical aggregates with sizes close to those measured by DLS. **DHP[G2+3](NH$_3^+$Cl$^-$)$_{120}$/pDNA** dendriplexes have diameters around 160 nm at the ratio ($w_{dend.}/w_{pDNA}$) 10/1 and diameters around 130 nm at the ratio 100/1 while **DHP[G3+3](NH$_3^+$Cl$^-$)$_{248}$/pDNA** dendriplexes have diameters around 70 nm at the ratio 10/1 and diameters around 100 nm at the ratio 100/1 and, finally, **DHP[G4+3](NH$_3^+$Cl$^-$)$_{424}$/pDNA** dendriplexes have diameters around 70 nm at the ratio 10/1 and diameters around 50 nm at the ratio 100/1.

In all the cases, an additional population, less represented, composed of spherical aggregates with sizes superior to 200 nm were observed and corresponded to the aggregation of various dendriplexes. The proportion of this second population is higher in the case of **DHP[G2+3](NH$_3^+$Cl$^-$)$_{120}$/pDNA** dendriplexes as it can be observed in the cryoTEM images (**figure C$_5$-19-A**).

In the case of the dendriplexes containing siRNA (**figure C$_5$-19 B)**, two aggregate size-populations were observed for **DHP[G2+3](NH$_3^+$Cl$^-$)$_{120}$/siRNA** dendriplexes with sizes smaller than the ones measured by DLS. In any case, the small aggregate population appears as spherical objects with size *ca.* 30 - 40 nm

and the biggest one presents a more ovoidal shape with sizes *ca.* 60 - 90 nm. As occurred in the case of the ***bis*-GMPA** dendrimer, the siRNA dendriplexes showed a less spherical shape.

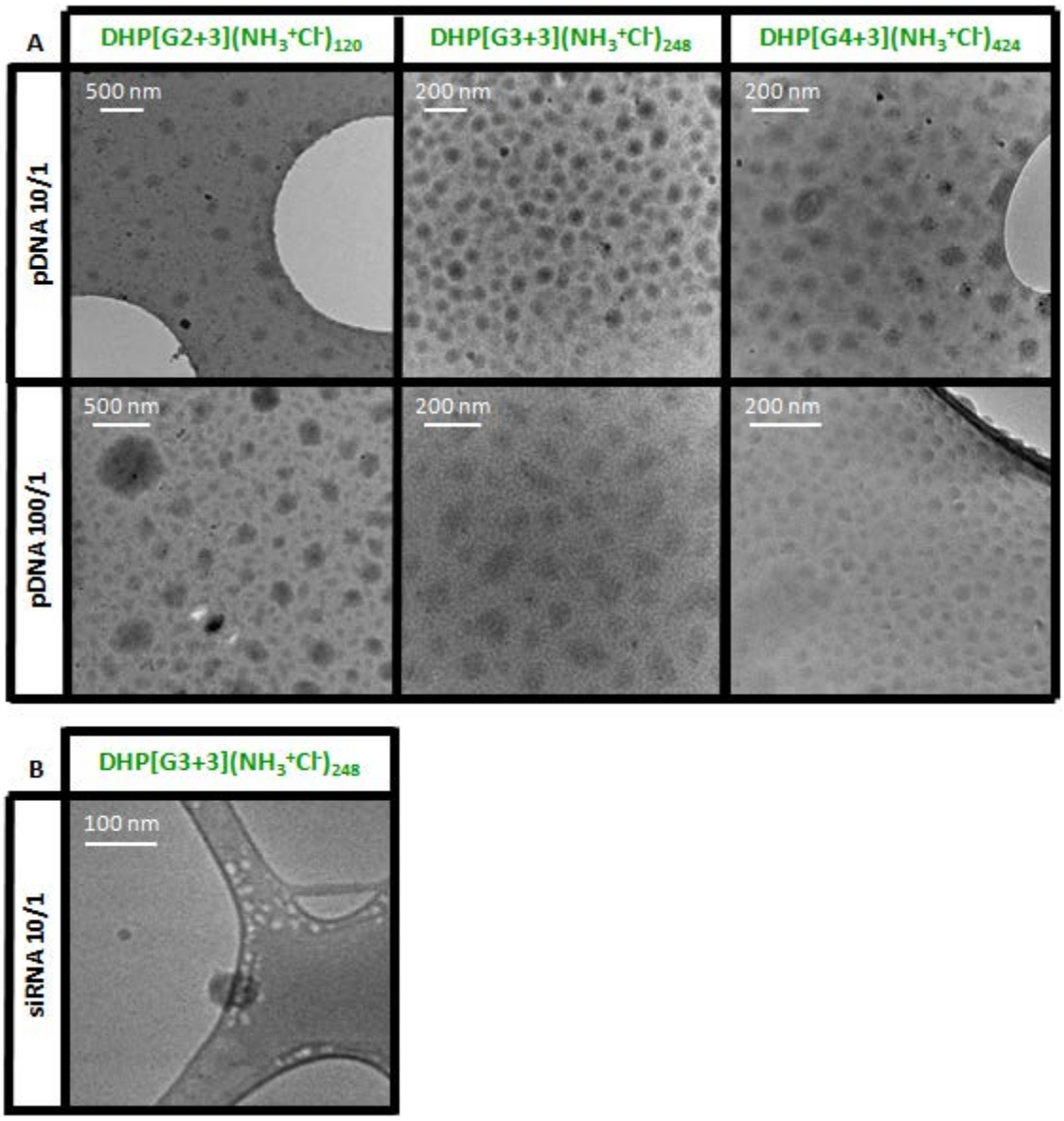

Figure C_5-19: CryoTEM images of the dendriplexes at different ($w_{dend.}/w_{pDNA}$) ratios (**A**) and ($w_{dend.}/w_{siRNA}$) ratios (**B**) at 1 mg/mL.

In all cases, the dendriplexes formed by the *bis*-MPA DHPs and the *bis*-GMPA dendrimers show sizes ranged from *ca.* 20 nm to 200 nm, and this may indicate that various dendritic compounds are involved during the formation of one dendriplex. The dendriplexes formed by the ***bis*-MPA DHPs** and pDNA appeared to be in general bigger than the ones formed by the ***bis*-GMPA dendrimers**. Fortunately, in each series, spherical dendriplexes showing sizes comprised between 50 and 100 nm with positive ζ potential, containing either pDNA or siRNA, were formed. These ideal characteristics should permit the dendriplexes cellular internalization by means of endocytic pathway.[223]

[223] A.P.R. De Garibay, Endocytosis in gene therapy with non-viral vectors, *Wien. Med. Wochenschr.*, **2016**, 166, 227-235.

5.2.2- siRNA and pDNA transfection

In vitro gene transfection was carried out with the *bis*-GMPA dendrimer of 4th generation, **D[G4]($NH_3^+Cl^-$)$_{48}$**, and with the two biggest *bis*-MPA DHPs, **DHP[G3+3]($NH_3^+Cl^-$)$_{248}$** and **DHP[G4+3]($NH_3^+Cl^-$)$_{424}$** as they presented better complexation abilities and formed less polydisperse dendriplexes with higher ζ potential.

For pDNA transfection, pEGFP plasmid was chosen. GFP is a green fluorescent protein and cells effectively transfected with this plasmid would emit green fluorescence. For siRNA transfection, siGFP and siLuc strands were chosen and transfection assays were performed with cells producing GFP or luciferase. When the cells were effectively transfected, they stopped producing GFP or luciferease and the global fluorescence or luminescence of the cells decreased.

Transfection efficiencies obtained with the different dendritic derivatives were compared to FuGene®, Lipofectamine 2000® and/or TransIT-X2® commercial agents.

5.2.2.1- siRNA transfection

siRNA transfection was studied for **D[G4]($NH_3^+Cl^-$)$_{48}$/siGFP** and **DHP[G3+3]($NH_3^+Cl^-$)$_{248}$/siGFP** and **DHP[G4+3]($NH_3^+Cl^-$)$_{424}$/siGFP** dendriplexes with epithelial kidney cells from dog expressing GFP (MDCK-GFP), and for **D[G4]($NH_3^+Cl^-$)$_{48}$/siLuc**, **DHP[G3+3]($NH_3^+Cl^-$)$_{248}$/siLuc** and **DHP[G4+3]($NH_3^+Cl^-$)$_{424}$/siLuc** dendriplexes with cancerous human ovary cells expressing luciferase (SOKV3-Luc) (**figure C_{IV}-20**). Transfection efficiency was compared with that obtained for commercial Lipofectamine® 2000 based complexes.

Although transfection values were lower than the ones obtained after transfection with Lipofectamine® 2000, *bis*-GMPA dendrimers and *bis*-MPA DHPs could reduce the fluorescence or luminescence of the cells, proving the effective GFP and luciferase gene silencing. **D[G4]($NH_3^+Cl^-$)$_{48}$/siGFP** and **D[G4]($NH_3^+Cl^-$)$_{48}$/siLuc** dendriplexes could reduce these proteins expression by up to 12 and 21 % respectively while **DHP[G3+3]($NH_3^+Cl^-$)$_{248}$/siGFP** and **DHP[G3+3]($NH_3^+Cl^-$)$_{248}$/siLuc** could reduce the expression of these proteins by up to 6 and 13 % respectively. No significant differences were observed when gene silencing was performed with either **DHP[G3+3]($NH_3^+Cl^-$)$_{248}$** or **DHP[G4+3]($NH_3^+Cl^-$)$_{424}$**.

In all cases, the cell viability after the transfection was high proving that the reduction of the fluorescence or the luminescence was due to siRNA transfection and not to cell death.

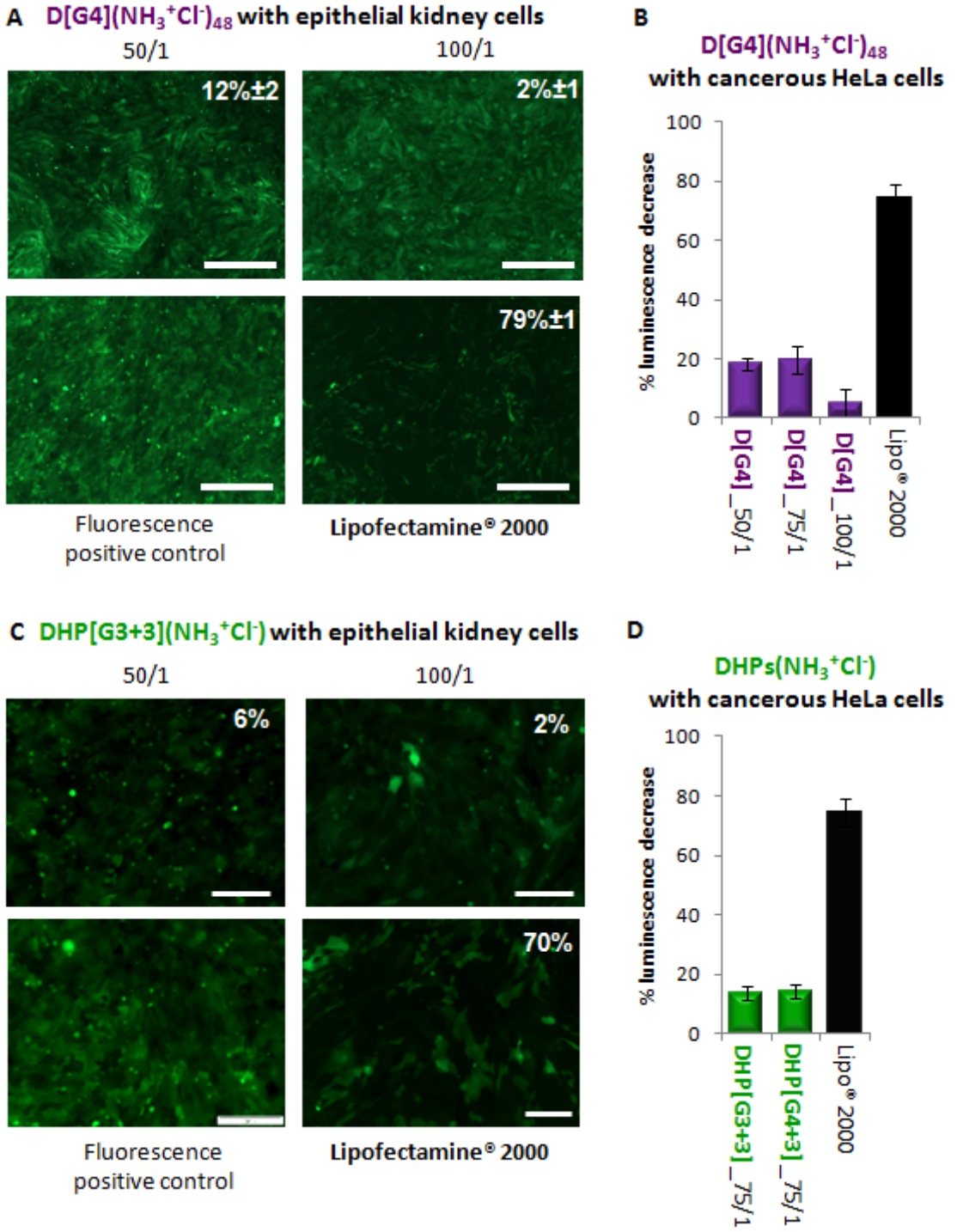

Figure C_5-20: Reduction of GFP expression (**A & C**) and luciferease expression (**B & D**) 48 hours after transfection with **D[*bis*GMPA,G4](NH$_3^+$Cl$^-$)$_{48}$**, **DHP[G3+3](NH$_3^+$Cl$^-$)$_{248}$** and **DHP[G3+3](NH$_3^+$Cl$^-$)$_{424}$** in MDCK-GFP and SOKV3-Luc cells at different ($w_{dend.}/w_{siRNA}$) ratios. Lipofectamine® 2000 was used as a positive control. Scale bar = 500 µM. The relative fluorescence of each sample (indicated in white at the right photo corner) was measured by flow cytometry.

Surprisingly, the transfection efficiencies obtained with **D[G4]($NH_3^+Cl^-$)$_{48}$** for both, GFP and luciferease, are higher at the ratio ($w_{dend.}/w_{siRNA}$) 50/1 than at the ratio 100/1, although siRNA appears to be not totally complexed at this lower ratio. Nevertheless, at the ratio 50/1, the dendriplexes formed are smaller (average diameters close to 60 nm) and more spherical (**figura C_5-18**, p. 237). These characteristics appear to be more appropriate to promote the cellular uptake of the dendriplexes, and the subsequent gene silencing than those of dendriplexes ay the ratio 100/1, which are bigger (with sizes superior to 100 nm) and less spherical .

D[G4]($NH_3^+Cl^-$)$_{48}$ shows better siRNA transfection efficiency in both cell lines than the two *bis*-MPA DHPs. This dendrimer could reach a siRNA 20 % transfection efficiency at the ratio ($w_{dend.}/w_{siRNA}$) (50/1) with cancerous cells, and 12 % with epithelial cells. The differences observed for the gene silencing obtained for the *bis*-GMPA dendrimers and the *bis*-MPA DHPs are difficult to explain and can be due to different parameters such as cellular uptake, siRNA release, *etc*.

5.2.2.2- pDNA transfection

pDNA transfection experiments were first performed with cancerous human HeLa cells with the **D[G4]($NH_3^+Cl^-$)$_{48}$/pEGFP** dendriplexes and with **DHP[G3+3]($NH_3^+Cl^-$)$_{248}$/pEGFP** and **DHP[G4+3]($NH_3^+Cl^-$)$_{424}$/pEGFP** dendriplexes. Transfection efficiencies were compared to those obtained for two commercial gene vectors (Lipofectamine® 2000 and FuGene®).

As for pEGFP transfection with HeLa cells (**figure C_5-21)**, some green cells could be observed in all the cases 48 hours after transfection proving the expression of the EGFP protein, and consequently a positive gene transfection. Nevertheless, the transfection levels remained low and inferior to the level obtained with FuGene® and Lipofectamine® 2000.

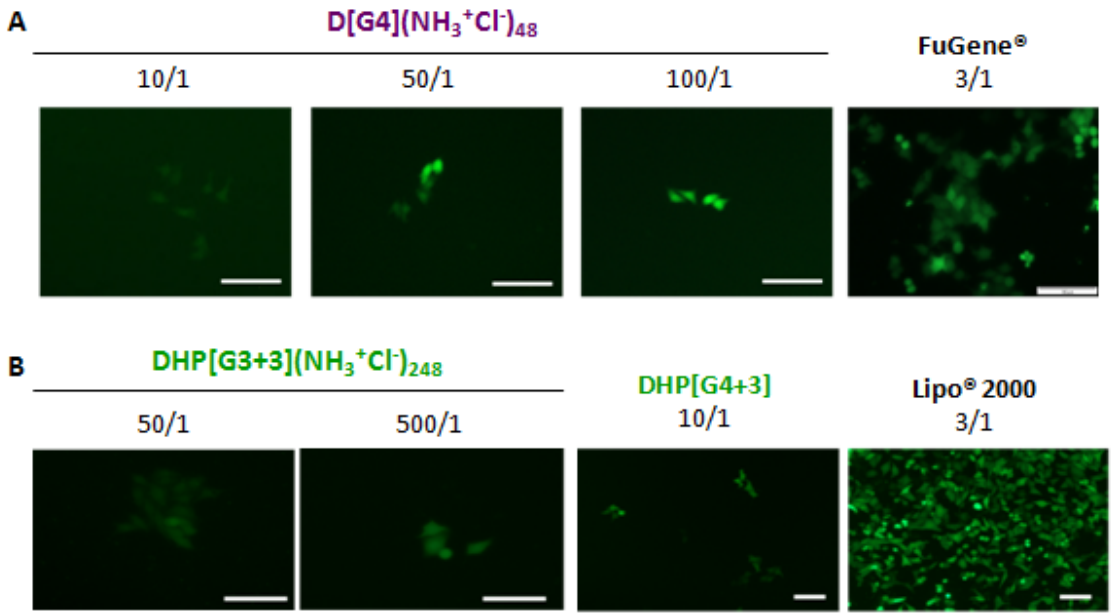

Figure C_5-21: GFP expression at 48 hours after transfection with **D[G4]($NH_3^+Cl^-$)$_{48}$** (**A**) and **DHP[G3+3]($NH_3^+Cl^-$)$_{248}$** and **DHP[G3]($NH_3^+Cl^-$)$_{424}$** (**B**) in HeLa cells at different ($w_{dend/DHPs.}/w_{pEGFP}$) ratios. FuGene® and Lipofectamine® 2000 were used as a positive control. Scale bar = 100 µm.

pEGFP transfection efficiency does not increase when the ratio ($w_{dend.}/W_{pEGFP}$) increases. However, **D[G4]($NH_3^+Cl^-$)$_{48}$/pEGFP** and **DHP[G4+3] ($NH_3^+Cl^-$)$_{424}$/pEGFP** dendriplexes can positively transfect HeLa cells with pEGFP starting from ratios lower (10/1) than **DHP[G3+3]($NH_3^+Cl^-$)$_{248}$/pEGFP**

dendriplexes that showed positive transfection at ratios superior or equal to 50/1.

pEGFP transfection was also carried out with **mesenchymal stem cells** (MSCs) from mousse origin with **DHP[G3+3]($NH_3^+Cl^-$)$_{248}$/pEGFP** and **DHP[G4+3]($NH_3^+Cl^-$)$_{248}$/pEGFP** dendriplexes. As they can still differentiate, MSCs show high potential to treat a large variety of diseases after transplantation. In particular, *ex-vivo* gene transfected MSCs can be used to favor their transplantation or locally induce the expression of therapeutic genes.[224]

Transfection experiments with MSCs were carried out with **DHP[G3+3]($NH_3^+Cl^-$)$_{248}$/pEGFP** and **DHP[G4+3]($NH_3^+Cl^-$)$_{424}$/pEGFP** dendriplexes at three ratios ($w_{DHPs.}/w_{DNA}$) 50/1, 100/1 and 200/1 and compared with two commercial agents: Lipofectamine® 2000 and TransIT-X2® as positive references (**figure C_5-22-A**).

48 hours after transfection, green cells were observed in all cases proving that the two *bis*-MPA DHPs could effectively transfect pDNA in MSCs. In particular, the GFP expression obtained after transfection with **DHP[G4+3] ($NH_3^+Cl^-$)$_{424}$/pEGFP** at the ration 200/1 reaches levels similar than the ones obtained after transfection with the complexes based on the commercial agents.

[224] C. Madeira, R.D. Mendes, S.C. Ribeiro, J.S. Boura, M.R. Aires-Barros, C.L. Da Silva, J.M.S. Cabral, Nonviral gene delivery to mesenchymal stem cells using cationic liposomes for gene and cell therapy, *J. Biomed. Biotechnol.*, **2010**, 2010, ID 735349.

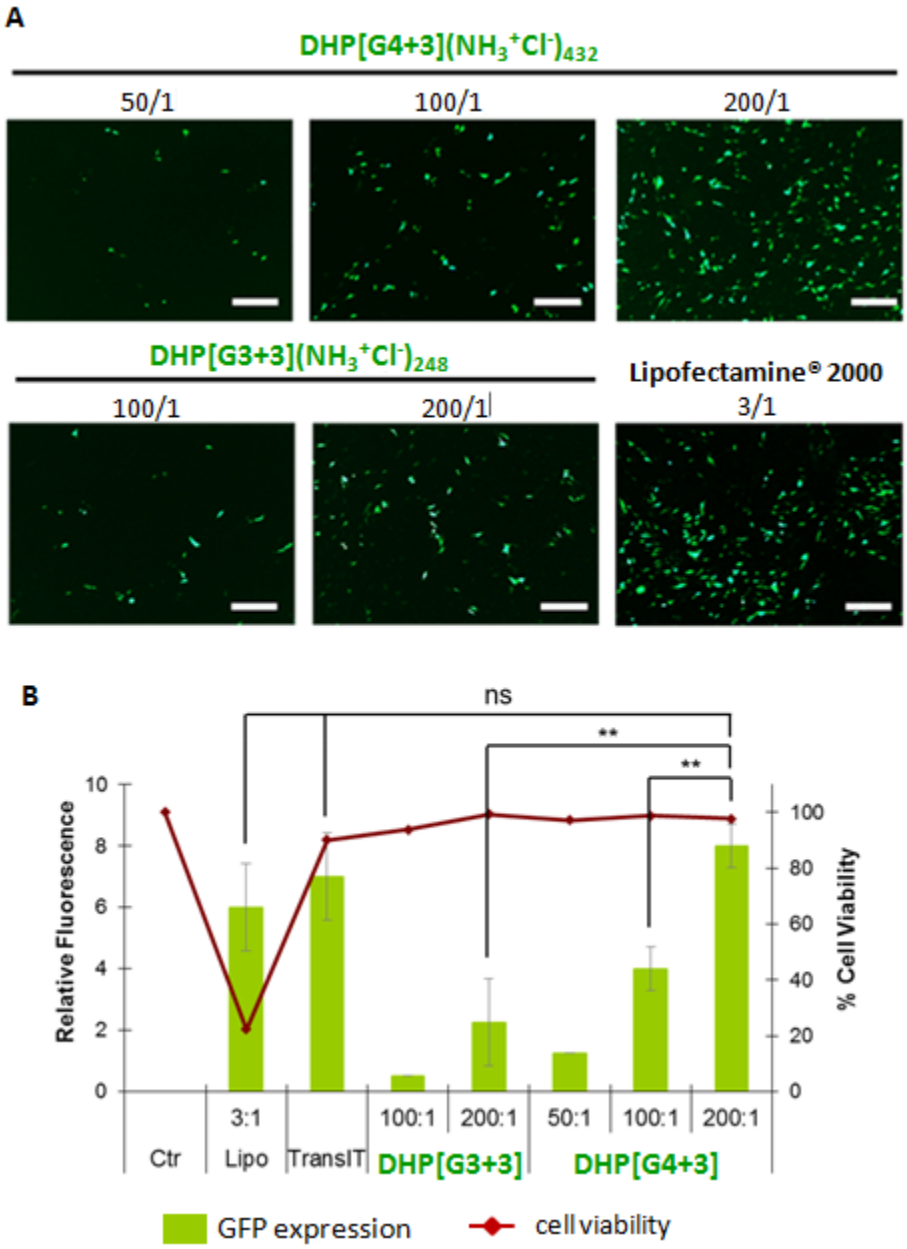

Figure C_5-22: (**A**) GFP expression 48 hours after transfection with **DHP[G3+3]$(NH_3^+Cl^-)_{248}$** and **DHP[G4+3]$(NH_3^+Cl^-)_{424}$** in MSCs at different ($w_{dend.}/w_{pEGFP}$) ratios. Lipofectamine 2000® was used as a positive reference control. Scale bar = 100 µm. (**B**) Relative fluorescence and cell viability of the samples 48 hours after transfection.

For both DHP based dendriplexes, the levels of the GFP relative fluorescence measured after transfection increase with the ($w_{dend.}/w_{pEGFP}$) ratio (**figure C_5-22-B**). The excellent biocompatibility of the *bis*-MPA DHPs with MSCs allows the use of dendriplexes with an elevated proportion of DHPs that have favored the pDNA transfection without affecting the cell viability.

Moreover, the GFP relative fluorescence levels measured after the pEGFP transfection with **DHP[G4+3]($NH_3^+Cl^-$)$_{424}$/pEGFP** dendriplexes were higher than the ones measured after transfection with the **DHP[G3+3]($NH_3^+Cl^-$)$_{248}$/pEGFP** regardless the ($w_{dend.}/w_{pEGFP}$) ratio. Thus, the dendriplexes formed by **DHP[G4+3]($NH_3^+Cl^-$)$_{424}$** at high ($w_{dend.}/w_{pEGFP}$) ratios that contain an elevated quantity of DHPs have shown the best transfection efficiency. Their smaller size (*ca.* 40-60 nm) might favor their internalization within the cells while the higher quantity of DHPs might favor their endosomal escape by proton sponge effect.

The cell viability was controlled after transfection (**figure C_5-22-B**). Whereas Lipofectamine® 2000 based dendriplexes showed low biocompatibility values (20 %), DHPs dendriplexes showed high biocompatibility values (> 90 %) similar to complexes containing the commercial TransIT-X2®. In conclusion, **DHP[G4+3]($NH_3^+Cl^-$)$_{424}$** shows similar transfection abilities for MSCs than two commercial agents and similar biocompatibility than TransIT-X2® and much higher biocompatibility than Lipofectamine® 2000.

The dendritic systems described herein show an interesting potential as vehicles to transfect siRNA and pDNA. In all cases, higher transfection efficiencies were obtained when the dendriplexes presented a small size close to 50 nm that might promote their cellular internalization. The small *bis*-GMPA dendrimers have shown better abilities than the *bis*-MPA DHPs to transfect siRNA whereas the *bis*-MPA DHPs were more efficient as pDNA vectors. These latter could even reach the transfection levels of two commercial agents with MSCs.

5.3- General remarks

Summary of results

Two *bis*-GMPA dendrimers of 3rd and 4th generation and three *bis*-MPA dendronized hyperbranched polymers (DHPs) of 5th, 6th and 7th generation with numerous terminal glycine moieties were synthesized. They showed high monodispersity and few defects.

The dendritic systems herein presented could complex and transfect pDNA and siRNA to cells. Better siRNA transfection efficiency was obtained employing the *bis*-GMPA dendrimers with HeLa cancerous cells whereas better pDNA transfection was obtained employing the *bis*-MPA DHPs with mesenchymal stem cells. In this last case, the dendritic systems were as efficient as two commercial agents.

Conclusion

Effective gene transfection can be performed with dendritic systems based on both polyester and poly(amidoester) architectures that show high bicompatibility. In particular, dendronized hyperbranched polymers (DHPs) appear as innovative systems as high generation dendritic systems can be reached avoiding long and tedious synthesis.

Future investigation

Dendronized hyperbranched polymers decorated with *bis*-GMPA might be investigated in gene transfection. Moreover, other commercial hyperbranched polymers containing internal amino groups, might be used as cores, such as polyester amide (Hybrane®) or poly(amidoamine) (Helux®).

Chapter 6:

bis-MPA and *bis*-GMPA HDLDBCs and bis-MPA DHPs as antimalarial drugs nanocarriers

In this chapter, the hybrid dendritic-linear-dendritic block copolymers (HDLDBCs) and the dendronized hyperbranched polymers (DHPs), previously presented in this thesis report, are described as antimalarial drug nanocarriers.

First, the encapsulation abilities and the targeting abilities of the nanocarriers are described. Second, the activity of the dendritic nanocarrier/antimalarial drug conjugates against the parasite replication is evaluated. The influence of heparin coating on these abilities is also commented.

Malaria is an infectious disease caused by *Plasmodium* type parasites principally affecting red blood cells (**RBCs**). It generally causes fever, headaches, muscular and articulation pains and digestive troubles and may also cause brain disorders, coma and/or death in some more severe cases. This disease, transfected to human via anopheles mosquito bites, has affected humanity for ages, and references dealing with it were found in documents dated from antic Egypt and China. Nowadays, it affects around 200 million people (~3% of the world population) almost exclusively spread in tropical regions and caused around 430 000 death in 2015, most of them being children under 15 with low economic resources.[225]

Four Nobel prizes were given to award important discoveries related with this disease: Ronald Ros (1902), Alphonse Laveran (1907), Paul Hermann Müller (1948) and Youyou Tu (shared with William Campbell and Satoshi Ōmura, 2015). Thanks to research, deaths attributed to malaria are decreasing since the last decades. Indeed, many efforts have been made to limit anopheles mosquito effects in the region infected by malaria by the use of mosquito nets and/or repellents and also by killing the mosquitoes. Prophylactic treatments also allow limiting the spread of the disease.[226]

Various drugs have been developed and used along History to treat malaria (**figure C_6-1**). **Quinine**, an alkaloid extracted from South American trees, which inhibits the enzymatic activity of the parasite, was the first drug used by the Europeans to treat this illness. Indeed, Jesuits started to use it during the XVII century to eradicate the disease from Rome. However, this drug is highly toxic and can cause cinchonism and severe or even lethal nervous, cardiac and

[225] a) X. Fernández-Busquets, a short (Hi)story of Malaria, IBEC seminars; b) WHO, Malaria fact sheet N°94.

[226] a) https://nobelprize.org; b) UNICEF & WHO, Achieving the malaria MDG target: reversing the incidence of malaria 2000–2015, **2015**, ISBN 978-92-4-150944-2.

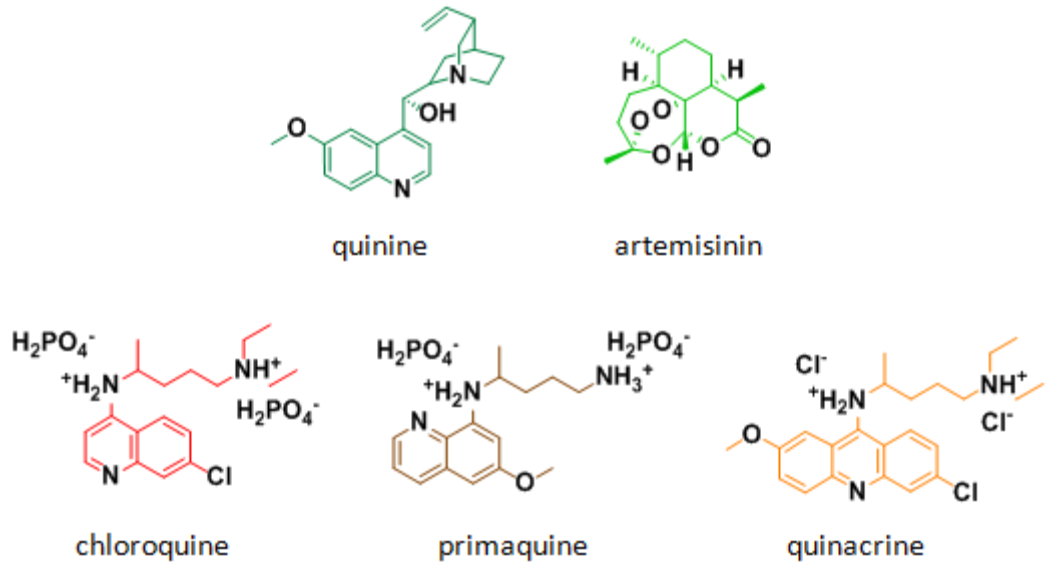

Figure C_6-1: Representation of various common antimalarial drugs: quinine, artemisinin, chloroquine, primaquine and quinacrine.

blood disorders. It has been gradually replaced since the XX century by other derivatives such as chloroquine, quinacrine (also called mepacrine) and primaquine.[227]

Chloroquine was developed during the World War II. It is still the most common drug used to prevent and treat malaria. It binds to heme residues that appear after hemoglobin digestion by the parasites, forming a complex highly toxic that induces cell death and impedes parasites replication. Chloroquine has important side effects, affecting the eyes, the brain, the ears, the skin, and the digestive system. When overdosed, it causes patient death.[227]

Quinacrine was used by the American soldiers during the World War II. Its mechanism of action against the parasites is not well understood although it is known that it binds with DNA and may affect the parasites' cell membranes. Quinacrine is far to be a first choice drug. It is more toxic than quinine and chloroquine and presents common serious side effects such as brain and psychological disorders, digestive issues and yellow skin coloration.[227]

[227] a) WHO, Guidelines for the treatment of malaria, **2006**, b) WHO, Prescribing information: drugs used in parasitic diseases - 2nd Edition, **1995**.

Primaquine was developed at the same period and is used to prevent disease infection and relapse. Indeed, although *plasmodium* principally affects red blood cells, it is also located in the liver in a dormant stage that may induce a new blood infection even after being cured. Its mechanism of action against the parasites remains unknown. Primaquine is less toxic than the other drugs but generally triggers nauseas, vomiting and painful stomach cramps.[227]

More recently, at the end of the XX century, **artemisinin** was re-introduced to treat malaria. This drug was isolated from a plant used in the Chinese traditional medicine for ages. Contrary to the other drugs, this one is well tolerated by the patients. Nevertheless, it is much more expensive that the other ones and its administration is challenging due to its low pharmacokinetical properties.[227,228]

The multiple side effects of these drugs are actually due to the little or inexistent abilities they present to target parasite infected red blood cells. Moreover, drug resistances have risen and forced the World Health Organization (WHO) to restrain the use of new artemisinin to chloroquine or quinine resistant infections. Thus, in the Institute for Bioengineering of Catalonia (IBEC) and in the Institute for Global Health (ISGlobal), Dr. Xavier Fernàndez-Busquets and collaborators are employing nanomedicine benefits in order to improve the targeting and efficacy of current antimalarial drugs to infected red blood cells.[229]

With this aim, antimalarial drugs have been encapsulated within nanoaggregates based on liposomes[230] and polymers[231] containing peripheral

[228] N.J. White, Artemisinin: current status, *Trans. R. Soc. Trop. Med. Hyg.*, **1994**, 88 Suppl. 1, S3-4.

[229] X. Fernàndez-Busquets, Novel strategies for Plasmodium-targeted drug delivery, *Expert Opin. Drug Deliv.*, **2016**, 13, 919-922

[230] E. Moles, K. Moll, J.H. Ch'ng, P. Parini, M. Wahlgren, X. Fernàndez-Busquets, Development of drug-loaded immunoliposomes for the selective targeting and elimination of rosetting Plasmodium falciparum-infected red blood cells, *J. Control. Release*, **2016**, 241, 57-67

amino groups. In particular, in a previous mutual collaboration, two hybrid dendritic-linear-dendritic block copolymers (HDLDBCs) based on Pluronic® F-127 and *bis*-MPA dendrons were successfully used to encapsulate chloroquine and primaquine. The HDLDBCs showed good targeting abilities for infected red blood cells and could enhance the drug activities against the parasite *in vitro* and *in vivo*.[95]

Another strategy developed by Fernàndez-Busquets's group consists on exploiting the use of polysaccharides as both antimalarial agents and as targeting agents for infected red blood cells.[232] In particular, heparin (**figure C_6-2**) has shown both antimalarial activity and targeting abilities.[233] Hence, the heparin coating of the surface of liposomes containing primaquine favored the targeting abilities of the liposome conjugate and enhanced the activity of the drug *in vitro*.[234] The anticoagulant properties of heparin have hinder its development as antimalarial drug. However, it has been demonstrated that the complexation of heparin with polycationic derivatives permits controlling this issue.[235,236]

---

[231] P. Urbán, J.J. Valle-Delgado, N. Mauro, J. Marques, A. Manfredi, M. Rottmann, E. Ranucci, P. Ferruti, Use of poly(amidoamine) drug conjugates for the delivery of antimalarials to Plasmodium, *J. Control. Release*, **2014**, 177, 84-95.

[95] J. Movellan, P. Urbán *et al.*, Biomaterials, 2014, 27, 7940.

[232] J. Marques, E. Vilanova, P.A.S Mourão, X. Fernàndez-Busquets, Marine organism sulfated polysaccharides exhibiting significant antimalarial activity and inhibition of red blood cell invasion by *Plasmodium*, *Sci. Rep.*, **2016**, 6, 24368.

[233]M.J. Boyle, J.S. Richards, P.R. Gilson, W. Chai, J.G. Beeson, Interactions with heparin-like molecules during erythrocyte invasion by Plasmodium falciparum merozoites, *Blood*, **2010**, 115, 4559-4568.

[234] J. Marques, E. Moles, P. Urbán, R. Prohens, M.A. Busquets, C. Sevrin, C. Grandfils, X. Fernàndez-Busquets, Applications of heparin as a dual agent with antimalarial and liposome targeting activities towards *Plasmodium*-infected red blood cells, *nanomedicine*, **2014**, 10, 1719-1728.

[235] X. Fernàndez-Busquets, Heparin-functionalized nanocapsules: enabling targeted delivery of antimalarial drugs, *Future Med. Chem.*, **2013**, 5, 737-9.

[236] K.T. Al-Jamal, W.T. Al-Jamal, K. Kostarelos, J.A. Turtonc, A.T. Florence, Anti-angiogenic poly-L-lysine dendrimer binds heparin and neutralizes its activity, *Res. Pharm. Sci.*, **2012**, 2, 9-15.

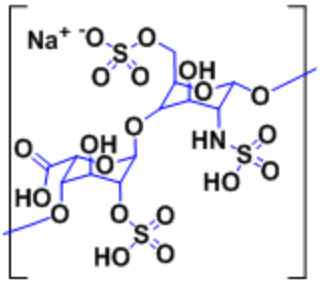

Figure C_6-2: Chemical structure of the most common repetitive units of heparin sodium salt polysaccharide.

According to these results, two ideas have been planned to search for novel nanocarriers for the targeted delivery of antimalarial drugs:

- As a continuation of the research on HDLDBCs the potential of HDLDBCs bearing *bis*-MPA and *bis*-GMPA dendrons previously presented in chapter 4 (**figure C_6-3-A**) has been investigated. Chloroquine (**CQ**), primaquine (**PQ**) and quinacrine (**QN**), three low molecular weight drugs, have been encapsulated in order to enhance their targeting to parasite infected red blood cells and activity against the parasite replication.

- The three dendronized hyperbranched polymers (DHPs) previously described in chapter 5 (**figure C_6-3-B**), which form unimolecular micelles in water and have demonstrated ability to form complexes with polyanionic biopolymers (*i.e.* DNA or RNA),[237] have been selected to prepare nanocarriers for the three antimalarial drugs, in which the targeting effect is reinforced by complexation with heparin.

A part of the studies described in this chapter (heparin complexation, targeting assays and antimalarial activity assays) were carried out in the laboratories of the Institute for Bioengineering of Catalonia (IBEC) and the Barcelona Institute for Global Health (ISGlobal) in collaboration with Dr. Xavier Fernàndez-Busquets during a 2 months stay financed by the Ministerio de Educación, Cultura y Deporte (MECD - scholarship with reference AP2012-5210).

[237] A.C. Rodrigo, A. Barnard, J. Cooper, D.K. Smith, Self-assembling ligands for multivalent nanoscale heparin binding, *Angew. Chem. Int. Ed.*, **2011**, 50, 4675-4679.

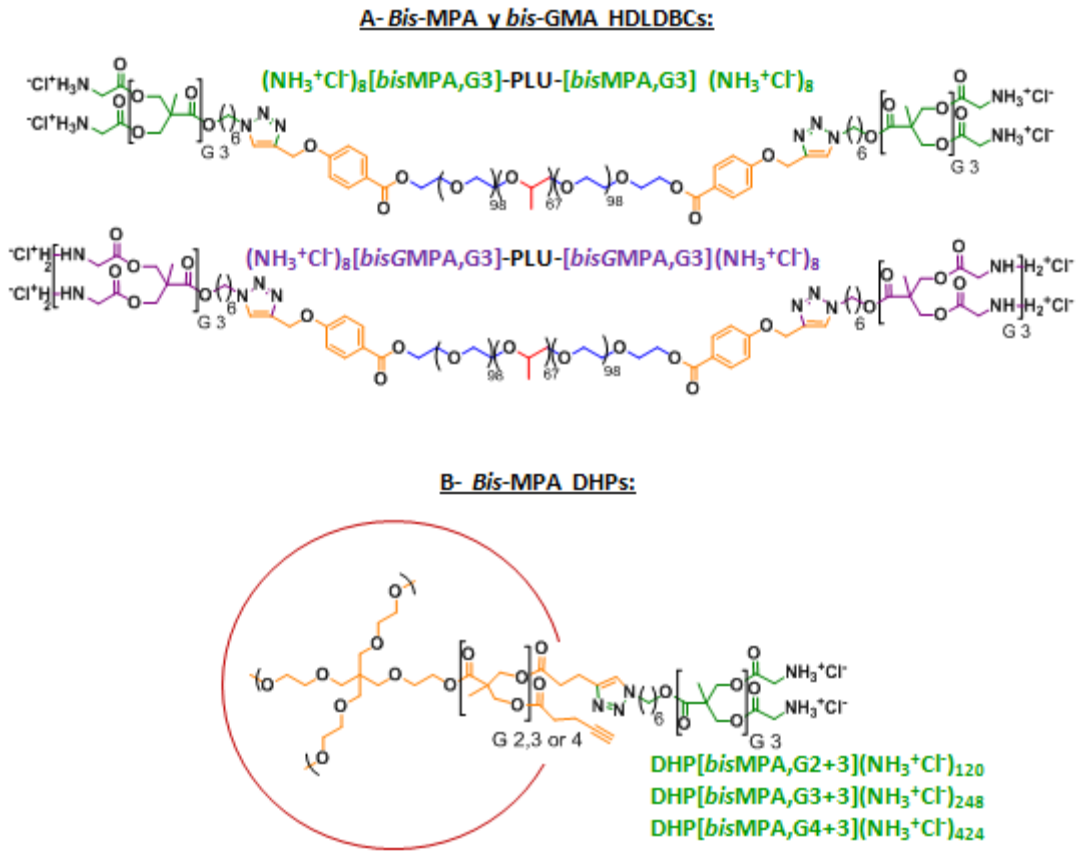

Figure C_6-3: Chemical structures of the HDLDBCs and the DHPs used as antimalarial drugs nanocarriers.

In particular, the study of the plasmodium growing inhibition activity of the dendritic nanocarrier/drug conjugates was performed by Elisabet Martí Coma-Cros and belongs to her thesis work. These results will be discussed at the end of this chapter in order to evaluate the potential of the dendritic nanocarriers to deliver antimalarial drugs.

6.1- Hybrid dendritic-linear-dendritic block copolymers (HDLDBCs)

The abilities of the HDLDBCs to encapsulate chloroquine, primaquine and quinacrine have been studied as well as their targeting abilities to infected red blood cells. The three antimalarial drugs have been encapsulated in their hydrophilic and lipophilic forms.

6.1.1- Chloroquine, primaquine and quinacrine encapsulation

Chloroquine, primaquine and quinacrine are generally administrated to patients in their hydrophilic salt form (**CQs**, **PQs** and **QNs**). Interestingly, their lipophilic base form (**CQb**, **PQb** and **QNb**) can be easily prepared starting from the commercial hydrophilic salt form. The encapsulation of both forms of the drugs into the dendritic nanocarriers may improve their pharmacokinetics properties when compared to the free drugs.

6.1.1.1- Preparation of the lipophilic base form of the drugs

After dissolution of the commercial (Sigma-Aldrich®) salt form of the drugs in water, NaOH (pellets) was added to the solution until pH 12 was reached. During this process, the drugs pass from their hydrophilic salt forms to their lipophilic base forms. Insoluble in water, this form precipitates and can be recovered by extraction with dichloromethane. The evaporation of the solvent yields the pure drugs in their lipophilic base forms with excellent yields, between 91 and 99 % (**figure C_6-4**).

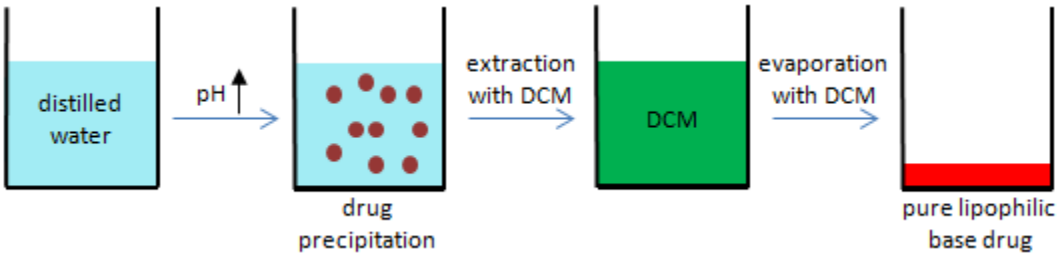

Figure C_6-4: Preparation of the lipophilic base forms of CQ, PQ y QN.

The correct preparation of the lipophilic base forms of the drugs was first of all controlled by the different solubility of the two forms: the hydrophilic form can be solubilized in polar solvent, such as water, whereas the lipophilic base form is only soluble into apolar organic solvents, such as dichloromethane. Furthermore, Fourier transform infrared spectroscopy (FTIR), ^{1}H nuclear magnetic resonance (NMR) spectroscopies and elemental analysis were performed to observe the differences between the two forms of the drugs.

In FTIR, the bands corresponding to the stretching vibration of the N-H bond (near 3270 cm^{-1}) changed when the amines were protonated or not. They passed from really large and unsymmetrical bands in the cases of N^+-H forms to more narrow and symmetrical bands in the case of the N-H forms (**figure C_6-5**).

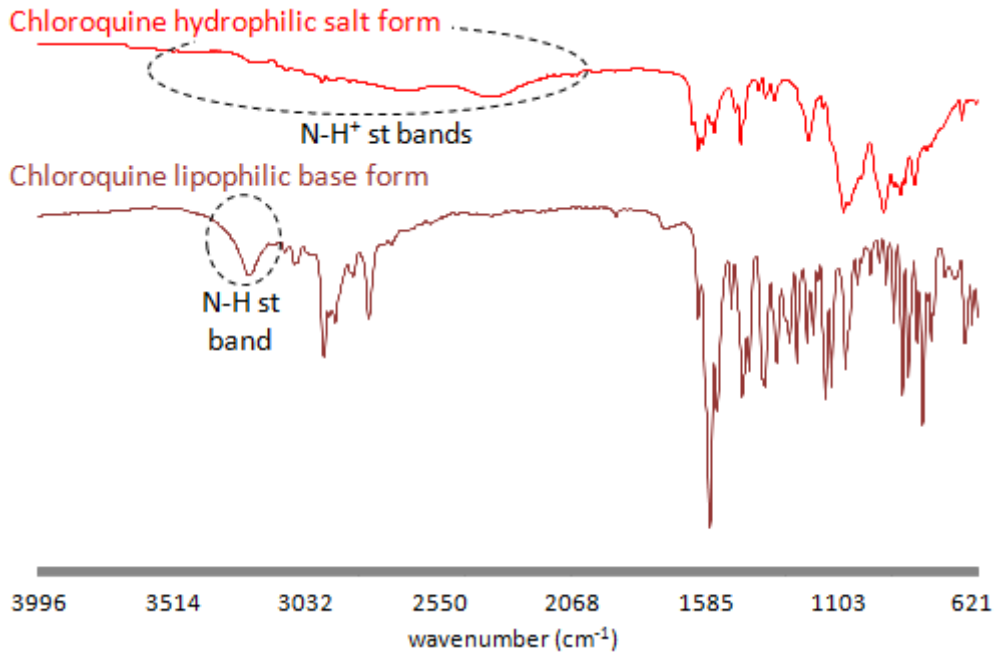

Figure C_6-5: FTIR spectra of chloroquine (CQ) in its hydrophilic salt form (up) and in its lipophilic base form (down).

In ^{1}H NMR, the C-H protons adjacent to the N atoms appear upfield shifted when the drugs pass from their salt form to their base form (**figure C_6-6**). In the case of chloroquine, *H-1* shifts from 3.31 to 3.25 ppm while *H-2* and *H-3* appear more resolved and shift from 2.30 to 1.91 ppm. In the case of primaquine, *H-4* and *H-5* shift, respectively, from 3.21 and 2.33 ppm to 3.14 and 2.09 ppm. Finally, in the case of quinacrine, H-6 shifts from 4.53 to 3.98 ppm while *H-7* and *H-8* appear more resolved and shift from 2.93 to 2.19 ppm.

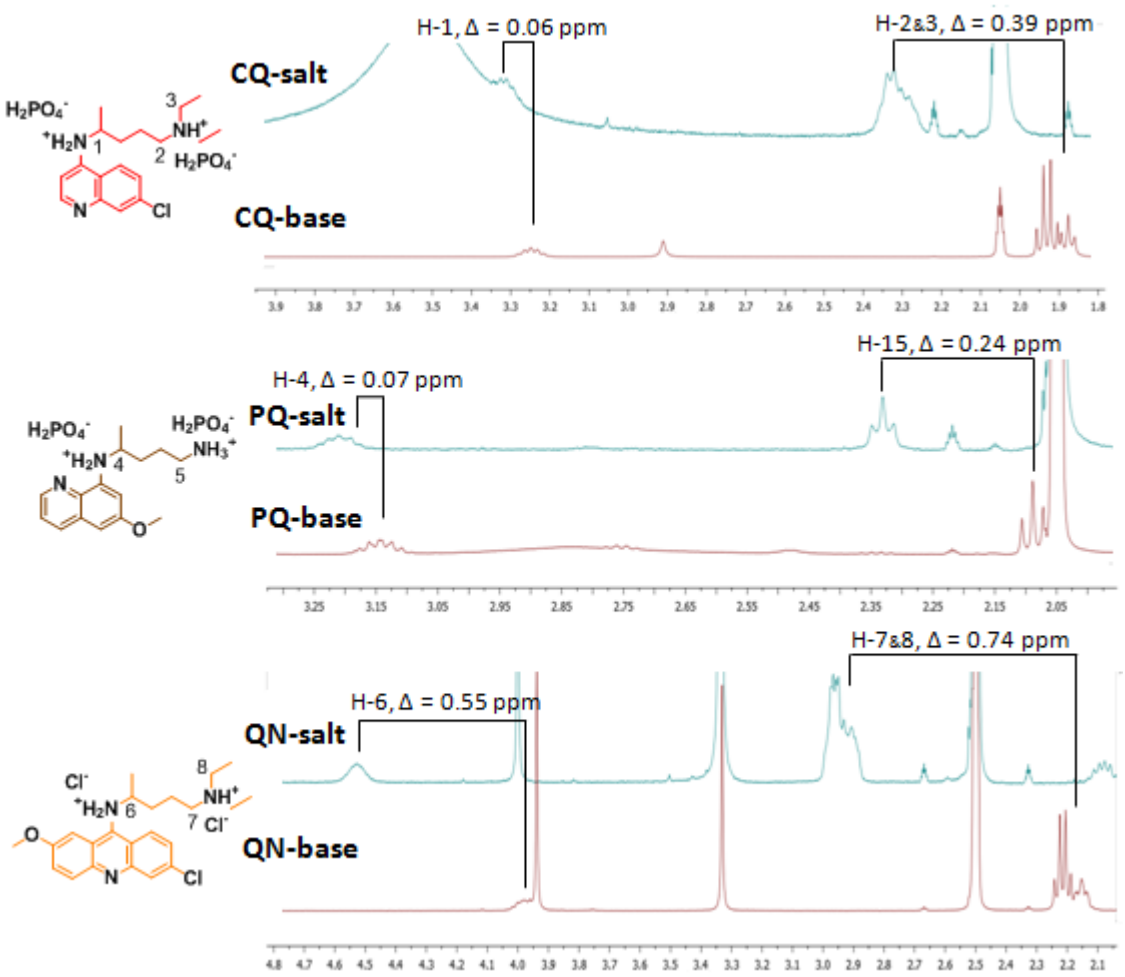

Figure C_6-6: ^{1}H NMR spectra of chloroquine (up), primaquine (middle) and quinacrine (down) in their salt and base forms and the respective structure of their salt from. Protons whose ^{1}H NMR signal were modified during the process are highlighted.

In elemental analysis, as the phosphate and chloride counterions were eliminated during the preparation of the lipophilic base form, the organic content of the three drugs increased (**table C_6-1**). Additionally, this treatment

allowed to increase the purity of the drugs, experimental values were measured closer to the theoretical ones for the lipophilic base forms than for the commercial hydrophilic salt forms.

Table C_6-1: Experimentally measured elemental analysis of C, H and N compared with the theoretic calculated ones for the three drugs in their hydrophilic salt and lipophilic base forms.

			% C	% H	% N	% other
chloroquine	hydrophilic salt form	*th.*	41.9	6.25	8.1	43.75
		exp.	39.6	6.5	7.8	16.1
	lipophilic base form	*th.*	67.6	8.2	13.1	11.1
		exp.	67.5	8.45	13.0	11.05
primaquine	hydrophilic salt form	*th.*	36.9	5.9	9.2	48.0
		exp.	38.8	6.1	9.35	45.75
	lipophilic base form	*th.*	69.5	8.2	16.2	6.1
		exp.	67.85	9.0	16.5	6.65
quinacrine	hydrophilic salt form	*th.*	58.4	6.8	8.9	25.9
		exp.	54.25	7.1	8.3	30.35
	lipophilic base form	*th.*	69.1	7.6	10.5	12.8
		exp.	67.7	7.8	9.9	14.6

6.1.1.2 - Drugs encapsulation

The hydrophilic salt forms (**CQs**, **PQs** and **QNs**) and the lipophilic base forms (**CQb**, **PQb** and **QNb**) of the three drugs were encapsulated within the micelles formed by ***bis*MPA-[PLU]-*bis*MPA** and ***bis*GMPA-[PLU]-*bis*GMPA**) according to the oil-in-water technique (**figure C_6-7**).[95]

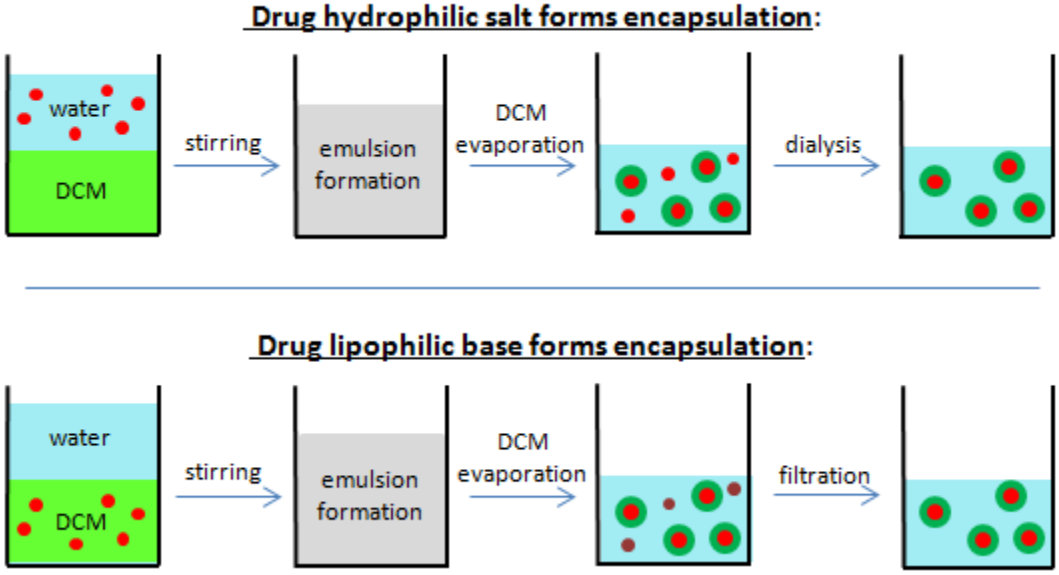

Figure C_6-7: Encapsulation procedures for the antimalarial drugs in their hydrophilic salt forms (up) and their lipophilic base forms (down).

The HDLDBC was dissolved in water (see section 4.2.2.2, p. 152) and the drugs in water or dichloromethane according to their hydrophilicity. The samples were vigorously stirred in order to form an emulsion from which the organic solvent was slowly evaporated, using a ventilation system, until a clear aqueous solution was obtained. The feeding ratio was of 1/1 (w_{drug}/w_{HDLDBC}) (see chapter 7 for detailed protocol).

The **hydrophilic form** of the drugs that was not encapsulated within the dendritic nanocarriers was removed by dialysis. The quantity of drug that could be effectively encapsulated within the nanocarriers was indirectly determined by measuring the UV absorbance of the dialysis waters.

[95] J. Movellan, P. Urbán *et al.*, *Biomaterials*, **2014**, 35, 7940.

The **lipophilic forms** of the drugs that were not encapsulated within the nanocarriers precipitated in the solution at pH 10 after the evaporation of dichloromethane and were removed by filtration. The quantity of drugs encapsulated within the nanocarriers was directly measured by dissolving an aliquot of the nanocarrier/drug complexes in dimehtyl sulfoxide. In this solvent the drugs were quickly released outside the nanocarriers and their concentrations were measured by UV absorbance.

The amounts of drugs encapsulated within the HDLDBC based nanocarriers was calculated in weight and in amount of substance while the encapsulation efficiencies (EE) were calculated by dividing the quantity of drugs encapsulated by the quantity used to perform the encapsulation (**table C_6-2**).

Regarding to the hydrophilic salt forms of the drugs, the quantities of all the three drugs (**CQs**, **PQs** and **QNs**) were high. Slightly higher quantities of **PQs** and **QNs** could be encapsulated within the two HDLDBCs (EE between 41 and 44 %) than **CQs** (EE between 31 and 35 %). Both HDLDBCs show similar encapsulation efficiencies.

Regarding to the lipophilic base forms of the drugs, the quantities of **PQb** encapsulated remained high and its EE, 43 %, was similar to the ones obtained for its hydrophilic salt form. Unfortunately, the quantities of **CQb** and **QNb** encapsulated were really lower and their EE were below 5 %.

All the solutions containing the HDLDBC/antimalarial drug conjugates were freeze-dried in order to facilitate their transport and conservation. After re-dissolution of the solid HDLDBC/drug conjugate, the correct encapsulation was checked again. In the case of the drugs in their hydrophilic form, it was asserted by comparing the fluorescence emission spectra of the free drugs in water with the one of the drugs encapsulated within the ***bis*GMPA-[PLU]-*bis*GMPA** HDLDBC. In all cases, differences are observed in the two spectra,

proving that interactions occurred between the nanocarrier and the hydrophilic drugs (see **annexes 11**). In the case of the drugs in their lipophilic form, the absence of any precipitate after the re-dissolution of the solids obtained after freeze-drying while containing low-water soluble drugs assessed the correct drug encapsulation.

Tables C_6-2: Amount of antimalarial drugs encapsulated within the HDLDBCs based nanocarriers in their hydrophilic salt forms (up) and in their lipophilic base forms (down). [a]EE means encapsulation efficiency.

	***bis*MPA-[PLU]-*bis*MPA**			
	drug	mg drug / mg HDLDBC	mol drug / mol HDLDBC	EE[a] (%)
hydrophilic salt form	**chloroquine**	0.348	17.75	35
	primaquine	0.412	25.92	41
	quinacrine	0.423	17.26	43
lipophilic base form	**chloroquine**	0.075	3.83	4
	primaquine	0.427	26.86	43
	quinacrine	0.009	0.37	1
	***bis*GMPA-[PLU]-*bis*GMPA**			
	drug	mg drug / mg HDLDBC	mol drug / mol HDLDBC	EE[a] (%)
hydrophilic salt form	**chloroquine**	0.307	16.33	31
	primaquine	0.408	26.76	41
	quinacrine	0.475	20.20	44
lipophilic base form	**chloroquine**	0.055	2.92	3
	primaquine	0.431	28.27	43
	quinacrine	0.008	0.34	1

6.1.2- *In vitro* targeting studies

In a previous work, *in vitro* targeting experiments were carried out with two HDLDBC labeled with commercial rhodamine B that showed that ***bis*MPA-[PLU]-*bis*MPA** was preferentially internalized within the infected red blood cells.[95]

6.1.2.1- Labeling with rhodamine B

In order to confirm the targeting abilities of the different systems towards parasite infected red blood cells, the two HDLDBCs were fluorescently labeled by encapsulating the low-water soluble modified rhodamine B, **RhB(C17)$_2$**, (see section 4.3.2.2, p. 181). Its encapsulation was carried out according to the oil-in-water technique in a way similar than that employed to encapsulate the antimalarial drugs in their lipophilic base forms (see p.). With a feeding ratio of 1/0.3 (w_{HDLDBC}/w_{LR}), no precipitate appeared after the encapsulation process and it was assumed that all **RhB(C17)$_2$** was encapsulated within the HDLDBC.

As before, the time-persistence of the **RhB(C17)$_2$** labeling was controlled by dialysis of a solution of ***bis*MPA-[PLU]-*bis*MPA/RhB(C17)$_2$** conjugate against a volume 100 times higher of distilled water ("*sink conditions*") (**figure C$_6$-8**). After 3 days, more than 90 % of **RhB(C17)$_2$** remained encapsulated within the micelles asserting the correct labeling. In contrast, after 72 hours only 30 % of commercial water soluble rhodamine B remained entrapped within the ***bis*MPA-[PLU]-*bis*MPA/RhB** conjugate.

[95] J. Movellan, P. Urbán *et al.*, *Biomaterials*, **2014**, 35, 7940.

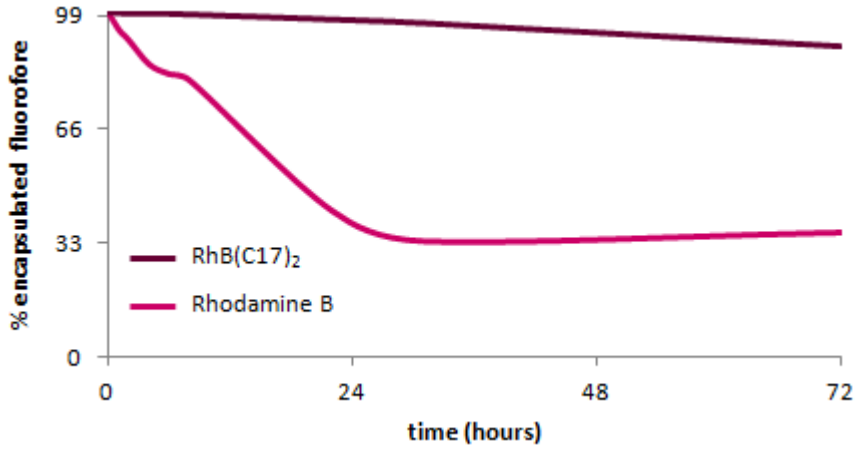

Figure C_6-8: RhB(C17)$_2$ and **RhB** releases curves from ***bis*MPA-PLU-*bis*MPA/RhB(C17)$_2$** and ***bis*MPA-PLU-*bis*MPA/RhB**.

6.1.2.2- Targeting experiments

The targeting ability of **RhB(C17)$_2$** labeled ***bis*MPA-[PLU]-*bis*MPA** and ***bis*GMPA-[PLU]-*bis*GMPA** nanocarriers to infected red blood cells, was then investigated by fluorescence microscopy (**figure C$_6$-9**). In this experiment, the red blood cells were treated with Hoechst (blue stain) that mark DNA. Healthy red blood cells that do not have DNA remain free of Hoechst whereas the DNA belonging to the *plasmodium* parasites is stained in blue. Thus, the infected red blood cells (blue fluorescence) can be easily distinguished from the healthy ones (no fluorescence). The **RhB(C17)$_2$** labeled **HDLDBC** appears in red.

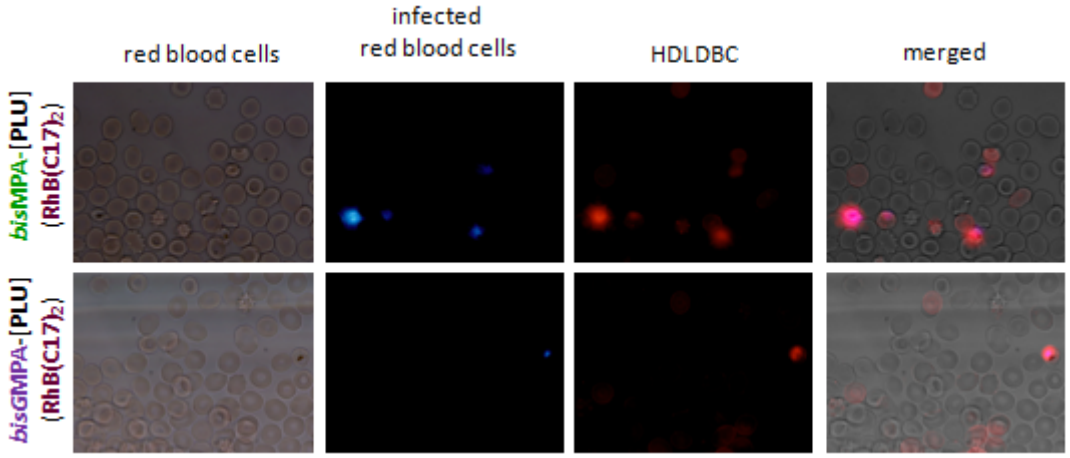

Figure C$_6$-9: Fluorescence microscopy images of the **HDLDBC/RhB(C17)$_2$** conjugates at 75 µg/mL after 90 minutes incubation. Infected RBCs appear in blue (Hoechst marking), **HDLDBC/RhB(C17)$_2$** conjugates appear in red.

Interestingly, all the infected red blood cells have internalized the labeled **HDLDBCs** and only a small portion of healthy red blood cells have internalized some labeled **HDLDBC**. These results confirm the previous targeting results obtained for ***bis*MPA-[PLU]-*bis*MPA**[95] and extend them to ***bis*GMPA-[PLU]-*bis*GMPA**.

The good HDLDBCs targeting abilities may be explained by the **modifications that the red blood cell membrane suffer** after the parasite

[95] J. Movellan, P. Urbán *et al.*, *Biomaterials*, **2014**, 35, 7940.

infection. Indeed, after having entered into a red blood cell, the parasite rapidly modifies the membrane of its host cell by means of effector proteins. Among other modifications, the cell membrane becomes much more permeable in order to favor the entry of nutrients into the cells.[238] Besides, the presence of new proteins from parasites origin at the membrane of the infected red blood cells might also favor some specific interactions between these modified membranes and the HDLDBCs.

The HDLDBCs appear as promising dendritic nanocarriers for the delivery of antimalarial drugs. On the one hand, they can encapsulate antimalarial chloroquine, primaquine and quinacrine in their hydrophilic salt form and primaquine in its lipophilic base form. On the other hand, they are favorably internalized within infected red blood cells and this must therefore increase the drug targeting of the encapsulated antimalarial drugs.

[238] a) P.R. Gilson, S.A. Chisholm, B.S. Crabb, T.F. de Koning-Ward, Host cell remodelling in malaria parasites: a new pool of potential drug targets, *Int. J. Parasitol.*, **2017**, 47, 119–127; b) K. Kirk, H.A. Horner, B.C. Elford, J.C. Ellory, C.I. Newbold, Transport of diverse substrates into malaria-infected erythrocytes via a pathway showing functional characteristics of a chloride channel, *J. Biol. Chem.*, **1994**, 269, 3339–3347.

6.2- Dendronized hyperbranched polymers (DHPs) coated with heparin

The unimolecular micelles formed by the biocompatible *bis*-MPA based dendronized hyperbranched polymers (DHPs) can be used as nanocarriers for drug delivery.[145,152,153,212] Moreover, their numerous peripheral cationic groups afford the possibility to conjugate them with polyanionic polymers. In particular, glycodendrimers have improved the targeting and/or activity of encapsulated anti-malarial primaquine[239] and chloroquine[240].

Accordingly, the DHPs **DHP[G2+3]($NH_3^+Cl^-$)$_{120}$**, **DHP[G3+3]($NH_3^+Cl^-$)$_{248}$** and **DHP[G4+3]($NH_3^+Cl^-$)$_{424}$** have been used to encapsulate chloroquine, primaquine and quinacrine in their hydrophilic and lipophilic forms in order to increase their targeting abilities and their antiparasite activity, as it has been carried out with the HDLDBCs. Furthermore, these DHP/drug conjugates have been coated with heparin (**figure C_6-10**).[226]

[145] A. Carlmark *et al.*, *Chem. Soc. Rev.*, **2013**, 42, 5858.
[152] O.L. Padilla de Jesús *et al.*, *Bioconjugate Chem.* **2002**, 13, 453.
[153] C. Kontoyianni *et al.*, *Macromol Biosci.*, **2008**, 8, 871.
[212] a) M. Prabaharan *et al.*, *Biomaterials*, **2009**, 30, 3009; b) G. Chen *et al.*, *Biomaterials*, **2015**, 47, 4.
[239] D. Bhadra , A.K. Yadav, S. Bhadra, N.K. Jain, Glycodendrimeric nanoparticulate carriers of primaquine phosphate for liver targeting, *Int. J. Pharm.*, **2005**, 295, 221–233.
[240] D. Bhadra, S. Bhadra, N.K. Jai, PEGylated peptide dendrimeric carriers for the delivery of antimalarial drug chloroquine phosphate, *Pharm. Res.*, **2006**, 23, 623–633.
[226] J. Marques *et al.*, *Sci. Rep.*, **2016**, 6, 24368.

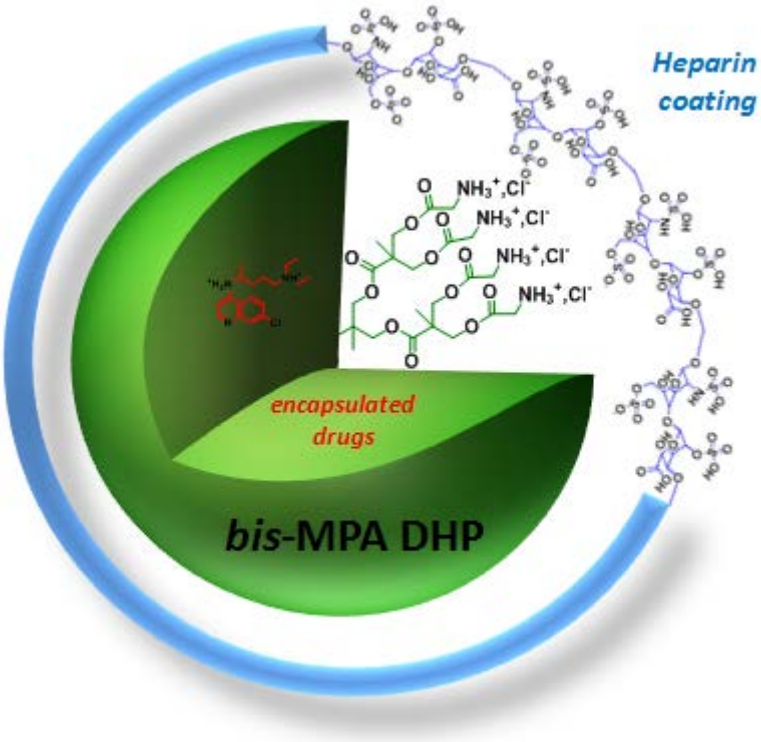

Figure C_6-10: Schematic representation of the DHP/antimalarial drug conjugates coated with heparin.

6.2.1- Chloroquine, primaquine and quinacrine encapsulation

Chloroquine, primaquine and quinacrine were encapsulated within the DHPs following the oil-in-water method as described for the HDLDBCS (see section 6.1.1.2, p. and chapter 7 for the detailed protocol).

Taking into account the data obtained during the encapsulation of the antimalarial drugs within the HDLDBCs, and in order to avoid the unnecessary waste of drugs, the hydrophilic forms of the antimalarial drugs were encapsulated within the three DHPs, **DHP[G2+3]$(NH_3^+Cl^-)_{120}$**, **DHP[G3+3]$(NH_3^+Cl^-)_{248}$** and **DHP[G4+3]$(NH_3^+Cl^-)_{424}$**, at a feeding ratio of 0.5/1 (w_{drug}/w_{DHP}) whereas their lipophilic base forms were encapsulated at a feeding ratio of 0.75/1 (w_{PQb}/w_{DHP}) for **PQb**, 0.50/1 (w_{CQb}/w_{DHP}) for **CQb** and 0.1/1 (w_{QNb}/w_{DHP}) for **QNb**.

The amount of drug encapsulated within the DHPs was calculated in weight and mole ratios, and the encapsulation efficiencies were calculated by dividing the quantity of drug encapsulated by the quantity used to perform the encapsulation (**table C_6-3**).

Tables C_6-3: Amount of antimalarial drugs encapsulated within the DHPs based nanocarriers in their hydrophilic salt forms (up) and in their lipophilic base forms (down). [a]EE means encapsulation efficiency.

	DHP[G2+3]$(NH_3^+Cl^-)_{120}$			
	drug	mg drug / mg DHP	mol drug / mol DHP	EE[a] (%)
Hydrophilic salt form	**chloroquine**	0.158	14.06	38
	primaquine	0.190	20.86	38
	quinacrine	0.129	9.18	26
Lipophilic base form	**chloroquine**	0.393	34.98	78
	primaquine	0.388	42.59	55
	quinacrine	0.007	0.50	7
	DHP[G3+3]$(NH_3^+Cl^-)_{248}$			
	drug	mg drug / mg DHP	mol drug / mol DHP	EE[a] (%)
Hydrophilic salt form	**chloroquine**	0.318	58.57	65
	primaquine	0.127	28.85	26
	quinacrine	0.233	34.32	46
Lipophilic base form	**chloroquine**	0.404	74.41	81
	primaquine	0.230	52.20	31
	quinacrine	0.012	1.77	13
	DHP[G4+3]$(NH_3^+Cl^-)_{424}$			
	drug	mg drug / mg DHP	mol drug / mol DHP	EE[a] (%)
Hydrophilic salt form	**chloroquine**	0.246	78.84	49
	primaquine	0.214	84.59	43
	quinacrine	0.229	58.70	46
Lipophilic base form	**chloroquine**	0.395	126.60	82
	primaquine	0.239	94.48	32
	quinacrine	0.007	1.79	7

All the drugs in their hydrophilic salt forms, **CQs**, **PQs** and **QNs**, can be encapsulated within the DHPs nanocarriers with high efficiencies, 26 to 49 %. The two biggest DHPs, **DHP[G3+3]($NH_3^+Cl^-$)$_{248}$** and **DHP[G4+3]($NH_3^+Cl^-$)$_{424}$**, show better encapsulation efficiencies than the smallest one. With respect to the lipophilic base forms of the drugs, high quantities of **CQb** can be encapsulated within the DHPs, showing encapsulation efficiencies between 78 and 82 %. Interestingly, the quantities of **CQb** encapsulated were higher than the quantities obtained with **CQs**. In the same manner, high quantities of **PQb** can be encapsulated within these nanocarriers. Unfortunately, and as observed for the HDLDBCs, **QNb** shows low level of encapsulation within the DHPs.

In general, **DHP[G3+3]($NH_3^+Cl^-$)$_{248}$** and **DHP[G4+3]($NH_3^+Cl^-$)$_{424}$** show higher encapsulation efficiencies than the smallest nanocarrier **DHP[G2+3]($NH_3^+Cl^-$)$_{120}$** for all the drugs, either in their hydrophilic or lipophilic form.

6.2.2- Heparin complex formation

Heparin (Hep) (**figure C_6-2, p.**) belongs to the family of the glycoaminoglycan and it is constituted of a repetition of various disaccharide units. Under physiological pH, heparin is negatively charged and can form complexes when mixed with polycationic dendrimers.[236,237] For this study, heparin sodium salt from porcine intestinal mucosa (≥ 180 U.S. Pharmacopeial (USP) units/mg) has been employed. Its molecular weight varies from 6 000 to 30 000 Da, with most chains being in the range of 17 000 to 19 000 Da, and presents an average of 2.3 negative charges per disaccharide unit at physiological pH although 4 sites are available.[241]

The formation of complexes with heparin was determined by the methylene blue (MB) spectroscopic competition assay. Heparin/MB complexes display an indigo color (absorption at λ_{max} = 565 nm). The addition of the corresponding DHP promotes the competition between DHP and MB to complex heparin. When all heparin is complexed by the DHP, MB is released and remains free in solution displaying a turquoise color (absorption at λ_{max} = 665 nm). The representation of the intensity ratio between the absorbance at 665 nm and the absorbance at 565 nm (A_{665}/A_{565}), and versus the w_{DHP}/w_{Hep} ratio permits to calculate the parameters that define the DHP/Hep complex formation, *i.e.* **EC_{50}**, the effective ratio at which 50 % of heparin is complexed by the DHP, and **EC_{100}**, the effective ratio at which 100 % of heparin is complexed by the DHPs (see chapter 7 for detailed protocol). The complexation experiments were carried out for the empty DHP nanocarriers as well as for the drug-loaded DHP nanocarriers.

[236] K.T. Al-Jamal *et al.*, *Res. Pharm. Sci.*, **2012**, 2, 9.

[237] A.C. Rodrigo *et al.*, *Angew. Chem. Int. Ed.*, **2011**, 50, 4675-4679.

[241] a) www.sigmaaldrich.com, ref. product H4784; b) R.A. Gelman, J.Blackwell, Heparin-polypeptide interactions in aqueous solution, *Arch. Biochem. Biophys.*, **1973**, 159, 427-33.

6.2.2.1 Bis-MPA DHP-heparin complexes

The study of the formation of the complexes between heparin and the three DHPs by the MB spectroscopic competition assay is represented in figure **C_6-11.**

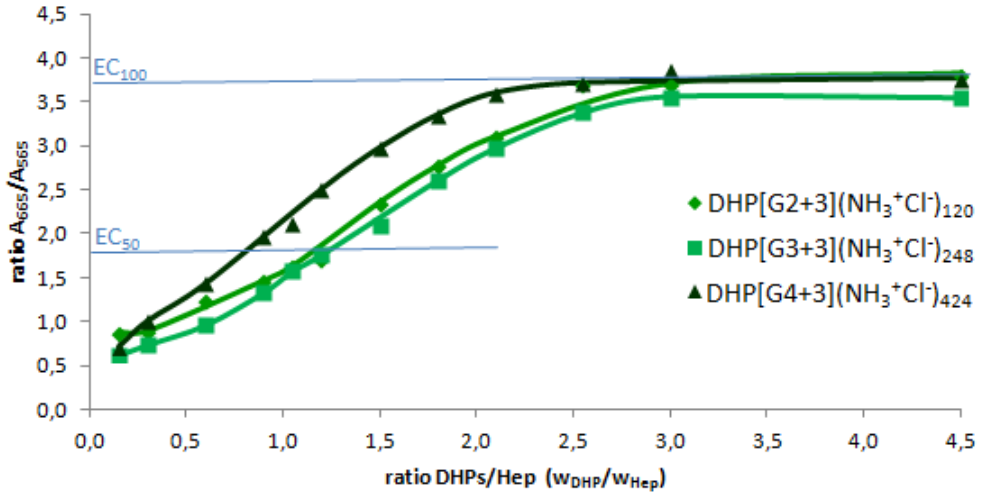

Figure C_6-11: Heparin complexation by the DHPs studied according to the MB spectroscopic assay. The EC_{100} corresponded to the ratio A_{665}/A_{565} ratio measured for free MB control in water.

In all cases, the ratio A_{665}/A_{565} reached a threshold that corresponded to the absorbance intensity of the free MB control in water, proving that heparin can be entirely complexed by the three DHPs. The biggest DHP, **DHP[G4+3]$(NH_3^+Cl^-)_{424}$** shows better heparin complexation abilities than the two other DHPs and can totally complex heparin from a (w_{DHP}/w_{Hep}) ratio of 2.5/1 whereas the two other DHPs can totally complex heparin from a ratio 3.0/1. Assuming that the average molecular weight of heparin used for this study is close to 18 000 Da and that 4 possible negative charges are present for each disaccharide units (corresponding to 6.20 x 10^{-3} negative charge per mole of heparin), the $^+/_-$ charges ratio at which all heparin is complexed by the DHPs were calculated: 1.2 for **DHP[G4+3]$(NH_3^+Cl^-)_{424}$** and 2.0 for **DHP[G3+3]$(NH_3^+Cl^-)_{248}$** and **DHP[2+3]$(NH_3^+Cl^-)_{120}$**. These values are slightly lower than the ones obtained for the pDNA complexation (N/P between 7 and 4, **figure C_5-16**, p. 231), certainly due to the

lower molecular weight of heparin. EC_{50} and EC_{100} values are gathered in **table C_6-4**.

6.2.2.2 - DHP/drug -heparin complexes

The ability of the different DHPs loaded with the hydrophilic drugs to form complexes with heparin was first investigated. The EC_{50} and EC_{100} values are gathered in **table C_6-4**.

Table C_6-4: EC_{50} and EC_{100} (w_{DHP}/w_{Hep}) ratios determined according to the MB spectroscopic competition assay for the three DHPs without drugs and with the antimalarial drugs encapsulated within them. The curves obtained for the MB spectroscopic competition assays are depicted in **annexes 12**.

	DHP[G2+3]$(NH_3^+Cl^-)_{120}$			
	no drug	**CQs**	**PQs**	**QNs**
EC_{50}	1.2/1	3.0/1	2.9/1	1.2/1
EC_{100}	3.0/1	7.5/1	7.5/1	4.5/1
	DHP[G3+3]$(NH_3^+Cl^-)_{248}$			
	no drug	**CQs**	**PQs**	**QNs**
EC_{50}	1.2/1	2.6/1	1.8/1	1.2/1
EC_{100}	3.0/1	4.5/1	4.5/1	3.5/1
	DHP[G4+3]$(NH_3^+Cl^-)_{424}$			
	no drug	**CQs**	**PQs**	**QNs**
EC_{50}	0.5/1	1.9/1	1.9/1	1.2/1
EC_{100}	2.5/1	4.5/1	4.5/1	3.0/1

As a general observation, the encapsulation of the antimalarial drugs in their hydrophilic salt form increases slightly the amount of DHP/drug necessary to complex the heparin.

Comparing the different DHPs, the heparin-complex formation is less altered for the two biggest DHPs. For instance, the (w_{DHP}/w_{Hep}) ratios at which the EC_{100} are reached for **DHP[G4+3]$(NH_3^+Cl^-)_{424}$/hydrophilic drug** and **DHP[G3+3]$(NH_3^+Cl^-)_{248}$/hydrophilic drug** conjugates increase, respectively, from

2.5/1 and 3.0/1 for the DHPs without drug to 3.5/1 and 4.5/1 after drug encapsulation. **DHP[G2+3]($NH_3^+Cl^-$)$_{120}$**, the smallest DHP, is more affected by the incorporation of the drugs and can totally complex heparin at ratios ranged from 4.5/1 to 7.5/1 after drug encapsulation.

Comparing the different drugs encapsulated within the DHPs, hydrophilic quinacrine (**QNs**) was the drug that less disturbed the formation of complexes between the DHPs and heparin, showing an increase of 0.5 points for the EC_{100} (w_{DHP}/w_{Hep}) ratios for the two biggest DHPs and of 1.5 point for the smallest one. Hydrophilic chloroquine (**CQs**) and primaquine (**PQs**) disturb a little more the formation of the complexes and the EC_{100} is reached from ratios comprised between 4.5/1 and 7.5/1.

At this point, it resulted necessary to confirm that the differences observed for heparin complexation between the DHPs without drug and DHPs with encapsulated hydrophilic drugs were actually due to drug encapsulation and not to the presence of free drug in solution. For this purpose, three MB spectroscopic competition assays were carried out with **DHP[G4+3]($NH_3^+Cl^-$)$_{424}$** in the presence of free **CQs**, **PQs** and **QNs**. In these conditions, the EC_{100} was reached for a ratio (w_{DHP}/w_{Hep}) 2.5/1, which is exactly the same than that determined for the DHP alone (**table C_6-4**).

Subsequently, the ability of the different **DHP/lipophilic drug** conjugates containing chloroquine (**CQb**) and primaquine (**PQb**) to form complexes with heparin was investigated according to the same assay. Unlike the **DHP/hydrophilic drug** conjugates, the two encapsulated lipophilic drugs strongly affected the formation of complexes (**figure C_6-12**).

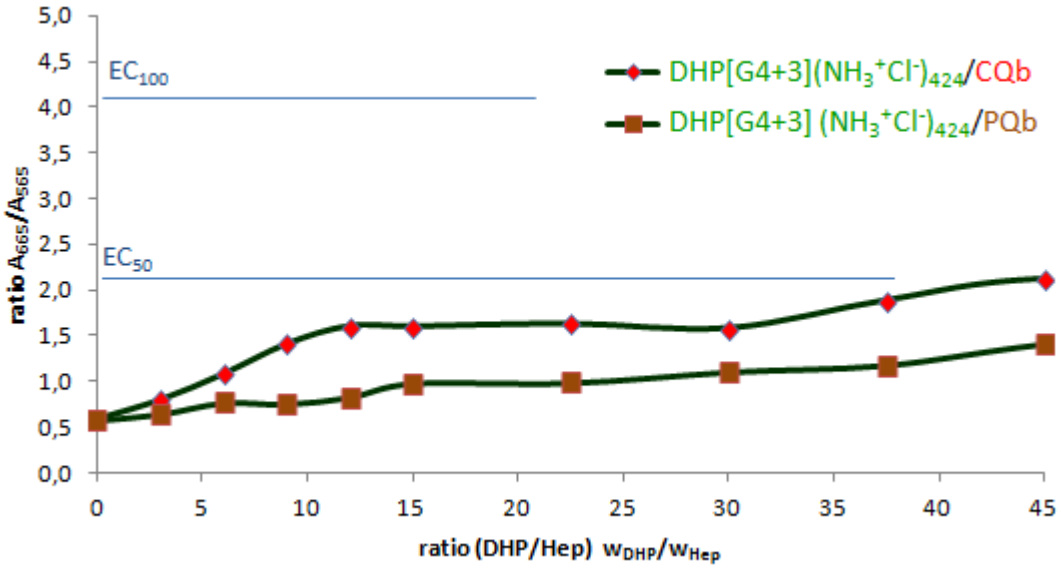

Figure C_6-12: Heparin complexation by **DHP[G4+3]/CQb** and **DHP[G4+3]/PQb** studied according to the MB spectroscopic competition assay. The EC_{100} corresponded to the ratio A_{665}/A_{565} ratio measured for free MB control in water.

Table C_6-5: Percentage of complexed heparin by the three DHPs/lipophilic base drugs conjugates at the ratio (w_{DHP}/w_{Hep}) 40/1.

	DHP[G2+3]	DHP[G3+3]	DHP[G4+3]
DHPs/CQb	48 %	52 %	47 %
DHP/PQb	45 %	25 %	30 %

Even at high (w_{DHP}/w_{Hep}) ratios, *i.e.* ≥ 40/1, more than 10 times higher than the ratios at which heparin is totally complexed by the DHPs alone, uncomplexed heparin remained present in the samples. At the ratio 40/1, between 25 and 52 % of heparin was complexed by the DHPs (**table C_6-5**). The encapsulation of lipophilic chloroquine (**CQb**) within the DHPs limits the heparin-complex formation is less extent than the introduction of lipophilic primaquine (**PQb**), and this although higher quantities of **CQb** than **PQb** were encapsulated within the DHPs (**table C_6-3)**.

As a summary, the three *bis*-MPA DHPs can form complexes with heparin by means of electrostatic interactions starting from low (w_{DHP}/w_{Hep}) ratios. The insertion of antimalarial drugs in their hydrophilic form within the DHPs only

slightly affects the formation of complexes with heparin. It still occurs from low ratios, demonstrating the effective post-functionalization of the nanocarrier/ antimalarial drug conjugates with heparin. In contrast, the presence of antimalarial drugs in their lipophilic form within the DHPs disturbs the heparin complexation that is uncompleted even at high ratios thus blocking their post-functionalization with heparin.

6.2.3- Morphological studies

Preliminary transmission electron microscopy (TEM) (**figure C_6-13**) and cryogenic transmission electron microscopy (cryoTEM) (**figure C_6-14**) observation was conducted to determine how the size and morphology of the unimicellar micelles formed by **DHP[G4+3]($NH_3^+Cl^-$)$_{424}$** were affected by the encapsulation of the primaquine drug in its hydrophilic salt form (**PQs**) and by the formation of the complexes with heparin (**Hep**).

In **TEM images**, the **diameter of the spherical aggregates slightly increases after the encapsulation** of hydrophilic primaquine or after the formation of the complexes with heparin. Whereas the unimolecular micelles formed by the DHP in water have an average size around 13.5 ± 3.5 nm, the **DHP[G4+3]($NH_3^+Cl^-$)$_{424}$/PQs** conjugates have average sizes around 18.7 ± 7.5 nm and **DHP[G4+3]($NH_3^+Cl^-$)$_{424}$/Hep** complexes have an average size around 23.5 ± 5.5 nm. Finally, **DHP[G4+3]($NH_3^+Cl^-$)$_{424}$/PQs/Hep** complexes are the biggest ones; they have an average size around 26.2 ± 6.2 nm. The higher polydispersity observed is due to the formation of a second size-population of bigger aggregates with sizes close to 50 nm that must correspond to the self-aggregation of various unimolecular micelles.

Additionally, the complexes formed with heparin were observed in **cryoTEM**. Like in TEM images, two size-population distributions are observed in these images. An abundant population of small aggregates, with diameters *ca.* 20 - 35 nm are visible for **DHP[G4+3]($NH_3^+Cl^-$)$_{424}$/Hep** and *ca.* 15 - 40 nm for **DHP[G4+3]($NH_3^+Cl^-$)$_{424}$/PQs/Hep**, together with another scarce size-population of bigger spherical aggregates with sizes *ca.* 60 - 90 nm.

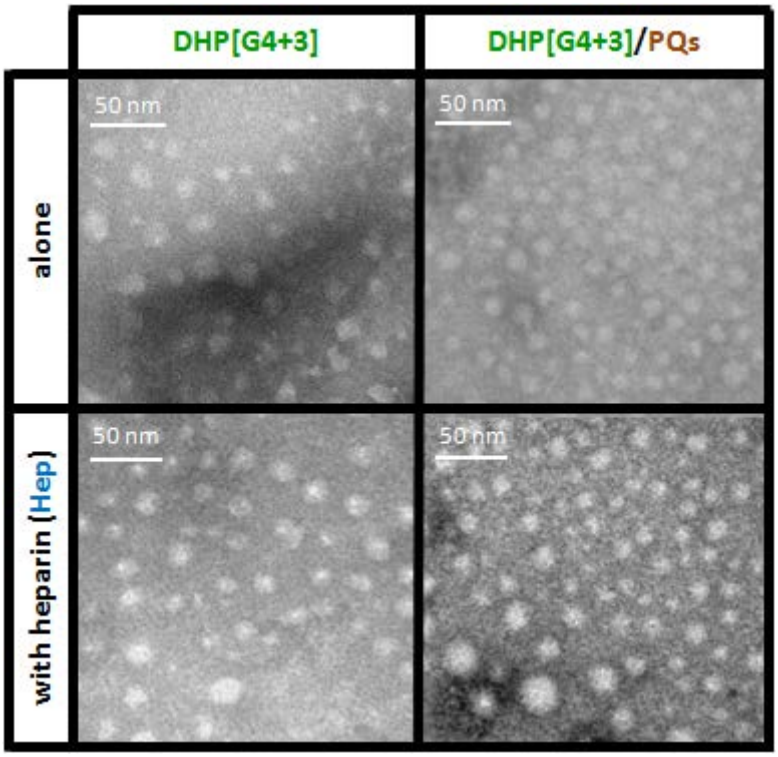

Figure C_6-13: TEM images of the aggregates formed by **DHP[G4+3]$(NH_3^+Cl^-)_{424}$** **DHP[G4+3]$(NH_3^+Cl^-)_{424}$/PQs**, **DHP[G4+3]$(NH_3^+Cl^-)_{424}$/Hep** and **DHP[G4+3]$(NH_3^+Cl^-)_{424}$/PQs/Hep** at 1 mg/mL in water.

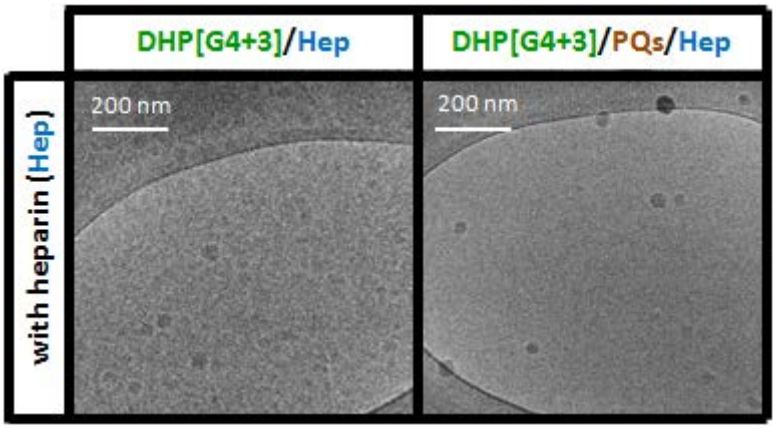

Figure C_6-14: CryoTEM images of the complexes formed by **DHP[G4+3]$(NH_3^+Cl^-)_{424}$/Hep** and **DHP[G4+3]$(NH_3^+Cl^-)_{424}$/PQs/Hep** at 1 mg/mL in water.

Interestingly, the unimolecular micelles formed by **DHP[G4+3]$(NH_3^+Cl^-)_{424}$** in water are only slightly affected by the encapsulation of the hydrophilic primaquine (**PQs**) and by the formation of the complexes with heparin (**Hep**). Their sizes remained small and only little aggregation between the dispersed particles is observed. These dendritic nanocarriers show attractive size and morphologic characteristics that should favor red blood cells internalization.

6.2.4- *In vitro* targeting studies

In order to confirm the targeting abilities of the different *bis*-MPA DHP towards parasite infected red blood cells, it was necessary to label the DHPs with a fluorescent probe. For this purpose **rhodamine B fluorophore** was covalently linked to **DHP[G3+3](NH$_3^+$Cl$^-$)$_{248}$.**

6.2.4.1- Synthesis of a bis-MPA DHP labeled with rhodamine B

The synthetic pathway is depicted in **figure C$_6$-15** (see section 5.1.1.2, p. 208, general procedure XII). The hyperbranched polyester of 3rd generation with an average of 31 alkyne groups at its periphery, **HP[G3]-≡$_{31}$**, was decorated with 3rd generation *bis*-MPA dendrons with 8 terminal glycine moieties and rhodamine B by means of two steps copper(I) azide-alkyne cycloaddition (CuAAC). In the first step, **HP[G3]-≡$_{31}$** was decorated with the dendrons but using an amount below the stoichiometric ratio, *i.e.* 0.77 mol of dendron per 1 mol of alkyne group. This allowed to ensure the presence of free alkyne groups after the 1st CuAAC. The catalytic system was then removed by various washings with aqueous solutions and the final DHP was precipitated into a mixture of hexanes and ethyl acetate in order to remove the dendrons that had not reacted. In the second step, a CuAAC was carried out with **N$_3$-RhB**, a rhodamine B derivative bearing an azide group (the synthesis of this derivatives is described in the section 4.3.3.2, p. 181). An excess of dye was used to ensure the sufficient labeling of the DHP (1.7 mol of dye per 1 mol of alkyne group). After completion of the reaction, the catalytic system and the excess of dye were removed by several washings with aqueous solutions and by dialysis against methanol in order to obtain pure **DHP[G3+3](NHBoc,RhB)**. Finally, the *t*-Boc protecting groups of the terminal amino groups were removed as before, in acidic conditions in ethyl acetate yielding the ammonium salts that precipitated from the reaction mixture. Pure dendronized hyperbranched polymer of generation 3+3 covalently labeled with rhodamine B, **DHP[G3+3](NH$_3^+$Cl$^-$,RhB)** was

obtained as a pink solid with a yield of 52 %, which is slightly lower than the one obtained for the DHP without dye (71 %).

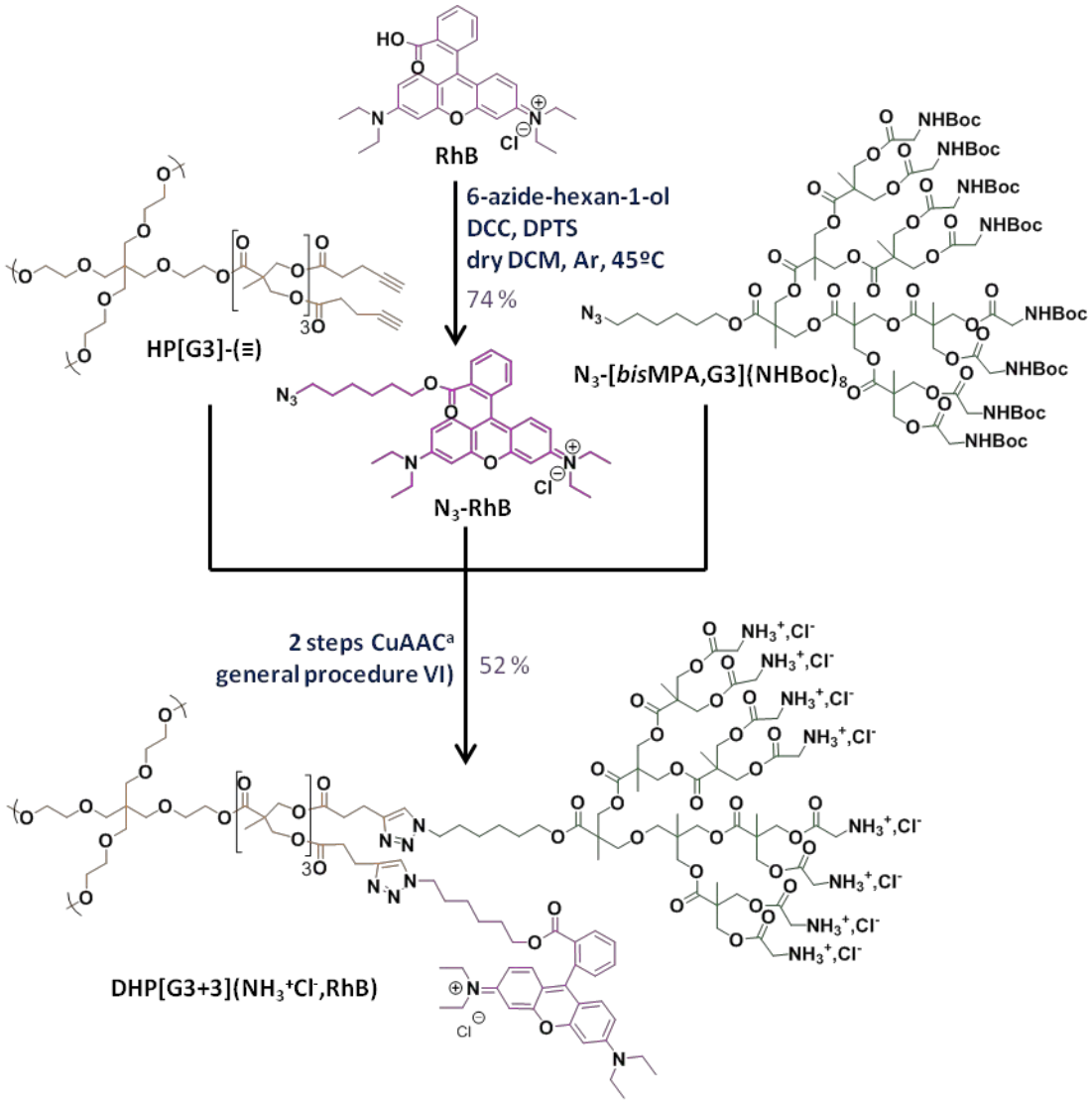

Figure C_6-15: Synthesis of the bis-MPA DHP covalently labeled with rhodamine B. [a]The 2 steps CuAAC was carried out in the same conditions described for the synthesis of the *bis*-MPA DHPs, general procedure XII detailed in the chapter 7).

As in the case of the DHPs without fluorescent label, ^{1}H-NMR (**figure C_6-16**) and FTIR spectroscopy were employed to confirm the formation of the final triazole rings. The complete chemical characterization data are gathered in chapter 7.

As before, the ^{1}H-NMR spectrum shows a peak at 7.40 ppm that corresponds to the proton of the triazole ring, *H-13*. The methylene protons

closed to the triazole ring (*H-10*, *H-11*, *H-14* and *H-15*) are downfield shifted. Additionally, peaks with low intensities corresponding to the aromatic protons of the dye can be observed between 6.5 and 8.5 ppm as well as a doublet corresponding to the methylene protons in the α-position of the N atoms of the dye, *H-29*, at 3.61 ppm. In the FTIR spectrum, the band corresponding to the stretching of the azide bond at 2100 cm^{-1} disappears completely while the two bands corresponding to the stretching of the bonds of the alkyne groups, ≡C-H and C≡C at 3292 and 2119 cm^{-1} respectively, are no longer observed.

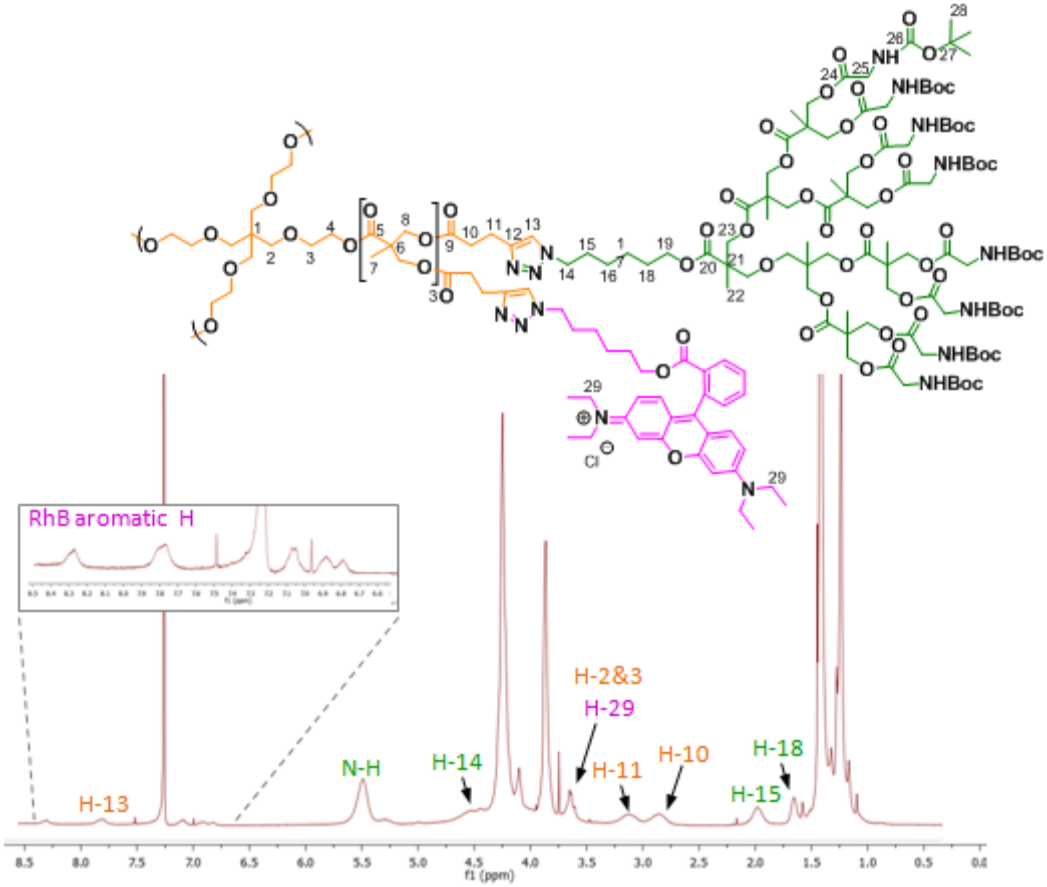

Figure C_6-16: ^{1}H NMR spectrum of **DHP[G3+3](NHBoc,RhB)** recorded at 400 MHz in $CDCl_3$.

The degree of functionalization of the *bis*-MPA hyperbranched polymers by the dendrons and then, by the rhodamine dye was calculated by ^{1}H-NMR. As for the DHPs without dye, the methylene protons in the α- and β-positions of the alkyne groups (*H-10'* and *H-11'*) or the proton of the triazole rings (*H-10* and *H-11*) can be used to determine the degree of dendrons and dye grafting (**figure**

C_6-17). When they are in the α- and β-positions of the alkyne groups, their corresponding peaks appear at 2.55 and 2.45 ppm and, after the formation of the triazole rings, they are downfield shifted to 2.90 and 3.19 ppm, respectively. Therefore, and as before, the degree of functionalization of the hyperbranched polymer can be determined by comparing the relative intensity of the different peaks. The degree of dendron functionalization during the 1st CuAAC step is equal to 78 % while the degree of rhodamine dye functionalization during the 2nd step is equal to 100 %. Thus, pure DHP of generation 3+3 bearing an average of 24 *bis*-MPA dendrons and labeled by 7 rhodamine dye moieties were obtained.

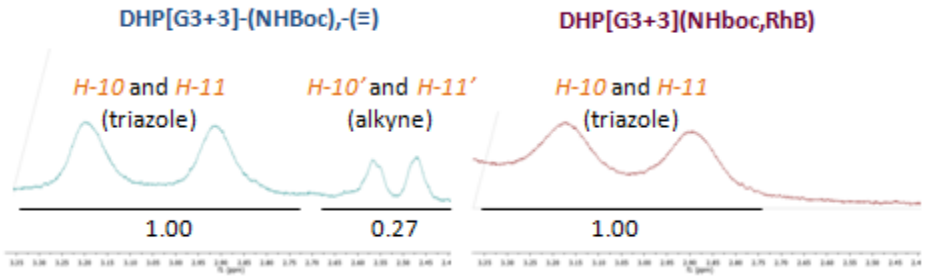

Figure C_6-17: ^{1}H-NMR spectra from 2.4 to 3.3 ppm of the DHP[G3+3] after the grafting of the *bis*-MPA dendrons (left) and after the grafting of rhodamine B dye (right).

6.2.4.2- Targeting experiments

Before carrying any targeting experiments, the abilities of **DHP[G3+3](NH$_3^+$Cl$^-$,RhB)** to form complexes with heparin was controlled by the methylene blue (MB) spectroscopic competition assay (see **annexes 13**). As this DHP has less dendrons and, as a consequence less peripheral glycine moieties than its respective DHP without dye (192 versus 248 terminal amino groups), it forms complexes with heparin at higher (w_{DHP}/w_{hep}) ratios. The EC_{50} and EC_{100} vales are 1.5 and 6.0, respectively, which correspond to a $^+/_-$ charge ratios of 0.8 and 3.2. Nevertheless, this DHP is still a good heparin binder and targeting experiments with heparin complexes could be conducted.

The abilities of **DHP[G3+3](NH$_3^+$Cl$^-$,RhB)** and its relative heparin complexes containing different quantities of heparin (5, 10 and 15 %w) to target parasites infected RBCs were studied by fluorescence microscopy and by flow cytometry (**figure C$_6$-18**). The infected RBCs were stained by Hoechst and appear in blue. **DHP[G3+3](NH$_3^+$Cl$^-$,RhB)** and its respective complexes appear in red.

The fluorescence microscopy images show that **DHP[G3+3](NH$_3^+$Cl$^-$,RhB)** is located in all the infected RBCs and only inside them. Moreover, the DHP is specifically located in the same area than the parasites within the infected cells. These results were confirmed by flow cytometry assays where more than 90 % of the infected red blood cells show red fluorescence whereas less than 10 % of the healthy ones show red fluorescence. As the DHP showed excellent properties for its own, the addition of heparin that specifically binds the infected RBCs didn't seem necessary for targeting.

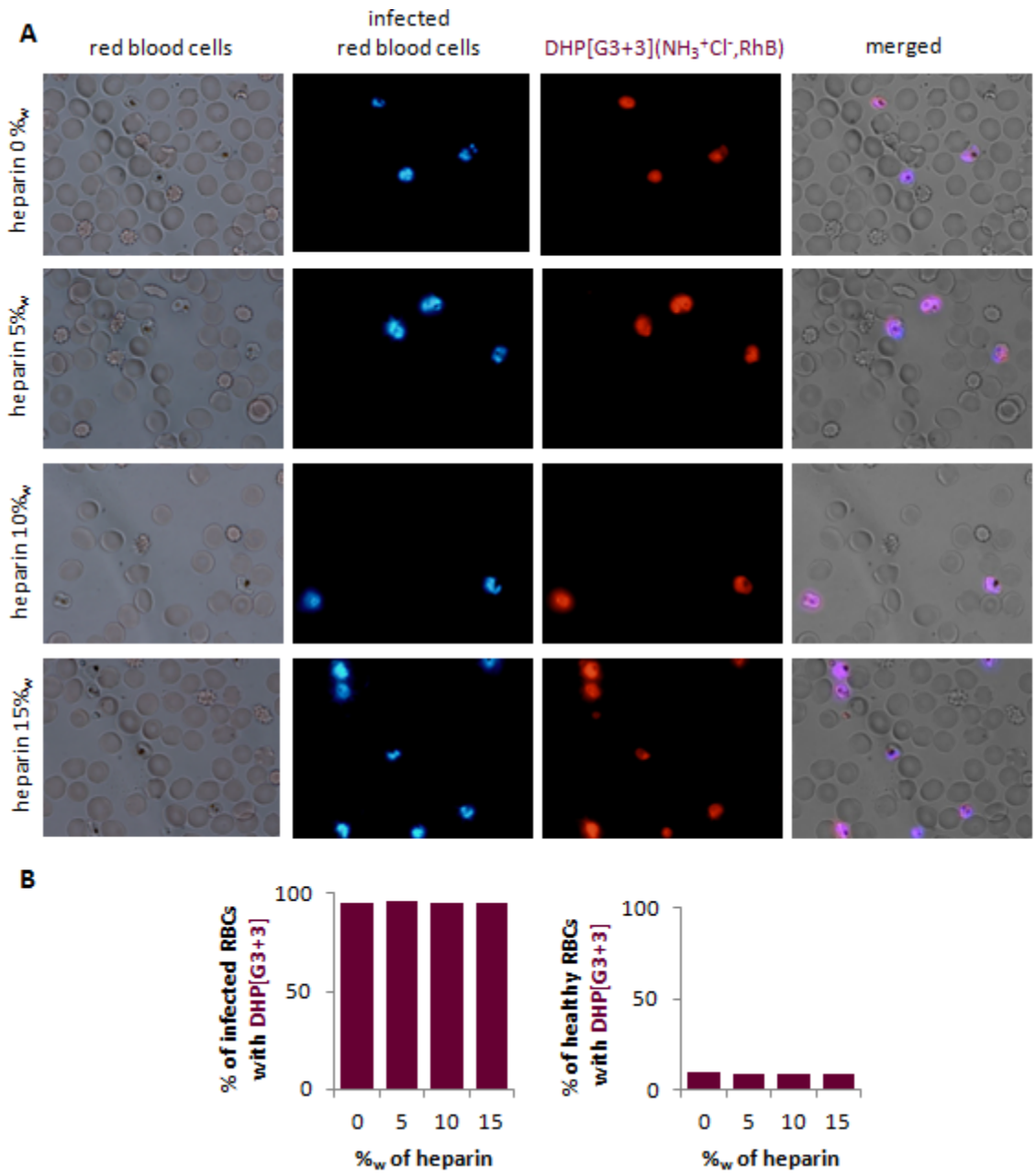

Figure C_6-18: Fluorescence microscopy images (**A**) of **DHP[G3+3]($NH_3^+Cl^-$,RhB)** with 0, 5, 10 and 15 $\%_w$ of heparin at 150 µg/mL after 90 minutes incubation. Infected RBCs appeared in blue and **DHP[G3+3]($NH_3^+Cl^-$,RhB)** appeared in red. (**B**) Percentage of DHP and complexes internalized within the infected (left) and healthy (right) red blood cells (RBCs) determined by flow cytometry assay.

An additional experiment was performed in which the targeting abilities of the complexes were conducted with **DHP[G3+3]($NH_3^+Cl^-$,RhB)-Hep**, in which the heparin is covalently marked with fluorescein isothiocyanate (Hep-FITC) (**figure C_6-19**).

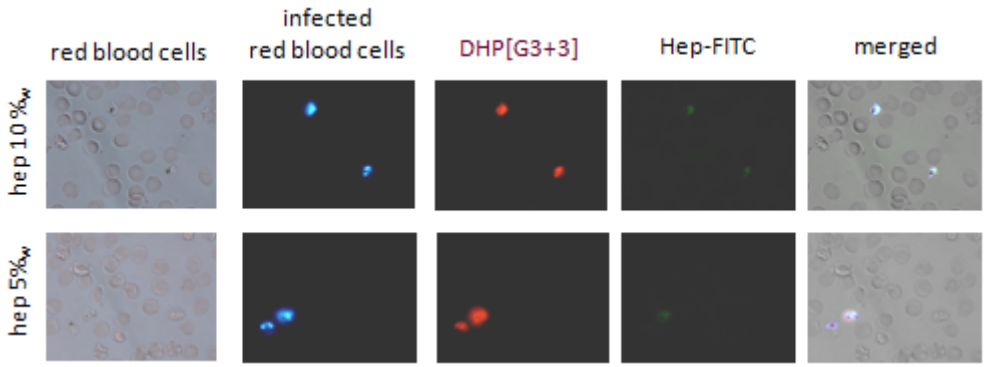

Figure C_6-19: Fluorescence microscopy images of **DHP[G3+3]($NH_3^+Cl^-$,RhB)-Hep** with 10 and 15 $\%_w$ of heparin at 150 µg/mL after 90 minutes incubation. Infected red blood cells appear in blue, **DHP[G3+3]($NH_3^+Cl^-$,RhB)** appears in red and Hep-FITC appears in green.

Green fluorescence due to heparin and red one due to the DHP were both located in the infected red blood cells confirming the entry of the whole **DHP-Hep** complexes within the infected red blood cells.

As it has occurred with the HDLDBCs, the cellular uptake of the DHPs into the parasite infected red blood cells is favored when compared with the cellular uptake of the non-infected ones. Thus, these two series of dendritic nanocarriers appear as alluring nanocarriers to deliver and increase the targeting of antimalarial drugs.

6.3- *In vitro plasmodium* growing inhibition assays (GIAs)

Preliminary studies have been undertaken in order to evaluate, the potential of the dendritic/antimalarial drug conjugates to inhibit plasmodium growing in infected RBCs for the conjugates based on **DHP[G4+3]($NH_3^+Cl^-$)$_{424}$** and on ***bis*GMPA-[PLU]-*bis*GMPA**.

First, the inhibition the replication of *plasmodium* was evaluated by measuring the *plasmodium* growth after being exposed to various concentrations of the corresponding dendritic derivative/chloroquine and dendritic derivative/primaquine conjugates for 48 hours and compare to the growth after exposition to the free drugs. The half-maximal inhibition effective concentrations (IC_{50}), which represents the concentrations at which the parasite growth decreases by 50% was evaluated for the dendritic derivatives/drug conjugates and their respective free drug control (**table C_6-6**). The Growing inhibition assays curves are gathered in **annexes 14**.

Table C_6-6: IC_{50} determined from the GIAs for the **DHP[G4+3]**/antimalarial drug conjugates, **HDLDBC**/antimalarial drug conjugates and for the **free drugs** controls.

	hydrophilic salts form			**lipophilic base form**		
primaquine	**free PQs**	**DHP[G4+3]**	**HDLDBC**	**free PQs**	**DHP[G4+3]**	**HDLDBC**
IC_{50}	15.5 µM	24.7 µM	22.9 µM	20.9 µM	20.7 µM	24.7 µM
chloroquine	**free CQs**	**DHP[G4+3]**	**HDLDBC**	**free CQs**	**DHP[G4+3]**	
IC_{50}	33.4 nM	72.9 nM	37.2 nM	37.8 nM	81.7 nM	

In almost all the cases, the **encapsulation of the antimalarial drugs** within the dendritic nanocarriers, in either their hydrophilic salt form or lipophilic salt form, does not affect negatively their activity

Second, the **DHP[G4+3]($NH_3^+Cl^-$)$_{424}$/QNs-Hep** conjugate was chosen to perform a preliminary *plasmodium* growing inhibition assay (GIA) when combined with heparin. The complex was prepared at a ratio (w_{DHP}/w_{Hep}) 5/1 at which all heparin is complexed. The plasmodium growing inhibition activity of plasmodium was measured after being exposed to the **DHP[G4+3]($NH_3^+Cl^-$)$_{424}$/ QNs/Hep** conjugate during 48 hours and the IC_{50} values were determined for all the drug conjugates and their respective free drug control (**table C_6-7)**. The GIAs curves are gathered **in annexes 15**.

Table C_6-7: IC_{50} determined from the GIA of the **DHP[G4+3]/QNs-Hep** conjugate.

Quinacrine	free QNs control	free QNs & Hep	DHP[G4+3] /Hep	DHP[G4+3] /QNs	DHP[G4+3] /QNs/Hep
IC_{50}	54.7 nM	132.2 nM	-	72.9 nM	35.0 nM

Interestingly, the activity of the drug is enhanced after the formation of the conjugate with heparin.

6.4- General remarks

Summary of results

The HDLDBCs based on commercial Pluronic® F127 and either *bis*-MPA or *bis*-GMPA dendrons and together with the *bis*-MPA DHPs, previously described chapters 4 and 5, respectively, can encapsulate three antimalarial drugs: chloroquine, primaquine and quinacrine. Furthermore, the polycationic DHPs can form complexes with heparin, a polyanionic polysaccharide, by means of electrostatic interactions from low (DHP/Heparin) ratios.

The HDLDBCs as well as the DHPs and DHP/heparin complexes labeled with rhodamine B fluorophore have shown interesting abilities to target red blood cells infected by the parasite that provokes malaria and subsequent cell internalization.

The antimalarial activity of the drugs was in general maintained after their encapsulation within the dendritic systems. The post-functionalization with heparin of DHP/quinacrine conjugate have enhanced the drug activity.

Conclusions

The HDLDBCs and the DHPs are promising nanocarriers for the delivery of antimalarial drugs. They are able to enhance the drug targeting to infected red blood cells without showing a decrease of the drug activity.

Future investigation

The promising results obtained for antimalarial drug delivery might be corroborate in order to extend the study to *in vivo* experiments. It might be interesting to perform *in vitro* studies in which parasite infected red blood cells are exposed 90 min to the drugs and drug nanocarriers. Moreover, the

administration of DHP/drug/heparin systems may be extended to chloroquine and primaquine in order to observe if the activity of these drugs could be improved as well. Following this idea, the pharmacokinetics of the drugs when encapsulated within the DHP or within the heparin post-functionalized DHPs might give critical results before making *in vivo* experiments.

Chapter 7

Experimental part

7.1- Synthesis and chemical characterization

7.1.1- Materials and equipments

The **reactive** were purchased form Sigma-Aldrich® or from Acros ™. In particular, the commercial *bis*-MPA hyperbranched polymers of generation 2, 3 and 4, camptothecin, hydrophilic chloroquine salt, hydrophilic primaquine salt and hydrophilic quinacrine salt were purchased from Sigma-Aldrich®. Rhodamine B fluorophore was purchased from Acros ™.

Organic solvents and silica gel were purchased from Sigma-Aldrich® or Scharlab S.L.; dichloromethane was distilled before use. Inorganic salts and mineral acids were purchased from Scharlab S.L. Bases were purchased from Panreac AppliChem®.

The **dialysis membranes** of cellulose acetate with 1000, 2000 or 3500 Da cut-off were purchased from Spectra/Por®.

^{1}H nuclear magnetic resonance (NMR) and **^{13}C NMR** experiments were performed using a Bruker AV-500 (^{1}H: 500 MHz, ^{13}C: 125 MHz), Bruker AV-400 (^{1}H: 400 MHz, ^{13}C: 100 MHz) or a Bruker AMX300 (^{1}H: 300 MHz, ^{13}C: 75 MHz) spectrometer employing deuterated chloroform ($CDCl_3$), deuterated dichloromethane (CD_2Cl_2), deuterated methanol (CD_3OD), deuterated dimethyl sulfoxide ($(CD_3)_2SO$) or deuterated water (D_2O) as solvents. The chemical shifts are given in ppm relative to TMS and the coupling constants in Hz. The solvent residual peak was used as internal standard.

Mass spectrometry (MS) were performed using an ESI Bruker Esquire 300^{+} or a Bruker Microflex system employing the MALDI-TOF technique with nitrogen laser (337 nm) and ditranol as matrix (expect otherwise specified).

Fourier transformed infrared (FTIR) spectra were performed using a Bruker Vertex 70 spectrophotometer in ATR mode and recorded between 4000 and 600 cm^{-1} or using a FTIR ATI-Mattson Genesis series II while the sample were suspended in nujol in NaCl cells and recorded between 4000 cm^{-1} and 600 cm^{-1}.

Elemental analysis (EA) were performed with a Perkin-Elmer 2400 series II microanalyser.

Size exclusion chromatography (SEC) were performed on a Waters e2695 Alliance system with two Styragel columns HR4 and HR1 (500 and 10^4 Å of pore size) in series and a Waters 2424 evaporation light scattering detector. The sample was dissolved into THF (HPLC grade) at the concentration of 1 $mg \cdot mL^{-1}$. The flow rate was set at 1 $mL \cdot min^{-1}$ and the temperature at 35 °C. PMMA was used as standard for calibration.

The **pH** of the solutions was measured after each addition by a Hanna HI 8424 pH meter with a HI 1110B electrode.

7.1.2- *Bis*-MPA and *bis*-GMPA dendrons

7.1.2.1- *bis*-MPA dendrons

General procedure I): growing up esterification reaction of the bis-MPA dendrons

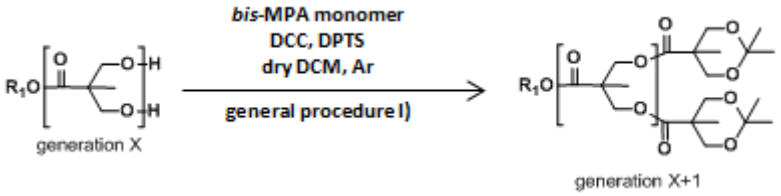

Alcohol was dissolved into dry dichloromethane. *Bis*-MPA(monomer)* (1.10, 1.05 or 1.50 mol per hydroxyl groups according to the dendron generation) and DPTS (0.40 mol per hydroxyl groups) were added. The reaction mixture was stirred under argon atmosphere and was cooled down to 0ºC. A solution of DCC (1.10, 1.05 or 1.50 mol per hydroxyl group according to the dendron generation) in dry dichloromethane was added drop wise. The reaction mixture was allowed to stir under argon atmosphere overnight at room temperature. The white precipitate, N,N'-dicyclohexylurea (DCU), was filtered off and the solvent was evaporated under vacuum to get a mixture of oil and solid. DCU was newly precipitated into hexane and filtered off. The solvent was evaporated under reduce pressure. The crude product was purified on silica gel (mixtures of hexane and ethyl acetate).

General procedure II): deprotection of the terminal hydroxyl groups

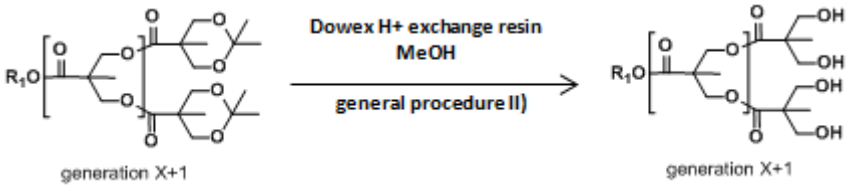

Dowex 50 WX2 hydrogen form 50.100 (mesh) (50 % mass equivalent) was washed by stirring it in MeOH and was recovered using filtration. Ketonide protected dendron (1.00 mol) was dissolved into MeOH. Washed Dowex resin H^+ was added and the reaction was stirred during 5, 10 or 24 hours according to the dendron generation. The resin was filtered off and the solvent was evaporated under vacuum to obtain the corresponding pure product.

General procedure III): functionalization of the dendron with t-Boc protected glycine moieties

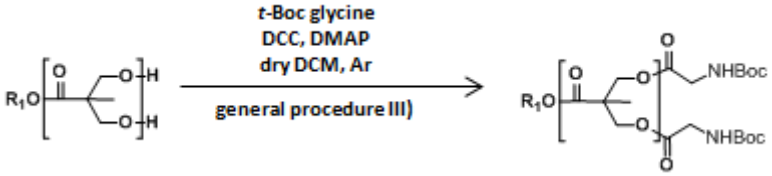

Alcohol (1.00 mol) was dissolved into dry dichloromethane. *t*-Boc Glycine (1.25 mol per hydroxyl groups) and DMAP (0.40 mol per hydroxyl groups) were added to it. The reaction mixture was stirred under argon atmosphere and cooled down to 0ºC. DCC (1.25 mol per hydroxyl groups) was dissolved into dry dichloromethane and was added drop wise to the reaction mixture. It was stirred at room temperature under argon atmosphere during 24 hours. The white precipitate, N,N'-dicyclohexylurea (DCU), was filtered off and the solvent was evaporated under vacuum to get a mixture of oil and solid. DCU was newly precipitated into a mixture of hexane and ethyl acetate (7:3) and filtered off. The solvent was evaporated under reduce pressure. The crude product was purified twice on silica gel with mixtures of hexane and ethyl acetate (ramp from 7:3 to 4:6) to get a white solid.

General procedure IV): functionalization of the dendron with stearic acid (C17 alkyl chains)

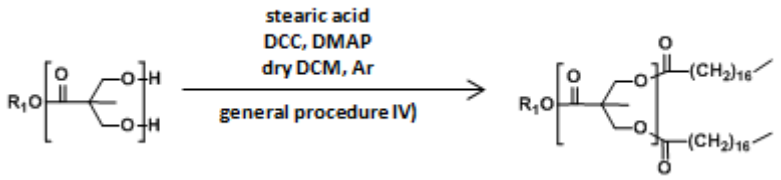

Alcohol (1.00 mol) was dissolved into dry dichloromethane. Stearic acid (1.50 mol per hydroxyl groups) and DMAP (0.4 mol per hydroxyl groups) were added to it. The reaction mixture was stirred under argon atmosphere and cooled down to 0ºC. DCC (1.50 eq. per hydroxyl groups) was dissolved into dry dichloromethane and was added drop wise to the reaction mixture. It was stirred at room temperature under argon atmosphere during 2 days. The white precipitate, N,N'-dicyclohexylurea (DCU), was filtered off and the solvent was evaporated under vacuum to get a mixture of oil and solid. DCU was newly precipitated into hexane and filtered off. The solvent was evaporated under reduce pressure. The crude product was purified by two successive precipitations into cold acetone.

ketal-protected *bis*-MPA(monomer), named as *bis*-MPA(monomer)*

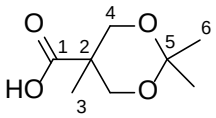

2,2-Bis(hydroxymethyl)propionic acid (60.00 g, 447.33 mmol, 1.00 eq.) was dissolved in dry acetone (300 mL). 2,2 dimethoxypropane (82.51 mL, 670.99 mmol, 1.50 eq.) and TsOH,H_2O (4.26 g, 22.37 mmol, 0.05 eq.) were added. The reaction mixture was stirred at room temperature during 2 hours. Then, the reaction was neutralized by adding a solution of NH_3/EtOH (1:1) (6 mL). The solvent was evaporated under vacuum. The white solid was dissolved in AcOEt (100 mL) and was washed twice with distillated water. The organic phase was dried over anhydrous $MgSO_4$. The solvent was evaporated under vacuum to get a white powder (54.07 g, 69 %).

^{1}H NMR (400 MHz, $CDCl_3$) δ (ppm): 1.21 (s, 3H, H-3), 1.41 (s, 3H, H-6), 1.44 (s, 3H, H-6'), 3.67 (d, J = 12 Hz, 2H, H-4), 4.19 (d, J = 12 Hz, 2H, H-4'), 9.95 (bs, COOH).

^{13}C NMR (100 MHz, $CDCl_3$) δ (ppm): 18.4 (C-3), 21.9 (C-6), 25.2 (C-6'), 41.8 (C-2), 65.8 (C-4), 98.3 (C-5), 180.2 (C-1).

MS (ESI^+): *m/z (%) 196.9 (100)* $[C_8H_{14}O_4,Na]^+$, *174.0 (33)* $[C_8H_{14}O_4,H]^+$.

FT-IR (ν_{max}/cm^{-1}, nujol): 3126 (COO-H st), 2924-2854 (C-H st), 1722 (C=O st), 1460 (CH_2, CH_3 δ).

EA (%): *Found*: C, 55.4; H, 8.4. *Calc. for* $C_8H_{14}O_4$: C, 55.2; H, 8.1%.

6-azidohexan-1-ol

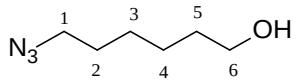

6-chlorohexan-1-ol (19.53 mL, 146 mmol, 1.00 eq.) was dissolved in DMF (60 mL). NaN_3 (19.99 g, 307 mmol, 2.10 eq.) was added. The reaction mixture was stirred at 140 ºC during 36 hours. Water (400 mL) was added. The product was extracted tree times using Et_2O (3 x 200 mL). Organic phases were collected, put together, washed twice using brine (2 x 200 mL) and dried over anhydrous $MgSO_4$. Solvent was evaporated to give an orange oil. The crude product was purified on silica gel (hexane : ethyl acetate = 7:3) to give a light yellow oil (15.32 g, 73 %).

^{1}H NMR (400 MHz, $CDCl_3$) δ (ppm): 1.34 (m, 4H, H-3 and H-4), 1.56 (m, 4H, H-2 and H-5), 1.76 (bs, -OH), 3.24 (t, J = 6.8 Hz, 2H, H-1), 3.61 (t, J = 6.4 Hz, 2H, H-6).

^{13}C NMR (400 MHz, $CDCl_3$) δ (ppm): 25.3 (C-4), 26.4 (C-3), 28.7 (C-5), 32.5 (C-2), 51.3 (C-1), 62.6 (C-6).

MS (ESI^+): *m/z (%) 166.0 (100)* $[C_6H_{13}N_3O_1,Na]^+$.

FTIR (ν_{max}/cm^{-1}, nujol): 3339 (O-H st), 2936-2861 (C-H st), 2097 (N_3 st), 1456 (CH_2, CH_3 δ).

EA (%): *Found:* C, 49.7; H, 9.2; N, 29.5. *Calc. for* $C_6H_{13}N_3O_1$: C, 50.3; H, 9.15; N, 29.35.

N_3-[*bis*MPA,G1]-(ketal)$_1$

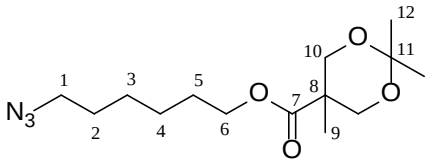

General procedure I) 6-azidohexan-1-ol (12.68 g, 88.58 mmol, 1.00 eq.); *bis*-MPA(monomer)* (16.97 g, 97.44 mmol, 1.10 eq.); DPTS (10.43 g, 35.43 mmol, 0.40 eq.); DCC (20.10 g, 97.44 mmol, 1.10 eq.); dry DCM (250 + 50 mL);time of reaction: overnight. The crude product was purified on silica gel (hexane : ethyl acetate = 8:2) to give a light yellow oil (25.68 g, 94 %).

^{1}H NMR (400 MHz, $CDCl_3$) δ (ppm): 1.18 (s, 3H, H-9), 1.38 (s, 3H, H-12), 1.40 (m, 4H, H-3 and H-4), 1.42 (s, 3H, H-12'), 1.61 (m, 2H, H-2) 1.67 (m, 2H, H-5), 3.26 (t, J = 6.8 Hz, 2H, H-1), 3.64 (d, J = 11.6 Hz, 2H, H-10), 4.14 (t, J =6.6 Hz, 2H, H-6), 4.18 (d, J = 11.6 Hz, 2H, H-10').

^{13}C NMR (100 MHz, $CDCl_3$) δ (ppm): 18.7 (C-9), 22.7 (C-12), 24.6 (C-12'), 25.4 (C-4), 26.3 (C-3), 28.4 (C-5), 28.7 (C-2), 41.8 (C-8), 51.3 (C-1), 64.6 (C-6), 66.0 (C-10), 98.0 (C-11), 174.3 (C-7).

MS (ESI$^+$): *m/z* (%): *322.1 (15)* $[C_{14}H_{25}N_3O_4,Na]^+$, *300.0 (52)* $[C_{14}H_{25}N_3O_4,H]^+$, *272.0 (100)* $[C_{14}H_{25}N_1O_{4,}H]^+$.

FTIR (ν_{max}/cm^{-1}, nujol): 2939-2864 (C-H st), 2096 (N_3 st), 1731 (C=O st), 1455 (CH_2, CH_3 δ), 1259 (CO-O st), 1160 (O-C-C st).

EA (%): *Found:* C, 55.9; H, 8.7; N, 13.8. *Calc. for* $C_{14}H_{25}N_3O_{4:}$ C, 56.2; H, 8.4; N, 14.0.

N_3-[*bis*MPA,G1]-$(OH)_2$

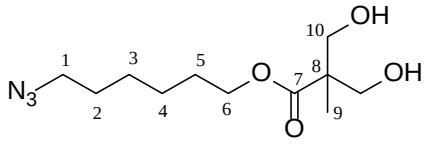

General procedure II) N_3-[*bis*MPA,G1]-$(ketal)_1$ (25.68 g, 85.78 mmol, 1.00 eq.); ion exchange resin Dowex H^+ (12.50 g, 50 % mass equivalent); MeOH (350 mL). Time of reaction: 5 hours. The product was obtained as a colorless oil (20.86 g, 97 %).

^{1}H NMR (300 MHz, $CDCl_3$) δ (ppm): 1.05 (s, 3H, H-9), 1.39 (m, 4H, H-3 and H-4), 1.61 (m, 2H, H-2), 1.67 (m, 2H, H-5), 3.02 (bs, -OH), 3.25 (t, J = 6.9 Hz, 2H, H-1), 3.68 (dd, J = 11.2 Hz and J = 5.7 Hz, 2H, H-10), 3.87 (dd, J = 11.2 Hz and J = 5.7 Hz, 2H, H-10'), 4.14 (t, J = 6.6 Hz, 2H, H-6).

^{13}C NMR (100 MHz, $CDCl_3$): δ (ppm)17.0 (C-9), 25.3 (C-4), 26.2 (C-3), 28.3 (C-5), 28.6 (C-2), 49.1 (C-8), 51.2 (C-1), 64.8 (C-6), 67.9 (C-10), 175.9 (C-7).

MS (ESI^+): *m/z(%)*: *282.0 (100)* $[C_{11}H_{21}N_3O_4,Na]^+$, *232.0 (72)* $[C_{11}H_{21}NO_4,H]^+$.

FTIR (ν_{max}/cm^{-1}, nujol): 3381 (O-H st), 2925-2855 (C-H st), 2097 (N_3 st); 1727 (C=O st), 1462 (CH_2,CH_3 δ), 1237 (CO-O st), 1131 (O-C-C st).

EA (%): *Found:* C. 50.4; H, 8.2; N, 16.4. *Calc. for* $C_{11}H_{21}N_3O_4$: C. 50.95; H. 8.2; N. 16.2.

N_3-[*bis*MPA,G2]-(ketal)$_2$

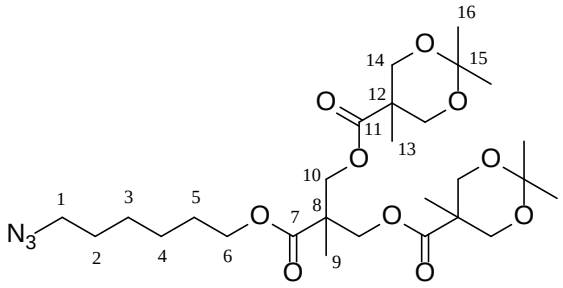

General procedure I) N_3-[*bis*MPA,G1]-$(OH)_2$ (16.78 g, 64.70 mmol, 1.00 eq.); *Bis*-MPA(monomer)* (24.80 g, 142.35 mmol, 2.10 eq.); DPTS (15.24 g, 51.76 mmol, 0.80 eq.); DCC (29.24 g, 142.35 mmol, 2.10 eq.); dry DCM (280 + 70 mL); time of reaction: overnight. The crude product was purified on silica gel (hexane : ethyl acetate = 7:3) to give a colorless oil (36.19 g, 98 %).

^{1}H NMR (400 MHz, $CDCl_3$) δ (ppm): 1.14 (s, 6H, H-13), 1.28 (s, 3H, H-9), 1.35 (s, 6H, H-16), 1.39 (m, 4H,H-3 and H-4), 1.41 (s, 6H, H-16'), 1.60 (m, 2H, H-2) 1.65 (m, 2H, H-5), 3.27 (t, J = 7.2 Hz, 2H, H-1), 3.62 (d, J = 12.8 Hz, 4H, H-14), 4.11 (t, J = 6.8 Hz, 2H, H-6), 4.15 (d, J = 12.0 Hz, 4H, H-14'), 4.32 (s, 4H, H-10).

^{13}C NMR (100 MHz, $CDCl_3$) δ (ppm): 17.7 (C-9), 18.5 (C-13), 22.2 (C-16), 25.0 (C-16'), 25.5 (C-4), 26.3 (C-3), 28.4 (C-5), 28.7 (C-2), 42.0 (C-12), 47.0 (C-8), 51.3 (C-1), 65.2 (C-6), 65.3 (C-10), 65.9 (C-14), 98.1 (C-15), 172.6 (C-7), 173.5 (C-11).

MS (MALDI$^+$): *m/z* (%): 594.3 (100) $[C_{27}H_{45}N_3O_{10}, Na]^+$.

FTIR (ν_{max}/cm^{-1}, nujol): 2940-2868 (C-H st), 2097 (N_3 st), 1736 (C=O st), 1457 (CH_2, CH_3 δ), 1252 (CO-O st), 1155 (O-C-C).

EA (%): *Found:* C, 56.5; H, 7.8; N, 7.0. *Calc. for* $C_{27}H_{45}N_3O_{10}$: C, 56.7; H, 7.9; N, 7.35.

N_3-[*bis*MPA,G2]-$(OH)_4$

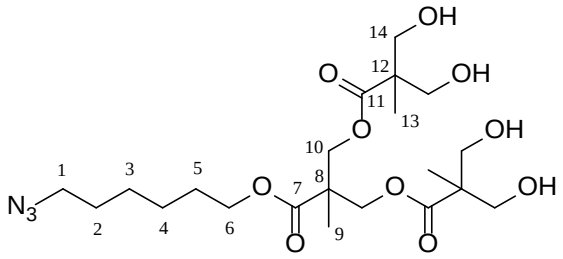

General procedure II) N_3-[*bis*MPA,G1]-$(ketal)_2$ (36.20 g, 63.30 mmol, 1.00 eq.); ion exchange resin Dowex H^+ (18.00 g, 50 % mass equivalent); MeOH (400 mL); time of reaction: 10 hours. The pure product was obtained as a white solid (28.96 g, 93 %).

^{1}H NMR (400 MHz, CD_3OD) δ (ppm): 1.05 (s, 6H, H-13), 1.30 (s, 3H, H-9), 1.40 (m, 4H, H-3 and H.4), 1.61 (m, 2H, H-2) 1.65 (m, 2H, H-5), 3.30 (t, J = 6.9 Hz, 2H, H-1), 3.64 (ABq, J = 10.8 Hz, Δ ν_{AB} = 26.7 Hz, 8H, H-14), 4.26 (t, J = 6.8 Hz, 2H, H-6), 4.43 (ABq, J = 11.2 Hz, Δ ν_{AB} = 15.1 Hz, 4H, H-10).

^{13}C NMR (100 MHz, $CDCl_3$) δ (ppm): 17.1 (C-13), 18.1 (C-9), 25.4 (C-3), 26.3 (C-4), 28.3 (C-5), 28.7 (C-2), 46.3 (C-8), 49.7 (C-12), 51.3 (C-1), 64.8 (C-10), 65.4 (C-6), 68.0 (C-14), 173.0 (C-7), 175.2 (C-11).

MS (MALDI$^+$) *m/z (%)*: *514.3 (100)* $[C_{21}H_{37}N_3O_{10},Na]^+$.

FTIR (ν_{max}/cm^{-1}, nujol): 3283 (O-H st), 2923-2854 (C-H st), 2098 (N_3 st), 1731 (C=O st), 1462 (CH_2, CH_3 δ), 1241 (CO-O st), 1137 (O-C-C st).

EA (%): *Found:* C, 51.5; H, 7.6; N, 8.7. *Calc. for* $C_{21}H_{37}N_3O_{10}$: C. 51.3; H, 7.6; N, 8.55.

N_3-[*bis*MPA,G3]-$(ketal)_4$

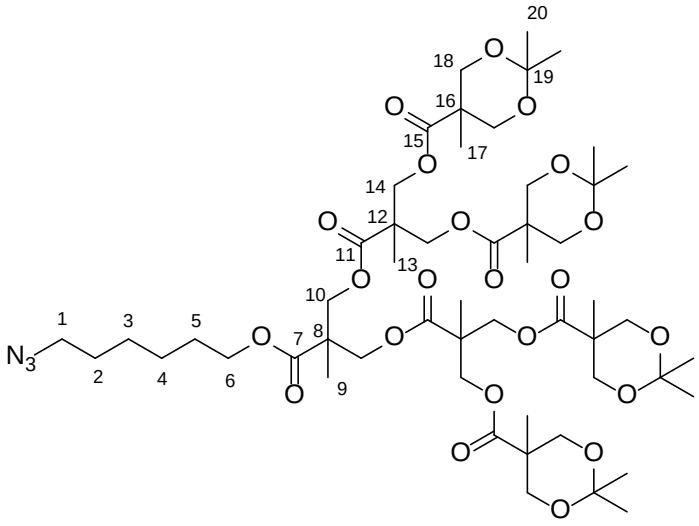

General procedure I) N_3-[bisMPA,G2]-$(OH)_4$ (15.00 g, 30.52 mmol, 1.00 eq.); *bis*-MPA(monomer)* (31.89 g, 183.11 mmol, 6.00 eq.); DPTS (14.37 g, 48.82 mol, 1.60 eq.); DCC (37.74 g, 183.11 mmol, 6.00 eq.); dry DCM (260 + 90 mL); time of reaction: overnight. The crude product was purified twice on silica gel (hexane : ethyl acetate = ramp from 7:3 to 6:4) to give a colorless gel (26.75 g, 79 %).

^{1}H NMR (400 MHz, $CDCl_3$) δ (ppm): 1.14 (s, 12 H, H-17), 1.25 (s, 3H, H-9), 1.26 (s, 6H, H-13), 1.35 (s, 12H, H-20), 1.40 (m, 16H, H-3, H-4 and H-20'), 1.60 (m, 2H, H-2) 1.65 (m, 2H, H-5), 3.27 (t, J = 6.6 Hz, 2H, H-1), 3.61 (d, J = 12 Hz, 8H, H-18), 4.10 (t, J = 7.2 Hz, 2H, H-6), 4.13 (d, J = 12.4 Hz, 8H, 18'), 4.27 (m, 12H, H-10 and H-14).

^{13}C NMR (100 MHz, $CDCl_3$) δ (ppm): 17.1 (C-9), 17.7 (C-13), 18.4 (C-17), 22.0 (C-20), 25.1 (C-20'), 25.4 (C-4), 26.3 (C-3), 28.3 (C-5), 28.7 (C-2), 42.0 (C-16), 46.6 (C-8), 46.8 (C-12), 51.3 (C-1), [64.9-65.4-65.9] (C-10, C-14 and C-18), 66.0 (C-6), 98.1 (C-19), 171.8 (C-11) , 172.1 (C-7), 173.4 (C-15).

MS (MALDI$^+$) *m/z(%)*: *1138.7 (100)* $[C_{53}H_{85}N_3O_{22},Na]^+$, *1115.7 (84)* $[C_{53}H_{85}N_3O_{22},H]^+$.

FTIR (ν_{max}/cm^{-1}, nujol): 2991-2940-2876 (C-H st), 2097 (N_3 st), 1739 (C=O st), 1457 (CH_2, CH_3 δ), 1253 (CO-O st), 1155 (O-C-C).

EA (%): *Found*: C, 57.05; H, 7.9; N, 3.7. *Calc. for* $C_{53}H_{85}N_3O_{22}$: C, 57.0; H, 7.7; N. 3.8.

N_3-[*bis*MPA,G3]-$(OH)_8$

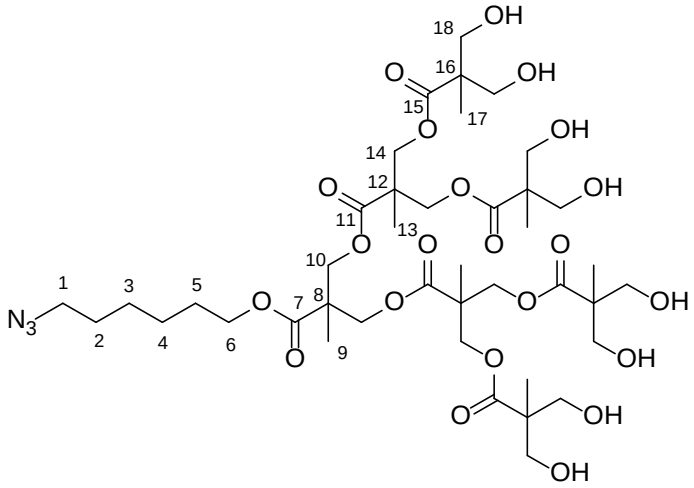

General procedure II) N_3-[*bis*MPA,G3]-$(OH)_8$ (22.88 g, 20.51 mmol, 1.00 eq.); ion exchange resin Dowex H^+ (11.00 g, 50 % mass equivalent); MeOH (300 mL). Time of reaction: 24 hours. The pure product was obtained as a white solid (17.45 g, 89 %).

^{1}H NMR (CD_3OD, 300 MHz) δ (ppm): 1.09 (s, 12H, H-17), 1.24 (s, 6H, H-13), 1.25 (s, 3H, H-9), 1.39 (m, 4H, H-3 and H-4), 1.57 (m,2H, H-2), , 1.65 (m, 2H, H-5), 3.26 (t, J = 6.8 Hz, H-1), 3.64 (ABq, J = 12 Hz, $\Delta\nu_{AB}$ = 32.0 Hz, 16H, H-18), 4.18 (t, J = 6.6 Hz, 2H, H-6), 4.29 (m, 12H, H-10 and H-14).

^{13}C NMR (CD_3OD, 75 MHz) δ (ppm): 17.3 (C-17), 18.2 (C-9), 18.3 (C-13), 26.7 (C-4), 27.5 (C-3), 29.6 (C-5), 29.8 (C-2), 48.0 (C-8 and C-12), 51.8 (C-16), 52.4 (C-1), 65.9 (C-18), 66.2 (C-14), 66.7 (C-10), 67.4 (C-6), 173.8 (C-11), 174.1 (C-7), 176.0 (C-15).

MS (MALDI$^+$) *m/z* (%): *978.5 (100)* $[C_{41}H_{69}N_3O_{22},Na]^+$.

FTIR (ν_{max}/cm^{-1}, nujol): 3289 (O-H st), 2924-2853 (C-H st), 2099 (N_3 st), 1732 (C=O st), 1461 (CH_2, CH_3 δ), 1237 (CO-O st), 1131 (O-C-C st).

EA (%): *Found:* C, 51.8; H, 7.3; N, 4.6. *Calc. for* $C_{41}H_{69}N_3O_{22}$: C, 51.5; H, 7.3; N, 4.4.

N_3-[*bis*MPA,G2]-$(NHBoc)_4$

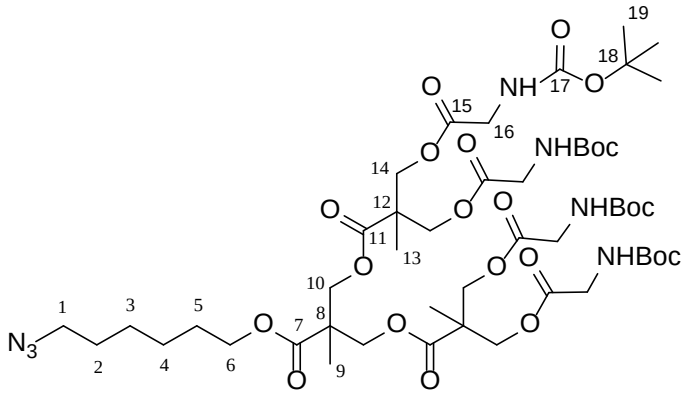

General procedure III) N_3-[*bis*MPA,G2]-$(OH)_4$ (2.50 g, 5.09 mmol, 1.00 eq.); Glyboc(OH) (4.46 g, 25.45 mmol, 5.00 eq.); DMAP (0.99 g, 8.14 mmol, 1.6 eq.); DCC (5.25 g, 25.45 mmol, 5.00 eq.); dry DCM (110 + 35 mL); time of reaction: 24 hours. The crude product was purified twice on silica gel (hexane : ethyl acetate = 7:3) to get a white solid (2.80 g, 49 %).

^{1}H (300 MHz, $CDCl_3$) δ (ppm): 1.25 (s, 6H, H-13), 1.27 (s, 3H, H-9), 1.45 (m, 40H, H-3, H-4 and H-19) 1.59 (m, 2H, H-2) 1.68 (m, 2H, H-5), 3.29 (t, J = 6.6 Hz, 2H, H-1), 3.89 (d, J = 5.7 Hz, 8H, H-16), 4.13 (t, J = 6.6 Hz, 2H, H-6), 4.27 (m, 12H, H-10 and H-14), 5.25 (bs, -NH).

^{13}C (75 MHz, $CDCl_3$) δ (ppm): [17.7-17.9] (C-9 and C-13), 25.4 (C-4), 26.3 (C-3), 28.3 (C-5 and C-19), 28.7 (C-2), 42.2 (C-16), 46.4 (C-12), 46.6 (C-8), 51.3 (C-1), [65.5-65.7] (C-6, C-10 and C-14), 80.0 (C-18), 155.8 (C-17), 170.0 (C-15), [171.8-172.2] (C-7 and C-11).

MS (MALDI$^+$) *m/z* (%): *1147.2 (100)* $[C_{49}H_{81}N_7O_{22},Na]^+$

FTIR (ν_{max}/cm^{-1}, ATR): 3394 (N-H st), 2918 (C-H st), 2100 (N_3 st), 1741 (C=O st ester), 1703 (C=O st carbamate), 1516 (N-H δ), 1471 (CH_2, CH_3 δ), 1247 (CO-O st), 1153 (N-CO-O st), 1130 (O-C-C st).

EA (%): *Found:* C. 52.6; H. 7.3; N, 8.55. *Calc. for* $C_{49}H_{81}N_7O_{22}$: C, 52.5; H, 7.3; N, 8.75.

SEC (*ref PMMA*): Mw 1352 g.mol^{-1}; Đ 1.02.

N_3-[*bis*MPA,G3]-$(NHBoc)_8$

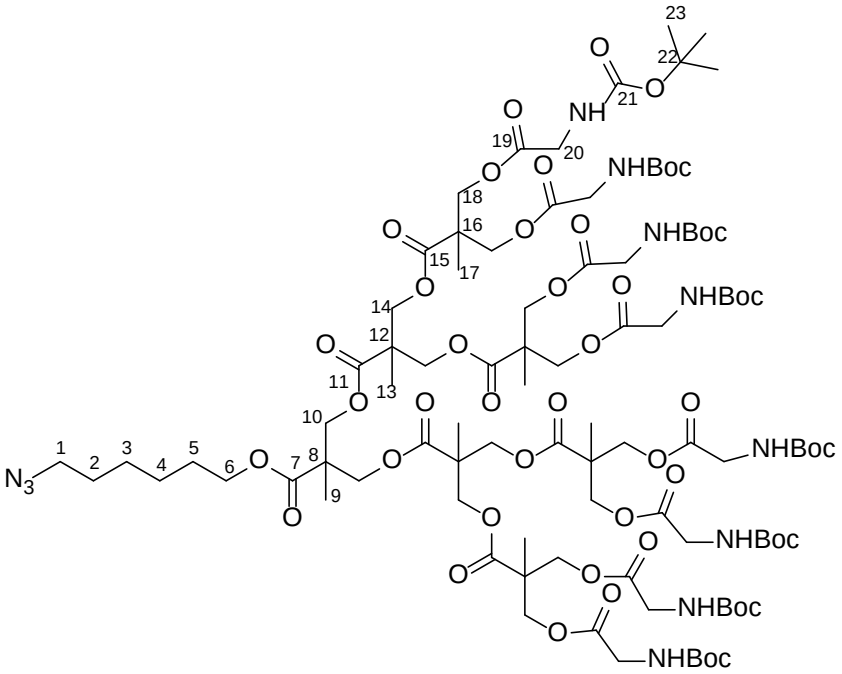

General procedure III) N_3-[bisMPA,G3]-$(OH)_8$ (15.00 g, 15.69 mmol, 1.00 eq.); Glyboc(OH) (27.49 g, 156.91 mmol, 10.00 eq.); DMAP (6.13 g, 50.21 mmol, 3.20 eq.); DCC (32.37 g, 156.91 mmol, 10.00 eq.); dry DCM (300 + 90 mL); time of reaction: 24 hours. The crude product was purified four times on silica gel (hexane : ethyl acetate = ramp from 7:3 to 4:6) to get a white solid (25.70 g, 74 %).

^{1}H NMR (400 MHz, $CDCl_3$) δ (ppm): 1.24 (s, 12H, H-17), 1.25 (s, 6H, H-13), 1.28 (s, 3H, H-9), 1.43 (s, 72H, H-23), 1.46 (m, 4H, H-3 and H-4,), 1.61 (m, 2H,H-2), 1.67 (m, 2H, H-5), 3.27 (t, J = 6.8 Hz, 2H, H-1), 3.88 (d, J = 6 Hz, 16H, H-20), 4.12 (t, J = 7.2 Hz, 2H, H-6), 4.25 (m, 28H, H-10, H-14 and H-18), 5.29 (bs, -NH).

^{13}C NMR (75 MHz, $CDCl_3$) δ (ppm): [17.4-17.7] (C-9, C-13 and C-17), 25.4 (C-4), 26.3 (C-3), 28.3 (C-5 and C-23), 28.7 (C-2), 42.2 (C-20), 46.3 (C-16), 46.4 (C-8), 46.6 (C-12), 51.1 (C-1), [65.2-66.1] (C-6, C-10, C-14 and C-18), 79.8 (C-22), 155.8 (C-21), 170.0 (C-19), [171.4-171.9] (C-7, C-11 and C-15).

MS (MALDI$^+$) *m/z* (%): *2236.3 (100)* $[C_{97}H_{157}N_{11}O_{46},Na]^+$.

FTIR (ν_{max}/cm^{-1}, ATR): 3383 (N-H st), 2980-2941 (C-H st), 2102 (N_3 st), 1742 (C=O st ester), 1717 (C=O st carbamate), 1520 (N-H δ), 1475 (CH_2, CH_3 δ), 1367 (C-N st), 1250 (CO-O st), 1155 (N-CO-O st), 1140 (O-C-C st).

EA (%): *Found:* C. 53.4; H. 7.7; N, 6.9. *Calc. for* $C_{97}H_{157}N_{11}O_{46}$: C, 52.6; H, 7.15; N, 7.0.

SEC: (*ref PMMA*): Mw 2469 g.mol^{-1}; Đ 1.02.

≡-[*bis*MPA,G1]-(ketal)$_1$

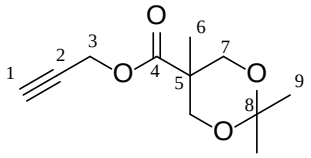

General procedure I) *Bis*-MPA(monomer)* (10.00 g, 53.1 mmol, 1.00 eq.); propargyl alcohol (3.23 mL, 55.8 mmol, 1.05 eq.); DPTS (6.24 g, 21.2 mmol, 0.40 eq.); DCC (10.96 g, 53.1 mmol, 1.05 eq.), dry DCM (80 + 20 mL); time of reaction: overnight. The crude product was purified on silica gel (hexane:ethyl acetate = 7:3) to give a light grey oil (10.77 g, 90 %).

^{1}H (400 MHz, $CDCl_3$) δ (ppm): 1.18 (s, 3H, H-6), 1.36 (s, 3H, H-9), 1.40 (d, 3H, H-9'), 2.46 (t, J = 2.4 Hz, 1H, H-1), 3.63 (d, J = 12 Hz, 2H, H-7), 4.17 (d, J = 12 Hz, 2H, H-7'), 4.71 (d, J = 2.4 Hz, 2H, H-3).

^{13}C (100 MHz, $CDCl_3$) δ (ppm): 18.3 (C-6), 22.5 (C-9), 24.5 (C-9'), 41.8 (C-5), 52.3 (C-3), 65.8 (C-7), 74.9 (C-1), 77.4 (C-2), 98.0 (C-8), 173.3 (C-4).

MS (ESI^+) *m/z (%)*: *235.0 (13)* $[C_{11}H_{16}O_4,Na]^+$, *213.0 (31)* $[C_{11}H_{16}O_4,H]^+$.

FTIR (ν_{max}/cm^{-1}, nujol): 3273 (≡C-H st), 2993 (C-H st), 2129 (C≡C st), 1739 (C=O st), 1456 (CH_2, CH_3 δ).

EA (%): *Found:* C, 61.6; H, 7.7. *Calc. for* $C_{11}H_{16}O_4$: C, 62.3; H, 7.6.

≡-[*bis*MPA,G1]-$(OH)_2$

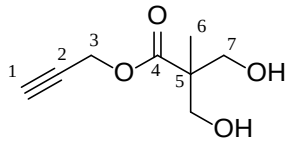

General procedure II) ≡-[*bis*MPA,G1]-$(ketal)_1$ (10.55 g, 49.71 mmol, 1.00 eq.); Dowex resin H^+ (5.22 g, 50 %mass equivalent); MeOH (150 mL); time of reaction: 5 hours. The pure product was obtained as a colorless oil (8.47 g, 99 %).

^{1}H (400 MHz, $CDCl_3$) δ (ppm): 1.09 (s, 3H, H-6), 2.50 (t, J = 2.4 Hz, 1H, H-1), 3.04 (bs, -OH), 3.71 (d, J = 10.6 Hz, 2H, H-7), 3.90 (d, J = 10.6 Hz, 2H, H-7'), 4.74 (d, J = 2.4 Hz, 2H, H-3).

^{13}C (100 MHz, $CDCl_3$) δ (ppm): 17.0 (C-6), 49.3 (C-5), 52.4 (C-3), 67.6 (C-7), 75.2 (C-1), 77.3 (C-2), 175.0 (C-4).

MS (ESI^+) *m/z (%)*: *194.9 (100)* $[C_8H_{12}O_4,Na]^+$.

FTIR (ν_{max}/cm^{-1}, nujol): 3293 (O-H st), 2945 (C-H st), 2128 (C≡C st), 1730 (C=O st), 1461 (CH_2, CH_3 δ).

EA (%): *Found*: C, 55.4; H, 7.3; *Calc. for* $C_8H_{12}O_4$: C, 55.8, H, 7.0.

≡-[*bis*MPA,G2]-(ketal)$_2$

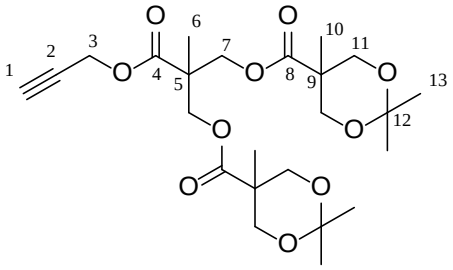

General procedure I) ≡-[*bis*MPA,G1]-(OH)$_2$ (6.87 g, 38.7 mmol, 1.00 eq.); *b*is-MPA(monomer)* (15.3 g, 81.3 mmol, 2.10 eq.); DPTS (9.11 g, 30.7 mmol, 0.80 eq.); DCC (16.77 g, 81.3 mmol, 2.10 eq.), dry DCM (160 + 40 mL); time of reaction: overnight. The crude product was purified on silica gel (hexane : ethyl acetate = 7:3) to obtain a white powder (18.57 g, 99 %).

^{1}H (300 MHz, $CDCl_3$): δ 1.16 (s, 6H, H-10), 1.20 (s, 3H, H-6), 1.39 (s, 6H, H-13), 1.41 (s, 6H, H-13'), 2.47 (t, J = 2.4 Hz, 1H, H-1), 3.62 (d, J = 12.3 Hz, 4H, H-11), 4.16 (d, J = 12.0 Hz, 4H, H-11'), 4.33 (s, 4H, H-7), 4.72 (d, J = 2.4 Hz, 2H, H-3).

^{13}C (75 MHz, $CDCl_3$): δ 17.6 (C-6), 18.5 (C-10), 22.2 (C-13), 24.9 (C-13'), 42.0 (C-9), 46.8 (C-5), 52.6 (C-3), 65.2 (C-7), 65.9 (C-11), 75.2 (C-1), 77.2 (C-2), 98.1 (C-12), 171.8 (C-4), 173.5 (C-8).

MS (MALDI$^+$) *m/z (%)*: *507.2 (100)* $[C_{24}H_{36}O_{10},Na]^+$.

FTIR (ν_{max}/cm^{-1}, nujol): 3249 (≡C-H st), 2923 (C-H st), 2121 (C≡C st), 1733 (C=O st), 1458 (CH_2, CH_3 δ).

EA (%): *Found*: C, 59.9; H, 8.1; *Calc. for* $C_{24}H_{36}O_{10}$: C, 59.5; H, 7.5.

≡-[*bis*MPA,G2]-(OH)$_4$

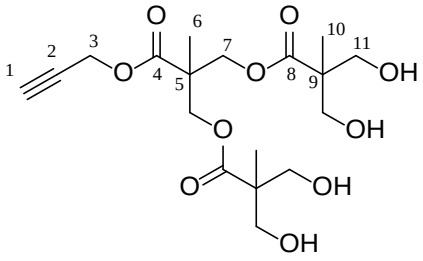

General procedure II) ≡-[*bis*MPA,G2]-(ketal)$_2$ (17.17 g, 35.44 mmol, 1.00 eq.); ion exchange resin Dowex H^+ (8.59 g, 50 %mass equivalent); MeOH (200 mL); time of reaction: 10 hours. The pure product was obtained as a white powder (13.03 g, 91 %).

^{1}H (400 MHz, CD_3OD) δ (ppm): 1.15 (s, 6H, H-10), 1.31 (s, 3H, H-6), 2.96 (t, J = 2.4 Hz, 1H, H-1), 3.64 (ABq, J = 11.2 Hz, $\Delta\nu_{AB}$ = 25.3 Hz, 8H, H-11), 4.29 (ABq, J = 10.8 Hz, $\Delta\nu_{AB}$ = 9.8 Hz, 4H, H-7), 4.76 (d, J = 2.4 Hz, 2H, H-3).

^{13}C (100 MHz, CD_3OD) δ (ppm): 17.3 (C-10), 18.1 (C-6), 40.5 (C-9), 47.9 (C-5), 51.8 (C-3), 65.8 (C-11), 66.4 (C-7), 76.7 (C-1), 78.6 (C-2), 173.7 (C-4), 175.9 (C-8).

MS ($MALDI^+$) *m/z* (%): *427.2 (100)* $[C_{18}H_{28}O_{10},Na]^+$.

FTIR (ν_{max}/cm^{-1}, nujol): 3403 (O-H st), 2923 (C-H st), 2125 (C≡C st), 1732 (C=O st), 1461 (CH_2, CH_3 δ).

EA (%): *Found:* C, 53.2; H, 7.45. *Calc. for* $C_{18}H_{28}O_{10}$: C, 53.5; H, 7.0.

≡-[*bis*MPA,G1]-$(C17)_2$

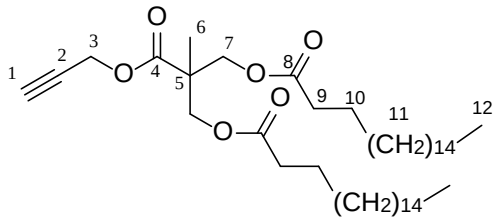

General procedure IV) ≡-[*bis*MPA,G1]-$(OH)_2$ (3.00 g, 17.49 mmol, 1.00 eq.); stearic acid (14.93 g, 52.47 mmol, 3.00 eq.); DMAP (1.71 g, 13.99 mmol, 0.80 eq.); DCC (10.83 g, 52.47 mmol, 4.00 eq.); dry DCM (120 + 30 mL); time of reaction: 2 days. The pure product was obtained as a white powder (7.73 g, 63%).

^{1}H ($CDCl_3$, 300 MHz) δ (ppm): 0.88 (t, J = 6.3 Hz, 6H, H-12), 1.25 (m, 59H, H-6 and H-11), 1.59 (m, 4H, H-10), 2.30 (t, J = 7.5 Hz, 4H, H-9), 2.45 (t, J = 2.1 Hz, 1H, H-1), 4.23 (ABq, J = 11.4 Hz, $\Delta\nu_{AB}$ = 6.0 Hz, 4H, H-7), 4.71 (d, J = 2.1 Hz, 2H, H-3).

^{13}C ($CDCl_3$, 75 MHz) δ (ppm): 14.1 (C-12), 17.7 (C-6), 22.7 (C-11), 24.9 (C-10), [29.1-29.7] (C-11), 31.9 (C-11), 34.1 (C-9), 46.4 (C-5), 52.5 (C-3), 65.1 (C-7), 75.1 (C-1), 77.2 (C-2), 172.1 (C-4), 173.2 (C-8).

MS ($MALDI^+$) *m/z* (%): *727.6 (100)* $[C_{44}H_{80}O_6,Na]^+$.

FTIR (ν_{max}/cm^{-1}, ATR): 3924 (≡C-H st), 2916 (C-H st), 2129 (C≡C st), 1734 (C=O st), 1473 (CH_2, CH_3 δ), 1250 (CO-O st), 1132 (O-C-C st).

EA: (%) *Found:* C, 75.5; H, 11.65. *Calc. for* $C_{44}H_{80}O_6$: C, 74.95; H, 11.4.

SEC: (*ref PMMA*): Mw 1211 $g.mol^{-1}$; Đ 1.02.

≡-[*bis*MPA,G2]-(C17)$_4$

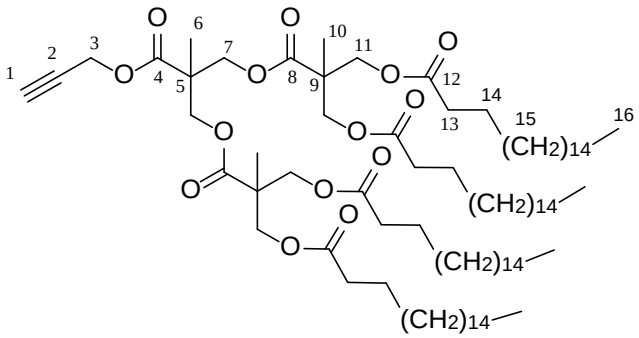

General procedure IV) ≡-[*bis*MPA,G2]-(OH)$_4$ (1.50 g, 3.71 mmol, 1.00 eq.); stearic acid (6.33 g, 22.26 mmol, 6.00 eq.); DMAP (7.25 g, 5.94 mmol, 1.60 eq.); DCC (4.59 g, 22.27 mmol, 6.00 eq.); dry DCM (90 + 10 mL). The pure product was obtained as a white powder (3.67 g, 67 %).

^{1}H (400 MHz, $CDCl_3$) δ (ppm): 0.88 (t, J = 6.6 Hz, 12H, H-16), 1.25 (m, 121 H, H-6, H-10 and H-15), 1.58 (m, 8H, H-14), 2.29 (t, J = 7.5 Hz, 8H, H-13), 2.50 (t, J = 2.4 Hz, 1H, H-1), 4.19 (ABq, J = 10.5 Hz, $\Delta\nu_{AB}$ = 6.8 Hz, 8H, H-11), 4.26 (ABq, J = 8.1 Hz, $\Delta\nu_{AB}$ = 12.0 Hz, H-7), 4.72 (d, J = 2.4 Hz, H-3).

^{13}C (100 MHz, $CDCl_3$) δ (ppm): 14.1 (C-16), 17.4 (C-6), 17.8 (C-10), 22.7 (C-15), 24.8 (C-14), [29.1-29.7] (C-15), 31.9 (C-15), 34.0 (C-13), 46.4 (C-9), 46.7 (C-5), 52.8 (C-3), 65.0 (C-11), 65.6 (C-7), 75.4 (C-1), 77.1 (C-2), 171.4 (C-4), 172.0 (C-8), 173.1 (C-12).

MS (MALDI$^+$): *m/z* (%): *1492.4 (100)* $[C_{90}H_{164}O_{14},Na]^+$.

FTIR (ν_{max}/cm^{-1}, ATR): 3292 (≡C-H st), 2916 (C-H st), 2141 (C≡C st), 1736 (C=O st), 1472 (CH_2, CH_3 δ), 1236 (CO-O st), 1119 (O-C-C st).

EA (%): *Found:* C, 74.0; H, 11.6. *Calc. for* $C_{90}H_{164}O_{14}$: C, 73.5, H, 11.2.

SEC: (*ref PMMA*): Mw 2428 g.mol^{-1}; Đ 1.02.

7.1.2- *Bis*-GMPA dendrons

General procedure V): growing up amide coupling reaction of the bis-GMPA dendrons

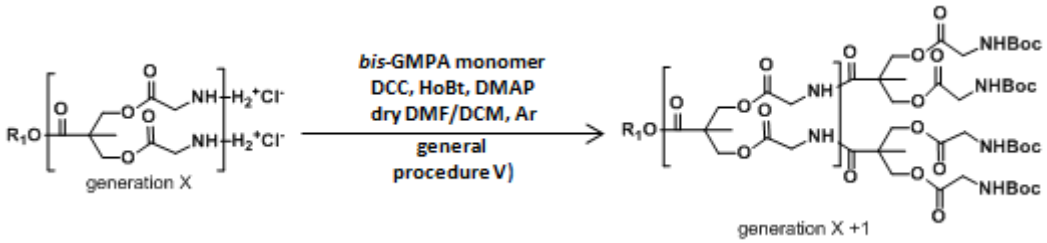

Amine (1.00 mol) was dissolved into a mixture of dry dimethylformamide and dry dichloromethane. *Bis*-GMPA(monomer)* (1.20, 1.50 and 1.75 mol per amino groups according to the dendron generation), HOBt (1.20, 1.50 and 1.75 mol per amino groups according to the dendron generation) and DMAP (1.4 mol per amino groups) were added to it. The reaction mixture was stirred under argon atmosphere and cooled down to 0ºC. DCC (1.20, 1.50 and 1.75 mol per amino groups according to the dendron generation) was dissolved into dry dichloromethane and was added drop wise to the reaction mixture. It was stirred at room temperature under argon atmosphere during 24 hours. The white precipitate, N,N'-dicyclohexylurea (DCU), was filtered off and the solvent was evaporated under vacuum to get an orange oil. Remaining DCU and HOBt were precipitated into a mixture of hexane and ethyl acetate and filtered off. The organic phase was washed 3 times with brine, dried over anhydrous $MgSO_4$ and the solvent were evaporated. Remaining HOBt was precipitated into cold AcOEt (-16ºC) and filtered off. The solvent was evaporated under reduce pressure. The crude product was purified on silica gel. In the case of the 3rd generation, the crude product was precipitate into a mixture of hexane and ethyl acetate before purification on silica gel.

General procedure VI): deprotection of the terminal amino groups

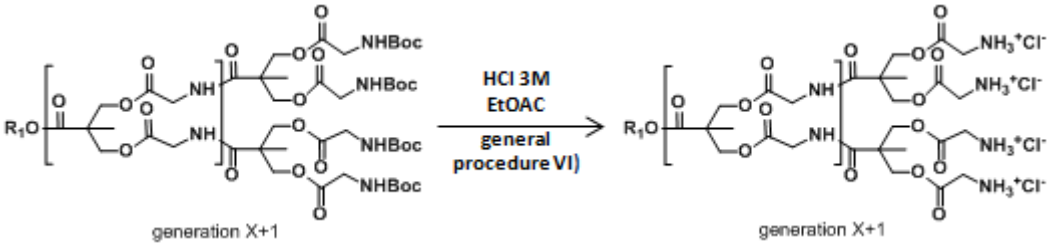

t-Boc protected dendron (1 mol) was dissolved into ethyl acetate. HCl into ethyl acetate (3M) was carefully added to it. The reaction mixture was stirred at room temperature during 1 hour. A white precipitate appeared. The reaction mixture was diluted into ethyl acetate and was stirred during another 30 min. Then, it was stirred under vacuum to remove the hydrochloric acid. The white residue was recovered by centrifugation and was washed twice with pure ethyl acetate.

BnOOC-[*bis*MPA,G1]-$(OH)_2$

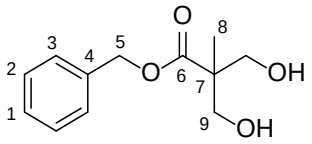

Bis-MPA (20.00 g, 149.2 mmol, 1.00 eq.) was dissolved into DMF (100 mL). KOH (10.20 g, 179.0 mmol, 1.20 eq.) was added to it. The reaction was stirred at 100ºC during 1 hour. Then, BnBr (26.55 mL, 223.7 mmol, 1.50 eq.) was added drop wise. The reaction mixture was stirred overnight at 100ºC. A white precipitate appeared. It was filtered off. Water (450 mL) was added to the filtrate and the product was extracted three times with ethyl acetate, (3 x 200 mL) and then washed three times with brine (3 x 150 mL) to give a yellow oil. The crude product was recristalized into toluene to get white crystals (23.20 g, 69 %).

^{1}H (400 MHz, $CDCl_3$) δ (ppm): 1.02 (s, 3H, H-8), 2.82 (bs, -OH), 3.74 (d, J = 10.8 Hz, 2H, H-9), 3.94 (d, J= 11.2 Hz, 2H, H-9'), 5.21 (s, 2H, H-5), 7.36 (m, 5H, H-1, H-2 and H-3).

^{13}C (100 MHz, $CDCl_3$) δ (ppm): 17.1 (C-8), 49.2 (C-7), 66.7 (C-5), 68.6 (C-9), 127.9 (C-3), 128.3 (C-1), 128.6 (C-2), 135.6 (C-4), 175.7 (C-6).

MS (ESI^+) *m/z (%): 246.8 (100)* $[C_{12}H_{16}O_4,Na]^+$.

FTIR (ν_{max}/cm^{-1}, nujol): 3352 (O-H st), 2923-2853 (C-H st and arC-H), 1701 (C=O st).

EA (%): *Found*: C, 63.9; H, 7.3. *Calc. for* $C_{12}H_{16}O_4$: C, 64.3; H, 7.2.

BnOOC-[*bis*MPA,G1]-$(NHBoc)_2$

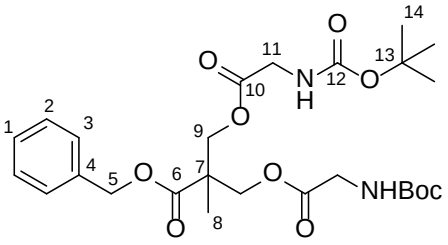

BnOOC-[*bis*MPA,G1]-$(OH)_2$ (10.00 g, 44.62 mmol, 1.00 eq.) was dissolved into dry DCM (230 mL). Glyboc(OH) (19.54 g, 111.56 mmol, 2.50 eq.) and DPTS (10.51 g, 35.70 mmol, 0.80 eq.) were added to it. The reaction mixture was stirred under argon atmosphere and cooled down to 0ºC. DCC (22.99 g, 111.56 mmol, 2.50 eq.) was dissolved into dry DCM (70 mL) and was added drop wise to the reaction mixture. The reaction mixture was stirred at room temperature overnight. The white precipitate, N,N'-dicyclohexylurea (DCU), was filtered off and the solvent was evaporated under vacuum to get a mixture of oil and solid. DCU was newly precipitated into a mixture of hexane : ethyl acetate (10:2) (240 mL) and was filtered off. The solvents were evaporated under reduce pressure. The crude powder was purified on silica gel (hexane : ethyl acetate = 8:2) to get a colorless oil (22.00 g, 92 %).

^{1}H (300 MHz, $CDCl_3$) δ (ppm): 1.27 (s, 3H, H-8), 1.45 (s, 18 H, H-14), 3.81 (d, J = 4Hz, 4H, H-11), 4.31 (ABq, J = 10.8 Hz, $\Delta\nu_{AB}$ = 22.4 Hz, 4H, H-9), 5.03 (bs, -NH), 5.17 (s, 2H, H-5), 7.36 (m, 5H, H-1, H-2 and H-3).

^{13}C (75 MHz, $CDCl_3$) δ (ppm): 17.9 (C-8), 28.3 (C-14), 42.2 (C-11), 46.3 (C-7), 65.8 (C-9), 67.0 (C-5), 80.0 (C-13), 128.3 (C-3), 128.5 (C-1), 128.6 (C-2), 135.4 (C-4), 155.7 (C-12), 169.9 (C-10), 172.1 (C-6).

MS (ESI^+) *m/z (%)*: *561 (42)* $[C_{26}H_{38}N_2O_{10},Na]^+$.

FTIR (ν_{max}/cm^{-1}, ATR): 3379 (N-H st), 2980-2932 (C-H st and C-H_{ar} st), 1757 (C=O st aliphatic ester), 1720 (C=O st aromatic ester), 1690 (C=O st carbamate), 1512 (N-H δ), 1456 (CH_2, CH_3 δ), 1365 (C-N st), 1250 (CO-O st), 1153 (N-CO-O st), 1132 (O-C-C st).

EA (%): *Found:* C, 57.8; H, 7.2; N, 5.4. *Calc. for* $C_{26}H_{38}N_2O_{10}$: C, 58.0; H, 7.1; N, 5.2.

t-Boc protected *Bis*-GMPA(monomer), named as *bis*-GMPA(monomer)*

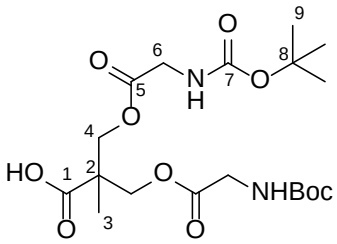

BnOOC-[*bis*MPA,G1]-$(NHBoc)_2$ (16.75 g, 31.10 mmol, 1.00 eq.) was dissolved into ethyl acetate (150 mL) under argon atmosphere. Pd/C (837 mg, 0.05 eq. in weight) was added carefully to the reaction mixture. Firstly, three cycles of argon - vacuum were made and secondly three cycles vaccum-H_2 were made. The reaction mixture was stirred overnight under H_2 pressure using a globe. Then, it was filtered on celite© with ethyl acetate flow. The solvent was evaporated under reduce pressure to give a colorless gel (13.39 g, 96 %).

^{1}H (400 MHz, $CDCl_3$) δ (ppm): 1.26 (s, 3H, H-3), 1.43 (s, 18H, H-9), 3.89 (d, J = 5.6 Hz, 4H, H-6), 4.32 (ABq, J = 11.2 Hz, $\Delta\nu_{AB}$ = 23.7 Hz, 4H, H-4), 5.27 (bs, -NH).

^{13}C (100 MHz, $CDCl_3$) δ (ppm): 17.9 (C-3), 28.3 (C-9), 42.2 (C-6), 45.9 (C-2), 65.8 (C-4), 80.2 (C-8), 156.0 (C-7), 170.1 (C-5), 176.1 (C-1).

MS (ESI^+) *m/z (%)*: *471 (100)* $[C_{19}H_{32}N_2O_{10},Na]^+$.

FTIR (ν_{max}/cm^{-1}, ATR): 3381 (N-H st), 2980-2937 (C-H st), 1745 (C=O st aliphatic ester), 1699 (C=O st carbamate), 1522 (N-H δ), 1458 (CH_2, CH_3 δ), 1367 (C-N st), 1250 (CO-O st), 1151 (N-CO-O st), 1140 (O-C-C st).

EA (%): *Found:* C, 50.6; H, 7.5; N, 5.9. *Calc. for* $C_{19}H_{32}N_2O_{10}$: C, 50.9; H, 7.2; N, 6.25.

N_3-[*bis*GMPA,G1]-$(NHBoc)_2$

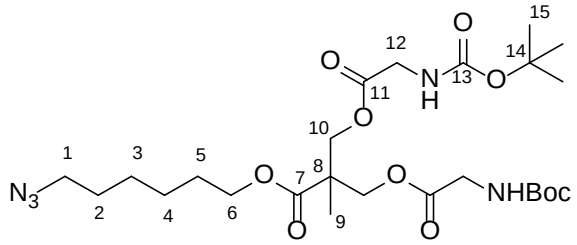

General procedure III) N_3-[*bis*MPA,G1]-$(OH)_2$[A] (3,69 g, 14.2 mmol, 1.00 eq.); Glyboc(OH) (6.23 g, 35.6 mmol, 2.50 eq.); DPTS (3.35 g, 11.4 mmol, 0.80 eq.); DCC (7.33 g, 35.6 mmol, 2.50 eq.); dry DCM (85 + 15 mL); time of reaction: 24 hours. The crude product was purified on silica gel (hexane : ethyl acetate = 8:2) to get a colorless and viscous oil (7.50 g, 92 %).

[A] The synthesis of N_3-[*bis*MPA,G1]-$(OH)_2$ is described at page 307.

^{1}H (300 MHz, $CDCl_3$) δ (ppm): 1.24 (s, 3H, H-9), 1.37 (m, 4H, H-3 and H-4), 1.44 (s, 18H, H-15), 1.60 (m, 2H, H-2), 1.64 (m, 2H, H-5), 3.27 (t, J = 6.8 Hz, 2H, H-1), 3.88 (d, J = 5.3 Hz, 4H, H-12), 4.12 (t, J = 6.6Hz, 2H, H-6), 4.32 (ABq, J = 11.1 Hz and $\Delta\nu_{AB}$ = 21.6 Hz, 4H, H-10), 5.08 (bs, -NH).

^{13}C (100 MHz, $CDCl_3$) δ (ppm): 18.0 (C-9), 25.4 (C-4), 26.3 (C-3), 28.3 (C-5 and C-15), 28.7 (C-2), 42.2 (C-12), 46.2 (C-8), 51.3 (C-1), 65.2 (C-6), 65.7 (C-10), 80.0 (C-14), 156.7 (C-13), 170.0 (C-11), 172.4 (C-7).

MS (ESI^+) *m/z (%)*: *596 (24)* $[C_{25}H_{43}N_5O_{10},Na]^+$.

FT-IR (cm^{-1}, ATR): 3410-3339 (N-H st), 2984-2949-2872 (C-H st), 2093 (N_3 st), 1771-1757 (C=O st ester), 1722-1688 (C=O st carbamate), 1539-1510 (N-H δ), 1472 (CH_2, CH_3 δ), 1367 (C-N st), 1228 (CO-O st), 1161 (N-CO-O st), 1128 (O-C-C st).

EA (%): *Found:* C, 52.7; H, 7.6; N, 12.0. *Calc. for* $C_{25}H_{43}N_5O_{10}$: C, 52.35; H, 7.6; N, 12.2.

SEC (*ref PMMA*): Mw 747 $g.mol^{-1}$; Đ: 1.01.

N_3-[*bis*GMPA,G1]-($NH_3^+Cl^-$)$_2$

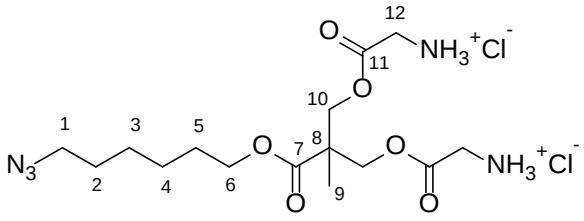

N_3-[*bis*GMPA,G1]-(NHBoc)$_2$ (4.54 g, 7.91 mmol, 1.00 eq.) was dissolved into AcOEt (15 mL). A dissolution of HCl 3M into AcOEt (15 mL) was added to it. It was stirred at room temperature during 4 hours. A precipitate appeared. AcOEt (100 mL) was added to the reaction mixture and it was stirred at room temperature for 1 hour more. Then, it was stirred under vacuum to remove HCl vapors. Ethyl acetate was removed under reduce pressure. The white precipitate was washed by being newly dispersed into ethyl acetate and stirred during 15 min. The ethyl acetate was evaporated under reduce pressure to give a white powder (2.67 g, 76 %).

^{1}H (400 MHz, CD_3OD) δ (ppm): 1.31 (s, 3H, H-9), 1.43 (m, 4H, H-3 and H-4), 1.61 (m, 2H, H-2), 1.65 (m, 2H, H-5), 3.89 (s, 4H, H-12), 4.16 (t, J = 6.4 Hz, 2H, H-6), 4.45 (ABq, J = 19.2 Hz, $\Delta\nu_{AB}$ = 7.0 Hz, 4H, H-10).
note: H-1 signal (~3.2 ppm) is overlapped with the CH_3 signal of CD_3OD but the correlation between H-1 and H-2 is observed in ^{1}H-^{1}H COSY and the correlation between H-1 and C-1 is observed in ^{1}H-^{13}C HSQC.

^{13}C (100 MHz, CD_3OD): δ (ppm): 17.9 (C-9), 26.5 (C-4), 27.3 (C-3), 29.4 (C-5), 29.7 (C-2), 40.9 (C-12), 47.5 (C-8), 52.3 (C-1), 66.6 (C-6), 67.7 (C-10), 168.3 (C-11), 173.8 (C-7).

MS (ESI^+) *m/z (%)*: *374.1 (100)* $[C_{20}H_{30}N_2O_6,H]^+$.

FTIR (ν_{max}/cm^{-1}, ATR): 3441-2505 (N-H^+), 2943-2860-2702-2625 (C-H st), 2097 (N_3 st), 1744 (C=O st ester), 1605-1574 (N-H^+ δ), 1466 (CH_2, CH_3 δ), 1420 (C-N st), 1224 (CO-O st), 1137 (O-C-C st).

EA (%): *Found:* C, 40.1; H, 6.6; N, 14.2. *Calc. for* $C_{15}H_{29}Cl_2N_5O_6$: C, 40.4; H, 6.55; N, 15.7.

N_3-[*bis*GMPA,G2]-$(NHBoc)_4$

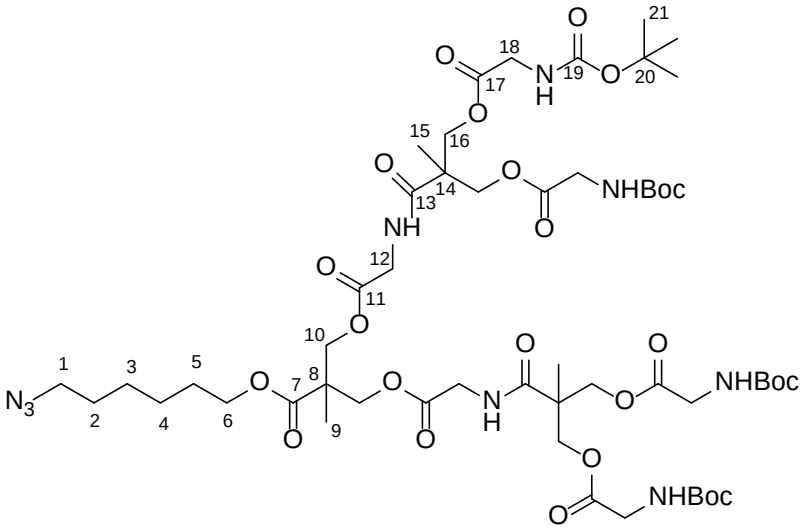

General procedure V) N_3-[*bis*GMPA,G1]-$(NH_3^+Cl^-)_2$ (3.59 g, 8.04 mmol, 1.00 eq.); *Bis*-GMPA(monomer)* (7.96 g, 17.70 mmol, 2.20 eq.); HOBt,nH_2O (2.71 g, 17.70 mmol, 2.20 eq.); DMAP (2.42 g, 19.82 mmol, 2.80 eq.); DCC (3.65 g, 17.70 mmol, 2.20 eq.); dry DMF (40 mL); dry DCM (90 + 10 mL). The crude product was purified on silica gel (hexane : ethyl acetate = ramp from 5:5 to 2:8) to obtain a white powder (7.64 g, 77 %).

^{1}H (400 MHz, $CDCl_3$) δ (ppm): 1.27 (s, 3H, H-9), 1.29 (s, 6H, H-15), 1.41 (m, 4H, H-3 and H-4), 1.45 (m, 36H, H-21), 1.62 (m, 2H, H-2), 1.67 (m, 2H, H-5), 3.29 (t, 2H, J = 6.8Hz, H-1), 3.91 (d, J = 5.6Hz, 8H, H-18), 3.98 (d, J = 5.2Hz, 4H, H-12), 4.15 (t, J = 6.4 Hz, 2H, H-6), 4.17 (m, 2H, H-10), [4.17-4.38] (m, 10H, H-10' and H-16), 5.29 (bs, -NHBoc), 7.08 (bs, -NHCO).

^{13}C (100 MHz, $CDCl_3$) δ (ppm): 17.8 (C-15), 18.1 (C-9), 25.4 (C-4), 26.3 (C-3), 28.3 (C-5 and C-21), 28.7 (C-2), 41.0 (C-18), 42.4 (C-12), 46.1 (C-8), 46.3 (C-14), 51.3 (C-1), 64.9 (C-16), 65.3 (C-10), 66.5 (C-6), 80.1 (C-20), 155.9 (C-19), 169.6 (C-17), 170.3 (C-11), 172.5 (C-7), 172.8 (C-13).

MS (MALDI$^+$) *m/z (%)*: *1256 (100)* $[C_{53}H_{87}N_9O_{24},Na]^+$.

FTIR (ν_{max}/cm^{-1}, ATR): 3379 (N-H st), 2980-2943-2864 (C-H st), 2098 (N_3 st), 1742 (C=O ester st), 1699 (C=O st carbamate), 1676 (C=O st amide), 1520 (N-H δ), 1458 (CH_2, CH_3 δ), 1367 (C-N st), 1246 (CO-O st), 1155 (N-CO-O st).

EA (%): *Found:* C, 52.2; H, 7.5; N, 10.1. *Calc. for* $C_{53}H_{87}N_9O_{24}$: C, 51.6; H, 7.1; N, 10.2.

SEC (*ref PMMA*): Mw 1581 $g.mol^{-1}$; Đ: 1.02.

N_3-[*bis*GMPA,G2]-($NH_3^+Cl^-$)$_4$

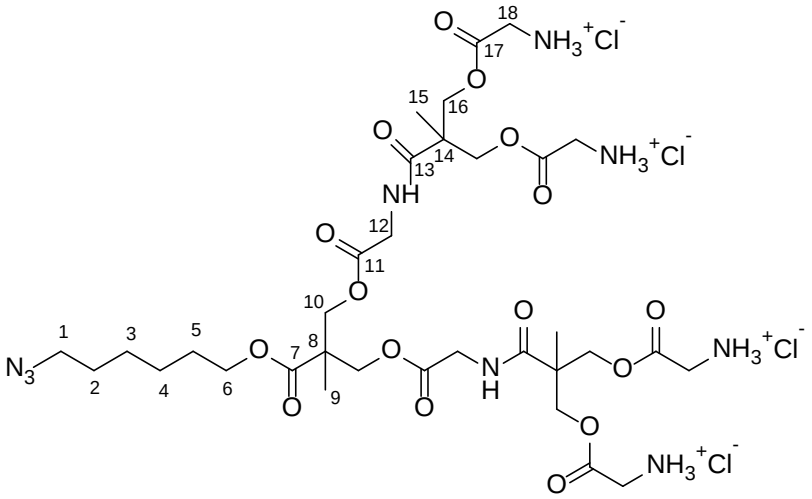

General procedure VI) N_3-[*bis*GMPA,G2]-(NHBoc)$_4$ (6.00 g, 2.58 mmol, 1.00 eq.); HCl 3M into ethyl acetate (20 mL); ethyl acetate (10 mL). The pure product was obtained as a white powder (3.77 g, 81 %).

^{1}H (400 MHz, CD_3OD) δ (ppm): 1.27 (s, 3H, H-9), 1.37 (s, 6H, H-15), 1.43 (m, 4H, H-3 and H-4), 1.62 (m, 2H, H-2), 1.69 (m, 2H, H-5), 3.93 (m, 8H, H-18), 3.96 (m, 4H, H-12), 4.16 (t, J = 6.8 Hz, 2H, H-6), 4.32 (ABq, J = 11.6 Hz, $\Delta\nu_{AB}$ = 9.4 Hz, 4H, H-10), 4.45 (ABq, J = 11.2 Hz, 8H, H-16), 8.35 (bs, -NHCO).

*note: H-1 signal (~3.2 ppm) is overlapped with the CH_3 signal of CD_3OD but the correlation between H-1 and H-2 is observed in ^{1}H-^{1}H COSY and the correlation between H-1 and C-1 is observed in ^{1}H-^{13}C HSQC (see **annexes 1**).*

^{13}C (100 MHz, CD_3OD) δ (ppm): 17.8 (C-15), 18.1 (C-9), 26.5 (C-4), 27.3 (C-3), 29.4 (C-5), 29.7 (C-2), 41.1 (C-18), 42.1 (C-12), 47.3 (C-14), 47.6 (C-8), 52.3 (C-1), 66.6 (C-6), 67.2 (C-10), 68.5 (C-16), 168.2 (C-17), 170.9 (C-11), 174.0 (C-7), 174.9 (C-13).

MS (MALDI$^+$) *m/z (%)*: *834.7 (100)* $[C_{33}H_{55}N_9O_{16},H]^+$.

FTIR (ν_{max}/cm^{-1}, ATR): 3222 (N-H st), 2941-2861 (C-H st and bs N-H$^+$ st), 2098 (N_3 st), 1747 (C=O st ester), 1662 (C=O st amide and N-H$^+$ δ), 1541 (N-H δ), 1478 (CH_2, CH_3 δ), 1407 (C-N st), 1246 (CO-O st), 1138 (O-C-C st) .

EA (%): *Found:* C, 39.9; H, 6.5; N, 12.9. *Calc. for* $C_{33}H_{59}Cl_4N_9O_{16}$: C, 40.5; H, 6.1; N, 12.9.

N_3-[*bis*GMPA,G3]-$(NHBoc)_8$

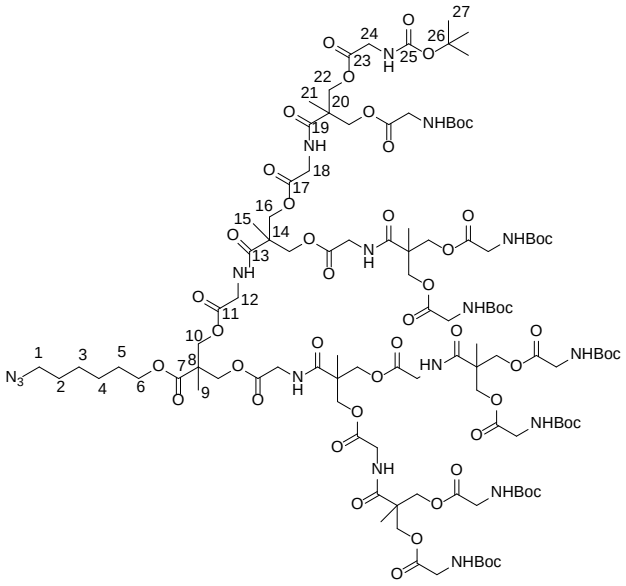

General procedure V) N_3-[*bis*GMPA,G2]-$(NH_3^+Cl^-)_4$ (2.00 g, 2.04 mmol, 1.00 eq.); *Bis*-GMPA(monomer)* (5.50 g, 12.25 mmol, 6.00 eq.); HOBt,nH_2O (1.88 g, 12.25 mmol, 6.00 eq.); DMAP (1.40 mg, 11.43 mmol, 5.60 eq.); DCC (2.53 g, 12.25 mmol, 6.00 eq.); dry DMF (33 mL); dry DCM (56 + 10 mL). The crude product was purified on silica gel (DCM : MeOH = 95:5) to obtain a white solid (3.88 g, 74 %).

^{1}H (400 MHz, $CDCl_3$) δ (ppm): 1.25 (s, 6H, H-15), 1,26 (s, 3H, H-9), 1.28 (s, 12H, H-21), 1.44 (m, 76H, H-3, H-4 and H-27), 1.61 (m, 2H, H-2), 1.66 (m, 2H, H-5), 3.27 (t, 2H, J = 6.8 Hz, H-1), 3.90 (d, J = 5.2 Hz, 16H, H-24), 3.95 (d, J = 5.2 Hz, 4H, H-12), 4.00 (d, J = 5.2 Hz, 8H, H-18), 4.13 (t, J = 6.4 Hz, 2H, H-6), [4.20-4.38] (m, 28H, H-10, H-16 and H-22), 5.42 (bs, -NHBoc), 7.19 (bs, -NHCO).

^{13}C (75 MHz, $CDCl_3$) δ (ppm): 17.7 (C-21), 18.0 (C-15), 18.3 (C-9), 25.3 (C-4), 26.2 (C-3), 28.3 (C-5 and C-27), 28.6 (C-2), 41.3 (C-24), 42.3 (C-12 and C-18), 46.0 (C-8 and C-14), 46.1 (C-20), 51.2 (C-1), 65.2 (C-22), 66.4 (C-6, C-10 and C-16), 80.0 (C-26), 156.0 (C-25), 170.6 (C-11, C-17 and C-23), 172.5 (C-7), 172.8 (C-13 and C-19).

MS (MALDI$^+$) *m/z (%)* : *2580 (100)* $[C_{109}H_{175}N_{17}O_{52},Na]^+$.

FTIR (ν_{max}/cm^{-1}, ATR): 3356 (N-H st), 2978-2928-2854 (C-H st), 2106 (N_3 st), 1742-1718 (C=O ester st), 1699 (C=O carbamate st), 1664 (C=O amide st), 1528 (N-H δ), 1458 (CH_2, CH_3 δ), 1367 (C-N st), 1250 (CO-O st), 1157 (N-CO-O st).

EA (%): *Found:* C, 51.3; H, 7.3; N, 9.6. *Calc. for* $C_{109}H_{175}N_{17}O_{52}$: C, 51.2; H, 6.9; N, 9.3.

SEC (*ref PMMA*): Mw 2966 $g.mol^{-1}$; Đ: 1.02

N_3-[*bis*GMPA,G3]-$(NH_3^+Cl^-)_8$

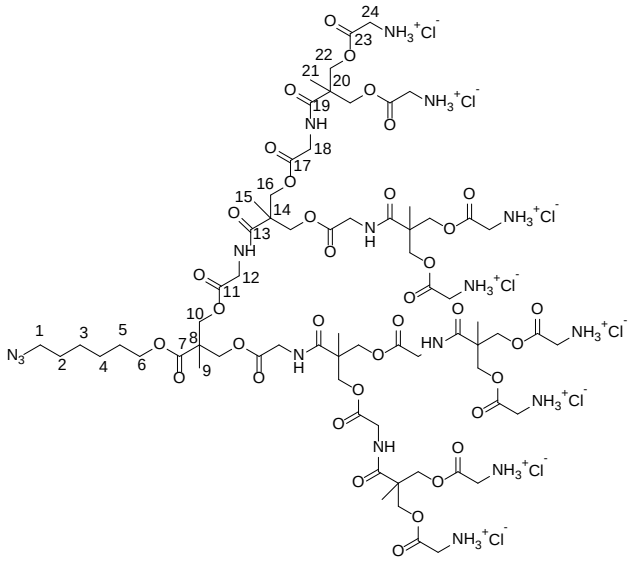

General procedure VI) N_3-[*bis*GMPA,G3]-$(NHBoc)_8$ (1.50 g, $5.86x10^{-1}$ mmol, 1.00 eq.); HCl 3M into ethyl acetate (10 mL); ethyl acetate (5 mL). The pure product was obtained as a white powder was obtained (1.12 g, 93 %).

^{1}H (400 MHz, CD_3OD) δ (ppm): 1.28 (s, 3H, H-9), 1.33 (s, 6H, H-15), 1.38 (s 12H, H-21), 1.43 (m, 4H, H-3 and H-4), 1.62 (m, 2H, H-2), 1.69 (m, 2H, H-5), 3.93 (s, 16H, H-24), 3.97 (s, 4H, H-12), 4.01 (s, 8H, H-18), 4.16 (t, J = 6.4 Hz, 2H, H-6), 4.32 (m, 12H, H-10 and H-16), 4.45 (ABq, 16H, H-22).
note: H-1 signal (~3.2 ppm) is overlapped with the CH_3 signal of CD_3OD but the correlation between H-1 and H-2 is observed in ^{1}H-^{1}H COSY and the correlation between H-1 and C-1 is observed in ^{1}H-^{13}C HSQC.

^{13}C (100 MHz, CD_3OD): δ 17.8 (C-21), 18.1 (C-9 and C-15), 26.6 (C-4), 27.4 (C-3), 29.4 (C-5), 29.8 (C-2), 41.2 (C-24), 42.2 (C-12 and C-18), 47.4 (C-14 and C-20), 47.7 (C-8), 52.4 (C-1), 66.5 (C-6), 67.2 (C-10), 67.8 (C-16), 68.5 (C-22), 168.3 (C-23), 170.8 (C-11), 171.1 (C-17), 174.1 (C-7), 175.0 (C-19), 175.2 (C-13).

MS (MADLI$^+$, DHB) *m/z (%)*: *1775.2 (100)* $[C_{69}H_{111}N_{17}O_{36},Na]^+$.

FTIR (ν_{max}/cm^{-1}, ATR): 3342 (N-H st), 2984-2928 (C-H and bs N-H$^+$), 2091 (N_3 st), 1755 (C=O st ester), 1659 (C=O st amide and N-H$^+$ δ), 1541 (N-H δ), 1475 (CH_2, CH_3 δ), 1406 (C-N st), 1236 (ν_{as} CO-O), 1171 (O-C-C st).

EA (%): *Found:* C, 39.7; H, 6.5; N, 11.5. *Calc. for* $C_{69}H_{119}Cl_8N_{17}O_{36}$: C, 40.5; H, 5.9; N, 11.6.

N_3-[*bis*GMAP,G4]-$(NHBoc)_{16}$

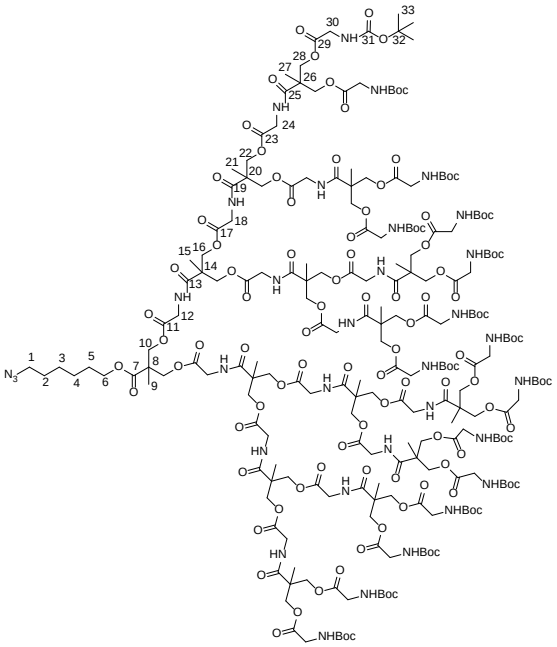

General procedure V) N_3 -[*bis*GMPA,G3]-$(NH_3^+,Cl^-)_8$ (1.02 g, 4.99x10^{-1} mmol, 1.00 eq.); *Bis*-GMPA(monomer)* (3.14 g, 6.92 mmol, 14.00 eq.); HOBt,nH2O (1.07 g, 6.92 mmol, 14.00 eq.); DMAP (878 mg, 7.19 mmol, 14.4 eq.); DCC (1.44 g, 6.92 mmol, 14.00 eq.); dry DMF (7 mL); dry DCM (63 mL) The crude product was dissolved in ethyl acetate (30 mL) and hexane (70 mL) was added slowly under agitation until the formation of a gel. This operation was repeated twice. Then, it was purified on silica gel (DCM : MeOH = ramp from 95:5 to 9:1) to obtain a white solid (2.29 g, 88 %).

^{1}H (400 MHz, $CDCl_3$) δ (ppm): [1.24-1.28] (m, 45H, H-9, H-15, H-21 and H-27) 1.45 (s, 148H, H-3, H-4 and H-33), 1.61 (m, 4H, H-2 and H-5), 3.27 (t, 2H, J = 7.2 Hz, H-1), 3.88 (m, 32H, H-30), 3.98 (m, 28H, H-12, H-18 and H-24), 4.11 (t, J = 6.4 Hz, 2H, H-6), [4.20-4.45] (m, 60H, H-10, H-16, H-22 and H-28), 5.55 (bs, -NHBoc), 7.38 (bs, -NHCO).

^{13}C (100 MHz, $CDCl_3$) δ (ppm): [17.7-18.0] (C-9, C-15, C-21 and C-27), 25.3 (C-4), 26.3 (C-3), 28.3 (C-5 and C-33), 28.3 (C-2), 41.3 (C-30), 42.3 (C-12, C-18 and C-24), [46.0-46.1] (C-8, C-14, C-20 and C-26), 51.3 (C-1), 65.3 (C-28), [66.3-66.5] (C-6, C-10, C-16 and C-22), 80.0 (C-32), 156.1 (C-31), 169.6 (C-29), [170.2-170.3] (C-11, C-17 and C-23), 172.6 (C-7), [172.9-173.2] (C-13, C-19 and C-25).

MS (MALDI$^+$, DCTB) *m/z (%)*: *5220.2 (100)* $[C_{221}H_{351}N_{33}O_{108},Na]^+$.

FTIR (ν_{max}/cm^{-1}, ATR): 3362 (N-H st), 2978-2930-2852 (C-H st), 2098 (N_3 st), 1749 (C=O st ester), 1695 (C=O st carbamate), 1668 (C=O st amide), 1520 (N-H δ), 1456 (CH_2, CH_3 δ), 1367 (C-N st), 1284 (CO-O st), 1155 (N-CO-O st).

EA (%): *Found:* C, 52.2; H, 7.1; N, 8.8. *Calc. for* $C_{221}H_{351}N_{33}O_{108}$: C, 51.1; H, 6.8; N, 8.9.

SEC (*ref PMMA*): Mw 4463 g.mol^{-1}; Đ: 1.04.

N_3-[*bis*GMPA,G4]-(NH_3^+,Cl^-)$_{16}$

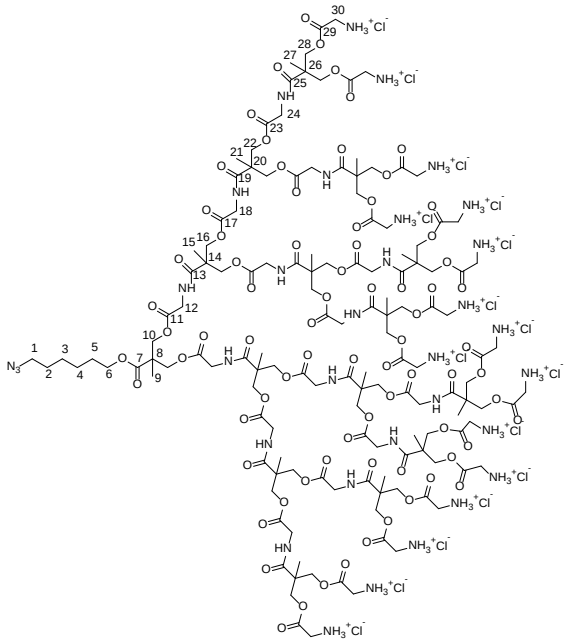

General procedure VI) N_3-[*bis*GMPA,G4]-$(NHBoc)_{16}$ (708 mg, 1.36x10^{-1} mmol, 1.00 eq.); HCl 3M into ethyl acetate (10 mL); ethyl acetate (5 mL). The pure product was obtained as a white powder (506 mg, 89 %).

^{1}H (400 MHz, CD_3OD) δ (ppm): 1.23 (s, 3H, H-9), 1.28 (s, 6H, H-15), 1.33 (s, 12H, H-21) 1.38 (s, 24H, H-27), 1.43 (m, 4H, H-3 and H-4), 1.62 (m, 2H, H-2), 1.69 (m, 2H, H-5), 3.95 (s, 32H, H-30), 4.01 (m, 28H, H-12, H-18 and H-24), 4.16 (t, J = 6.4 Hz, 2H, H-6), 4.33 (m, 28H, H-10, H-16 and H-22), 4.46 (m, 32H, H-28), 8.35 (bs, -NHCO).
note: H-1 signal (~3.2 ppm) is overlapped with the CH_3 signal of CD_3OD but the correlation between H-1 and H-2 is observed in ^{1}H-^{1}H COSY and the correlation between H-1 and C-1 is observed in ^{1}H-^{13}C HSQC.

^{13}C (100 MHz, CD_3OD) δ (ppm): [17-9-18.2] (C-9, C-15, C-21 and C-27), 26.6 (C-4), 27.4 (C-3), 29.4 (C-5), 29.8 (C-2), 41.2 (C-30), 42.2 (C-12, C-18 and C-24), [47.3-47.7] (C-8, C-14, C-20 and C-26), 52.4 (C-1), 66.4 (C-6), [67.2-67.9] (C-10, C-16 and C-22), 68.5 (C-28), 168.3 (C-29), [170.8-171.3] (C-11, C-17 and C-23), 174.2 (C-7), [174.9-175.3] (C-13, C-19 and C-25).

FTIR (ν_{max}/cm^{-1}, ATR): 3318 (N-H st), 2986-2883-2615 (C-H and bs N-H^+), 2102 (N_3 st), 1744 (C=O ester st), 1655 (C=O st amide and N-H^+ δ), 1539 (N-H st), 1479 (CH_2, CH_3 δ), 1410 (C-N st), 1230 (CO-O st), 1176 (O-C-C st).

EA (%): *Found:* C, 39.4; H, 6.5; N, 10.7. *Calc. for* $C_{141}H_{239}Cl_{16}N_{33}O_{76}$: C, 40.5; H, 5.8; N, 11.1.

7.1.3- Amphiphilic dendritic derivatives for camptothecin delivery

7.1.3.1- Amphiphilic Janus dendrimers

General procedure VII): copper(I) azide-alkyne cyloaddition reaction (CuAAC) for the synthesis of the Janus dendrimers

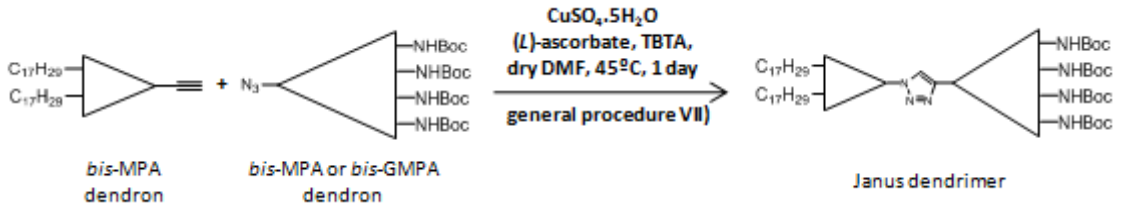

Pre-hydrophilic azido-dendron (1.00 mol) and lipophilic alkyno-dendron (1.20 or 1.50 mol) were dissolved into dimethylformamide (7 mL) in a Schlenk flask. 3 cycles vacuum-argon were made to remove O_2. The reaction mixture was allowed to stir under argon atmosphere at 45ºC. $CuSO_4 5.H_2O$ (0.1 mol), L-ascorbate (0.2 mol) and TBTA (0.1 mol) were dissolved into DMF (3 mL) in a second Schlenk flask. 3 cycles vacuum-Argon were made in order to remove O_2 and the copper solution was stirred at 45ºC during 15 min. Then, it was added through a cannula to the previous azide-alkyne reaction mixture. The reaction mixture was stirred at 45ºC during 2 days. Then, brine was added (100 mL) and the product was extracted 2 times with ethyl acetate (2 x 70 mL). The organic phase was washed three times with brine (3 x 100 mL), once with a KCN aqueous solution (15 mg into 100 mL of water) and twice with brine (2 x 100 mL), dried over anhydrous $MgSO_4$ and the solvent was evaporated under reduce pressure. Finally, the crude product was purified on silica gel (refer to the product to see the solvents that were employed and their proportions.

The *t*-Boc protective groups were removed according to the ***general procedure VI)*** (see page 321).

(NHBoc)$_4$[*bis*MPA,G2]-[*bis*MPA,G1](C17)$_2$

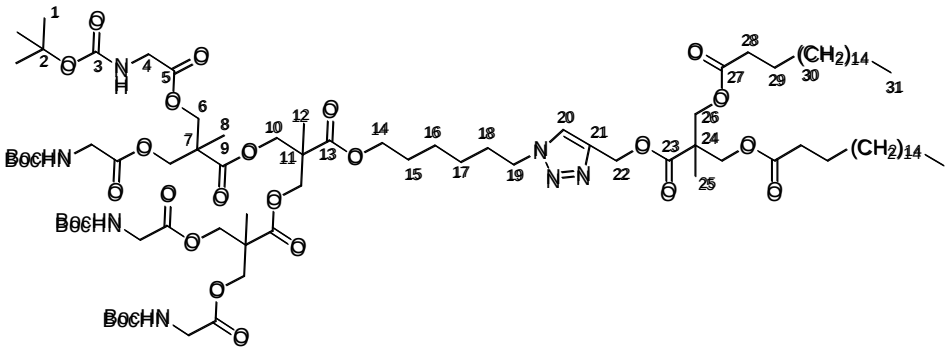

General procedure VII) N_3-[*bis*MPA,G2]-$(NHBoc)_4$ (1,531 g, 1.36 mmol, 1.00 eq.); ≡-[*bis*MPA,G1]-$(C17)_2$ (1,439 g, 2.04 mmol, 1.50 eq.); $CuSO_4$, $5H_2O$ (34 mg, 0.12 mmol, 0.10 eq), (*L*)-ascorbate (46 mg, 0.23 mmol, 0.20 eq.), TBTA (61mg, 0.12 mmol, 0,10 eq.). The crude product was purified on silica gel (hexane : ethyl acetate = ramp from 7:3 to 5:5) to give a white solid (1.896 g, 76 %).

^{1}H (300 MHz, $CDCl_3$) δ (ppm): 0.89 (t, J = 6Hz, 6H, H-31), 1.27 (m, 70H, H-8, H-12, H-17, H-25 and H-30), 1.43 (m, 2H, H-16), 1.46 (s, 36H, H-1), 1.58 (m, 4H, H-29), 1.67 (m, 2H, H-15), 1.96 (m, 2H, H-18), 2.27 (t, J = 7.8 Hz, 4H, H-28), 3.91 (d, J = 5.7 Hz, 8H, H-4), 4.13 (t, J = 6.6 Hz, 2H, H-14), 4.25 (m, 16H, H-6, H-10 and H-26), 4.38 (t, J = 7.2 Hz, 2H, H-19), 5.24 (s, 2H, H-22), 5.28 (bs, -NHBoc), 7.63 (s, 1H, H-20).

^{13}C (100 MHz, $CDCl_3$) δ (ppm): 14.1 (C-31), [17.7-17.9] (C-8, C-12 and C-25), 22.7 (C-30), 24.9 (C-29), 25.3 (C-17), 26.1 (C-16), 28.3 (C-1 and C-15), [29.1-29.7] (C-30), 30.1 (C-18), 31.9 (C-30), 34.1 (C-28), 42.3 (C-4), 46.3 (C-24), 46.4 (C-11), 46.6 (C-7), 50.2 (C-19), 58.4 (C-22), 65.0 (C-26), 65.4 (C-10), 65.6 (C-14), 65.7 (C-6), 80.0 (C-2), 123.7 (C-20), 142.4 (C-21), 155.8 (C-3), 170.1 (C-5), [172.2-172.8] (C-9, C-13 and C-23), 173.3 (C-27).

MS (MALDI$^+$) *m/z (%)*: *1848.1 (100)* $[C_{93}H_{161}N_7O_{28},Na]^+$.

FTIR (ν_{max}/cm^{-1}, ATR): 3393 (N-H st), 2978-2918-2851 (C-H st), 1738 (C=O st ester), 1724 (C=O st carbamate), 1514 (N-H δ), 1468 (CH_2-, CH_3 δ), 1367 (C-N st), 1250 (CO-O st as), 1155 (N-CO-O st), 1130 (O-C-C st).

EA (%): *Found* C. 60.92; H. 8.43; N. 5.34. *Calcd for* $C_{93}H_{161}N_7O_{28}$: C. 61.20; H. 8.89; N. 5.37.

SEC (*ref PMMA*): Mw 2702 g.mol^{-1}; Đ: 1.02.

$(NHBoc)_8$[*bis*MPA,G3]-[*bis*MPA,G1](C17)$_2$.

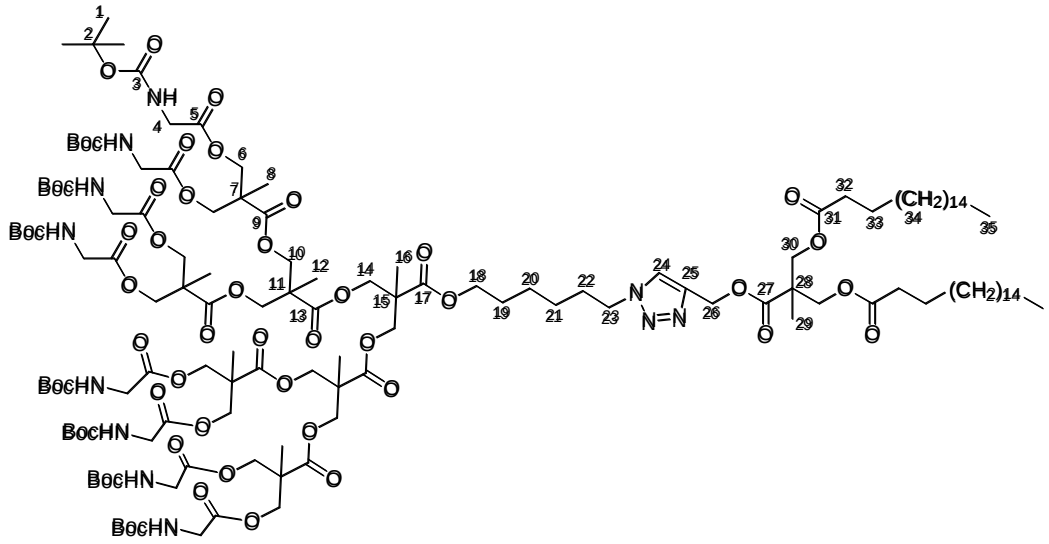

General procedure VII) N_3-[3G]-$(glyBoc)_8$ (1.200 g, 5.67x10^{-1} mmol, 1.00 eq.); ≡-[1G]-(C17) (600 mg, 8.51x10^{-1} mmol, 1.00 eq.); $CuSO_4$, $5H_2O$ (16.7 mg, 5.67x10^{-2} mmol, 0.10 eq); (*L*)-ascorbate (22.5 mg, 1.13x10^{-1} mmol, 0.20 eq.); TBTA (30.1 mg, 5.67x10^{-2} mmol, 0.10 eq.); dry DMF (10 mL). The crude product was purified on silica gel (hexane : ethyl acetate = ramp from 6:4 to 4:6) to give a white solid (1.344 g, 81 %).

^{1}H (400 MHz, $CDCl_3$) δ (ppm):0.87 (t, J = 6Hz, 6H, H-35), 1.27 (m, 80H, H-8, H-12, H-16, H-29 and H-34), 1.43 (m, 76H, H-1, H-20 and H-21), 1.56 (m, 4H, H-33), 1.69 (m, 2H, H-19), 1.96 (m, 2H, H-22), 2.25 (t, J = 7.8 Hz, 4H, H-32), 3.91 (d, J = 5.7 Hz, 16H, H-4), 4.13 (t, J = 6.6 Hz, 2H, H-18), 4.25 (m, 32H, H-6, H-10, H-14 and H-30), 4.36 (t, J = 7.2 Hz, 2H, H-23), 5.25 (s, 2H, H-26), 5.27 (bs, -NHBoc), 7.62 (s, 1H, H-24).

^{13}C (100 MHz, $CDCl_3$) δ (ppm): 14.1 (C-35), [17.5 - 17.9] (C-8, C-12, C-16 and C-29), 22.6 (C-34), 24.8 (C-33), 25.3 (C-21), 26.1 (C-20), 28.3 (C-1 and C-19), [29.1-29.7] (C-34), 30.1 (C-22), 31.9 (C-34), 31.9 (C-32), 42.2 (C-4), [46.3-46.7] (C-7, C-11, C-15 and C-28), 50.3 (C-23), 58.3 (C-26), 65.0 (C-30), 65.4 (C-10 and C-14), 65.6 (C-6), 66.1 (C-18), 79.9 (C-2), 123.8 (C-24), 142.2 (C-25), 155.9 (C-3), 170.1 (C-5), [171.5-172.8] (C-9, C-13, C-17 and C-27), 173.2 (C-31).

MS (MALDI$^+$) *m/z (%)*: *2939.1 (100)* $[C_{141}H_{237}N_{11}O_{52},Na]^+$.

FTIR (ν_{max}/cm^{-1}, ATR): 3373 (N-H st), 2980-2926-2854 (C-H st), 1738 (C=O st ester), 1720 (C=O st carbamate), 1516 (N-H δ), 1464 (CH_2, CH_3 δ), 1367 (C-N st), 1232 (CO-O st as), 1151 (N-CO-O st), 1132 (O-C-C st).

EA (%): *Found* C. 57.90; H. 8.02; N. 5.27; *Calcd for* $C_{141}H_{237}N_{11}O_{52}$: C. 58.03; H. 8.19; N. 5.28.

SEC (*ref PMMA*): Mw 3653 g.mol^{-1}; Đ: 1.02.

(NHBoc)$_4$[*bis*MPA,G2]-[*bis*MPA,G2](C17)$_4$

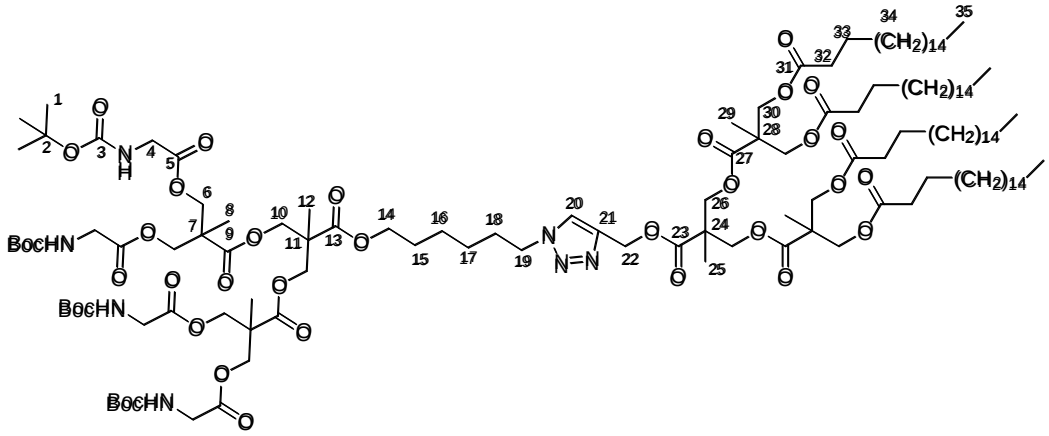

General procedure VII) N_3-[*bis*MPA,G2]-(NHBoc)$_4$ (1.027 g, 9.24x10^{-1} mmol, 1.00 eq.); ≡-[*bis*MPA,G2]-(C17)$_4$ (1.630 g, 1.10 mmol, 1.20 eq.); $CuSO_4$,5H_2O (27 mg, 9.24x10^{-2} mmol, 0.10 eq); (L)-ascorbate (37 mg, 1.85x10^{-1} mmol, 0.20 eq.) and TBTA (49 mg, 9.24x10^{-2} mmol, 0.10 eq.) into dry DMF (10 mL). The crude product was purified on silica gel (hexane : ethyl acetate; ramp from 8:2 to 6:4) to give a white solid (1.641 g, 69 %).

^{1}H ($CDCl_3$, 300 MHz) δ (ppm): 0.88 (t, J = 6.3 Hz, 12H, H-35), 1.24 (m, 130H, H-8, H-12, H-25, H-29 and H-34), 1.39 (m, 4H, H-16 and H-17), 1.44 (s, 36H, H-1), 1.57 (m, 8H, H-33), 1.65 (m, 2H, H-15), 1.93 (m, 2H, H-18), 2.28 (t, J = 7.5 Hz, 8H, H-32), 3.89 (d, J = 5.7 Hz, 8H, H-4), 4.07 – 4.31 (m, 26H, H-6, H-10, H-14, H-26 and H-30), 4.37 (t, J = 7.2 Hz, 2H, H-19), 5.24 (s, 2H, H-22), 5.25 (bs, -NHBoc), 7.69 (s, 1H, H-20).

^{13}C ($CDCl_3$, 100 MHz) δ (ppm): 14.1 (C-35), 17.5 (C-29), [17.7-17.9] (C-8, C-12 and C-25), 22.7 (C-34), 24.8 (C-33), 25.2 (C-17), 26.1 (C-16), 28.3 (C-1 and C-15), [29.1-29.7] (C-34), 30.1 (C-18), 31.9 (C-34), 34.0 (C-32), 42.3 (C-4), 46.4 (C-28), 46.4 (C-7), 46.6 (C-24), 46.6 (C-11), 50.2 (C-19), 58.4 (C-22), [64.9 – 65.7] (C-6, C-10, C-14, C-26 and C-30), 79.9 (C-2), 124.0 (C-20), 142.0 (C-21), 155.8 (C-3), [170.0-172.2] (C-5, C-9, C-13, C-23 and C-27), 173.2 (C-31).

MS (MALDI$^+$) *m/z (%)*: *2612.8 (100)* [$C_{139}H_{245}N_7O_{36}$,Na]$^+$.

FTIR (ν_{max}/cm^{-1}, ATR): 3404 (N-H st), 2960-2918-2851 (C-H st), 1740 (C=O st ester), 1707 (C=O st carbamate), 1524 (N-H δ), 1470 (CH_2, -CH_3 δ), 1367 (C-N st), 1252 (CO-O st as), 1159 (N-CO-O st), 1140 (O-C-C st).

EA: *Found* C, 64.54; H, 9.54; N, 3.78; *Calcd for* $C_{139}H_{245}N_7O_{36}$: C. 64.45; H. 9.53; N. 3.78.

SEC (*ref PMMA*): Mw 3743 g.mol^{-1}; Đ: 1.02.

$(NHBoc)_8$[*bis*MPA,G3]-[*bis*MPA,G2](C17)$_4$

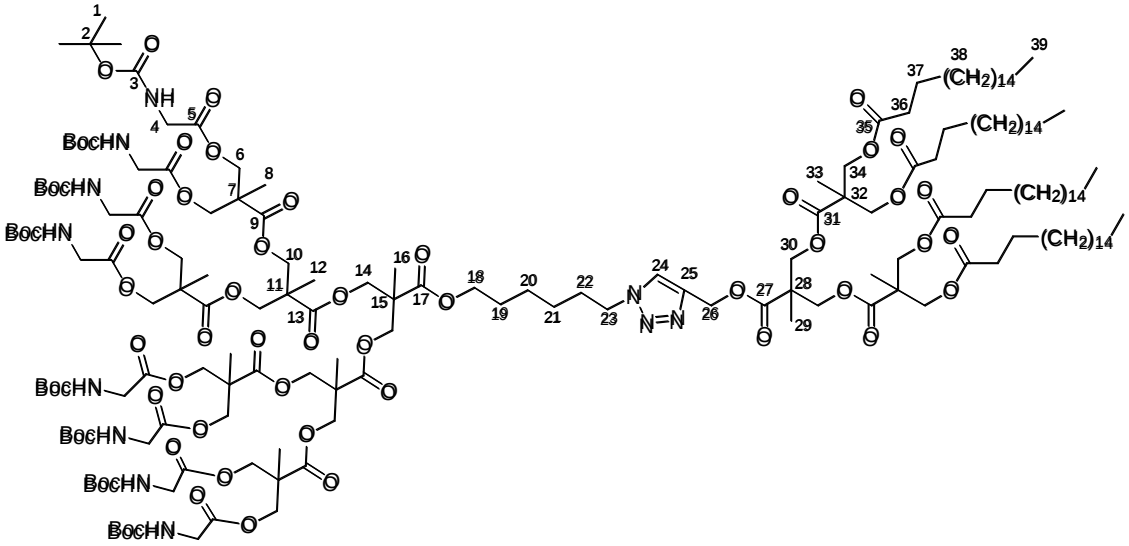

General procedure VII) N_3-[*bis*MPA,G3]-$(NHBoc)_8$ (960 mg, 0.45 mmol, 1.00 eq.); ≡-[*bis*MPA,G2]-(C17) (1000 mg, 0.68 mmol, 1.50 eq.); $CuSO_4$,$5H_2O$ (13.36 mg, $4.5x10^{-1}$ mmol, 0.10 eq.); (*L*)-ascorbate (17.97 mg, $9.0x10^{-1}$ mmol, 0.20 eq.) and TBTA (24.05 mg, $4.5x10^{-1}$ mmol,0.10 eq.) into DMF (10 mL). The crude product was purified on silica gel (hexane : ethyl acetate = ramp from 8:2 to 5:5) to give a white solid (1.604 g, 92 %).

^{1}H (300 MHz, $CDCl_3$) δ (ppm): 0.87 (t, J = 8.0 Hz, 12H, H-39), 1.24 (m, 142H, H-8, H-12, H-16, H-29, H-33 and H-38), 1.43 (m, 76H, H-1, H-20 and H-21), 1.57 (m, 8H, H-37), 1.67 (m, 2H, H-19), 1.93 (m, 2H, H-22), 2.28 (t, J = 6.0 Hz, 8H, H-36), 3.88 (d, J = 4.0 Hz, 16H, H-4), [4.13-4.25] (m, 42H, H-6, H-10, H-14, H-18, H-30 and H-34), 4.36 (t, J = 6.9 Hz, 2H, H-23), 5.23 (s, 2H, H-26), 5.36 (bs, -NHBoc), 7.68 (s, 1H, H-24).

^{13}C (75 MHz, $CDCl_3$) δ (ppm): 14.1 (C-39), [17.5-17.8] (C-8, C-12, C-16, C-29 and C-33), 22.6 (C-38), 24.8 (C-37), 25.3 (C-21), 26.1 (C-20), 28.3 (C-1 and C-22), [29.1 - 29.7] (C-38), 30.1 (C-19), 31.9 (C-38), 34.0 (C-36), 42.2 (C-4), [46.3-46.7] (C-7, C-11, C-15, C-28 and C-32), 50.2 (C-23), 58.4 (C-26), [64.9 - 66.0] (C-6, C-10, C-14, C-18, C-30 and C-34), 79.9 (C-2), 124.1 (C-24), 141.9 (C-25), 155.9 (C-3), [170.1-172.1] (C-5, C-9, C-13, C-17, C-27 and C-31), 173.2 (C-35).

MS (MALDI$^+$) *m/z (%)*: *3706.5 (100)* $[C_{187}H_{321}N_{11}O_{60},Na]^+$.

FTIR (ν_{max}/cm^{-1}, ATR): 3391 (N-H st), 2978-2918-2849 (C-H st), 1740 (C=O st ester), 1724 (C=O st carbamate), 1516 (N-H δ), 1468 (δ-CH_2-, δ_{as} -CH_3), 1367 (C-N st), 1250 (CO-O st as), 1155 (N-CO-O st), 1142 (O-C-C st).

EA (%): *Found* C, 60.95; H, 8.64; N, 4.17; *Calcd for* $C_{187}H_{321}N_{11}O_{60}$: C, 60.97; H, 8.78; N, 4.18.

SEC (*ref PMMA*): Mw 4590 g.mol^{-1}; Đ: 1.02.

(NHBoc)$_4$[*bis*GMPA,G2]-[*bis*MPA,G1](C17)$_2$

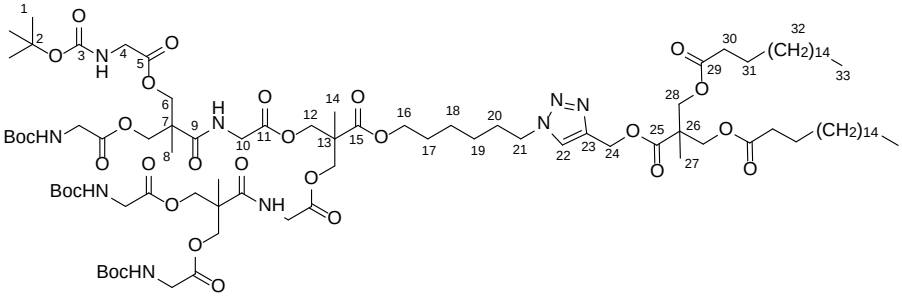

General procedure VII) N_3-[*bis*GMPA,G2]-$(NHBoc)_4$ (1000 mg, $8.10x10^{-1}$ mmol, 1.00 eq.); ≡-[*bis*MPA,G1]-$(C17)_2$ (686 mg, $9.72x10^{-1}$ mmol, 1.20 eq.), $CuSO_4$,$5H_2O$ (20.23 mg, $8.10x10^{-2}$ mmol, 0.10 eq.); (*L*)-ascorbate (32.11 mg, $1.62x10^{-2}$ mmol, 0.20 eq.) and TBTA (42.97 mg, $8.10x10^{-2}$ mmol, 0.10 eq.) into dry DMF (10 mL). The crude product was purified on silica gel (DCM : MeOH = ramp from 98:2 to 95:5) to give a yellow solid (1193 mg, 76 %).

^{1}H (400 MHz, $CDCl_3$) δ (ppm): 0.86 (t, J = 6.8Hz, 6H, H-33), 1.20 (s, 3H, H-27), 1.23 (m, 59H, H-14 and H-32), 1.27 (s, 6H, H-8), 1.35 (m, 4H, H-18 and H-19), 1.42 (s, 36H, H-1), 1.54 (m, 4H, H-31), 1.63 (m, 2H, H-17), 1.92 (m, 2H, H-20), 2.23 (t, J = 7.6 Hz, 4H, H-30), 3.91 (d, J 0 5.6 Hz, 8H, H-4), 3.96 (d, J = 4.8 Hz, 4H, H-10), 4.11 (t, J = 6.4 Hz, 2H, H-16), 4.19 (ABq, J = 11.2 Hz, $\Delta\nu_{AB}$ = 18.5 Hz, 4H, H-28), [4.24-4.39] (m, 14H, H-4, H-12 and H-21), 5.23 (s, 2H, H-24), 5.27 (bs, -NHBoc), 7.10 (bs, -NHCO), 7.59 (s, 1H, H-22).

^{13}C (100 MHz, $CDCl_3$) δ (ppm): 14.1 (C-33), [17.7-17.9] (C-8, C-14 and C-27), 22.7 (C-32), 24.9 (C-31), 25.3 (C-18), 26.1 (C-19), 28.3 (C-1 and C-17), [29.1-29.7] (C-32), 30.1 (C-20), 31.9 (C-32), 34.1 (C-30), 41.1 (C-10), 42.4 (C-4), [46.1-46.3] (C-7, C-13 and C-26), 50.2 (C-21), 58.4 (C-24), [65.0-65,7] (C-6, C-12, C-16 and C-28), 80.1 (C-2), 123.7 (C-22), 142.4 (C-23), 155.9 (C-3), 170.3 (C-5), [172.5-173.2] (C-9, C-11, C-15, C-25 and C-29).

MS ($MALDI^+$) *m/z (%)*: *1962.3 (100)* $[C_{97}H_{167}N_9O_{30},Na]^+$.

FTIR (ν_{max}/cm^{-1}, ATR): 3366 (N-H st), 2980-2916-2851 (C-H st), 1744 (C=O st ester), 1717 (C=O st carbamate), 1664 (C=O st amide), 1528 (N-H δ), 1468 (CH_2, CH_3 δ), 1367 (C-N st), 1254 (CO-O st), 1157 (N-CO-O st).

EA: *Found* C. 61.3; H. 9.4; N. 6.8; *Calcd for* $C_{97}H_{167}N_9O_{30}$: C. 60.1; H. 8.7; N. 6.5.

SEC (*ref PMMA*): Mw 2718 $g.mol^{-1}$; Đ: 1.02.

$(NHBoc)_8$[*bis*GMPA,G3]-[*bis*MPA,G1]$(C17)_2$

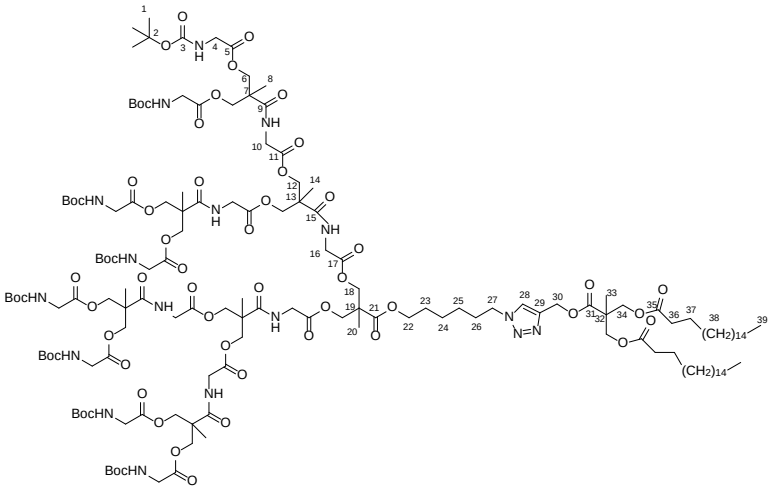

General procedure VII) N_3-[*bis*GMPA,G3]-$(NHBoc)_8$ (600 mg, $2.35x10^{-1}$ mmol, 1.00 eq.); ≡-[*bis*MPA,G1]-$(C17)_2$ (199 mg, $2.82x10^{-1}$ mmol, 1.20 eq.), $CuSO_4,5H_2O$ (6.92 mg, $2.35x10^{-2}$ mmol, 0.10 eq.); (*L*)-ascorbate (9.30 mg, $4.69x10^{-2}$ mmol, 0.20 eq.) and TBTA (12.45 mg, $2.35x10^{-2}$ mmol, 0.10 eq.) into dry DMF (10 mL). The crude product was purified on silica gel (DCM : MeOH = ramp from 95:5 to 90:1) to give a yellow solid (646 mg, 84 %).

^{1}H (400 MHz, CD_2Cl_2) δ (ppm): 0.87 (t, J = 8.0 Hz, 6H, H-39), 1.21 (s, 3H, H-33), 1.26 (m, 65H, H-14, H-20 and H-38), 1.28 (s, 12H, H-8), 1.37 (m, 4-H, H-24 and H-25), 1.42 (s, 72H, H-1), 1.54 (m, 8H, H-37), 1.64 (m, 2H, H-22), 1.91 (m, 2H, H-27), 2.24 (t, J = 7.6 Hz, 4H, H-36), 3.88 (d, J = 6.0 Hz, 16H, H-4), 3.95 (d, J = 5.6 Hz, 4H, H-16), 4.00 (d, J= 5.2 Hz, 8H, H-10), 4.11 (t, J = 6.4 Hz, 2H, H-22), 4.18 (ABq, J = 10.8 Hz, $\Delta\nu_{AB}$ = 19.7 Hz, 4H, H-34). [4.21-4.37] (m, 30H, H-6, H-12, H-18 and H-22), 5.22 (s, 2H, H-30), 5.46 (bs, -NHBoc), 7.10 (bs, -NHCO), 7.62 (s, 1H, H-28).

^{13}C (100 MHz, CD_2Cl_2) δ (ppm): 14.5 (C-39), [18.1-18.7] (C-8, C-14, C-20 and C-33), 23.3 (C-38), 25.4 (C-37), 25.8 (C-24), 26.6 (C-25), 28.6 (C-1), 28.8 (C-23), [29.7-30.3] (C-38), 30.6 (C-26), 32.5 (C-38), 34.5 (C-36), [41.8-41.9] (C-10 and C-16), 42.9 (C-4), [46.6-46.8] (C-7, C-13 and C-19), 47.7 (C-32), 50.8 (C-1), 58.9 (C-30), [65.3-67.1] (C-6, C-12, C-18, C-22 and C-34), 80.3 (C-2), 124.3 (C-28), 142.9 (C-29), 156.6 (C-3), [170.1-170.2] (C-11 and C-17),170.8 (C-5), 173.1 (C-21), [173-2-173.6] (C-9, C.15 and C-35).

FTIR (ν_{max}/cm^{-1}, ATR): 3360 (N-H st), 2980-2928-2854 (C-H st), 1747 (C=O st ester), 1713 (C=O st carbamate), 1670 (C=O st amide), 1518 (N-H δ), 1466 (CH_2, CH_3 δ), 1367 (C-N st), 1250 (CO-O st), 1157 (N-CO-O st).

EA: *Found* C. 57.0; H. 8.5; N. 7.7; *Calcd for* $C_{153}H_{255}N_{17}O_{58}$: C. 56.4; H. 7.9; N. 7.3.

SEC (*ref PMMA*): Mw 4056 $g.mol^{-1}$; Đ: 1.02

$(NHBoc)_8$[*bis*GMPA,G3]-[*bis*MPA,G2]$(C17)_4$

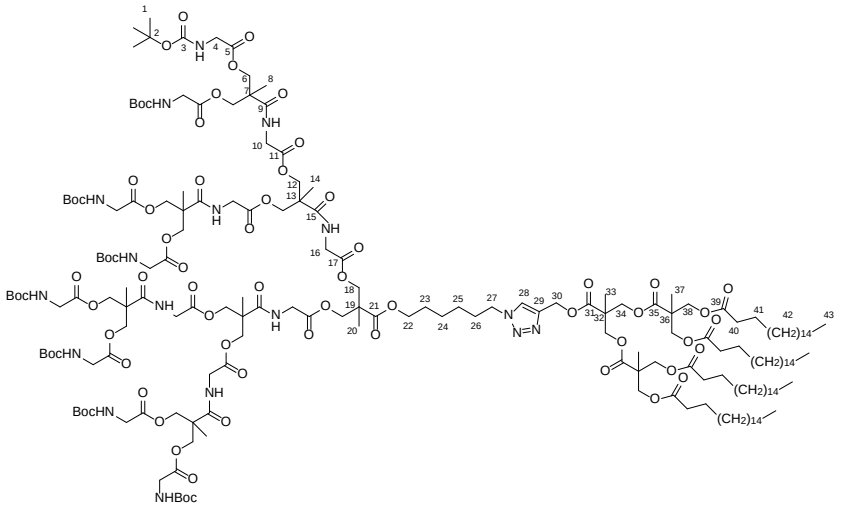

General procedure VII) N_3-[*bis*GMPA,G3]-$(NHBoc)_8$ (1000 mg, $3.91x10^{-1}$ mmol, 1.00 eq.); ≡-[*bis*MPA,G2]-$(C17)_4$ (690 mg, $4.69x10^{-1}$ mmol, 1.20 eq.), $CuSO_4$,$5H_2O$ (11.53 mg, $3.91x10^{-2}$ mmol, 0.10 eq.); (*L*)-ascorbate (15.50 mg, $7.82x10^{-2}$ mmol, 0.20 eq.) and TBTA (20.75 mg, $3.91x10^{-2}$ mmol, 0.10 eq.) into dry DMF (10 mL). The crude product was purified on silica gel (DCM : MeOH = ramp from 98:2 to 95:5) to give a yellow solid (1070 mg, 68 %).

^{1}H ($CDCl_3$, 400 MHz) δ (ppm): 0.86 (t, J = 6.4 Hz, 12H, H-43), [1.16-1.26] (m, 130H, H-14, H-20, H-33, H-37 and H-42), 1.27 (s, 12H, H-8), 1.37 (m, 4H, H-24 and H-25), 1.44 (s, 72H, H-1), 1.56 (m, 8H, H-41), 1.63 (m, 2H, H-23), 1.92 (m, 2H, H-26), 2.27 (t, J = 7.6 Hz, 8H, H-40), 3.88 (d, J = 5.6 Hz, 16H, H-4), 3.94 (d, J = 5.2 Hz, 4H, H-16), 3.98 (d, J = 5.2 Hz, 8H, H-10), 4.11 (t, J = 6.0 Hz, 2H, H-22), 4.12 (ABq, J = 11.2 Hz, $\Delta\nu_{AB}$ = 9.8 Hz, 8H, H-38), [4.19-4.37] (m, 34H, H-6, H-12, H-18, H-27 and H-34), 5.22 (s, 2H, H-30), 5.25 (bs, -NHBoc), 7.19 (bs, -NHCO), 7.67 (s, 1H, H-28).

^{13}C ($CDCl_3$, 100 MHz) δ (ppm): 14.1 (C-43), [17.7 -18.3] (C-8, C-14, C-20, C-33 and C-37), 22.7 (C-42), 24.8 (C-41), 25.2 (C-24), 26.0 (C-25), 28.3 (C-1 and C-23), [29.1-29.7] (C-42), 30.1 (C-28), 31.9 (C-42), 34.0 (C-40), [41.2-41.3] (C-10 and C-16), 42.3 (C-4), [46.0-46.6] (C-7, C-13, C-19, C-32 and C-36), 50.1 (C-27), 58.4 (C-30), [64.9-66.7] (C-6, C-12, C-18, C-22, C-34 and C-38), 80.0 (C-2), 124.1 (C-28), 141.9 (C-29), 156.0 (C-3), [169.5-173.1] (C-5, C-9, C-11, C-15, C-17, C-21, C-31, C-35 and C-39).

MS (MALDI$^+$) *m/z (%)*: *4046-4067 (100)* $[C_{199}H_{339}N_{17}O_{66},Na]^+$.

FTIR (ν_{max}/cm^{-1}, ATR): 3362 (N-H st), 2976-2918-2851 (C-H st), 1744 (C=O st ester), 1717 (C=O st carbamate), 1663 (C=O st amide), 1526 (N-H δ), 1470 (CH_2, CH_3 δ), 1367 (C-N st), 1252 (CO-O st), 1159 (N-CO-O st).

EA: *Found* C. 60.1; H. 8.9; N. 6.2; *Calcd for* $C_{199}H_{339}N_{17}O_{66}$: C. 59.4; H. 8.5; N. 5.9.

SEC (*ref PMMA*): Mw 4952 $g.mol^{-1}$; Đ: 1.02.

$(NH_3^+Cl^-)_4$[*bis*MPA,G2]-[*bis*MPA,G1]-$(C17)_2$

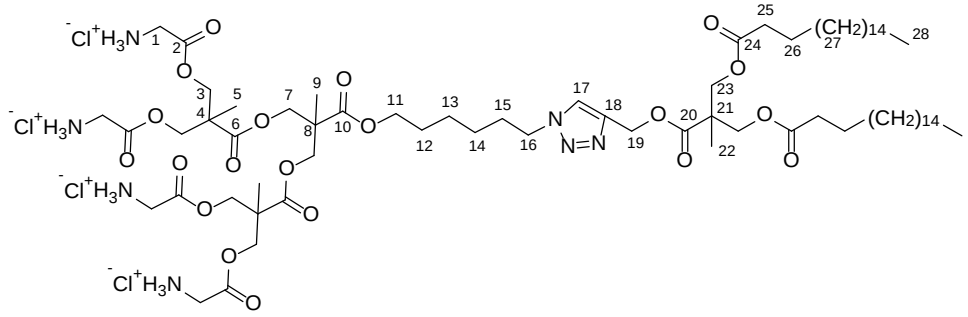

General procedure VI) $(NHBoc)_4$[*bis*MPA,G2]-[*bis*MPA,G1]-$(C17)_2$ (500 mg, 0.27 mmol, 1 eq.) and HCl 3M into ethyl acetate (20 mL) into ethyl acetate (5 mL). The product was obtained as a white solid (430 mg, 99 %).

^{1}H NMR (400 MHz, CD_3OD) δ (ppm): 0.90 (t, J = 6.4Hz, 6H, H-28), 1.24 (s, 3H, H-22), 1.29 (m, 59H, H-9 and H-27), 1.31 (s, 6H, H-5), 1.46 (m, 4H, H-13 and H-14), 1.56 (m, 4H, H-26), 1.69 (m, 2H, H-12), 1.94 (m, 2H, H-15), 2.26 (t, J = 7.2Hz, 4H, H-25), 3.94 (s, 8H, H-1), 4.16 (t, J = 6.4 Hz, 2H, H-11), 4.22 (ABq, J = 10.8 Hz, $\Delta\nu_{AB}$ = 26.0 Hz, 4H, H-23), 4.32 (ABq, J = 11.2 Hz, $\Delta\nu_{AB}$ = 17 Hz, 4H, H-7), 4.44 (m, 10H, H-16 and H-3), 5.25 (s, 2H, H-19), 8.06 (s, 1H, H-17).

^{13}C NMR (75 MHz, $CDCl_3$) δ (ppm): 14.1 (C-28), [17.7-17-9] (C-5, C-9 and C-22), 22.7 (C-17), 24.9 (C-26), 25.3 (C-13), 26.1 (C-14), 28.3 (C-12), [29.1-29.7] (C-27), 30.1 (C-15), 31.9 (C-27), 34.1 (C-1 and C-25), [46.0-46.3] (C-4, C-8 and C-21), 50.3 (C-16), 58.4 (C-19), [64.7-65.5] (C-3, C-7, C-11 and C-23), 123.7 (C-17), 142.3 (C-18), 167.6 (C-2), [172.0-173.6] (C-6, C-10, C-20), 173.3 (C-24).

MS (MALDI$^+$) *m/z (%)*: *1447.1 (100)* $[C_{73}H_{129}N_7O_{20},Na]^+$; *1425.1 (16)* $[C_{73}H_{129}N_7O_{20},H]^+$.

FTIR (ν_{max}/cm^{-1}, ATR): 3000-2600 (bs N-H^+ st), 2959-2918-2851 (C-H st), 1736 (C=O st ester), 1589 (N-H^+ δ), 1468 (CH_2, CH_3 δ), 1379 (C-N st), 1236 (CO-O st as), 1134 (O-C-C st).

pH (1 mg·mL^{-1} in distilled water): 3.54.

$(NH_3^+Cl^-)_8$[*bis*MPA,G3]-[*bis*MPA,G1](C17)$_2$

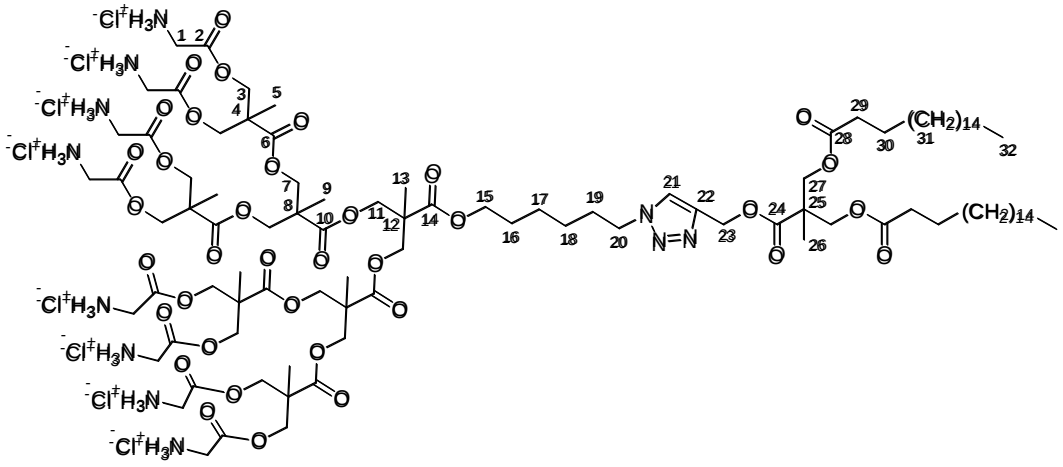

General procedure VI) $(NHBoc)_8$[*bis*MPA,G3]-[*bis*MPA,G1]$(C17)_2$ (1000 mg, 0.27 mmol, 1.00 eq.) and HCl 3M into ethyl acetate (5 mL) into ethyl acetate (3 mL) The product was obtained as a white solid (737 mg, quantitative yield).

^{1}H (400 MHz, CD_3OD) δ (ppm): 0.90 (t, J = 6.4Hz, 6H, H-32), 1.24 (s, 3H, H-26), 1.29 (m, 65H, H-9, H-13 and H-31), 1.33 (s, 12H, H-5), 1.45 (m, 4H, H-17 and H-18), 1.56 (m, 4H, H-30), 1.70 (m, 2H, H-16), 1.95 (m, 2H, H-19), 2.27 (t, J = 7.2Hz, 4H, H-29), 3.96 (s, 16H, H-1), 4.16 (t, J = 6.8 Hz, 2H, H-15), 4.22 (ABq, J = 11.2 Hz, $\Delta\nu_{AB}$ = 28.7 Hz, 4H, H-27), 4.33 (m, 12H, H-7 and H-11), 4.45 (m, 18H, H-3 and H-20), 5.26 (s, 2H, H-23), 8.08 (s, 1H, H-21).

^{13}C (100 MHz, CD_3OD) δ (ppm): 14.1 (C-32), [18.1-18.2] (C-5, C-9, C-13 and C-26), 23.7 (C-31), 26.0 (C-30), 26.5 (C-17), 27.1 (C-18), 28.3 (C-16), [29.5-31.2] (C-31), 33.1 (C-19), 34.8 (C-29), 41.1 (C-1), [47.5-48.1] (C-4, C-8, C-12 and C-25), 51.3 (C-20), 58.9 (C-23), [65.9-67.7] (C-7, C-11, C-15 and C-27), 67.6 (C-3), 126.2 (C-21), 143.6 (C-22), 168.3 (C-2), [173.2-174.0] (C-6, C-10, C-14 and C-24), 174.6 (C-28).

MS ($MALDI^+$) *m/z (%)*: *2140.1 (100)* $[C_{101}H_{173}N_{11}O_{36},Na]^+$.

FTIR (ν_{max}/cm^{-1}, ATR): 3000-2600 (bs N-H^+ st), 2962-2922-2852 (C-H st), 1738 (C=O st ester), 1593 (N-H^+ δ), 1468 (CH_2, CH_3 δ), 1373 (C-N st), 1229 (CO-O st as), 1130 (O-C-C st).

pH (1 mg·mL^{-1} in distilled water): 3.72.

$(NH_3^+Cl^-)_4$[*bis*MPA,G2]-[*bis*MPA,G2](C17)$_4$

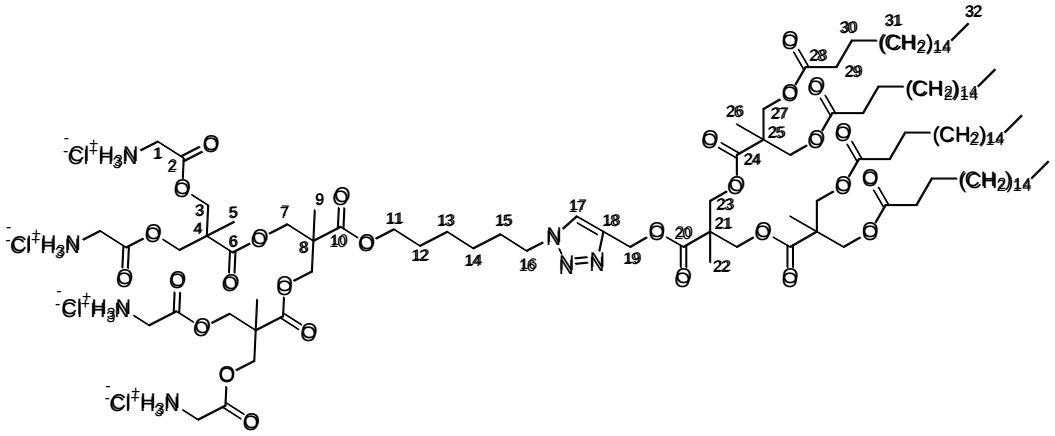

General procedure VI) (NHBoc)$_4$[*bis*MPA,G2]-[*bis*MPA,G2]-(C17)$_4$ (470 mg, 0.18 mmol, 1.00 eq.); HCl 3M into ethyl acetate (20 mL) into ethyl acetate (5 mL).The pure product was obtained as a white solid (423 mg, quantitative yield).

^{1}H NMR (400 MHz, CD_3OD, 40 ºC) δ (ppm): 0.90 (t, J = 6.4Hz, 12H, H-32), 1.21 (s, 6H, H-26), 1.30 (m, 124H, H-5, H-9, H-22 and H-31), 1.43 (m, 4H, H-13 and H-14), 1.60 (m, 8H, H-30), 1.70 (m, 2H, H-12), 1.94 (m, 2H, H-15), 2.32 (t, J = 7.6 Hz, 8H, H-29), 3.93 (m, 8H, H-1), 4.18 (m, 10H, H-11 and H-27), [4.18-4.50] (m, 18H, H-3, H-7, H-16, H-23), 5.27 (s, 2H, H-19), 8.00 (s, 1H, H-17).

^{13}C NMR (75 MHz, $CDCl_3$): δ (ppm) 14.0 (C-32), [17.5-17.7] (C-5, C-9, C-22 and C-26), 22.6 (C-31), 24.8 (C-30), 25.3 (C-13), 26.1 (C-14), 28.3 (C-12), [29.1-29.7] (C-31), 30.2 (C-15), 31.9 (C-31), 34.0 (C-1 and C-29), [46.0-46.6] (C-4, C-8, C-21 and C-25), 50.2 (C-16), 58.3 (C-19), [64.8-65.3] (C-3, C-7, C-11, C-23 and C-27), 124.1 (C-17), 142.0 (C-18), 167.5 (C-2), [171.9-172.3] (C-6, C-10, C-20 and C-24), 173.1 (C-28).

MS (MALDI$^+$) *m/z (%)*: *2212.8 (100)* $[C_{119}H_{213}N_7O_{28},Na]^+$; *2155.7 (7)* $[C_{117}H_{210}N_6O_{27},Na]^+$.

FTIR (ν_{max}/cm^{-1}, ATR): 3000-2600 (bs N-H$^+$ st), 2959-2918-2851 (C-H st), 1738 (C=O st ester), 1585 (N-H$^+$ δ), 1468 (CH_2, CH_3 δ), 1385 (C-N st), 1236 (CO-O st as), 1134 (O-C-C st).

pH (1 mg·mL^{-1} in distilled water): 3.08.

$(NH_3^+Cl^-)_8$[*bis*MPA,G3]-[*bis*MPA,G2](C17)$_4$

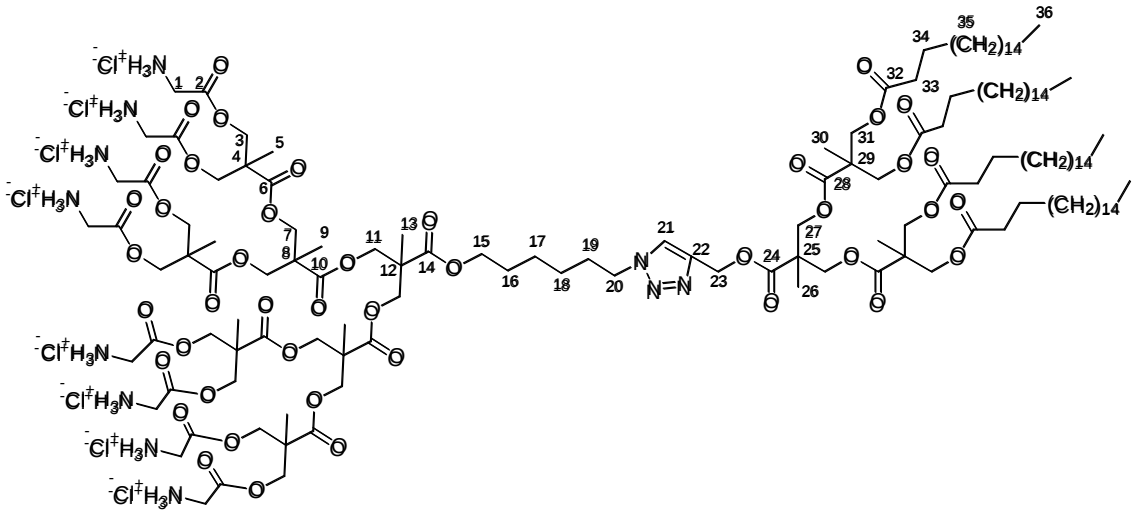

General procedure VI) $(NHBoc)_8$[*bis*MPA,G3]-[*bis*MPA,G2](C17)$_4$ (1282 mg, 0.35 mmol, 1.00 eq.); HCl 3M into ethyl acetate (25 mL) into ethyl acetate (8 mL). The pure product was obtained as a white solid (430 mg, 96 %).

^{1}H NMR (400 MHz, CD_3OD, 35ºC) δ (ppm): 0.90 (t, J = 6,8Hz, 12H, H-36), 1.21 (s, 6H, H-30), 1.25 (m, 124H, H-9, H-13, H-26 and H-35), 1.34 (s, 12H, H-5), 1.45 (m, 4H, H-17 and H-18), 1.60 (m, 8H, H-34), 1.70 (m, 2H, H-16), 1.96 (m, 2H, H-19), 2.33 (t, J = 7.2Hz, 8H, H-33), 3.95 (s, 16H, H-1), 4.16 (m, 10H, H-15 and H-31), [4.28-4.38] (m, 16H, H-7, H-11 and H-27), 4.45 (m, 18H, H-3 and H-20), 5.28 (s, 2H, H-23), 8.07 (s, 1H, H-21).

^{13}C NMR (75 MHz, $CDCl_3$): δ (ppm) 14.1 (C-36), [17.6-18.3] (C-5, C-9, C-13, C-26 and C-30), 22.7 (C-35), 24.9 (C-34), 25.3 (C-17), 26.2 (C-18), 28.3 (C-16), [29.1-29.7] (C-35), 30.2 (C-19), 31.9 (C-35), 34.0 (C-1 and C-33), [46.1-46.6] (C-4, C-8, C-12, C-25 and C-29), 50.0 (C-20), 58.3 (C-23), [64.7-64.3] (C-3, C-7, C-11, C-15, C-27 and C-31), 124.0 (C-21), 142.0 (C-22), 167.7 (C-2), [173.4-171.9] (C-6, C-10, C-14, C-24 and C-28), 173.1 (C-32).

MS (MALDI$^+$) *m/z (%)*: *2905.0 (100)* $[C_{147}H_{257}N_{11}O_{44},Na]^+$; *2847.9 (13)* $[C_{145}H_{254}N_{11}O_{43},Na]^+$.

FTIR (ν_{max}/cm^{-1}, ATR): 3000-2600 (bs N-H$^+$ st), 2959-2916-2849 (C-H st), 1736 (C=O st ester), 1601 (N-H+ δ), 1470 (CH_2, CH_3 δ), 1377 (C-N st), 1236 (CO-O st as), 1136 (O-C-C st).

pH (1 mg·mL^{-1} in distilled water): 3.21.

$(NH_3^+Cl^-)_4$[*bis*GMPA,G2]-[*bis*MPA,G1](C17)$_2$

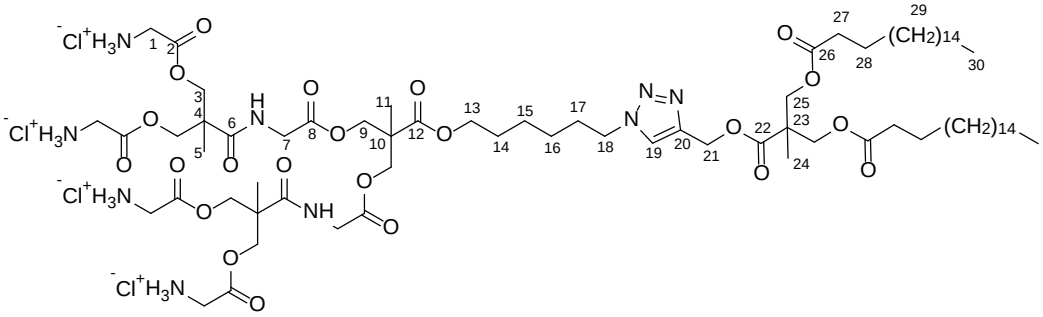

General procedure VI) $(NHBoc)_4$-[*bis*GMPA,G1]-[*bis*MPA,G2]-$(C17)_2$ (214 mg, $1.11x10^{-1}$ mmol, 1.00 eq.); HCl 3M into AcOEt (10 mL) into ethyl acetate (5 mL). The product was obtained as a white solid (187 mg, quantitative yield).

^{1}H NMR (400 MHz, $CDCl_3$) δ (ppm): 0.90 (t, J = 6.4Hz, 6H, H-30), 1.24 (s, 3H, H-24), 1.27 (s, 3H, H-11), 1.29 (s, 56H, H-29), 1.37 (s, 6H, H-5), 1.43 (m, 4H, H-15 and H-16), 1.55 (m, 4H, H-28), 1.66 (m, 2H, H-14), 1.94 (m, 2H, H-17), 2.26 (t, J = 7.2 Hz, 4H, H-27), 3.94 (s, 8H, H-3), 3.96 (s, 4H, H-9), 4.13 (t, J = 6.4 Hz, 2H, H-13), 4.21 (ABq, J = 11.2 Hz, $\Delta\nu_{AB}$ = 24.8 Hz, 4H, H-25), 4.31 (m, 4H, H-9), [4.37-4.47] (m, 10H, H-3 and H-18), 7.36 (bs, -NHCO), 8.06 (s, 1H, H-19).

^{13}C NMR (75 MHz, CD_3OD) δ (ppm): 14.5 (C-30), [17.8-18.2] (C-5, C-11 and C-24), 23.7 (C-29), 26.0 (C-28), 26.4 (C-15), 27.0 (C-16), 29.4 (C-14), [30.2-31.4] (C-29), 31.1 (C-17), 33.1 (C-29), 34.8 (C-29), 41.1 (C-1), 42.1 (C-7), [47.4-47.6] (C-4, C-10 and C-23), 51.3 (C-18), 58.9 (C-21), [66.2-68.4] (C-3 and C-9), 67.3 (C-9), 68.5 (C-3), 126.1 (C-19), 143.5 (C-20), 168.3 (C-2), [170.9-174.9] (C-6, C-8, C-12, C-22 and C-26).

MS (MALDI$^+$): *m/z (%)*: $[C_{77}H_{135}N_9O_{22},Na]^+$ *1561.5 (100)*.

FTIR (ν_{max}/cm^{-1}, ATR): 3000-2600 (bs N-H^+ st), 2953-2916-2851 (C-H st), 1742 (C=O st ester), 1657 (C=O st amide and N-H^+ δ), 1543 (N-H δ), 1470 (CH_2, CH_3 δ), 1229 (CO-O st), 1134 (O-C-C st).

pH (1 mg·mL^{-1} in distilled water): 3.20.

$(NH_3^+Cl^-)_8$[*bis*GMPA,G3]-[*bis*MPA,G1](C17)$_2$

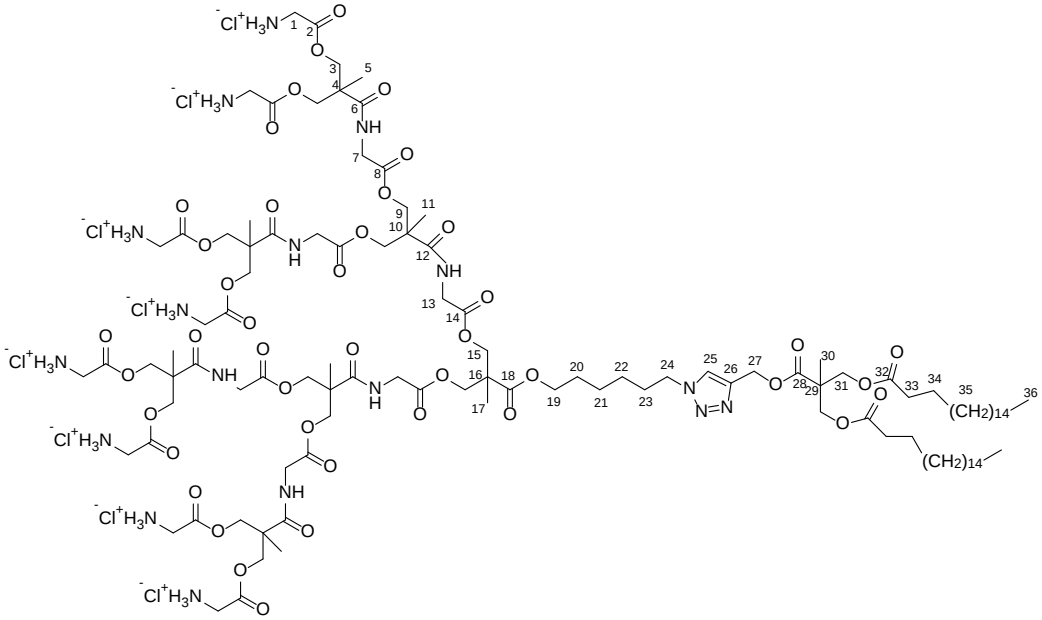

General procedure VI) $(NHBoc)_8$-[*bis*GMPA,G3]-[bisMPA,G1]-$(C17)_2$ (424 mg, $1.30x10^{-1}$ mmol, 1.00 eq.) and HCl 3M into ethyl acetate (10 mL) into ethyl acetate (5 mL). The product was obtained as a white solid (313 mg, quantitative yield).

^{1}H (400 MHz, CD_3OD) δ (ppm): 0.90 (t, J = 6.8 Hz, 6H, H-36), 1.24 (s, 3H, H-30), 1.27 (s, 3H, H-17), 1.29 (m, 56H, H-35), 1.32 (s, 6H, H-11), 1.38 (s, 12H, H-5), 1.44 (m, 4H, H-21 and H-22), 1.55 (m, 4H, H-34), 1.67 (m, 2H, H-20), 1.94 (m, 2H, H-23), 2.26 (t, 4H, J = 7.2 Hz, H-33), 3.95 (s, 16H, H-1), 3.97 (s, 4H, H-13), 4.01 (s, 8H, H-7), 4.13 (t, J = 6.4 Hz, 2H, H-19), 4.21 (ABq, J = 11.2 Hz, $\Delta\nu_{AB}$ = 27.7 Hz, 4H, H-31), 4.32 (m, 12H, H-9 and H-16), 4.45 (m, 18H, H-3 and H-24), 5.26 (s, 2H, H-27), 8.08 (s, 1H, H-25).

^{13}C (100 MHz, CD_3OD) δ (ppm):14.5 (C-36), [17.8-18.2] (C-5, C-11, C-17 and C-30), 23.7 (C-35), 26.0 (C-34), 26.4 (C-21), 27.0 (C-22), 29.4 (C-20), [30.1-30.8] (C-35), 31.1 (C-23), 33.1 (C-35), 34.8 (C-33), 41.2 (C-1), 42.2 (C-7 and C-13), [47.4-47.6] (C-4, C-10, C-16 and C-29), 51.4 (C-24), 58.9 (C-27), [66.2-66.4] (C-19 and C-31), 67.2 (C-15), 67.8 (C-9), 68.5 (C-3), 126.2 (C-25), 143.5 (C-26), 168.3 (C-2), [170.8-171.1] (C-8 and C-14), [174.0-174.1] (C-19 and C-28), [174.6-175.2] (C-6, C-14 and C-32).

FTIR (ν_{max}/cm^{-1}, ATR): 3600-2600 (bs N-H^+ st), 2920-2852 (C-H st), 1745 (C=O st ester), 1653 (C=O st amide and N-H^+ δ), 1537 (N-H δ), 1468 (CH_2, CH_3 δ), 1229 (CO-O st).

pH (1 mg·mL^{-1} in distilled water): 3.66.

$(NH_3^+Cl^-)_8$[*bis*GMPA,G3]-[*bis*MPA,G2](C17)$_4$

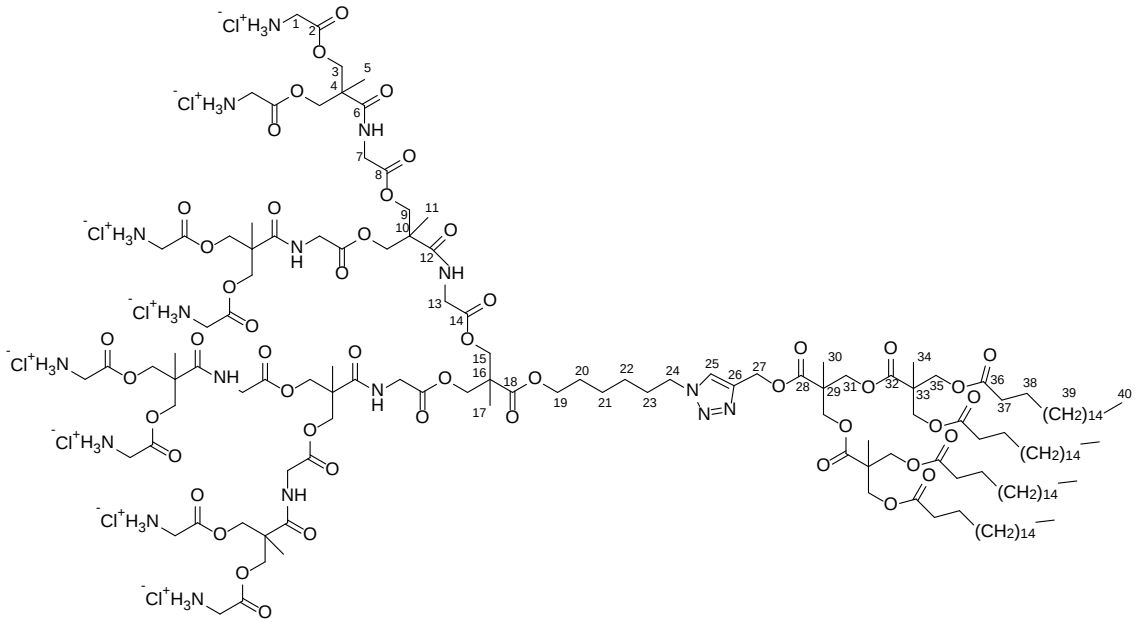

General procedure VI) $(NHBoc)_8$-[*bis*GMPA,G2]-[*bis*MPA,G3]-$(C17)_4$ (290 mg, $7.20x10^{-2}$ mmol, 1.00 eq.) and HCl 3M into ethyl acetate (10 mL) into ethyl acetate (5 mL). The pure product was obtained as a white solid (253 mg, quantitative yield).

^{1}H NMR (400 MHz, CD_3OD) δ (ppm): 0.90 (t, J = 6.8Hz, 12H, H-40), 1.20 (s, 6H, H-34), [1.28-1.33] (m, 124H, H-11, H-17, H-30 and H-39), 1.38 (s, 12H, H-5), 1.43 (m, 4H, H-21 and H-22), 1.59 (m, 8H, H-38), 1.67 (m, 2H, H-20), 1.95 (m, 2H, H-23), 2.33 (t, J = 7.2Hz, 8H, H-37), 3.94 (s, 16H, H-1), 3.97 (m, 4H, H-13), 4.00 (m, 8H, H-9), 4.13 (m, 10H, H-19 and H-35), 4.27 (ABq, 4H, H-31), 4.32 (m, 12H, H-9 and H-15), 4.45 (m, 18H, H-19 and H-24), 8.08 (bs, -NHCO).

^{13}C NMR (100 MHz, $CDCl_3$) δ (ppm): 14.5 (C-40), [17.8-18.3] (C-5, C-11, C-17, C-30 and C-34), 23.8 (C-39), 26.1 (C-38), 26.4 (C-21), 27.1 (C-22), 29.4 (C-23), [30.2-30.9] (C-31), 31.2 (C-20), 33.1 (C-39), 34.9 (C-37), 41.2 (C-1), 42.2 (C-7 and C-13), [47.4-47.9] (C-4, C-10, C-16, C-29 and C-33), 51.4 (C-24), 59.1 (C-27), [66.3-68.6] (C-3, C-9, C-15, C-19, C-31 and C-35), 126.3 (C-25), 143.5 (C-26), 168.3 (C-2), [170.8-175.3] (C-6, C-8, C-12, C-14, C-18, C-28 and C-32).

MS ($MALDI^+$) *m/z (%)*: *3248.6 (100)* $[C_{159}H_{275}N_{17}O_{50},Na]^+$.

FTIR (ν_{max}/cm^{-1}, ATR): 3000-2600 (bs N-H^+ st), 2959-2918-2851 (C-H st), 1738 (C=O st ester), 1653 (C=O st amide and N-H^+ δ), 1539 (N-H δ) 1470 (CH_2, CH_3 δ), 1217 (CO-O st as), 1132 (O-C-C st).

pH (1 mg·mL^{-1} in distilled water): 3.33.

7.1.3.2 - Amphiphilic hybrid dendritic-linear-dendritic blocks copolymers (HDLDBCs)

General procedure VIII): copper(I) azide-alkyne cyloaddition reaction (CuAAC) for the synthesis of the HDLDBCs

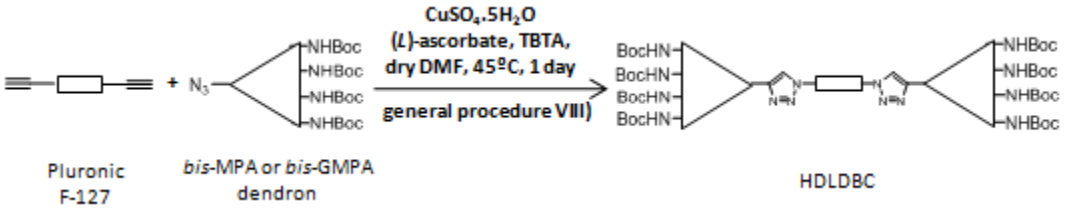

Alkyne functionalized F-127 Pluronic (1.00 mol) and pre-hydrophilic dendrons (2.60 mol) were dissolved into dimethylformamide (8 mL) in a Schlenk flask. 3 cycles vacuum-argon were made to remove the O_2. The reaction mixture was allowed to stir under argon atmosphere at 45ºC. $CuSO_45.H_2O$ (0.40 mol), L-ascorbate (0.80 mol) and TBTA (0.40 mol) were dissolved into DMF (5 mL) in a second Schlenk flask. 3 cycles vacuum-argon were made in order to remove the O_2 and the copper solution was stirred at 45ºC during 15 min. Then, it was added through a cannula to the previous azide-alkyne reaction mixture. The reaction mixture was stirred at 45ºC during 2 days under argon atmosphere. Then, hot brine (100 mL) was added to the reaction mixture and the product was extracted 3 times with dichloromethane (3 x 100 mL). Organic phases were washed two times with hot brine (2 x 100 mL), dried over anhydrous $MgSO_4$ and the solvent was evaporated under reduce pressure to give a yellow solid. The crude product was precipitated into cold diethyl ether and allowed to decant overnight at 4ºC. It was filtered and washed with cold diethyl ether to give a white powder. Finally, the product was dialyzed (cellulose membrane, 1000 Da) against methanol during 24 hours to give a light yellow solid.

General procedure IX): deprotection of the terminal amino groups

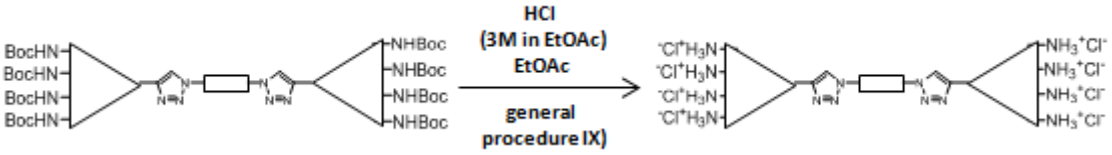

t-Boc protected HDLDBC (1 mol) was dissolved into ethyl acetate. HCl (3M into ethyl acetate) was carefully added to it. The reaction mixture was stirred at room temperature during 45 min. A white gel appeared. The reaction mixture was diluted into ethyl acetate and was stirred during another 30 min. Then, it was stirred under vacuum to remove the hydrochloric acid and the solvent was evaporated under reduce pressure. The gel was washed firstly with pure ethyl acetate and secondly with pure methanol. In each case, the solution was stirred under vacuum to remove the residual hydrochloric acid and then, the solvent was evaporated under reduce pressure to obtain a dried gel.

4-propargyloxybenzoate

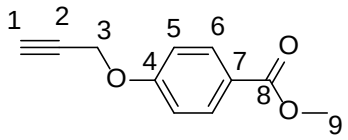

4-hydroxybenzoate (5.00 g, 32.9 mmol, 1.00 eq) was dissolved into DMF (100 mL). K_2CO_3 (6.82 g, 49.4 mmol, 1.50 eq.) was added to it. The reaction mixture was heated up to 105ºC. Propargyl bromide (80% in toluene) (4.74 mL, 36.1 mmol, 1.10 eq.) was added drop wise. The reaction was stirred at 105ºC overnight. The reaction was cooled down to room temperature and a mixture of water and brine (3:1) (400 mL) was added to it. The product was extracted two times with AcOEt (2 x 200 mL). The organic phases were washed two times with a mixture of water and brine (1:1) (2 x 200 mL), dried over anhydrous $MgSO_4$ and the solvent was evaporated under vacuum. The crude product was purified on silica gel (hexane : ethyl acetate = ramp from 9:1 to 8:2) to give a light orange solid (4.34 g, 69 %).

^{1}H (400 MHz, $CDCl_3$) δ (ppm): 2.55 (t, J = 2.4 Hz, 1H, H-1), 3.88 (s, 3H, H-9), 4.75 (d, J = 2.4 Hz, 2H, H-3), 6.99 (dt, J_1 = 9.2 Hz, J_2 = 2.8 Hz, 2H- H-5), 8.01 (dt, J_1 = 9.2 Hz, J_2 = 2.8 Hz, 2H, H-6).

^{13}C (100 MHz, $CDCl_3$) δ (ppm): 51.9 (C-9), 55.8 (C-3), 76.0 (C-1), 77.8 (C-2), 114.4 (C-5), 122.4 (C-7), 131.5 (C-6), 161.1 (C-4), 166.6 (C-8).

FTIR (ν_{max}/cm^{-1}, ATR): 3246 (≡C-H st), 2959 (C-H st), 2129 (C≡C-H st), 1705 (C=O st ester), 1286-1250 (CO-O st), 1175(C-O-C st).

4-propargyloxybenzoic acid

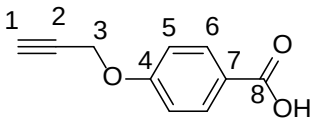

4-propargyloxybenzoate (4.13 g, 21.75 mmol, 1.00 eq) was dissolved into MeOH (133 mL). Distilled water (66 mL) is slowly added. The reaction mixture was cooled down to 0ºC. LiOH (3.65 g, 87.04 mmol, 4.00 eq.) was slowly added. The reaction mixture was slowly heated up to reflux temperature and stirred during 6 hours. It was diluted with NaOH (2M in water) in an ice bath. HCl (12M in water) is carefully added to pH 1. A white precipitate appeared. It was filtered and washed with HCl (0.5M in water) (2.59 g, 81 %).

^{1}H (400 MHz, $(CD_3)_2SO$): δ 3.61 (t, J = 2.0 Hz, 1H, H-1), 4.88 (d, J = 2.0 Hz, 2H, H-3), 7.10 (d, J= 8.8 Hz, 2H, H-5), 7.92 (d, J = 8.8 Hz, 2H, H-6), 12.69 (bs, -COOH).

^{13}C (100 MHz, $(CD_3)_2SO$): δ 55.7 (C-3), 78.1 (C-1), 78.8 (C-2), 114.7 (C-5), 123.7 (C-7), 131.3 (C-6), 160.8 (C-4), 166.9 (C-8).

FTIR (ν_{max}/cm^{-1}, ATR): 3244 (≡C-H st), 3200-2300 (O-H st), 2825 (C-H st), 2131 (C≡C-H st), 1672 (C=O st acid), 1296-1242 (CO-O st), 1182 (C-O-C st).

≡-PLU-≡

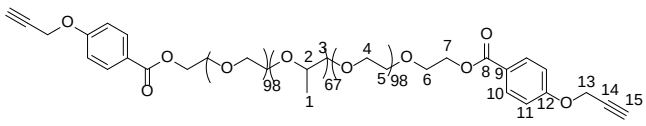

Pluronic® F-127 (10.00 g, 0.794 mmol, 1.00 eq) was heated during 2 hours at 105ºC to remove the water that are contained inside the polymer. It was cooled to room temperature and dissolved into a mixture of dry dichloromethane : dry tetrahydrofurane (1:1) (20 mL) and stirred at 45ºC under argon atmosphere. DMAP (118 mg, 0.953 mmol, 1.20 eq.) and 4-propargyloxybenzoic acid (560 mg, 3.12 mmol, 4.00 eq.) were added to it. DCC (655 mg, 3.12 mmol, 4.00 eq.) was dissolved into dry tetrahydrofurane (1 mL) and added drop wise. The reaction mixture was stirred at 45ºC under argon atmosphere during 48 hours. The white precipitate, N,N'-dicyclohexylurea (DCU), was filtered off and the product was precipitate into cold diethyl ether (1 L) and it was allowed to decant overnight at 4ºC. The white precipitate was recovered by filtration at atmospheric pressure and was washed with cold diethyl ether. Then, it was dissolved into toluene (20 mL) and filtered in order to remove the entrapped DCU that is insoluble in toluene. The solvent was evaporated under reduce pressure to obtain a white powder (8.47, 75 %).

^{1}H ($CDCl_3$, 400 MHz) δ (ppm): 1.13 (m, 201H, H-1), 2.55 (t, J = 2.4 Hz, 2H, H-15), 3.37 (m, 67H, H-2), [3.42-3.74] (m, ~1000H, H-3, H-4 and H-5), 3.79 (t, 4H, H-6), 4.41 (m, 8H, H-7), 4.72 (d, J = 2.4 Hz, 4H, H-13), 6.97 (dt, J = 9.2 Hz, J = 2.0 Hz, 4H, H-11), 7.99 (dt, J_1 = 9.2 Hz, J = 9.2 Hz, J = 2.0 Hz, 4H, H-10).

^{13}C ($CDCl_3$, 100 MHz) δ (ppm): [17.1-17.2] (C-1), 55.6 (C-13), [63.7-75.3] (C-2 to C-7), 76.1 (C-15), 77.6 (C-14), 114.3 (C-11), 123.2 (C-9), 131.5 (C-10), 161.0 (C-12), 165.9 (C-8).

MS ($MALDI^+$): distribution with max at m/z 13800.

FTIR (ν_{max}/cm^{-1}, ATR): 3240 (≡C-H st), 2883 (C-H st), 1717 (C=O st ester), 1466 (CH_2, CH_3 δ), 1279 (CO-O st), 1101 (C-O-C st).

SEC (*ref PMMA*): 2 populations; Mw 17006 $g.mol^{-1}$; Đ: 1.10.

$(NHBoc)_8$[*bis*MPA]-PLU-[*bis*MPA]$(NHBoc)_8$

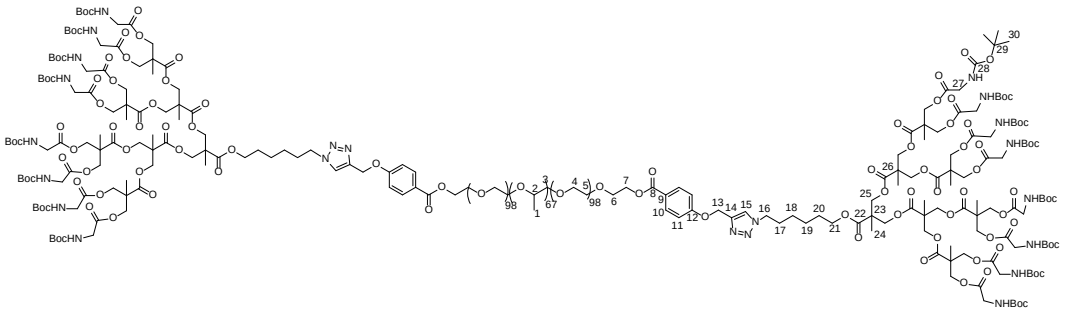

General procedure VIII) ≡-(PLU)-≡ (2.000 g, $1.55x10^{-1}$ mmol, 1.00 eq.); N_3-[*bis*MPA,G3]-$(NHBoc)_8$ (891 mg, $4.03x10^{-1}$ mmol, 2.60 eq.); $CuSO_4$,$5H_2O$ (32.8 mg, $6.20x10^{-2}$ mmol, 0.40 eq), (*L*)-ascorbate (24.5 mg, $1.24x10^{-1}$mmol, 0.80 eq.) and TBTA (32.8 mg, $6.20x10^{-2}$, 0.40 eq.) into DMF (12 mL). The product was obtained as a white powder (1.024 g, 38%).

^{1}H (400 MHz, $CDCl_3$) δ (ppm): 1.13 (m, 201H, H-1), 1.23 (s, 18H, H-24_{G3}), 1.28 (s, 12H, H-24_{G2}), 1.33 (s, 6H, H-24_{G1}), 1.43 (m, 152H, H-18, H-19 and H-30), 1.67 (m, 4H, H-20), 1.95 (m, 4H, H-17), 3.39 (m, 67H, H-2), 3.44-3.74 (m, ~1000H, H-3, H-4 and H-5), 3.81 (t, J = 4.8 Hz, H-6), 3.87 (d, J = 5.6 Hz, 32H, H-27), 4.11 (t, J = 6.4 Hz, 4H, H-7), [4.18-4.29] (m, 56H, H-25), 4.37 (t, J = 7.2 Hz, 4H, H-16), 4.43 (t, J = 4.8 Hz, 4H, H-7) 5.25 (s, 4H, H-13), 5.35 (bs, ~NH), 7.01 (d, J = 9.2 Hz, 4H, H-11), 7.67 (s, 2H, H-15), 8.00 (d, J = 9.2Hz, 4H, H-10).

^{13}C NMR (75 MHz, $CDCl_3$) δ (ppm): [17.3-17.8] (C-1 and C-24), 25.3 (C-19), 26.1 (C-18), 28.3 (C-20 and C-30), 30.1 (C-17), 42.2 (C-25_{G3}), [46.4-46.7] (C-23), 50.2 (C-16), [62.1-75.3] (C-2 to C-7, C-13, C-21 and C-$25_{G1,G2}$), 79.9 (C-29), 114.3 (C-11), 122.7 (C-15), 123.1 (C-9), 131.7 (C-10), 143.4 (C-14), 155.8 (C-28), 162.0 (C-12), 166.1 (C-8), 170.0 (C-26_{G3}), [171.5-172.0] (C-21 and C-$26_{G1,G2}$).

MS (MALDI$^+$): distribution with max at m/z 17550.

FTIR (ν_{max}/cm^{-1}, ATR): 3321 (N-H st), 2974-2883 (C-H st), 1745 (C=O st ester), 1717 (C=O st carbamate), 1670 (C=O st amide), 1514 (N-H δ), 1466 (δ -CH_2-, δ_{as} -CH_3), 1101 (C-O-C st).

(NHBoc)$_8$[*bis*GMPA]-PLU-[*bis*GMPA](NHBoc)$_8$

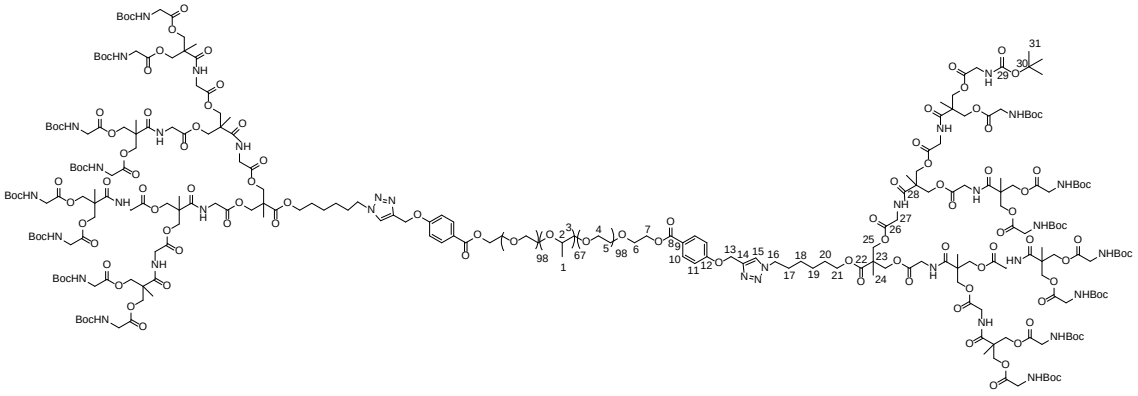

General procedure VIII) ≡-(PLU)-≡ (1.000 g, 7.74x10^{-1} mmol, 1.00 eq.); N_3-[*bis*GMPA,G3]-(NHBOC)$_8$ (514 mg, 2.01x10^{-1} mmol, 2.60 eq.); $CuSO_4$,5H_2O (18.2 mg, 6.19x10^{-2} mmol, 0.80 eq), (*L*)-ascorbate (24.05 mg, 1.24x10^{-1}mmol, 1.60 eq.) and TBTA (32.8 mg, 6.19x10^{-2}, 0.80 eq.) into dry DMF (12 mL). The product was obtained as a light yellow solid (855 mg, 61%).

^{1}H (400 MHz, $CDCl_3$) δ (ppm): 1.11 (m, 201H, H-1), 1.26 (m, 36H, H-24), 1.41 (m, 152H, H-18, H-19 and H-31), 1.62 (m, 4H, H-20), 1.94 (m, 4H, H-17), 3.38 (m, 67H, H-2), [3.44-3.74] (m, ~1000H, H-3, H-4 and H-5), 3.81 (t, 4H, J = 4.8 Hz, H-6), 3.88 (m, 32H, H-27$_{G3}$), 3.94 (m, 8H, H-27$_{G1}$), 3.88 (m, 16H, H-27$_{G2}$), 4.11 (t, J = 6.4 Hz, 4H, H-21), [4.18-4.35] (m, 60H, H-16 and H-25), 4.43 (t, J = 4.8 Hz, 4H, H-7) 5.29 (s, 4H, H-13), 5.35 (bs, ~NHBoc), 7.02 (d, J = 8.8 Hz, 4H, H-11), 7.17 (bs, ~CONH), 7.82 (s, 2H, H-15), 8.00 (d, J = 8.0 Hz, 4H, H-10).

FTIR (ν_{max}/cm^{-1}, ATR): 3360 (N-H st), 2883 (C-H st), 1755 (C=O st ester), 1718 (C=O st carbamate), 1670 (C=O st amide), 1533 (N-H δ), 1468 (δ -CH_2-, δ_{as} -CH_3), 1101 (C-O-C st).

SEC (*ref PMMA*): 2 populations; Mw 19745 g.mol^{-1}; Đ: 1.08.

$(NH_3^+Cl^-)_8$[*bis*MPA]-PLU-[*bis*MPA] $(NH_3^+Cl^-)_8$

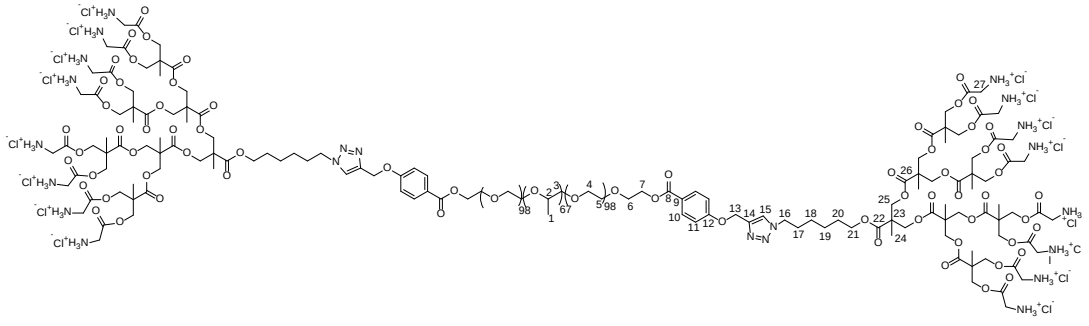

General procedure IX) $(NHBoc)_8$[*bis*MPA]-PLU-[*bis*MPA]$(NHBoc)_8$ (500 mg, $2.88x10^{-2}$ mmol, 1.00 eq.) and HCl (3M in ethyl acetate) (7 mL) into ethyl acetate (3 mL).The product was obtained as a colorless dried gel (470 mg, quantitative yield).

^{1}H NMR (400 MHz, CD_3OD) δ (ppm): 1.14 (m, 201H, H-1), 1.34 (m, 42H, H-24), 1.43 (m, 8H, H-18 and H-19), 1.67 (m, 4H, H-20), 1.96 (m, 4H, H-17), 3.46 (m, 67H, H-2), [3.44-3.74] (m, ~1000H, H-3, H-4 and H-5), 3.83 (m, 4H, H-6), 4.05 (m, 32H, H-27), 4.14 (t, J = 5.6 Hz, 4H, H-21), [4.27-4.37] (m, 24H, H-$25_{G1,G2}$), 4.41 (m, 4H, H-16), 4.46 (m, 32H, H-25_{G3}), 5.32 (s, 4H, H-13), 7.16 (d, J = 8.8 Hz, 4H, H-11), 8.02 (d, J = 8.8 Hz, H-10), 8.21 (m, 2H, H-15).

MS ($MALDI^+$): distribution with max at m/z 16260.

FTIR (ν_{max}/cm^{-1}, ATR): 3441 (N-H st), 2887 (C-H st), 1742 (C=O st ester), 1468 (CH_2, CH_3 δ), 1103 (C-O-C st).

pH (1 mg·mL^{-1} in distilled water): 3.82.

$(NH_3^+Cl^-)_8$[*bis*GMPA]-PLU-[*bis*GMPA]$(NH_3^+Cl^-)_8$

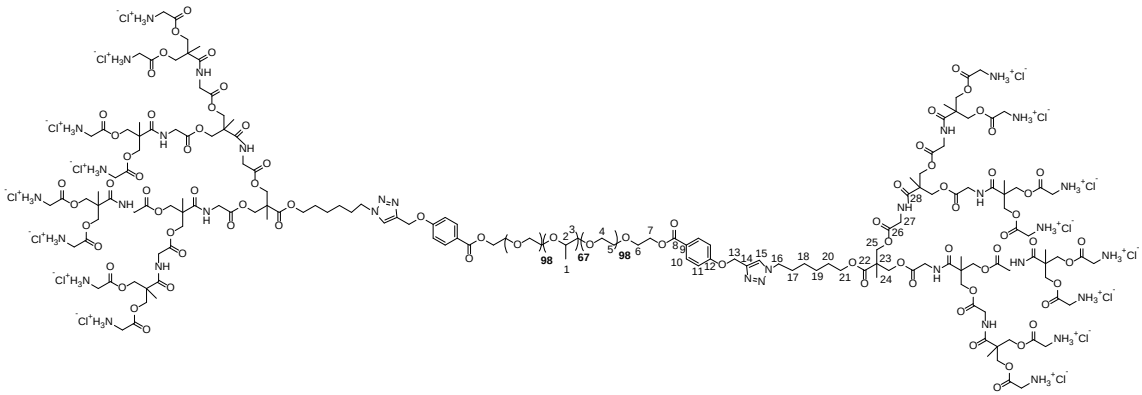

General procedure IX) $(NHBoc)_8$-[*bis*GMPA,G2]-PLU-[*bi*-GMPA,G2]-$(NHBoc)_8$ (653 mg, $3.62x10^{-2}$ mmol, 1.00 eq.) and HCl (3 M in ethyl acetate) (7 mL) into ethyl acetate (3 mL). The product was obtained as a light yellow dried gel (212) (615 mg, quantitative yield).

^{1}H (400 MHz, CD_3OD) δ (ppm): 1.14 (m, 201H, H-1), 1.27 (s, 6H, H-24_{G1}), 1.32 (s, 20H, H-18, H-19 and H-24_{G2}), 1.39 (s, 24H, H-24_{G2}), 1.64 (m, 4H, H-20), 1.95 (m, 4H, H-17), 3.47 (m, 67H, H-2), 3.51-3.73 (m, ~1000H, H-3, H-4 and 5), 3.84 (t, J = 4.8 Hz, 4H, H-6), 3.96 (s, 8H, H-27_{G0}), 4.00 (s, 16H, H-27_{G1}), 4.03 (s, 32H, H-27_{G2}), 4.12 (t, J = 6.0 Hz, 4H, H-21), 4.31 (m, 24H, H-$25_{G0,G1}$), 4.45 (m, 40H, H-7, H-16 and H-25_{G3}) 5.30 (s, 4H, H-13), 7.38 (d, J = 8.8 Hz, 4H, H-11), 8.23 (d, J = 8.8 Hz, 4H, H-10), 8.19 (s, 2H, H-15).

^{13}C NMR (125 MHz, CD_3OD) δ (ppm): [17.4-18.3] (C-1 and C-24), 26.3 (C-19), 26.9 (C-18), 29.3 (C-20), 31.1 (C-17), 41.5 (C-25_{G2}), 42.2 (C-$25_{G0,G1}$), 47.3 (C-23), 51.3 (C-16), [62.6-76.8] (C-2 to C-7, C-13, 21 and C-25), 115.9 (C-11), 124.2 (C-9), 125.8 (C-15), 132.8 (C-10), 140.4 (C-14), 163.7 (C-12), 167.6 (C-8), 168.8 (C-26_{G2}), [170.8-171.2] (C-$26_{G0,G1}$), 174.0 (C-21), [174.7, 175.0] (C-28).

FTIR (ν_{max}/cm^{-1}, ATR): 2885 (C-H st), 1751 (C=O st ester), 1663 (C=O st amide and N-H^+ δ), 1545 (N-H δ), 1468 (CH_2-, CH_3 δ), 1099 (C-O-C st).

pH (1 mg·mL^{-1} in distilled water): 3.43.

7.1.4- Globular dendritic derivatives for gene transfection

7.1.4.1- *B*is-GMPA dendrimers

General procedure X): copper(I) azide-alkyne cyloaddition reaction (CuAAC) for the synthesis of the 3-arms dendrimers

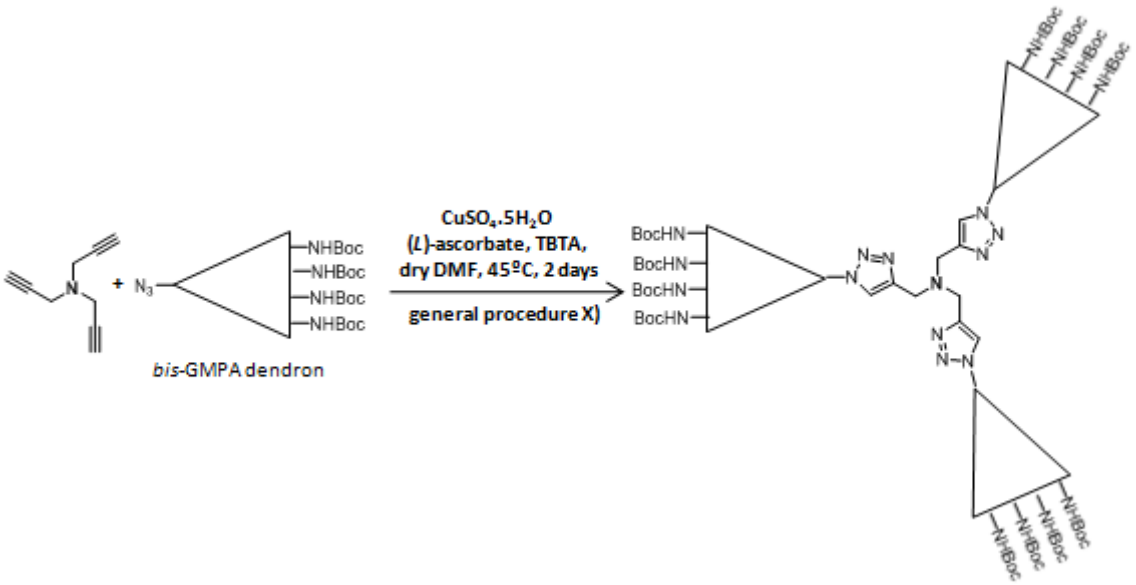

Tripropargylamine (1.00 mol) and azido-dendron (1.10 mol) were dissolved into dimethylformamide (7 mL) in a Schlenk flask. 3 cycles vacuum-argon were made to remove the O_2. The reaction mixture was allowed to stir under argon atmosphere at 45ºC. $CuSO_4 5.H_2O$ (0.3 or 1.5 mol), L-ascorbate (0.6 or 3.0 mol) and TBTA (0.3 mol) were dissolved into DMF (3 mL) in a second Schlenk flask. 3 cycles vacuum-Argon were made in order to remove the O_2 and the copper solution was stirred at 45ºC during 15 min. Then, it was added through a cannula to the previous azide-alkyne reaction mixture. The reaction mixture was stirred at 45ºC during 2 days. Then, brine was added (100 mL) and the product was extracted 2 times with ethyl acetate (2 x 70 mL). The organic phase was washed three times with brine (3 x 100 mL), once with a KCN

aqueous solution (15 mg into 100 mL of water) and twice with brine (2 x 100 mL), dried over anhydrous $MgSO_4$ and the solvent was evaporated under reduce pressure. Finally, the crude product was precipitated into a mixture of hexane and ethyl acetate (refer to the product to see the solvents proportion, 100 mL); the crude product was first dissolved into ethyl acetate and then, hexane was slowly added into the dissolution. The product was recovered by centrifugation and the solid was washed once with the same mixture of hexane and ethyl acetate. Finally, the product was dialyzed against methanol (cellulose acetate, MW 1000 Da) to give a white or light yellow powder.

The *t*-Boc protective groups were removed according to *the* ***general procedure VI)*** (see page 321).

D[*bis*GMPA,G3](NHBoc)$_{24}$ and D[*bis*GMPA,G4]-(NHBoc)$_{48}$

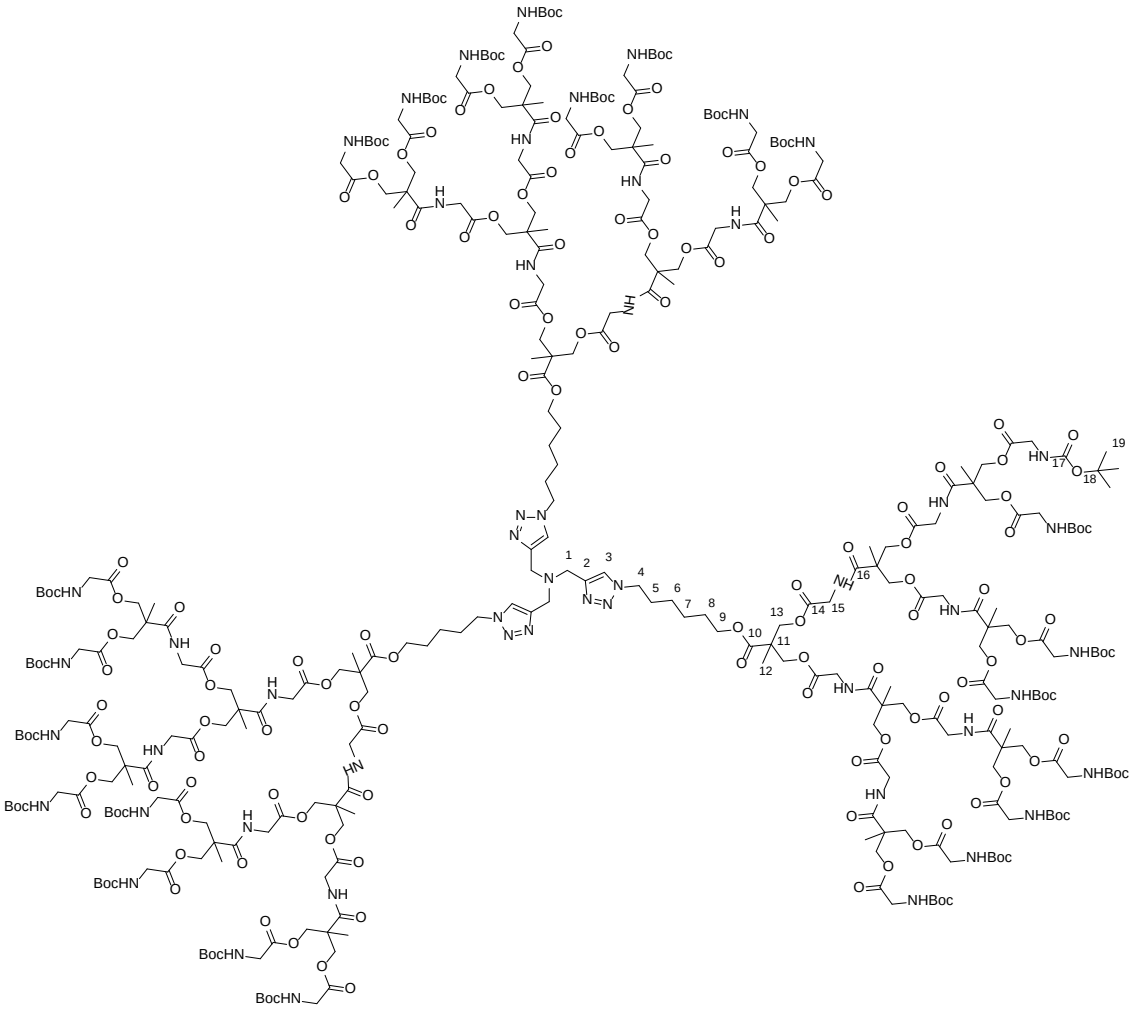

D[*bis*GMPA,G3](NHBoc)$_{24}$

General procedure X) Triporpargylamine amine (6.71 µL, 4.74x10^{-2} mmol, 1.00 eq.); N_3-[*bis*GMPA,G3]-(NHBoc)$_8$ (400 mg, 1.57x10^{-1} mmol, 3.30 eq.); $CusO_4.5H_2O$ (17.8 mg, 7.11x10^{-2} mmol, 1.50 eq.), (*L*)-ascorbate (28.2 mg, 1.42x10^{-2} mmol, 3.00 eq.); TBTA (7.53 mg, 1.42x10^{-2} mmol, 0.30 eq.); dry DMF (10 mL). The crude product was purified by precipitation into a mixture of hexane and ethyl acetate (4:6) and by dialysis against methanol to give a white powder (313 mg, 85 %).

For ^{1}H and ^{13}C number, refer to the scheme C_{VI}-1.

^{1}H (400 MHz, $CDCl_3$) δ (ppm): [1.22-1.27] (m, 63H, H-12), 1.38 (m, 12H, H-6 and H-7), 1.42 (m, 216H, H-19), 1.63 (m, 6H, H-8), 1.93 (m, 2H, H-5), 3.70 (m, 6H, H-1), 3.88 (d, J = 5.2 Hz, 48H, H-15[G3]), 3.94 (d, J = 4.4 Hz, 6H, H-15[G1]), 3.98 (d, J = 4.0 Hz, H-15[G2]), 4.11 (m, 6H, H-9), [4.19-4.34] (m, 90H, H-13 and H-4), 5.48 (-NHBoc), 7.33 (-NHCO), 7.82 (s, 3H, H-3).

^{13}C (100 MHz, $CDCl_3$) δ (ppm): [17.8-18.3] (C-12), 25.2 (C-7), 26.0 (C-6), 28.3 (C-8 and C-19), 30.1 (C-5), 41.3 (C-15[G1,2]), 42.3 (C-15[G2]), [46.0-46.1] (C-11), 46.8 (C-1), 50.2 (C-1), [65.2-66.5] (C-9 and C-13), 80.0 (C-16), 123.0 (C-3), 156.1 (C-17), 169.6 (C-14[G3]), [170.3-171.1] (C-14[G1,G2]), 172.6 (C-10), 172.9 (C-16).
Note: The signals of the carbons C-1, C-2, C-3 and C-4 could not be observed in the ^{13}C NMR spectrum. However, coupling signals between H-1 and C-1, H-2 and C-2 and H-4 and C-4 were observed in ^{1}H-^{13}C HSQC experiment.

FTIR (ν_{max}/cm^{-1}, ATR): 3375 (N-H st), 2979-2927-2868 (C-H st), 1749 (C=O st ester), 1699 (C=O st carbamate), 1660 (C=O st amide), 1522 (N-H δ), 1457 (CH_2, CH_3 δ), 1366 (C-N st), 1287 (CO-O st), 1161 (N-CO-O st).

EA (%): *Found:* C, 51.2; H, 6.9; N, 9.2. *Calc. for* $C_{335}H_{532}N_{52}O_{156}$: C, 51.7; H, 6.9; N, 9.4.

SEC (*ref PMMA*): Mw 6895 g.mol^{-1}; Đ: 1.05.

D[*bis*GMPA,G4]-(NHBoc)$_{48}$

General procedure X) Triporpargylamine amine (3,45 µL, 2.33x10^{-2} mmol, 1.00 eq.); N_3-[*bisG*MPA,G4]-$(NHBoc)_{16}$ (400 mg, 7.69x10^{-1} mmol, 3.30 eq.); $CusO_4.5H_2O$ (8.73 mg, 3.50x10^{-2} mmol, 1.50 eq.), (*L*)-ascorbate (13.9 mg, 7.00x10^{-2} mmol, 3.00 eq.); TBTA (3.71 mg, 7.00x10^{-3} mmol, 0.30 eq.); dry DMF (10 mL). The crude product was purified by precipitation into a mixture of hexane and ethyl acetate (5:5) (100 mL) and by dialysis against methanol to give a light yellow powder (287 mg, 78 %).

For ^{1}H and ^{13}C number, refer to the scheme C_{VI}-1.

^{1}H (400 MHz, CDCl3) δ (ppm): [1.22-1.28] (m, 135H, H-12), 1.43 (m, 444H, H-17, H-6 and H-7), 1.64 (m, 6H, H-8), 1.96 (m, 6H, H-5), 3.69 (m, 6H, H-1), 3.89 (m, 96H, H-15[G4]), 3.98 (m, 84H, H-15[G1,2,3]), 4.12 (m, 6H, H-9), [4.17-4.40] (m, 180H, H-13), 4.35 (m, 6H, H-4), 5.54 (-NHBoc), 7.70 (s, 3H, H-3).

^{13}C (100 MHz, $CDCl_3$) δ (ppm): [17.7-18.8] (C-12), 28.3 (C-19), 42.4 (C-15[G4]), 42.4 (C-15[G1,2,3]), 46.0 (C-11), [65.3-66.1] (C-9 and C-13), 80.0 (C-18), 156.1 (C-17), 170.1 (C-14_{G3}), [169.6-173.1] (C-10, C-14 and C-16).
Note: The signals of the carbons C-1 to C-9 could not be observed in the ^{13}C NMR spectrum and their ^{1}H-^{13}C correlations could not be observed in the ^{1}H-^{13}C HSQC spectrum.

FTIR (ν_{max}/cm^{-1}, ATR): 3367 (N-H st), 2978-2927 (C-H st), 1749 (C=O st ester), 1699 (C=O st carbamate), 1675 (C=O st amide), 1525 (N-H δ), 1469 (CH_2, CH_3 δ), 1369 (C-N st), 1249 (CO-O st), 1159 (N-CO-O st).

EA (%): *Found:* C, 52.0; H, 7.3; N, 8.0. *Calc. for* $C_{672}H_{1062}N_{100}O_{324}$: C, 51.3; H, 6.8; N, 8.9.

SEC (*ref PMMA*): Mw 13102 g.mol^{-1}; Đ: 1.05.

D[*bis*GMPA,G3](NH$_3^+$Cl$^-$)$_{24}$ and D[*bis*GMPA,G4]-(NHBoc)$_{48}$

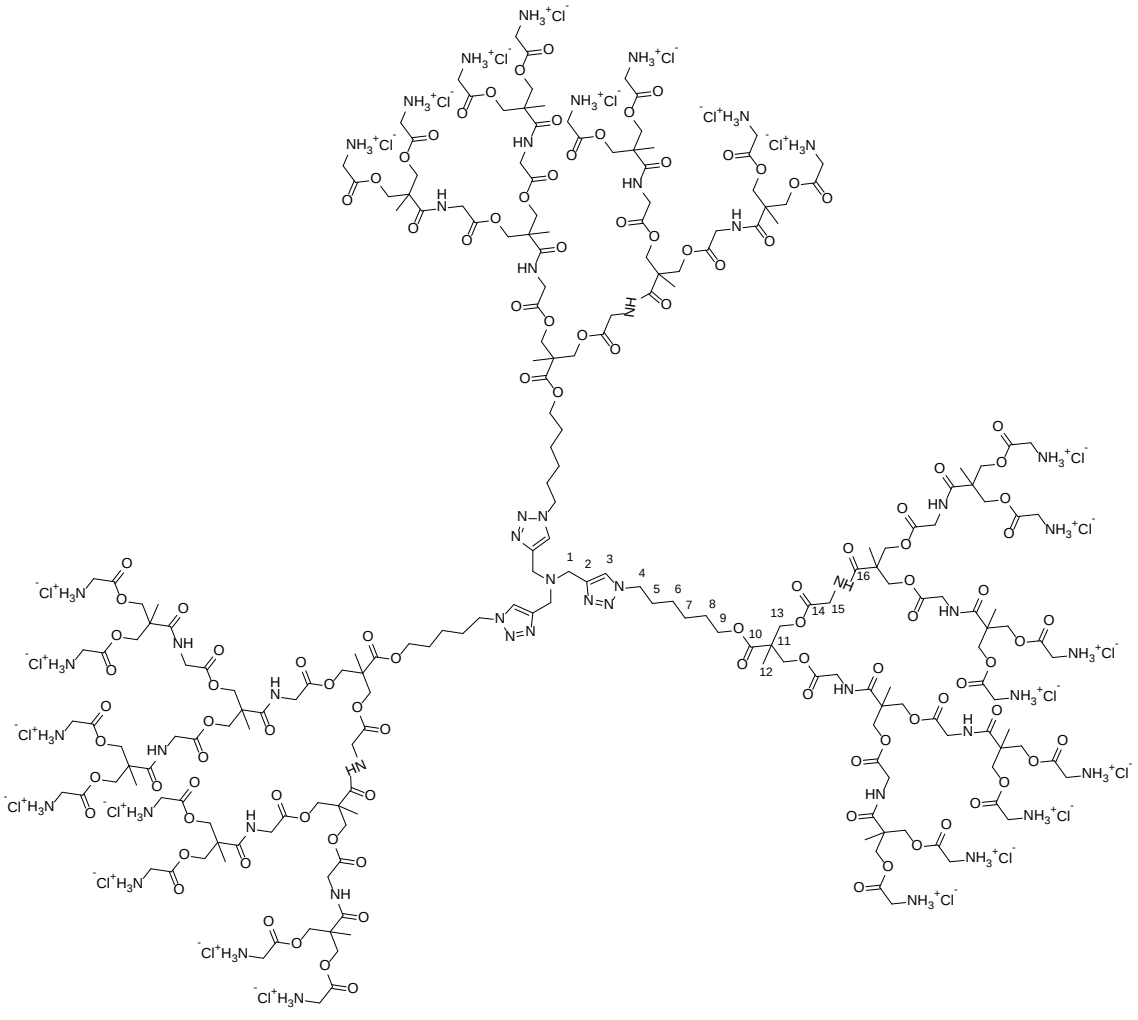

D[*bis*GMPA,G3](NH$_3^+$Cl$^-$)$_{24}$

General procedure VI) D-[*bis*GMPA,G3](NHBoc)$_8$ (154 mg, 7.38x10^{-2} mmol, 1.00 eq.); HCl 3M into ethyl acetate (5 mL); ethyl acetate (5 mL). The product was obtained as a white powder (123 mg, quantitative yield).

^{1}H (500 MHz, CD_3OD) δ (ppm): 1.28 (s, 9H, H-12$_{[G0]}$), 1.33 (s, 18H, H-12$_{[G1]}$), 1.38 (s, 36H, H-12$_{[G2]}$), 1.43 (m, 12H, H-6 and H-7), 1.68 (m, 6H, H-8), 1.99 (m, 6H, H-5), 3.95 (s, 48H, H-15$_{[G2]}$), 3.97 (s, 12H, H-15$_{[G0]}$), 4.01 (s, 24H, H-15$_{[G1]}$), 4.15 (m, 6H, H-9), 4.33 (m, 36H, H-13$_{[G0,1]}$), 4.46 (m, 48H, H-13$_{[G2]}$), 4.52 (m, 12H, H-1 and H-4), [8.26-8.34] (bs, N-H), 8.42 (s, 3H, H-3).

^{13}C (125 MHz, CD_3OD) δ (ppm): [17.9-18.2] (C-12), 26.4 (C-7), 27.1 (C-6), 29.4 (C-8), 31.2 (C-5), 41.2 (C-15$_{[G2]}$), 42.2 (C-15$_{[G0,1]}$), [47.4-47.9] (C-1 and C-11), 51.6 (C-4), 66.4 (C-9), [67.2-68.6] (C-13), 128.7 (C-3), 137.9 (C-2), 168. 3 (C-14$_{[G2]}$), [170.8-174.1] (C-10 and C-14$_{[G0,G1]}$) [174.0-175.2] (C-16).

FTIR (ν_{max}/cm^{-1}, ATR): 3600-2600 (bs N-H^+ st), 2947-2633 (C-H st), 1749 (C=O st ester), 1655 (C=O st and N-H^+ δ), 1545 (N-H δ), 1473 (CH_2, CH_3 δ), 1379 (C-N st), 1221 (CO-O st).

D[*bis*GMPA,G4]-$(NH_3^+Cl^-)_{48}$

General procedure VI) D-[*bis*GMPA,G4](NHBoc)$_{16}$ (163 mg, 1.04x10^{-2} mmol, 1.00 eq.); HCl 3M into ethyl acetate (5 mL); ethyl acetate (5 mL). The product was obtained as a white powder (131 mg, quantitative yield).

^{1}H (500 MHz, CD_3OD) δ (ppm): 1.23 (s, 9H, H-12[G1]), 1.28 (s, 18H, H-12[G2]), 1.33 (s, 36H, H-12[G3]), 1.38 (s, 72H, H-12[G4]), 1.45 (m, 12H, H-6 and H-7), 1.68 (m, 6H, H-8), 1.99 (m, 6H, H-5), 3.96 (s, 96H, H-15[G4]), 4.01 (m, 84H, H-15[G1,2,3]), 4.15 (m, 6H, H-9), 4.33 (m, 84H, H-13[G1,2,3]), 4.46 (m, 96H, H-13[G4]), 4.56 (m, 12H, H-1 and H-4), [8.24-8.33] (bs, N-H), 8.44 (s, 3H, H-3).
Note: Some ^{1}H signals can be detected near 3.77 ppm, they result to the degradation of the bis-GMPA dendrons but they do not integrate for more than 5 % percent of the total of the bis-GMPA dendrons.

^{13}C (125 MHz, CD_3OD) δ (ppm): [17.9-18.2] (C-12), 26.4 (C-7), 27.1 (C-6), 29.4 (C-8), 31.2 (C-5), 41.2 (C-15[G4]), 42.3 (C-15[G1,2,3]), [47.4-47.7] (C-1 and C-11), 51.6 (C-4), [65.7-68.6] (C-9 and C-13), 128.9 (C-3), 137.7 (C-2), 168.3 (C-14[G4]), [170.9-174.1] (C-10 and C-14[G1,2,3]) [175.0-177.0] (C-16).

FTIR (ν_{max}/cm^{-1}, ATR): 3600-2600 (bs N-H^+ st), 3391 (N-H st), 2935-2615 (C-H st), 1749 (C=O st ester), 1655 (C=O st and N-H^+ δ), 1545 (N-H δ), 1477 (CH_2, CH_3 δ), 1385 (C-N st), 1211 (CO-O st).

7.1.4.2 - *Bis*-MPA dendronized hyperbranched polymers (DHPs)

General procedure XI): Alkyne functionalization of the commercial hyperbranched polyesters

Commercial hyperbranched polyesters (1.00 mol) were dissolved into dry THF. DPTS (0.50 mol per hydroxyl groups) and 4-pentynoic acid (1.25 mol per hydroxyl groups) were dissolved in dry THF. The reaction mixture was stirred under argon atmosphere and was cooled down to 0ºC. EDC·HCl (1.25 mol per hydroxyl groups) was added. The mixture was stirred under argon atmosphere at room temperature for 72 h. Then, the solvent was evaporated and the resulting product was dissolved in dichloromethane (100 mL) and washed twice with water (70 mL) and once with brine (70 mL). The organic layer was dried over anhydrous $MgSO_4$ and the dichloromethane was partially evaporated. The solution was carefully precipitated into cold hexane and recovered by further centrifugation at 4000 rpm for 30 min. The alkyne functionalized hyperbranched polymer was washed twice with cold hexane.

General procedure XII): copper(I) azide-alkyne cyloaddition reaction (CuAAC) for the synthesis of the DHPs

Alkyne functionalized hyperbranched polymer (1.00 mol) and N_3-[*bis*MPA,G3]-$(NHboc)_8$ (1.20 mol per mol of alkyne group) were dissolved into dimethylformamide in a Schlenk flask. 3 cycles vacuum-argon were made to remove O_2 and the reaction mixture was allowed to stir at 45ºC under argon atmosphere. $CuSO_4 5.H_2O$ (0.10 mol per mol of alkyne group), (*L*)-ascorbate (0.20 mol per mol of alkyne group) and TBTA (0.10 mol per mol of alkyne grous) were added to the copper dissolution. 3 cycles vacuum-Argon were made in order to remove the O_2 and the copper solution was stirred at 45ºC until it became yellow. Then, it was added through a cannula to the previous azide-alkyne reaction mixture. The reaction mixture was stirred under argon atmosphere at 45ºC during 2 days. Brine (250 mL) was added to the reaction

mixture and the product was extracted 3 times with ethyl acetate (3 x 150 mL). The organic phases were collected and combined and washed 3 times with brine (3 x 200 mL). The organic phase was dried over anhydrous $MgSO_4$ and the solvent was evaporated under reduce pressure to give a yellow oil. The crude product was filtrated through silica gel (DCM 100%) and the solvent was evaporated under reduced pressure to give a light yellow oil. The product was then dissolved in ethyl acetate (250 mL) and was washed twice with a solution of KCN (15 mg) in water (150 mL) and twice with brine (150 mL). The organic phase was dried over anhydrous $MgSO_4$ and concentrated by evaporation under reduced pressure. The product was precipitated by pouring into a mixture of hexane and ethyl acetate (9:1) and recovered by filtration. The products were obtained as white solids.

The *t*-Boc protective groups were removed according to the **general *procedure VI)*** (see page 321).

HPs[G2,G3,G4]-≡

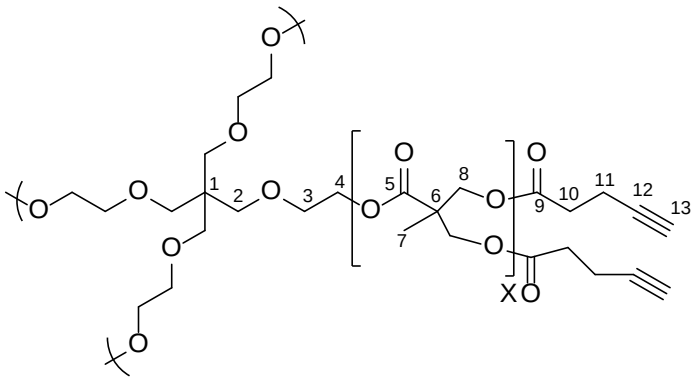

HP[G2]-≡

General procedure XI) HP[G2]-$(OH)_{16}$ (1.25 g, 0.74 mmol, 1.00 eq.); DPTS (1.79 g, 5.72 mmol, 12.00 eq.); 4-pentynoic acid (1.40 g, 14.29 mmol, 19.20 eq.) and EDC·HCl (2.74 g, 14.20 mmol, 19.20 eq.) into THF (100 mL). The product was obtained as a yellow solid (1.74 g, 81%).

^{1}H NMR ($CDCl_3$, 400 MHz) δ (ppm): 1.24 (m, 36H, H-7), 1.99 (m, 15H, H-13), 2.44 (m, 30H, H-11), 2.54 (m, 30H, H-10), 3.64 (m, 16H, H-2 and H-3), 4.24 (m, 56H, H-4 and H-8).

^{13}C NMR ($CDCl_3$, 100 MHz) δ (ppm): 14.4 (C-11), 17.9 (C-7), 33.3 (C-10), 46.7 (C-6), 65.5 (C-8), 69.5 (C-13), 82.5 (C-12), 171.3 (C-8 and C-9).

FTIR (ν_{max}/cm^{-1}, KBr): 3287 (≡C−H st), 2122 (C≡C st), 1740 (C=O st), 1245 (CO-O st).

SEC (*ref PMMA*): M_w 5000 g mol^{-1}; $Đ_M$ = 1.20.

HP[G3]-≡

General procedure XI) HP[G3]-$(OH)_{32}$ (1.25 g, 0.35 mmol, 1.00 eq.); DPTS (1.73 g, 5.54 mmol, 16.00 eq.); 4-pentynoic acid (1.36 g, 13.86 mmol, 39.60 eq.) and EDC·HCl (2.66 g, 13.86 mmol, 39.60 eq.) into THF (100 mL). The product was obtained as a yellow solid (1.66 g, 78%).

^{1}H NMR ($CDCl_3$, 400 MHz) δ (ppm): 1.24 (m, 84H, H-7), 1.99 (m, 31H, H-13), 2.44 (m, 64H, H-11), 2.54 (m, 64H, H-10), 3.64 (m, 16H, H-2 and H-3), 4.24 (m, 120H, H-4 and H-8).

^{13}C NMR ($CDCl_3$, 100 MHz) δ (ppm): 14.4 (C-11), 17.9 (C-7), 33.3 (C-10), 46.7 (C-6), 65.5 (C-8), 69.5 (C-13), 82.5 (C-12), 171.3 (C-8 and C-9).

FTIR (ν_{max}/cm^{-1}, KBr): 3285 (≡C−H st), 2119 (C≡C st), 1740 (C=O st), 1243 (CO-O st).

SEC (*ref PMMA*): M_w 7700 g mol^{-1}; $Đ_M$ 1.43.

HP[G4]-≡

General procedure XI) HP[G4]-$(OH)_{64}$ (1.25 g, 0.17 mmol, 1.00 eq.); DPTS (1.71 g, 5.46 mmol, 32.00 eq.); 4-pentynoic acid (1.34 g, 13.66 mmol, 80.35 eq.) and EDC·HCl (2.62 g, 13.66 mmol 80.35 eq.) into THF (100 mL). The product was obtained as a yellow solid (1.33 g, 64%).

^{1}H NMR ($CDCl_3$, 400 MHz) δ (ppm): 1.24 (m, 180H, H-7), 1.99 (m, 61H, H-13), 2.44 (m, 128H, H-11), 2.54 (m, 128H, H-10), 3.64 (m, 16H, H-2 and H-3), 4.24 (m, 248H, H-4 and H-8).

^{13}C NMR ($CDCl_3$, 100 MHz) δ (ppm): 14.4 (C-11), 17.9 (C-7), 33.3 (C-10), 46.7 (C-6), 65.5 (C-8), 69.5 (C-13), 82.5 (C-12), 171.3 (C-8 and C-9).

FTIR (ν_{max}/cm^{-1}, KBr): 3287 (≡C−H st), 2121 (C≡C st), 1741 (C=O st), 1243 (CO-O).

SEC (*ref PMMA*): M_w 15600 g mol^{-1}; $Đ_M$ 1.91.

DHPs[G 2+3, 3+3, 4+3](NHBoc)

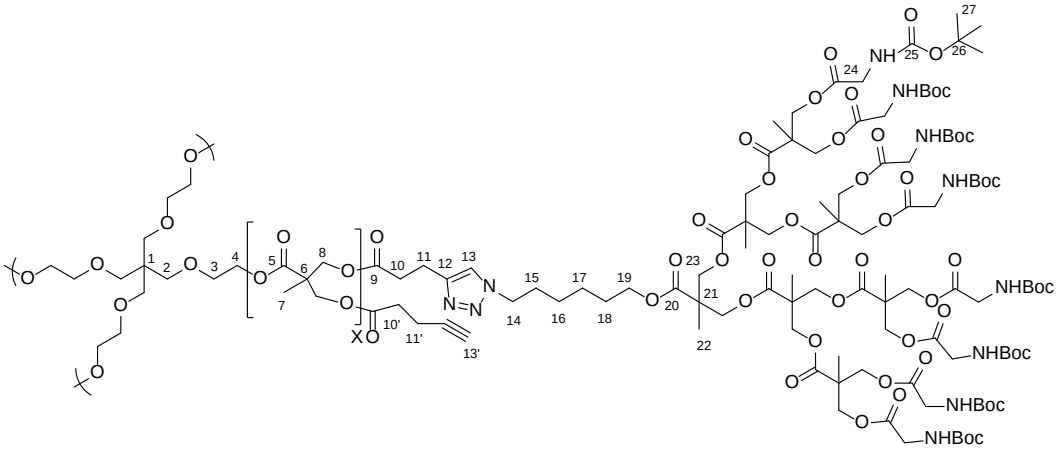

DHP[G2+3](NHBoc)

General procedure XII). HP[G2]-≡ (208 mg, $7x10^{-2}$ mmol, 1.00 eq.); N_3-[*bis*MPA,G3]-$(NHBoc)_8$ (3.00 g, 1.36 mmol, 19.2 eq.); $CuSO_4{,}5H_2O$ (33 mg, $1.13x10^{-1}$ mmol, 1.60 eq.); (*L*)-ascorbate (48 mg, $2.30x10^{-1}$ mmol, 6.40 eq.) and TBTA (60 mg, $1.13x10^{-1}$ mmol, 1.60 eq.) into dimethylformamide (15 mL). The product was obtained as a white solid (1.755 g, 65 %).

^{1}H NMR (400 MHz, $CDCl_3$) δ (ppm): 1.24 (411H, m, H-7, H-16, H-17 and H-22), 1.45 (1080H, s, H-28), 1.60 (30H, m, H-18), 1.90 (30H, m, H-15), 2.73 (30H, m, H-10), 2.97 (30H, m, H-11), 3.63 (16H, m, H-2 and H-3), 3.87 (240 H, d, J = 4.8 Hz, H-25), 4.26 (506H, m, H-4, H-8, H-19 and H-23), 4.43 (30H, m, H-14), 5.46 (bs, -NHBoc), 7.41 (15H, s, H-13).

^{13}C NMR (75 MHz, $CDCl_3$) δ (ppm): [17.5-17.7] (C-7 and C-22), 20.8 (C-11), 25.3 (C-17), 26.2 (C-16), 28.3 (C-18 and C-27), 30.2 (C-15), 33.3 (C-10), 42.2 (C-24), [46.4-46.6] (C-6 and C-21), 50.0 (C-14), [65.4-65.6] (C-8, C-19, C-23), 79.8 (C-26), 121.2 (C-12), 145.9 (C-13), 155.9 (C-25), [170.1- 171.5-171.8-172.1] (C-5, C-9, C-20 and C-24).

FTIR (ν_{max}/cm^{-1}, ATR): 3367 (N-H st), 2988-2935 (C-H st), 1738 (C=O st ester), 1711 (C=O st carbamate), 1514 (N-H δ), 1470 (CH_2, CH_3 δ), 1367 (C-N st), 1248 (CO-O st), 1155 (N-CO-O st), 1142 (O-C-C st).

EA (%): *Found:* C, 53.1; H, 7.6; N, 6.3; *Calc. for* $C_{1603}H_{2539}N_{165}O_{749}$: C, 53.3; H, 7.1; N, 6.4.

SEC (*ref PMMA*): Mw 32698 $g.mol^{-1}$; $Đ_M$ 1.16.

DHP[G3+3](NHBoc)

General procedure V) HP[G3]-≡ (215 mg, 3.53x10^{-2} mmol, 1.00 eq.); N_3-[*bis*MPA,G3]-$(NHBoc)_8$ (3.00 g, 1.36 mmol, 38.4 eq.); $CuSO_4$,$5H_2O$ (33 mg, 1.13x10^{-1} mmol, 3.20 eq.); (*L*)-ascorbate (48 mg, 2.30x10^{-1} mmol, 6.40 eq.) and TBTA (60 mg, 1.13x10^{-1}mmol, 1.60 eq.) into dimethylformamide (15 mL). The product was obtained as a white solide (1.937 g, 71 %).

^{1}H NMR (400 MHz, $CDCl_3$) δ (ppm): 1.24 (859H, m, H-7, H-16, H-17 and H-22), 1.43 (2232H, s, H-28), 1.65 (62H, m, H-18), 1.89 (62H, m, H-15), 2.73 (62H, m, H-10) 2.86 (62H, m, H-11), 3.64 (16H, m, H-2 and H-3), 3.87 (496H, m, H-25), 4.26 (1050H, m, H-4, H-8, H-19 and H-23), 4.44 (62H, m, H-14), 5.48 (bs, -NHBoc), 7.42 (31H, s, H-13).

^{13}C NMR (75 MHz, $CDCl_3$) δ (ppm): [17.5-17.8] (C-7 and C-22), 20.8 (C-11), 25.3 (C-17), 26.2 (C-16), 28.3 (C-18 and C-27), 30.2 (C-15), 33.3 (C-10), 42.2 (C-24), [46.4-46.7] (C-6 and C-21), 50.0 (C-14), [65.4-65.6] (C-8, C-19, C-23), 79.8 (C-26), 121.2 (C-12), 145.8 (C-13), 155.9 (C-25), [170.1-171.5-171.8-172.0] (C-5, C-9, C-20 and C-24).

FTIR (ν_{max}/cm^{-1}, ATR): 3354 (N-H st), 2986-2947 (C-H st), 1736 (C=O ester st), 1711 (C=O st carbamate), 1518 (N-H δ), 1462 (CH_2, CH_3 δ), 1367 (C-N st), 1244 (CO-O st), 1155 (N-CO-O st), 1124 (O-C-C st).

EA (%): *Found:* C, 53.2; H, 7.35; N, 6.5; *Calc. for* $C_{3317}H_{5247}N_{341}O_{1550}$: C, 53.3; H, 7.1; N, 6.4.

SEC (*ref PMMA*): Mw 42745 g.mol^{-1}; $Đ_M$ 1.14.

DHP[G4+3](NHBoc)

General procedure XII) HP[G4]-≡ (217 mg, 1.78x10^{-2} mmol, 1.00 eq.); N_3-[*bis*MPA,G3]-$(NHBoc)_8$ (3.00 g, 1.36 mmol, 76.8 eq.); $CuSO_4$,5H_2O (33 mg, 1.13x10^{-1}mmol, 6.40 eq.); (*L*)-ascorbate (48 mg, 2.30x10^{-1}mmol, 12.80 eq.); TBTA (60 mg, 1.13x10^{-1}mmol, 6.40 eq.). The product was obtained as a white solid (1.834 g, 77 %).

^{1}H NMR (400 MHz, $CDCl_3$) δ (ppm): 1.27 (1505H, m, H-7, H-16, H-17 and H-22), 1.43 (3816H, s, H-28), 1.66 (106H, m, H-18), 1.90 (106H, m, H-15), 2.44 (16H, m, H-11') 2.54 (16H, m, H-10'), 2.73 (106H, m, H-10) 2.96 (106H, m, H-11), 3.64 (16H, m, H-3 and H-4), 3.87 (848H, m, H-25), 4.26 (1838H, m, H-4, H-8, H-19 and H-23), 4.43 (106H, m, H-14), 5.51 (bs, -NHBoc), 7.41 (53H, s, H-13).

^{13}C NMR (75 MHz, $CDCl_3$) δ (ppm): [17.5-17.8] (C-7 and C-22), 20.8 (C-11), 25.3 (C-17), 26.2 (C-16), 28.3 (C-18 and C-27), 30.2 (C-15), 33.3 (C-10), 42.2 (C-24), [46.4-46.6] (C-6 and C-21), 50.0 (C-14), [65.4-65.6] (C-8, C-19, C-23), 79.8 (C-26), 121.2 (C-12), 145.8 (C-13), 155.9 (C-25), [170.0- 171.5-171.8-172.0] (C-5, C-9, C-20 and C-24).

FTIR (ν_{max}/cm^{-1}, ATR): 3393 (N-H st), 2980-2932 (C-H st), 1740 (C=O st ester), 1713 (C=O st carbamate), 1512 (N-H δ), 1460 (CH_2, CH_3 δ), 1365 (C-N st), 1244 (CO-O st), 1155 (N-CO-O st), 1136 (O-C-C st).

EA (%): *Found:* C. 53.3; H. 7.2; N. 6.4. *Calc. for* $C_{5761}H_{9077}N_{583}O_{2688}$: C, 53.4; H, 7.1; N, 6.3.

SEC (*ref PMMA*): Mw 58703 g.mol^{-1}; $Đ_M$ 1.21.

DHPs[G2+3,G3+3,G4+3]($NH_3^+Cl^-$)

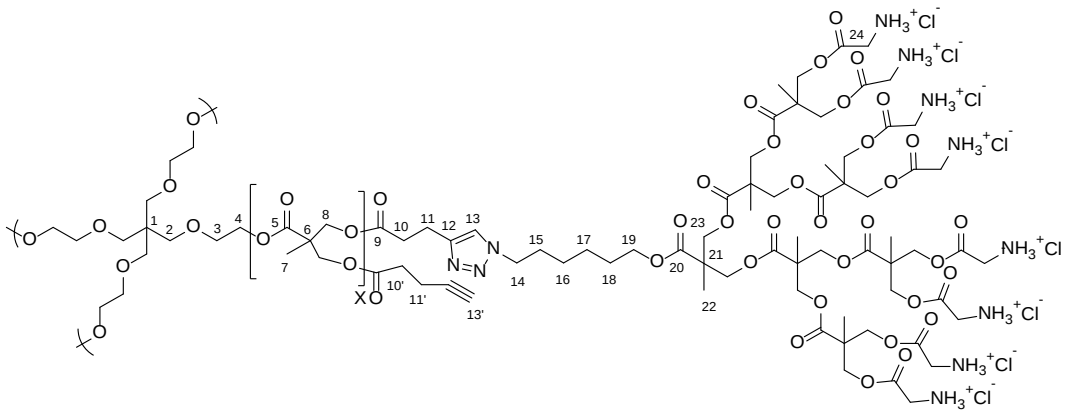

DHP[G2+3]($NH_3^+Cl^-$)

General procedure VI) DHP[G2+3](NHBoc) (873 mg, $2.42x10^{-2}$ mmol) and HCl 3M into ethyla acetate (20 mL) into ethyl acetate (5 mL). The product was obtained as a white powder (688 mg, quantitative yield).

^{1}H NMR (400 MHz, CD_3OD) δ (ppm): 1.34 (351H, m, H-7 and H-22), 1.44 (60H, m, H-16 and H-17), 1.70 (30H, m, H-18), 1.94 (30H, m, H-15), 2.76 (30H, m, H-10), 3.02 (30H, m, H-11), 3.66 m (16H, m, H-2 and H-3), 3.98 (240H, m, H-25), 4.17 (30H, m, H-19), 4.35 (236H, m, H-4, H-8 and H-23[G1,2]), 4.46 (270H, m, H-14 and H-23[G3]) 7.94 (15H, s, H-13).

^{13}C NMR (75 MHz, C_2D_6SO) δ (ppm): [17.1-17.4] (C-7 and C-22), 21.1 (C-11), 25.3 (C-17), 25.6 (C-16), 27.9 (C-18), 29.8 (C-15), 32.8 (C-10), [45.9-46.3] (C-6, C-24 and C-21), 49.3 (C-14), 65.7 (C-8, C-19, C-23), 122.1 (C-12), 145.1 (C-13), 167.1 (C-20[G3]), [171.6-172.1] (C-5, C-9 and C-20[G0,1,2]).

FTIR (ν_{max}/cm^{-1}, ATR): 3000-2600 ($N\text{-}H^+$ st), 2984-2941 (C-H st), 1732 (C=O st ester), 1605-1514 ($N\text{-}H^+$ δ), 1472 (CH_2, CH_3 δ), 1369 (C-N st), 1236 (CO-O st), 1128 (O-C-C st).

EA (%) *Found:* C, 41.5; H, 6.8; N, 7.9; *Calc. for* $C_{1003}H_{1699}N_{165}Cl_{120}O_{509}$: C, 42.3; H, 6.0; N, 8.1.

DHP[G3+3](NH$_3^+$Cl$^-$)

General procedure VI) DHP[G3+3]-(NHBoc) (1287 mg, 1.72x10^{-2} mmol) and HCl 3M into ethyl acetate (20 mL) into ethyl acetate (5 mL). The product was obtained as a white powder (1014 mg, quantitative yield).

^{1}H NMR (400 MHz, CD_3OD) δ (ppm): 1.35 (735H, m, H-7 and H-22), 1.43 (124H, m, H-16 and H-17), 1.71 (62H, m, H-18), 1.93 (62H, m, H-15), 2.77 (62H, m, H-10), 3.00 (62H, m, H-11), 3.68 (16H, m, H-2 and H-3), 3.99 (496H, m, H-25), 4.17 (62H, m, H-19), 4.35 (492H, m, H-4, H-8 and H-23[1,2G]), 4.46 (558H, m, H-14 and H-23[3G]), 7.94 (31H, s, H-13).

^{13}C NMR (75 MHz, C_2D_6SO) δ (ppm): [17.1-17.4] (C-7 and C-22), 24.8 (C-11), 25.6 (C-16), 27.9 (C-18), 30.0 (C-15), 32.8 (C-10), [45.9-46.3] (C-6, C-24 and C-21), 49.3 (C-14), 65.7 (C-8, C-19, C-23), 122.1 (C-12), 145.1 (C-13), 167.1 (C-20[G3]), [171.6-172.1] (C-5, C-9 and C-20[G0,1,2]).

FTIR (ν_{max}/cm^{-1}, ATR): 3000-2600 (bs, N-H$^+$ st), 3001-2851 (C-H st), 1734 (C=O st ester), 1605-1510 (N-H$^+$ st), 1474 (CH_2, CH_3 δ), 1302 (C-N st), 1223 (CO-O st), 1126 (O-C-C st).

EA (%): *Found*: C, 41.5; H, 7.0; N, 7.6; *Calc. for* $C_{2077}H_{3507}N_{341}O_{1054}$: C, 42.3; H, 6.0; N, 8.1.

DHP[G4+3](NH$_3^+$Cl$^-$)

General procedure VI) DHP[G4+3]-(NHBoc) (1184 mg, 9.14x10^{-3} mmol) and HCl 3M into ethyl acetate (20 mL) into ethyl acetate (5 mL).The product was obtained as a white powder (937 mg, quantitative yield).

^{1}H NMR (400 MHz, CD_3OD) δ (ppm): 1.35 (1293H, m, H-7 and H-22), 1.45 (212H, m, H-16 and H-17), 1.70 (106H, m, H-18), 1.95 (106H, m, H-15), 2.34 (16H, m, H-11'), 2.48 (16H, m, H-12'), 2.78 (106H, m, H-10) 3.02 (106H, m, H-11), 3.68 (16H, m, H-2 and H-3), 3.99 (848H, m, H-25), 4.17 (106H, m, H-19), 4.35 (884H, m, H-4, H-8 and H-23[1,2G]), 4.47 (954H, H-14 and H-23[3G]), 7.94 (53H, s, H-13).

^{13}C NMR (75 MHz, C_2D_6SO) δ (ppm): [17.2-17.5] (C-7 and C-22), 21.1 (C-11), 24.8 (C-17), 25.7 (C-16), 28.0 (C-18), 29.8 (C-15), 32.9 (C-10), [46.0-46.3] (C-6, C-24 and C-21), 49.3 (C-14), 65.8 (C-8, C-19, C-23), 122.1 (C-12), 145.2 (C-13), 167.2 (C-20[G3]), [171.6-172.2] (C-5, C-9 and C-20[G0,1,2]).

FTIR (ν_{max}/cm^{-1}, ATR): 3000-2600 (bs, N-H$^+$ st), 2999-2947 (C-H st), 1730 (C=O st ester), 1605-1514 (N-H$^+$ δ), 1472 (CH_2, CH_3 δ), 1369 (C-N st), 1225 (CO-O st), 1128 (O-C-C st).

EA (%): *Found:* C, 41.9; H, 6.7; N, 7.6; *Calc. for* $C_{3641}H_{6105}Cl_{424}N_{583}O_{1840}$: C. 42.65; H, 6.0; N, 8.0.

7.1.5- Other derivatives

7.1.5.1- Rhodamine B derivatives

azido rhodamine B (N_3-RhB)

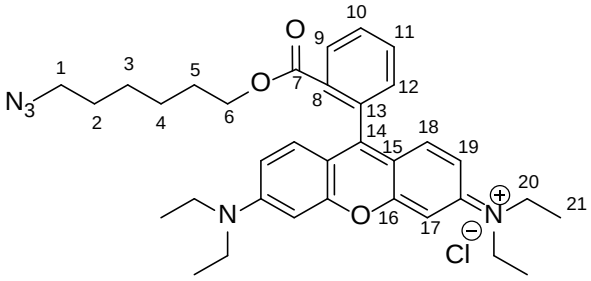

Rhodamine B (1.00g, 2.09 mmol, 1.00 eq.) was dissolved into dry dichloromethane (70 mL). 6-azidohexan-1-ol (602 mg, 4.18 mmol, 2.00 eq.) and DPTS (492 mg, 1.67 mmol, 0.80 eq.) were added to it. The reaction mixture was stirred at 45ºC under argon atmosphere. DCC (861 mg, 4.18 mmol, 2.00 eq.) was dissolved into dry dichloromethane (10 mL) and added drop wise to the reaction mixture. It was stirred at 45ºC under atmosphere overnight, protected from the light. Then, the white precipitate, N,N'-dicyclohexylurea (DCU), was filtered off. Dichloromethane was added (20 mL) to the filtrate. It was washed once with HCl 0.1 M (100 mL) and twice with brine (2 x 100 mL). The organic phase was dried over anhydrous $MgSO_4$ and the solvent was evaporated under reduce pressure. The crude product was purified on silica gel (DCM : MeOH = ramp from 10:0 to 9:1) to give a purple solid (934 mg, 74 %).

^{1}H NMR (400 MHz, $CDCl_3$) δ (ppm): 1.32 (t, J = 8 Hz, 12H, H-21), 1.49 (m ,4H, H-3 and H.4), 1.65 (m, 2H, H-2), 1.87 (m, 2H, H-5), 3.23 (t, J = 4 Hz, 2H, H-1), 3.63 (q, J = 8 Hz, H-20), 4.02 (t, J = 8 Hz, 2H, H-6), 6.84 (d, J = 2.4 Hz, 2H, H-17), 6,90 (dd, J =9,6 Hz, J = 2.4 Hz, 2H, H-19), 7.07 (d, 2H, H-18), 7.31 (dd, J = 7.6 Hz, J = 1.2 Hz, 1H, H-12), 7.74 (td, J = 8.0 Hz, J = 1.2 Hz, 1H, H-10), 7.82 (td, J = 7.6 Hz, J = 1.2 Hz, 1H, H-11), 8.29 (dd, J = 8.0 Hz, J = 1.2 Hz, 1H, H-9).

^{13}C NMR (75MHz, $CDCl_3$) δ (ppm): 12.6 (C-21), 25.4 (C-4), 26.3 (C-3), 28.2 (C-5), 28.6 (C-2), 46.2 (C-20), 51.3 (C-1), 65.5 (C-6), 96.5, 113.6, 114.3, 126.3, 128.5, 130.0, 130.3, 130.4, 131.3, 133.1, 133.5, 155.5, 157.7, 165.1 (C-7).

Note: the counter-ions are a mixture of $C_7H_7SO_3^-$ and Cl^-; $C_7H_7SO_3^-$ was observed in ^{1}H NMR (2.26 (s, 2.4H), 7.07 (d, J = 8.0 Hz, 1.6H), 7.90 (d, J = 8.0 Hz, 1.6H)), and ^{13}C NMR (21.3, 127.0, 129.7, 139.4, and 158.9).

FTIR (ν_{max}/cm^{-1}, ATR): 2928-2852 (C-H st), 2095 (N_3 st), 1715 (C=O st), 1645-1585 (C-Car).

MS (ESI^+) *m/z (%)*: *568.4 (100)* $[C_{34}H_{42}N_5O_3]^+$.

EA (%): *Found:* C, 66.3; H, 7.0; N, 10.0; S, 3.7; *Calc. for* $C_{34}H_{42}N_5O_3^+$,Cl^-/$C_7H_7SO_3^-$: C, 66.8; H, 6.7; N, 9.9; S, 3.5.

low-water soluble modified rhodamine B (RhB(C17)$_2$)

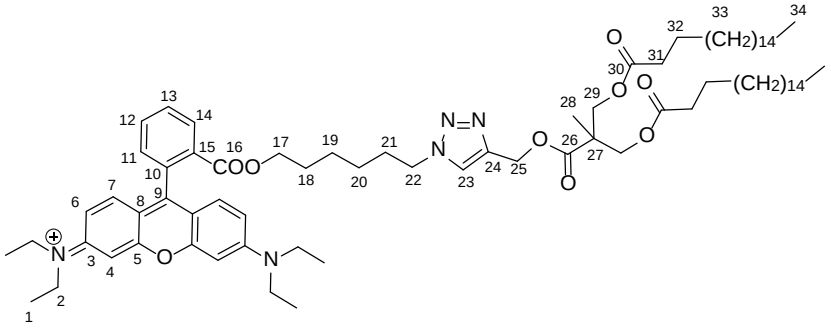

N_3-RhB (200 mg, 0.33 mmol, 1.00 eq.) and ≡-[*bis*MPA,G1]-$(C17)_2$ (280 mg, 0.40 mmol, 1.20 eq.)were dissolved into dimethylformamide (7 mL) in a Schlenk flask. 3 cycles vacuum-argon were made to remove the O_2. The reaction mixture was allowed to stir under argon atmosphere at 45ºC. 3 cycles of vacuum–argon were made to remove O_2. $CuSO_4.5H_2O$ (9.8 mg, 0.03 mmol, 0.10 eq.), (*L*)-ascorbate (13.1 mg, 0.07 mmol, 0.20 eq.) and TBTA (17.6 mg, 0.003 mmol, 0.01 eq.) were dissolved into dimethylformamide (3 mL) in a second Schlenk flask. 3 cycles vacuum-argon were made in order to remove the O_2 and the copper solution was stirred at 45ºC during 15 min. Then, it was added through a cannula to the previous azide-alkyne reaction mixture. The reaction mixture was stirred at 45ºC during 1 day under argon atmosphere protected from the light. Then, brine (100 mL) was added to the reaction mixture. The product was extracted three times with ethyl acetate (3 x 70 mL). The organic phases were dried over anhydrous $MgSO_4$ and the solvent was evaporated under reduced pressure. The crude product was purified on silica gel (DCM:MeOH = ramp from 100:0 to 92:8) to give a purple solid (199 mg, 46%).

^{1}H NMR (400 MHz, $CDCl_3$) δ (ppm): 0.87 (t, J = 6.4 Hz, 6H, H-34), 1.24 (m, 59H, H-28 and H-33), 1.33 (m, 16H, H-1, H-19 and H-20), 1.42 (m, 2H, H-18), 1.55 (m, 4H, H-32), 1.88 (m, 2H, H-21), 2.26 (t, J = 7.2 Hz, 4H, H-31), 3.65 (m, 8H, H-2), 4.00 (t, J = 6.0 Hz, H-17), 4.20 (ABq, J = 11.2 Hz, ΔνAB = 17.4 Hz, 4H, H-29), 4.40 (t, J = 5.6 Hz, 2H, H-22), 5.24 (s, 2H, H-25), 6.92 (m, 4H, H-4 and H-6), 7.08 (d, J = 9.6 Hz, 2H, H-7), 7.29 (d, J = 6.8 Hz,

1H, H-11), 7.74 (t, J = 8.0 Hz, 1H, H-13), 7.79 (t, J = 7.2 Hz, 1H, H-12), 7.97 (s, 1H, H-23), 8.28 (d, J = 8.0 Hz, 1H, H-14).

^{13}C NMR (100 MHz, $CDCl_3$) δ (ppm): 12.7 (C-1), 14.1 (C-34), 17.8 (C-28), 22.6 (C-33), 24.8 (C-32), 25.2 (C-19), 26.1 (C-20), 28.12(C-18), [29.1-29.7] (C-33), 30.0 (C-21), 31.9 (C-33), 34.0 (C-31), 46.3 (C-2), 50.7 (C-22), 58.2 (C-26), 64.9 (C-29), 65.5 (C-17), 96.5 (C-4), 113.5 (C-6), 130.1, 130.2, 130.4, 131.3, 131.4, 133.0, 133.4, 155.5, 157.7, 158.8, 165.1 (C-16), 172.6 (C-26), 173.2 (C-30).
Note: The signals of the carbons C-23 and C-24 could not be observed in the ^{13}C NMR spectrum. The ^{1}H-^{13}C correlation could be observed in the ^{1}H-^{13}C HSQC spectrum at 7.97(^{1}H signal)-125.6 (^{13}C signal).

FTIR (ν_{max}/cm^{-1}, ATR): 2916-2 851 (C–H st), 1 740-1 715 (C=O), 1 649-1 587 (C–Car).
Note: a peak corresponding to water is observed at 3406 cm^{-1}.

MS (MALDI$^+$) *m/z (%)*: *1273.1 (100)* $[C_{78}H_{122}N_5O_8]^+$.

EA (%): *Found:* C, 69.6; H, 9.4; N, 5.45; *Calc. for* $C_{78}H_{122}N_5O_9Cl_1$: C, 71.6; H, 9.4; N, 5.35.

DHP[G3+3](NHBoc),(RhB)

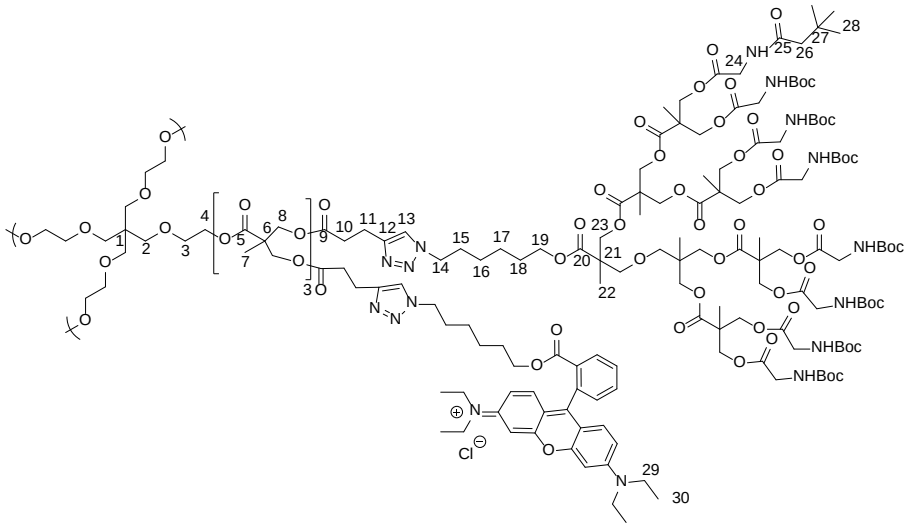

First, HP[G3]-≡ (60.37 mg, 9.92x10^{-2} mmol, 1.00 eq.) and N_3-[*bis*MPA,G3]-(NHboc)$_8$ (526 mg, 2.38x10^{-2} mmol, 24.00 eq.) were dissolved into dimethylformamide (4 mL) in a Schlenk flask. 3 cycles vacuum-argon were made to remove air and the reaction mixture was allowed to stir at 45ºC under argon atmosphere. $CuSO_45.H_2O$ (7.01 mg, 2.38x10^{-2} mmol, 2.40 eq.), (*L*)-ascorbate (9.42 mg, 4.76x10^{-2} mmol, 4.80 eq.) and TBTA (12.61 mg, 2.38x10^{-2} mmol, 2.40 eq.) were dissolved into dimethylformamide (3 mL). 3 cycles vacuum-Argon were made in order to remove the O_2 and the copper solution was stirred under argon pressure at 45ºC during 15 min. Then, it was added through a cannula to the previous azide-alkyne reaction mixture. The reaction mixture was stirred under argon atmosphere at 45ºC during 2 days. The crude products were purified in the same manner than the one described in the general procedure **XII**).

Second, the obtained solids with free alkynes remaining, DHP[G3+3](NHBoc),-(≡), (435 mg, 7.35x10^{-2} mmol, 1.00 eq.) and N_3-RhB (53 mg, 1.88x10^{-2} mmol, 12.00 eq.) were dissolved into dimethylformamide (4 mL). 3 cycles vacuum-argon were made to remove air and the reaction mixture was stirred under argon atmosphere at 45ºC. $CuSO_4$, 5.H_2O (4.12 mg, 1.39x10^{-2} mmol, 2.40 eq.), (*L*)-ascorbate (5.51 mg, 2.78x10^{-2} mmol, 4.80 eq.) and TBTA (3.70 mg, 6.98x10^{-2} mmol, 0.80 eq.) were dissolved into dimethylformamide (3 mL). 3 cycles vacuum-argon were made to remove air and the copper dissolutions were stirred under argon atmosphere at 45ºC during 15 min. Then,

it was added through a cannula to the previous azide-alkyne reaction mixture. The reaction mixture was stirred under argon atmosphere at 45ºC during 2 day keeping it away from the light. Then, a dissolution of $NaHSO_4$ (saturated in water) (100 mL) was added to the reaction mixture. The product was extracted 3 times with a mixture of hexane and ethyl acetate (1:2). The organic phases were collected and combined together. They were washed 3 times with brine (3 x 150 mL), once with a solution of KCN (15 mg) in water (150 mL) and repetitively with brine (150 mL) until the aqueous phase remained colorless. The organic phases were dried over anhydrous $MgSO_4$ and the solvent were evaporated to give dark pink solids. The crude products were dialyzed (cellulose membrane, 3500 Da) against methanol during 2 days to give the pure product as dark pink solid (349 mg, 50 %).

^{1}H NMR (400 MHz, $CDCl_3$) δ (ppm): 1.24 (m, 796H, H-7, H-16, H-17, H-22 and H-30), 1.42 (s, 1728H, H-28), 1.65 (m, 62H, H-18), 2.00 (m, 62H, H-15), 2.89 (m, 62H, H-10), 3.17 (m, 62H, H-11), 3.64 (m, 72H, H-2, H-3 and H-29), 3.87 (m, 384H, H-24), 4.25 (m, 854H, H-4, H-8, H-19 and H-23), 4.55 (m, 62H, H-14), 5.50 (bs, -NHBoc), [6.7-7.2] (bs, H_{ar} RhB), [7.30-8.29] (m, bs, H-13 and H_{ar} RhB).

FTIR (ν_{max}/cm^{-1}, ATR): 3383 (N-H st), 2978-2933 (C-H st), 1740 (C=O st ester), 1713 (C=O st carbamate), 1512 (N-H δ), 1460 (CH_2, CH_3 δ), 1367 (C-N st), 1248 (CO-O st), 1157 (N-CO-O st), 1130 (O-C-C st).

DHPs[G3+3]-($NH_3^+Cl^-$),(RhB)

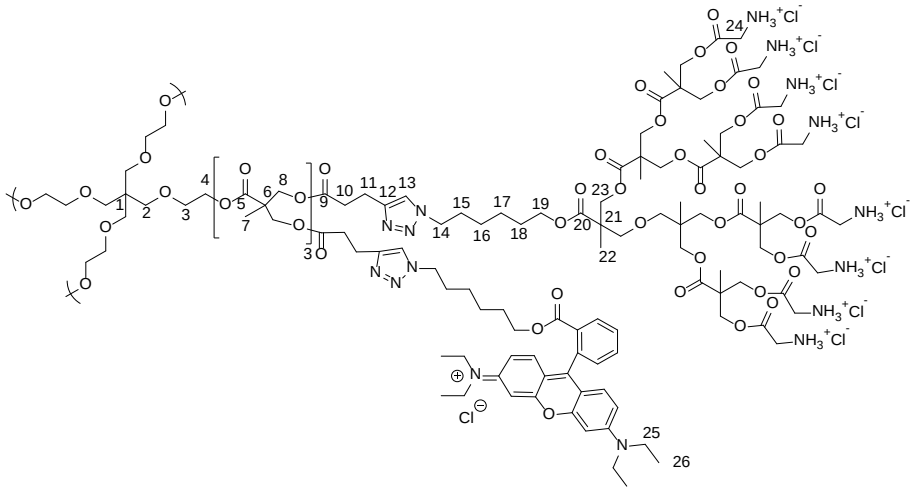

General procedure VI) DHP[G3+3](NHBoc),(RhB) (261 mg, $3.75x10^{-3}$ mmol) and HCl 3M into ethyl acetate (8 mL) into ethyl acetate (2 mL).The product was obtained as a pink solid (193 mg, quantitative yield).

^{1}H NMR (400 MHz, CD_3OD) δ (ppm): 1.34 (m, 796H, H-7, H-16, H-17, H-22 and H-26), 1.70 (m, 62H, H-18), 1.95 (m, 62H, H-15), 2.77 (m, 62H, H-10), 3.03 (m, 62H, H-11), 3.67 (m, 72H, H-2, H-3 and H-25), 3.98 (m, 384H, H-24), 4.16 (m, 62H, H-19), 4.34 (m, 408H, H-4, H-8 and H-23[G1,2]), 4.45 (m, 446H, H-14 and H-23[G3]), [6.7-7.2] (bs, H_{ar} RhB), [7.30-8.29] (bs, H-13 and m H_{ar} RhB).

FTIR (ν_{max}/cm^{-1}, ATR): 3600-2600 (N-H^+ st), 2947-2870 (C-H st), 1736 (C=O st ester), 1512 (N-H^+ δ), 1472 (CH_2, CH_3 δ), 1242 (CO-O st), 1132 (O-C-C st).

7.1.5.2- Antimalarial drugs in their base form

General procedure XIII): synthesis of the lipophilic base antimalarial drugs forms starting from their hydrophilic salt forms

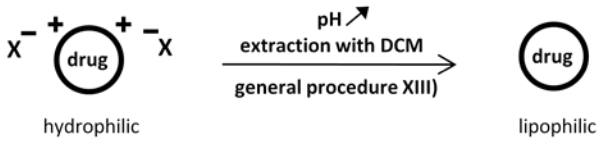

Commercial antimalarial drug in its salt form was dissolved into distilled water (25 mL) NaOH was added to brought pH up to 12. A precipitate appeared. The product was extracted 3 times with dichloromethane (3 x 10 mL). The organic phase was dried over anhydrous MgSO4 and the dichloromethane was evaporated under reduce pressure to give the pure antimalarial drug in its lipophilic base form.

Chloroquine base (CQb)

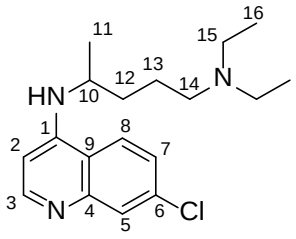

General procedure XIII). CQ-salt (1000 mg, 1.94 mmol). The pure product was obtained as a white solid (566 mg, 91 %).

^{1}H NMR (400 MHz, CD_2Cl_2) δ (ppm): 0.98 (t, J = 9.6 Hz, 6H, H-16), 1.30, (d, J = 6.4 Hz, 3H, H-11), 1.59 (m, 2H, H-13), 1.65 (m, 1H, H-12), 1.74 (m, 1H, H-12'), 2.42 (t, J = 6.8 Hz, 2H, H-14), 2.49 (q, J = 6.8 Hz, 4H, H-15), 3.71 (m, 1H, H-10), 5.47 (d, J = 6.8 Hz, 1H, N-*H*), 6.46 (d, J = 5.2 Hz, 1H, H-2), 7.34 (dd, J = 9.2 Hz and J = 2.4 Hz, 1H, H-7), 7.75 (d, J = 8.8 Hz, 1H, H-8), 7.89 (d, J = 2Hz, 1H, H-5), 8.47 (d, J = 5.6 Hz, H-3).

^{1}H NMR (400 MHz, $(CD_3)_2SO$) δ (ppm): 0.89 (t, J = 7.2 Hz, 6H), 1.22 (d, J = 6.4 Hz, 3H), 1.46 (m, 3H), 1.67 (m, 1H), 2.33 (t, J = 6.8 Hz, 2H), 3.38 (q, J = 7.6 Hz, 4H), 3.36 (s, 1H), 3.70 (m, 1H), 6.49 (d, J = 5.6 Hz, 1H), 6.91 (d, J = 8.0 Hz, 1H), 7.41 (dd, J = 8.8 Hz and J = 2.0 Hz, 1H), 7.76 (d, J = 2.0 Hz, 1H), 8.35 (s, 1H), 8.37 (d, J = 2.4 Hz, 1H).

^{13}C NMR (100 MHz, CD_2Cl_2) δ (ppm): 11.9 (C-16), 20.4 (C-11), 24.4 (C-13), 35.0 (C-12), 47.3 (C-15), 48.9 (C-10), 53.0 (C-14), 99.9 (C-2), 118.1 (C-9), 122.2 (C-8), 125.2 (C-7), 129.2 (C-5), 134.9 (C-6), [149.7-150.1] (C-1 and C-4), 152.6 (C-3).

FTIR (ATR, cm^{-1}): 3244 (N-H st), 2968 and 2800 (C-H C-H_{ar} st), 1466 (-CH_2-, CH_3 δ).

EA (%): *Found:* C, 67.5; H, 8.45; N, 13.0; *Calc. for* $C_{18}H_{26}N_3Cl_1$: C, 67.6; H, 8.2; N, 13.1.

Chloroquine salt (CQs)

Commercial product (Aldrich), white solid.

^{1}H NMR (400 MHz, $(CD_3)_2SO$) δ (ppm): 0.89 (t, J = 7.2 Hz, 6H), 1.08 (d, J = 6.0 Hz, 3H), 1.42 (m, 3H), 1.56 (m, 1H), 2.62 (m, 6H), 3.36 (s, 1H), 3.60 (m, 1H), 3.80 (bs), 6.38 (d, J = 5.6 Hz, 1H), 6.91 (d, J = 7.6 Hz, 1H), 7.28 (dd, J = 8.8 Hz and J = 2.4 Hz, 1H), 7.61 (d, J = 2.4 Hz, 1H), 8.22 (d, J = 5.6 Hz, 1H), 8.26 (d, J = 9.2 Hz, 1H).

FTIR (ATR, cm^{-1}): 3658-2052 (bs, N-H^+ st), 2970 and 2865 (C-H, C-H_{ar} st) 1458 (-CH_2-, CH_3 δ).

EA (%): *Found:* C, 39.6; H, 6.5; N, 7.8; *Calc. for* $C_{18}H_{32}N_3O_8Cl_1P_2$: C, 41.9; H, 6.25; N, 8.1.

Primaquine base (PQb)

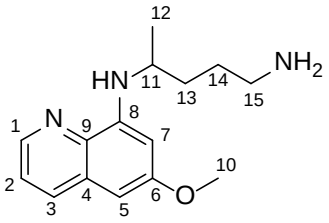

General procedure XIII). PQ-salt (350 mg, 0.77 mmol). The product was obtained as a brown gel (199 mg, 99 %).

^{1}H NMR (400 MHz, CD_2Cl_2) δ (ppm): 1.29 (d, J = 6.4 Hz, 3 H, H-12), 1.56 (bs, H-13, H-14 and
-NH_2), 1.70 (m, 1H, H-13), 2.68 (t, J = 6.8 Hz, 2H, H-15), 3.62 (qd, 1H, H-11), 3.87 (s, 3H, H-10), 6.06 (d, J = 7.6 Hz, 1H, -NH), 6.28 (d, J = 2.4 Hz, H-5), 6.35 (d, J = 2.4 Hz, 2H, H-7), 7.31 (dd, J = 8 Hz and J = 4 Hz, 1H, H-2), 7.94 (dd, J = 8.0 Hz and J = 1.6 Hz, 1H, H-3), 8.50 (dd, J = 4.4 Hz and J = 1.6 Hz, 1H, H-1).

^{1}H NMR (400 MHz, $(CD_3)_2SO$) δ (ppm): 1.21 (d, J = 6.0 Hz, 3 H), [1.35-1.71] (m, 4H), 2.54 (t, J = 6.8 Hz, 2H), 3.59 (m, 1H), 3.82 (s, 3H), 6.12 (d, J = 8.4 Hz, 1H), 6.24 (d, J = 2.4 Hz, 1H), 6.35 (d, J = 2.4 Hz, 1H), 7.42 (m, 1H), 8.07 (dd, J = 8.4 Hz and J = 1.6 Hz, 1H), 8.53 (dd, J = 4.4 Hz and J = 1.6 Hz, 1H).

^{13}C NMR (100 MHz, CD_2Cl_2) δ (ppm): 20.8 (C-12), 30.9 (C-14), 34.6 (C-13), 42,8 (c-15), 48.5 (C-11), 55.7 (C-10), 92.0 (C-7), 97.0 (C-5), 1223 (C-2), 130.5 (C-4), 130.5 (C-4), 135.2 (C-3), 135.9 (C-9), 144.8 (C-1), 145.7 (C-8), 160.1 (C-6).

FTIR (ATR, cm^{-1}): 3385 (N-H st), 2933 and 2852 (C-H, C-H_{ar} st), 1456 (-CH_2-, CH_3 δ).

EA (%): *Found:* C, 67.85; H, 9.0; N, 16.5; *Calc. for* $C_{15}H_{21}N_3$: C, 69.5; H, 8.2; N, 16.2.

Primaquine salt (PQs)

Commercial product (Aldrich), orange solid.

^{1}H NMR (400 MHz, $(CD_3)_2SO$) δ (ppm): 1.22 (d, J = 6.4 Hz, 3 H), [1.55-1.73] (m, 4H), 2.78 (t, J = 7.2 Hz, 2H), 3.66 (m, 1H), 3.82 (s, 3H), 4.89 (bs), 6.16 (d, J = 9.2 Hz, 1H), 6.29 (d, J = 2.4 Hz), 6.49 (d, J = 2.4 Hz, 1H), 7.43 (m, 1H), 8.08 (dd, J = 8.4 Hz and J = 1.6 Hz, 1H), 8.54 (dd, J = 4.4 Hz and J = 1.6 Hz, 1H).

FTIR (ATR, cm^{-1}): 3416-2154 (bs, N-H^+ st), 2866 (C-H, C-H_{ar} st).

EA (%): *Found:* C, 38.8; H, 6.1; N, 9.35; *Calc. for* $C_{15}H_{21}N_3O_9P_2$: C, 39.6; H, 5.9; N, 9.2.

Quinacrine base (QNb)

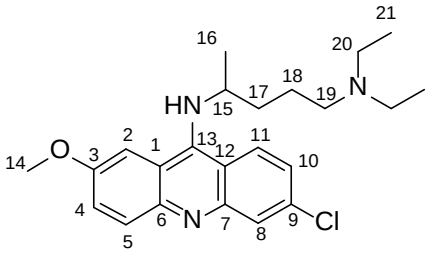

General procedure XIII). QN-salt (1000 mg, 2.11 mmol). The pure product was obtained as a yellow gel (822 mg, 97 %).

^{1}H NMR (400 MHz, CD_2Cl_2) δ (ppm): 0.91 (t, J = 7.2 Hz, 6H, H-21), 1.28 (d, J = 6.4 Hz, 3H, H-16), 1.57 (m, 2H, H-18), 1.70 (m, 2H, H-17), 2.34 (td, J = 7.2 Hz and J = 1.2 Hz, 2H, H-19), 2.41 (q, J = 7.2 Hz, 4H, H-20), 3.97 (s, 3H, H-14), 4.05 (qd, 1H, H-15), 4.56 (d, J = 10.4 Hz, 1H, -NH), 7.27 (d, J = 2.8 Hz, H-11), 7.34 (dd, J = 9.2 Hz and J = 2.4 Hz, 1H, H-3), 7.41 (dd, J = 9.6 Hz and 2.8 Hz, 1H, H-9), 7.96 (d, J = 9.2 Hz, 1H, H-8), 8.02 (d, J = 2.0 Hz, 1H, H-5), 8.06 (d, J = 9.6 Hz, 1H, H-2).

^{1}H NMR (400 MHz, $(CD_3)_2SO$) δ (ppm): 0.75 (t, J = 6.8 Hz, 6H), 1.25 (m, 1H), 1.35 (m, 3H), 1.56 (m, 1H), 1.73 (m, 1H), 2.15 (t, J = 6.4 Hz, 2H), 2.21 (q, J = 7.2 Hz, 4H), 3.94 (s, 3H), 3.98 (m, 1H), 6.30 (d, J = 10.0 Hz, 1H), 7.38 (dd, J = 9.2 Hz and J = 2.0 Hz), 7.43 (dd, J = 9.6 Hz and J = 2.8 Hz, 1H), 7.59 (d, J = 2.4 Hz, 1H), 7.87 (d, J = 9.2 Hz, 1H), 7.92 (d, J = 2.0 Hz, 1H), 8.31 (d, J = 9.2 Hz, 1H).

^{13}C NMR (100 MHz, CD_2Cl_2) δ (ppm): 12.1 (C-21), 22.6 (C-16), 24.7 (C-17), 37.5 (C-18), 47.4 (C-20), 53.3 (C-19), 56.1 (C-14), 56.6 (C-15), 99.9 (C-11), 117.9 (C-1), 119.9 (C-9), [124.9-125.1-125.2] (C-2, C-3 and C-9), 128.9 (C-5), 132.2 (C-8), 134.9 (C-4), [147.6-148.9] (C-6 and C-7), 149.9 (C-13), 156.7 (C-10).

FTIR (ATR, cm^{-1}): 3312 (N-H st), 2968 and 2800 (C-H $C\text{-}H_{ar}$ st), 1466 ($\text{-}CH_2\text{-}$, CH_3 δ).

EA (%): *Found:* C, 67.7; H, 7.8; N, 9.9; *Calc. for* $C_{23}H_{30}N_3OCl$: C, 69.1; H, 7.6; N, 10.5.

Quinacrine salt (QNs)

Commercial product (Aldrich), yellow solid.

^{1}H NMR (400 MHz, $(CD_3)_2SO$) δ (ppm): 1.08 (t, J = 7.2 Hz, 6H), 1.58 (m, 2H), 1.64 (d, J = 6.5 Hz, 3H), 1.82 (m, 1H), 2.08 (m, 1H), [2.86-3.01] (m, 6H), 4.00 (s, 3H), 4.53 (m, 1H), 7.56 (dd, J = 9.2 Hz and J = 2.0 Hz), 7.71 (dd, J = 9.2 Hz and J = 1.0 Hz, 1H), 7.96 (d, J = 9.2 Hz, 1H), 8.04 (d, J = 2.0 Hz, 1H), 8.43 (bs, 1H), 9.44 (bs, 1H), 10.07 (bs, 1H).

FTIR (ATR, cm^{-1}): 3533-2490 (bs, $N\text{-}H^{+}$ st).

EA (%): *Found:* C, 54.25; H, 7.1; N, 8.3; *Calc. for* $C_{23}H_{32}N_3OCl_3$: C, 58.4; H, 6.8; N, 8.9.

7.1.5.3- Tris(benzyltriazolylmethyl)amine (TBTA)

Benzyl azide (BnN_3)

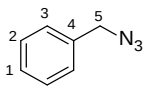

Sodium azide (2.09 g, 32.15 mmol, 1.10 eq.) was dissolved into dimethyl sulfoxide (200 mL) at 50ºC. Benzyl bromide (3.47 mL, 29.23 mmol, 1.00 eq.) was added drop wise. The reaction mixture was stirred at 50ºC during 3 hours. Then, water (200 mL) was added to it and the product was extracted with diethyl ether (3 x 100 mL). The organic phase was washed with brine (3 x 100 mL) and was dried over anhydrous MgSO4. The solvent was evaporated under reduce pressure. The product was obtained as a light yellow oil (3.81 g, 98%).

^{1}H NMR (400 MHz, $CDCl_3$) δ (ppm): 4.35 (s, 2H, H-5), [7.32-7.43] (m, 5H, H-1 to H-3).

^{13}C NMR (100 MHz, $CDCl_3$) δ (ppm): 54.7 (C-5), 128.2 (C-3), 128.3 (C-1), 128.8 (C-2), 135.3 (C-4).

Tris(benzyltriazolylmethyl)amine (TBTA)

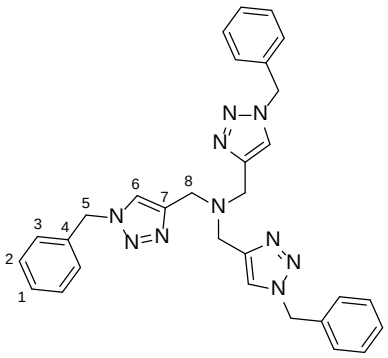

Tripropargylamine (1.26 mL, 8.89 mmol, 1.00 eq.) was dissolved into acetonitrile (15 mL). Benzylbromide (3.82 g, 28.71 mmol, 4.50 eq.), 2,6-lutidine (1.03 mL, 8.89 mmol, 1.00 eq.) and $Cu(MeCN)_4^+$,PF_6^- (129 mg, $3.6x10^{-1}$ mmol, $3.9x10^{-2}$ mmol) were successively added to the reaction mixture. The reaction mixture was stirred at room temperature during 2 days. The product precipitated as white needle crystals. It was recovered by filtration and was washed with cold methanol (2.00 g, 42 %).

^{1}H NMR (400 MHz, $CDCl_3$) δ (ppm): 3.65 (s, 6H, H-8), 5.48 (s, 6H, H-5), [7.23-7.35] (m, 15H, H-1, H-2 and H-3), 7.62 (s, 3H, H-6).

^{13}C NMR (100 MHz, $CDCl_3$) δ (ppm): 47.2 (C-8), 54.0 (C-5), 123.7 (C-6), 128.02 (C-3), 128.5 (C-1), 129.0 (C-2), 135.4 (C-4), 144.5 (C-7).

MS (ESI^+) *m/z (%)*: *553.0 (15)* $[C_{30}H_{30}N_{10},Na]^+$; *531.1 (100)* $[[C_{30}H_{30}N_{10},H]^+$.

7.2- Working protocols

7.1.1- General working protocols and apparatus

Ultraviolet-visible absorbance measurements were performed with a Varian Cary50 Probe UV-visible spectrophotometer (unless otherwise specified) and **Fluorescence** measurements were performed with a Perkin Elmer LS 55 fluorescent spectrophotometer (unless otherwise specified) using quartz cells. UV-Vis and fluorescence measurements were performed in distilled water or DMSO spectrophotometric grade (Sigma-Aldrich®).

Liophilization processes were performed with a Teslar Cryodos 50 liofilizador. Samples were frozen in liquid nitrogen prior to liophilization.

Vigorous **rotational stirring** was performed with an IKA KS 130 basic orbital shaker.

Dynamic light scattering measurements of the amphiphilic Janus and pDNA/siRNA dendriplexes samples were performed with a Brookhaven Instruments Corporation 90 plus particle size analyzer with a laser with a wavelength of 658 nm at concentrations of 1 mg/mL and at 25ºC. Dynamic light scattering measurements of the HDLDBCs samples were performed with Malvern Instruments Nano ZS with a laser with a wavelength of 633 nm at concentrations of 1 mg/mL at 25, 37 and 45ºC. Dynamic light scattering measurements of the Pluronic® F-127 sample were performed in the same conditions but at a concentration of 2 mg/mL, *i.e.* > CMC. The samples were not filtrated before measurements and the results are given applying two mathematical data treatments, the intensity average and the number average.

Transmission electron microscopy (TEM) images were obtained with a FEI TECNAI T20 with beam power 200kV using holey carbon film 300 mesh coppered grids provided by Agar Scientific Ltd. A droplet of an aqueous solution of the samples at the concentration of 1 mg/mL was deposited on the grid and let penetrate during 30 seconds; the excess of the aqueous solution was removed using a filter paper. A phosphotungstic acid, 3% aqueous solution was used as negative stain; a droplet of the stain solution was deposited on the sample grid and let penetrate during 10 seconds; the excess of the staining aqueous solution was removed using a filter paper. The grid was dried during at least 24 hours under atmospheric pressure. The average size of the different aggregates measured by TEM was obtained by comparing at least 100 aggregates in at least 4 photos.

Cryogenic transmission electron microscopy (cryoTEM) images were obtained with a FEI TECNAI T20 with beam power 200kV using quantifoil carbon film 300 mesh coppered grid or lacey carbon film 300 mesh coppered grids provided by Agar Scientific Ltd. Quantifoil grids were previously ionized using a plasma cleaner whereas lacey carbon grids were previously ionized using UV light irradiation or using a glow-discharge apparatus. A droplet (60 µL) of an aqueous solution of the samples was deposited on the grid. Sample vitrification was automatically processed using a vitrobot (FEI) and performed in liquid ethane. A specific sample holder, Gatan for cold samples, was used to stock the grids in liquid nitrogen prior to observation with the microscope.

7.2.2- Study of the amphiphilic dendritic derivatives for camptothecin delivery

Bis-GMPA dendrons degradation

The *bis*-GMPA dendrons degradation was observed by ^{1}H NMR. 10 mg of the dendrons were dissolved into 0.7 µL of D_2O or D_2O+H_2SO_4. The samples were stocked at 37ºC while ^{1}H NMR spectra were recorded at different times.

Formation of the aggregates in water

As the majority of the **Janus dendrimers** could not be directly solubilized in water at room temperature, all the aggregates formed in water by the Janus dendrimers were prepared following the oil-in-water procedure.[95] Each Janus dendrimer was dissolved at a concentration of 1 mg/mL in dichloromethane, a volatile and water-immiscible solvent. An appropriate volume of distilled water was added to obtain a final concentration of 1 mg/mL in water. The mixtures were vigorously rotationally stirred at room temperature under ventilation until the organic solvent was completely evaporated.

The aggregates formed by the **HDLDBCs** and the Pluronic® F-127 were prepared taking advantages of the LCST of the materials. An appropriate volume of distilled water was added to each derivative in order to obtain a final concentration of 1 or 2 mg/mL in water. The samples were placed 30 min at 4ºC to favor the total dissolution of the derivatives in water. Then, they were slowly heated to room temperature.[193]

[95] J. Movellan, P. Urbán *et al.*, *Biomaterials*, **2014**, 35, 7940.

[193] I Jiménez-Pardo, Hidrogeles termosensibles y fotopolimerizables derivados de Pluronic® para aplicaciones biomédicas, **2014**, Univerisdad de Zaragoza.

Determination of the critical aggregation concentration (CAC) using the nile red technique

The CAC of the amphiphilic Janus dendrimers, HDLDBCs and Pluronic® F-127 was determined using nile red as a solvatochromic fluorophore which fluorescence spectrum (λ_{ext} = 550 nm) is different according to the hydrophilicity of its environment.[191] Below the CAC, the nile red is in a hydrophilic environment, *i.e.* water, and presents low fluorescence emission (λ_{max} = 653 nm). In contrast, above the CAC, Nile red migrates to the lipophilic inner part of the aggregates and presents intense fluorescence emission (λ_{max} ≈ 630 nm) (**figure C_7-1**).

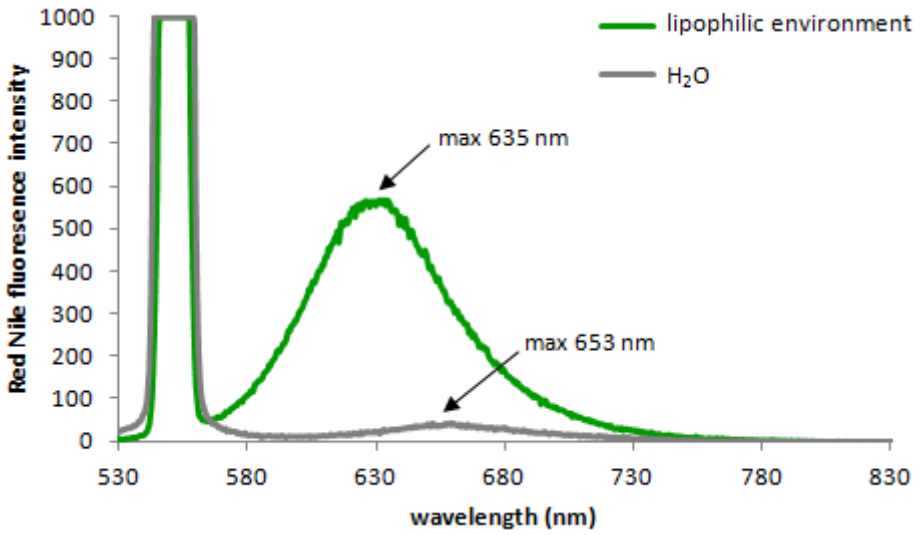

Figure C_7-1: Fluorescence spectra of Nile red after excitation at 550 nm in an hydrophilic environment, *i.e.* water, (λ_{max} = 653 nm) and in an lipophilic environment, *i.e.* after encapsulation within **$(NH_3^+Cl^-)_8$[*bis*MPA,G3]-[*bis*MPA,G2]$(C17)_4$** (λ_{max} = 635 nm).

The aqueous dissolution of the samples with a volume of 2 mL and an adequate concentrations ranging were prepared as described before (protocol A). Nile red was dissolved in ethanol at a concentration of 2.5 x 10^{-1} mM and 10 µL of this solution was added to the dendritic derivatives solutions. In the specific case of **$(NH_3^+Cl^-)_4$[*bis*MPA,G2]-[*bis*MPA,G2]$(C17)_4$**, the concentration of the Nile red solution was lower (0.83 x 10^{-1} mM) in order to avoid precipitation.

[191] M.C.A. Stuart, *J. Phys. Org. Chem.*, **2005**, 18, 929.

The mixtures were vigorously rotationally stirred at room temperature for 1 hour in the dark with an orbital shaker. The emission spectrum of each sample dissolution was measured (λ_{max} ≈ 660 nm or λ_{max2} = 635 nm) after excitation at λ_{exc} = 550 nm.

This technique was preferred to the pyrene technique[242] employed before in the Crystal Liquid and Polymers group due to interactions between the terminal amino groups of the dendritic derivatives and pyrene that modified the pyrene fluorescent properties.

Encapsulations of camptothecin (CPT) and modified rhodamine B (RhB(C17)$_2$)

The solvent diffusion technique was employed to **encapsulate camptothecin (CPT)** inside the aggregates.[203] Firstly, CPT was dissolved in DMSO and was added to the previously prepared aggregates under the following conditions: 100 µg of CPT per mg of dendritic derivatives were added and the volume of DMSO was adjusted to obtain a final concentration of CPT in DMSO of 200 µg/mL. The mixtures were stirred at 4 °C for 12 hours to allow CPT to reach the lipophilic core of the aggregates. DMSO was removed by dialysis against distilled water at 4 °C using a 1000 Dalton membrane. The volume of the samples after dialysis was measured. The non-encapsulated camptothecin precipitated during the dialysis and was removed by filtration to obtain the dendrimer/CPT conjugates.

The concentration of encapsulated camptothecin was directly measured by fluorescence (λ_{max} = 436 nm and λ_{exc} = 368 nm) in DMSO. Two aliquots, 400 µL each, were freeze-dried and then redissolved in DMSO for to break down the aggregates and allow the immediate and total release of camptothecin.

[242] J. Aguiar, P. Carpena, J.A. Molina-Bolívar, C. Carnero Ruiz, On the determination of the critical micelle concentration by the pyrene 1:3 ratio method, *J. Coll. Interface Sci.*, **2003**, 258, 116-122.

[203] I. Jiménez-Pardo *et al.*, *Macromol. Biosci.*, **2015**, 15, 1381.

The encapsulation process was repeated at least two times for each dendritic derivatives/CPT conjugate.

The oil-in-water technique was employed to **encapsulate modified rhodamine (*RhB(C17)$_2$*)** within the amphiphilic Janus. Each Janus dendrimer was dissolved at a concentration of 1 mg/mL in dichloromethane. An appropriate amount of RhB(C17)$_2$ was added to each dissolution in order to obtain a concentration of RhB(C17)$_2$ equal to 0.15 mg/mL in dichloromethane. Then, an appropriate volume of distilled water was added to obtain a final concentration of 1 mg/mL of amphiphilic Janus dendrimer in water. The mixtures were vigorously rotationally stirred at room temperature under ventilation until the organic solvent was completely evaporated. As any precipitate was observed in the final aqueous dissolution, it was assumed that all RhB(C17)$_2$ was encapsulated. The encapsulation process was repeated at least two times for each dendritic derivatives/RhB(C17)$_2$ conjugate.

The two previous encapsulation protocols were employed for the **RhB(C17)$_2$ and CPT co-encapsulation** within the amphiphilic Janus dendrimers. Firstly, RhB(C17)$_2$ was encapsulated within the dendrimers according to the oil-in-water procedure and secondly, CPT was encapsulated within the dendrimers/RhB(C17)$_2$ conjugates following the solvent diffusion procedure. The quantity of CPT that could be encapsulated within the dendritic nanocarriers was directly determined by fluorescence as explained before. As the excitation and maximal fluorescence emission wavelengths of CPT were lower (368 and 413 nm, respectively) than the ones of RhB(C17)$_2$ (540 and 580 nm respectively), any interference occurred during the measurements.

The encapsulation process was repeated at least two times for each dendritic derivatives/RhB(C17)$_2$/CPT conjugate.

Modified rhodamine B (RhB(C17)$_2$) and rhodamine B releases

The **RhB(C17)$_2$ release** outside the dendrimer/RhB(C17)$_2$ conjugates was studied by dialysis. 2 mL of the dendrimer/RhB(C17)$_2$ conjugates containing 0.15 mg/mL of encapsulated RhB(C17)$_2$ were dialyzed against distilled water (200 mL) using a dialysis membrane (1000 Da cut-off). Aliquots (2mL) were withdrawn from the water dialysis at different times during 72 hours. The quantity of RhB(C17)$_2$ in the water dialysis was measured by fluorescence at different times (λ_{exc} = 540 and λ_{max} =580 nm). Additionally, unmodified water soluble rhodamine B fluorophore was encapsulated within **(NH$_3^+$Cl$^-$)$_4$ [*bisG*MPA,G2]-[*bis*MPA,G1](C17)$_2$** in order to compare its release profile with RhB(C17)$_2$.

Evaluation of the anti-Hepatitis C activity of the dendritic derivatives/ camptothecin conjugates

(protocol carried out by Rafael Clavería-Gimeno)

These biological studies were performed with the highly permissive **cell clone Huh 7-Lunet**, as well as **Huh 7 cells containing subgenomic (HCV) replicons** I389luc-ubi-neo/NS3-3'/5.1 (Huh 5-2), I377NS3-3'/wt (Huh 9-13), or I389/hygro-ubi-NS3-3/5.1 (a kind gift from Dr. V. Lohmann and Dr. R. Bartenschlager).[243] Briefly, this system allowed the efficient propagation of genetically modified HCV RNAs (replicons) in a human hepatoma cell line (Huh).

[243] a) J. Courcambeck, M. Bouzidi, R. Perbost, B. Jouirou, N. Amrani, P. Cacoub, G. Pepe, J.M. Sabatier, P. Halfon, Resistance of hepatitis C virus to NS3-4A protease inhibitors: mechanisms of drug resistance induced by R155Q, A156T, D168A and D168V mutations, *Antiviral Therapy*, **2006**, 11, 847-855; b) S. Susser, J. Vermehren, N. Forestier, M.W. Welker, N. Grigorian, C. Fuller, D. Perner, S. Zeuzem, C. Sarrazin, Analysis of long-term persistence of resistance mutations within the hepatitis C virus NS3 protease after treatment with telaprevir or boceprevir, *J. Clin. Virol.*, **2011**, 52,321-327; c) K.J. Blight, J.A. McKeating, C.M. Rice, Highly permissive cell lines for subgenomic and genomic hepatitis C virus RNA replication, *J. Virol.*, **2002**, 76, 13001-13014; d) V. Lohmann, F. Korner, J. Koch, U. Herian, L. Theilmann, R. Bartenschlager, Replication of subgenomic hepatitis C virus RNAs in a hepatoma cell line, *Science*, **1999**,285,110-113.

The amount of RNA that has been transcribed and translated is determined through the quantification of a reporter contained in the replicon system (luciferase). The amount of luminescence detected (after adding the substrate specific for this enzyme) is proportional to the virus replication rate. Cells were grown in Dulbecco's Modified Eagle's Medium (DMEM) supplemented with 10% heat-inactivated fetal bovine serum, 1x non-essential amino acids, 100 IU/mL penicillin, 100 μg/mL streptomycin, and 250 μg/mL geneticin (G418).

The **antiviral assays** for determining the efficacy of the dendritic derivative/CPT conjugates were performed as described in the literature.[243,244] Briefly, Huh5-2 cells were seeded at a density of 7.10^3 cells per well in a tissue culture-treated white 96-well view plate (Techno Plastic Products AG) in complete DMEM supplemented with 250 μg/mL G418. After incubation for 24 h at 37 °C, the medium was removed and two-fold serial dilutions in complete DMEM (without G418) of the dendritic derivative/CPT and dendritic derivatives/ RhB$(C17)_2$/CPT conjugates were added in a total volume of 100 μL (final CPT concentrations from 1 or 2 μM to 0 μM). After 3 days of incubation at 37 °C, luciferase activity was determined using the Bright-Glo Luciferase Assay System (20 μL). The luciferase signal was measured using a Synergy HT 50 Multimode Reader (BioTek Instruments). Luciferase signal levels obtained in each assay were normalized using internal patterns previously determined in Huh5-2 cells. The 50 % effective concentration (EC_{50}) was defined as the concentration of compound that reduced the luciferase signal by 50%.

The **cytostatic assays** for measuring the cell viability of all the dendritic derivatives/CPT and dendritic derivatives/RhB$(C17)_2$/CPT conjugates were performed as described in the literature.[243,244] Briefly, Huh5-2 cell lines were seeded at a density of $7x10^3$ cells per well of a 96-well plate in complete DMEM

[244] A. Urbani, R. Bazzo, M. C. Nardi, D. O. Cicero, R. De Francesco, C. Steinkuhler, G. Barbato, The metal binding site of the hepatitis C virus NS3 protease. A spectroscopic investigation, *J. Biol. Chem.* **1998**, 273, 18760-18769.

(with the appropriate concentrations of G418 in the case of Huh 5-2). Serial dilutions of the dendrimer/CPT aggregates in complete DMEM (without G418) were added 24 h after seeding. Cells were allowed to proliferate for 3 days at 37 °C. Cell culture medium was removed and cell number was determined by CellTiter 96 AQueous One Solution Cell Proliferation Assay. The 50% cytostatic concentration (CC_{50}) was determined employing the dose–response equation (*i.e.*, Hill equation). All experiments on Huh5-2 cells were carried out in triplicate and each experiment was repeated on three different days.

Cellular uptake of the dendrimer/CPT and dendrimer/RhB(C17)$_2$/CPT conjugates *(protocol carried out by Rafael Clavería-Gimeno)*

The cellular uptake of the dendrimer/CPT conjugates and dendrimer/ RhB(C17)$_2$/CPT conjugate were studied by **flow cytometric assays** performed with an ImageStream X Amnis® Cytometer and the results were analyzed with an IDEAS® software. Cytometry assays were performed in a similar way that antiviral and cytostatic assays. After being seeded, cells were incubated with free CPT, dendrimer/CPT conjugates, dendrimer/RhB(C17)$_2$ conjugates and dendrimer/RhB(C17)$_2$/CPT conjugates with a concentration of 2 µM of CPT for 3 days at 37ºC. A control treated only with DMEM was made. Then, cells were picked up in a volume of 200 µl and were washed three times with PBS by centrifugation at 1500 rpm. 30 µL of propidium iodide (PI) solution (1 mg/mL) was added to the cells and the samples were shaken in a vortex and incubated in darkness for 3 minutes to mark the cellular cycle before being introduced into the cytometer. RhB(C17)$_2$ (λ_{ext} = 507 nm, λ_{dect} = 529 nm) and PI (λ_{ext} = 535 nm, λ_{dect} = 610 nm) were detected in two different channels.

7.2.3- Study of the globular dendritic derivatives for gene transfection

Determination of the amount of copper in the globular dendritic derivatives after the CuAAC

The quantities of copper that remained entrapped in the final globular dendritic derivatives after the CuAAC were determined by **inductively coupled plasma atomic emission spectroscopy (ICP-AES)** performed on a Thermo elemental IRIS intrepid apparatus, with a limit of quantification (LOQ) of 15 ppm.

pH measurements

The pH of the solutions was measured after each addition by a Hanna HI 8424 pH meter with a HI 1110B electrode.

The **titrations** were carried out by adding small volumes of NaOH (0.1 M) into an aqueous dissolution of the dendritic derivatives. After each addition of NaOH, the pH of the samples was measured. Theoretical pKA calculations were performed by MarvinSketch® program.[245]

The **"*buffer sponge*" ability** of the dendritic derivatives was determined by dissolving 4 mg of them into 20 mL of a 0.1 M NaCl aqueous dissolution. pH was set to 11 using NaOH (1M) and titrated to 3.2 by successive additions of 10 µL of HCl 0.1M.[215a]

[245] Mª Elena Fuentes Paniagua, Tesis Mª Elena Fuentes Paniagua - Síntesis de marcromléculas dendríticas catiónicas de estructuras carbosilano y sus aplicaciones en biomedicina, **2015**, Univerisdad de Alcalá de Henares,
[215a] J.C. Sunshine *et al*., *Mol. Pharm.*, **2012**, 9, 3375.

Complexation of pDNA and siRNA by the globular dendritic derivatives *(protocols carried out in collaboration with Rebeca González)*

Dendriplexes were freshly prepared by adding pDNA or siRNA to dendritic derivatives solutions diluted in serum-free medium (SFM). The solutions were mixed by vigorous pipetting and incubated for 20 min at room temperature. **Gel retardation assays**[246] were performed to study pDNA and siRNA complexation by the dendritic derivatives. 15 µL of freshly prepared dendriplexes at different ratios, from 1:1 to 200:1 (w:w), containing 0.25 µg of pDNA (pEGFP) or 0.3 µg siRNA (siGFP), were mixed with appropriate amounts of 6X loading buffer (Takara, UK) and then electrophoresed on a 0.8% (w/v) agarose gel in 1X TAE (40 mM TRIS/HCl, 1% acetic acid, 1 mM EDTA, pH 7.4) containing SyberSafe for 30 min at 95 V. The location of pDNA and siRNA in the gel was analyzed on a G:Box UV transilluminator (Syngene, UK).

Dendriplexes were freshly prepared by adding pDNA or siRNA to dendritic derivatives solutions diluted in a NaCl-HEPES buffer, containing 6 mM of HEPES buffer pH 7.4 and 144 mM of NaCl, filtered through a 0.2 µm pore size cellulose membrane 25 mm filter (ChemLab®). The solutions were mixed by vigorous pipetting and incubated for 30 min at room temperature. **ζ potential** measurements[246] were performed to study the pDNA and siRNA complexation with a Malvern™ Instruments Nano ZS using DTS 1070 folded capillary cells (provided by Iesmat, S.A.). The dendriplexes were prepared at a concentration of 10 µg/mL of pDNA or siRNA and with concentrations of pseudodendrimers comprised between 4.5 and 2000 µg/mL. Three measurements with a minimum of 10 scans were carried out for each sample.

[246] D. Shcharbin, E. Pedziwiatr, M. Bryszewska. How to study dendriplexes I: Characterization, *J. Control. Release*, **2009**, 135, 186-97.

Biocompatibility of the bis-GMPA dendrons and globular dendritic derivatives *(protocols carried out by Rebeca González)*

Mesenchymal stem cells (MSCs) from mousse origin (Lonza) were grown in DMEM/F12 (Biowest) supplemented with 10% FBS (Gibco), 1% Penicillin/ Streptomycin/Amphotericin (Biowest) and 2 mM L-glutamine (Biowest) and maintained under hypoxic conditions (3% O_2). Human cervix cancer cell line HeLa were maintained in DMEM High Glucose (w/Glutamine, Biowest) supplemented with 10% FBS and 1% Pencillin/Streptomycin/Amphotericin at 37 ºC and 5% CO_2 in a humidified atmosphere.[184]

For **cytotoxicity evaluation**, cells were seeded at a density of 5×10^3 cells per well in 96 multiwell culture plates. After 24 h incubation, the culture medium was removed and 100 µL of DMEMc with increasing concentrations of the corresponding dendritic derivatives were added (0.1–1 mg/mL). After 24–72 h the solutions were replaced by 100 µL of fresh DMEM and 10 µL of Alamar Blue® dye solution (Thermo Fisher Scientific). Upon entering the cells, resazurin, the active ingredient of the dye, was reduced to resorufin, which produced very bright red fluorescence. After incubation for 3 h at 37 ºC, fluorescence was read (λ_{ext} = 530, λ_{em} = 590) on a Synergy HT (BioTek, USA) plate reader. Untreated cells incubated with medium without dendritic derivatives were used as control and cytotoxicity is expressed as the relative viability of the cells compared to control cells (considered as 100% viability). Four replicates per concentration were assayed in each of the three independent experiments performed.

[184] R. González, Estudio de dendrímeros y nanopartículas de oro para su uso en tratamientos antitumorales, **2017**, Universidad de Zaragoza.

In vitro transfection

(protocols carried out by Rebeca González)

Mesenchymal stem cells (MSCs) from mousse origin (Lonza) were grown in DMEM/F12 (Biowest) supplemented with 10% FBS (Gibco), 1% Penicillin/ Streptomycin/Amphotericin (Biowest) and 2 mM L-glutamine (Biowest) and maintained under hypoxic conditions (3 % O_2). Human cervix cancer cell line HeLa, MDCK-GFP (Madin-Darby Canine Kidney expressing GFP) and SKOV3-Luc derived from human ovarian carcinoma and expressing Luciferase (kindly obtained from Cancer Research-UK Cell services) were maintained in DMEM High Glucose (w/Glutamine, Biowest) supplemented with 10% FBS and 1% Pencillin/ Streptomycin/Amphotericin at 37 ºC and 5% CO_2 in a humidified atmosphere.[184]

MSCs and HeLa were seeded at a density of 1×10^4 cells per well in 96-well plates 24 h prior to *in vitro* transfection. In positive control experiments, pEGFP, siGFP and siLuc were mixed with Lipofectamine (Thermo Fisher Scientific) at a 3:1 w:w ratio in SFM. 50 µL of dendriplexes consisting of 0.1–0.4 µg of pEGFP and the adjusted amount of dendritic derivatives to obtain the desired ($w_{dend.}/w_{pDNA/siRNA}$) ratios were prepared in SFM. After incubation at room temperature for 20 min, complexes were added in duplicate to each well and incubated for 4 h. EGFP expression was evaluated by fluorescence microscopy (Olympus IX81 Olympus, Spain) at 24-48 h. For quantification of EGFP by flow cytometry, cells were seeded at a density of 5×10^5 cells per well in 6-well plates and incubated with 750 µL of dendriplexes with 5-100 nM siGFP for 4h. For quantification of Luciferase with Bright-Glo™ Assay Reagent (Promega), after 72h of transfection with siLuc, media was changed for 100 µL fresh complete DMEM, 100 µL of Bright-Glo™ Assay Reagent (lysis buffer and luciferin) were added and cells were lysed by pipetting. After 5 minutes, all the content was transferred to an opaque 96 well plate (Nunc) in dark. Luminiscence was read was read on a Synergy HT (Biotek).

7.2.4- Study of the dendritic derivatives as antimalarial nanocarriers

Encapsulation of the antimalarial drug within the dendritic derivatives

The oil-in-water procedure was employed to **encapsulate** the hydrophilic form of the antimalarial drugs **(PQ-salt, QN-salt and CQ-salt)** within the **HDLDBCs**.[95] The HDLDBCs were dissolved into DCM at a concentration of 1 mg/mL. An appropriate volume of a dissolution of the hydrophilic drugs in distilled water (1 mg/mL) was added to obtain final concentrations of HDLDBC of 1 mg/mL in water. The samples were vigorously rotationally stirred at room temperature under ventilation until complete evaporation of DCM (around 2 hours). The non-encapsulated drugs were removed by dialysis (regenerated cellulose membrane, MW 1000 Da cut off) against distilled water (200 mL) at 4ºC during 16h. The final volumes of the dissolutions were measured. The amounts of encapsulated drug were indirectly measured: the quantities of drugs were determined in the dialysis water by UV-VIS spectrometry (λ_{CQs} = 345 nm, λ_{PQs} =259 nm, λ_{Qns} = 280 nm) and were subtracted to the initial quantity of drug.

The oil-in-water procedure was employed to **encapsulate** the hydrophilic form of the antimalarial drugs **(PQ-salt, QN-salt and CQ-salt)** within the **DHPs** was performed following the oil-in-water procedure. The DHPs and the hydrophilic drugs were dissolved into distilled water at the respective concentrations of 5 mg/mL of DHPs and 2.5 mg/mL of drugs. A volume of dichloromethane equivalent to the one of distilled water was added. The samples were vigorously rotationally stirred at room temperature under ventilation until complete evaporation of DCM. The non-encapsulated drugs

[95] J. Movellan, P. Urbán *et al.*, *Biomaterials*, **2014**, 35, 7940.

were removed by dialysis (regenerated cellulose membrane, MW 1000 Da cut-off) against distilled water (200 mL) at 4ºC during 16h. The final volumes of the dissolutions were measured. The final volume of the dissolutions was measured. The amounts of encapsulated drugs were indirectly measured: the quantities of drugs were determined in the dialysis water by UV-VIS spectrometry (λ_{CQs} = 345 nm, λ_{PQs} =259 nm, λ_{Qns} = 280 nm) and were subtracted to the initial quantity of drug.

The oil-in-water procedure was performed to **encapsulate** the hydrophobic form of the antimalarial drugs **(PQ-base, QN-base and CQ-base)** within the **HDLDBCs**. The HDLDBCs were dissolved in water at the concentration of 1.00 mg/mL. The lipophilic drugs were dissolved into dichloromethane at the concentration of 1.00 mg/mL and were mixed with the HDLDBCs dissolutions at the ratio ($w_{HDLDBCs}/w_{drug}$) 1/1. The samples were vigorously rotationally stirred at room temperature under ventilation until complete evaporation of dichloromethane. NaOH (1 M in distilled water) was added to the dissolutions until pH 10 was reached. The non-encapsulated drugs precipitated and were removed by filtration through 0.2 µm pore size cellulose membrane 25 mm filter (ChemLab®). The final volumes of the dissolutions were measured. The amounts of encapsulated drugs were directly measured: the quantities of drugs were determined by withdrawing two aliquots of 100 µL, diluting them with 1.90 mL of DMSO and measuring their UV-VIS absorbance (λ_{CQb} = 340 nm, λ_{PQb} = 366 nm, λ_{Qnb} = 420 nm).

The oil-in-water procedure was performed to **encapsulate** the hydrophobic form of the antimalarial drugs **(PQ-base, QN-base and CQ-base)** within the **DHPs**. The DHPs were dissolved in water at the concentration of 5.00 mg/mL. The lipophilic drugs were dissolved into dichloromethane at the concentration of 2.50 mg/mL for CQ-base, 3.75 mg/mL for PQ-base and 0.50 mg/mL for QN-base and were mixed with the DHPs dissolutions at the ratios (w_{HDLDBC}/w_{CQb}) 1/0.5, (w_{DHPs}/w_{PQb}) 1/0.75 and (w_{HDLDBC}/w_{QNb}) 1/0.1. The samples

were vigorously rotationally stirred at room temperature under ventilation until complete evaporation of dichloromethane. NaOH (1 M in distilled water) was added to the dissolutions until pH 10 was reached. The non-encapsulated drugs precipitated and were removed by filtration through 0.2 µm pore size cellulose membrane 25 mm filter (ChemLab®). The final volumes of the dissolutions were measured. The amounts of encapsulated drugs were directly measured: the quantities of drugs were determined by withdrawing two aliquots of 100 µL, diluting them with 1.90 mL of DMSO and measuring their UV-VIS absorbance (λ_{CQb} = 340 nm, λ_{PQb} = 366 nm, λ_{Qnb} = 420 nm).

Complexation of heparin by the DHPs

The formation of the complexes between the DHPs and heparin was studied employing the **methylene blue (MB) spectroscopic competition assay process**.[236] MB is a cationic metachromatic dye that presents a good affinity for polyanions. In particular, MB can complex heparin forming a complex that displays an indigo color (λ_{max} = 565 nm). When a potential heparin binder is added to a MB/heparin complex dissolution, it may compete with MB and bind heparin; thus, MB would be released in the solution and displays its natural sky blue color (λ_{max} = 665 nm) (**figure C_7-2**).

In the Heparin/MB spectrum, two maximums can be observed, one at 565 nm that corresponds to the MB/heparin complexes and another one at 665 nm that correspond to the free MB in excess, assuring that all heparin is complexed by the MB. When all heparin was complexed by one DHP, MB was totally released in the medium and displayed the same UV/Vis spectra that the free MB. In addition, DHP/heparin complexes do not present absorbance between 400 and 800 nm that could have affected the presence of DHPs do not affect the same UV/Vis spectrum of MB.

[236] Al-Jamal KT *et al.*, *Results in Pharma Sci.*, **2012**, 2, 9.

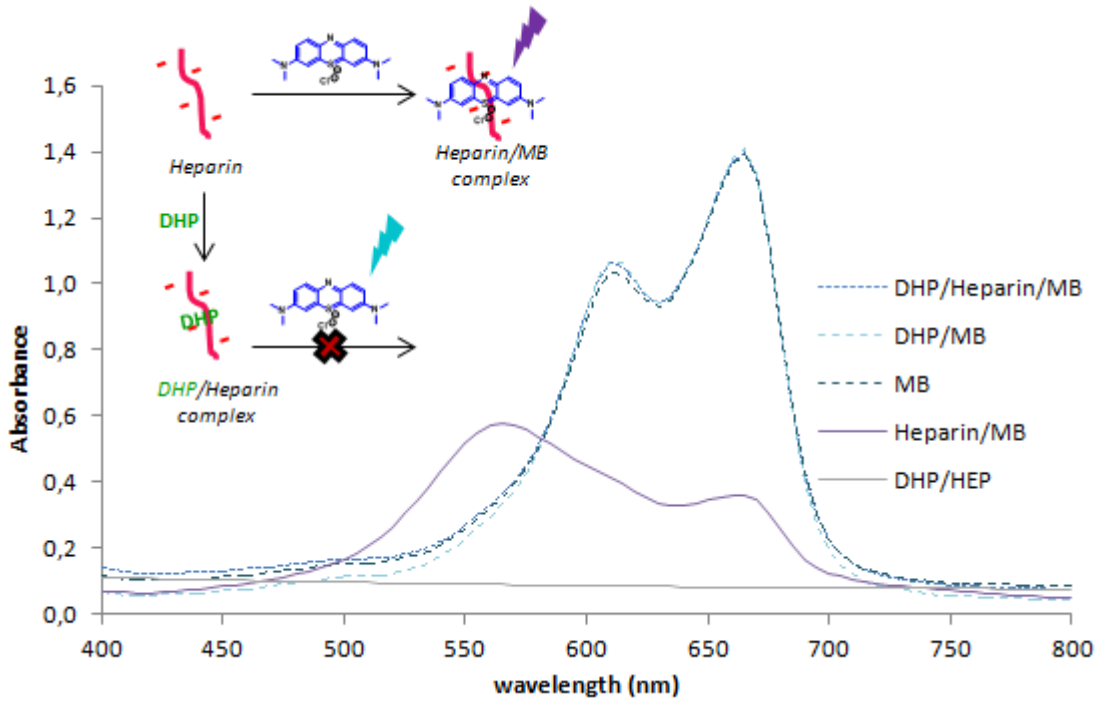

FigureC$_7$-2: UV/Vis spectra of DHP/Heparin/MB (λ_{max} = 665 nm), DHP/MB (λ_{max} = 665 nm), free MB (λ_{max} = 665 nm), Heparin/MB (λ_{max} = 565 nm) and DHP with heparin (no absorbance).

*S*amples containing heparin (10 µg/mL) and methylene blue (50 µM) was dissolved into TRIS.HCl pH 7.4 (10 mM) buffer were prepared in 96 multiwell culture plates and were gently rotationally stirred at room temperature for 15 min to allow MB to fully complex heparin. Then, DHPs were added to the samples at different (w_{DHPs}/w_{Hep}) ratios and the final sample volumes were adjusted to 150 µL. They were newly stirred for another 30 min. UV/Vis spectra was recorded between 400 and 800 nm with an EPOCH UV/Vis spectrophotometer. A_{665}/A_{565} ratio was calculated to determine the complexation between the DHPs and heparin. The experiments were replicated in triplicate in the case of the DHPs alone and in duplicate with the DHPs containing the encapsulate antimalarial drugs in their salt and base form.

Parasite infected red blood cells targeting

(protocols carried out in collaboration with Elisabet Martí Coma-Cros)

The oil-in-water procedure was employed to **encapsulate** modified rhodamine **(RhB(C17)$_2$)** within the **HDLDBCs**.[95] Each HDLDBC was dissolved at a concentration of 1 mg/mL in water. RhB(C17)$_2$ was dissolved in dichloromethane at a concentration of 0.15 mg/mL. An appropriate volume of the RhB(C17)$_2$ solution was added to each HDLBC solution in order to obtain a ($w_{HDLDBC}/W_{RhB(C17)}$) ratio of 1/0.15. The mixtures vigorously rotationally stirred at room temperature under ventilation until the organic solvent was completely evaporated. As any precipitate was observed in the final aqueous dissolution, it was assumed that all RhB(C17)$_2$ was encapsulated.

Parasite infected red blood cells **targeting** was studied by fluorescence microscopy.[95] Living P. falciparum cultures were synchronized to mature stages of the parasite (trophozoites). They were incubated with Hoechst during 30 minutes in RPMIc in dark at room temperature to stain the parasite nuclei. After three washings with RPMIc, parasitemia was decreased to 2 %. Parasite infected red blood cells (pRBCs) were incubated during 90 min at 37ºC with gentle stirring in dark with the presence of 150 μg/mL of DHP[G3+3]($NH_3^+Cl^-$,RhB) with 0, 5, 10 and 15 %w of heparin or with 75 μg/mL of HDLDBC/RhB(C17)$_2$ conjugates in RPMIc. After three washings with RPMIc, samples were observed in RPMIc in an 8 chambered borosilicate coverglass system in fluorescence microscopy. Hoechst fluorescence was observed at λ = 461 nm (λ_{ext} = 340 nm), FITC fluorescence was observed at λ = 518 nm (λ_{ext} =492 nm) and rhodamine fluorescence was observed at λ = 575 nm (λ_{ext} = 558 nm). Time of exposure was of 100 ms for Hoechst and rhodamine derivatives fluorescence and of 1000 ms for FITC fluorescence.

[95] J. Movellan, P. Urbán *et al.*, *Biomaterials*, **2014**, 35 7940.

***In vitro* plasmodium growing inhibition assays (GIAs)** *(protocols carried out by Elisabet Martí Coma-Cros)*

Plasmodium falciparum strains 3D7 was grown *in vitro* in human red blood cells (RBCs) type B, haematocrit 3%, using previously described conditions.[247] Parasites, thawed from glycerol stocks, were cultured at 37°C in T25 flasks with RBCs in Roswell Park Memorial Institute (RPMI) complete medium and incubated under a gas mixture of 92% N_2, 5% CO_2, and 3% O_2. Culture was synchronize with 5% sorbitol lysis[248 and maintained below 5% parasitemia by dilution with washed RBCs.

For standard **growth inhibition assays** (GIAs), parasitemia was adjusted to 1.5% parasitemia with more than 90% of rings stages after sorbitol synchronization. 150 µL of living parasite in complete medium with different concentrations of free drug and dendrimer encapsulating drug were plated in 96-well plate and incubated for 48h at 37°C, at same gas mixture than maintenance. Parasitemia was determined by fluorescent-assisted cell sorting (FACS) after staining pRBCs DNA with Syto 11 a nucleic acid dye dilution 1:1000 for FACS Calibur.

[247] C. Lambros, J.P. Vanderber, Synchronization of *Plasmodium falciparum* erythrocytic stages in culture, *J. Parasitol.*, **1979**, 65, 418-420.

[248] P. Urbán, J. Estelrich, A. Cortés, X. Fernàndez-Busquets A nonovector with complete discrimination for targeted delivery to *Plasmodium falciparum* versus non-infected red blood cells in vitro, *J. Control. Release*, **2011**, 151, 202-211.

Capitulo 8

Resumen y conclusiones

Resumen de la tesis

Introducción

El transporte y la liberación controlada de fármacos y la terapia génica son nuevas herramientas que permiten tratar enfermedades de manera más específica limitando los efectos secundarios de los tratamientos. En ambos casos, se requiere el empleo de vectores para transportar los genes o los fármacos. Estos vectores tienen que proteger su carga del sistema inmune, dirigirla de manera específica hacia las células enfermas y liberarla, reduciendo por lo tanto las dosis necesarias para obtener un efecto terapéutico y los efectos secundarios de las terapias. Además, en el caso del transporte de fármacos se puede emplear nuevos fármacos que no pueden ser inyectados directamente al paciente por su falta de solubilidad o su inestabilidad en el suero fisiológico.[1,2]

Dentro de la familia de los polímeros, los dendrímeros presentan características muy interesantes para convertirlos en buenos vectores para el transporte de genes y de fármacos. De hecho, al contrario de los polímeros lineares, los dendrímeros se sintetizan por etapas sucesivas formando macromoléculas hiperramificadas que tienen una topología repetitiva en forma de árbol. Sus estructuras finales están perfectamente controladas y se obtiene macromoléculas uniformes y monodispersas que presentan un alto número de grupos terminales en su superficie. Además, presentan unas propiedades muy interesantes tales como alta solubilidad, baja viscosidad, forma tridimensional globular que contiene huecos en su estructura capaces de contener moléculas pequeñas, *etc*.

[1] V.P. Torchilin, *Nat. Rev. Drug. Discov.* **2014**, *13*, 813.

[2] H. Yin, R.L. Kanasty, A.A. Eltoukhy, A.J. Vegas, J.R. Dorkin, D.G. Anderson, *Nat. Rev. Genet.* **2014**, *15*, 541.

Los dendrímeros de tipo polilisina (PLL), poliamidoamina (PAMAM), polipropileneimina (PPI) y poliésteres (*bis*-MPA) han sido ampliamente

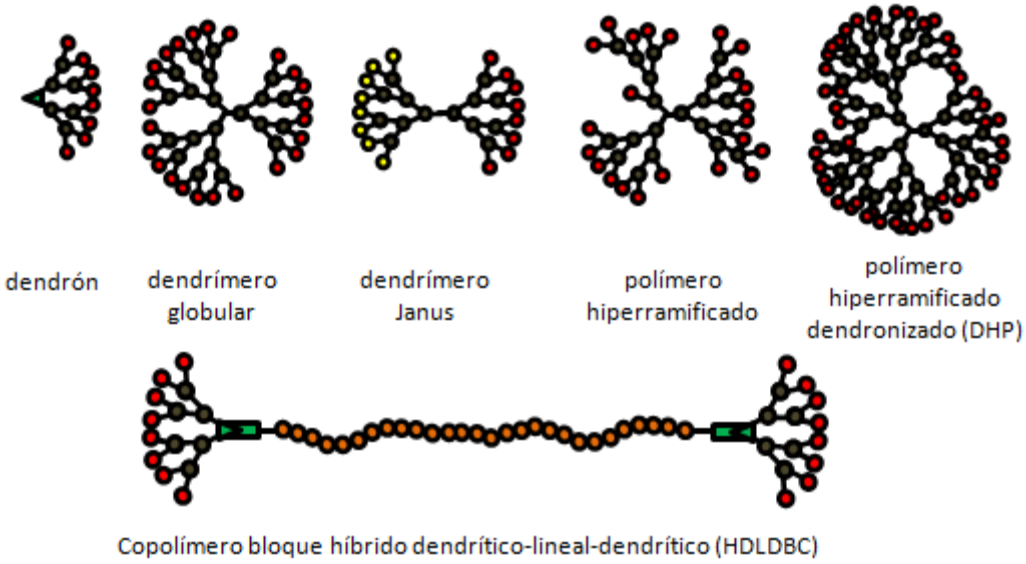

Figura 1: Representación esquemática de algunas derivados dendríticos.

investigados para sus aplicaciones en nanomedicina. Dado la dificultad de sintetizar dendrímeros globulares de altas generaciones, se han sintetizado e investigado nuevos derivados dendríticos: polímeros hiperramificados y polímeros hiperramificados dendrónizados (DHPs), dendrímeros Janus, híbridos de copolímeros bloque dendrítico-lineal-dendrítico (HDLDBCs), *etc*. (**figura 1**).[3]

Los dendrímeros de tipo Janus y los HDLDBCs son particularmente interesantes para el transporte de fármacos. Estas estructuras permiten la síntesis de macromoléculas anfífilas que pueden autoensamblarse en agua formando nanoestructuras cuyo núcleo es lipófilo y cuya periferia es hidrófila. Por una parte, pueden encapsular unos fármacos lipófilos en su núcleo y por lo tanto aumentar su solubilidad en medios acuosos y, por otra parte, pueden encapsular unos fármacos hidrófilos en su periferia aumentado su actividad. Previamente en nuestro grupo de investigación, unos dendrímeros de tipo Janus y HDLDBCs, ambos anfífilos, basados en *bis*-MPA han sido sintetizados para el

[3] F. Vögtle, G. Richardt, N. Werner, *Dendrimer chemistry, concepts, synthesis, properties, applications*, **2009**, WILEY-VCH Verlag GmbH & Co. Weinheim.

transporte de dos fármacos lipófilos insolubles en agua, la plitidepsina y la camptotecina, y dos hidrófilos, la primaquina y la cloroquina, para el tratamiento de diversos cánceres, de la hepatitis C y de la malaria.[4,5,6]

Los dendrímeros de *bis*-MPA funcionalizados con aminas terminales en su periferia han sido utilizados también en terapia génica. Así, se han utilizado polímeros hiperramificados y macromoléculas dendríticas iónicas o covalentes basadas en *bis*-MPA. Estas estructuras presentan buenas propiedades para formar complejos con el ADN pero su eficiencia en transfección génica sigue siendo nula o limitada.[7,8,9]

Objetivos

En esta tesis doctoral, se ha empleado derivados dendríticos del ácido 2,2-*bis*-hidroximetilpropiónico (*bis*-MPA) funcionalizados en su periferia con glicina y otros derivados dendríticos originales derivado del ácido 2,2-*bis*-gliciloximetilpropiónico (*bis*-GMPA) para sus aplicaciones en terapia génica y en transporte de fármacos (**figura 2**).

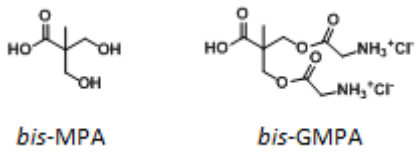

bis-MPA *bis*-GMPA

Figura 2: Representación del ácido 2,2-*bis*-hidroximetilpropiónico (*bis*-MPA) y del ácido 2,2-*bis*-gliciloximetilpropiónico (*bis*-MPA).

[4] E. Fedeli, A. Lancelot, J.L. Serrano, P. Calvo, T. Sierra, *New J. Chem.* **2015**, *39*, 1960.

[5] I. Jiménez, R. González, A. Lancelot, R. Clavería, A. Velázquez, O. Abián, M.B. Ros, T. Sierra, *Macromol. Biosci.* **2015**, *15*, 1381.

[6] J. Movellan, P. Urbán, E. Moles, J.M. de la Fuente, T. Sierra, J.L. Serrano, X. Fernàndez, *Biomaterials,* **2014**, *35*, 7940.

[7] J. Movellan, R. González, P. Martín, T. Sierra, J.M. de la Fuente, J.L. Serrano, *Macromol. Biosci.* **2015**, *15*, 657.

[8] A. Barnard, P. Posocco, S. Pricl, M. Calderon, R. Haag, M.E. Hwang, V.W.T. Shum, D.W. Pack, D.K. Smith, *J. Am. Chem. Soc.* **2011**, *133*, 20288.

[9] R. Reul, J. Nguyen, T. Kissel, *Biomaterials* **2009**, *30*, 5815.

En un primer lugar, se han sintetizado y empleado siete dendrímeros de tipo Janus y dos híbridos de copolímeros bloque dendrítico-lineal-dendrítico (HDLDBCs) anfífilos basados en *bis*-MPA y *bis*-GMPA para el transporte un fármaco lipófilo, la camptotecina, y se ha evaluado su potencial para el tratamiento *in vitro* de la hepatitis C.

En un segundo lugar, se han sintetizado y empleado dos dendrímeros globulares de *bis*-GMPA y tres polímeros hiperramificados dendronizados (DHPs) de *bis*-MPA para su uso como vectores sintéticos de siARN y pADN.

En un tercer lugar, se ha empleado los HDLDBCs basados en *bis*-MPA y *bis*-GMPA y los DHPs basados en *bis*-MPA sintetizados previamente para formar complejos con la heparina y encapsular tres fármacos antimaláricos, cloroquina, primaquina y quinacrina en sus formas hidrófila y lipófila, los cuales son.

Sistemas anfifílos para el transporte de la camptotecina, fármaco usado como antiviral en el tratamiento de la hepatitis C

La **camptotecina** es un inhibidor alostérico de la protease NS3 perteneciendo al virus de la hepatitis C y por lo tanto impide la replicación de este virus. Sin embargo, este **fármaco lipófilo** presenta una baja solubilidad en agua, una inestabilidad al suero fisiológico y una elevada citotoxicidad.[10]

Para superar estos inconvenientes, se ha planteado encapsular el fármaco dentro de nuevos sistemas dendrítico anfifílos, conteniendo un bloque lipófilo y un otro bloque hidrófilo. Por eso, se han sintetizado los siguientes sistemas dendríticos de tipo Janus y los siguientes HDLDBCs basados en Pluronic® F-127 (**figura 3**):

[10] O. Abián, S. Vega, J. Sancho, A. Velázquez-Campoy, Allosteric Inhibitors of the NS3 Protease from the Hepatitis C Virus. *PLoS ONE*. **2013**, 8, e69773.,

- $(NH_3^+Cl^-)_4$[*bis*MPA,G2]-[*bis*MPA,G1]-$(C17)_2$
- $(NH_3^+Cl^-)_4$[*bis*MPA,G2]-[*bis*MPA,G2]-$(C17)_4$
- $(NH_3^+Cl^-)_8$[*bis*MPA,G3]-[*bis*MPA,G1]-$(C17)_2$
- $(NH_3^+Cl^-)_8$[*bis*MPA,G3]-[*bis*MPA,G2]-$(C17)_4$
- $(NH_3^+Cl^-)_4$[*bis*GMPA,G2]-[*bis*MPA,G1]-$(C17)_2$
- $(NH_3^+Cl^-)_8$[*bis*GMPA,G3]-[*bis*MPA,G1]-$(C17)_2$
- $(NH_3^+Cl^-)_8$[*bis*GMPA,G3]-[*bis*MPA,G2]-$(C17)_4$

dendrímeros de tipo Janus

- $(NH_3^+Cl^-)_8$[*bis*MPA,G3]-PLU-[*bis*MPA,G3]$(NH_3^+Cl^-)_8$
- $(NH_3^+Cl^-)_8$[*bis*GMPA,G3]-PLU-[*bis*GMPA,G3]$(NH_3^+Cl^-)_8$

HDLDBCs

Todos los derivados anfifílos sintetizados pudieron **auto-ensamblarse en agua** formando diversos agregados supramoleculares tales como micelas esféricas o ovoidales, bicapas flexibles o rígidas y vesículas.

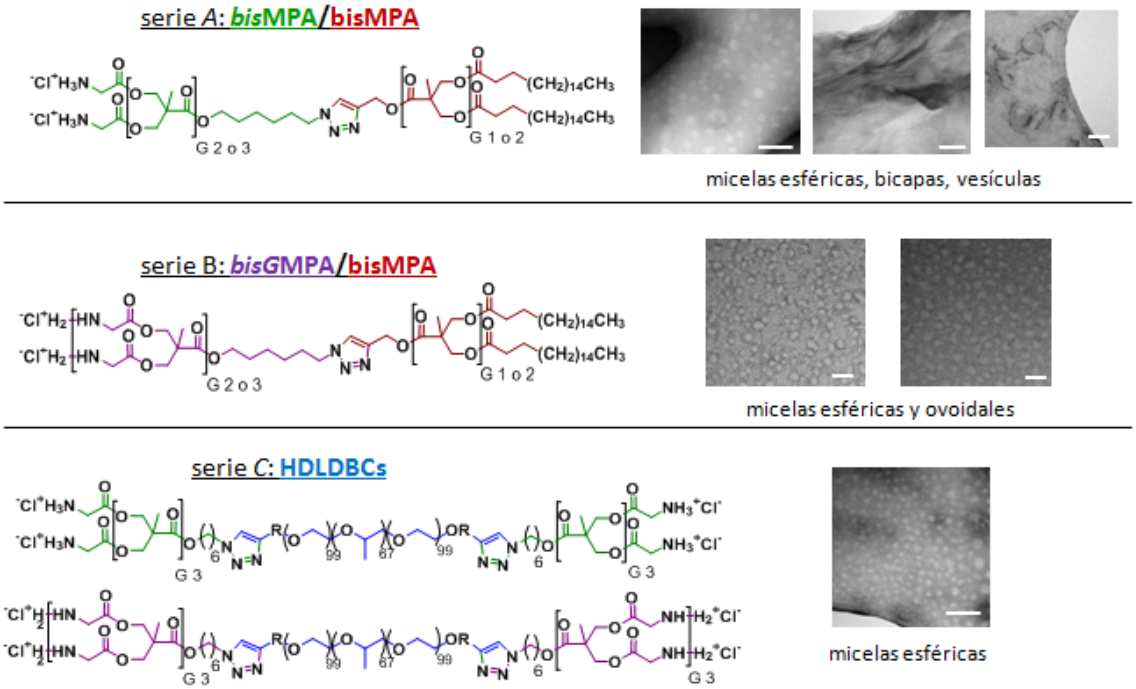

Figura 3: Representación esquemática de los derivados dendríticos sintetizados y fotos de microscopia de transmisión de electrones de los diversos agregados que forman en agua. Barra de escala = 50 nm.

Se ha logrado encapsular la camptotecina dentro de 8 de los 9 derivados dendríticos sintetizados, **aumentando la solubilidad y la estabilidad del fármaco lipófilo en medio acuoso**. Los dendrímeros de tipo Janus constituidos por el dendrón hidrófilo de ***bis*-GMPA** (*serie B*) han demostrado la **mayor capacidad para encapsular el fármaco** con una eficiencia de encapsulación (EE) siendo entre el 54 y el 60 % mientras que la EE ha sido entre el 29 y el 46 % por los HDLDBCs (*serie C*) y entre el 0 y el 14 % por los dendrímeros de tipo Janus constituidos por el dendrón hidrófilo de *bis*-MPA (*serie A*). Claramente, la presencia del dendrón de *bis*-GMPA ha favorecido la encapsulación del fármaco dentro de los agregados supramoleculares y la estabilidad del conjugado "*derivado dendrítico/fármaco*" formado.

Además, se ha observado durante ensayos *in vitro* **un aumento de la actividad antiviral del fármaco encapsulado**, en respeto a la actividad del fármaco libre, cuando estaba encapsulado dentro de los dendrímeros de tipo Janus constituidos por el dendrón de *bis*-MPA hidrófilo (*serie A*) y dentro de los HDLDBCs (*serie C*).

De todos los sistemas estudiados, el HDLDBC, **$(NH_3^+Cl^-)_8$[*bis*GMPA,G2]-PLU-[*bis*GMPA,G2]$(NH_3^+Cl^-)_8$,** aparece como el **mejor vector para el transporte de la camptotecina** para tratar la hepatitis C, dado que presenta una buena eficiencia de encapsulación del fármaco (46 %) y que ha permitido mejorar la actividad del fármaco.

En un estudio paralelo, se ha sintetizado un nuevo **fluoróforo lipófilo**, derivado de un fluoróforo comercial: la rodamina B. Este fluoróforo original ha demostrado su potencial para **marcar eficazmente por simples interacciones lipófilas**, los agregados de tipo Janus sin alterar su formación, su morfología y la actividad del fármaco encapsulado.

Sistemas dendríticos globulares para su uso como vectores sintéticos de siARN y pADN

Para transfectar siARN y pADN, se ha sintetizado dos series de derivados dendríticos globulares con numerosos cationes localizados en su periferia. Los cationes de los derivados dendríticos forman interacciones electrostáticas con los grupos fosfato aniónicos del **siARN o del pADN permitiendo su transporte y protección** hacía las partes internas de las células. Por eso, se ha sintetizado los siguientes dendrímeros de *bis*-GMPA y polímeros hiperramificados dendronizados (DHPs) de *bis*-MPA con glicinas terminales (**figura 3**):

- **D[*bis*GMPA,G2] $(NH_3^+Cl^-)_{24}$**
- **D[*bis*GMPA,G3] $(NH_3^+Cl^-)_{48}$**

dendrímeros de *bis*-GMPA

- **DHP[*bis*MPA,G2+3]$(NH_3^+Cl^-)_{120}$**
- **DHP[*bis*MPA,G3+3]$(NH_3^+Cl^-)_{248}$**
- **DHP[*bis*MPA,G4+3]$(NH_3^+Cl^-)_{424}$**

***bis*-MPA DHPs con glicinas terminales**

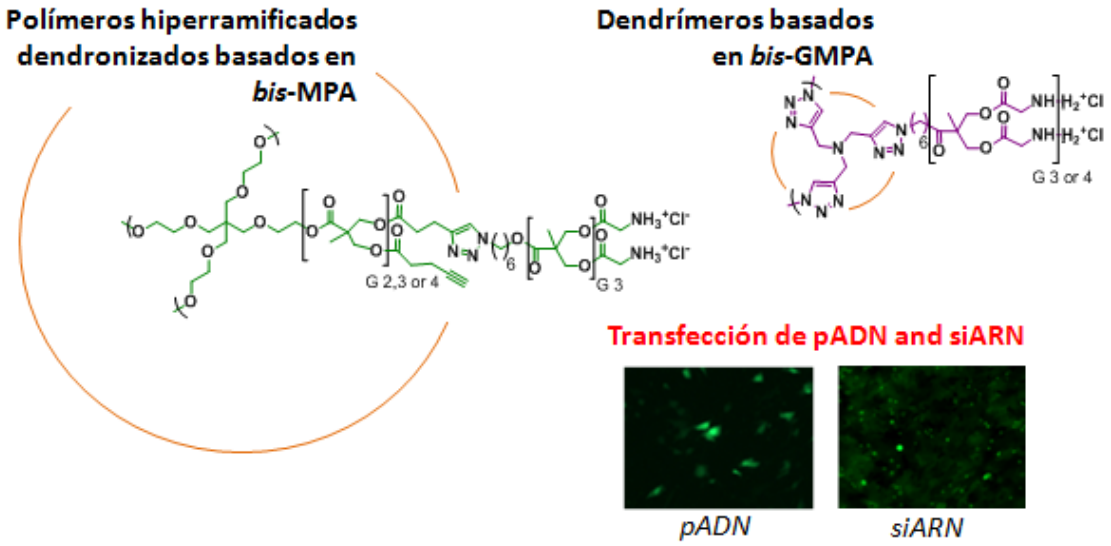

Figura 3: Polímeros hiperramificados dendronizados (DHPs) basados en *bis*-MPA y dendrímeros basados en *bis*-GMPA para su uso como transportadores de pADN y siARN.

La **biocompatibilidad** de todos los derivados dendríticos ha sido comprobada en varias líneas celulares y todos los derivados han podido **formar**

complejos con pADN y siARN, llamados "*dendriplexos*". Sin embargo, los derivados dendríticos de las generaciones más altas de ambas series, **D[*bis*GMPA,G3] $(NH_3^+Cl^-)_{48}$** y **DHP[*bis*MPA,G4+3]$(NH_3^+Cl^-)_{424}$** han formado complejos más pequeños y con una carga superficial más altas, características favorables a una eficiente transfección génica.[2]

En cuanto a la transfección del siARN, el dendrímero de *bis*-GMPA, **D[*bis*GMPA,G3]$(NH_3^+Cl^-)_{48}$**, ha presentado los mejores resultados, **transfectando el siARN** en células cancerígenas con una eficiencia igual al cuarto de la eficiencia de la lipofectamina® 2000, un agente comercial, e igual al séptimo de la eficiencia de este mismo agente en células no tumorales.

En cuanto a la transfección de pADN, el DHP basado en *bis*-MPA, **DHP[*bis*MPA,G3+3]$(NH_3^+Cl^-)_{424}$**, ha presentado los mejores resultados. Si la transfección génica no fue muy eficiente en células cancerígenas, este derivado dendrítico ha conseguido transferir el pADN en células madre mesenquimatosas con la **misma eficiencia que la lipofectamina® 2000 y el Transit-X2®**, presentando además una mejor biocompatibilidad que el primer agente comercial. Estos DHPs han sido los primeros derivados dendríticos basados en *bis*-MPA que pudieron demonstrar una eficiencia de transfección de pADN similar a la de dos agentes comerciales.

Sistemas dendríticos para el transporte de fármacos antimaláricos

Una amplia librería de fármacos se ha usado para el tratamiento de la malaria. No obstante, estos fármacos presentan un direccionamiento insuficiente hacía los glóbulos rojos infectados por el parásito responsable de la malaria. En consecuencia, unas altas dosis de fármacos son necesarias para tratar la enfermedad, lo cual resulta en numerosos y penosos efectos secundarios para los pacientes y en la aparición de cepas de parásitos resistentes a los tratamientos.

Con el fin de mejorar su direccionamiento y su actividad, tres fármacos antimaláricos, la cloroquina (CQ), la primaquina (PQ) y la quinacrina (QN), han sido encapsulados tanto en su forma de sal (soluble en agua) como en su forma básica (insoluble en agua) dentro de los tres **DHPs** basados en *bis*-MPA y de los dos **HDLDBCs** basados en *bis*-MPA y *bis*-GMPA presentados anteriormente en esa memoria (**figura 4**).

Todos los derivados dendríticos estudiados **han podido encapsular los tres fármacos en sus formas hidrófilas y la primaquina en su forma base con buenas eficiencias de encapsulación** (EE entre el 26 y el 44 %). Solo los DHPs han sido capaces encapsular la cloroquina en su forma básica (EE entre el 78 y el 82 %) mientras que no se ha conseguido encapsular la quinacrina en su forma básica en ninguno de los derivados estudiados.

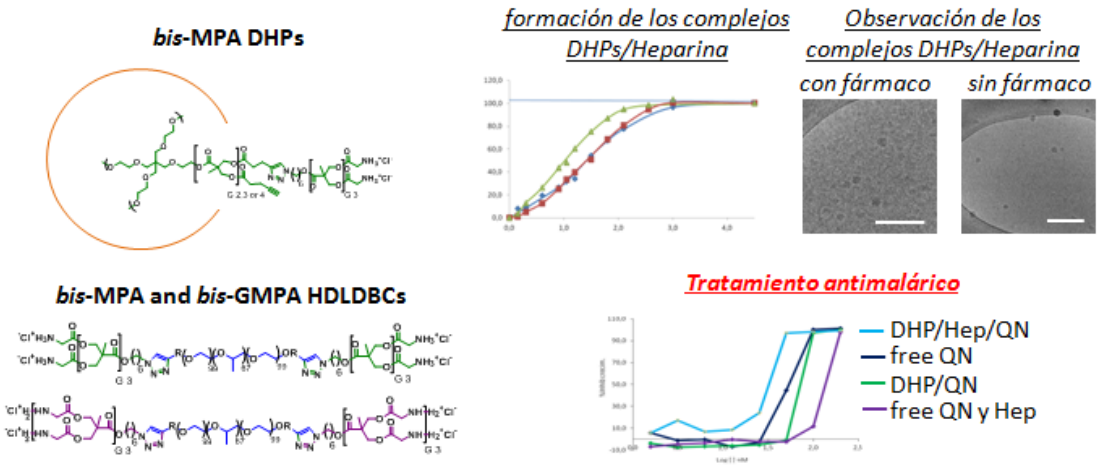

Figura 4: Representación esquemática de los derivados dendríticos dendronizados para la formación de complejos con heparina (Hep) y el transporte de fármacos antimaláricos (cloroquina (CQ), primaquina (PQ) y quinacrina (QN)). Barra de escala = 200 nm.

En paralelo, la **formación de complejos con la heparina** y los DHPs ha sido estudiada. La heparina es un polímero que tiene una actividad antimalárica y se dirige con preferencia hacia los glóbulos rojos infectados con el parásito

responsable de la malaria.[11] Los tres DHPs han sido capaces de formar complejos basados en interacciones electrostáticas con la heparina. Similarmente a lo observado con anterioridad con el ADN, el DHP más grande **DHP[*bis*MPA,G4+3]($NH_3^+Cl^-$)$_{424}$** ha presentado las **mejores eficiencias para formar los complejos con la heparina**. La presencia de los fármacos encapsulados en sus formas salinas dentro de los DHPs retarda levemente la formación de los complejos con heparina mientras que la presencia de los fármacos encapsulados en sus formas básicas impide la formación de los complejos con heparina. El tamaño de los complejos es pequeño (inferior a 50 nm) lo cual es interesante para su internalización eficaz dentro de los glóbulos rojos infectados.[12]

Tanto los DHPs como los HDLDBCs han demostrado un **buen direccionamiento hacia los glóbulos rojos infectados** por el parásito, siendo casi exclusivo por los DHPs. En la mayoría de los casos, se ha conseguido mantener la actividad de los fármacos en comparación con la de los fármacos libres. Además, se ha conseguido mejorar la actividad de la quinacrina encapsulada dentro de un DHP mientras estaba asociada con la heparina demostrando el potencial de los complejos "*DHP/heparina*" para transportar fármacos antimaláricos. Sería relevante seguir con estos estudios, probando si la formación de los complejos DHP/heparina, permite mejorar la actividad de la cloroquina y de la primaquina.

[11] J. Marqués, E. Moles, P. Urbán, R. Prohens, M.A. Busquets, C. Sevrin, C. Grandfils, X. Fernàndez-Busquets, *nanomedicine* **2014**, 10, 1719.

[12] P.R. Gilson, S.A. Chisholm, B.S. Crabb, T.F. de Koning-Ward, *Int. J. Parasitol.* **2017**, 47, 119.

Conclusiones

En esta tesis doctoral, se ha estudiado el potencial de nuevos sistemas dendríticos de tipo poliéster basados en el ácido 2,2'-bis-hidroximetilpropiónico (bis-MPA) o de tipo poli(esteramido) basados en el ácido 2,2'-bis-gliciloximetilpropiónico (bis-GMPA) para su aplicación como transportadores de material genético como de fármacos. Todos los sistemas sintetizados, dendrímeros globulares y Janus, copolímeros bloques híbrido dendrítico-lineal-dendrítico (HDLDBCs) y polímeros hiperramificados dendronizados (DHPs), han demostrado su biocompatibilidad y biodegradabilidad.

En terapia anti-hepatitis C, los derivados dendríticos de tipo Janus y HDLDBCs han podido encapsular la camptotecina, un fármaco lipófilo, y mejorar su actividad contra la replicación del virus del la hepatitis C. En particular, los HDLDBCs han demostrado un buen balance, mejorando a la vez la solubilidad del fármaco en agua y su actividad.

En terapia génica, los derivados dendríticos de tipo dendrímero globular y DHPs, han permitido la transfección de pADN y de siARN. En particular, los polímeros hiperramificado dendronizados (DHPs) basados en bis-MPA han destacado como compuestos innovadores para la síntesis de sistemas dendríticos de alta generación con aplicaciones en terapia génica que pueden competir con los agentes comerciales.

En terapia antimalárica, los derivados dendríticos basados en bis-MPA y bis-GMA han demostrado su potencial para encapsular fármacos antimaláricos y su alta selectividad hacia los glóbulos rojos infectados con el parásito plásmodium, responsable de la enfermedad. Además, los DHPs han podido formar complejos con la heparina, un polisacárido que favorece el direccionamiento de los transportadores de fármacos antimaláricos hacia los glóbulos rojos infectados, mejorando su actividad.

La adición de cadenas lipófilas mediante un dendrón de bis-MPA sobre la rodamina permite marcar de manera eficaz y duradera varios agregados basados en sistemas dendríticos sin necesidad de emplear química covalente y sin alterar sus propiedades biológicas.

Annexes

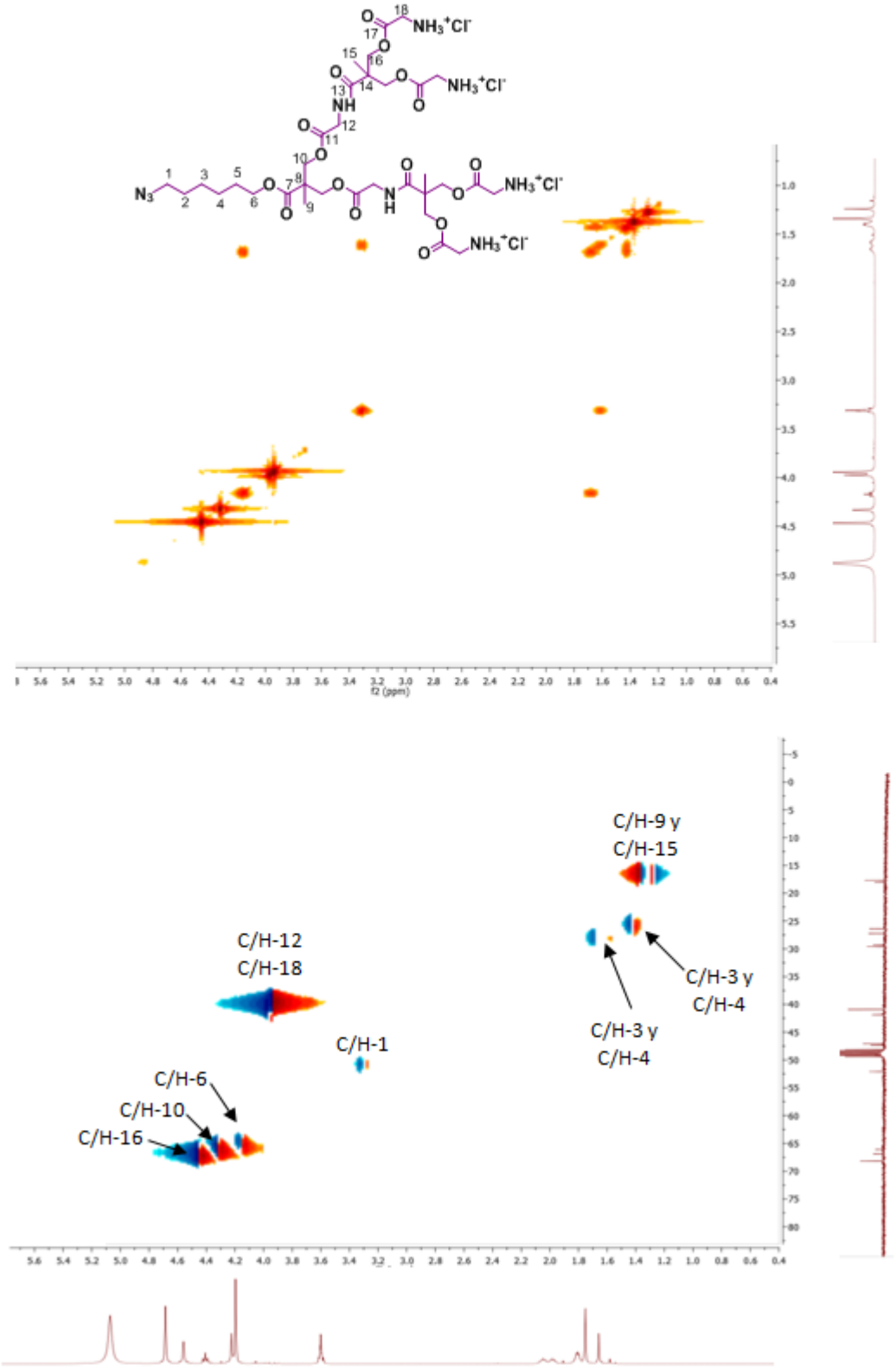

Annexes 1: ^{1}H-^{1}H COSY and ^{1}H-^{13}C HSQC NMR experiments of N_3-[*bis*GMPA,G1]-$(NH_3^+Cl^-)_4$.

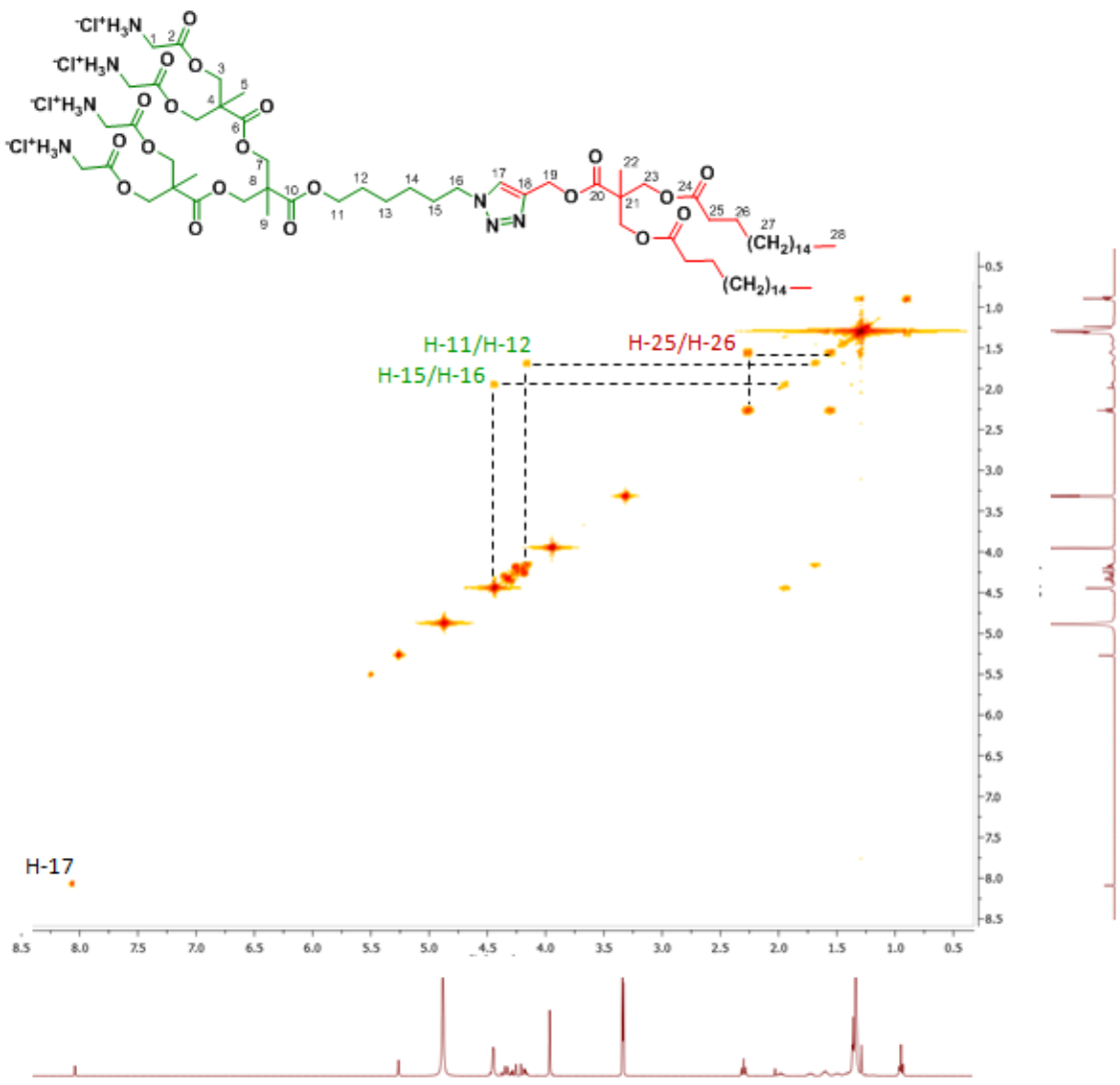

Annexes 2: ^{1}H-^{1}H COSY of **($NH_3^+Cl^-$)$_4$ [*bis*MPA,G2]-[*bis*MPA,G1](C17)$_2$.**

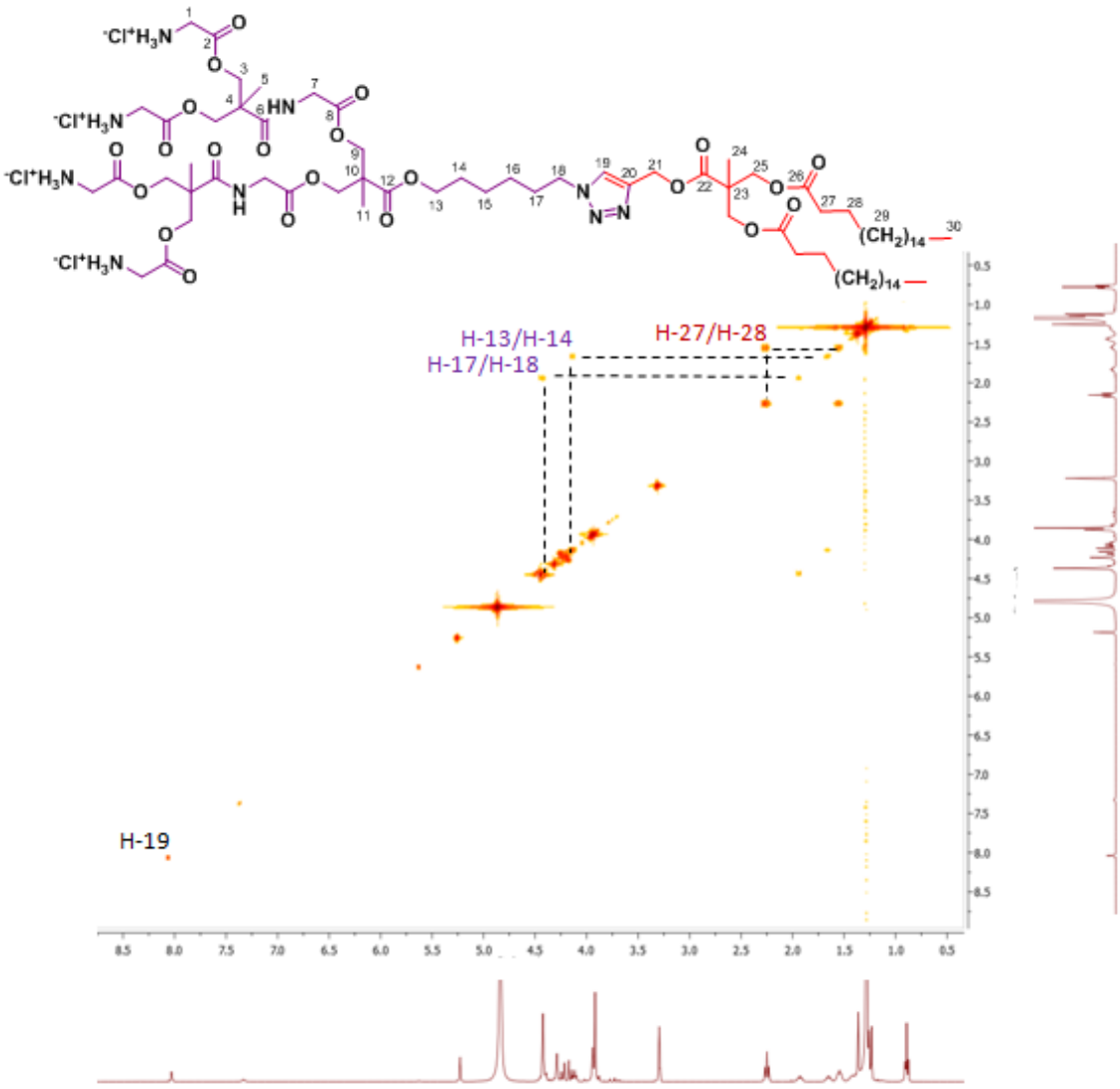

Annexes 3: ^{1}H-^{1}H COSY of **$(NH_3^+Cl^-)_4$ [*bis*GMPA,G2]-[*bis*MPA,G1](C17)$_2$.**

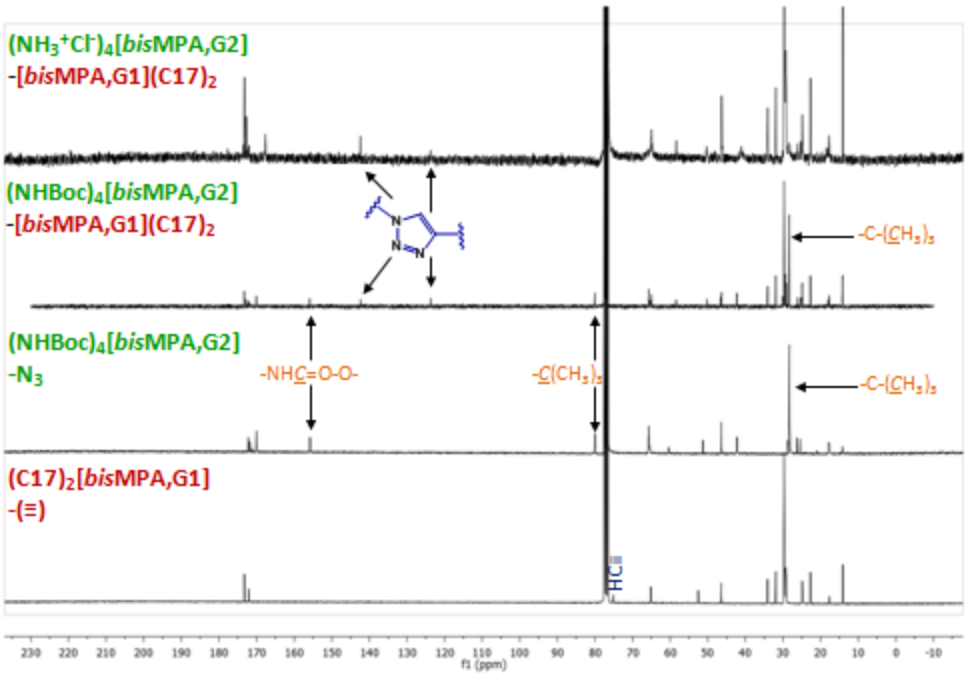

Annexes 4: ^{13}C-NMR spectra of **(NHBoc)$_4$[*bis*MPA,G2]-[*bis*MPA,G1](C17)$_2$** and the two starting dendrons **(NH$_3^+$Cl$^-$)$_4$[*bis*GMPA,G2]-N$_3$** and **(C17)$_2$[*bis*MPA,G1]-(≡)** in $CDCl_3$ and **(NH$_3^+$Cl$^-$)$_4$[*bis*MPA,G2]-[*bis*MPA,G1](C17)$_2$** in CD_3OD, at 75 or 100 MHz.

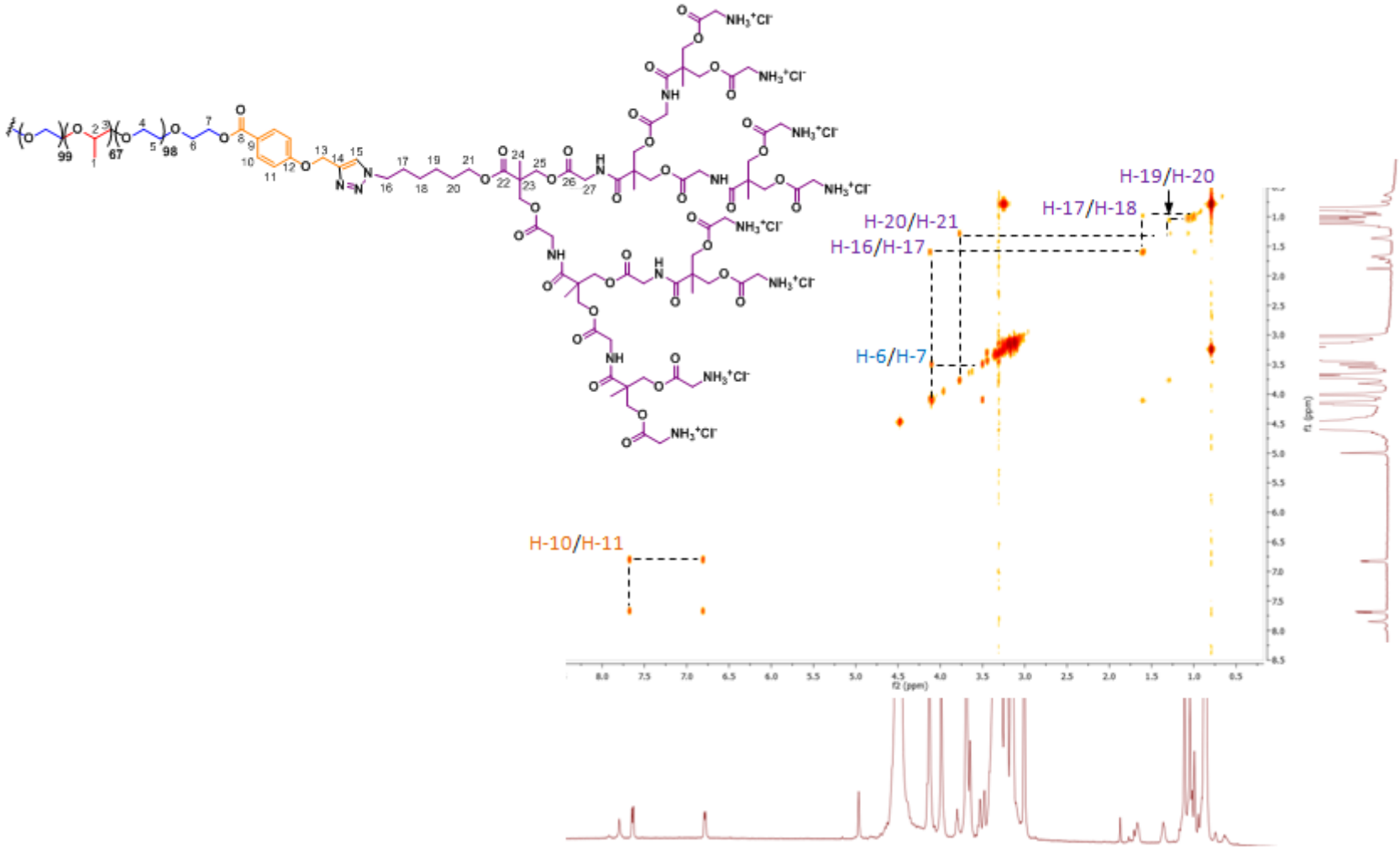

Annexes 5: ^{1}H-^{1}H COSY of ***bis*GMPA-PLU-*bis*GMPA** recorded in CD_3OD at 500 MHz.

	***bis*-MPA/*bis*-MPA series with CPT**		
	[G2]-[G1]	**[G3]-[G1]**	**[G3]-[G2]**
number	160 nm	140 nm	120 nm
intensity	400 - 800 nm	800 - 1400 nm	600 - 1500 nm
	***bis*-GMPA/*bis*-MPA series with CPT**		
	[G1]-[G1]	**[G2]-[G1]**	**[G2]-[G1]**
number	45 nm	140 nm	25 nm
intensity	100 - 900 nm	500 - 700 nm	100 - 700 nm
	HDLDBCs with CPT		
	***bis*MPA-[PLU]-*bis*MPA**	***bis*GMPA-[PLU]-*bis*GMPA**	
number	15 nm (100%)	12 nm (100%)	
intensity	30 nm (24 %) 150 - 250 nm (76 %)	40 nm (8 %) 220 - 300 nm (92 %)	

Annexes 6: Hydrodynamic diameter (nm) of the nanocarrier/**CPT** conjugates measured with DLS according to two different mathematical data treatments (number average and intensity average).

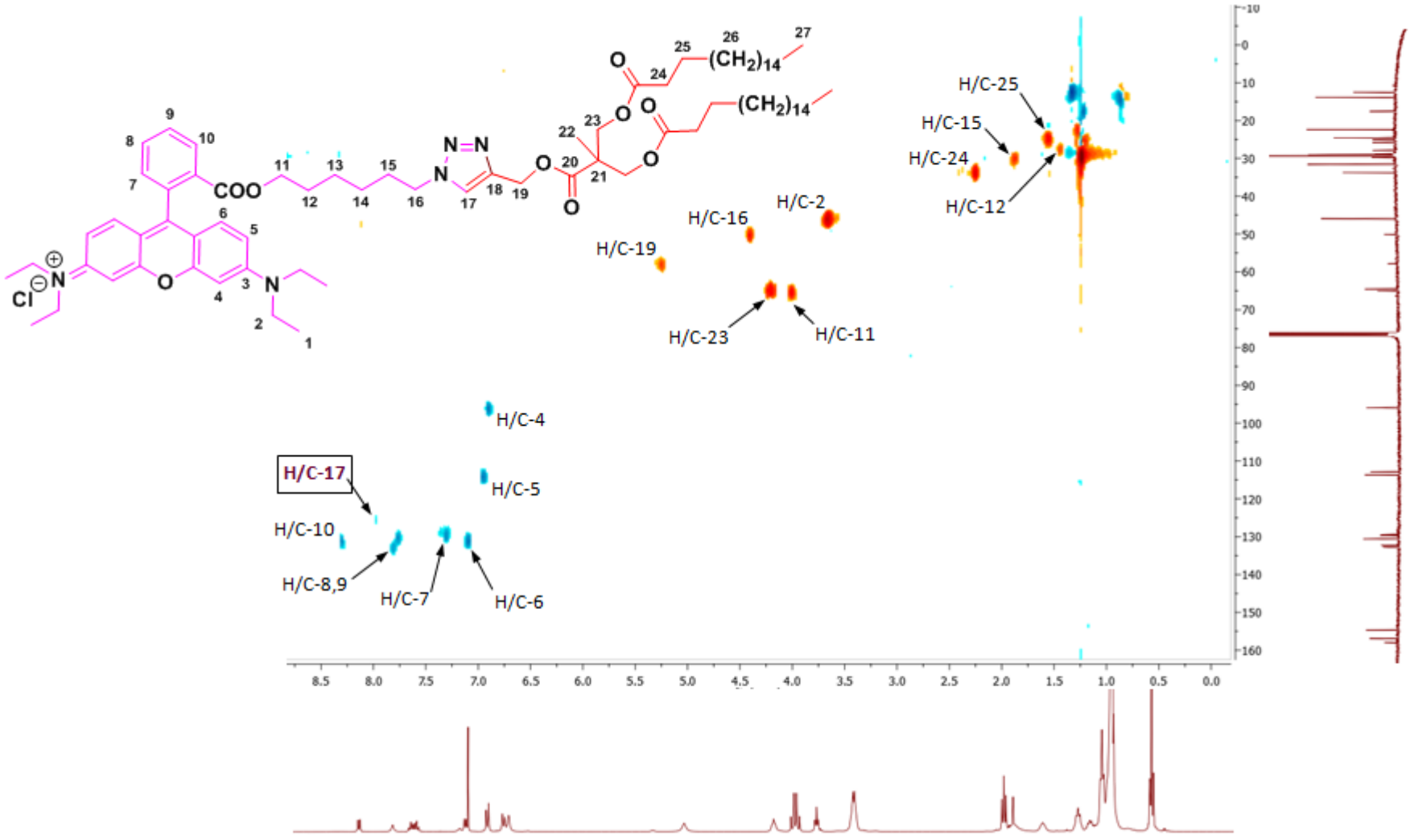

Annexes 7: ^{1}H-^{13}C HSQC spectrum of low-water soluble rhodamine B (**RHB(C17)$_2$**).

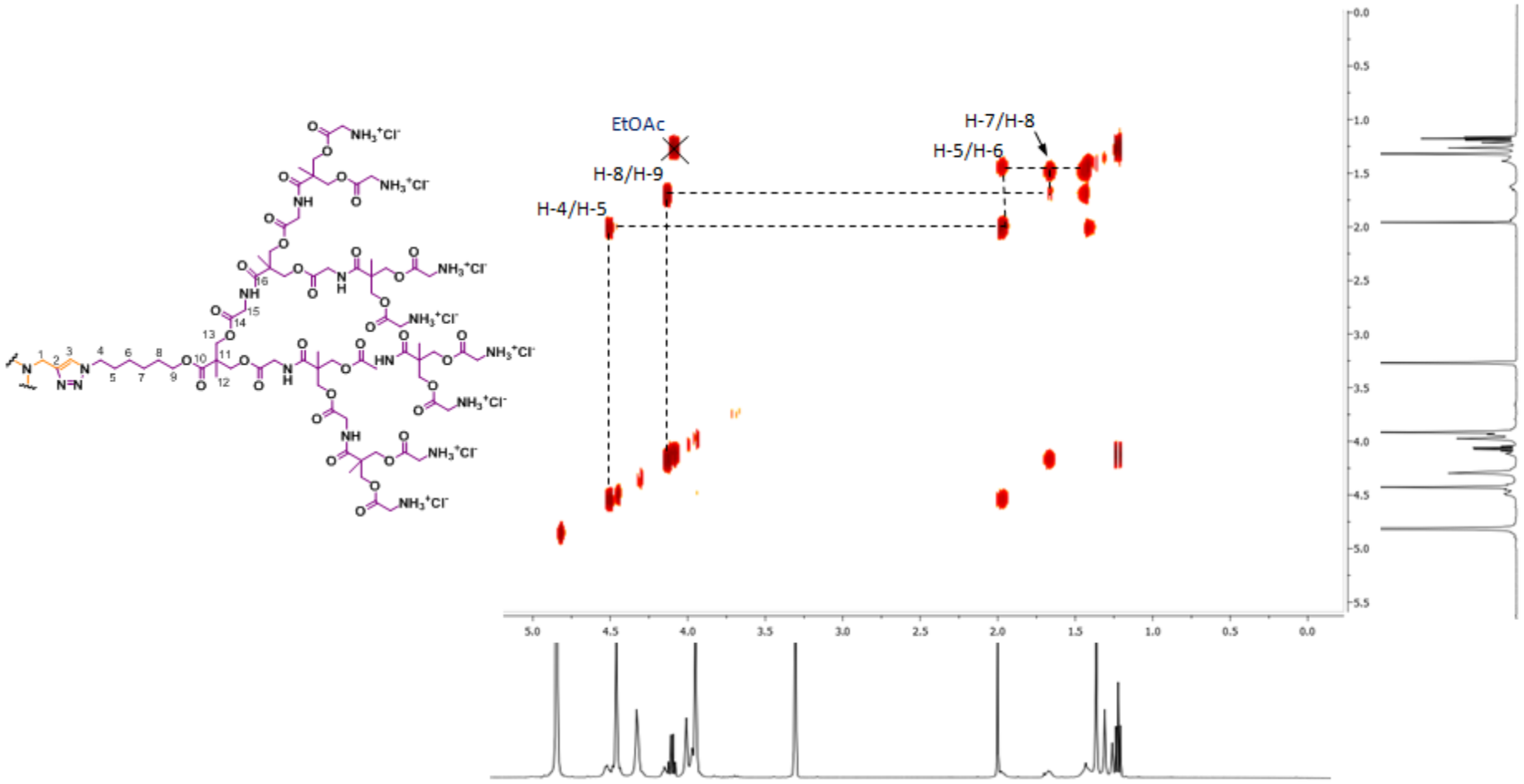

Annexes 8: $^{1}H\text{-}1^{H}$ NMR COSY of the 2nd generation *bis*-GMPA dendrimer, **D[G2]($NH_3^+Cl^-$)$_{24}$**, recorded in CD_3OD at 500 MHz.

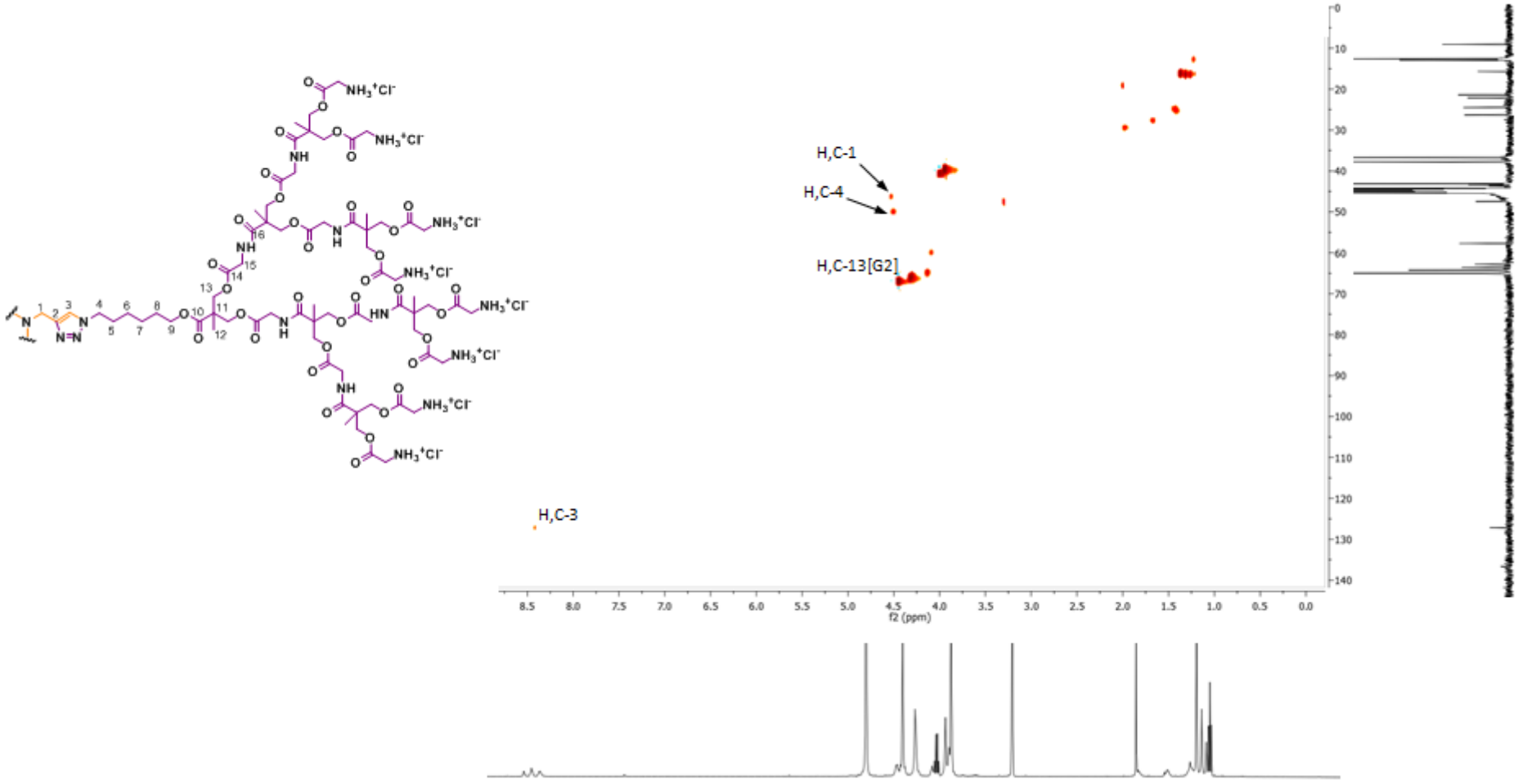

Annexes 9: ^{1}H-^{13}C NMR HSQC of the 2nd generation *bis*-GMPA dendrimer, **D[G2]($NH_3^+Cl^-$)$_{24}$**, recorded in CD_3OD at 500/100 MHz.

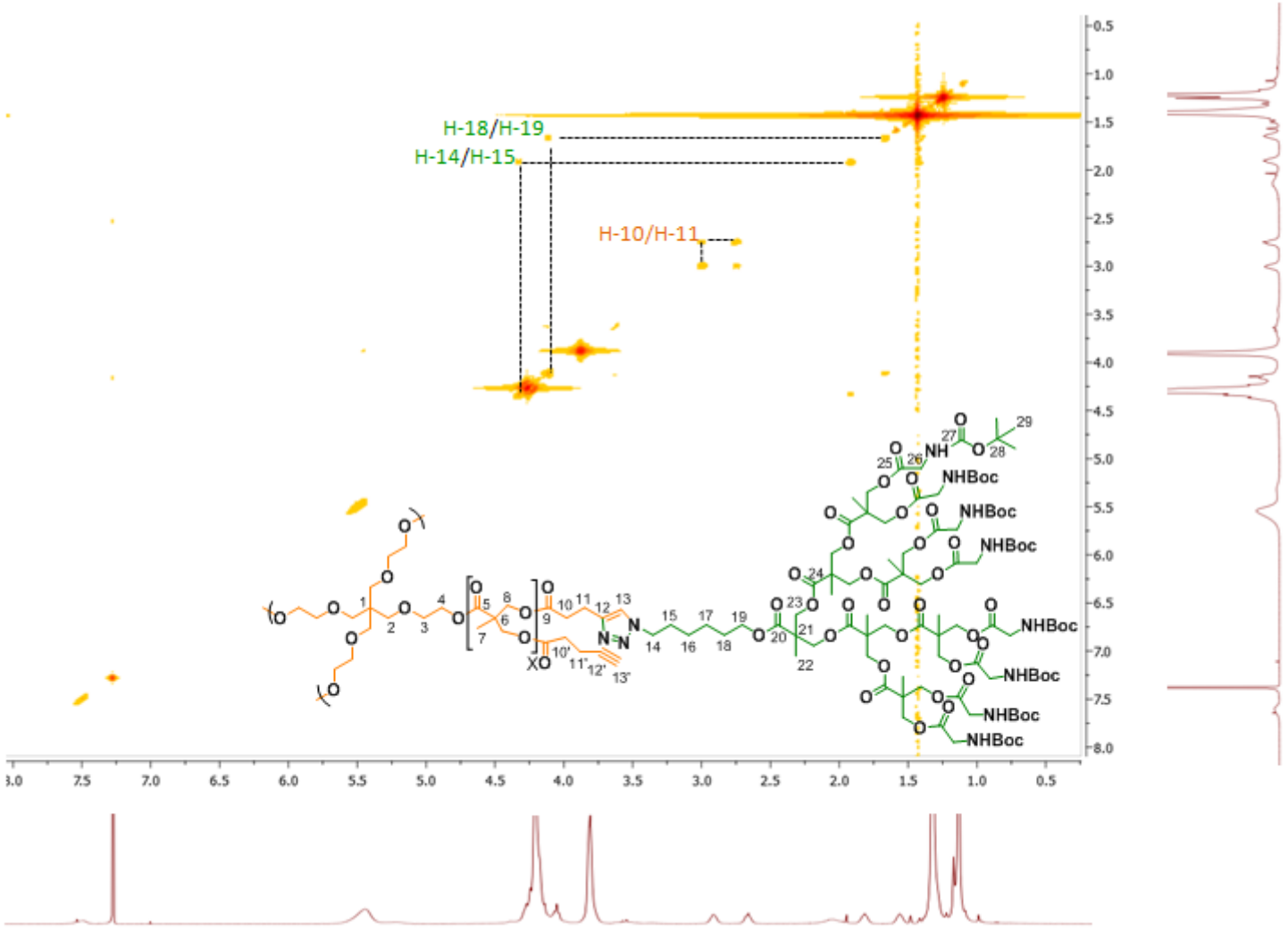

Annexes 10: ^{1}H-^{1}H COSY spectrum of **DHP[*bis*MPA,G2+3](NHBoc)$_{120}$** recorded in $CDCl_3$ at 400 MHz.

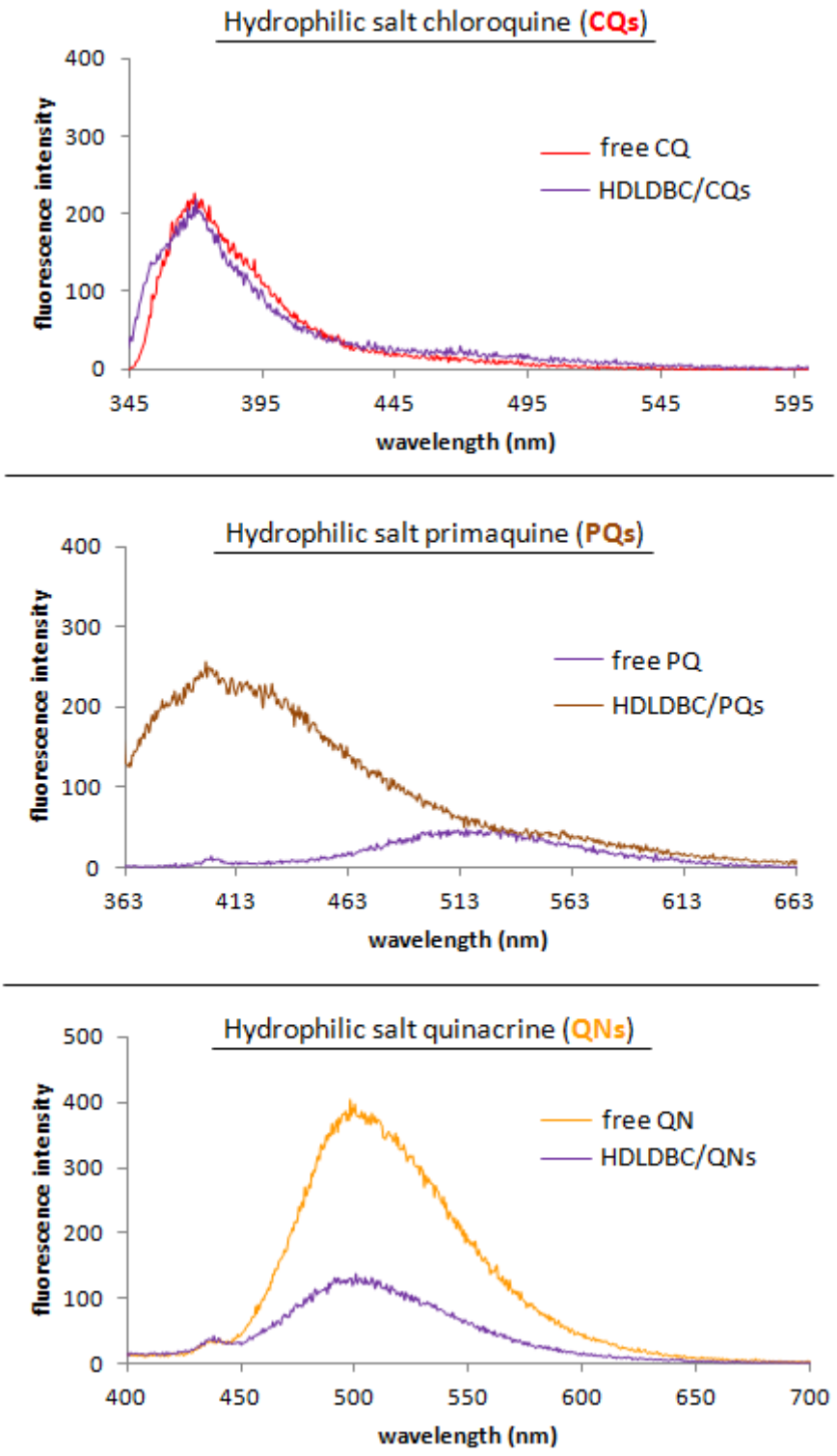

Annexes 11: Fluorescence spectra of the free antimalarial drugs (**CQs**, **PQs** and **QNs**) and of the ***bis*GMPA-[Plu]-*bis*GMPA**/hydrophilic antimalarial drug conjugates (**HDLDBC/CQs**, **HDLDBC/PQs** and **HDLDBC/QNs**).

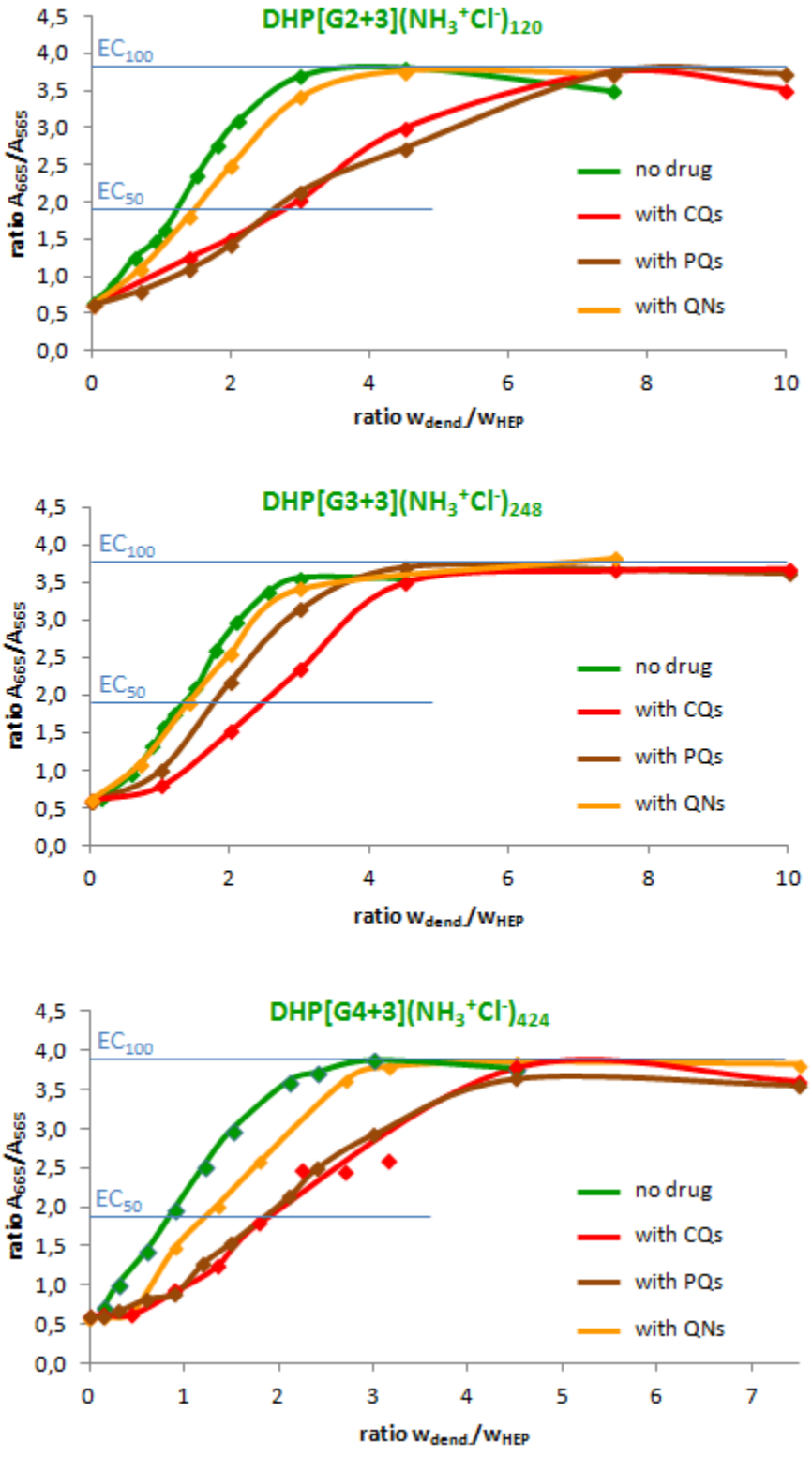

Annexes 12: Heparin complexation by the DHP/hydrophilic drug conjugates studied according to the MB spectroscopic competition assay. The EC_{100} corresponded to the ratio A_{665}/A_{565} ratio measured for free MB in water.

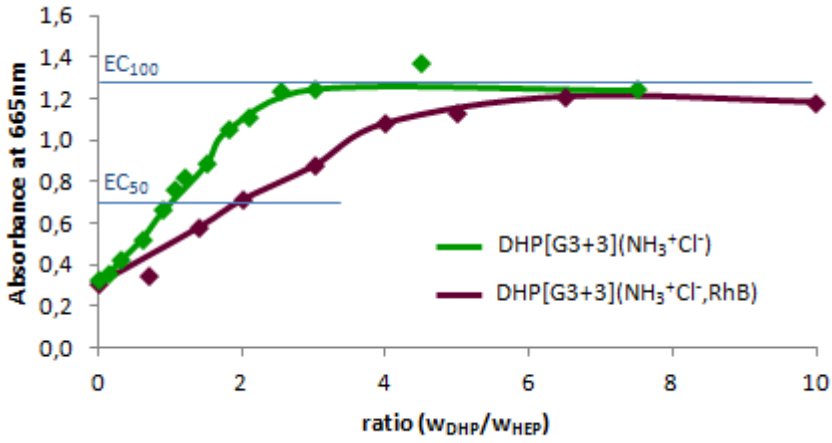

Annexes 13: Heparin complexation by the **DHP[G3+3](NH$_3^+$Cl$^-$)$_{248}$** and **DHP[G3+3](NH$_3^+$Cl$^-$,RhB)**, bearing 192 terminal amino groups. As the rhodamine showed intense absorbance at 565 nm, the complexation was studied only measuring the absorbance at 665 nm. The EC_{100} corresponded at the absorbance intensity of free MB in water at 665 nm.

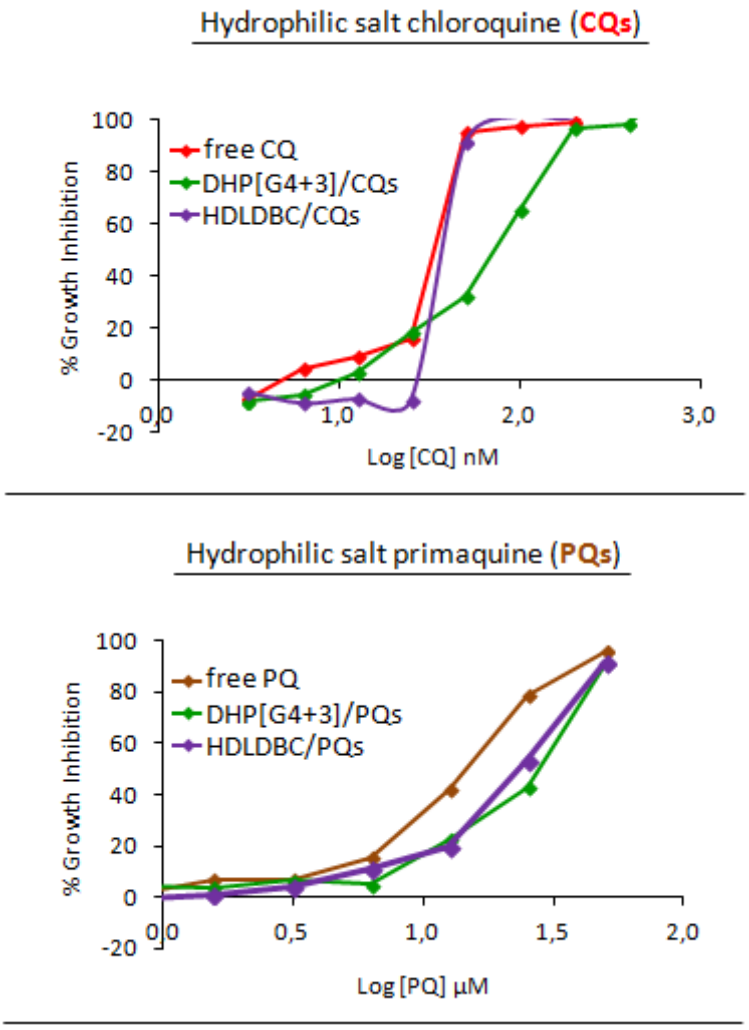

Annexes 14: Growing inhibition assays (GIAs) of free chloroquine (**CQ**) (up), primaquine (**PQ**) (middle) and quinacrine (**QN**) (down) and encapsulated within their hydrophilic salt form in **DHP[G4+3]($(NH_3^+Cl^-)_{424}$** and ***bis*GMPA-[PLU]-*bis*GMPA**.

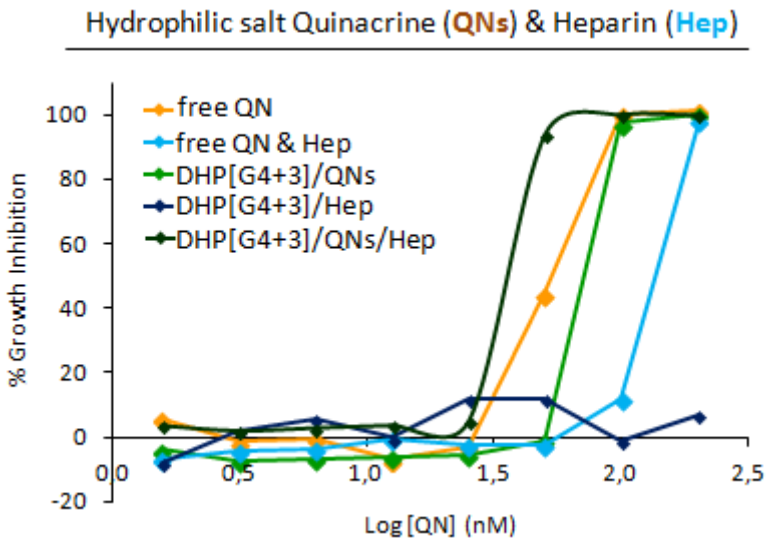

Annexes 15: Growing inhibition assays (GIAs) of free quinacrine without (**QN**) and with heparin (**QN** & **Hep**), **DHP[G4+3]/Hep** complexe, **DHP[G4+3]/QNs** conjugate and **DHP[G4+3]/QNs/Hep** conjugate.